Corrosion fatigue of a C-Mn steel.

Richard Joseph Appleton

PhD thesis

October 1985

Department of Mechanical Engineering

University of Glasgow

To Helen

Acknowledgments

This work was funded through the SERC Marine Technology Directorate under grant numbers GR/B/8872.3 and GR/C/7139.2, and also by the Department of Energy (Petroleum Engineering Division) through project OT/F/918. The financial support of these bodies is gratefully acknowledged.

I would also like to thank Professors J.D.Robson and B.F.Scott, as well as the University of Glasgow, for the provision of research facilities.

Messrs A.Torry, N.Flaherty and A.Birbeck provided invaluable assistance with the experiments.

I am very grateful to Dr. M.J.Cowling for his help and advice as superviser during the past few years.

These acknowledgements would not be complete without a very big "thank-you" to my wife for her patience and understanding during the past year.

Summary

The work reported in this thesis consists of three related studies relevant to the fatigue performance of offshore structures;

(a) a fundamental investigation into the mechanisms of corrosion fatigue crack growth in a C-Mn structural steel in the marine environment,

(b) a study of the effects of bacterial activity on corrosion fatigue crack growth rates,

(c) determination of stress intensity factors for surface breaking defects, and crack profile development.

Manipulation of solution chemistry, achieved by the use of solution additives, has shown that for the C-Mn steel studied both anodic dissolution and hydrogen embrittlement may cause enhanced crack growth rates in 3% NaCl solution. The dominant mechanism is determined by the solution chemistry and specimen potential. Results from fractography, slow strain rate testing, and crack propagation studies investigating the effects of oxygen concentration, waveform and specimen potential were shown to be consistent with this conclusion. Doubt has been expressed by other workers as to the applicability of an anodic dissolution mechanism to the system studied. However the current work has shown that these doubts are largely unfounded. In particular it was shown that the environmental enhancement of crack growth attributed to a dissolution mechanism could be completely accounted for on the basis of the bare surface current densities observed in such systems.

The effects of several significant engineering variables on crack growth rates produced by each of these mechanisms were also investigated. An important result was the lack of dependence on R ratio ($0.1 < R < 0.7$) for growth rates due to either mechanism. This has significant implications for design and the results are at variance with some previous work. For the case of crack growth enhancement due to hydrogen embrittlement a phenomenological model was outlined.

The activity of a mixed bacterial community including sulphate reducing bacteria was found to produce crack growth rates of up to 10 times faster than those found in plain synthetic seawater. This result was very reproducible, despite the variability in the naturally occurring initial bacterial population. The attainable concentration of bacterial sulphide was shown to be sensitive to the experimental procedure. The procedure adopted was chosen to model the offshore environment.

Development of preferred shapes by surface breaking cracks was shown to result from the distribution of stress intensity factors pertaining to these cracks.

The overall objectives and achievements of this study were the better understanding of the mechanisms of corrosion fatigue crack growth in a salt water environment, and an initial appreciation of crack growth rates in the more realistic situation involving bacterial activity. Together with the study of surface breaking cracks this work contributes to progress towards greater compatibility between the fracture mechanics approach to corrosion fatigue and the traditional engineering S-N approach.

Part I

Corrosion fatigue -

mechanisms and effect of environmental/loading variables.

1.0 Introduction.

1.1 Background.

With the exploitation of offshore oil and gas reserves, there arose the need for reliable fatigue data in order to be able to guarantee the structural integrity of the platform structures. This was especially true for the northern North Sea oilfields, where conditions are far more severe than in any offshore oil or gas field previously exploited. As a result of the uncertainty about the effect of the seawater environment upon the fatigue life of welded steel jacket structures, the United Kingdom government set up the United Kingdom Offshore Steel Research Project (UKOSRP 1). The main aim of the first phase of UKOSRP 1 was to provide S-N data suitable for use in the fatigue guidance notes, issued by the Department of Energy for designers. Because the traditional S–N approach to fatigue is of little use in predicting the residual life of a cracked structure a limited number of crack propagation studies were undertaken as a subsidiary part of UKOSRP I.

In addition to the UKOSRP programme, the United Kingdom Science and Engineering Research Council embarked on a special initiative in all areas of Marine Technology, including that of fatigue in offshore structures. A particular concern in the fatigue research programme has been to undertake the fundamental studies of corrosion fatigue necessary to be able to apply the principles of fracture mechanics to the prediction of residual life of a structure that has been found to contain a flaw.

The work reported in this thesis forms part of the SERC Marine Technology Directorate's programme in fatigue relevant to offshore structures. The work involving biologically active environments was a joint SERC/Department of Energy project.

1.2 Overview of linear elastic fracture mechanics (LEFM).

1.2.1 Fast Fracture.

Fracture mechanics is the branch of engineering mechanics that deals with the behaviour of cracks in materials. A crack in a stressed body has an associated "stress intensity factor", K, which characterizes the crack tip stress field [1-3]. The stress intensity factor is given by :

$$K = Y\sigma\sqrt{(\pi a)} \qquad (1.1)$$

where σ is the (remote) applied stress
a is the crack length
Y is a geometrical correction factor.

Opposing crack surfaces can be moved in a combination of three basic modes of opening and these are shown in figure 1. Mode I, the opening tensile mode is the most important mode practically and usually dominates the growth of a crack in a real component. Consequently, Mode I is the most studied mode of crack opening, and it has been used in this work. Usually a suffix, I,II, or III is added to K to indicate the mode of loading referred to. For a stressed body containing a crack, catostrophic failure occurs when :

$$K_I = K_{IC} \qquad (1.2)$$

where K_{IC} is the "critical stress intensity factor" for plane strain Mode I loading. K_{IC} is a material property that measures the ability of a material to withstand the propagation of a crack, and is usually called the "fracture toughness" of the material. It is found that the resistance of a material to crack propagation is greater in plane stress than in plane strain, and so a thickness effect on K_I at fracture exists. A consequence of this is that a size requirement must be met for the specimens used to measure K_{IC} if that measurement is to be considered valid [4]. It is possible to relate a critical value of applied stress intensity, K_C, to the "critical strain energy release rate" for fracture, G_C by the equation :

$$G_C = \frac{K_C^2}{E}(1-\nu^2) \quad \text{(plane strain)} \qquad (1.3)$$

Furthermore, G_C is related to the surface energy of the newly created crack faces and the energy absorbed by the plastic deformation at the

crack tip :

$$G_c = 2(\gamma_s+\gamma_p) \qquad (1.4)$$

where γ_s = the surface energy of the new crack surface
γ_p = the energy absorbed by plastic deformation.

Because of the dependence of the fracture toughness on the state of stress a thickness criteria exists for applicability of LEFM :

$$B \geq 2.5\left[\frac{K_I}{\sigma_y}\right]^2 \qquad (1.5)$$

where B is the thickness
σ_y is the material's yield stress.

If a cracked component is subjected to varying loads, corrosive environments, or a steady load and a high temperature, the crack may grow even though $K_I<K_{IC}$. This is called "sub-critical crack growth" because the crack growth is much slower than for catastrophic failure ($K_I>K_{IC}$). The useful life of the cracked component in these situations is then determined by the amount of allowable crack growth.

1.2.2 Fatigue.

A common form of sub-critical crack growth is fatigue, which is caused by varying loads being applied to the component. For constant amplitude loading the notation used is defined in figure 1.2. For a statically loaded crack, there exists a plastic zone ahead of the crack tip whose size is determined by the applied K. When the load varies with time, as in fatigue, there is a region within the plastic zone which experiences reversed plasticity, and this region is proportional in size to the square of ΔK, the applied stress intensity factor range. As strain is important in fatigue crack propagation it is not surprising that the fatigue crack growth rate is found to depend on ΔK, as shown in figure 1.3. Figure 1.3 also illustrates the three commonly observed stages of fatigue crack growth. For stage II crack growth the Paris law [5] applies :

$$\frac{da}{dN} = A\,\Delta K^{m} \qquad (1.6)$$

where $\frac{da}{dN}$ is the crack growth per cycle
and A,m are constants

It has been conclusively shown that the range of applied stress intensity resulting from a varying applied load, ΔK, is the controlling parameter for fatigue crack growth, rather than any other function of stress and crack length [6,7].

Equation 1.6 may be integrated to estimate the residual life of a flawed structure or component. The final crack length is taken as that at which failure would occur under the applied loading, whereas the initial crack size used for the calculation is that of the largest possible existing defect within the structure or component.

Equation 1.6 only holds over an intermediate range of ΔK. At low values of ΔK the crack growth rate is less than that predicted by eqn 1.6 as a threshold effect is found for fatigue crack propagation. As ΔK increases so that K_{max} approaches K_{1C} static modes of fracture cause the crack growth rate to exceed that given by equation 1.6.

The crack surface of a material that has failed by fatigue often exhibits a series of ridges, called "striations", when viewed in an electron microscope. The spacing of these striations often correlates with the macroscopic crack growth rate, da/dN, ie. one striation corresponds to the crack growth increment during one load cycle. An empirical equation has been developed to relate striation spacing to

the value of $\Delta K/E$ [8] :

$$\text{Striation spacing} \approx 6 \left[\frac{\Delta K}{E}\right]^2 \qquad (1.7)$$

When crack growth occurs during a load cycle by mechanisms other than striation formation the crack growth rate may be increased [9,10]. The crack growth rate, da/dN, may then be written as :

$$\frac{da}{dN} = Af_1(K)_{\substack{\text{striation}\\\text{mechanism}}} + Bf_2(K)_{\substack{\text{void}\\\text{coalescence}}} + Cf_3(K)_{\text{cleavage}} + Df_4(K)_{\text{corrosion}} \qquad (1.8)$$

The predominance of striation formation associated with the crack growth mechanism for fatigue in air, and its dependence upon the strain at the crack tip, is demonstrated by the close similarity in crack growth rates, da/dN, as a function of $\Delta K/E$ [8] for many materials.

1.2.3 Environmentally assisted cracking.

The application of fracture mechanics to stress corrosion cracking (SCC) has resulted in much work being done on SCC crack propagation. The results are usually plotted on a graph of log da/dt vs. log K, where da/dt is the crack growth velocity. Commonly the results are of the form shown in figure 1.4. A threshold value of K is often found below which no SCC crack growth occurs, the threshold value of K is designated K_{1SCC}. For an applied K greater than K_{1SCC} three distinct regions of crack growth are usually observed, as indicated on figure 1.4. The region II crack growth velocity is commonly independent of the applied value of K, unlike for regions I and III. In region III the crack growth velocity increases as K approaches K_{1C}.

However non-propagating cracks can occur for $K_1<K_{1SCC}$ which is due to the importance of the effective strain rate at the crack tip upon SCC [11]. A small oscillating load superimposed upon the static load can cause SCC to occur when $K_1<K_{1SCC}$, as any protective film that is formed at the crack tip may be disrupted by the strain occurring there. This last example also serves to illustrate the fact that SCC and corrosion fatigue are closely related phenomena, with no clear cut boundary between them : SCC is the limiting case of corrosion fatigue as the stress ratio R-1, or the frequency f-0 [12,37].

Previous research into corrosion fatigue has divided it into two regimes [13,14] :

(a) "Stress corrosion fatigue" for materials that exhibit SCC in that particular environment.

(b) "True corrosion fatigue" when $K_{max}<K_{1SCC}$ and environmentally enhanced crack growth rates are observed.

"Stress corrosion fatigue" is thought to be caused by the operation of a SCC mode of fracture when $K_{max}>K_{1SCC}$ [15], and a superposition model of Wei and Landes [15] was partially successful at modelling this situation. The concept of the superposition model was altered by Austen and McIntyre [16] and reformulated as a "process competition model". As recently amended [17] the "process competition model" has been fairly sucessful in modelling the effects of R ratio, waveform and frequency for this situation.

In "true corrosion fatigue" as $K_{max}<K_{1SCC}$, a static environmental

mode of fracture does not occur, and a truly synergistic effect of the material, loading and environment must exist. Low strength high toughness structural steels, such as the C-Mn steel used in this study, do not appear to exhibit SCC in seawater. However, such steels do exhibit true corrosion fatigue crack growth rates that are many times those found in air. For this situation two possible mechanisms of corrosion fatigue crack growth have been postulated, namely anodic slip dissolution and hydrogen embrittlement.

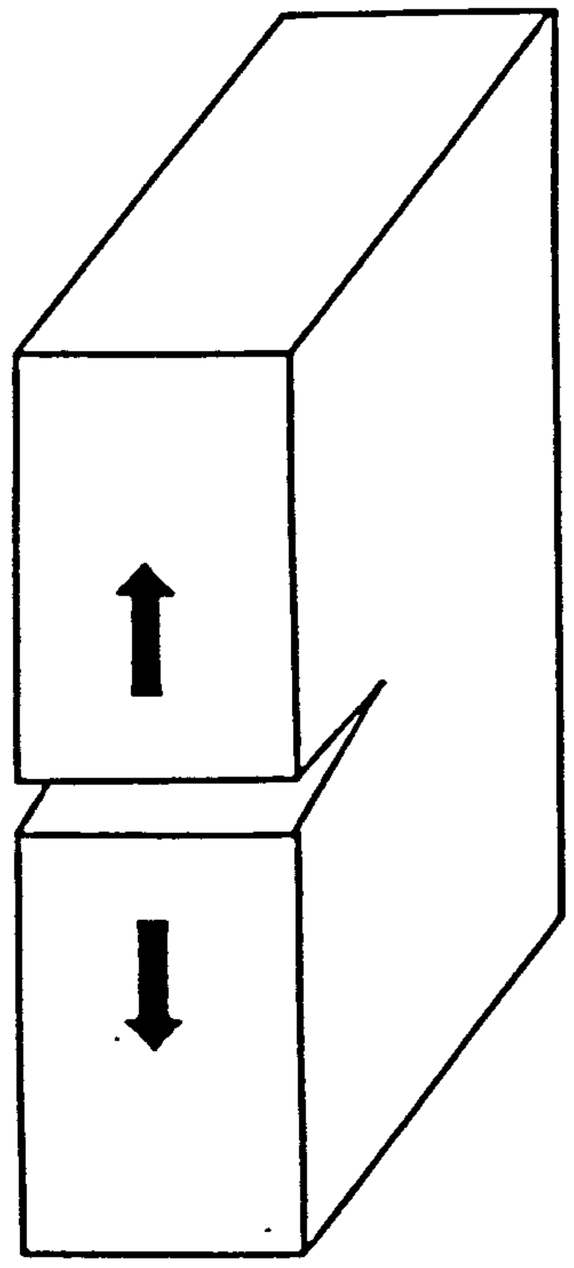

Mode I

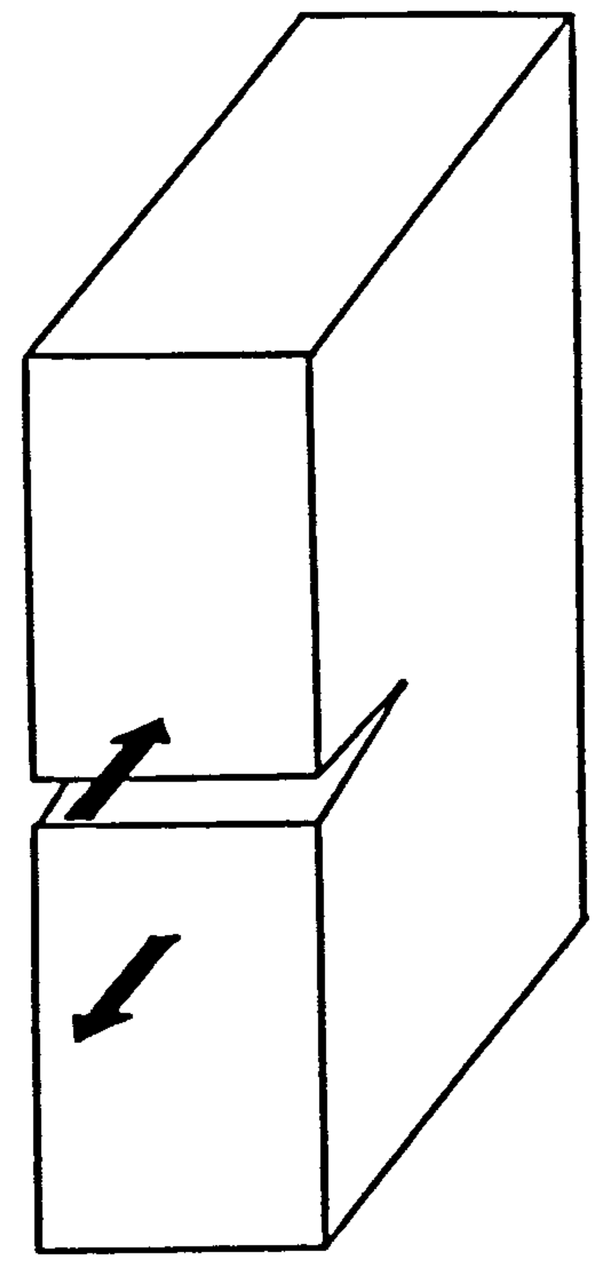

Mode II

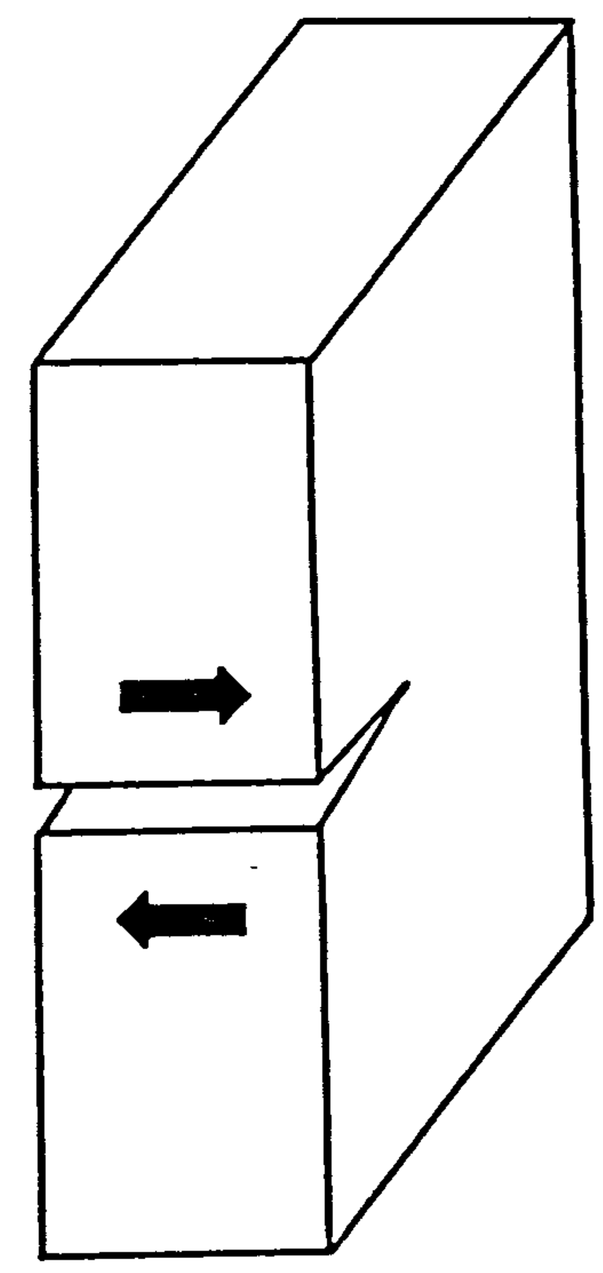

Mode III

Figure 1.1 Possible modes of loading

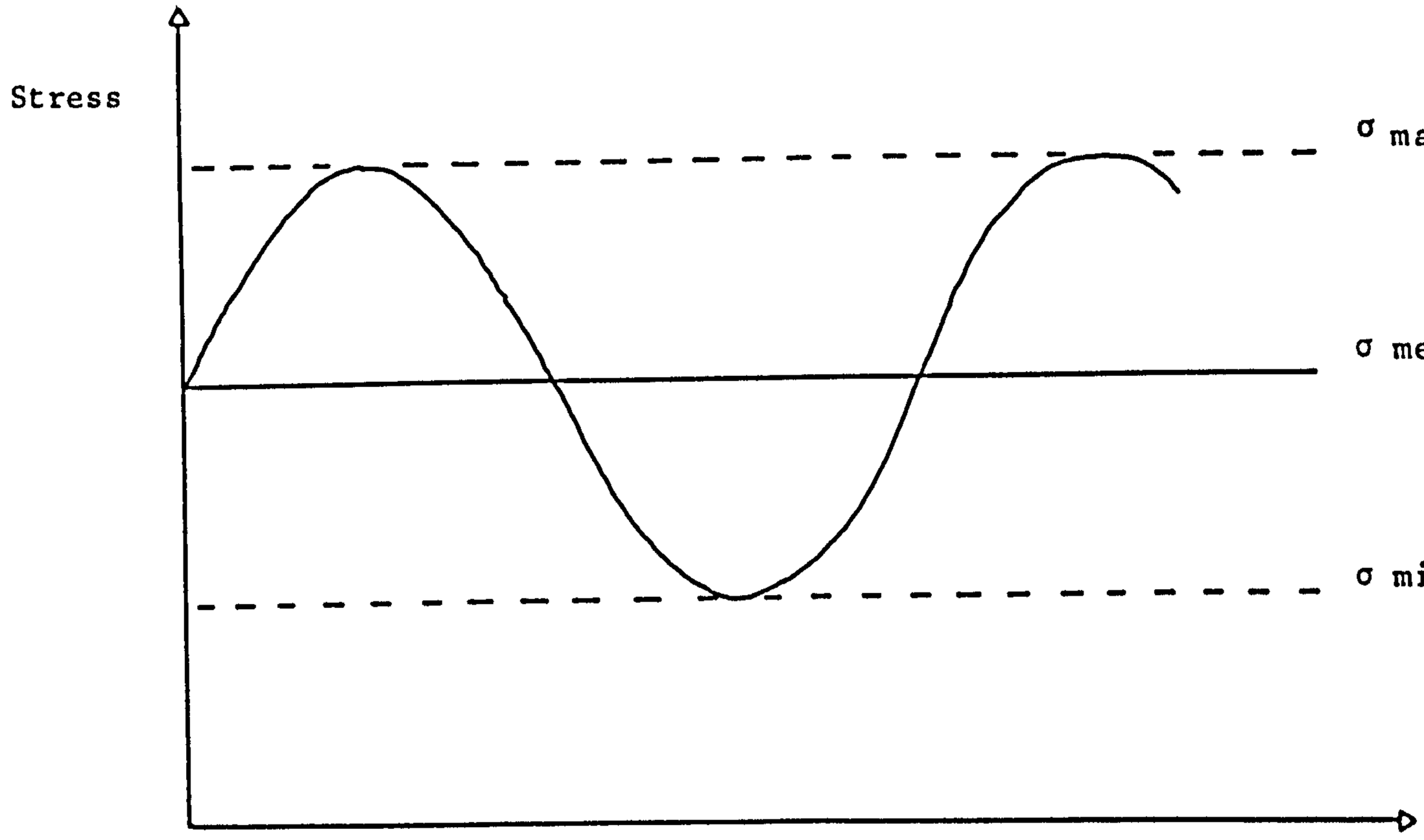

$$\Delta\sigma = \sigma max - \sigma min$$

$$\Delta K = Y \, \Delta\sigma \, \sqrt{\pi a}$$

$$R = \sigma min / \sigma max$$

Figure 1.2 Notation relating to stress cycling

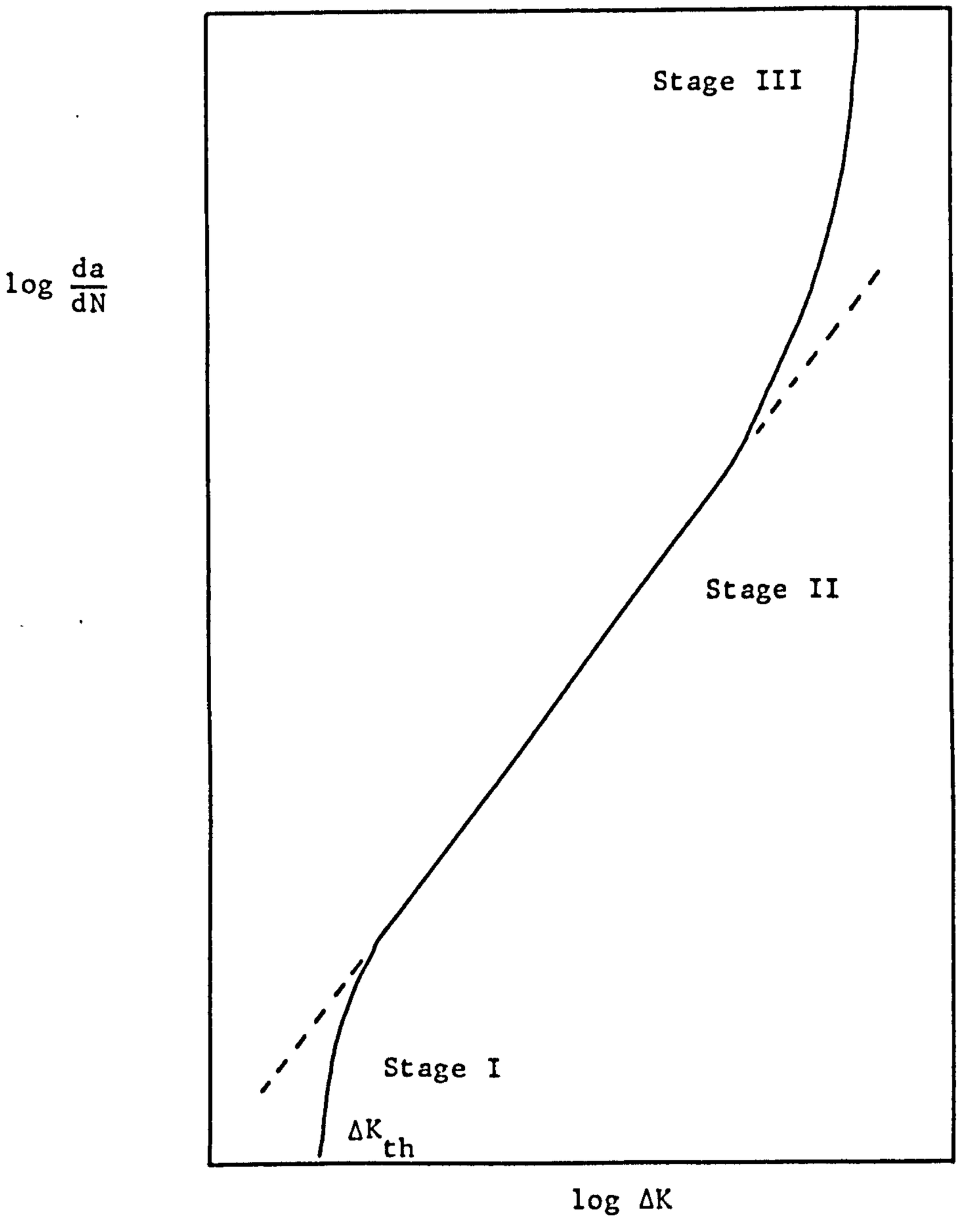

Stage I = threshold as da/dN approaches 1 atomic spacing

Stage II = $da/dN = A\Delta K^m$

Stage III= static modes of fracture occur

Figure 1.3 Schematic diagram of fatigue crack growth regimes

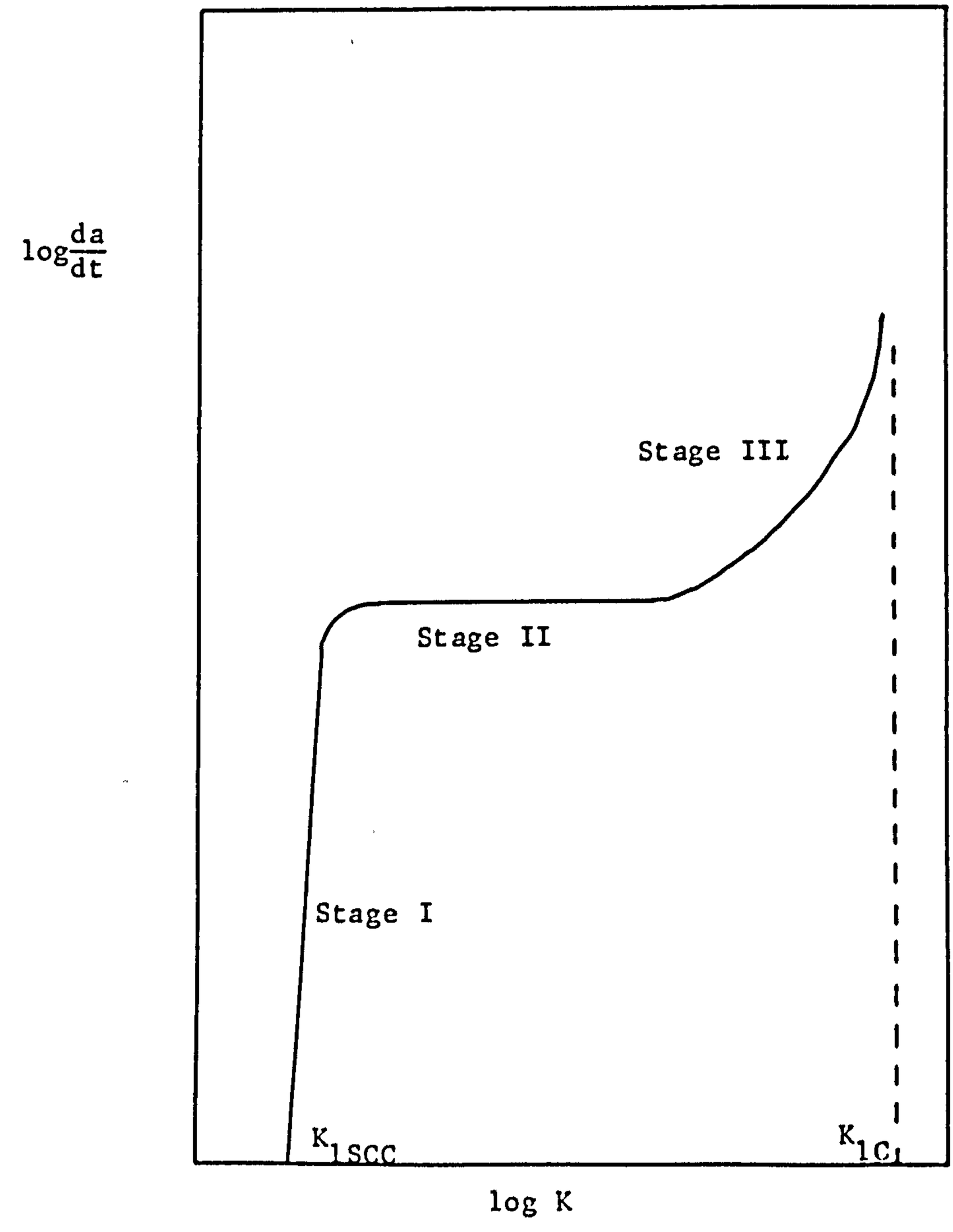

Figure 1.4 Schematic diagram of stress corrosion cracking (SCC) regimes

2.0 Mechanisms of environmentally assisted crack growth.

2.1 Introduction.

The purpose of this chapter is to present an overview of the proposed mechanisms of environmentally assisted crack growth. For each mechanism the possible processes that control the rate of crack growth are reviewed. The chapter is concluded by a review of methods that have been proposed in order to determine which mechanism of environmentally assisted crack growth operates in a specific situation. This review has been restricted to processes that are relevant to the environmentally assisted cracking of C-Mn structural steels in seawater or NaCl solution.

2.2 Electrochemical conditions within cracks.

Many studies have shown that the electrochemical conditions within cracks may be significantly different from those pertaining to the bulk solution. In this section a brief review is given of crack electrochemistry.

2.2.1 Crack tip potential.

Within cracks or crevices the potential of the metal at the end of the crack or crevice may be significantly different from that at the exterior surface. For instance, Bernstein and Pickering [18,19] claimed to have found evidence that anodic dissolution can occur within cracks in Ferrovac-E iron, even when the specimen is held at a strongly cathodically protected potential. Solid corrosion products and gas bubbles have been held to significantly alter the crack tip potential by constricting the current path down the crack [20,21].

Most experimental measurements of potentials within cracks or crevices have employed artificial crevices, sometimes with side wall movement to simulate pumping due to load cycling, because of the greater ease with which measurements may be made. Parkins et. al. have observed no difference between the results from artificial crevices and from real cracks [22]. They found that no large potential drops existed within cracks so long as the specimen potential was such that the passage of a large current along the crack was not required [22,23]. This was true for both HY80 in natural seawater and

for a C-Mn steel in a CO_3^{2-}/HCO_3^- solution, although for the case of the C-Mn steel several hours were required for the potential within a crack to reach a steady state. This was due to the progressive formation of a passive film along the crack faces [23]. For HY80 in natural seawater zero potential drop within the crack was found for potentials between the free corrosion potential and about -1.1V(scc) [22,24].

Turnbull has obtained similar results in his work on BS4360:50D in 3% NaCl and seawater [25,26]. No significant differences were observed between the results obtained for 3.5% NaCl, ASTM artificial seawater and natural seawater. No potential drop was found in artificial crevices for specimen potentials between ≈-0.7V(scc) and -1V(scc). At specimen potentials more positive than -0.7V(sce) a limiting crack tip potential of about -0.625V(scc) was reached. The results for specimen potentials more negative than -1V(sce) indicated that the most negative crack tip potential it is possible to achieve would be ≈-1.1V(sce). The measurements of Hodgkiess et. al. [27] on real fatigue cracks (for BS4360:50D in artificial seawater) agree with Turnbull's observations for crevices in that little potential variation was observed between the crack tip potential and the specimen potential.

The electrochemical conditions within cracks, including potential, are discussed in more detail in references [28-30]. Turnbull and Gardner [31] have also reported polarization data for BS4360:50D in 3.5% NaCl.

2.2.2 Crack tip pH.

For AISI 4340 steel undergoing stress corrosion cracking in 3.5% NaCl at free corrosion Brown et. al. [32,33] have measured the crack tip solution as having a pH within the range 3.6 to 3.8. It had been commonly assumed before these results were reported that the crack tip solution would be acidic as a result of the dissolution reactions. Acidic crack tip pH values have been found for HY80 in seawater, when the specimen is anodically polarized [22,24]. When the specimen was cathodically protected the crack tip pH became alkaline as a result of the reduction of either oxygen or water.

The most acidic crack tip pH found by Turnbull and Gardner in their work utilizing artificial crevices of BS4360:50D [25,26] was 6.5 to 6.75 at potentials anodic to the free corrosion potential. At the

free corrosion potential the crack tip pH was around 7, but became significantly higher under cathodic protection conditions. At -1V(sce) the crack tip pH was as high as 11 for the 3.5% NaCl solution, and about 10.5 for seawater. The difference between 3.5% NaCl and seawater was attributed [25] to the reduced cathodic protection current in seawater that is a consequence of calcareous deposits forming on the crack face. As the cathodic reduction current is less the formation of OH^- ions as a result of water reduction is reduced, and so the pH is slightly lower. This effect only occurs at potentials below about -0.8V(sce), at higher potentials the results from 3.5% NaCl and seawater were identical. The time required to reach a steady state value of pH within the crevice was usually less than 24hrs, but in some cases was as much as 40hrs. In their *in situ* measurements of cracks in artificial seawater Hodgkiess et. al. [27] found that cathodic protection caused the crack tip pH to increase to about 12 or more. In free corrosion, with load cycling, the crack tip pH was between 8 and 9.

2.2.3 Solution composition.

It had been expected that the sodium chloride concentration might alter within a crack or crevice, but no such change was found by Alavi and Cottis [34] for an artificial crevice of high strength steel in either NaCl solution or artificial seawater. No other *in situ* measurements of solution composition within cracks or crevices are known to the author, although it is obvious that dissolution at the crack tip would increase the amount of iron dissolved in the solution within the crack.

2.3. Anodic Dissolution.

The rapid dissolution of freshly exposed metal at the tip of a crack is often advanced as an explanation of SCC in many alloy/environment conditions [35-38]. The fresh metal surface is often assumed to be created as a result of creep and rupture of a passive film, or of a protective oxide layer [35-38]. The crack growth rate is then given by [39,40] :

$$v = \frac{M}{n\rho F} \cdot \frac{Q}{t^*} \qquad (2.1)$$

where M = molecular weight of metal at the crack tip
ρ = density of metal at the crack tip
n = charge on the dissolving cation
F = Faraday constant
t^* = periodicity of film rupture at the crack tip
Q = charge density passed at the crack tip in time t^*.

When a bare surface continuously exists at the crack tip equation 2.1 can be rewritten as :

$$v = \frac{M}{n\rho F} \cdot i_a \qquad (2.2)$$

where i_a is the bare surface current density.

By assuming that a bare surface always exists at the crack tip [41] equation 2.2 defines the maximum theoretical crack propagation rate for an anodic dissolution mechanism. In practice the crack growth rate caused by a dissolution mechanism may be limited by factors such as passivation, solution renewal and crack blunting [40,42].

The different factors that limit dissolution controlled crack growth are discussed below.

2.3.1 Bare surface current density.

Howard and Pyle [43] have shown that the dissolution of atoms from steps on the surface of a metal may occur at rates up to $\approx 10^4$ times faster than for atoms on the plane of a surface. Such effects were held to be important in transgranular SCC [44]. They have also observed current transients during the cyclic straining of various metals [45], these are due to the increased current densities that occur at bare metal surfaces.

In the absence of any other rate controlling process equation 2.2 indicates that the crack propagation rate is controlled by the bare surface current density. When a fresh metal surface is exposed to the environment a corrosion current transient occurs. The peak of the transient defines the bare surface current density, and is followed by the passivation of the bare surface as surface films form on it. Bare surface current densities of up to 10 A/cm^2 [42,46,47] have been measured. For mild steels in chloride solutions at 20°C bare surface current densities of up to 1 A/cm^2 have been found [48], which compare with current densities of the order of 10^{-5} A/cm^2 for a normal surface [49]. The current transient decayed by 90% of its peak value in only 10-15ms [48]. It was also found [48] that the bare surface current densities for iron and steels, in chloride and sulphate solutions, were primarily determined by the iron content, and so were only marginally affected by the exact composition of the steel. Another feature of bare surface corrosion behaviour is that the reversible potential, E_0, is shifted to more negative values [42,48,50]. This implies that crack growth by a dissolution mechanism could still occur when the metal potential is below the normal reversible potential for a filmed surface. For steels in chloride solutions, Burstein and Davies [50] indicate that dissolution may still occur at a bare surface at potentials up to ≈250mV more negative than the reversible potential for a filmed surface, whereas a figure of ≈400mV is suggested by Trant's results [48].

A number of methods of measuring bare surface current densities have been used. The fast straining of wires [51,52] suffers from the difficulty of calculating the exact area of bare surface formed. The most commonly used method has been the scratching electrode technique [47,50,53,54] in which a rotating disc electrode is scratched by a diamond. The area of bare surface formed is known from the scratch width, time of contact and speed of rotation of the disc electrode.

Although for some alloy/environment systems bare surface current densities have been successfully correlated with crack growth [12,42,51] very little data relevant for use with offshore steels in seawater exists. Trant [53], following the method of Ford [42,54], has determined the maximum theoretical crack propagation rate (which is a function of potential, cf. figure 5.26) by a dissolution mechanism for X65 steel in 3.5% NaCl at 23°C. Due to the similarity between X65 and the material used in this work, BS4360:50D, as well as the relative independence of the maximum rate with respect to chloride and sulphate concentration, this data should be applicable for the conditions used in the present work.

2.3.2 Crack tip strain.

The rate of crack growth by a dissolution mechanism may be limited by the time necessary to accumulate a sufficient amount of strain at the crack tip to rupture any film there. For SCC the strain is a result of creep processes that are caused by the material's time dependent response to the last film rupture event [38,55]. The rate of crack growth is described by equation 2.1. The rate at which strain accumulates at the crack tip affects the periodicity, t^*, of film rupture. As t^* decreases (ie. film rupture rate increases) dissolution controlled SCC crack growth rates increase, and the potential range over which cracking occurs is extended in both the anodic and cathodic directions [39]. The imposition of a dynamic load on the crack would cause the accumulation of strain at the crack tip and so would reduce t^*. As a result dynamic loading would be expected to result in dissolution controlled environmentally assisted cracking occurring at potentials that are outside of the range over which SCC occurs [39]. It is indeed well known that corrosion fatigue is much less material/environment specific than SCC. The application of a small oscillating load to a nominally statically loaded test has been shown to cause crack growth under conditions where crack growth is not observed during a normal SCC test [56]. Another illustration of this type of behaviour is the occurrence of crack growth during slow strain rate testing [57,58] even where no SCC crack growth is expected.

For corrosion fatigue behaviour the crack tip strain rate has been proposed [59] as a controlling parameter of crack growth enhancement caused by a dissolution mechanism. If the applied crack tip strain rate is very slow film growth may occur at the crack tip, so preventing rapid dissolution from occurring there until the film is strained beyond its failure strain. The crack tip strain rate was proposed [59] to explain the "plateaus" (cf. footnote) observed in the

---

"plateaus" are regions of crack growth where the crack growth per cycle (da/dN) does not depend upon the range of applied stress intensity factor (ΔK), and are so called from their appearance on the usual log da/dN vs. log ΔK plot.

corrosion fatigue behaviour of PWR pressure vessel steels at 288°C, rather than offshore steels in seawater. However, the results of Atkinson and Lindley [60,61] indicate that it could be important for C-Mn steels in seawater for frequencies less than 0.01Hz. For crack tip strain rates that are large enough to prevent a film forming at the crack tip the crack growth rate caused by dissolution is limited by either the bare surface current density or the solution renewal rate.

2.3.3 Passivation.

During SCC the passivation rate, or rate of film formation, controls the amount of charge that flows after each film rupture event. If the passivation rate is too fast the crack will not grow by a sufficient amount to enable subsequent crack tip strain (due to creep processes) to rupture the film formed there. In such circumstances the crack will arrest unless a dynamic load is applied [62]. As mentioned in the previous section if the applied crack tip strain rate in dynamic loading is not great enough film formation may occur at the crack tip. The film deforms as it forms, in order to accommodate the strain at the crack tip until it exceeds its failure strain. Obviously there is competition between the crack tip strain rate in providing fresh bare surface at the crack tip, and the rate of film formation. Thus the rate of film formation determines the critical frequency (at a given R ratio) for corrosion fatigue, below which the crack tip strain rate limits the amount of dissolution controlled enhanced crack growth.

2.3.4 Mass transport and solution renewal.

For corrosion metal dissolution occurs via the anodic reaction :

$$Fe \rightarrow Fe^{2+} + 2e^{-} \qquad (2.3)$$

(There must also be a corresponding cathodic reaction with the anodic and cathodic areas in electrical contact). The Fe^{2+} ion is present in solution as a complex ion and so a supply of solvating water molecules is required at the crack tip. If the rate of supply of water to the crack tip is not great enough then the amount of dissolution able to occur at the crack tip is restricted. This happens during SCC when the flux of metal cations leaving the bare surface equals the necessary flux of water molecules to solvate them [42], ie. when :

$$\frac{i_a}{nF} = -\frac{1}{Z}.D.\frac{dC}{dx} \qquad (2.4)$$

where Z = hydration number
D = diffusion coefficient for water (10^{-5} cm^2/s @ 25°C)
$-\frac{dC}{dx}$ = concentration of water molecules in the crack tip region.

In his work Ford [42] quotes the hydration number for aluminium as 6, the number for iron would also be 6. However this is an underestimate due to the secondary ligand shell that forms around a solvated ion. Equation 2.4 may be used, together with an estimate of -dC/dx, to define the SCC crack growth rate at which the supply of water to the crack tip becomes the rate determining step [42].

For corrosion fatigue conditions diffusion is not the only mechanism by which water molecules can reach the crack tip. An effect of the oscillating load is to cause the crack faces to pump solution into and out of the crack. The pumping action would increase the supply of water molecules to the crack tip, and so increase the rate of crack growth possible before this becomes the rate determining step. At the crack tip region the crack pumping would be expected to be more effective at renewing the crack tip solution as the loading frequency increases and as R→0 (or is <0).

If solvated Fe^{2+} ions are not removed rapidly enough from the crack tip region then the rate of metal dissolution may be limited by the concentration of Fe^{2+} ions at the crack tip. In a situation similar to the supply of water molecules to the crack tip discussed before, the Fe^{2+} ions are removed by diffusion for SCC and by diffusion assisted crack pumping for dynamic loading.

2.3.5 Crack blunting.

The potential range over which SCC occurs may be bounded by the regimes of general dissolution or of pitting [39]. Either of these regimes cause the SCC crack tip to blunt, and so the crack growth arrests as the associated stress concentration decreases. For corrosion fatigue conditions the crack would be expected to resharpen during the unloading part of the cycle, even if the potential is in the pitting or general dissolution regimes. It has been proposed that a limit to dissolution controlled crack growth exists of one half of the crack tip opening displacement per cycle [63,64]. It was reasoned that if the crack growth by dissolution was greater than this the crack would not resharpen upon unloading, and so subsequent crack growth would be diminished. The results of Atkinson and Lindley [60] were held to confirm the proposal [64] in that the crack growth rate decreased below a critical frequency, and the maximum enhancement was approximately one half the crack tip opening displacement. However, it is hard to see why the crack growth rate should decrease with decreasing frequency below the critical frequency, rather than remain at a constant value of half the crack tip opening displacement. Radon [65] has claimed to have observed crack blunting arresting corrosion fatigue crack growth. It is possible that this may have been a result of crack closure rather than crack blunting per se.

2.3.6 Crack closure.

If a voluminous corrosion product accumulates on the crack surfaces during corrosion fatigue crack growth a crack closure effect may occur [66]. In this case the crack becomes fully closed before the minimum load is reached, thus reducing the effective range of applied stress intensity factor. Crack closure has been shown to be important at low values of the applied stress intensity factor range, in the vicinity of the fatigue threshold [67-71].

Erroneously low crack growth rates due to crack closure were observed in this study with R=0.1.

2.3.7 Crack branching.

Crack branching may occur during environmentally assisted crack growth [72-74]. This may lead to the effective value of ΔK at the crack tip being reduced. McClintock [75] states that the reduction in the effective ΔK due to crack branching is not more than a factor of 2.

2.4 Hydrogen embrittlement.

The presence of hydrogen may severely affect the fracture properties of many metals [76-78]. This phenomena, called hydrogen embrittlement, can be responsible for environmentally assisted crack growth in metals in aqueous environments [74,80]. In SCC or corrosion fatigue hydrogen may be formed in the vicinity of the crack tip by the reduction of water molecules or protons. The resulting hydrogen adatoms are then responsible for embrittling the metal at the crack tip, although it is not clear whether the embrittling process occurs at the surface or the interior of the metal.

Although the phenomena is called "hydrogen embrittlement" the term "embrittlement" only refers to macroscopic parameters which are measures of ductility, such as elongation (failure strain) or reduction of area. The microscopic fracture modes involved in hydrogen embrittlement all involve localized plasticity, and all can occur in the absence of hydrogen [81,82]. Thus the macroscopic embrittlement that is observed is the result of the localization of plasticity along the fracture plane. It is obviously not possible to conclude that hydrogen embrittlement occurred from solely fractographic studies since hydrogen may or may not cause a change in the microscopic mode of failure [81,83,84]. If hydrogen causes a change of microscopic fracture mode the new mode is generally one associated with less macroscopic ductility [82].

Although much work has been done in studying hydrogen embrittlement there is still a lack of mechanistic understanding of the phenomena. Thus although a large amount of phenomenological data has been gathered [83] there are also a number of proposed models for hydrogen embrittlement. In the next section the various models for hydrogen embrittlement are briefly discussed. The succeeding sections review the possible rate controlling steps involved in hydrogen embrittlement.

2.4.1 Hydrogen embrittlement models.

(a) Internal pressure.

Blisters, containing high pressure hydrogen, occur in steels that are exposed to hydrogen containing environments at high fugacity. This has led to the proposal [85-87] that crack propagation in hydrogen containing environments is caused, or enhanced, by the pressure of hydrogen in voids or traps. Thus the hydrogen migrates through the lattice towards the region of high triaxiality, where it recombines inside voids to provide an additional component of stress.

Although internal pressurization of voids by hydrogen is definitely the cause of blistering it cannot be a universal mechanism of hydrogen embrittlement. This is because crack propagation has been observed in dry hydrogen at sub-atmospheric pressure [88]. From thermodynamic considerations the pressure of hydrogen at the void or trap should not rise above the external hydrogen pressure. It has been countered that hydrogen may be carried as a Cottrell atmosphere on moving dislocations, and that this may cause supersaturation to occur [89,90]. Although supersaturation can be considerable at low temperatures it now appears that supersaturation by a factor of only 2 or 3 times can be obtained at room temperature [91]. Supersaturation by dislocation transport is only a transient phenomena as diffusion restores the hydrogen pressure in the voids to its equilibrium value. Thus a continual influx of dislocations is required to maintain the supersaturation.

(b) Surface energy.

This model states that as adsorption of hydrogen lowers the surface free energy then the fracture stress should also be lowered [92,93], in accordance with Griffith's model for cracks in a brittle material [94]. Oriani [95] has claimed that data for the adsorption of hydrogen upon iron has not confirmed this model.

It is also difficult to see how the model can explain the discontinuous nature of hydrogen cracking (as determined by sonic emissions), the reversibility of hydrogen effects and the effect of other species such as chlorine and oxygen. For instance, oxygen has a greater heat of adsorption than hydrogen, but fails to promote cracking and even blocks the effect of hydrogen [96,97].

Another difficulty with the surface energy model is that in essence it is a thermodynamic model and consequently does not specify a kinetic pathway. Thus it is of limited use for SCC or corrosion fatigue studies. Also irreversible effects such as the large plastic energy required to propagate a crack in a ductile material cast further doubts upon the applicability of this model [98,99]. It can be shown that the surface energy model is a necessary, but not sufficient, condition according to decohesion models.

(c) Decohesion.

Troiano [100] originally proposed that decohesion could be responsible for hydrogen embrittlement. Oriani and others [101-106] have developed this model into a semi-quantitative form. SCC tests on an AISI-SAE 4130 low alloy steel by Nelson and Williams [107] have provided data that substantially agrees with Oriani's theory.

Oriani's theory is based upon the postulate that hydrogen dissolved in iron at sufficiently high concentrations decreases the maximum cohesive force between iron atoms. It is also assumed that there are transient regions near the crack tip where the elastic stress approaches that at which the cohesive force between atoms is reached. The number of these regions, and their lifetime, increases as the strength level of the material increases. This provides a rationale for the often observed effect of strength level on susceptibility to hydrogen embrittlement.

The model infers that a stationary crack may be restarted either by increasing the applied stress, or by increasing the pressure of hydrogen gas : this effect is observed [101]. The theory does not predict crack growth rates, only if crack growth will or will not occur. Oriani [101] states that the crack growth rate is determined by the kinetic processes that govern the entry and transport of hydrogen to the cracking site. It would appear that Oriani's results [101] are quite consistent with the cracking site being between the crack tip and the region of maximum triaxial stress [108].

Rice [109] has presented an arguement that most cases of hydrogen embrittlement can be explained on the basis of a loss of cohesion of interfaces. As the cohesive strength of interfaces and plastic flow are important for all failure modes then hydrogen embrittles by affecting these processes. It is probable that hydrogen only has a minor effect on plastic flow at room temperature, leaving its effect on

the cohesive strength of interfaces (eg. grain boundaries, phase boundaries and particle-matrix interfaces) as being of prime importance. Furthermore he suggests that hydrogen is not unique per se in its effect on cohesion. A much greater impairment of cohesion occurs when the embrittling element is mobile on the surface. Thus hydrogen's uniqueness is its high mobility at room temperatures : other elements could cause similar decohesion of interfaces if they were as mobile.

(d) Enhanced plasticity.

Beachem observed evidence of plasticity on fracture surfaces and so proposed that hydrogen aids failure by augmenting dislocation motion [110,111]. He proposed that the crack tip plasticity is aided by hydrogen entry into the metal matrix, and that plastic deformation aids the entry of hydrogen into the crack tip region. Thus he proposes that these two mutually abetting processes localize the plasticity and so cause less overall deformation. The enhanced plasticity aids the operation of the usual form of failure in the metal and so causes enhanced cracking. It is noteworthy that this mechanism requires the prime effect of hydrogen to be on the plastic flow of the metal, rather than on the cohesive strength of interfaces. This is in contrast to Rice's model [109] mentioned in the previous section.

In some situations dislocation motion is definitely enhanced by hydrogen. In particular the motion of screw dislocations is enhanced and it is possible that the injection of dislocations at free surfaces is also abetted [112]. However, it is established that hydrogen does not always enhance the plasticity of metals, it is possible for it to cause hardening effects as well [103,112,113]. Hardening (as well as the generation of dense dislocation tangles) has been caused by hydrogen at large plastic strains [103]. This could be important for the reversed plastic zone at the tip of a fatigue crack.

Although it is probable that the effect of hydrogen on plasticity can be important in some situations, it is not clear that hydrogen always enhances plasticity. Another problem with Beachem's proposal is that, like the surface energy model, it contains no provision for calculating the possible crack velocity caused by hydrogen embrittlement.

An alternative model of hydrogen embrittlement based on enhanced plasticity has been put forward by Lynch [99,114-120]. Like Beachem

[111] Lynch observed plastic markings in fractographic studies of hydrogen embrittlement. He also observed that these fracture surfaces were very similar to fracture surfaces produced by liquid metal embrittlement. Consequently he proposed that as hydrogen embrittlement and liquid metal embrittlement have a number of other similarities in behaviour they are caused by a common mechanism. He states that liquid metal embrittlement is "almost certainly caused by an effect of chemisorption at crack tips" [114], and by analogy proposes that hydrogen embrittlement is also caused by chemisorption. It is proposed [114] that this would explain the effect of environmental factors on hydrogen embrittlement such as the blocking action of oxygen.

The mechanism by which chemisorption of hydrogen or liquid metal atoms enhances crack growth is that, it is suggested, this would facilitate the nucleation of dislocations at the crack tip [114,115]. It is argued [114,115] that the chemisorption of atoms at the crack tip provides more neighbours for the surface atoms of the metal and that this reduces the hindrance to the egress and nucleation of dislocations at the surface. Enhanced crack growth then occurs by an alternate shear mechanism similar to that for fatigue crack growth, not by a process of generally enhanced plasticity as suggested by Beachem [110,111]. Furthermore it is argued that the effect of chemisorption is limited only to the slip systems that intersect the crack tip, and so general plasticity is not enhanced. This means that the chemisorption effect does not lead to an enhancement of crack blunting as this would require generally enhanced plasticity (ie. 5 active slip systems). The work of Clum [121] suggests that hydrogen may indeed aid the nucleation of dislocations in iron. This mechanism of hydrogen embrittlement could operate at internal flaws as the hydrogen diffuses through the lattice to the flaw, where it can chemisorb at the crack tip [114].

An important point about Lynch's mechanism is that it is a surface phenomena. Thus for a crack that connects with the bulk environment the crack growth rate should not be dependent on the transport of hydrogen through the lattice.

Eastman et. al. [122] have extensively studied the hydrogen related fracture of nickel. They report that a high degree of local ductility is involved in these processes. An interesting point is that, for specimens containing solute hydrogen that failed by an intergranular mode of fracture, crack nucleation ahead of the main

crack was observed. For the transgranular mode of fracture hydrogen was observed to cause the fracture surface to be highly crystallographic, with the fracture planes parallel to the {111} direction. For both modes of fracture hydrogen was held to induce highly localized plastic processes, probably as a result of enhanced slip.

(e) Hydride formation.

Some metals, including Ti, Nb and Zr, exhibit a form of hydrogen embrittlement that involves the formation of a stable hydride [123]. The hydrides are often brittle and may cause cracking to occur in the matrix, the phase boundaries or at the crack tip [124]. The hydrostatic stress at a crack tip may help to stabilize any hydride formed there [125], but even so it is unlikely that any stable iron hydrides may form there [112]. It has been suggested [98,112] that the coverage of adsorbed hydrogen at a crack tip is so great that it amounts to being essentially a hydride layer, so far as mechanical properties are concerned. Therefore, although there is no known formation of a stable hydride in iron at crack tips this mechanism cannot be definitely ruled out.

(f) Conclusion.

It is obvious from the preceeding discussion that hydrogen embrittlement is far from understood. The present understanding does not allow a kinetic model of hydrogen embrittlement to be applied to the situation of corrosion fatigue [98]. It is not even possible to say definitely where the site of embrittlement occurs - at the crack tip, point of maximum triaxiality or elsewhere in the plastic zone ahead of the crack. This is because it is still not known which of the above mechanisms are actually responsible for hydrogen embrittlement in steels [98], indeed it is easy to think of situations where more than one mechanism operates simultaneously.

Much more work requires to be performed before a satisfactory model of hydrogen embrittlement is available, to compare with corrosion fatigue crack growth rates. However, it is clear that factors such as the rate of formation, and transport of hydrogen could limit the crack growth rate [126].

2.4.2 Rate of hydrogen formation.

The severity of embrittlement depends upon the amount of hydrogen charging of the steel that occurs, whichever of the proposed mechanisms it is caused by. For steel immersed in seawater or 3% to 3.5% NaCl solution the source of hydrogen is the cathodic corrosion reaction. The amount of hydrogen charging that occurs is a function of the solution pH, applied potential and steel composition (including inclusions, especially manganese sulphide inclusions). Hydrogen atoms are deposited on the metal surface and either recombine to form $H_{2(gas)}$ or dissolve into the matrix. The amount of hydrogen entering the matrix can be increased by poisoning the recombination reaction, so preventing gaseous hydrogen from leaving the surface.

It is not really possible to relate a given overpotential or current density to a hydrogen fugacity at the metal surface, as cathodic charging is not yet fully understood [103].

An additional complication in calculating the amount of hydrogen entering the steel at the tip of a corrosion fatigue crack is the formation and rupture of films on the metal surface. Obviously the permeability of the film to hydrogen, the crack tip strain rate, and the rate of film formation are all important parameters. Most entry of hydrogen into the steel [127] would probably occur whilst no film is present at the crack tip. If the film is relatively impermeable to hydrogen then the only significant source of hydrogen is at the crack tip, rather than hydrogen entry occuring at the crack sides or through the bulk of the component.

As the rate of formation of hydrogen on the metal surface depends on the solution composition, it is possible that the transport (either by pumping or by diffusion) of fresh solution down the crack could limit crack growth. The presence of hydrogen gas as bubbles inside a crack [19] would severely restrict the rate at which fresh solution is transported to the crack tip, as would any other deposit on the crack surface (eg. calcareous deposits [128]). Solution renewal has been suggested as a rate determining step during corrosion fatigue (by a hydrogen embrittlement mechanism) of a pipeline steel [129].

2.4.3 Rate of hydrogen transport.

After hydrogen has been formed on the metal surface it must be transported to the embrittlement site if any degradation of material properties is to occur. Most of the hydrogen embrittlement models reviewed require the hydrogen to be present inside the bulk of the metal for it to be embrittled. The exceptions to this are any effect of a "psuedo-hydride" layer at the crack tip, and Lynch's proposed mechanism. For these mechanisms some of the hydrogen at the crack tip would arrive via surface diffusion along the crack face. This is so rapid that it is unlikely to limit crack growth rates in any region of practical interest [98].

Although there have been some reports of crack growth being a result of surface hydrogen [130,131] most workers believe that dissolved hydrogen is essential for the occurrence of hydrogen embrittlement [127,132,133]. For this situation the rate at which hydrogen is transported from the surface to the site of embrittlement may control the crack velocity. Hydrogen may be transported through the lattice either by diffusion or by dislocation transport.

The rate at which hydrogen can diffuse through pure iron is greater than for commercial alloys [112,134]. This is because of the presence of "traps" in such impure materials. Any structural inhomogenity such as grain boundaries, dislocation cores, voids or particle/matrix interfaces will act as a trap for hydrogen. This affects both the solubility and diffusivity of hydrogen in the metal. (A review of the solubility and diffusivity of hydrogen in metals is given in reference [134]).

The presence of traps in steel, reduces the diffusivity to 10^{-8}-10^{-10} m^2/s [112,134]. Tensile stress enhances the diffusion of hydrogen [135-137] through the metal (and also possibly the entry of hydrogen into the lattice [138]). Thus, hydrogen would be assisted in diffusing to the point of maximum triaxial stress by the stress gradient around the crack tip. Also, at the point of maximum triaxiality the large hydrostatic component of stress would increase the solubility of hydrogen in the lattice.

If the crack growth is under diffusion control then the maximum crack growth rate is given by :

$$v = \frac{x}{t} = \frac{x}{\left[\frac{x^2}{D}\right]} = \frac{D}{x} \qquad (2.5)$$

where v = crack velocity
t = time
x = distance of crack extension
D = diffusion coefficient of hydrogen in steel
($\approx 10^{-8} \rightarrow 10^{-10}$ m^2/s [112,134]).

Therefore if the site of embrittlement is <100nm from the crack tip, as suggested in reference [130], the maximum crack velocity is of the order $10^{-1} \rightarrow 10^{-3}$ m/s. Similarly, if the embrittlement occurs at the point of maximum triaxiality (10^{-5} m from the crack tip for K_{max}=40MPa$\sqrt{m}$ and the material used in this study) the maximum crack velocity would be $10^{-3} \rightarrow 10^{-5}$ m/s.

Although lattice diffusion is able to provide hydrogen transport at a rate that exceeds any crack growth velocity observed in this study, there are cases of hydrogen embrittlement in other materials where hydrogen is only required to initiate a cleavage crack, which then propagates mechanically before being arrested. Thus the average growth rate can exceed the rate at which hydrogen could diffuse through the lattice, even though hydrogen embrittlement is occurring [127].

As well as hydrogen diffusing through the lattice, or through more favourable regions such as dislocation cores or grain boundaries [135], a model has been developed of hydrogen transport as Cottrell atmospheres on moving dislocations [89,133]. Although it was claimed [89] that this could result in a large supersaturation of hydrogen in voids, and the consequential growth of the voids, this has been contested [91]. If hydrogen transport by dislocations occurs it is more likely to lead to the rapid attainment of the equilibrium concentration of dissolved hydrogen throughout the plastic zone, rather than to any large degree of supersaturation. An interesting feature of dislocation transport is that the rate of hydrogen transport increases with increasing strain rate. Above a critical strain rate the hydrogen cloud around the dislocation core cannot keep pace with the moving dislocation, and so the amount of hydrogen transported decreases sharply [89]. In a manner similar to that for lattice diffusion, the presence of traps in steels should reduce the rate of hydrogen transported by dislocations.

2.4.4 Crack closure.

Crack closure effects have been observed during corrosion fatigue crack growth by a hydrogen embrittlement mechanism [139,140]. Cathodic protection with seawater can cause the deposition of a calcareous deposit on the crack faces [128] which reduces the effective range of applied stress intensity factor. Therefore the crack growth rate is reduced.

This effect is not observed in NaCl solutions as it is not possible to form calcareous deposits from them. Although the formation of calcareous deposits has a beneficial effect on the fatigue life because of the induced crack closure, it is not an effect that can be depended upon [128,139].

2.4.5 Crack branching.

Crack branching has been observed in crack growth by a hydrogen embrittlement mechanism [72,107,141]. This would reduce the applied stress intensity factor in the same manner as for the anodic dissolution case previously discussed.

2.4.6 Mechanics limitation.

Tomkins [64] has proposed that a mechanics controlled limit to crack growth by a hydrogen embrittlement mechanism exists. An empirical upper bound of $3\Delta\delta$ has been suggested for some steels in low pressure hydrogen gas [142]. The concept of a mechanics limit to environmentally assisted crack growth by a hydrogen embrittlement mechanism is discussed more fully in section 5.4.

2.5 Reduction of slip reversibility.

Stage II fatigue crack growth by a striation mechanism is a result of alternate slip on two planes that intersect the crack tip [121,143,144]. The process is shown diagrammatically in figure 2.1. In a vacuum the possibility exists that a degree of "rewelding" occurs during the closing part of the cycle [144,145]. Adsorption of gases on the crack face, or the formation of corrosion products, whilst the crack is opening would reduce the amount of rewelding that could occur. This mechanism of reduced slip reversibility has been proposed [60] as an explanation of the enhancement of crack growth rates for En56C steel in air relative to those observed in a vacuum. In air an oxide film forms on the crack face, modifying the slip reversibility. Fatigue crack growth rates in air were independent of frequency and temperature changes, which was taken to suggest an effect connected with cyclic crack growth processes [60]. It is known that air and other environments can affect how much Stage I crack propagation occurs, although the details of this are still unclear [144,145].

Although frequency independent regimes are seen in corrosion fatigue [72,146], it is difficult to see how a mechanism of reduced slip reversibility could account for the observed effects of potential and waveform.

2.6 Methods of determining the mechanism of environmentally assisted crack growth.

From the preceding sections it can be seen that anodic dissolution and hydrogen embrittlement share common possible rate controlling processes. For instance both hydrogen embrittlement and anodic dissolution depend upon the crack tip potential. For anodic dissolution the potential determines the bare surface current density whereas for hydrogen embrittlement it controls the hydrogen atom coverage of the crack tip (and so the concentration of hydrogen in the lattice). Again, the competition between crack tip strain rate and the passivation rate can control the extent to which both of these advancement mechanisms operate. The presence of a film on the crack tip surface reduces both the dissolution current and the permeation of hydrogen into the metal. Both mechanisms may be limited by the rate at which fresh solution is transported to the crack tip region. Also for either mechanism the effective K or ΔK can be reduced by crack closure or crack branching.

A consequence of the dependence of anodic dissolution and hydrogen embrittlement on common processes is that it is difficult to determine which mechanism is responsible for environmentally enhanced crack growth in any given situation [40,42]. Thus whilst high strength steels are generally supposed to fail by a hydrogen embrittlement mechanism in aqueous solutions the situation for brasses and aluminium alloys remains controversial [74], and is also unclear for lower strength steels. Several methods that have been proposed in order to distinguish between mechanisms are now discussed.

2.6.1 Polarization method.

Brown and others have proposed a criteria [147,148] that if the cracking is enhanced by a slight anodic shift in the specimen's polarization and reduced by a slight cathodic shift, then the crack growth is caused by a dissolution mechanism. If the opposite effect is observed the mechanism of crack growth is assumed to be hydrogen embrittlement. This criteria fails to meet its objective as what is observed is not the dependence of the mechanism of crack advancement on potential, but the dependence of the intervening rate limiting step (which as previously noted could be common to both mechanisms).

2.6.2 Mode I/Mode III testing.

A number of investigations have used different loading modes as a means of determining the mechanism of crack growth in SCC [136,149-156]. Under Mode III loading no hydrostatic component of stress exists at the crack tip, in contrast to Mode I loading. Dissolved hydrogen accumulates in regions of hydrostatic stress, because of its increased solubility in these regions. As discussed before, the influence of hydrostatic stress (ie. triaxiality) is thought by many workers to cause hydrogen embrittlement to occur at these regions [150,151]. Thus it is proposed that a pure Mode III loading should eliminate the occurrence of hydrogen embrittlement, leaving only the effects of any anodic dissolution.

Although the studies mentioned [136,149-156] have reported a hydrogen embrittlement and a mixed anodic dissolution/hydrogen embrittlement mechanism for many systems, only one result of a pure dissolution mechanism has been reported [150]. The method has not been proved beyond doubt, in that no tests to date have been performed in situations where only one mechanism is known to operate (such as in H_2 gas) [149]. Also confirmation is required that the loading mode does not affect a dissolution mechanism. It is very likely that the passivation rate, crack tip strain rate and solution access are affected by loading mode [150,151]. From the preceding sections it is clear that both mechanisms could be affected by loading mode. In particular the solution access to the crack tip could be much reduced in Mode III experiments. This is because Mode III loading does not allow any opening of the crack faces similar to that in Mode I loading. Several of the investigations [150,151] also used additions to the solution, as discussed in the next section. The results appear to confirm the Mode I/Mode III method's viability.

Care must be taken experimentally when using this method [149] to ensure that as pure as possible Mode III loading is obtained. Even so a nominal hydrostatic stress probably exists in all practical tests, although this should not be great enough to significantly affect the results. A consequence of the care needed to obtain Mode III loading, is that special apparatus is needed before this diagnostic method can be used. The use of additions to the solution does not require this.

2.6.3 Solution additives.

The relative amount of hydrogen entry into the metal can be affected by additions to the solution. Many substances "poison" the hydrogen evolution reaction. This results in a larger fraction of the adsorped hydrogen entering the metal, rather than recombining to form hydrogen gas. Thus if these substances are added to the solution the crack growth rate should increase if crack growth is due to a hydrogen embrittlement mechanism. Such poisons include arsenic, thiourea and hydrogen sulphide. A platinum deposit on the metal surface should decrease the hydrogen entry into the steel because of its effect on the overpotential required for hydrogen evolution. A platinum deposit is therefore expected to decrease the crack growth rate if a hydrogen embrittlement mechanism occurs. Solution additions have been used in several studies [74,150,151]. Concern has been expressed [42] that the passivation rate may also be altered by solution additions. It was suggested that this was only of concern for SCC tests, as a bare surface can be continuously maintained during the opening part of a fatigue cycle. Therefore the use of solution additives is a useful diagnostic method, especially for corrosion fatigue. (As solution additives were used in this study their effects are considered in more detail in the next chapter).

2.6.4 Other methods.

Ford established [42,54] that the mechanism of environmentally assisted crack growth in an aluminium alloy was that of anodic dissolution. This was done by comparing the observed crack growth rates with those predicted from equation 2.2 and measurements of the bare surface current density.

Parkins [74] concluded that a mixed mechanism of environmentally assisted crack growth occurred for a C-Mn steel in phosphate. The bounds to the cracking regime were compared on a Pourbaix diagram with those corresponding to likely controlling chemical reactions.

2.6.5 Conclusions.

Both the use of solution additives and Mode I/Mode III loading are useful diagnostic methods for distinguishing between anodic dissolution and hydrogen embrittlement. Other techniques, such as comparing the cracking regime on a Pourbaix diagram with possible bounding chemical reactions [74], or fractography [72,146,157], are also useful. Fractography is not a sufficient method of distinguishing between the two mechanisms, but can provide supporting evidence [79]. The determination of activation energies for environmental crack growth is of little use, because of the common possible rate controlling processes [61,158].

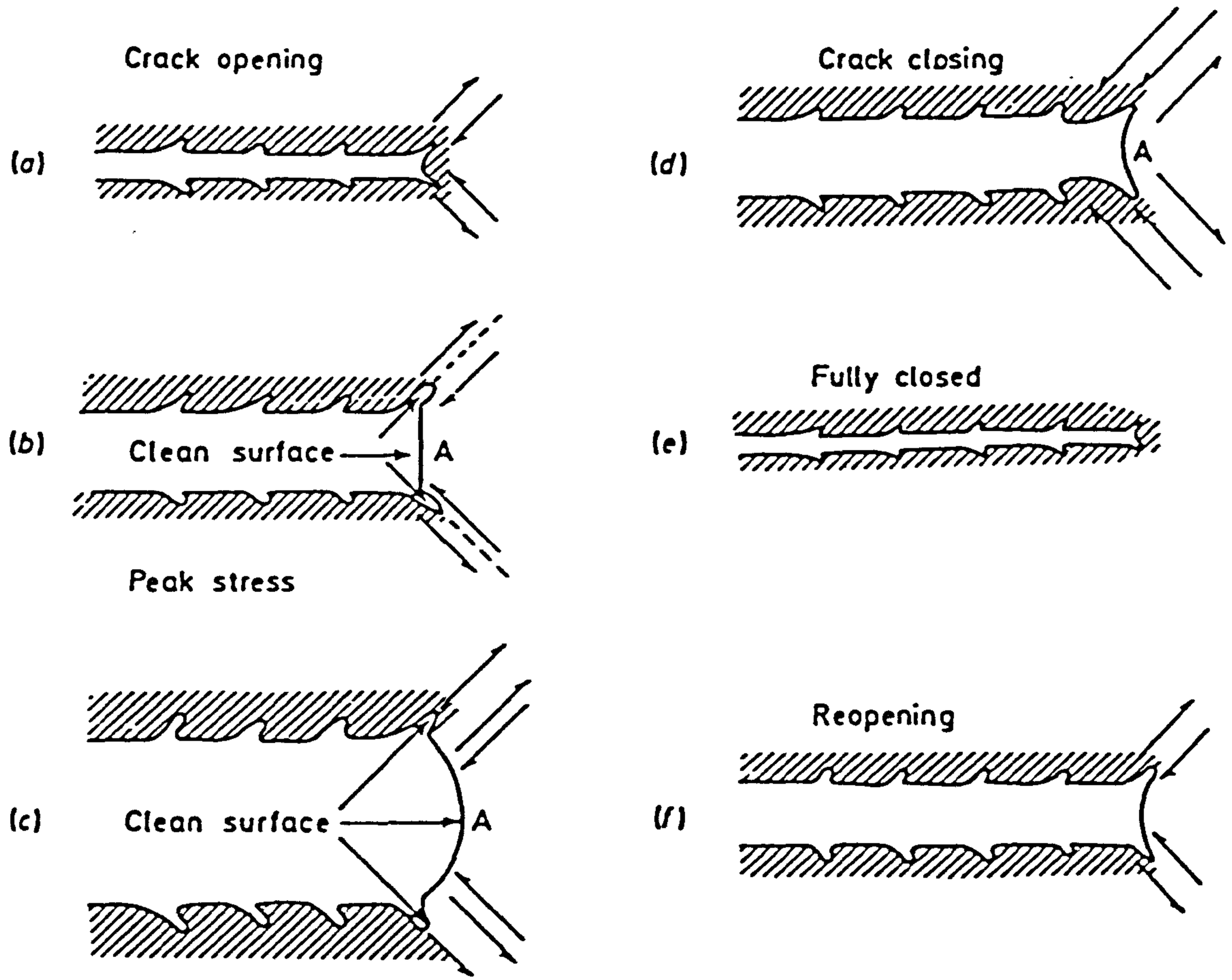

Figure 2.1 Schematic representation of fatigue crack advance by plastic blunting process, from Knott [159]

3.0 Experimental arrangement and theory.

3.1 Experimental.

The experimental arrangement and procedures used are given in reasonable detail in the following sections. Hopefully this will enable the results of this study to be compared with other future studies, and the reasons for any discrepancies due to experimental method to be discovered.

3.1.1 Material.

The material used was node quality BS4360 grade 50D steel. It was supplied in the form of a 25mm thick plate. The material composition and properties are given in table 3.1. Other investigators [160] have reported a wide variation in grain size (3-30μm) for 50D steel. A grain size of 18μm was reported for the material used in this study [161]. BS4360:50D is a structural steel widely used in the fabrication of offshore structures.

3.1.2 Specimens.

The fatigue crack growth rate experiments were performed using standard 3 point bend specimens. The specimen was cut in the long transverse (LT) direction. The specimen dimensions are given in figure 3.1. Before the corrosion fatigue experiments were begun the specimen was precracked in air to a depth of approximately 3mm.

The specimens used for the slow strain rate testing were standard tensile specimens of guage length 38mm. They were cut from broken fatigue specimens, as illustrated in figure 3.2.

3.1.3 Crack length measurement.

The crack length was measured during the fatigue experiments by a DC potential drop (PD) method [162] using a current of 58A. It has been reported that this method does not affect the crack tip conditions [163-165], and has been used in other corrosion fatigue studies [160,163,164,166]. In these other studies the DC potential drop technique gave results that were similar to those obtained using other methods.

When using a DC potential drop method of crack length measurement the measurement leads must be accurately positioned in order to ensure good reproducibility [167]. In this work the leads were spot welded onto the specimen as shown in figure 3.3, and a jig was made up to aid the positioning of the spot welding. A sleeving was then put over the lead and the connection was encapsulated with an epoxy adhesive to protect the lead and spot weld from environmental attack and mechanical breakage.

Commonly a reference voltage is used in this method [162] to eliminate temperature effects. This is not practicable for corrosion fatigue experiments, and so was not used. However, as mentioned later, the temperature control of the specimens was excellent and so this should not have introduced any significant errors. For tests at other than room temperature the change in the specimen's resistivity with temperature altered the measured PD. This was accounted for by multiplying the measured PD by a factor, so as to adjust it to a nominal room temperature value. The factor was determined from a special calibration test, the results of which are shown in figure 3.4.

The calibration curve for crack length against measured PD had been previously determined [168]. As the calibration was determined in air, a check was made upon its applicability for corrosion fatigue experiments. This was done by breaking open fatigue specimens at the end of corrosion fatigue experiments, and measuring the crack length with a travelling microscope. The results are shown in figure 3.5, and confirm the calibration for use in this corrosion fatigue study. (The scatter results from errors in measuring the final PD, specimen corrosion and effects of the crack front shape. The DC potential drop method measures an average crack length [169] and so minimizes errors due to changes in the shape of the crack front).

Originally the potential developed across the crack was measured

using a Solartron 7045 DVM. This was not completely satisfactory because :

(i) corrosion fatigue experiments suffer from transient effects, and so should be run continuously [170]. Thus the use of a DVM led to overnight gaps in the gathered data.

(ii) as the crack opened and closed a slight variation occurred in the potential measured. This was as much as 5μV in extreme cases, although ususally around 2μV. As a result of this variation in potential errors could have been introduced from readings taken manually.

As a result of these potential measurement problems a computerized data logging system was obtained. This consisted of an AIM 65 microprocessor linked to a A-D converter. The A-D board had a resolution capability of 0.75μV. It was necessary to also purchase a clock board as the measurement board interfered with the use of the microprocessor's internal timers. Two signal input boards were purchased with eight input channels available on each board. It was recommended that for floating signals (such as the potential measurements here) the "low" terminal should be strapped to earth. However it was discovered that in conjuction with the cathodic protection system used this caused an earth loop to be formed. Consequently on one board the "low" terminals were left unconnected to earth, and this board was used for the corrosion fatigue work. This had no detectable effect on the measured potentials. A program was written for the AIM 65 to enable measurements to be made; the frequency of readings could be determined independently for each channel. The program listing is included in Appendix 1. Each reading recorded was the average of 100 readings taken over approximately an 18 second period. As averaging n measurements reduces the error by $\sqrt{n}$ this considerably improved the measurement accuracy. Tests on a static crack showed that the error involved in the computerized data logging system was less than 1μV, which corresponds to a resolution of the crack length to within 0.05mm. This system was used for the majority of the work reported in this thesis.

3.1.4 Data analysis.

The method used to reduce the crack length, a, versus the number of cycles, N, data is very important [171]. For instance, use of the standard ASTM 7 point incremental polynomial method may lead to spurious points appearing if the crack growth rate changes abruptly. This method may also lead to a "smoothing" of any sharp change of gradient of the da/dN vs. ΔK curve [172,173]. On the other hand linear difference techniques lead to a lot of scatter in the results [172,173]. The ASTM 7 point incremental polynomial method also results in more loss of data at the beginning and end of the test, and may give false results when either large gaps exist in the experimental readings, or the number of readings are small. A 3 point linear difference technique was used because it was concluded [172,173] that it was the best compromise between the need to reduce experimental scatter, and the need to avoid excessive smoothing off of real changes in the crack growth rate. Also, as mentioned earlier, the earliest experimental data contained overnight gaps in it, and only a limited number of readings were taken. For these experiments the standard ASTM method was definitely inappropriate. However the two methods of data reduction have been compared using experimental data obtained with the computerized data logging system. The results are shown in figures 3.6 to 3.10. Whilst the scatter is slightly greater using the 3 point linear difference technique the two methods of data reduction give results that agree closely. The use of a numerical data reduction method allowed the use of a microcomputer system for data analysis. A Hewlett-Packard HP87 computer system, incorporating a plotter, was used. A program was developed that allowed a choice of data analysis method. A graph of a vs. N was output as well as of log da/dN vs. log ΔK, to serve as a check of the results. The program listing is included in Appendix 1, together with a listing of a file creation program written to ease data entry from the output of the data logging system.

The effect of experimental errors upon log da/dN vs. log ΔK curves has not been widely considered. However some workers have attempted to investigate this question [172-177]. In most of these studies a systematically varying errror was added to a correct "reading", and the resultant errors in the log da/dN vs. log ΔK curves compared. The introduction of a systematic error is obviously unrealistic for true experimental errors. Following Austen's example [172], the crack

growth curve of figure 3.11 was numerically integrated on a microcomputer to provide "correct" a vs. N data. This was then converted into PD vs. N "experimental results". These "results" obtained therefore contained no significant error. Whereas Austen used a systematic error in his comparison of data reduction methods [172] for this work a random error has been used. As the number of cycles, N, could be measured accurately experimentally, the experimental errors were simulated by a normally distributed error superimposed on the PD "results". The results are shown in figures 3.12 to 3.16 for different values of the standard deviation of the error. The envelope of the results shown in figures 3.12 to 3.16 provides an indication of the degree of experimental scatter expected as a result of measurement errors. Other sources of possible error include the effects of environment temperature variation and variation in the current supply through the specimen. Generally these were not significant.

3.1.5 Environment.

Most testing was performed at ambient temperature (≈23°C). For some of the earlier work the air temperature varied somewhat, but most of the work was done after the installation of an air condition system in the laboratory. The ambient temperature was then 22-23°C, although occasionally it reached 21°C or 24°C. Thus the solution temperature was definitely within 23±2°C and usually within 23±1°C. For testing at other than ambient temperature the machine indenters and the solution around the specimen were heated or cooled. The test temperature was then maintained to within ±1°C.

The test solutions were contained around the specimen by a Perspex chamber, and were constantly circulated through the chamber from a 4 litre reservoir by a peristaltic pump. The solution flow rate was such that the solution in the tank was replaced every few minutes. The tests were performed using four different solutions :

(i) 3% NaCl
(ii) 3% NaCl + 5g/l sodium arsenate
(iii) 3% NaCl + 5g/l thiourea
(iv) 3% NaCl + 0.125% w/v platinum (iv) chloride (ie. chloroplatinic acid).

The solutions were fully aerated (≈7-8ppm O_2).

The specimen potential was controlled using a Wenking LT78 potentiostat, in conjunction with a saturated calomel reference electrode (sce) and platinum counter electrode.

Figure 3.17 is a photograph illustrating the experimental arrangement.

A large proportion of the testing was performed at a frequency of 0.167Hz, which is representative of North Sea wave loading. Constant amplitude loading was employed, using a sinusoidal waveform (except where stated otherwise).

The fatigue testing machines used were Dartec 100kN frames with servohydraulic actuators. Considerable experimental delay was experienced due to problems with the hydraulic circuit.

3.1.6 Fractography.

Fractographic investigation of corrosion fatigue specimens is hindered by the presence of corrosion products on the fracture surface. A variety of methods have been developed for specimen cleaning including :

(i) ultrasonic cleaning, followed by dry stripping using acetate film [178]

(ii) inhibited acid cleaning [160]

(iii) cathodic electrolytic cleaning, utilizing a propiety electrolyte (Endox 214) [179]

In the present work it was found that ultrasonic cleaning did not appreciably remove corrosion products. Also it was not possible to use the Endox 214 method, for safety reasons (Endox 214 contains cyanide). However the problem of fracture surface cleaning was circumvented as it was noticed that most of the fracture surface was still free of corrosion products at the end of the fatigue test. Removing the test solution quickly, and immediately cycling the specimen at around 10Hz with the tank refilled with methanol, enabled relatively clean fracture surfaces to be obtained. The fast cycling

with methanol replaced the water trapped inside the crack with methanol and so prevented further corrosion of the crack face. After the specimen was removed from the tank it was rinsed with acetone and stored in a desiccator. The advantage of this method is that no cleaning process is employed that could destroy fracture surface markings. A similar method has been used in other corrosion fatigue work [180].

The fracture surfaces were investigated using a Cambridge Steroscan 600 SEM.

3.1.7 Slow strain rate testing.

Some slow strain rate tests were performed in each of the four solutions using an Instron TT-KM universal testing machine. The experimental arrangement is illustrated in figure 3.18. The solutions were circulated, by a peristaltic pump, from a 4 litre reservoir through a Perspex tank surrounding the specimen. The specimen potential was controlled by the same means as for the fatigue specimens.

As the specimen gauge length was 38mm, and the slowest crosshead speed available on the testing machine was 0.01mm/min, the test was conducted at a nominal strain rate of 4.4×10^{-6}/s. Because the time to failure did not alter by much for these tests the degree of embrittlement was characterized by the percentage reduction of area. The specimen diameter was measured using a micrometer before insertion into the machine, and after failure the diameter of the neck was measured using an optical comparator.

3.2. Theory.

In the following sections a brief resume is given of some relevant aspects of electrochemistry. The effects of the various solution additives used are then considered.

3.2.1 Corrosion.

As mentioned in section 2.2.4, metal dissolution occurs through the anodic reaction :

$$Fe \rightarrow Fe^{2+} + 2e^- \qquad (3.1)$$

Metal dissolution will only occur if there is a corresponding cathodic reaction taking place simultaneously, with the anodic and cathodic areas in electrical contact. For aerated solutions the cathodic reaction is the oxygen reduction reaction :

$$O_2 + 2H_2O + 4e^- \rightarrow 4OH^- \qquad (3.2)$$

Generally it is thought [181] that crack tip conditions in structural C-Mn steels are such that the main cathodic reaction that occurs there is the hydrogen evolution reaction :

$$2H_3O^+ + 2e^- \rightarrow H_2 + 2H_2O \qquad (3.3)$$

The hydrogen evolution occurs at a potential below that given by :

$$E = -0.244 - 0.059[pH]\ V\ (sce) \qquad (3.4)$$

It is quite possible [74,98] for the theromodynamic conditions within the crack to be such that both hydrogen evolution and metal dissolution occur simultaneously. That is, the potential is below that given in equation 3.4 and above the minimum potential necessary for reaction 3.1 to occur.

3.2.2 The hydrogen evolution reaction.

The evolution of hydrogen from metal cathodes has been extensively studied. The overall reaction consists of several steps [182] :

(i) Diffusion of H_3O^+ ions from the bulk solution to the edge of the double layer.

(ii) Transfer of H_3O^+ ions across the layer.

(iii) Dehydration of H_3O^+.

(iv) Electron transfer from electrode to H^+.

(v) Formation of hydrogen molecules from adsorbed hydrogen atoms.

(vi) Desorption of hydrogen molecules and evolution of gas bubbles.

The complete reaction is :

$$2H_3O^+ + 2e^- \rightarrow H_2 + 2H_2O \qquad (3.3)$$

This consists of the reaction :

$$H_3O^+ + e^- \rightarrow H_{ads} + H_2O \qquad \text{(discharge)} \qquad (3.6)$$

followed by a chemical desorption reaction.

The discharge reaction comprises steps (ii)-(iv) in the hydrogen evolution reaction scheme above, whereas the chemical desorption reaction corresponds to step (v). There are two possible routes for the chemical desorption reaction :

$$2H_{ads} \rightarrow H_2 \qquad \text{(catalytic reaction)} \qquad (3.7)$$

$$H_{ads} + H_3O^+ + e^- \rightarrow H_2 + H_2O \qquad \text{(electrochemical reaction)} \qquad (3.8)$$

The rate of the overall reaction is usually governed by one of the steps (ii)-(iv). It appears [182] that for lower overvoltage metals, eg. platinized platinum, the catalytic reaction is the rate determining step. For the majority of metals, with higher overvoltages, steps (ii)-(iv) collectively (ie. the discharge

reaction) control the reaction rate. Occasionally the electrochemical reaction is rate controlling, though not for the conditions of this study.

The discharge reaction, equation 3.6, can be followed by the absorption of hydrogen into the metal :

$$H_{ads} \rightarrow H_{abs} \qquad (3.9)$$

Thus the amount of hydrogen entry into the metal is determined by the coverage of the surface by adsorbed hydrogen.

3.2.3 Effect of solution additives.

Platinic Chloride.

The addition of platinic chloride (chloroplatinic acid) to the solution results in platinum black being deposited at cathodically polarized sites. The platinum has a much lower overpotential for the hydrogen evolution reaction than iron, as well as a higher exchange current density [74,183]. This results in the platinic chloride promoting the evolution of hydrogen gas, at the expense of hydrogen entry into the metal. Thus the addition of platinic chloride to the solution would be expected to decrease any hydrogen embrittlement effects. The platinum deposit also results in a shift of the electrode potential in a more noble direction [74,183].

Arsenic.

Arsenic is well known to aid the entry of hydrogen into steel. Several theories have been proposed to explain this action. Smialowski [184] suggested that the presence of a volatile hydride is essential for the occurrence of promoted hydrogen entry. Other proposals include the strengthening of the bonding between the adsorped hydrogen atoms and the metal [185], although it has also been suggested that this bonding is weakened [186-188]. The usual view of the action of arsenic is that it prevents the formation of gaseous hydrogen, ie. it poisons the chemical desorption reaction [185,188]. If the formation of gaseous hydrogen occurs by the hydrogen recombination reaction (equation 3.7) then the configurational arguement of Evans could explain the action of arsenic [186,188]. If the hydrogen recombination reaction is poisoned then entry of hydrogen into the steel is promoted, as a consequence of the resultant increase in surface coverage by adsorbed hydrogen. It has been reported that in some circumstances, arsenic can also reduce hydrogen entry into the metal. At potentials more negative than ≈0V(sce), a film of metallic arsenic may form over the surface [184]. At anodic potentials arsenic may be desorbed and have no effect, this has been observed in alkaline solutions [185]. However, the poisoning action of arsenic only takes place at potentials that are more active (ie. negative) than ≈-0.644V(sce) [184], where AsH_3 is formed at low partial pressures.

A consequence of the poisoning of the hydrogen recombination

reaction, or of deposition of metallic arsenic, is that arsenic may inhibit the dissolution reaction (equation 3.1).

The effect of arsenic may be summarized as :

(i) negligable effect at anodic potentials

(ii) the promotion of hydrogen entry, and inhibition of metal dissolution, should encourage hydrogen embrittlement at cathodic potentials

(iii) a small promotion of hydrogen entry at the free corrosion potential, as at ≈-0.65V(sce) this is at the limit of the potential range over which arsenic promotes hydrogen entry.

Thiourea.

Thiourea derivatives have been used as inhibitors in acidic pickling, but have been found to promote hydrogen entry into the metal [186].

The inhibitory effect of thiourea is due to its adsorption at otherwise active sites [74,189]. However the effect of thiourea is also a function of concentration [189]. At high concentrations the inhibitory action is lost as effects due to a protonated form of thiourea become significant. Also thiourea does not alter the mechanism of the hydrogen evolution reaction [189]. Thiourea has been reported to decompose at a cathode, yielding H_2S [184]. Recent work has shown that H_2S is formed under anodic polarization [189]. The H_2S is formed as a result of a metal dissolution process that involves the protonated form of thiourea. At the concentration of thiourea used in this study (5g/l or 65.8 m molar) it is quite possible that this mechanism of H_2S formation occurs at anodic potentials.

Overall the action of thiourea should be to inhibit a dissolution mechanism, and to encourage a hydrogen embrittlement mechanism.

Composition.

C	Si	Mn	P	S	Nb
0.13	0.32	1.22	0.007	0.004	0.03

Mechanical properties.

yield stress : 368 MPa

ultimate tensile strength : 508 MPa

Charpy V notch @ -30°C : 235 - 268 J

Table 3.1 : Chemical composition and mechanical properties of material used in this study.

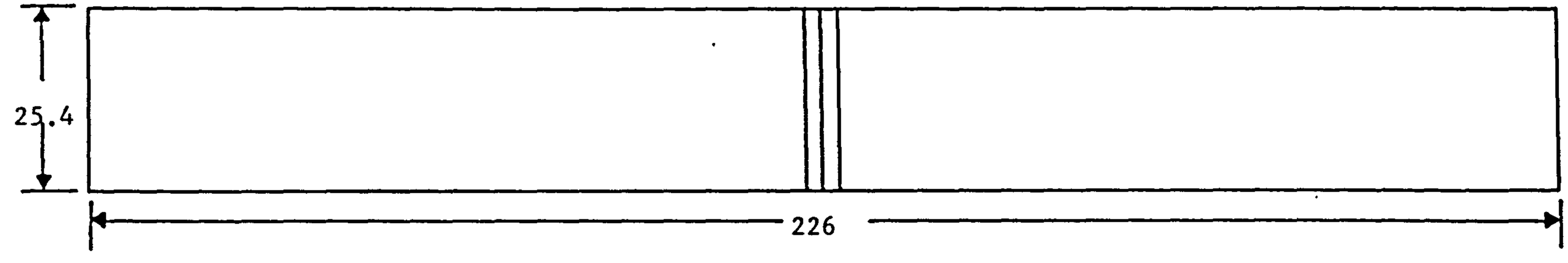

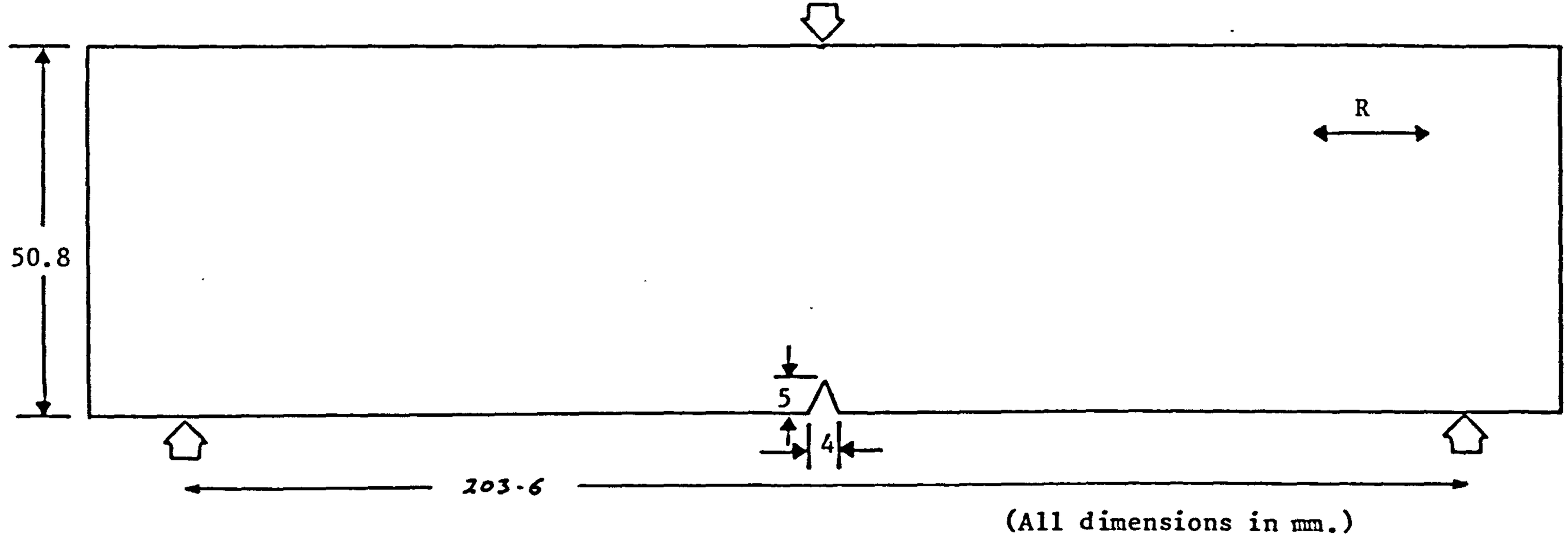

Figure 3.1 Fatigue specimen geometry

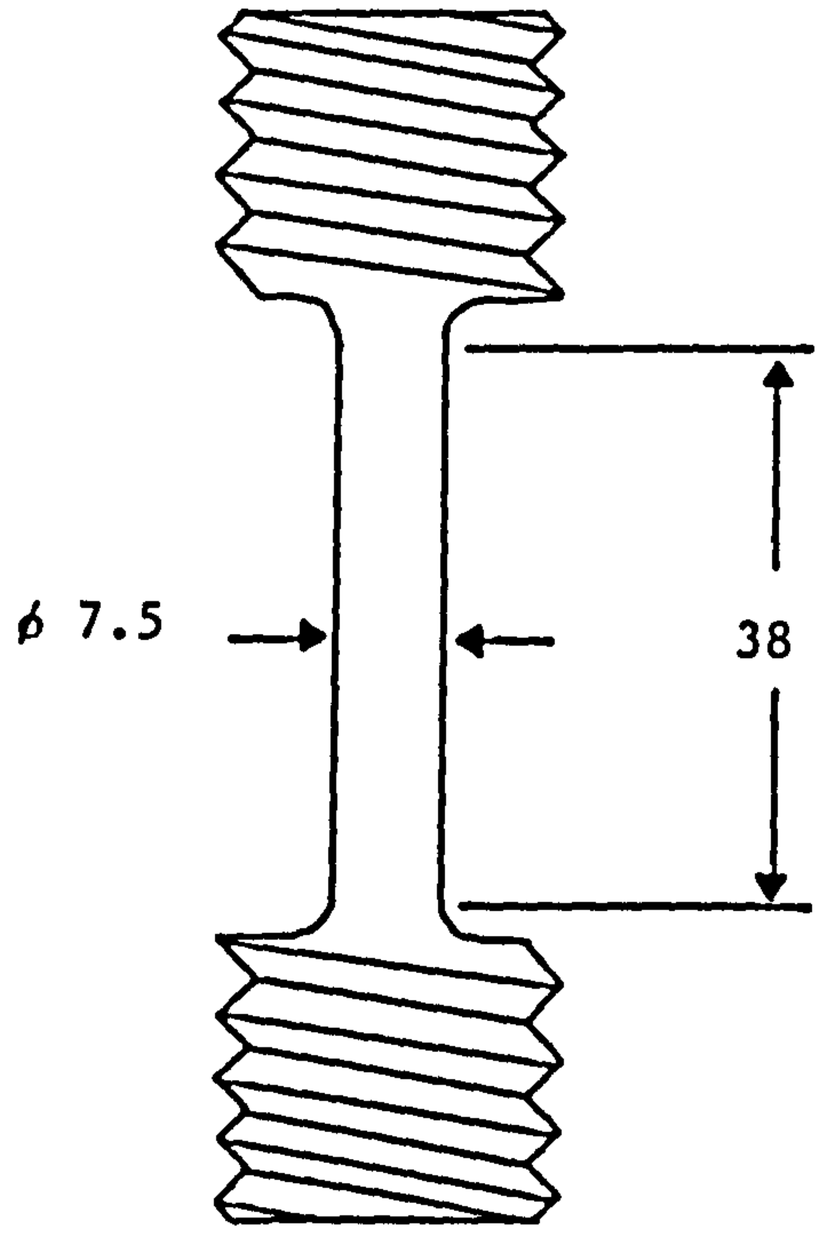

(All dimensions in mm.)

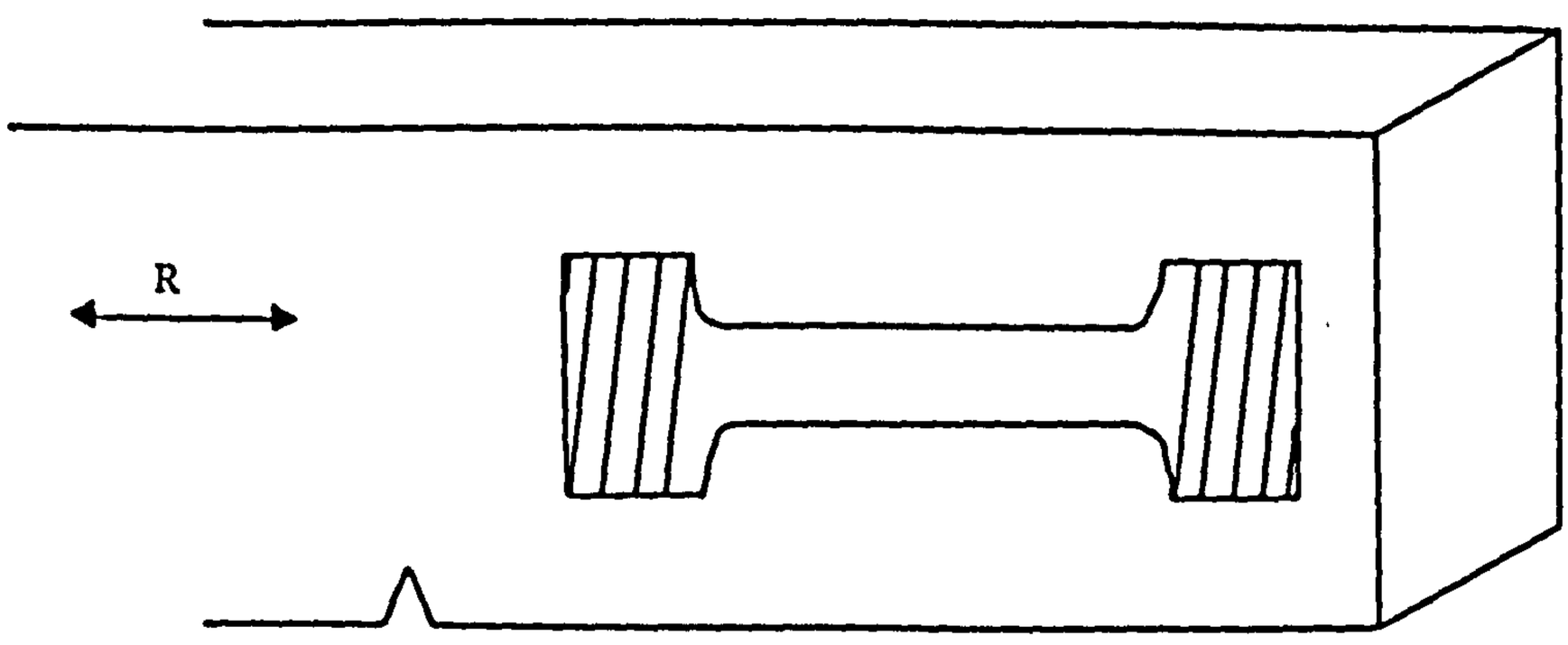

Figure 3.2 Slow strain rate tensile specimen geometry and orientation

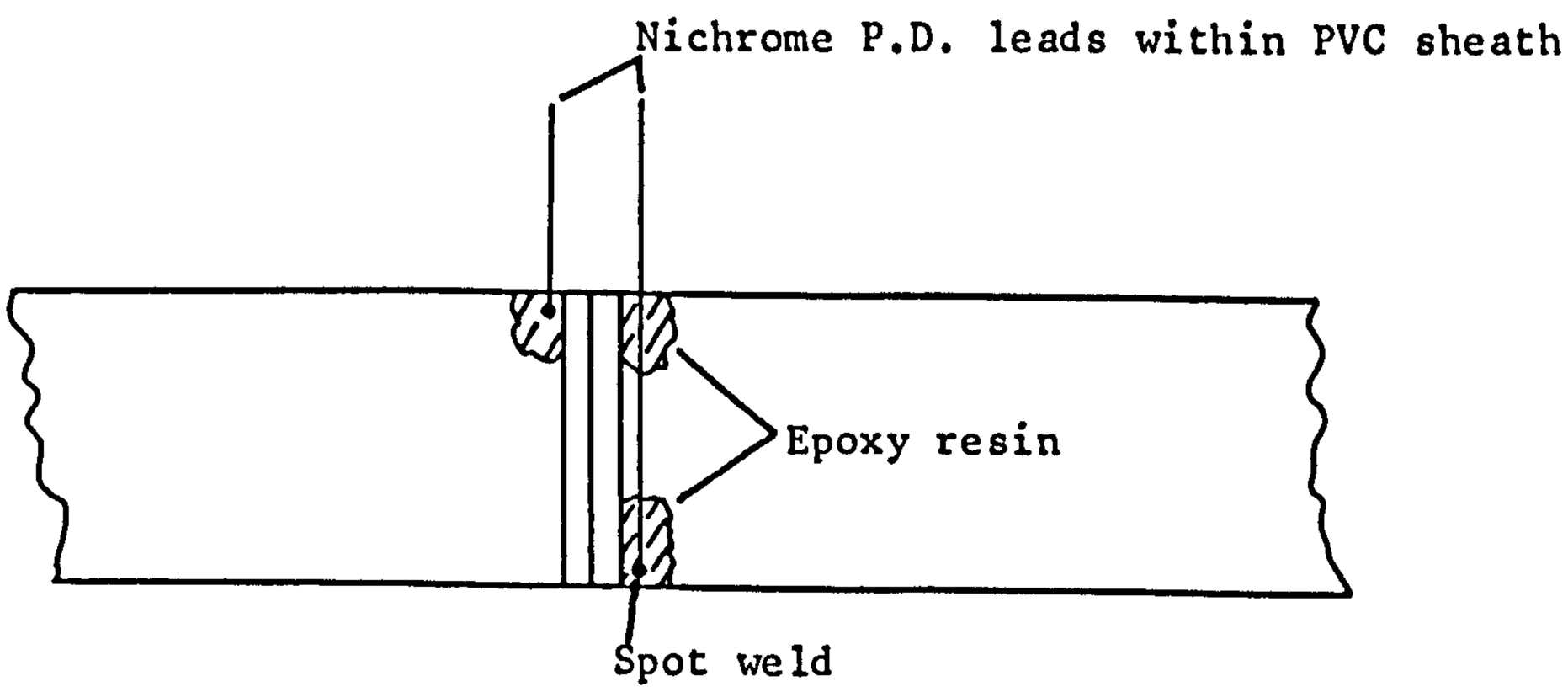

Figure 3.3 Diagram showing details of attachment of P.D. leads to fatigue specimen

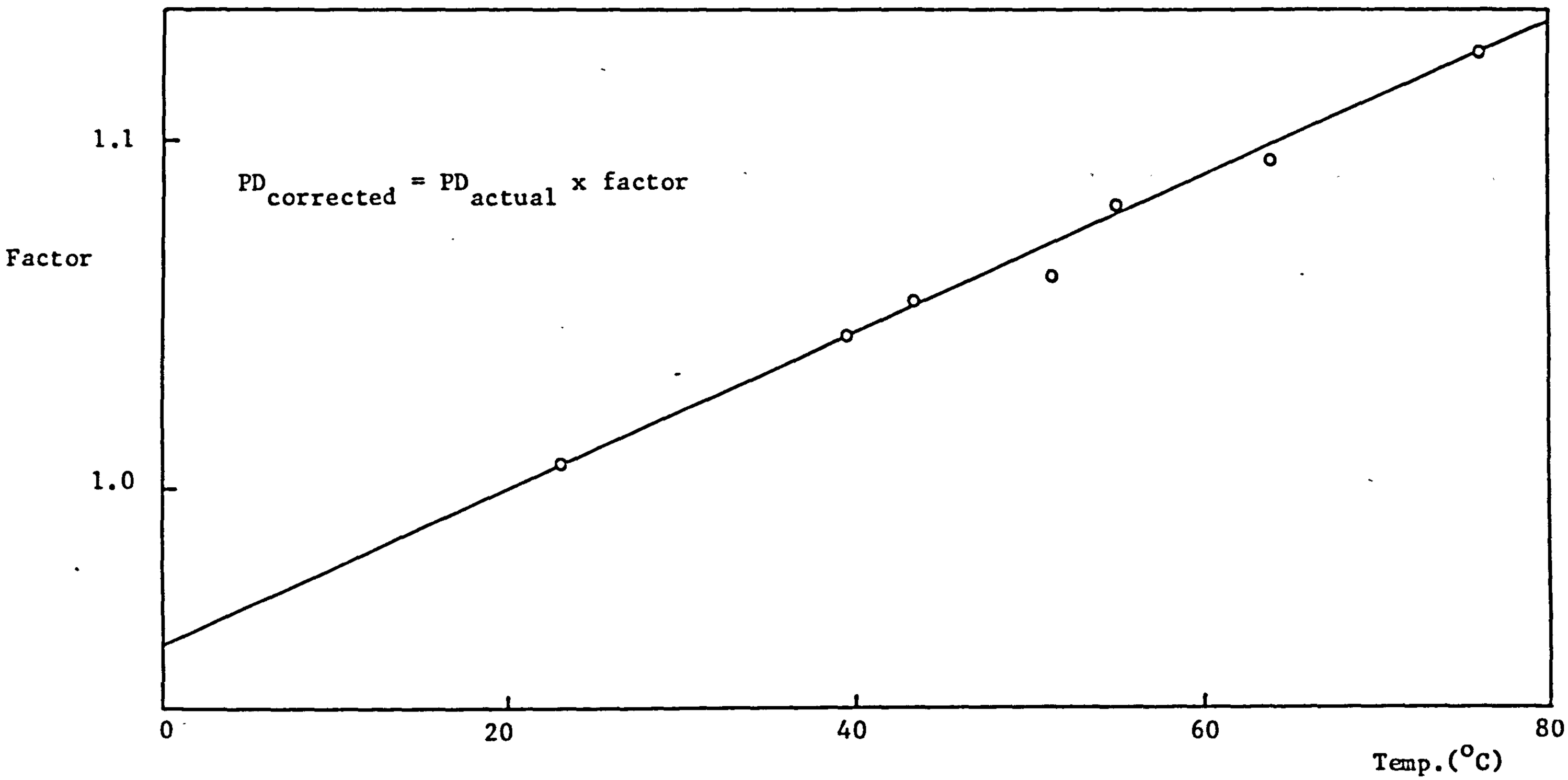

Figure 3.4 Potential vs. temperature calibration

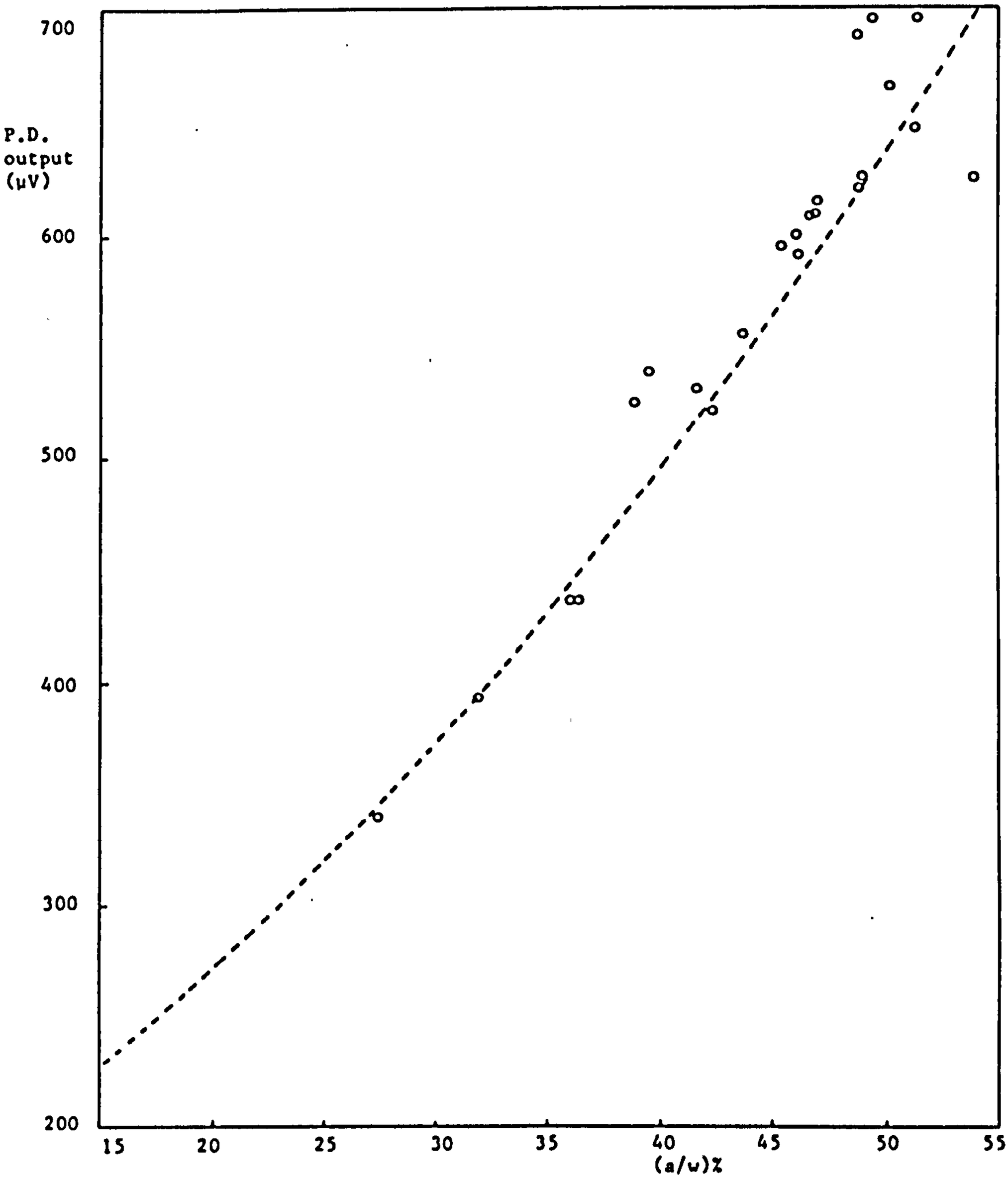

Figure 3.5 Comparison of P.D. calibration with final corrosion fatigue crack lengths and potentials.

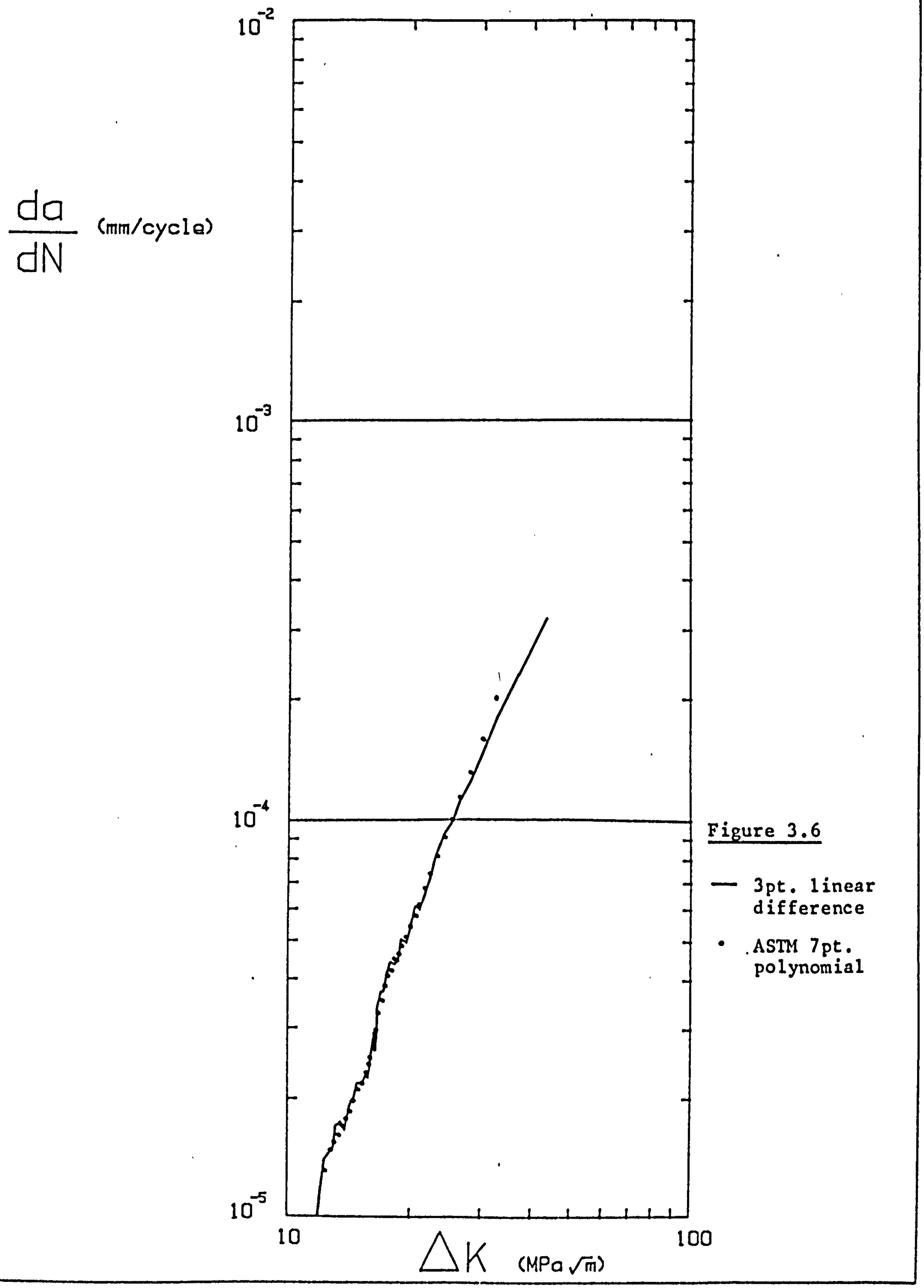
$\frac{da}{dN}$ (mm/cycle)
10^{-2}
10^{-3}
10^{-4}
10^{-5}
10
100
ΔK (MPa $\sqrt{m}$)
— 3pt. linear difference
• ASTM 7pt. polynomial

Figure 3.6

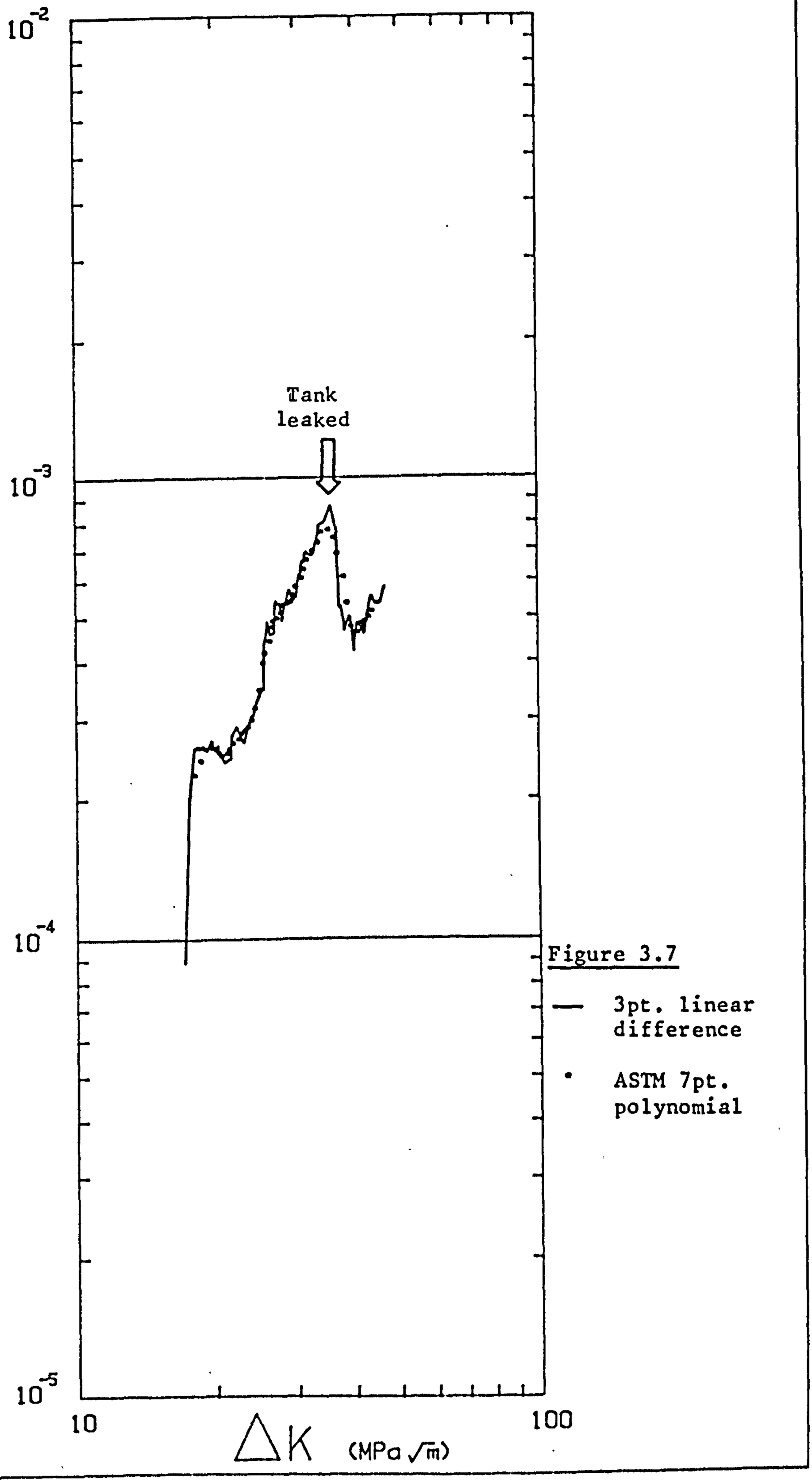

Figure 3.7

— 3pt. linear difference

• ASTM 7pt. polynomial

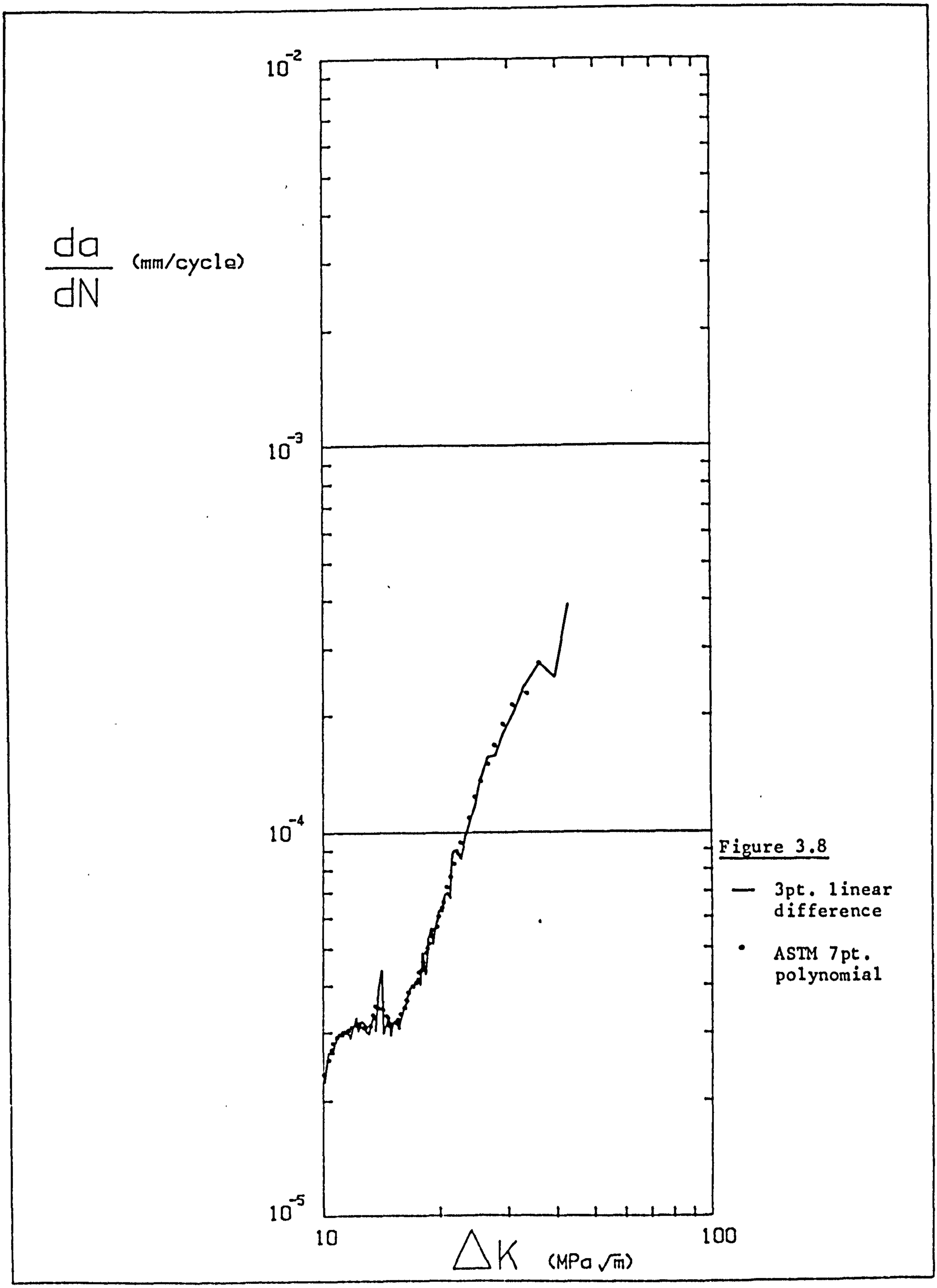

Figure 3.8

— 3pt. linear difference

• ASTM 7pt. polynomial

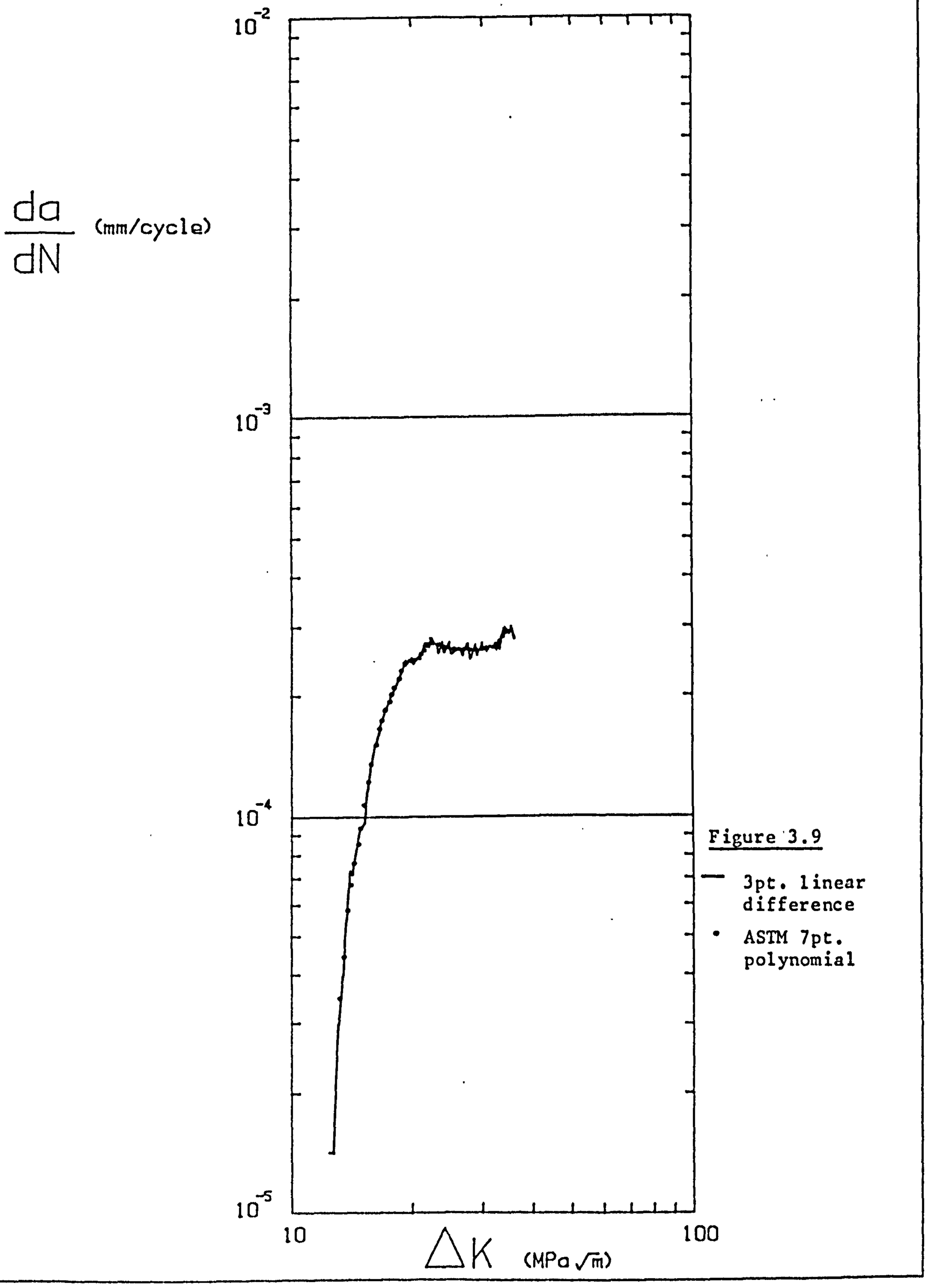
$\frac{da}{dN}$ (mm/cycle)
10^{-2}
10^{-3}
10^{-4}
10^{-5}
10
100
ΔK (MPa $\sqrt{m}$)
— 3pt. linear difference
• ASTM 7pt. polynomial

Figure 3.9

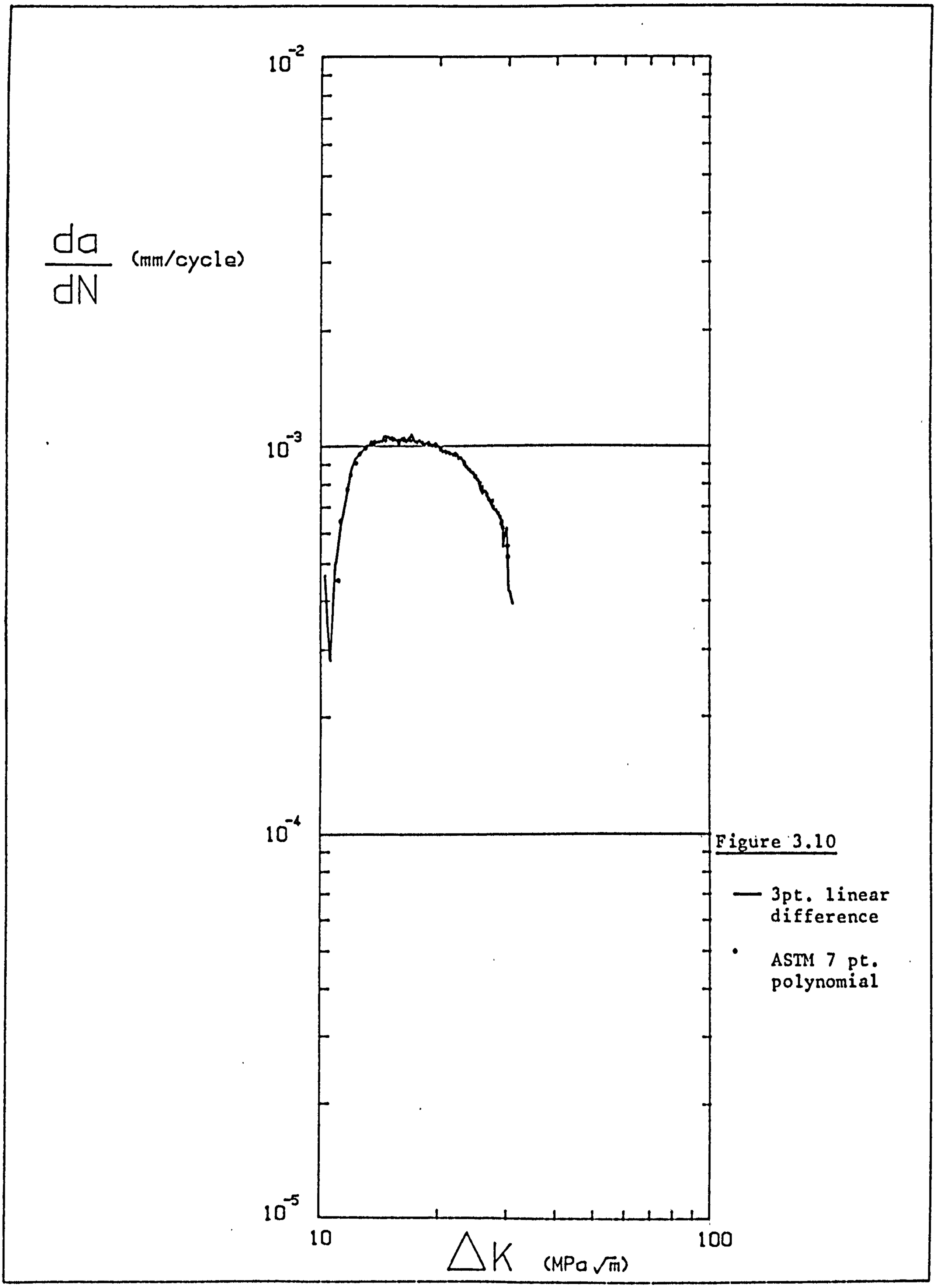
$\frac{da}{dN}$ (mm/cycle)
10^{-2}
10^{-3}
10^{-4}
10^{-5}
10
100
ΔK (MPa $\sqrt{m}$)
— 3pt. linear difference
• ASTM 7 pt. polynomial

Figure 3.10

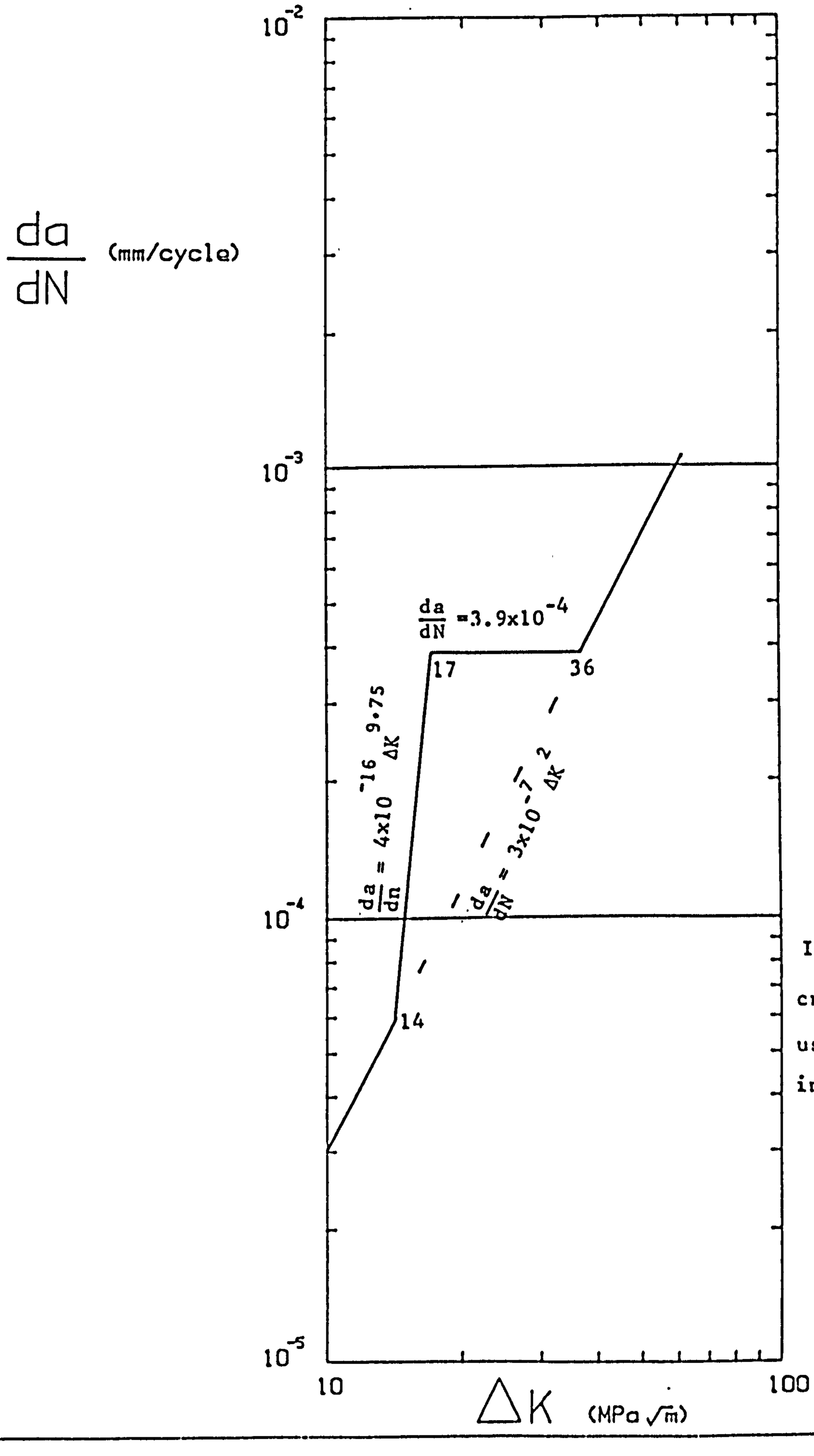

Figure 3.11

Idealised fatigue crack growth data used for numerical integration

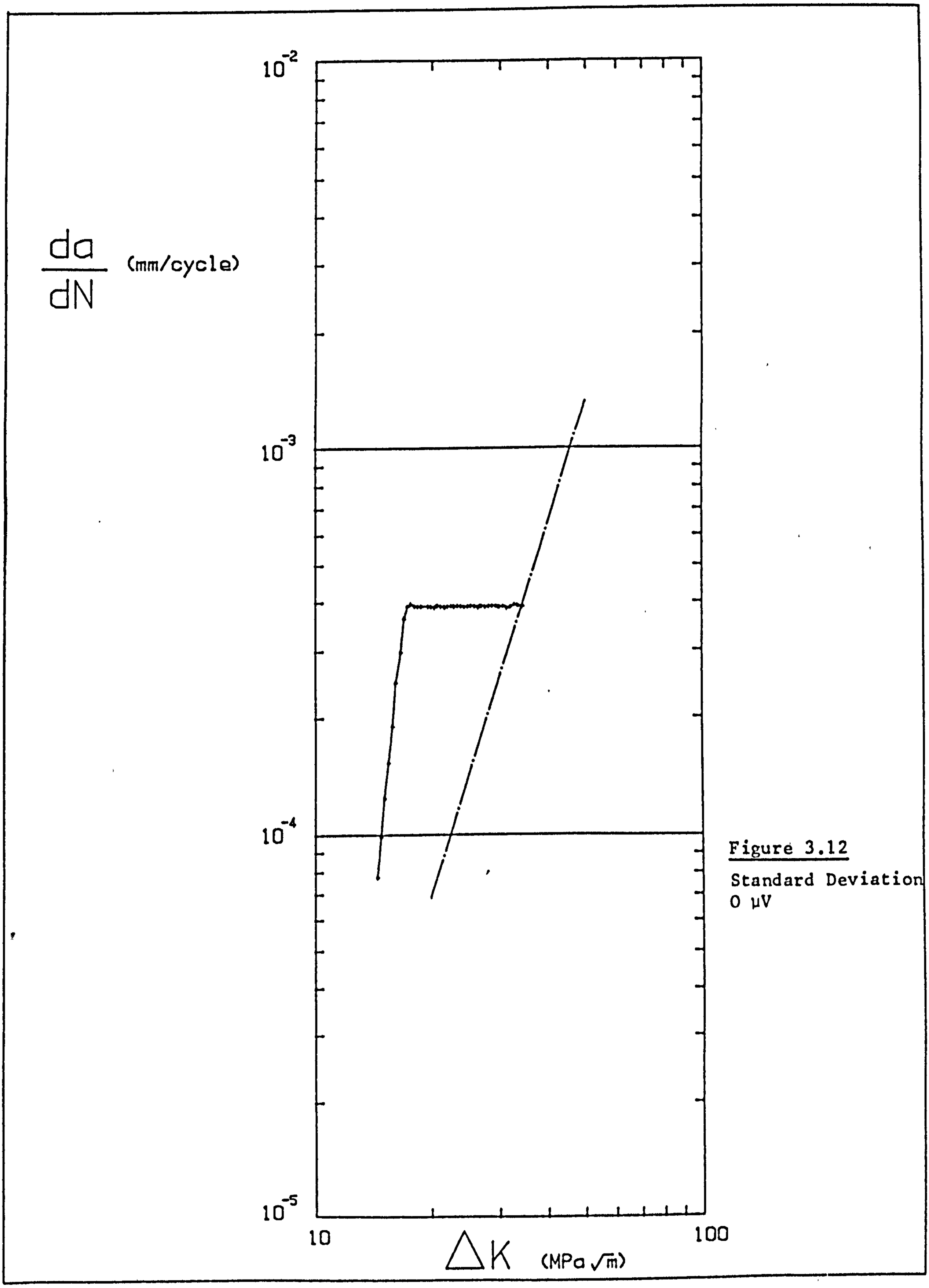

Figure 3.12

Standard Deviation
0 μV

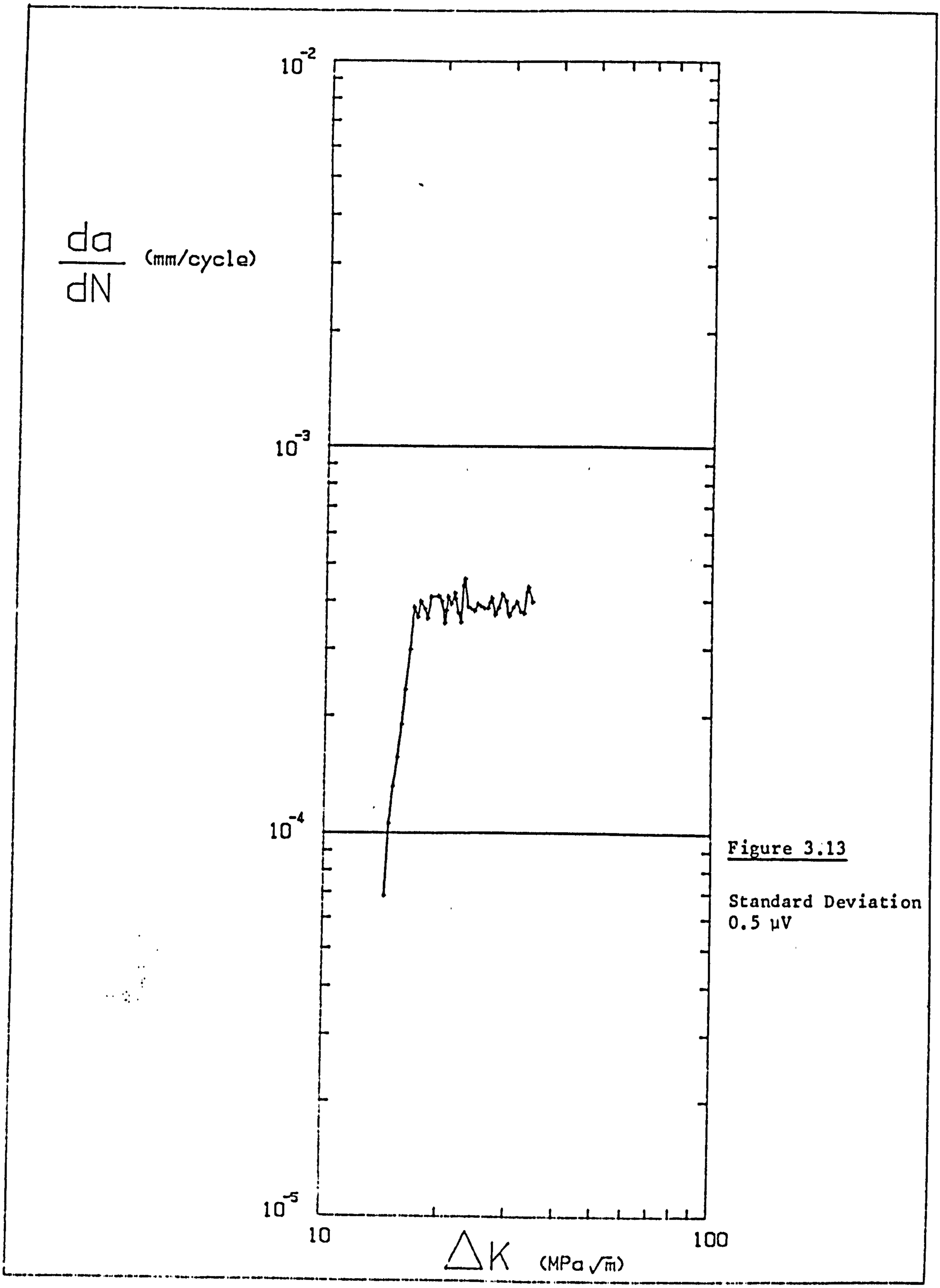

Figure 3.13

Standard Deviation
0.5 μV

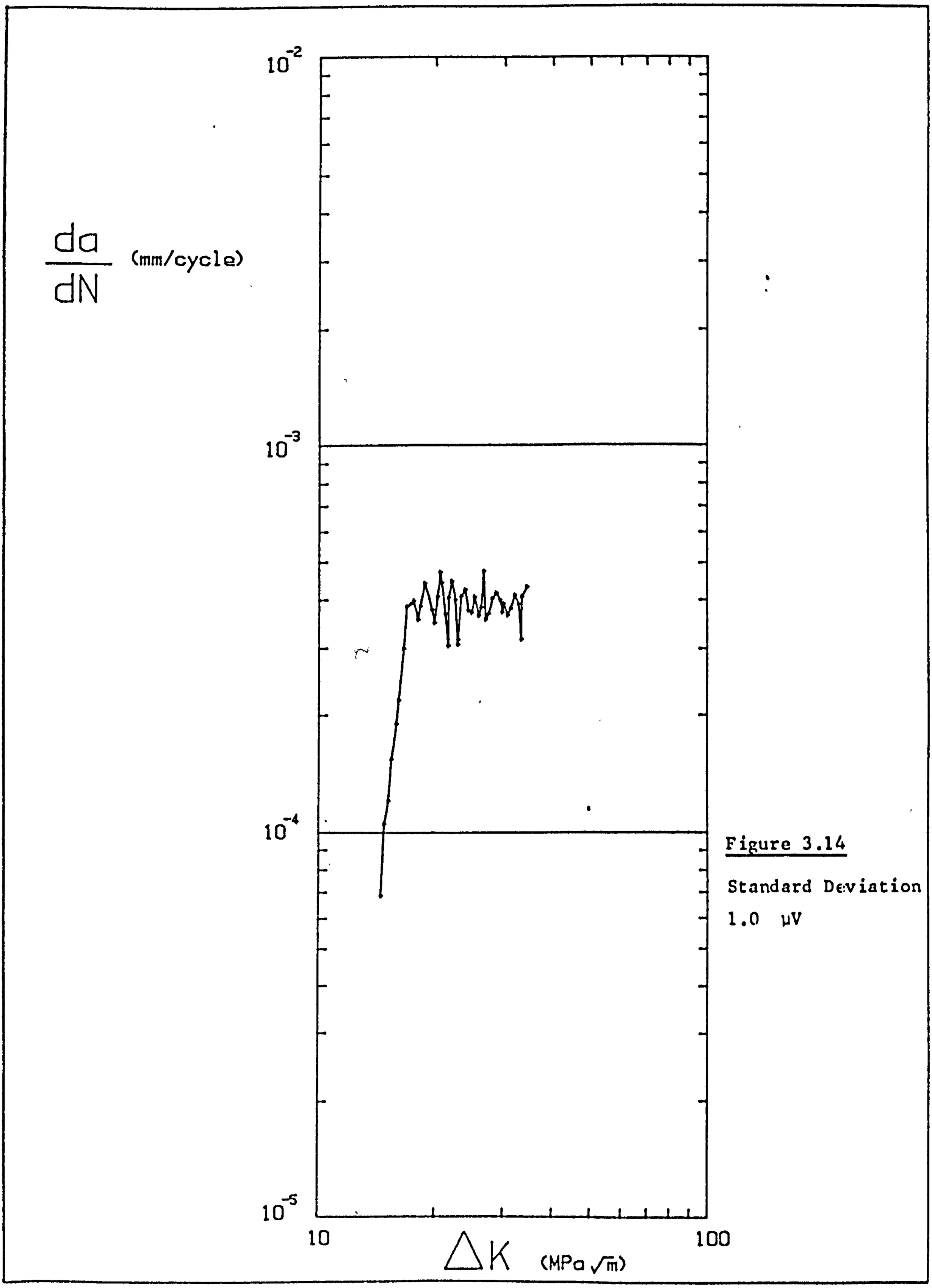

Figure 3.14

Standard Deviation

1.0 μV

Figure 3.15

Standard Deviation
2.0 μV

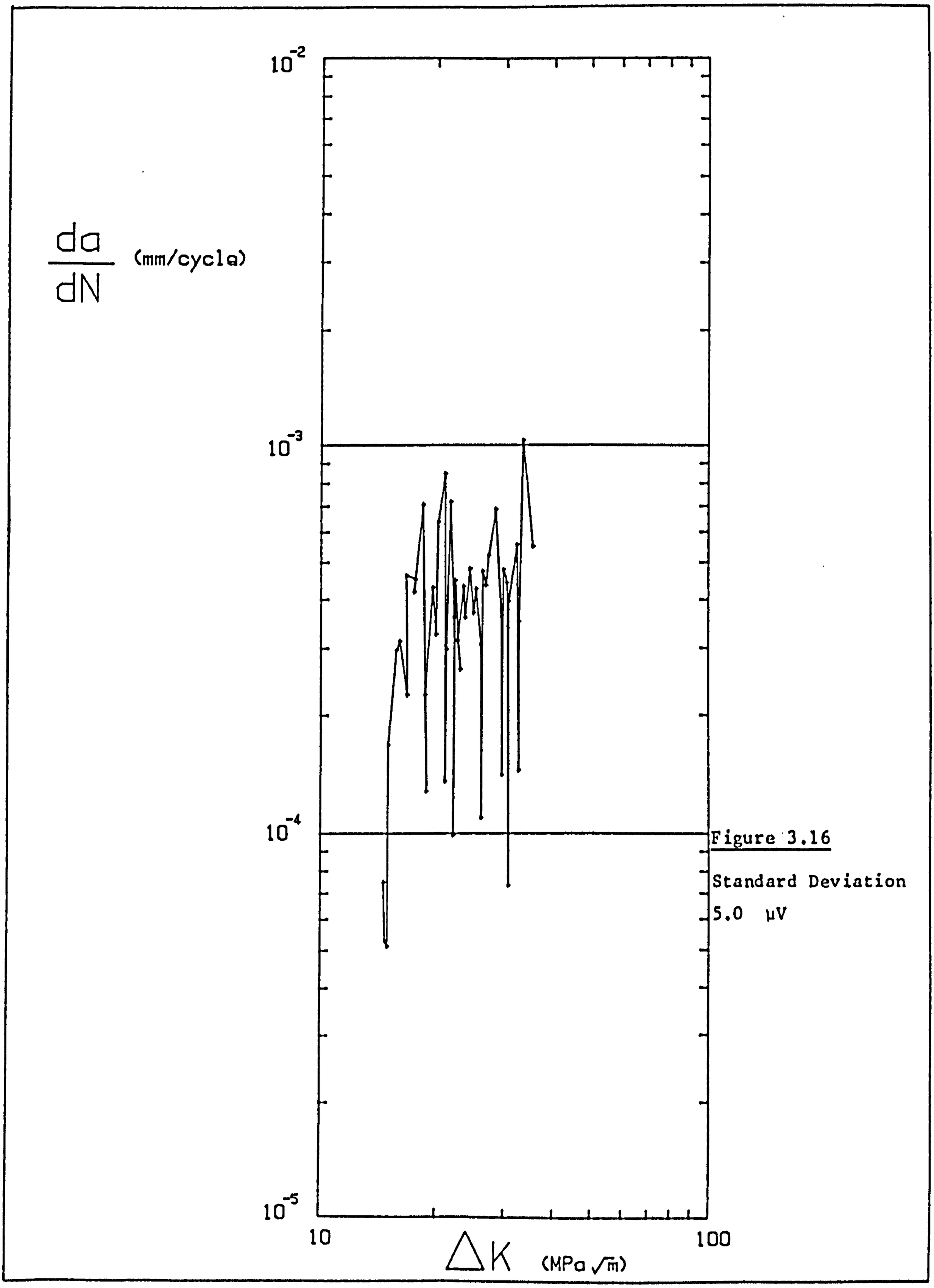

Figure 3.16

Standard Deviation

5.0 μV

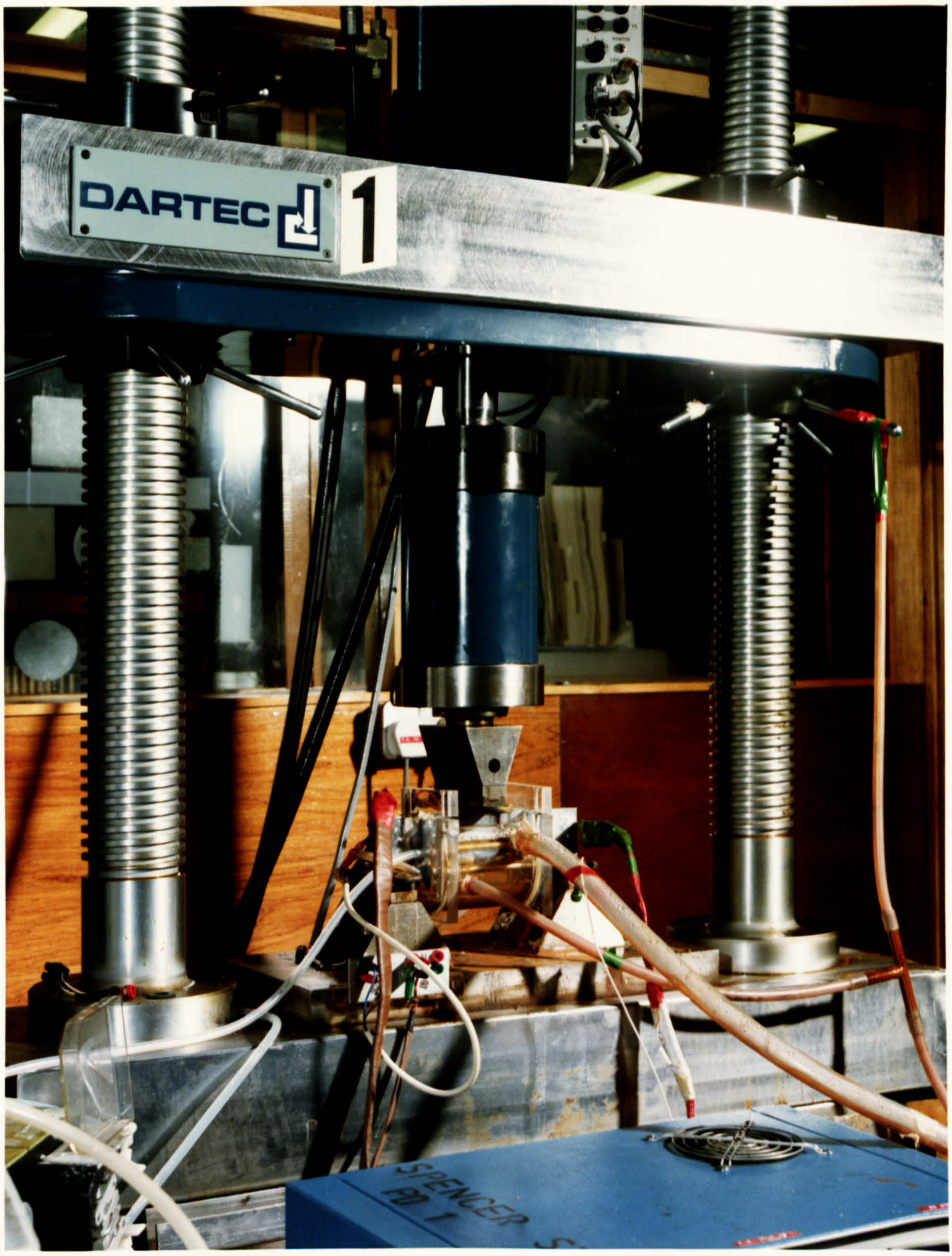

Figure 3.17 Photograph of experimental arrangement

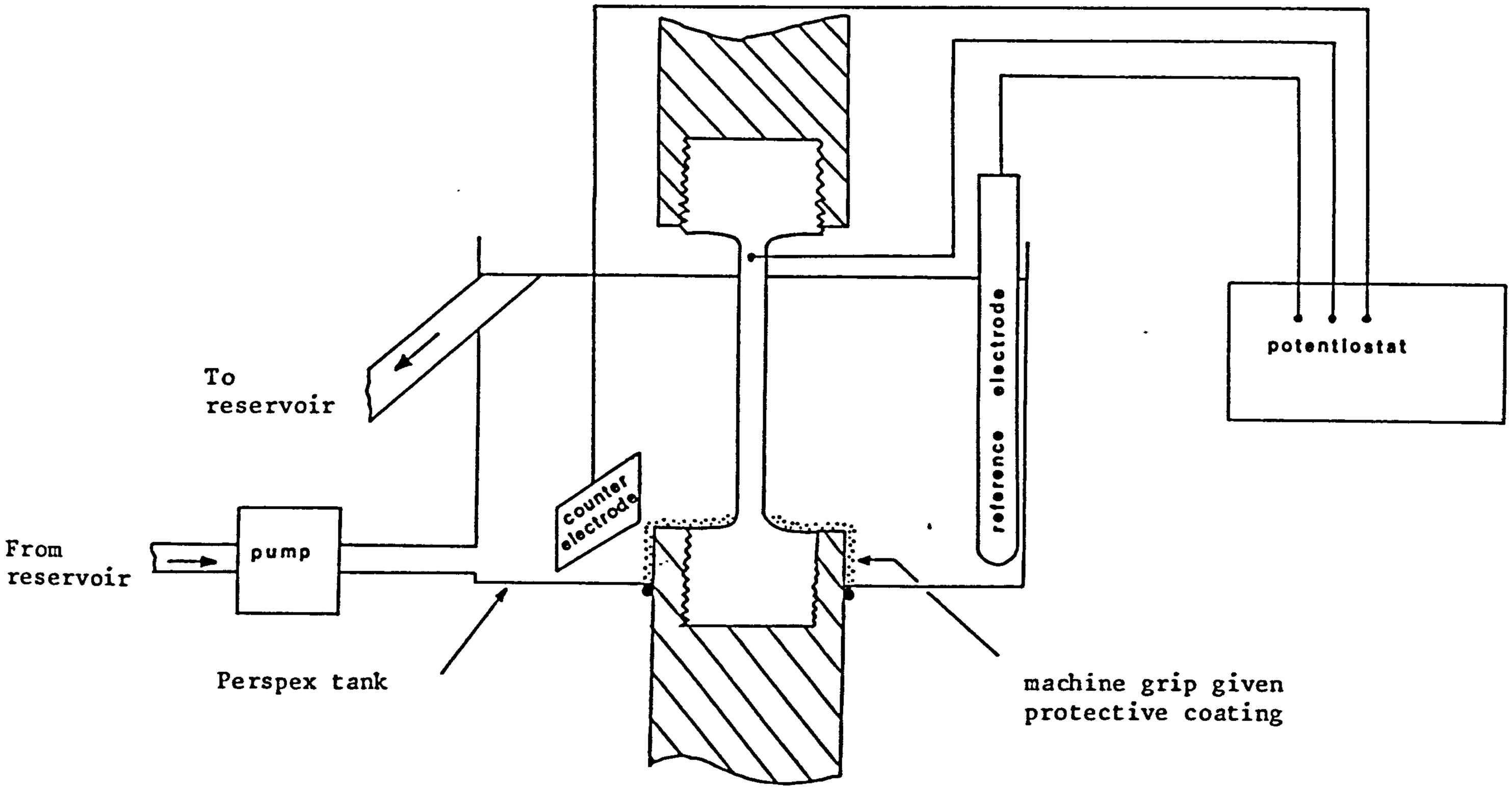

Figure 3.18 Slow strain rate experimental arrangement

4.0 Results.

4.1 Effect of solution additives.

The results of the fatigue crack growth rate experiments utilizing solution additives are shown in figures 4.1 to 4.8.

Figure 4.1 shows the effect of the different solutions on the crack growth rate in free corrosion. The addition of thiourea or arsenate to the solution gives a region of enhanced crack growth where the crack growth rates are significantly greater than those represented by the air upper bound line [190]. In the thiourea solution this occurs for ΔK between 15 and 20MPa$\sqrt{m}$, whilst for the arsenate solution it occurs at $\Delta K>15$MPa$\sqrt{m}$. For $\Delta K>20$MPa$\sqrt{m}$, the results in the thiourea solution lie just above the air upper bound line. The crack growth rate in the chloroplatinic acid solution is generally the same as in the plain NaCl, showing enhanced growth rates relative to the upper bound air data line for $\Delta K>15$MPa$\sqrt{m}$.

Some difficulty was observed in the reproducibility of crack growth rates at free corrosion in the arsenate solution. This is shown in figure 4.2; the crack growth rates are the same for $\Delta K>25$MPa$\sqrt{m}$, but differ below this value of ΔK.

The effects of the solutions at an impressed potential of -1V(sce) are seen in figure 4.3. For values of ΔK between 16 and 32MPa$\sqrt{m}$ both the NaCl and arsenate solutions gave a 'plateau' region, with $da/dN=5.1\times10^{-4}$ mm/cycle for the NaCl and $da/dN=3.1\times10^{-4}$ mm/cycle in the arsenate. This represents a maximum enhancement of crack growth rate relative to air of ≈12 times for the NaCl, and ≈9 times for the arsenate. For $\Delta K>32$MPa$\sqrt{m}$ the crack growth rate in the arsenate solution was the same as in air. A plateau region is also observed in the thiourea solution for $\Delta K>14.8$MPa$\sqrt{m}$ with $da/dN=4\times10^{-4}$ mm/cycle. This is a maximum enhancement of crack growth rate compared with air of ≈13 times. A plateau region is not observed in the chloroplatinic acid solution, and the maximum enhancement of crack growth rate compared with that in air is ≈4.5 times.

At an externally applied potential of +0.25V(sce) the crack growth rates are similar for the chloroplatinic acid, arsenate and NaCl solutions (figure 4.4). However, the thiourea solution gives markedly different results, with a plateau at $da/dN=6.1\times10^{-4}$ mm/cycle observed over a ΔK range of 14.5-22MPa$\sqrt{m}$. At values of $\Delta K>22$MPa$\sqrt{m}$ the crack

growth rate gradually decreases, and for $\Delta K>35MPa\sqrt{m}$ it is the same as in air. The maximum rate of crack growth compared to that in air is ≈20 times for the thiourea solution, and ≈4 times for the other solutions.

The results given in figure 4.5 indicate that for the range of potentials used in this study the specimen polarization has no effect on the crack growth rate in the chloroplatinic acid.

In figure 4.6 the results obtained in the arsenate solution are shown. Plateau regions were observed at free corrosion and -1V(sce), but not at +0.25V(sce). The crack growth rate at which the plateau occurred was $3.1x10^{-4}$ mm/cycle at -1V(sce), but varied over the range $2.6\rightarrow4.0x10^{-4}$ mm/cycle in free corrosion.

In the NaCl a plateau region was found at a potential of -1V(sce), but not in free corrosion or at +0.25V(sce), as seen in figure 4.7.

Figure 4.8 shows the results for the thiourea solution. For ΔK between 16 and 21 $MPa\sqrt{m}$ some variation in the crack growth rates in free corrosion was observed. At -1V(sce) and +0.25V(sce) plateaus were observed. For $\Delta K>22MPa\sqrt{m}$ at +0.25V(sce) the crack growth rate decreased from the plateau rate, becoming the same as in air at $\Delta K>35MPa\sqrt{m}$.

Figures 4.9 to 4.14 show that the solutions used could markedly alter the shape of the crack front. In air or in the chloroplatinic solution the crack front was always found to be convex. The thiourea solution and the arsenate solution could cause the crack front to become a concave shape. This did not always happen as shown by figures 4.11 to 4.14.

4.2. Slow strain rate tests.

The results of the slow strain rate testing are shown in figure 4.15. The results for the arsenate and NaCl solutions are similar over the range of potentials studied. Betwen the free corrosion potential and ≈-1V(sce) the results in the chloroplatinic acid solution are also similar to those in NaCl. However, at potentials more negative than -1V(sce) the reduction in area is ≈72% for the chloroplatinic acid solution compared to ≈55% for the NaCl and arsenate solutions. In air the reduction in area was found to be ≈78%. At potentials more positive than -0.9V(sce) the results from the thiourea solution were the same as for in air. However at potentials more

negative than this the thiourea soultion severely embrittled the specimen. The most severe case of embrittlement seen in the thiourea solution was at -1.9V(sce) when the reduction of area was found to be only ≈23%.

As the potential was decreased from the free corrosion potential the fracture surface changed from a "cup and cone" appearance typical of ductile fracture to a slanted fracture at 45° to the specimen axis. Extensive cracking in the neck of the specimen was associated with the slanted fracture. The amount of cracking and slanted fracture were reduced in the chloroplatinic acid solution, compared to the other solutions. These effects can be seen in figures 4.16 to 4.19.

4.3. Environmental/loading effects on fatigue crack propagation.

Further fatigue crack propagation studies were undertaken in order to investigate the effects of several environmental and loading parameters. Figure 4.20 gives a comparison between the upper bound air lines obtained by several workers, and the scatterband for results obtained at Glasgow University [190] is also shown.

The effect of frequency, for both free corrosion and -1V(sce), is shown in figures 4.21 and 4.22. For free corrosion the results lay along a common line above the air upper bound line. Above a critical rate of crack growth each curve deviated from the common line towards the air upper bound. For $\Delta K > 20 MPa\sqrt{m}$ the 5Hz free corrosion results lay along the lower bound to the air data scatterband. For a potential of -1V(sce) the results included a plateau region, which occurred at increased values of da/dN as the frequency decreased. For higher values of ΔK than those over which the plateau occurred the results lay just below the air data upper bound line.

A frequency of 1Hz was used in the investigation of the effects of specimen polarization. The results given in figure 4.23 show that the rate of crack growth at which a plateau occurred increased as the specimen polarization was made more negative. No plateau was observed at -0.8V(sce), and the results for -0.7V(sce) were similar to (but slightly below) those for free corrosion.

Figures 4.24 and 4.25 show that the value of R had almost no effect upon the observed crack growth rates. At low values of ΔK some of the results are experimental artefacts as discussed in section 4.5.

In figure 4.26, the results for different waveforms at the free

corrosion potential are presented. Triangular and sinusoidal waveforms gave identical results. A square waveform gave results that showed no environmental enhancement of crack growth rate. Indeed, the results for a square waveform lay along a straight line, the slope of which was less than that for the air data. Consequently for $\Delta K > 36 MPa\sqrt{m}$ the square waveform results lay below the air lower bound line.

The effects of waveform at a potential of -1V(sce) are shown in figure 4.27. The results for a triangular waveform were slightly below those for a sinusoidal waveform. However, an environmental enhancement of crack growth was also observed with a square waveform. The plateau crack growth rates were 5.1×10^{-4} mm/cycle for the sinusoidal waveform, 4.3×10^{-4} mm/cycle for the triangular waveform and 2.45×10^{-4} mm/cycle for the square waveform. For $\Delta K > 39 MPa\sqrt{m}$ the square waveform results followed the air data lower bound line.

Figure 4.28 shows the effect of potential on crack growth with a square waveform. The results at -0.85V(sce) lay slightly below those obtained in free corrosion. Neither of these potentials gave results that showed any environmental enhancement of crack growth rate which compares markedly with the results for -1V(sce).

Figure 4.29 compares the limited results obtained in free corrosion using 3% NaCl solution acidified to pH=5, with those in plain 3% NaCl (pH=6.5). No differences in crack growth rates were observed.

The concentration of NaCl did not significantly affect the crack growth rates observed in free corrosion, figure 4.30.

The results for different concentrations of NaCl at -1V(sce) are displayed in figure 4.31. The plateau crack growth rates are the same for 1% and 2% NaCl solutions, at $\approx 3.5 \times 10^{-4}$ mm/cycle. The plateau rate in the 5% NaCl solution was approximately the same as for the 3% NaCl solution.

For free corrosion the results at different temperatures and lower values of ΔK lay along a common line as seen in figure 4.32. At higher values of ΔK the crack growth rate tended towards that found in air. The crack growth rate at which this deviation began increased as the temperature increased.

Figure 4.33 shows that the plateau crack growth rate at -1V(sce) increased as the temperature increased. At crack growth rates greater than the plateau rate the crack growth behaviour was the same as in air.

4.4 Fractography.

Figures 4.34 to 4.36 display some of the fractographic evidence obtained from specimens that were fatigued in air. Ductile striations and much secondary cracking are clearly evident in these pictures.

The appearance of the fracture surfaces obtained in ASTM artificial seawater under free corrosion was somewhat different, as shown in figures 4.37 and 4.38. Some secondary cracking can be seen, but the surfaces have a pronounced brittle appearance. In figure 4.37 some corrosion products are evident, particularly in the lower left hand side of the photograph, but the fact that most of the surface shows no sign of corrosion products vindicates the fracographic experimental technique used (cf. section 3.1.6).

In order to examine the fracture surfaces the fatigue specimens were cooled in liquid nitrogen and broken open. Figure 4.39 shows an area of surface created by this process. Typical transgranular cleavage is seen.

Figure 4.40 shows what is believed to be a cleavage facet found on the surface of a specimen fatigued in arsenate at -1V(sce). Parallel V-shaped markings are seen on the surface of the facet. Figure 4.41 shows that these features occurred frequently upon the specimen surface, although small patches of quasi-cleavage and possible striations were also observed. No detailed investigation was made into the variation in the relative proportion of different fracture modes with ΔK. Transgranular cleavage was also seen at -1V(sce) in the arsenate solution, as shown in figure 4.42. Figure 4.43 gives another example of brittle features observed under these conditions.

An example of the results obtained from a specimen fatigued in ASTM artificial seawater at -0.85V(sce) is shown in figure 4.44. Whilst a small area of possible striations and the odd transgranular cleavage facet can be seen the majority of the surface appears to show a quasi-cleavage form of failure. An area of striations formed under these conditions is shown in figure 4.45.

Figures 4.46 and 4.47 show that the slow strain rate specimen strained in an air environment failed by the expected mechanism of void growth and coalescence. Figure 4.48 is included to indicate to which parts of the specimen surface the suceeding figures refer. The middle part of the surface obtained in NaCl at -1.2V(sce) showed a similar failure mechanism to that in air, this is shown by figures 4.49 and 4.50. However the environment altered the appearance of the fracture

surface near the edges of the specimen, as seen from figures 4.51 to 4.54. The surface has a pronounced "flaky" appearance, and the failure mode is probably a mixture of shear and of quasi-cleavage. In figure 4.54 some void coalescence can be seen.

4.5 Miscellaneous.

Experimental artefacts.

When corrosion fatigue testing is performed using a constant amplitude load, as in this study, the initial results may be experimental artefacts. This is because the crack growth rate accelerates to its true value during an initial period of growth. The effect is well illustrated by figure 4.55, which shows results from this study. Similar effects have been observed in other studies [139,191].

Incubation time.

Some tests, particulary those at potentials more negative than -0.85V(sce), showed an appreciable incubation time before crack growth began. Once crack growth had started the crack growth rate quickly reached its true value. Figure 4.56 shows an example of this effect. At free corrosion an incubation time was not observed, as illustrated by figure 4.57.

Environment.

The free corrosion potential was not measured for all of the experiments performed under this condition. For the experiments where it was measured the observed value in 3% NaCl was in the range -0.68V to -0.7V(sce). Likewise the solution pH was only measured during one test at free corrosion in 3% NaCl, for which the pH was found to remain within the range 6.8 to 7.1.

In the 3% NaCl solution a current of ≈5.5mA was required to maintain the specimen polarization at -1V(sce). An anodic current of between 98 to 120mA was necessary to keep the specimen polarized to +0.25V(sce).

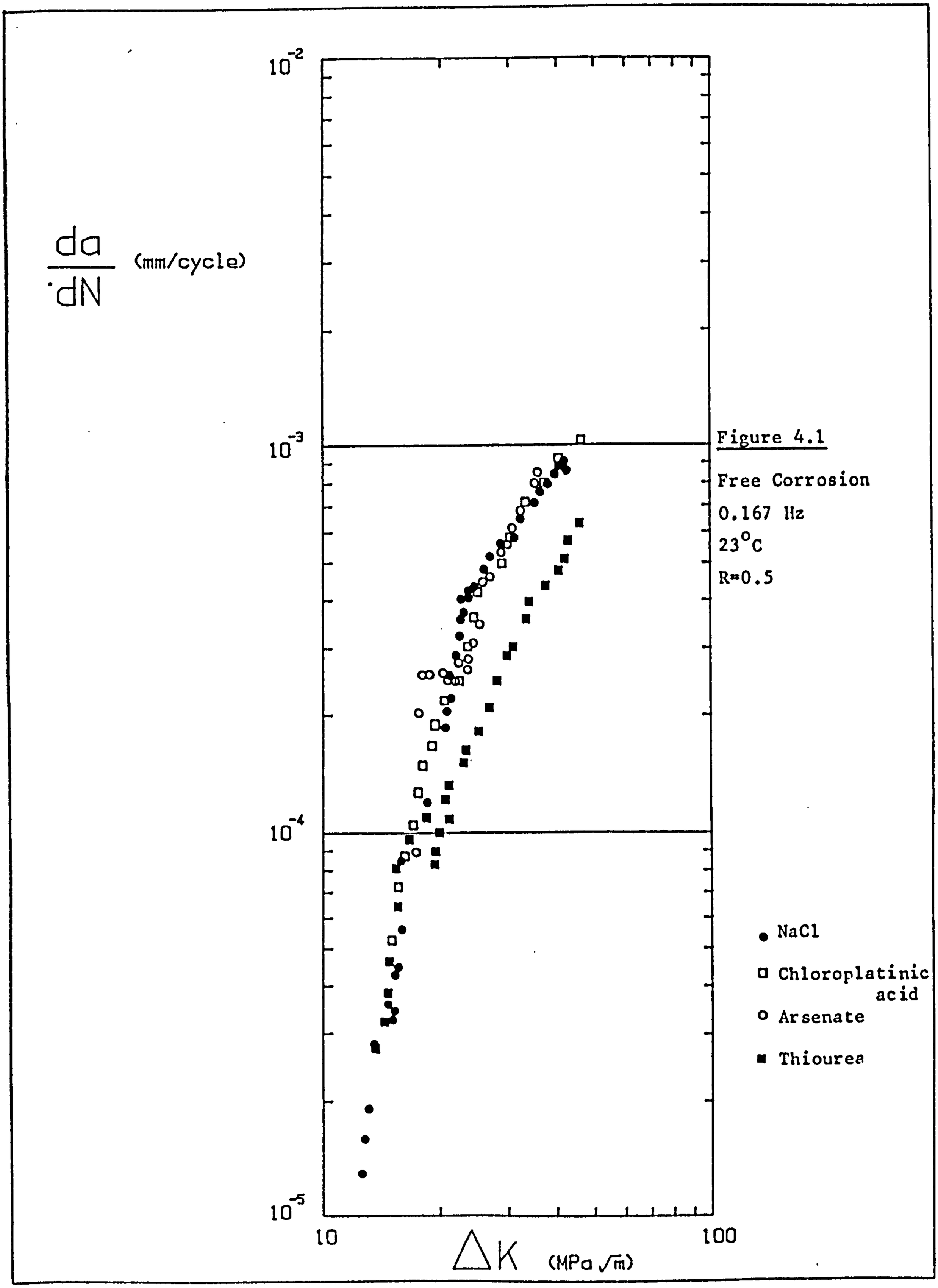
10^{-2}
10^{-3}
10^{-4}
10^{-5}
$\frac{da}{dN}$ (mm/cycle)
10
100
ΔK (MPa $\sqrt{m}$)
Free Corrosion
0.167 Hz
23°C
R=0.5
NaCl
Chloroplatinic acid
Arsenate
Thiourea

Figure 4.1

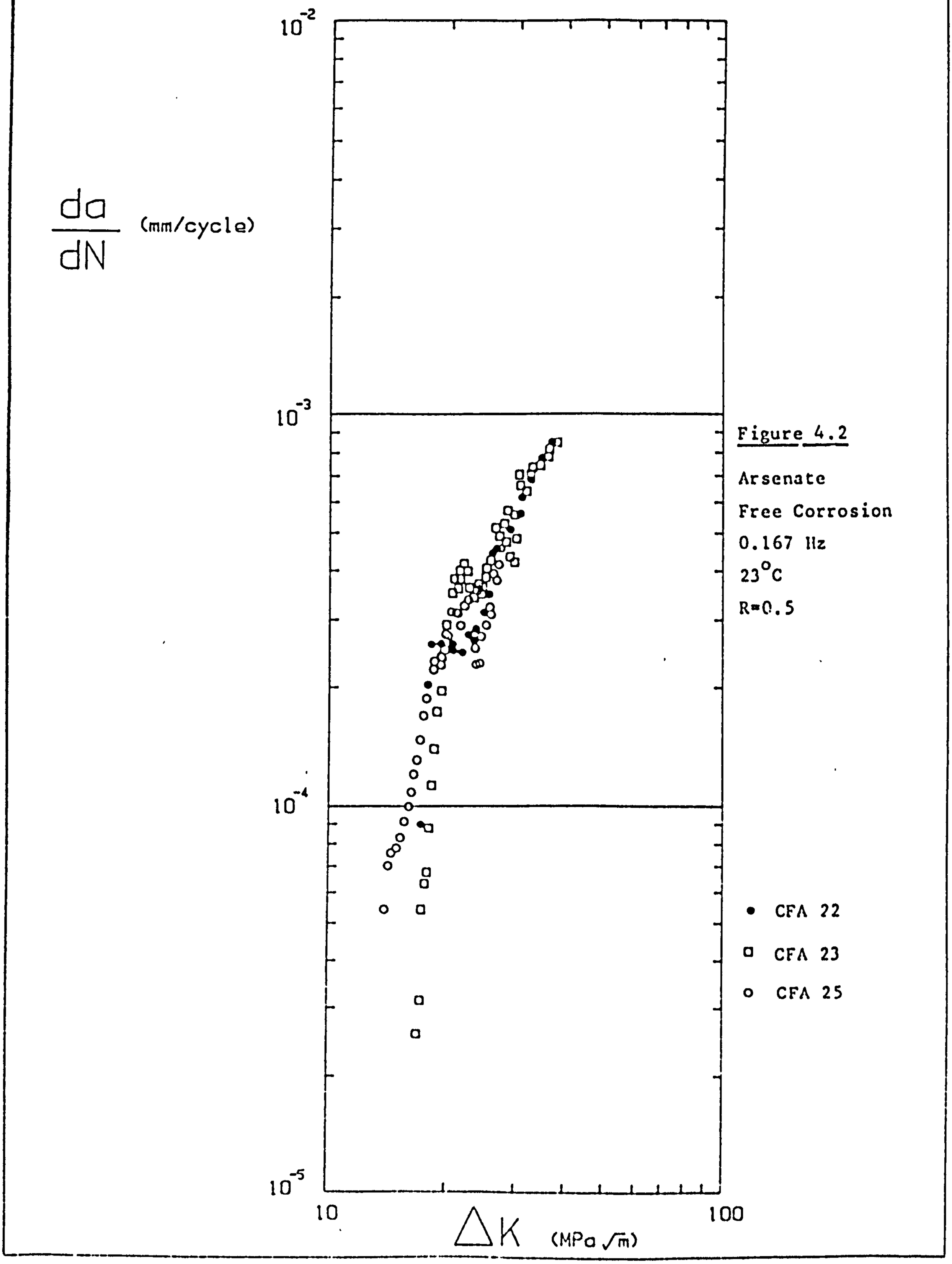

Figure 4.2

Arsenate

Free Corrosion

0.167 Hz

23°C

R=0.5

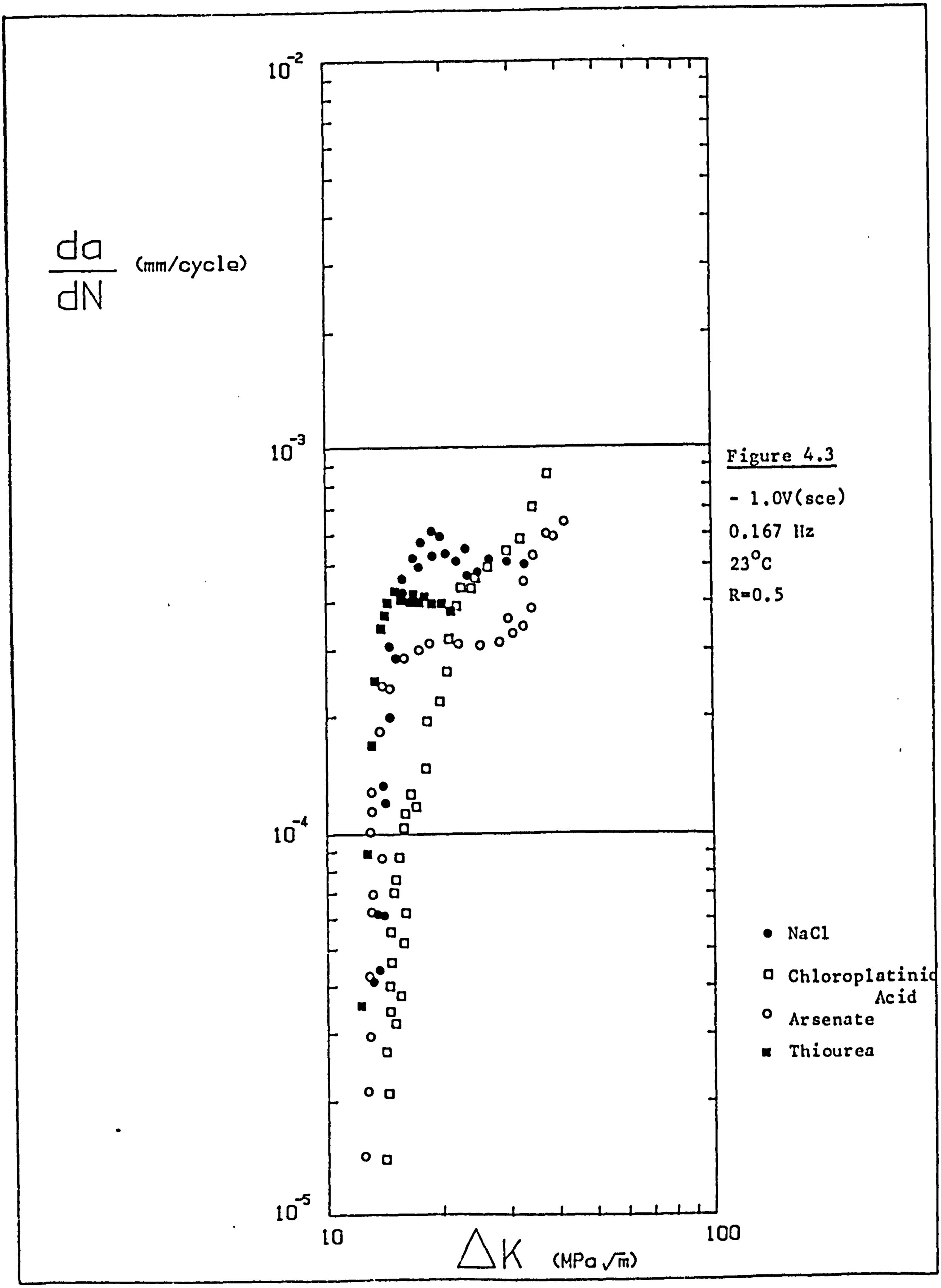
10^{-2}
10^{-3}
10^{-4}
10^{-5}
$\frac{da}{dN}$ (mm/cycle)
10
100
ΔK (MPa $\sqrt{m}$)
- 1.0V(sce)
0.167 Hz
23°C
R=0.5
NaCl
Chloroplatinic Acid
Arsenate
Thiourea

Figure 4.3

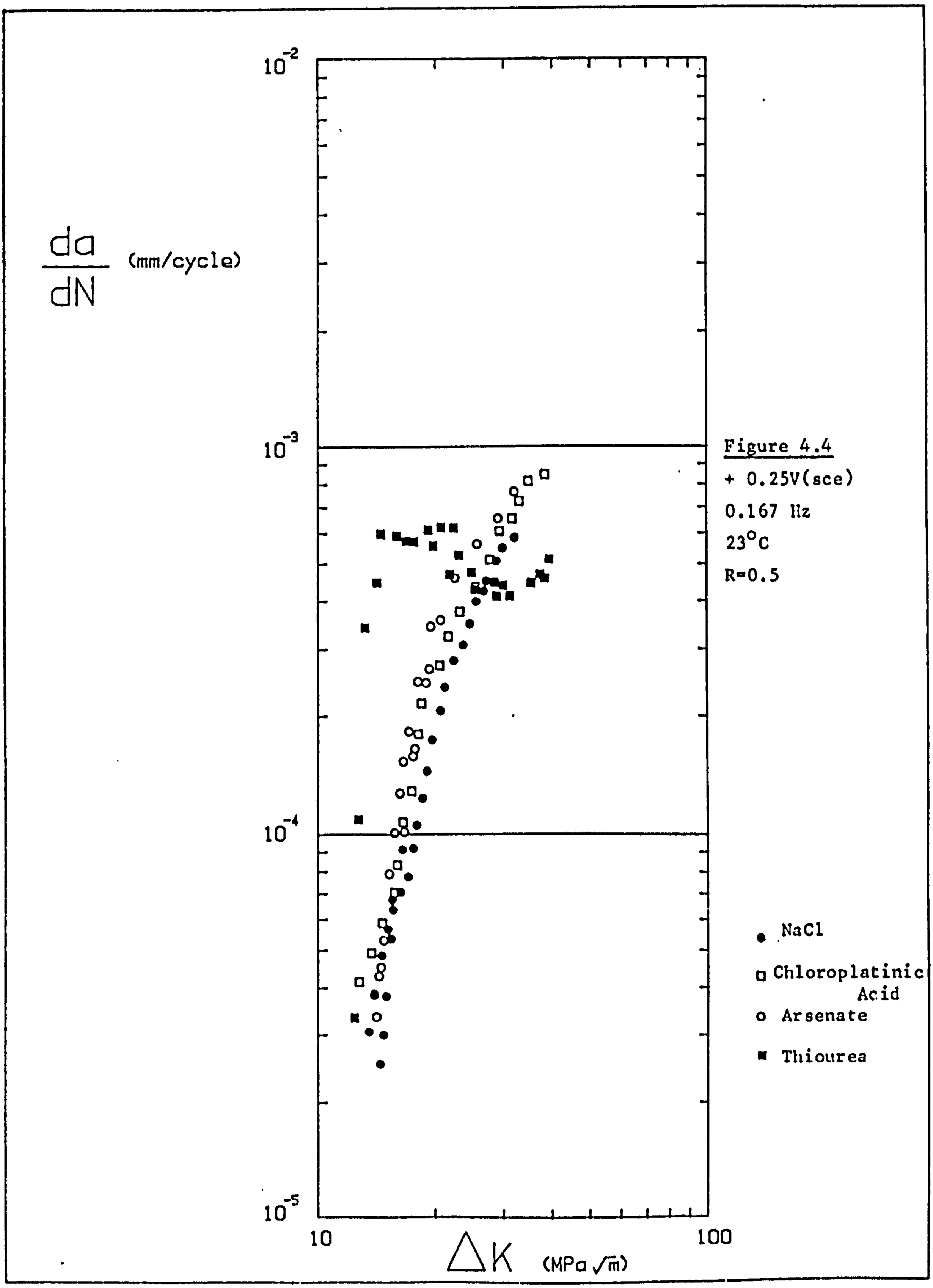
10^{-2}
10^{-3}
10^{-4}
10^{-5}
$\frac{da}{dN}$ (mm/cycle)
10
100
ΔK (MPa $\sqrt{m}$)
+ 0.25V(sce)
0.167 Hz
23°C
R=0.5
NaCl
Chloroplatinic Acid
Arsenate
Thiourea

Figure 4.4

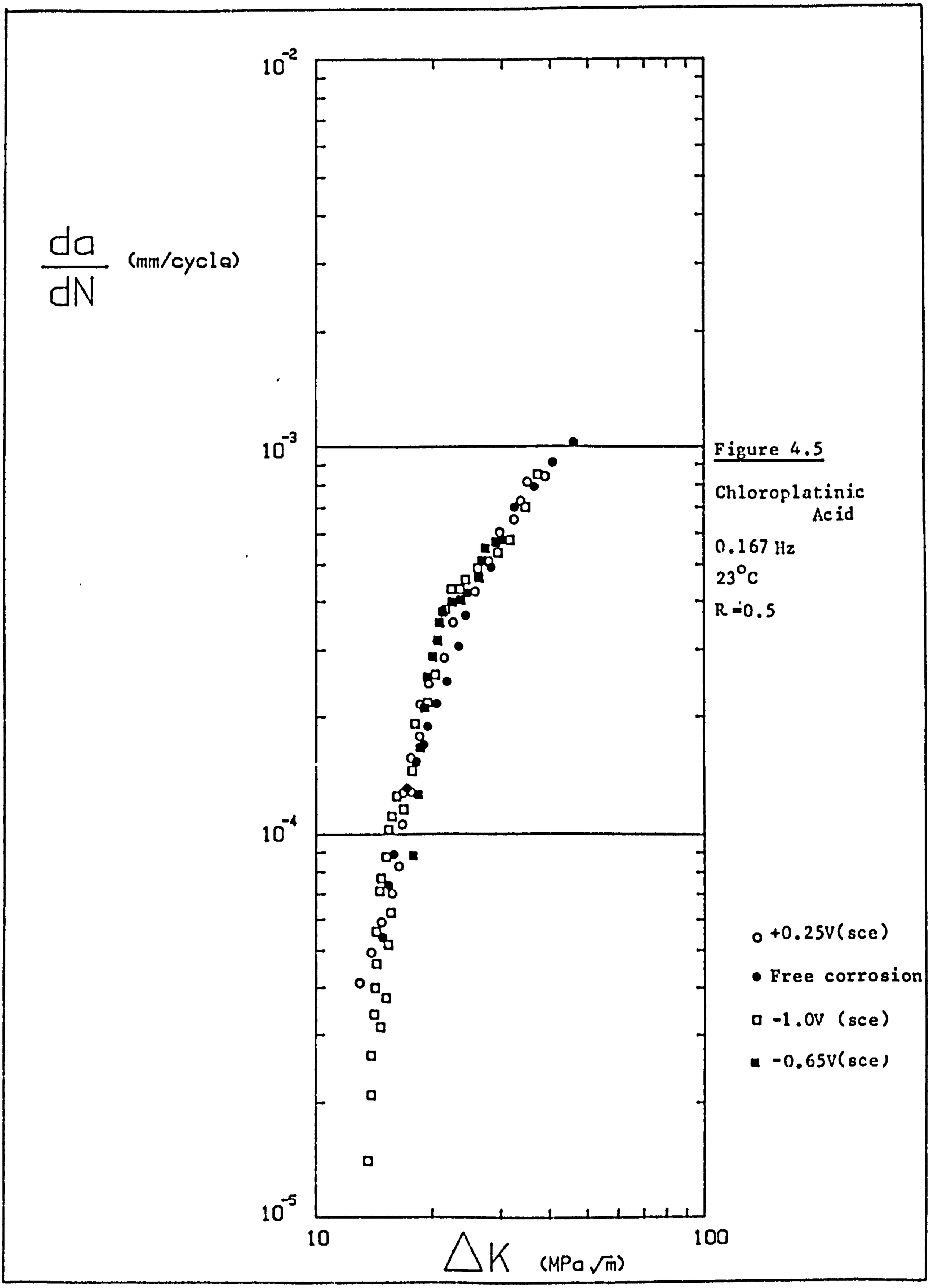

Figure 4.5

Chloroplatinic Acid

0.167 Hz

23°C

R=0.5

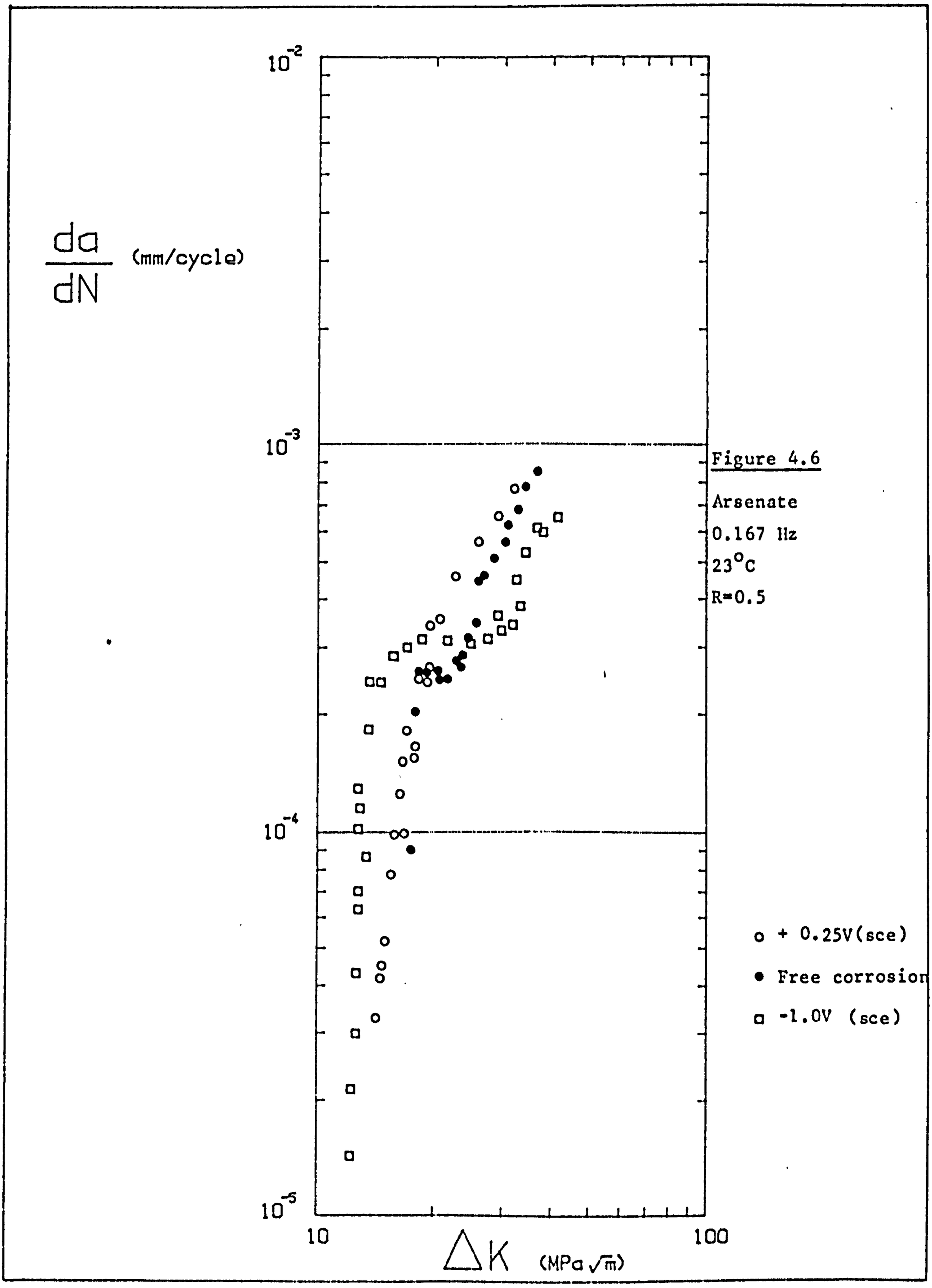
10^{-2}
10^{-3}
10^{-4}
10^{-5}
$\frac{da}{dN}$ (mm/cycle)
10
100
ΔK (MPa $\sqrt{m}$)
o + 0.25V(sce)
● Free corrosion
□ -1.0V (sce)
Arsenate
0.167 Hz
23°C
R=0.5

Figure 4.6

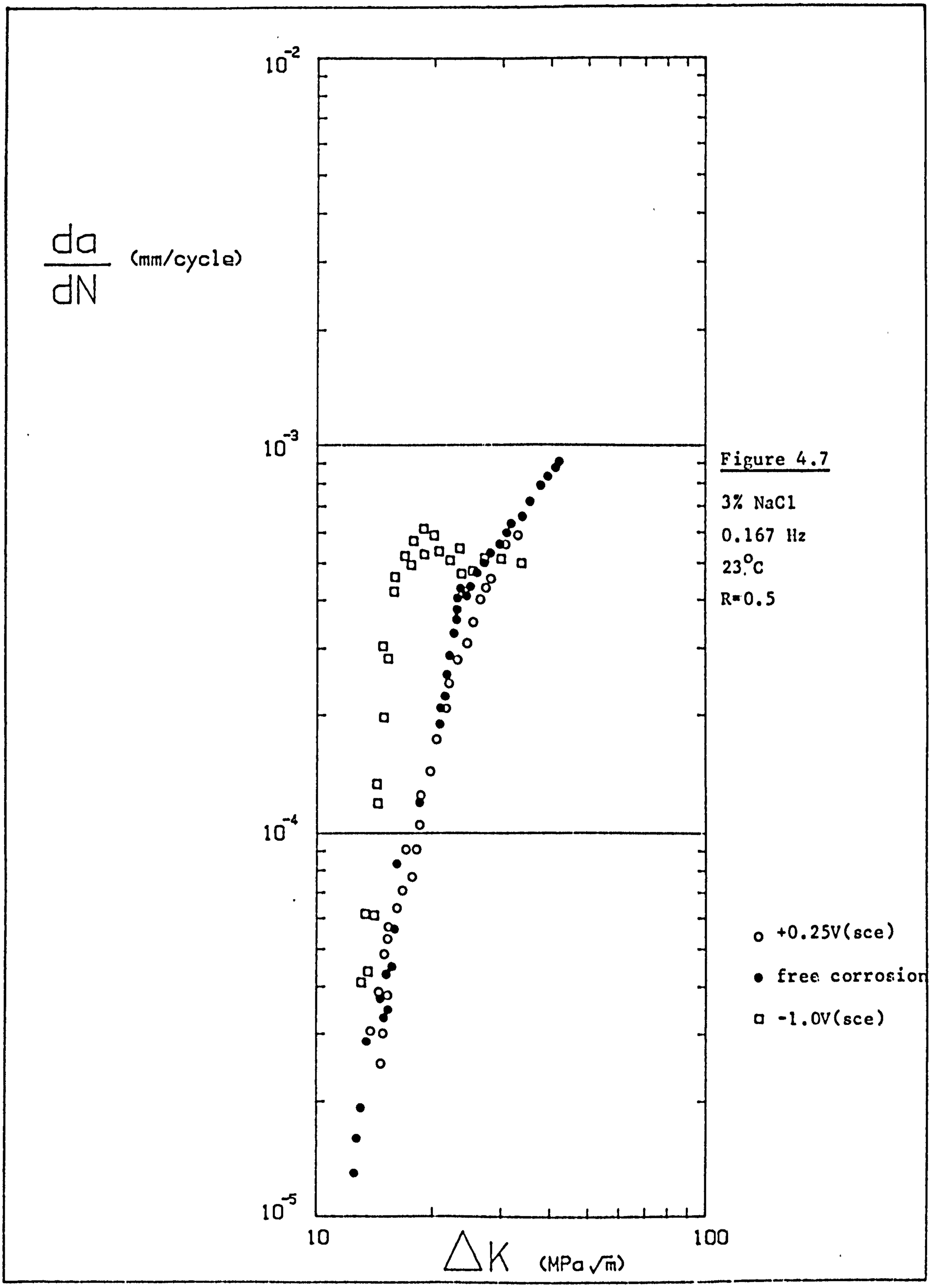

Figure 4.7

3% NaCl

0.167 Hz

23°C

R=0.5

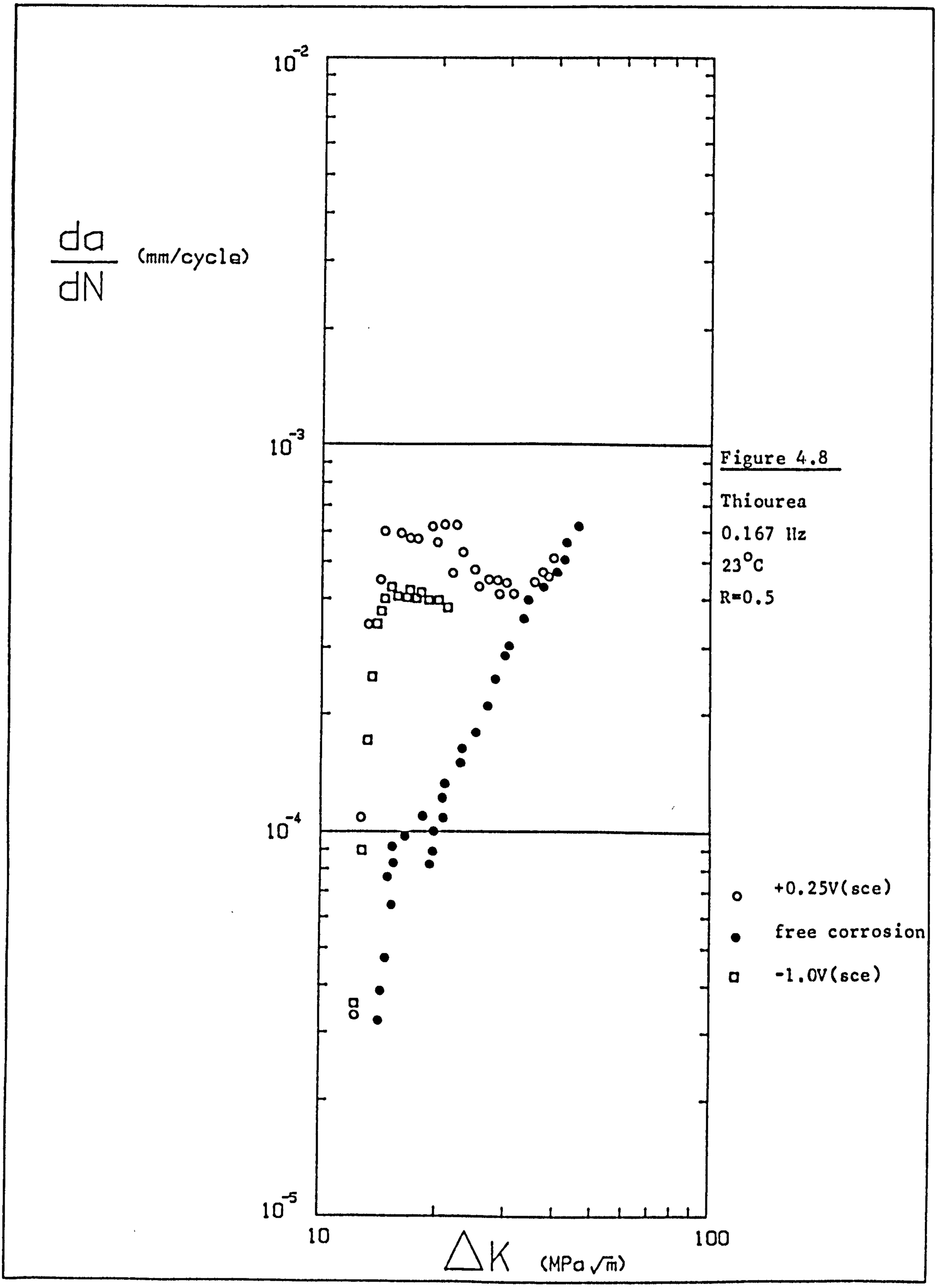
10^{-2}
10^{-3}
10^{-4}
10^{-5}
$\frac{da}{dN}$ (mm/cycle)
10
100
ΔK (MPa $\sqrt{m}$)
Thiourea
0.167 Hz
23°C
R=0.5
+0.25V(sce)
free corrosion
-1.0V(sce)

Figure 4.8

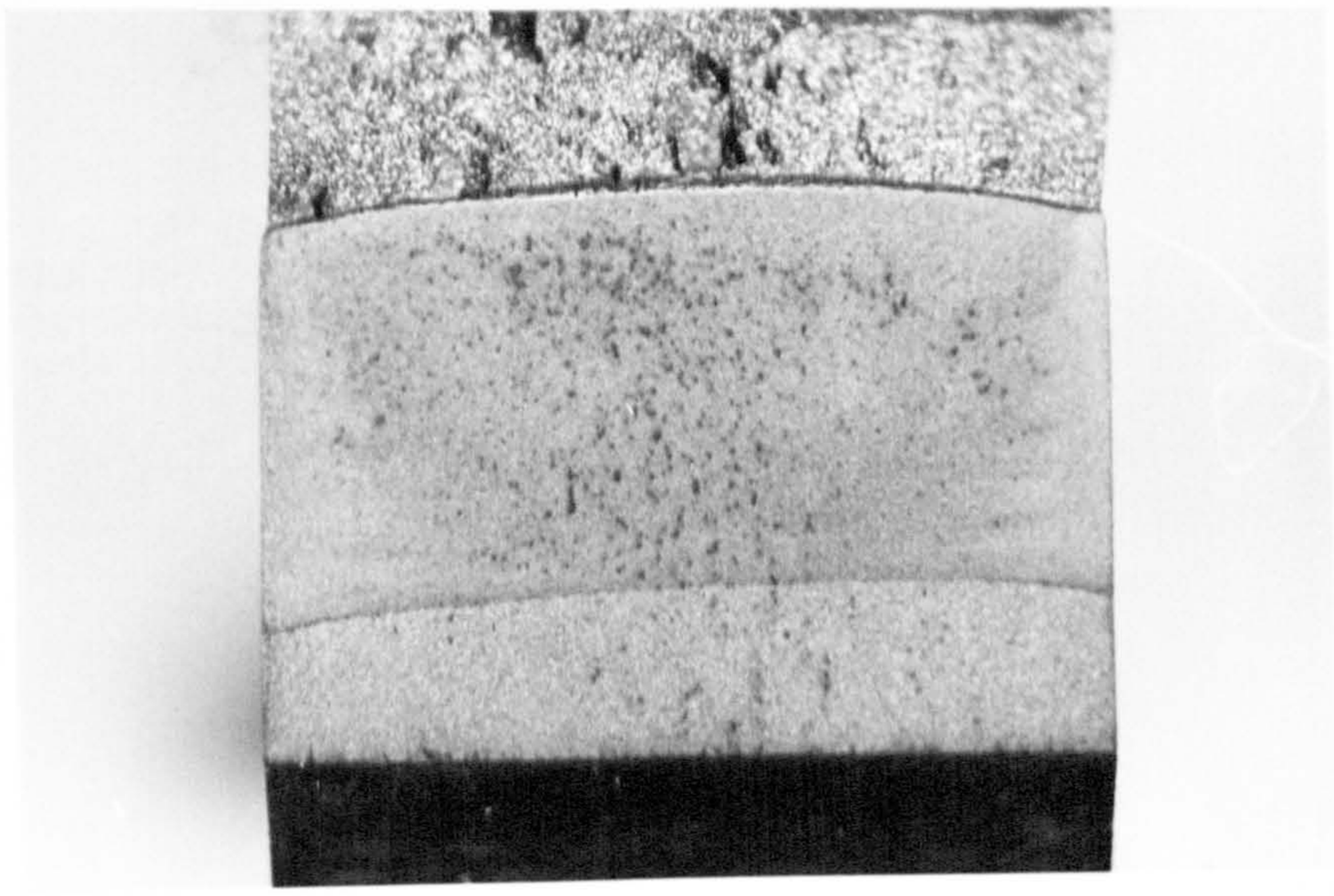

Figure 4.9 Air test 1
Photograph showing shape
of crack front.

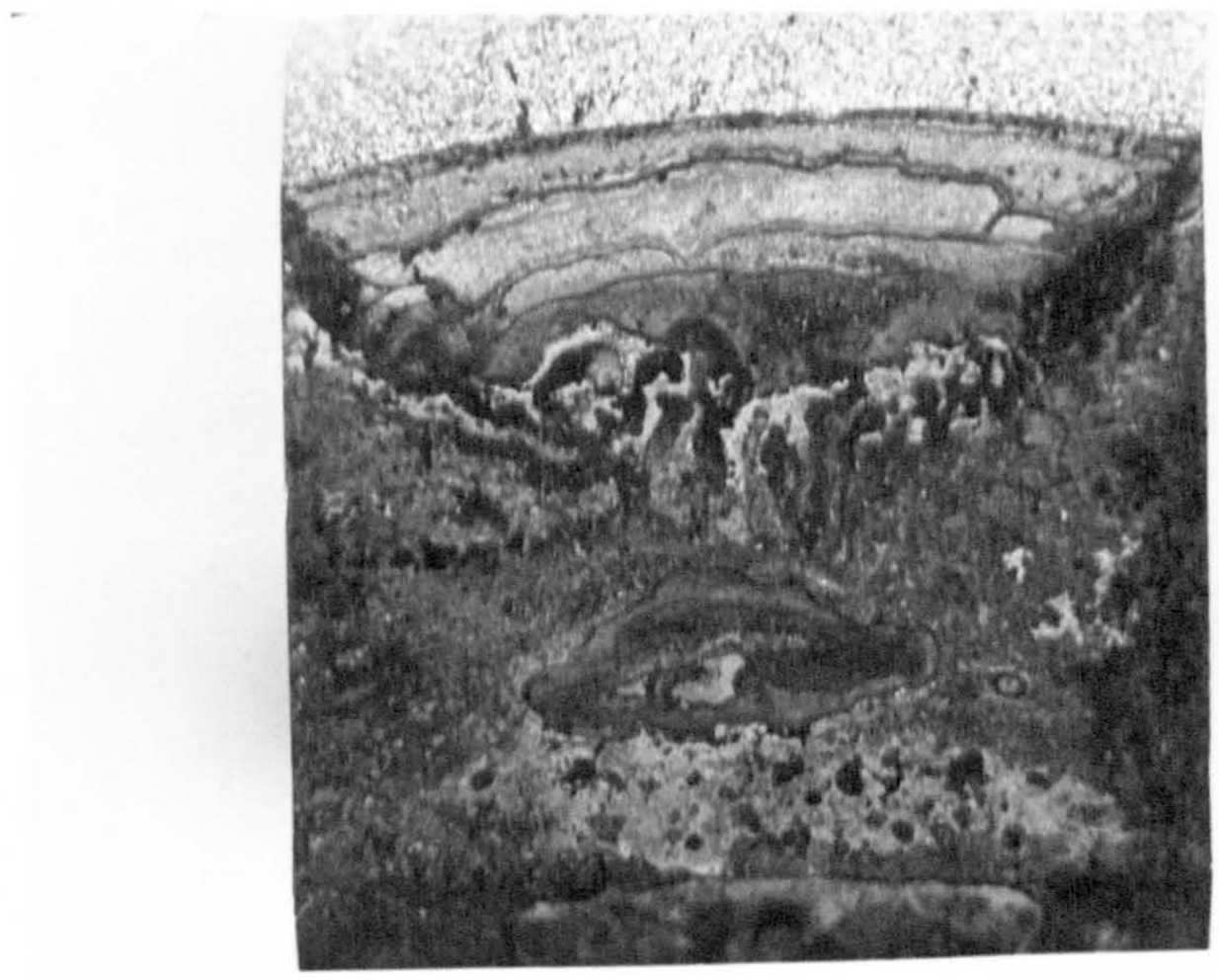

Figure 4.10 CFP 4
Chloroplatinic Acid, -1V (sce)
Photograph showing shape of
crack front.

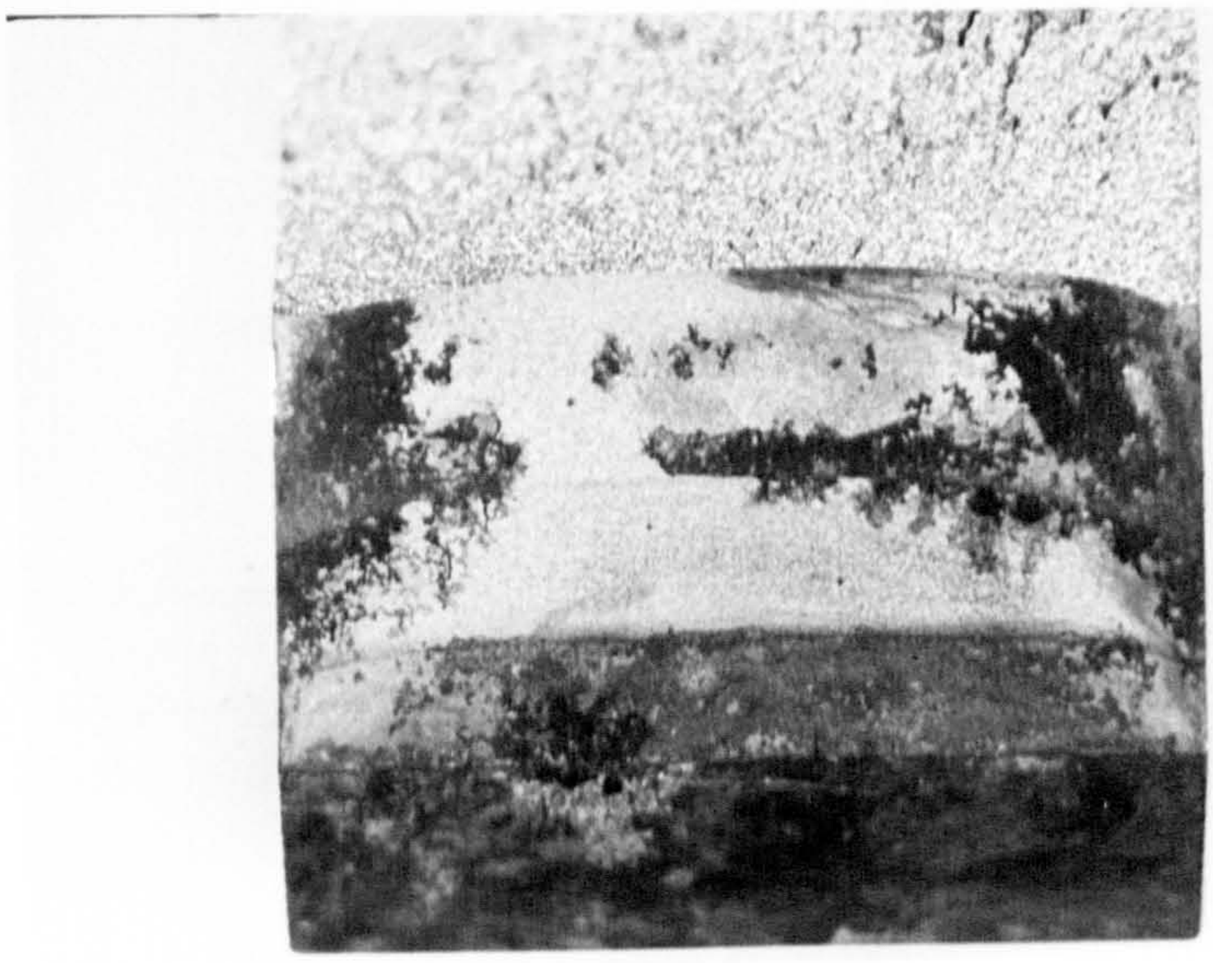

Figure 4.11 CFA 6
Arsenate, -1V (sce)
Photograph showing shape
of crack front.

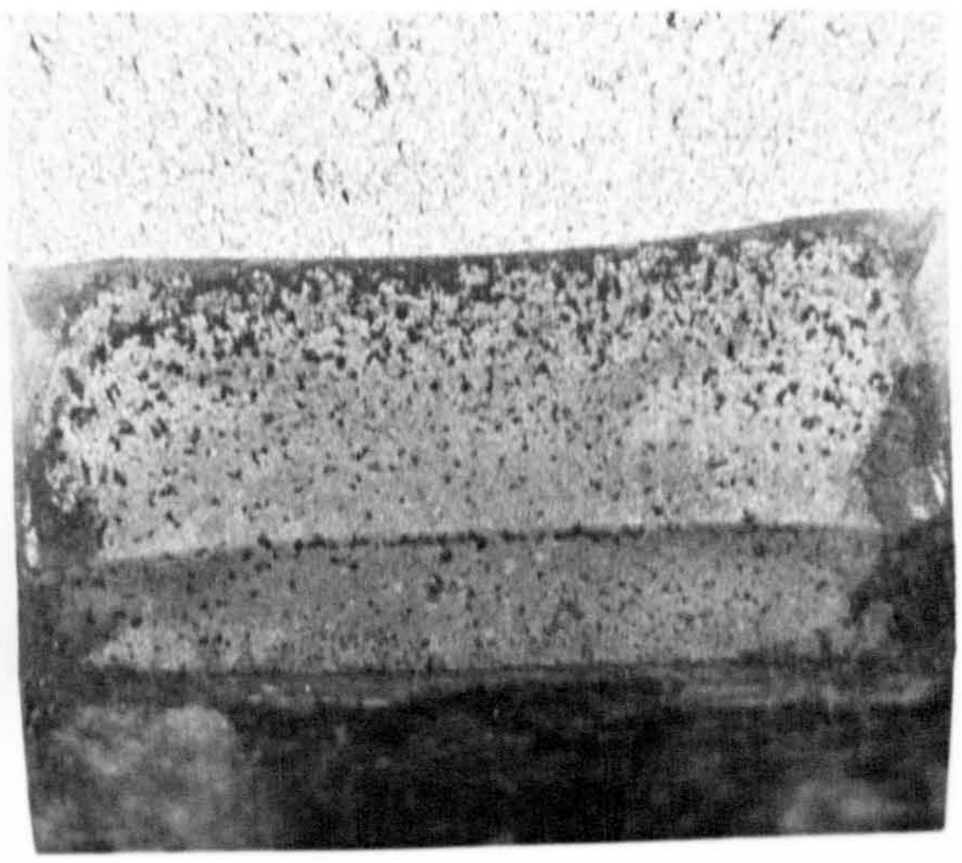

Figure 4.12 CFA 13
Arsenate, -1V (sce)
Photograph showing shape
of crack front.

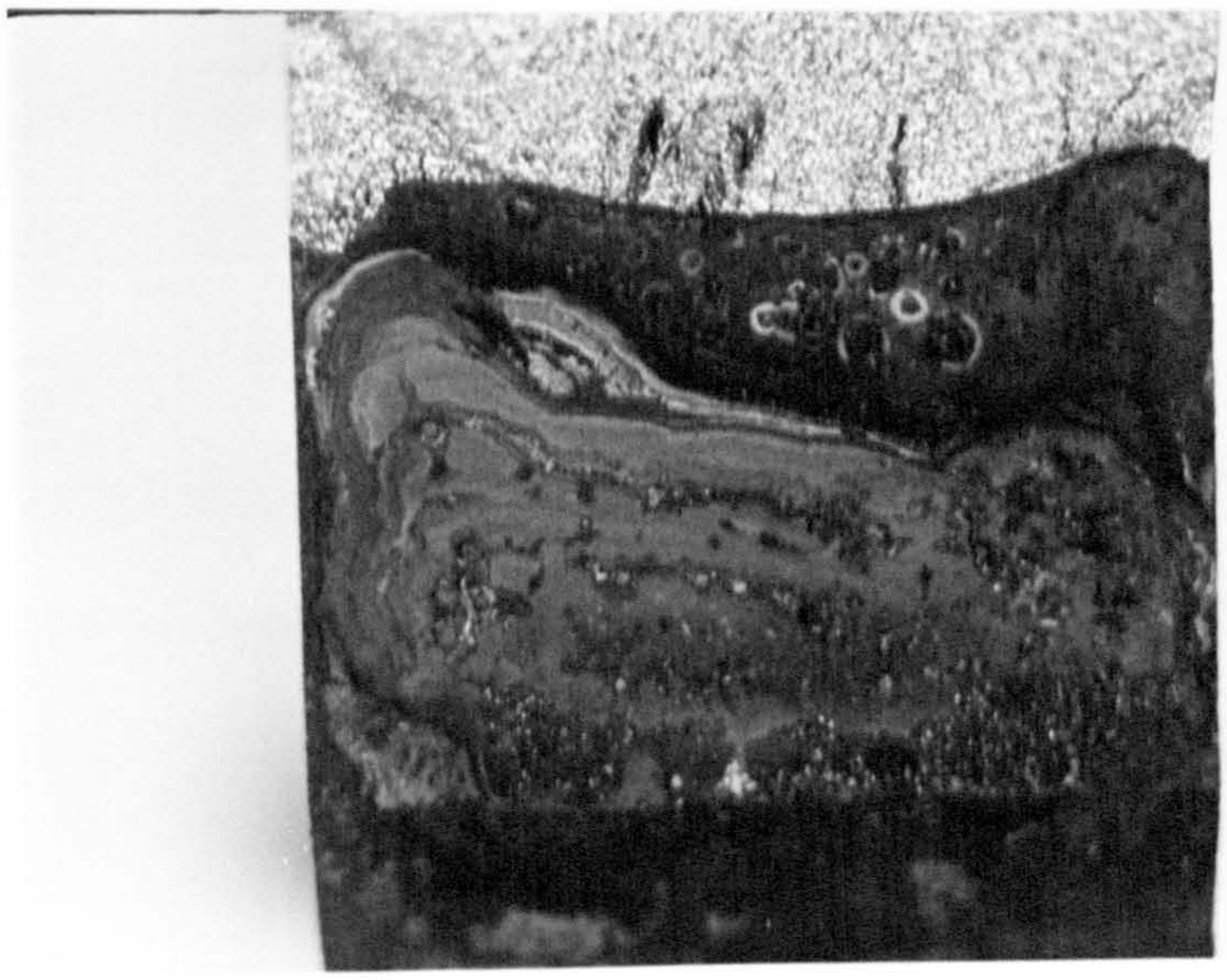

Figure 4.13 CFT 7
Thiourea, +0.25V (sce)
Photograph showing shape of crack front.

Figure 4.14 CFT 4
Thiourea, +0.25V (sce)
Photograph showing shape of crack front.

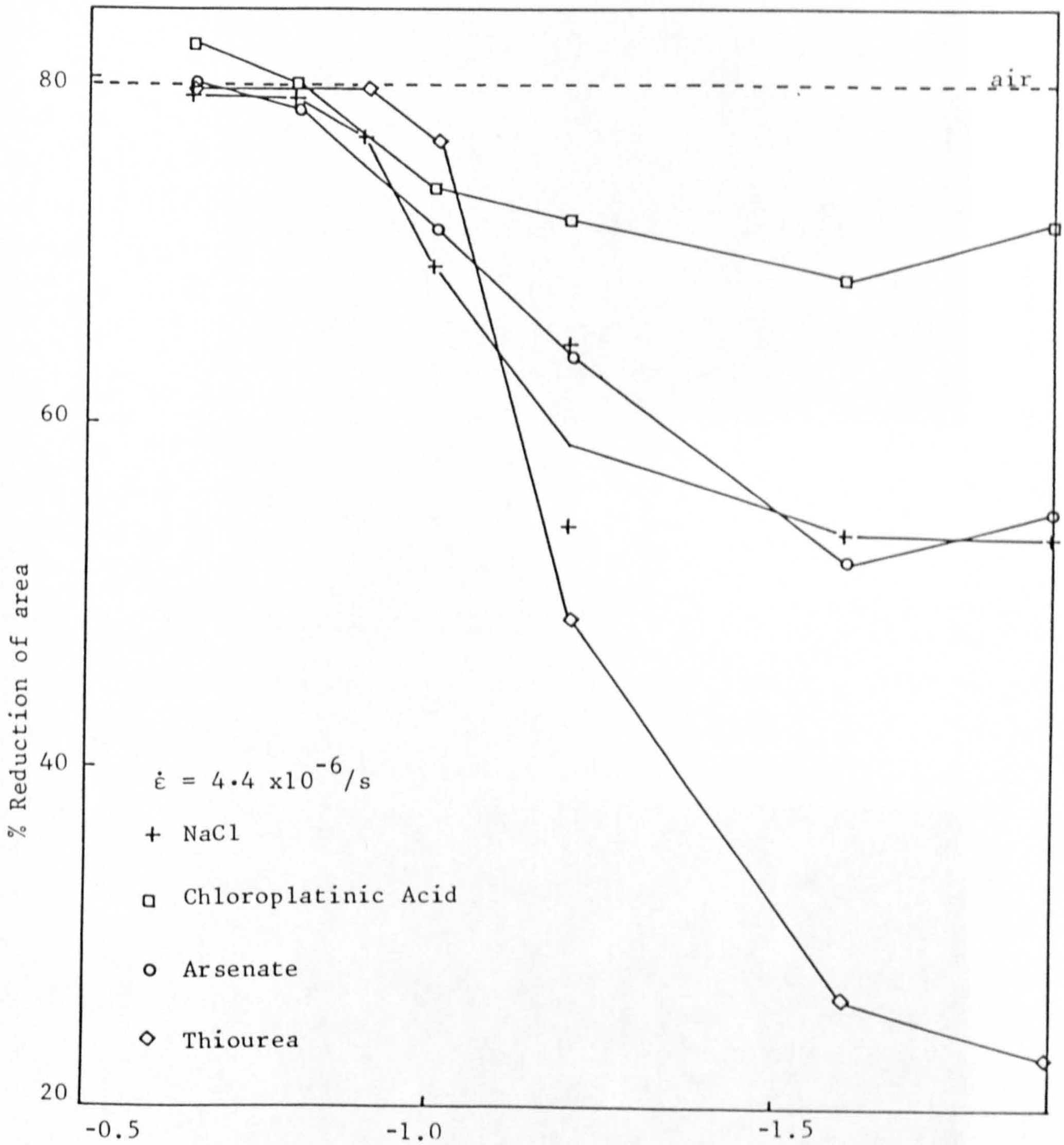

Figure 4.15 Slow strain rate results

(a) Side view

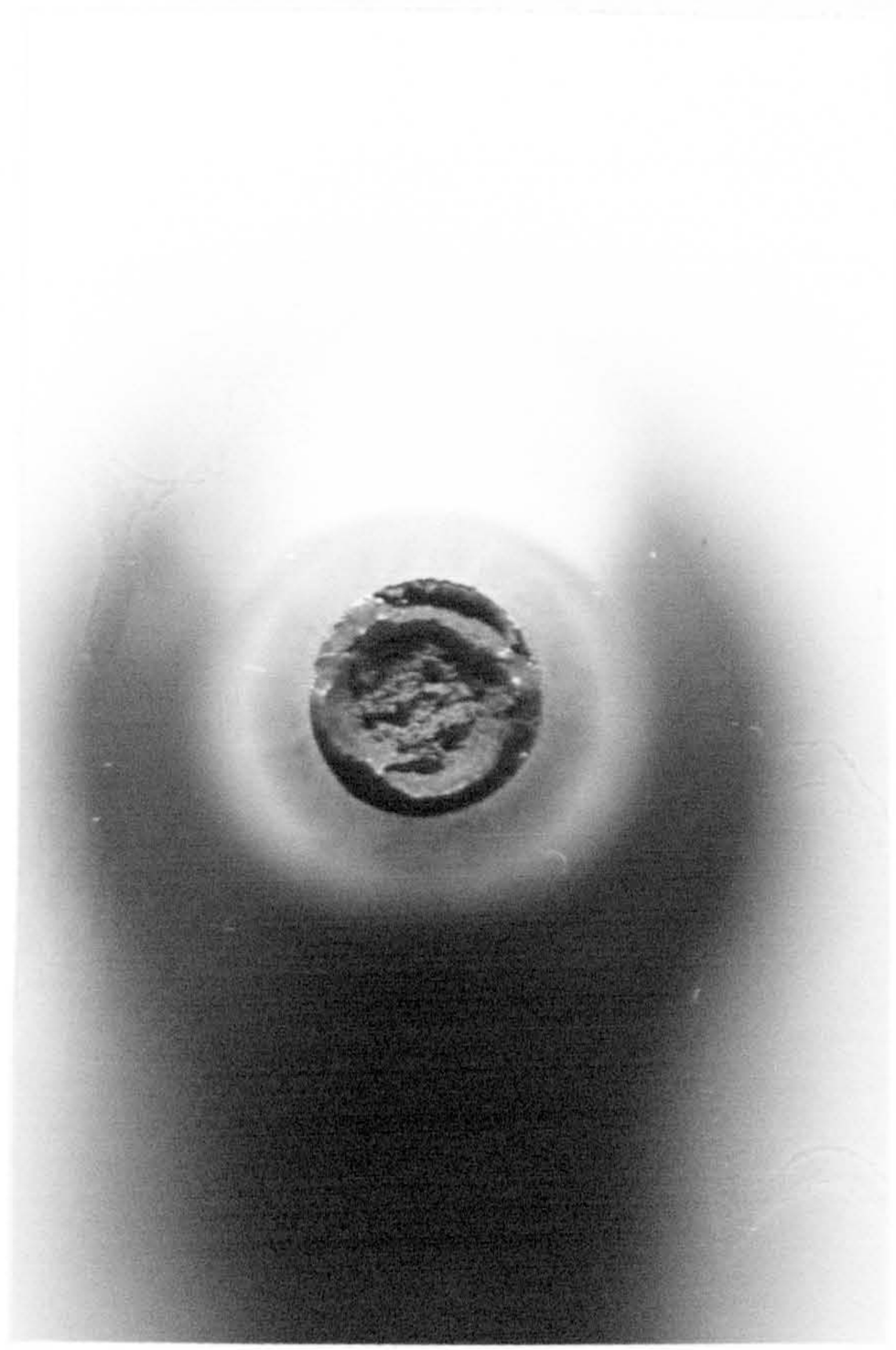

(b) Top view

Figure 4.16 Photographs of slow strain rate specimen tested in air

(a) Side view

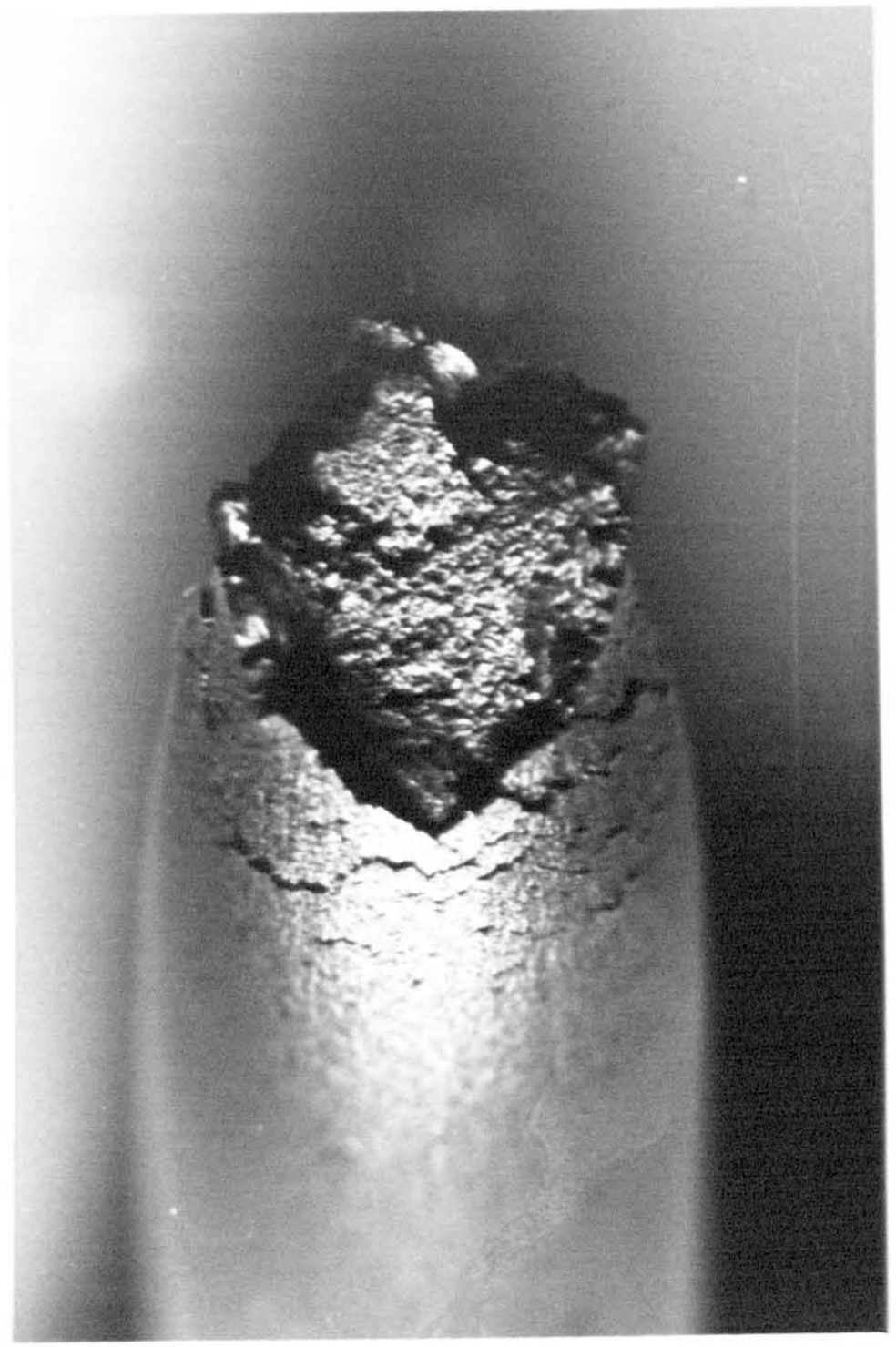

(b) View of failure surface

Figure 4.17 Photographs of slow strain rate specimen tested in arsenate at -1.2V (sce)

(a) Side view

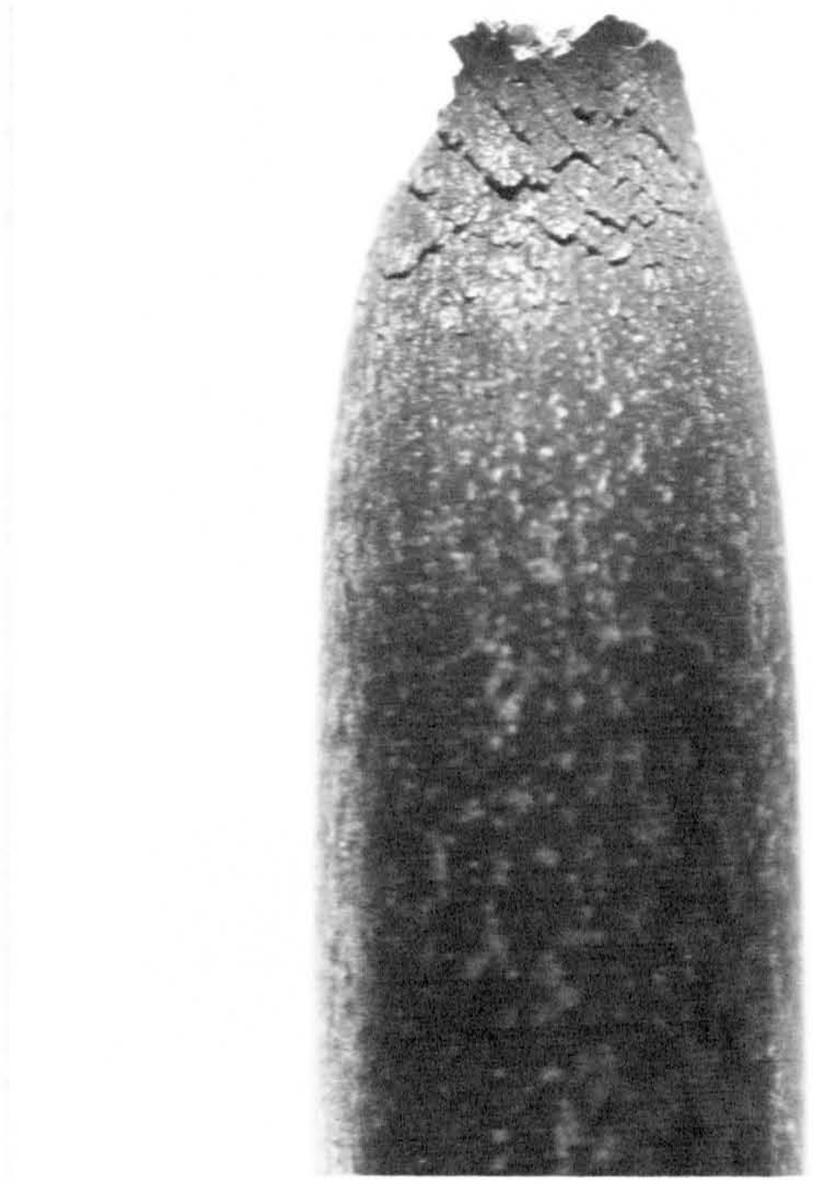

(b) Side view

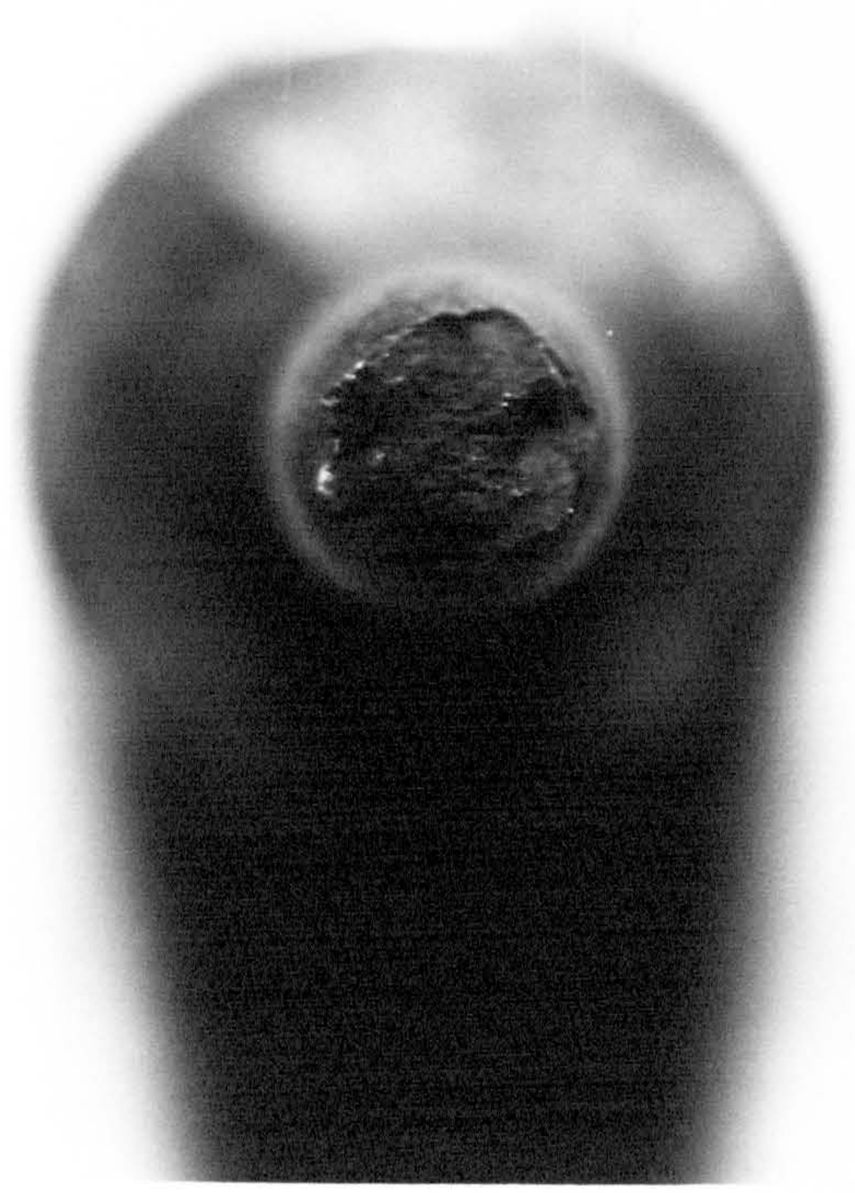

(c) Top view

Figure 4.18 Photographs of slow strain rate specimen tested in chloroplatinic acid at -1.9V (sce)

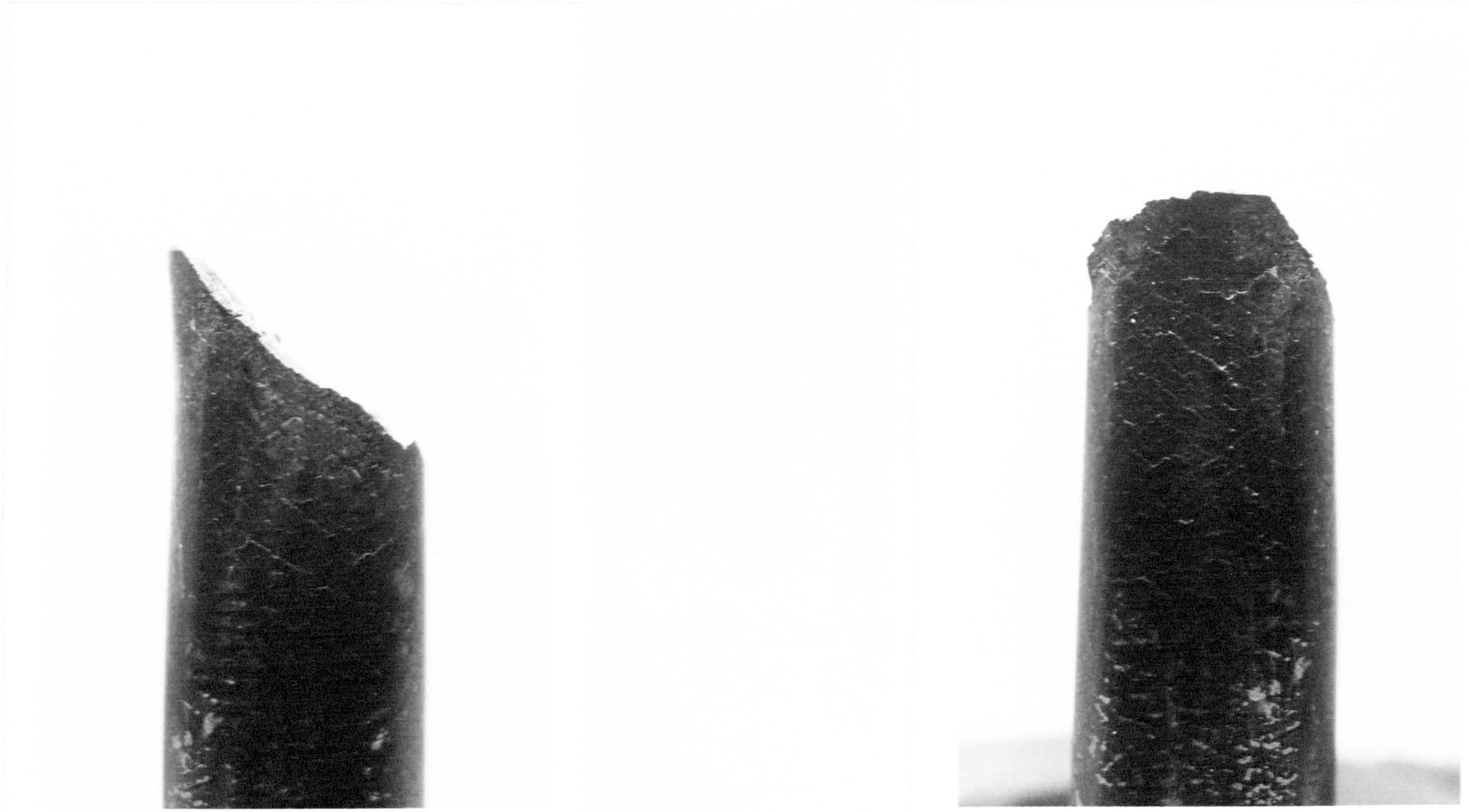

(a) Side view

(b) Side view

Figure 4.19 Photographs of slow strain rate specimen tested in thiourea at -1.9V (sce)

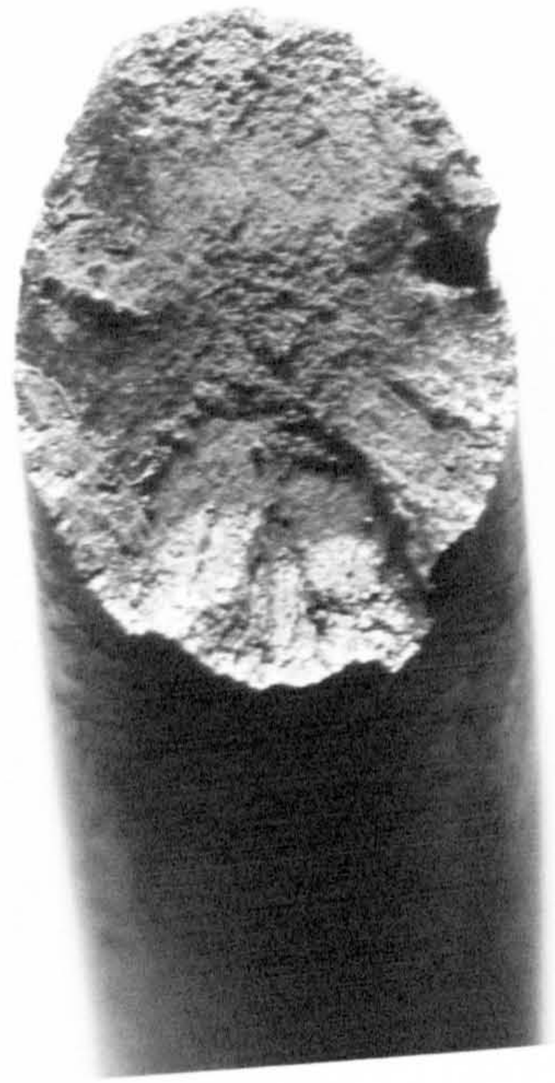

(c) View of failure surface

(d) View of failure surface

Figure 4.19 (Continued)

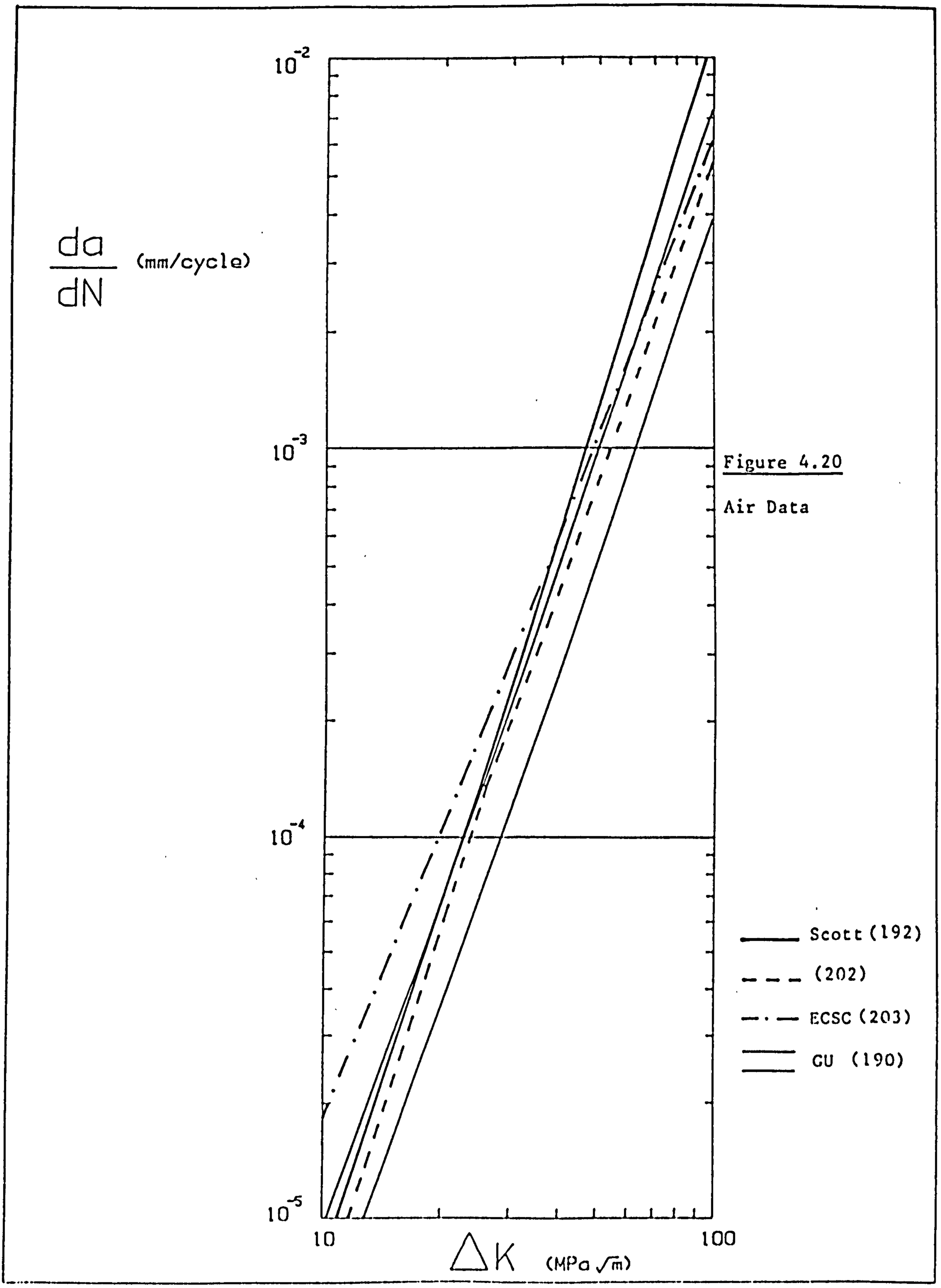

Figure 4.20

Air Data

(A transparency of this figure is included inside the front cover for reference purposes)

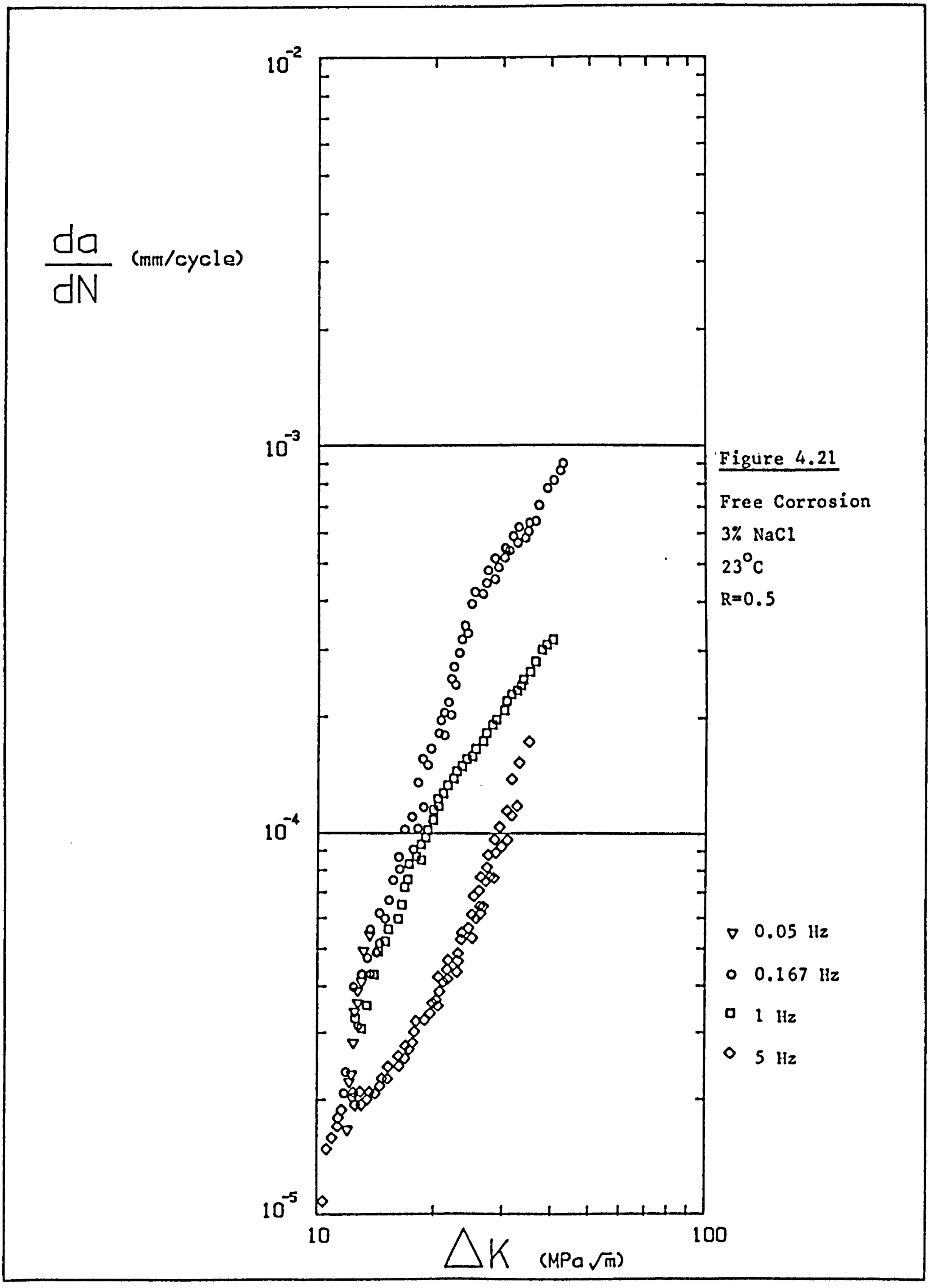

Figure 4.21

Free Corrosion
3% NaCl
23°C
R=0.5

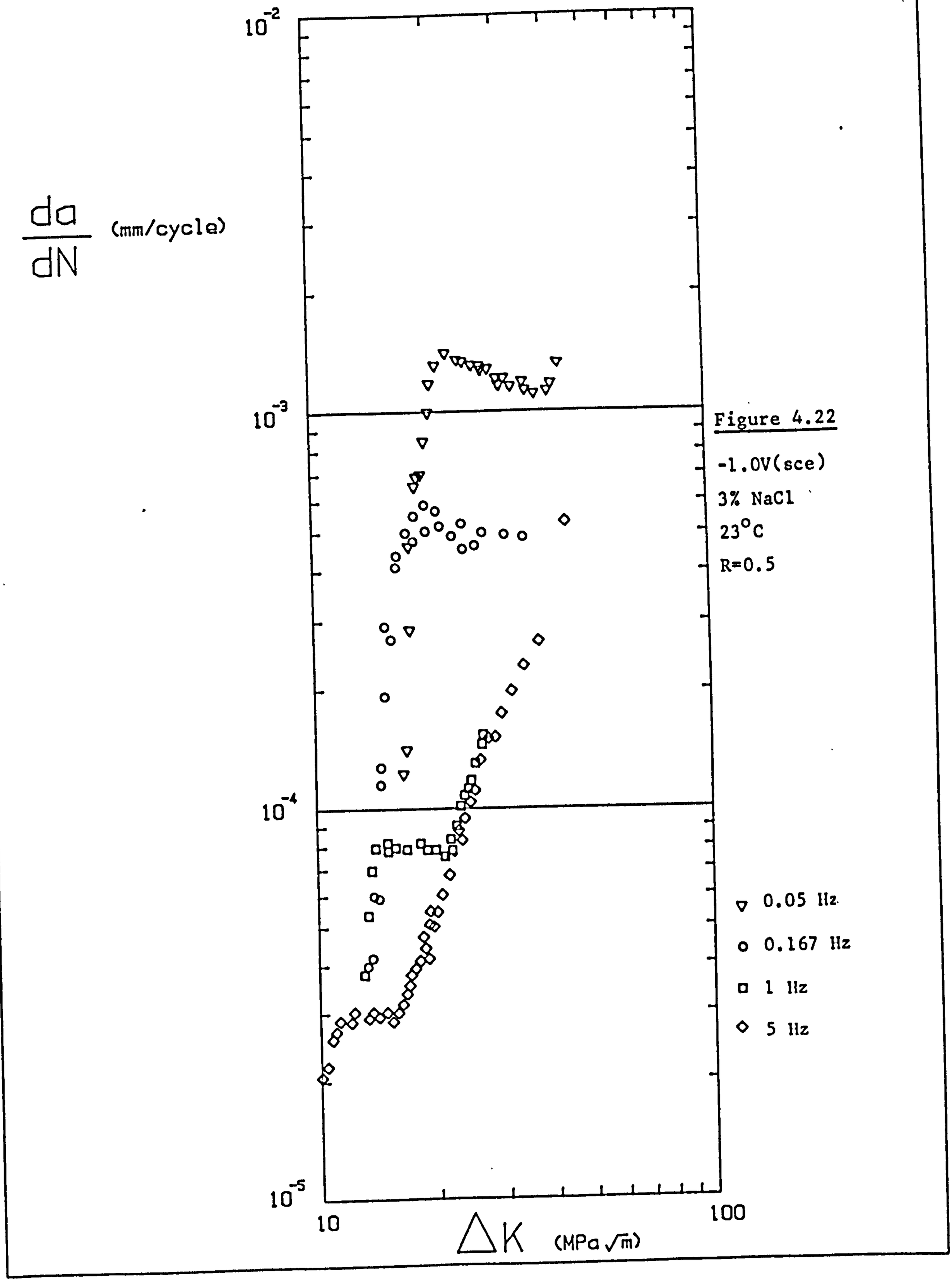
da/dN (mm/cycle)
10^-2
10^-3
10^-4
10^-5
10
100
ΔK (MPa √m)
-1.0V(sce)
3% NaCl
23°C
R=0.5
0.05 Hz
0.167 Hz
1 Hz
5 Hz

Figure 4.22

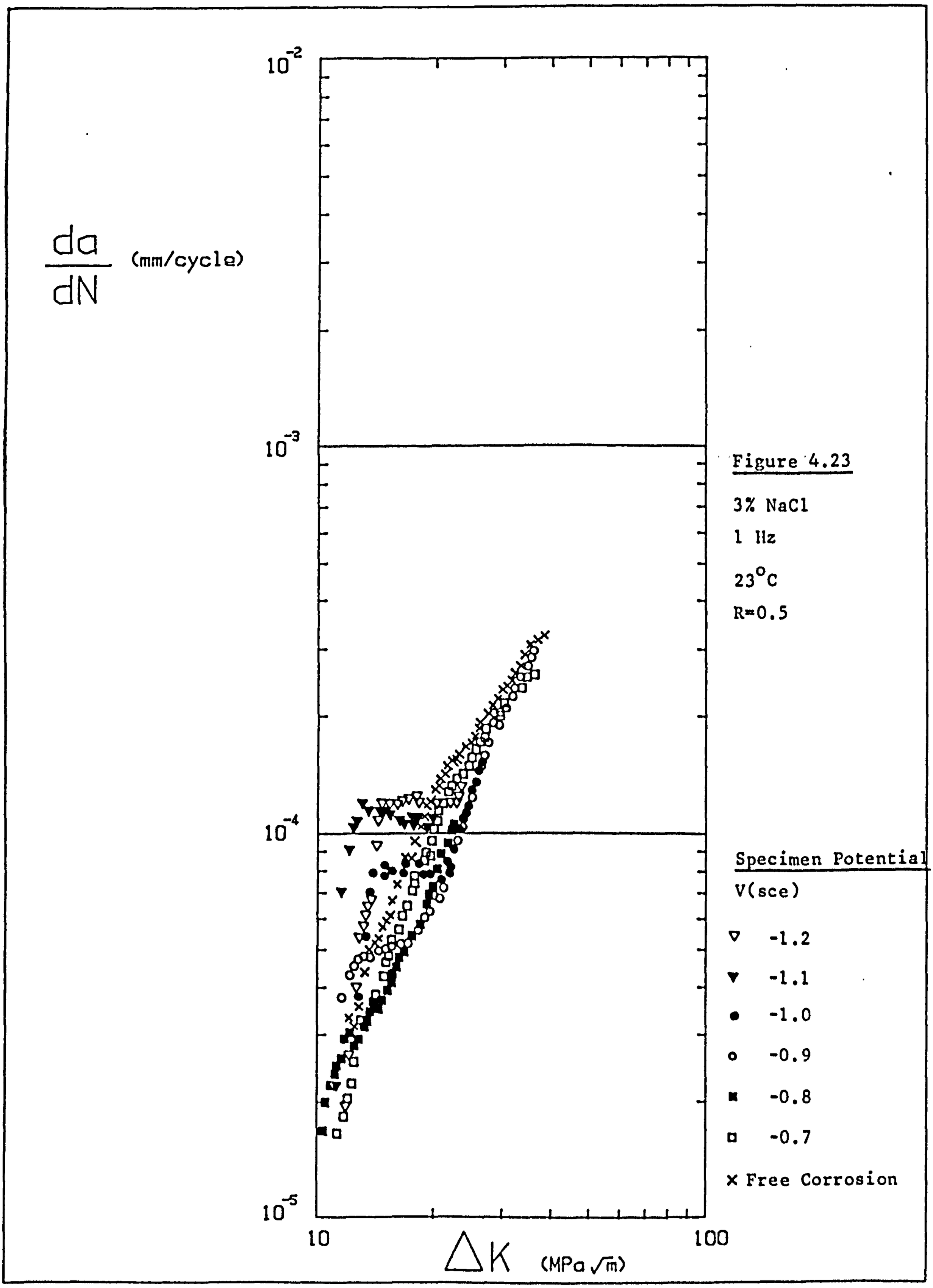
10^{-2}
10^{-3}
10^{-4}
10^{-5}
$\frac{da}{dN}$ (mm/cycle)
10
100
ΔK (MPa √m)
Figure 4.23
3% NaCl
1 Hz
23°C
R=0.5
Specimen Potential
V(sce)
-1.2
-1.1
-1.0
-0.9
-0.8
-0.7
Free Corrosion

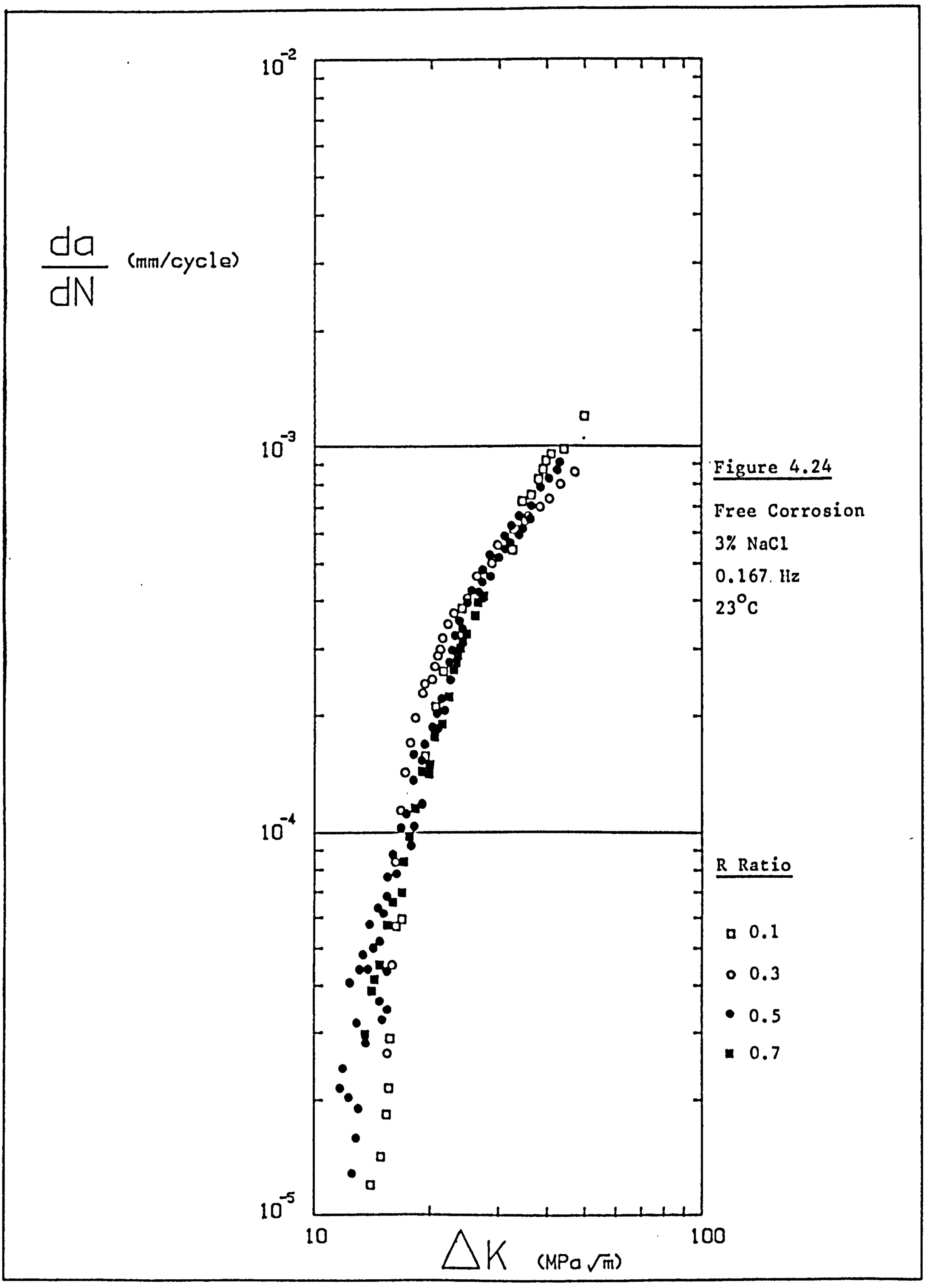
da/dN (mm/cycle)
10^-2
10^-3
10^-4
10^-5
10
100
ΔK (MPa √m)
R Ratio
0.1
0.3
0.5
0.7
Free Corrosion
3% NaCl
0.167 Hz
23°C

Figure 4.24

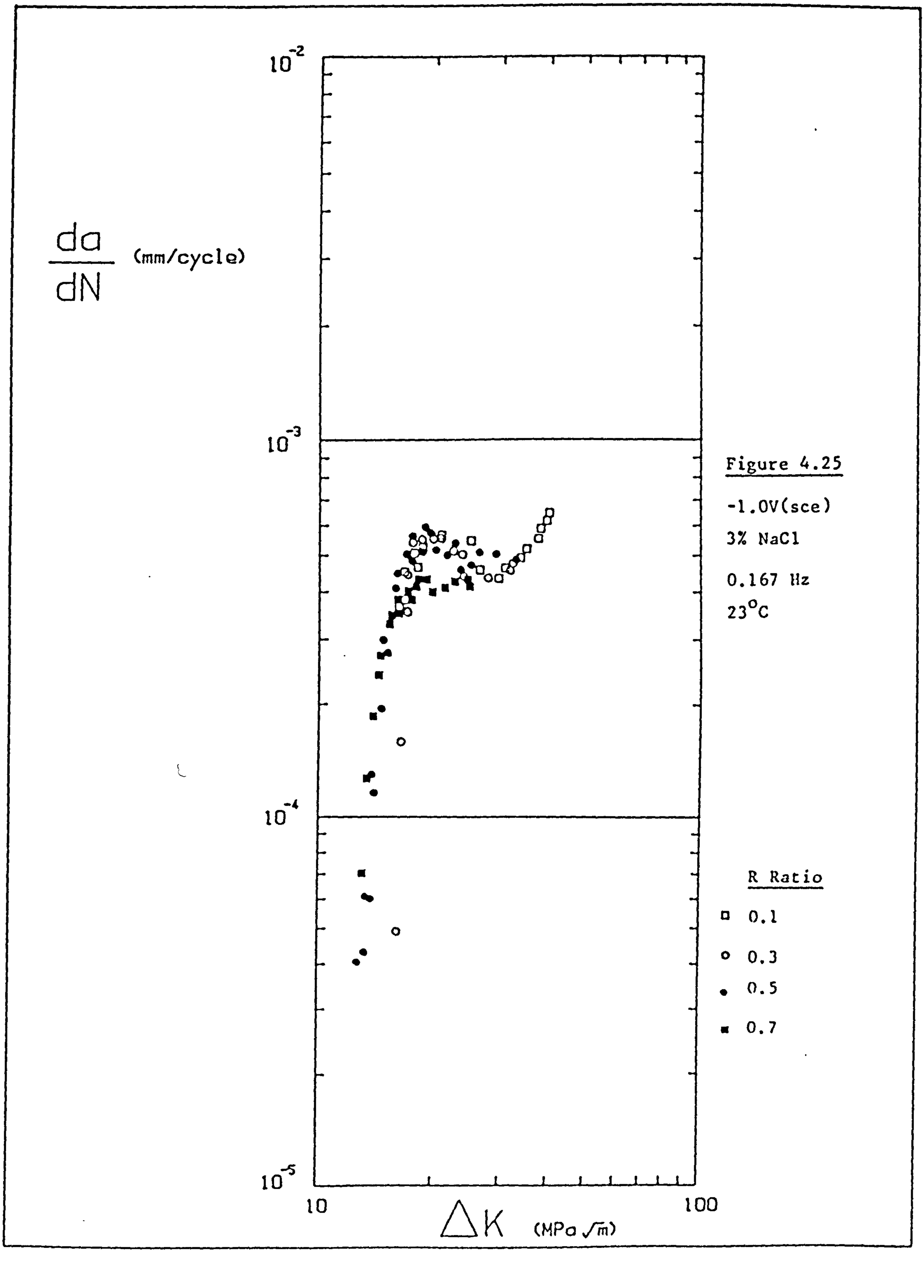
10^{-2}
10^{-3}
10^{-4}
10^{-5}
$\frac{da}{dN}$ (mm/cycle)
10
100
ΔK (MPa $\sqrt{m}$)
-1.0V(sce)
3% NaCl
0.167 Hz
23°C
R Ratio
0.1
0.3
0.5
0.7

Figure 4.25

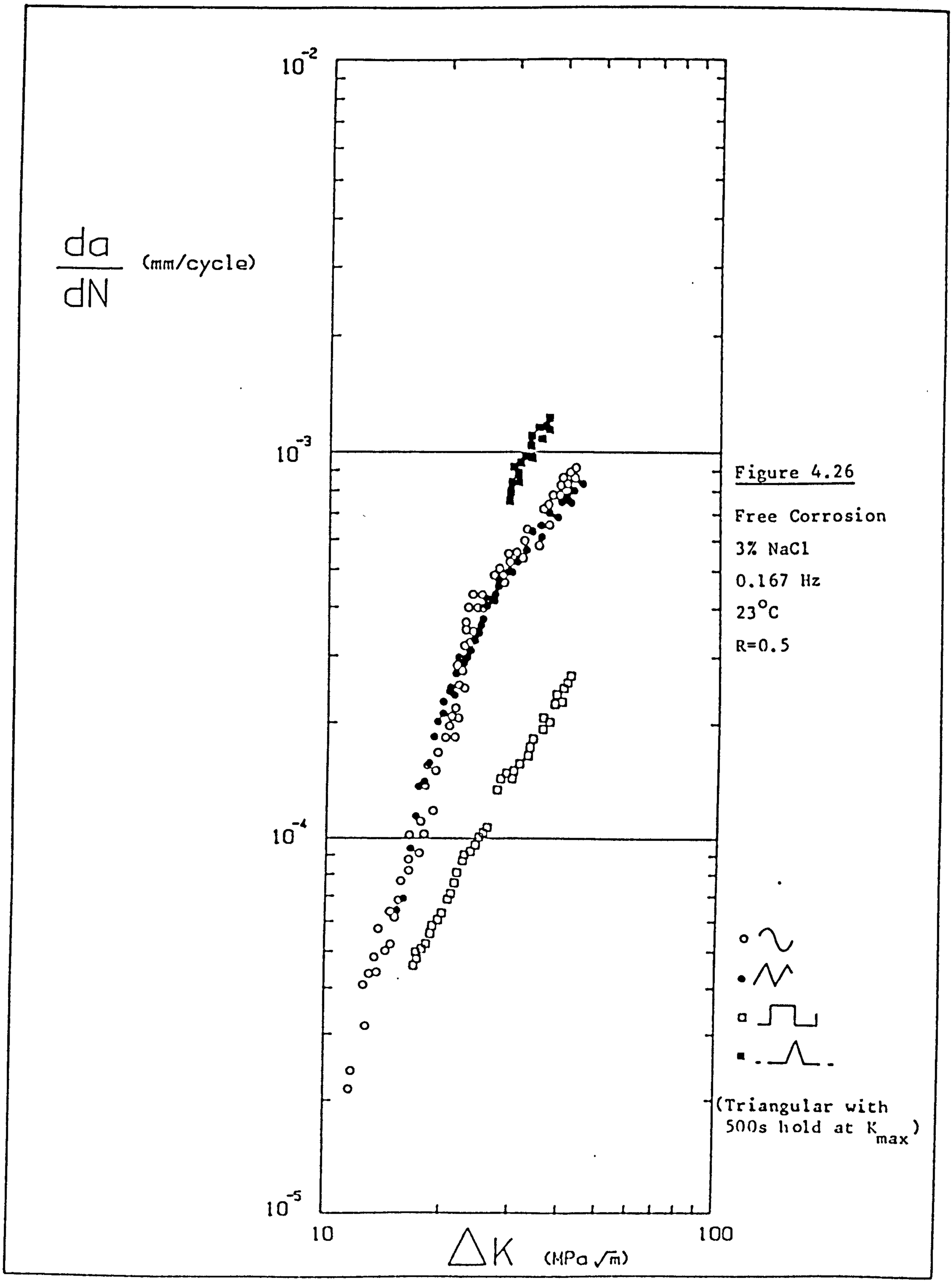

Figure 4.26

Free Corrosion

3% NaCl

0.167 Hz

23°C

R=0.5

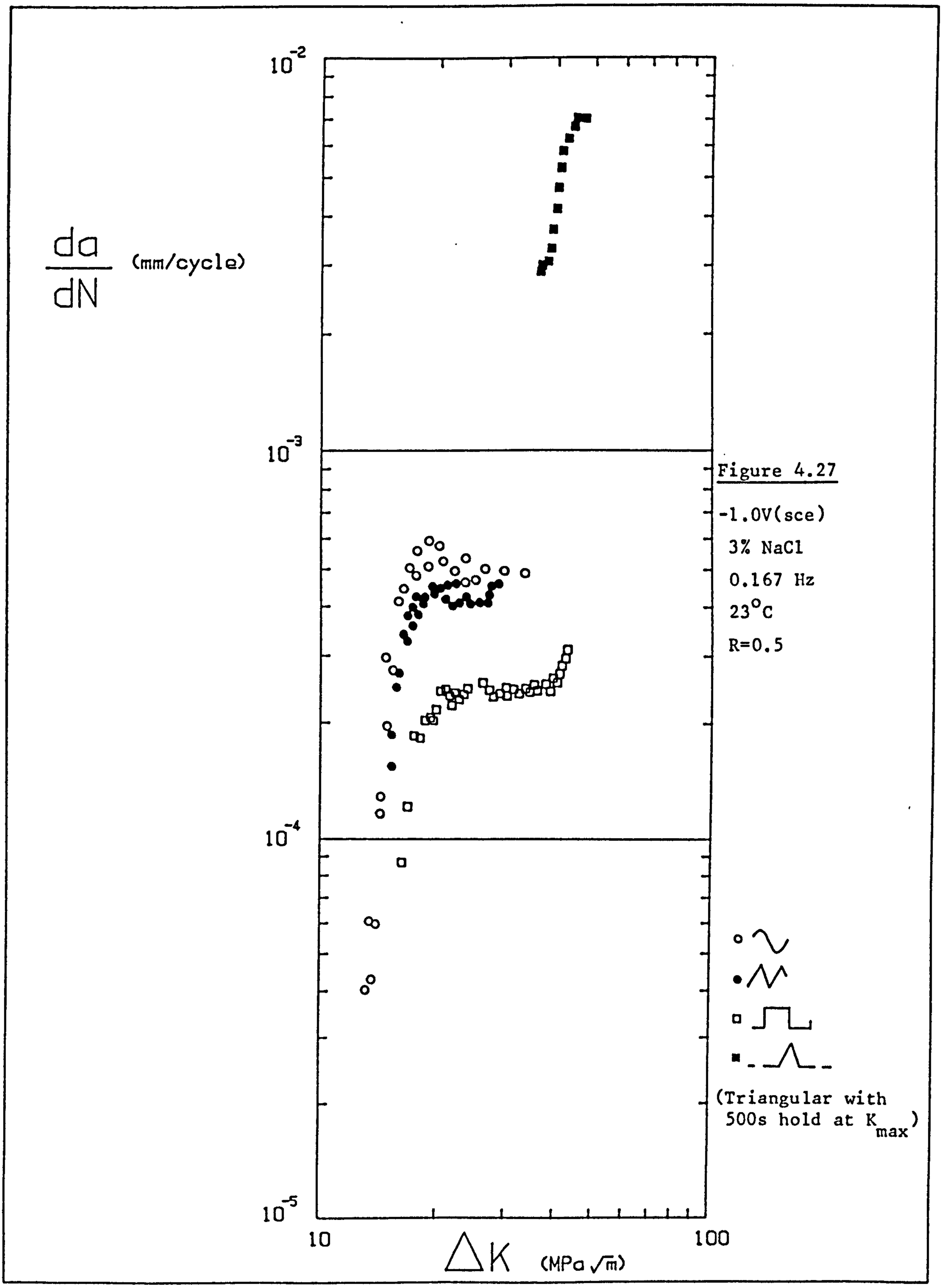
10^{-2}
10^{-3}
10^{-4}
10^{-5}
$\frac{da}{dN}$ (mm/cycle)
10
100
ΔK (MPa $\sqrt{m}$)
-1.0V(sce)
3% NaCl
0.167 Hz
23°C
R=0.5
(Triangular with 500s hold at K_{max})

Figure 4.27

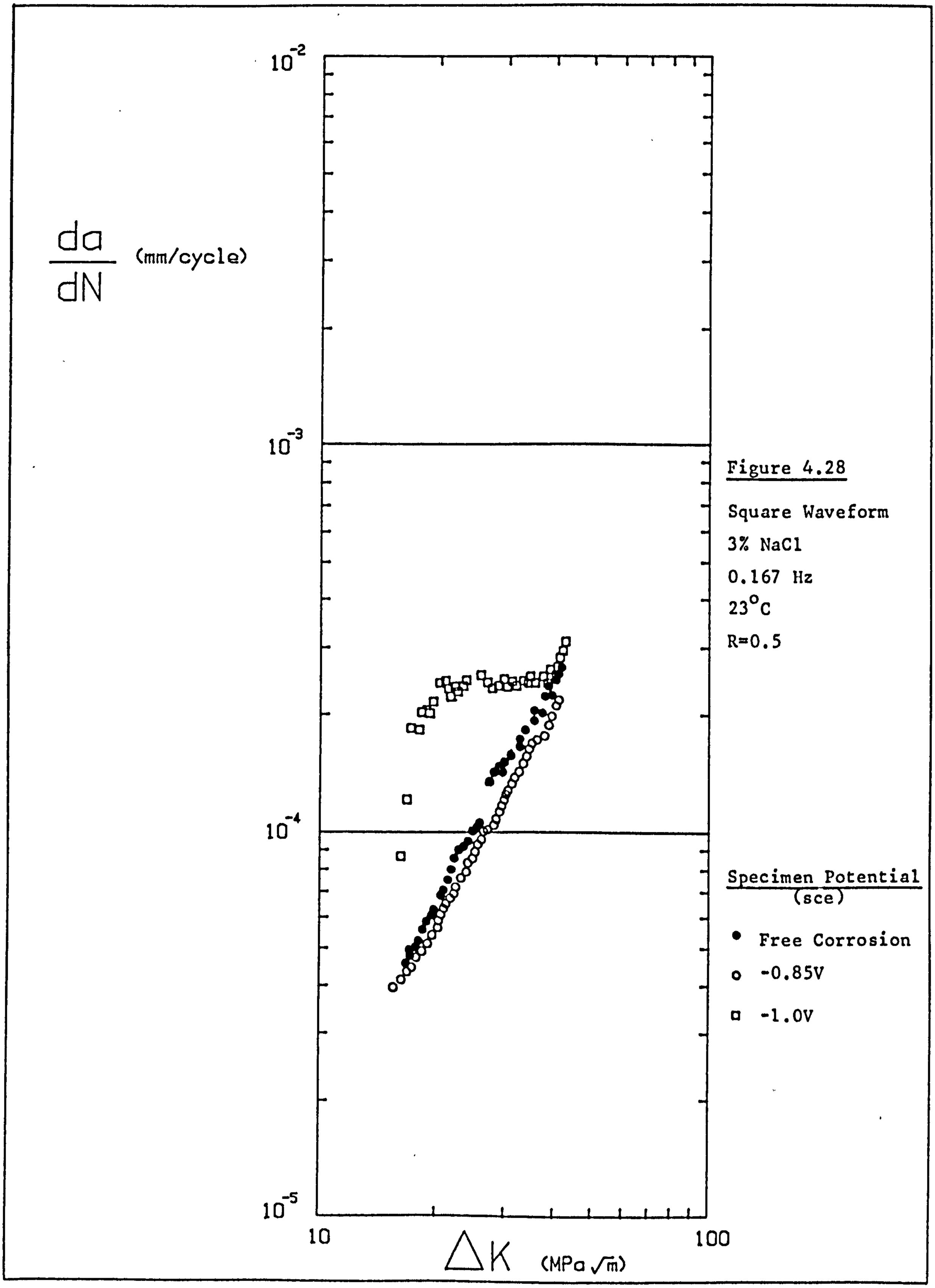
$\frac{da}{dN}$ (mm/cycle)
10^{-2}
10^{-3}
10^{-4}
10^{-5}
10
100
ΔK (MPa $\sqrt{m}$)
Figure 4.28
Square Waveform
3% NaCl
0.167 Hz
23°C
R=0.5
Specimen Potential (sce)
• Free Corrosion
o -0.85V
□ -1.0V

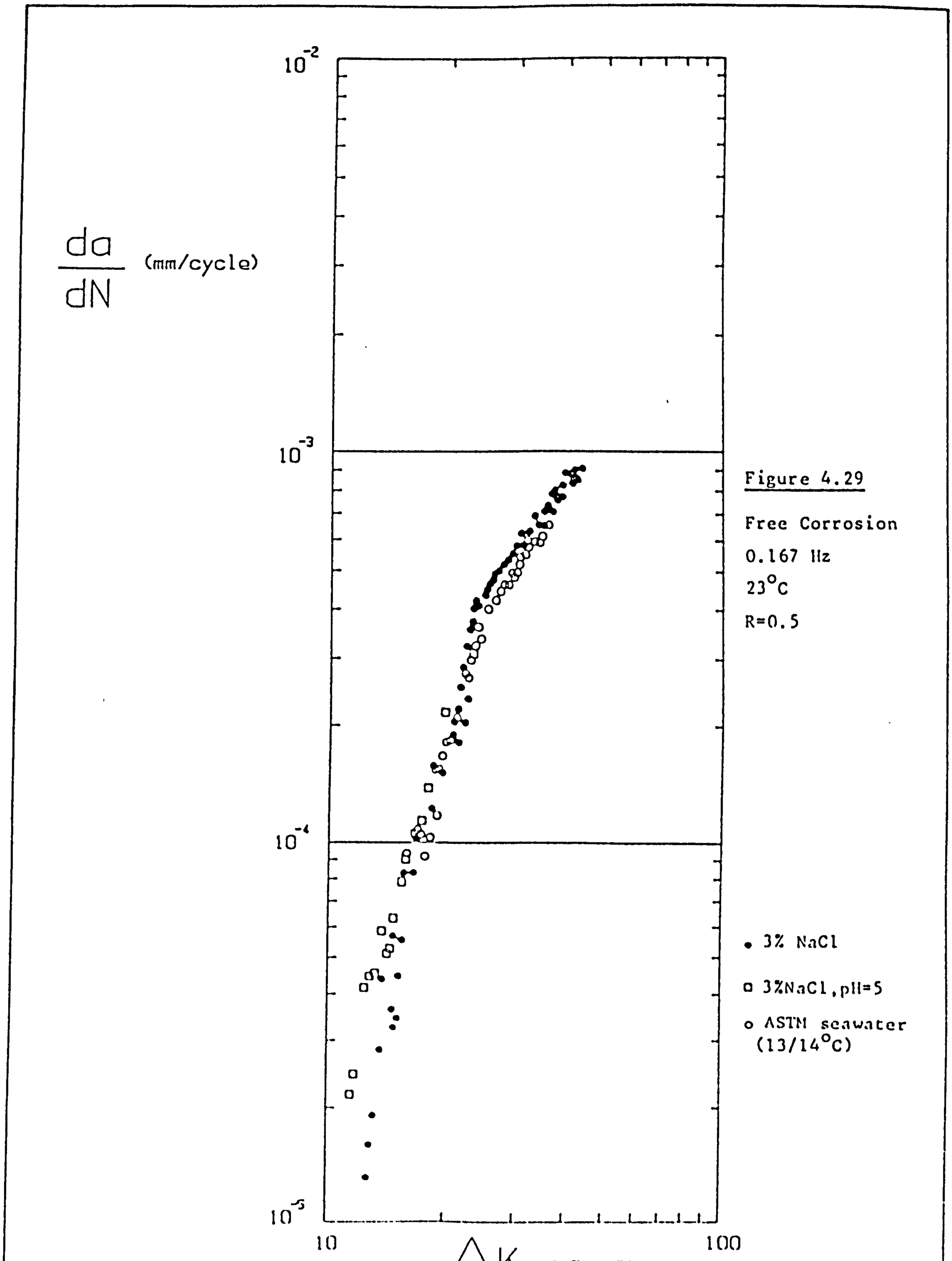

Figure 4.29

Free Corrosion

0.167 Hz

23°C

R=0.5

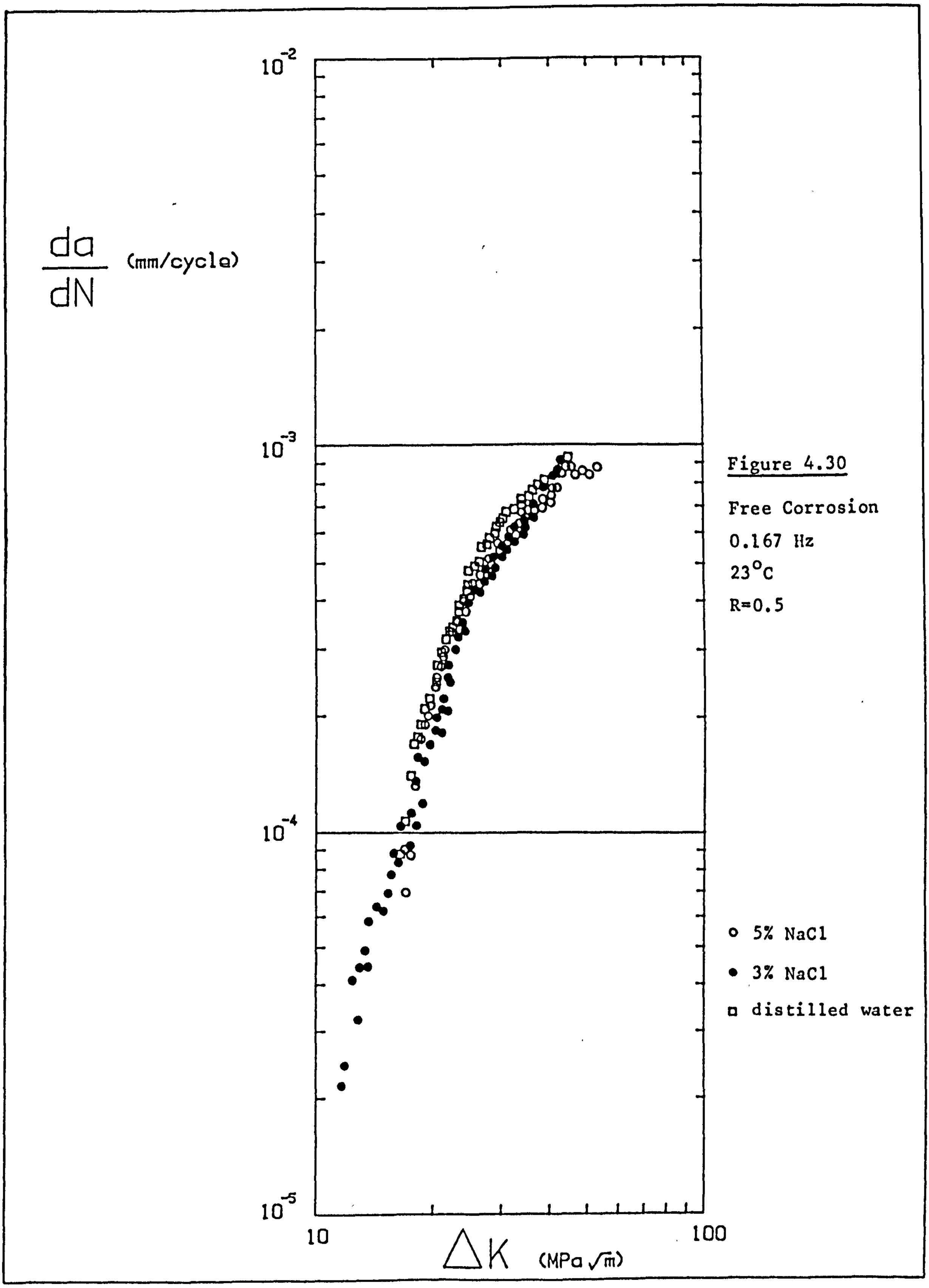

Figure 4.30

Free Corrosion

0.167 Hz

23°C

R=0.5

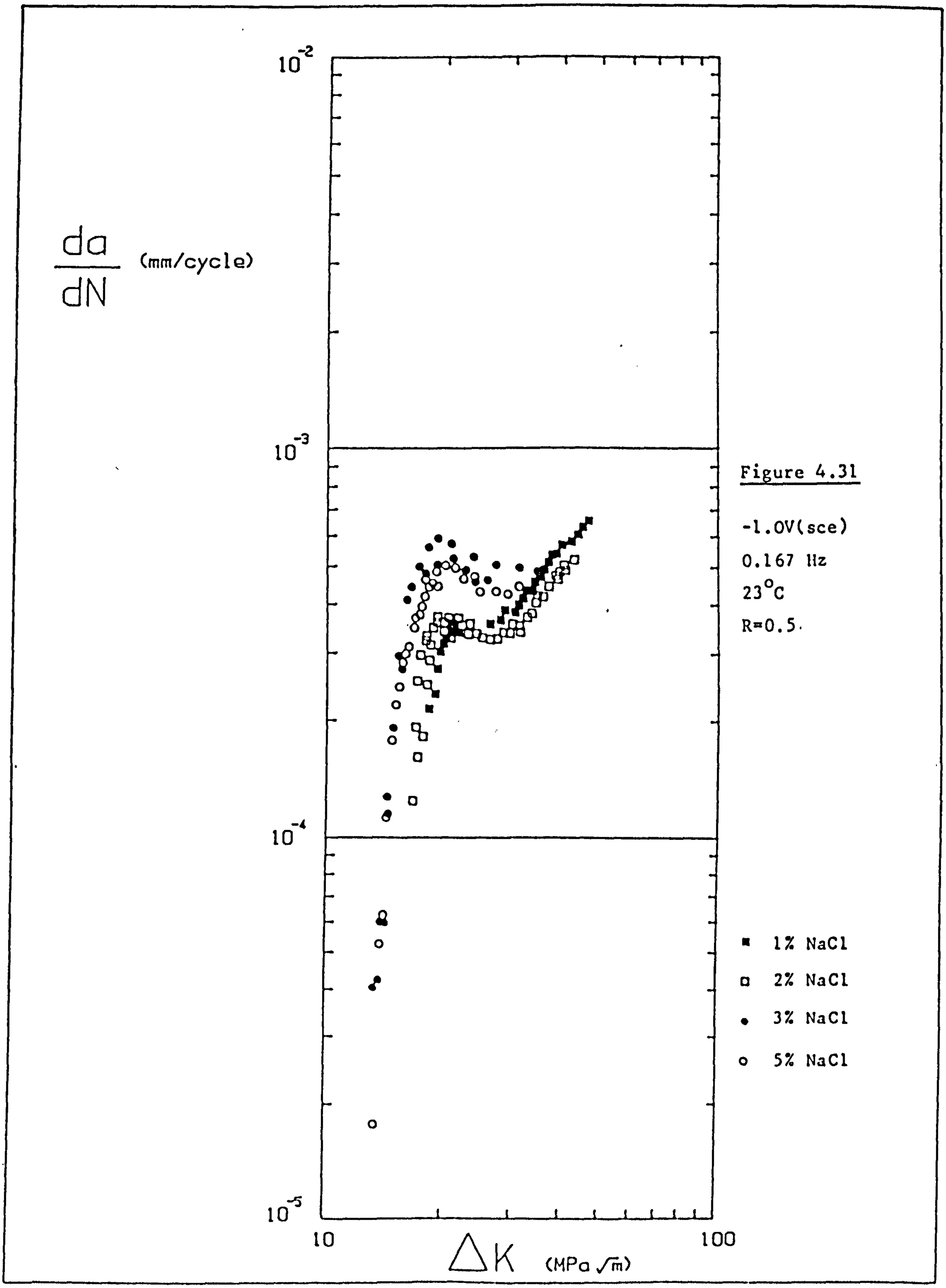

Figure 4.31

-1.0V(sce)

0.167 Hz

23°C

R=0.5

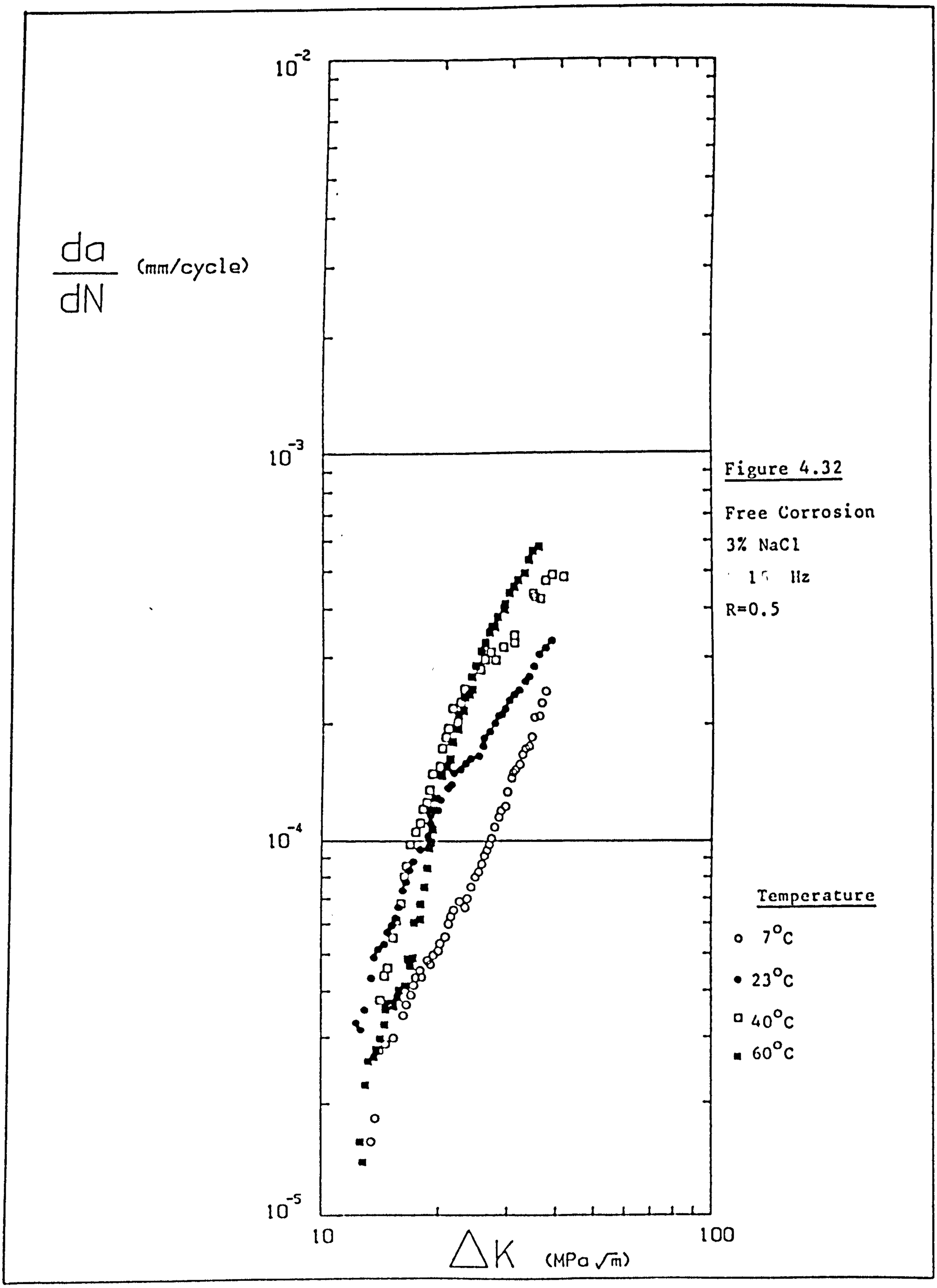

Figure 4.32

Free Corrosion

3% NaCl

1[illegible] Hz

R=0.5

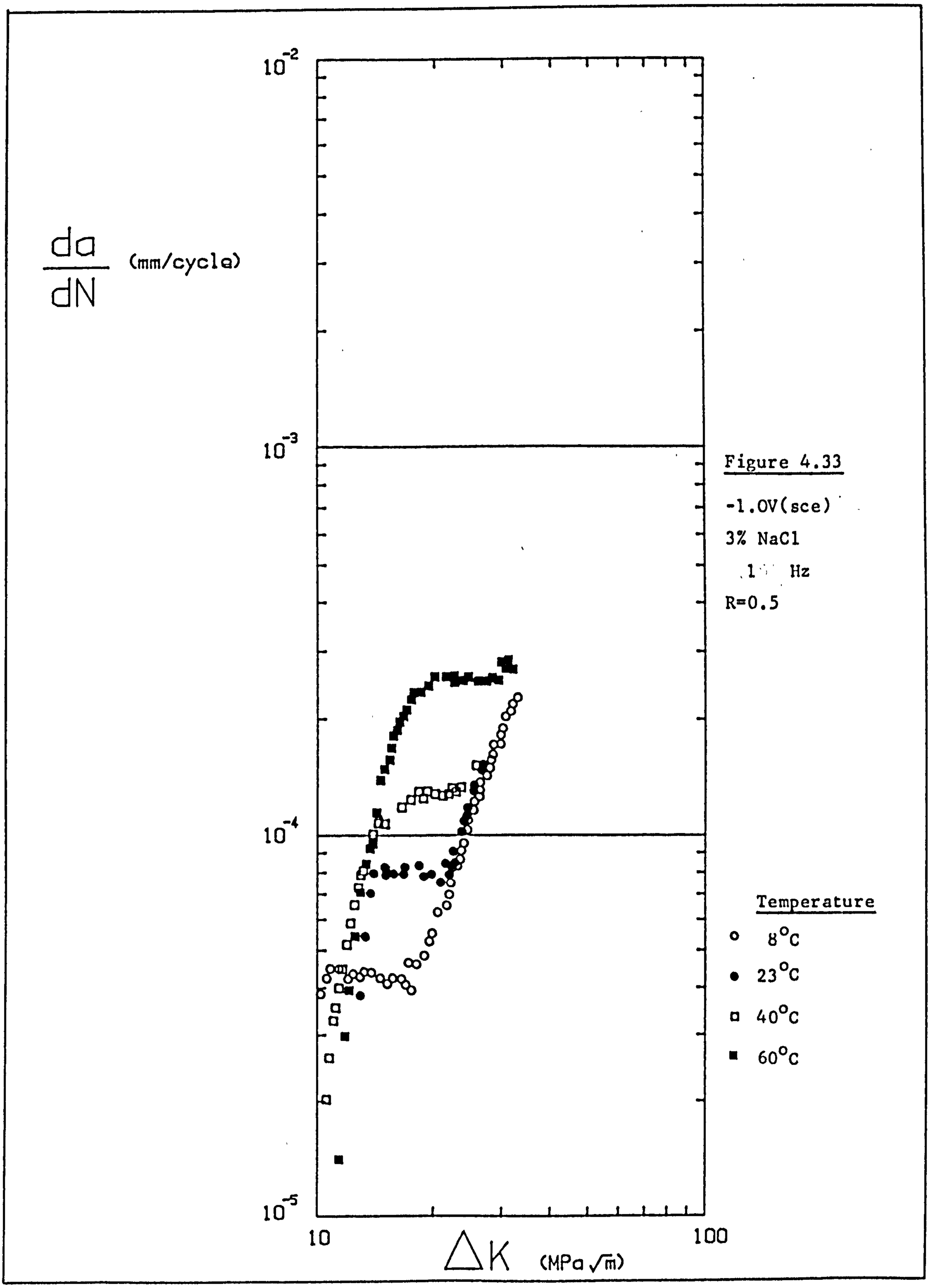
10^{-2}
10^{-3}
10^{-4}
10^{-5}
$\frac{da}{dN}$ (mm/cycle)
10
100
ΔK (MPa√m)
-1.0V(sce)
3% NaCl
1 Hz
R=0.5
Temperature
8°C
23°C
40°C
60°C

Figure 4.33

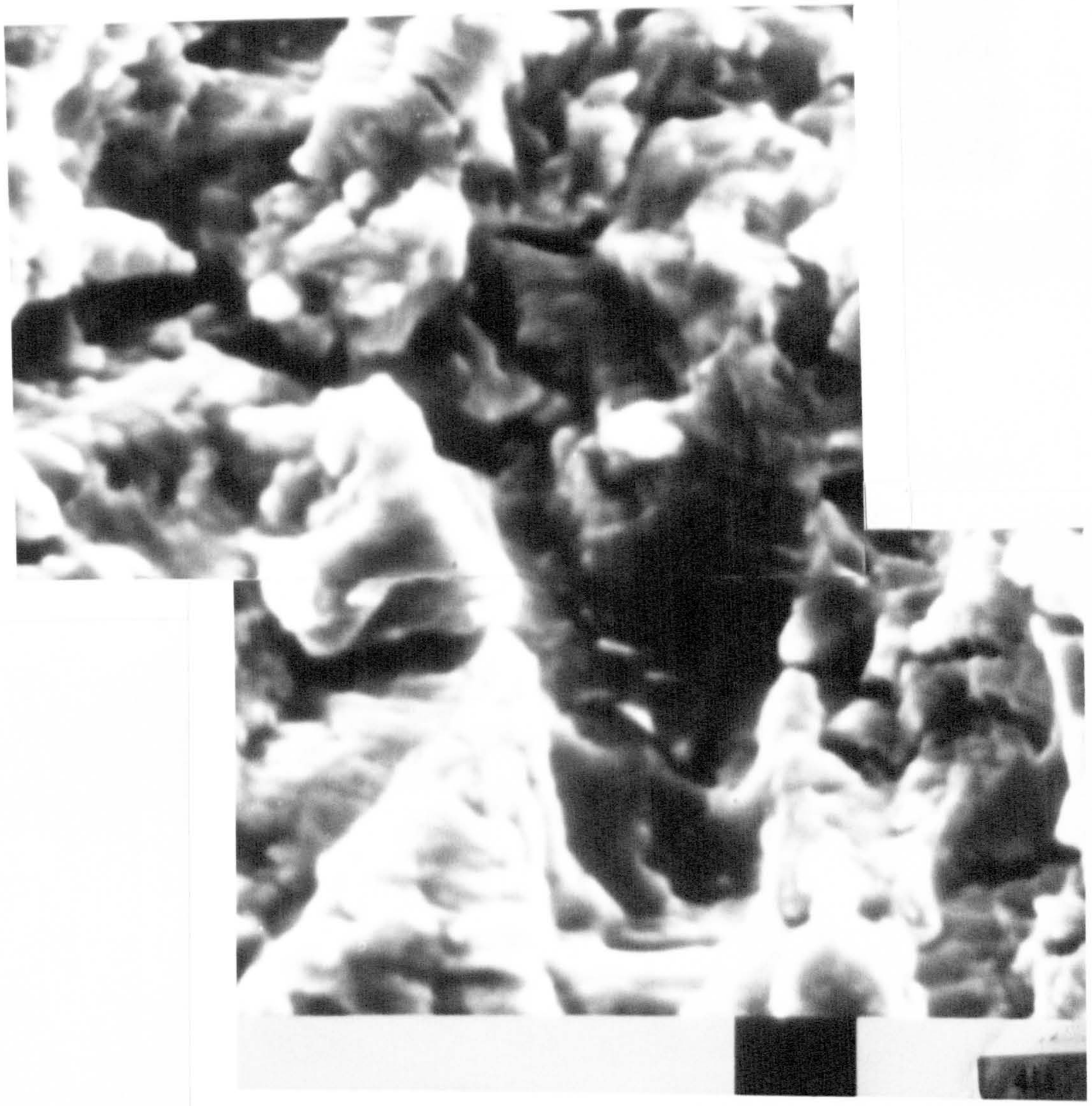

Air test 2

x3800 : 0^{o} tilt : crack growth direction ↑
ductile striations and secondary cracking
Figure 4.34

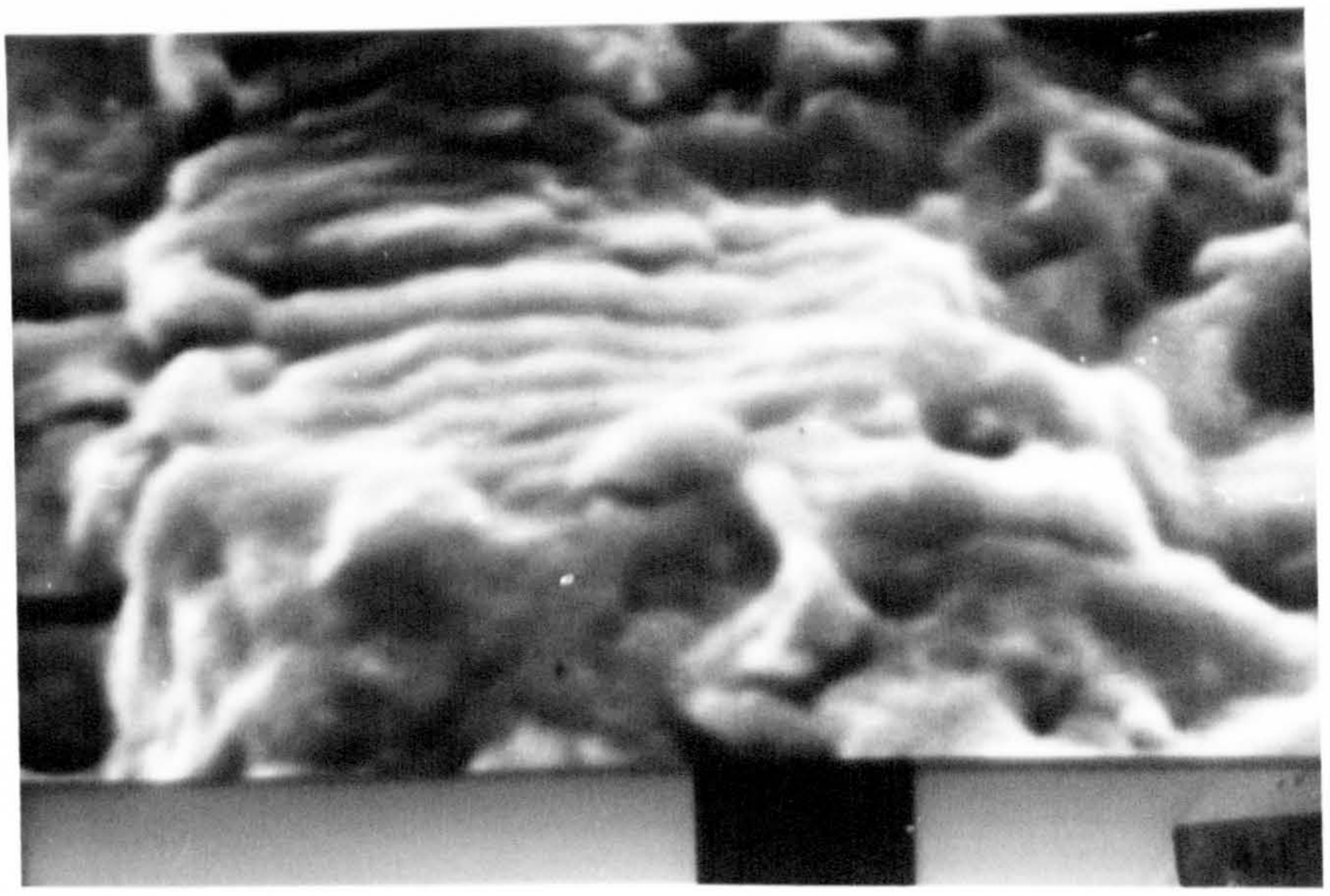

Air test 2

x4450 : 0^{o} tilt : crack direction ↑
pre-crack surface
ductile striations
Figure 4.35

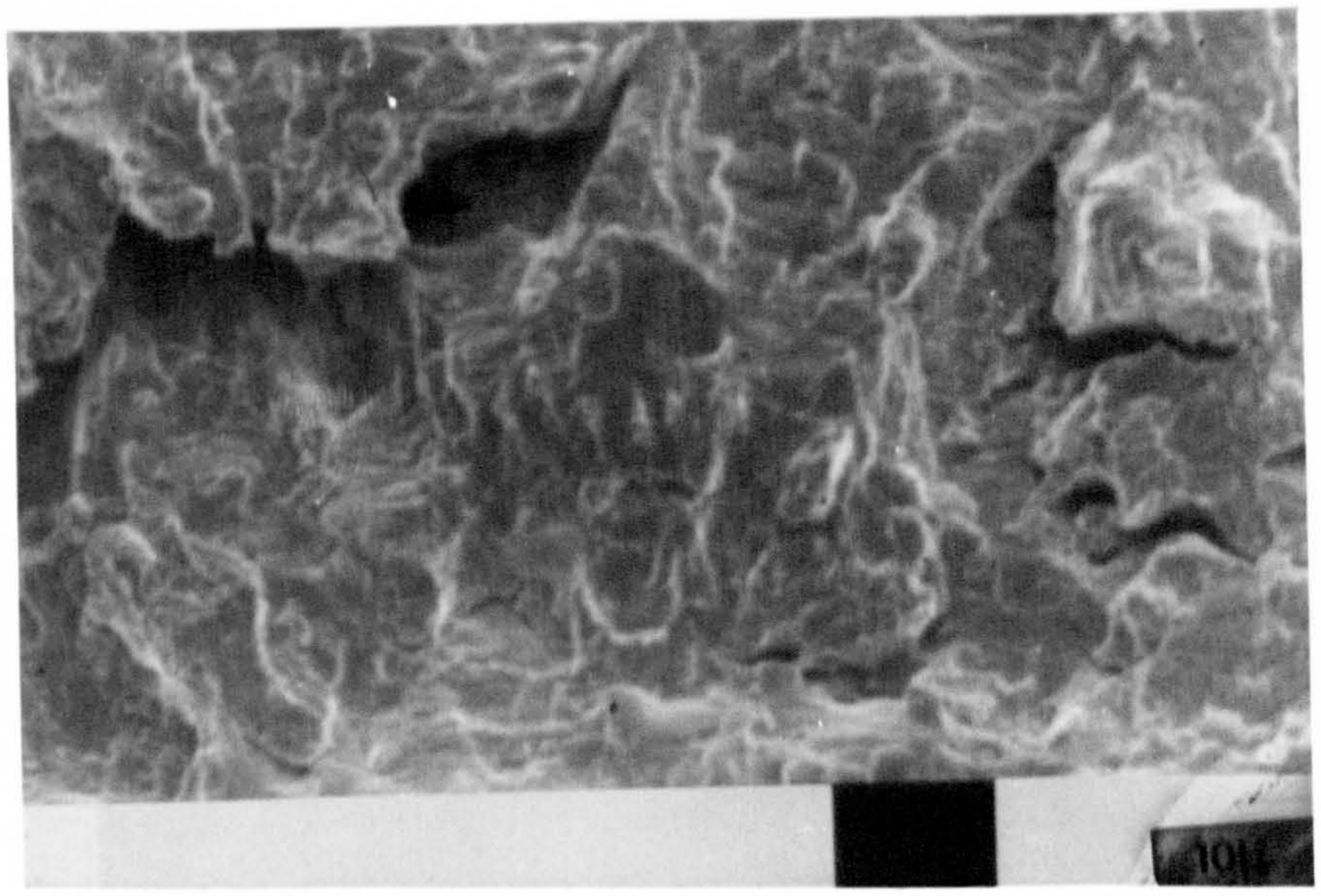

Air test 2

x2000 : 0^{o} tilt : crack direction ↑
$\Delta K = 13.1$ MPa$\sqrt{m}$
secondary cracking
Figure 4.36

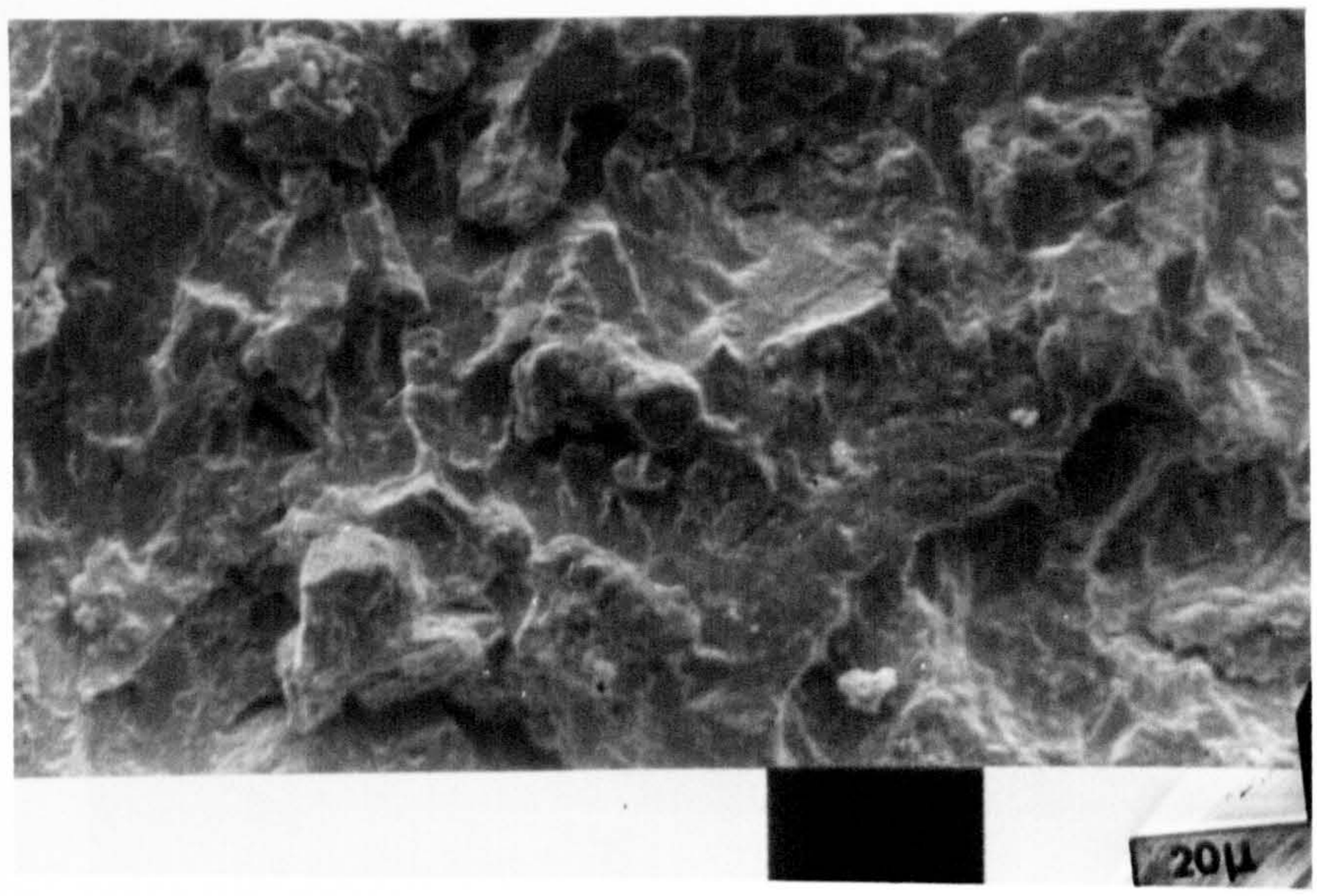

DOE 12 : Free corrosion : 8ppm O_2
x1000 : 0^o tilt : crack direction↑
$\Delta K = 29.8 MPa\sqrt{m}$
Figure 4.37

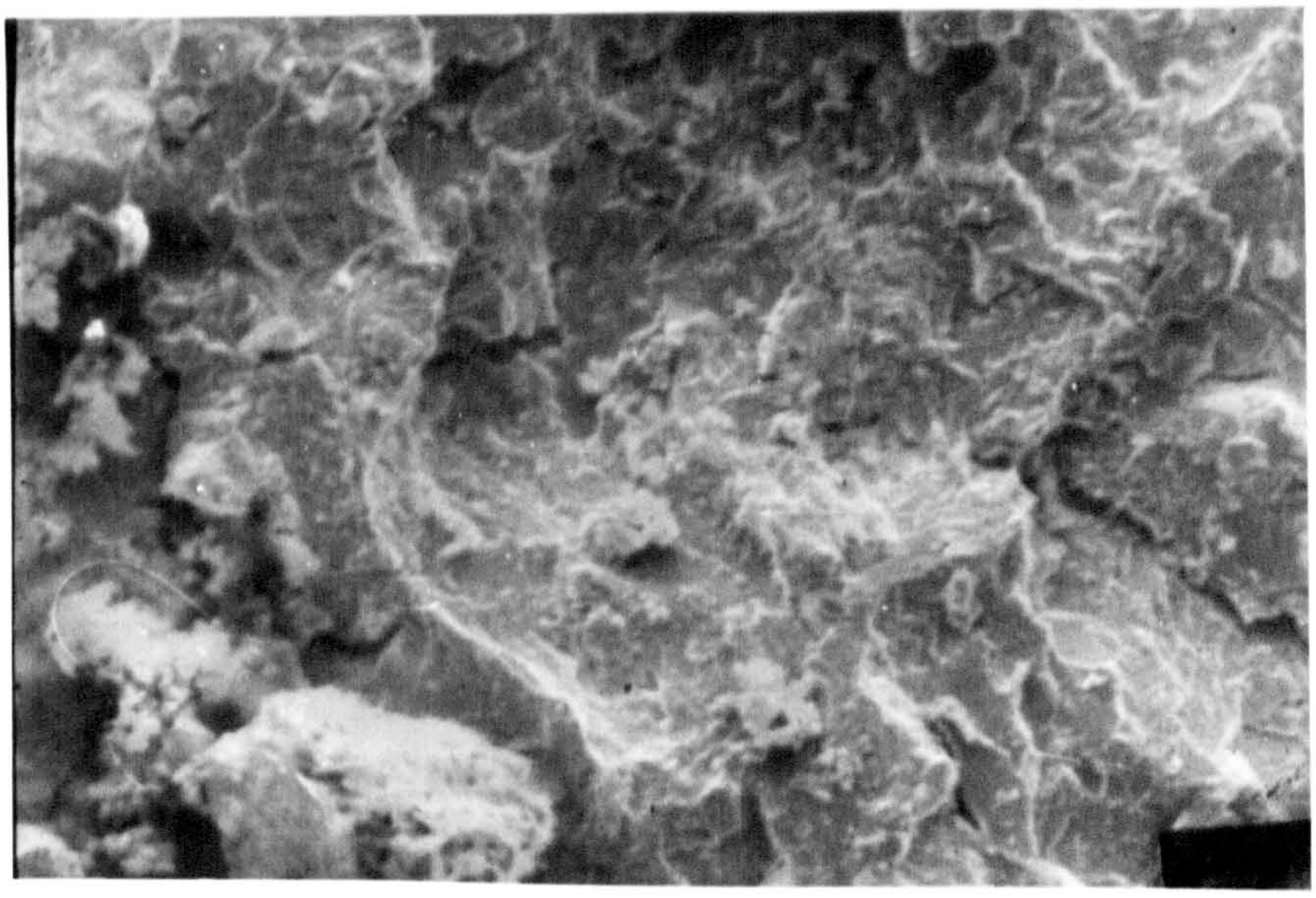

DOE 12 : Free corrosion : 8ppm O_2
x1000 : 0^o tilt : crack direction ↑
$\Delta K = 27.5\ MPa\sqrt{m}$
Figure 4.38

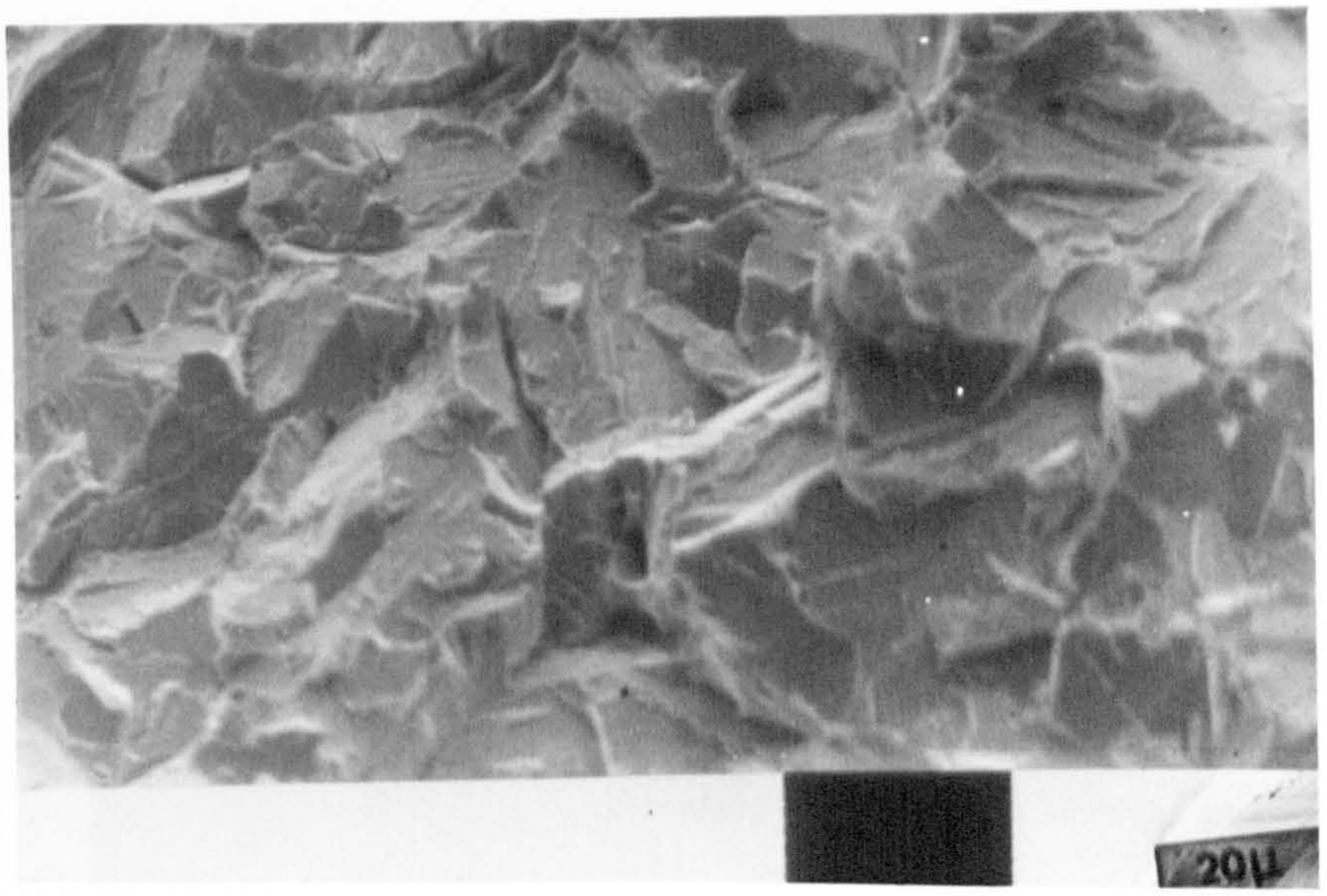

DOE 12

x1000 : 34° tilt : crack direction ↓
surface created by breaking specimen open in liquid nitrogen
Figure 4.39

CFA 14 : arsenate, -1V(sce)

x2000 : 0° tilt : crack direction ↑
cleavage facet
Figure 4.40

PAGES
MISSING
IN
ORIGINAL

CFA 14 : arsenate, -1V(sce)

x1100 : 0^{o} tilt : crack direction ↑
$\Delta K = 20.4 MPa\sqrt{m}$
general view of fracture surface showing cleavage facets
Figure 4.41

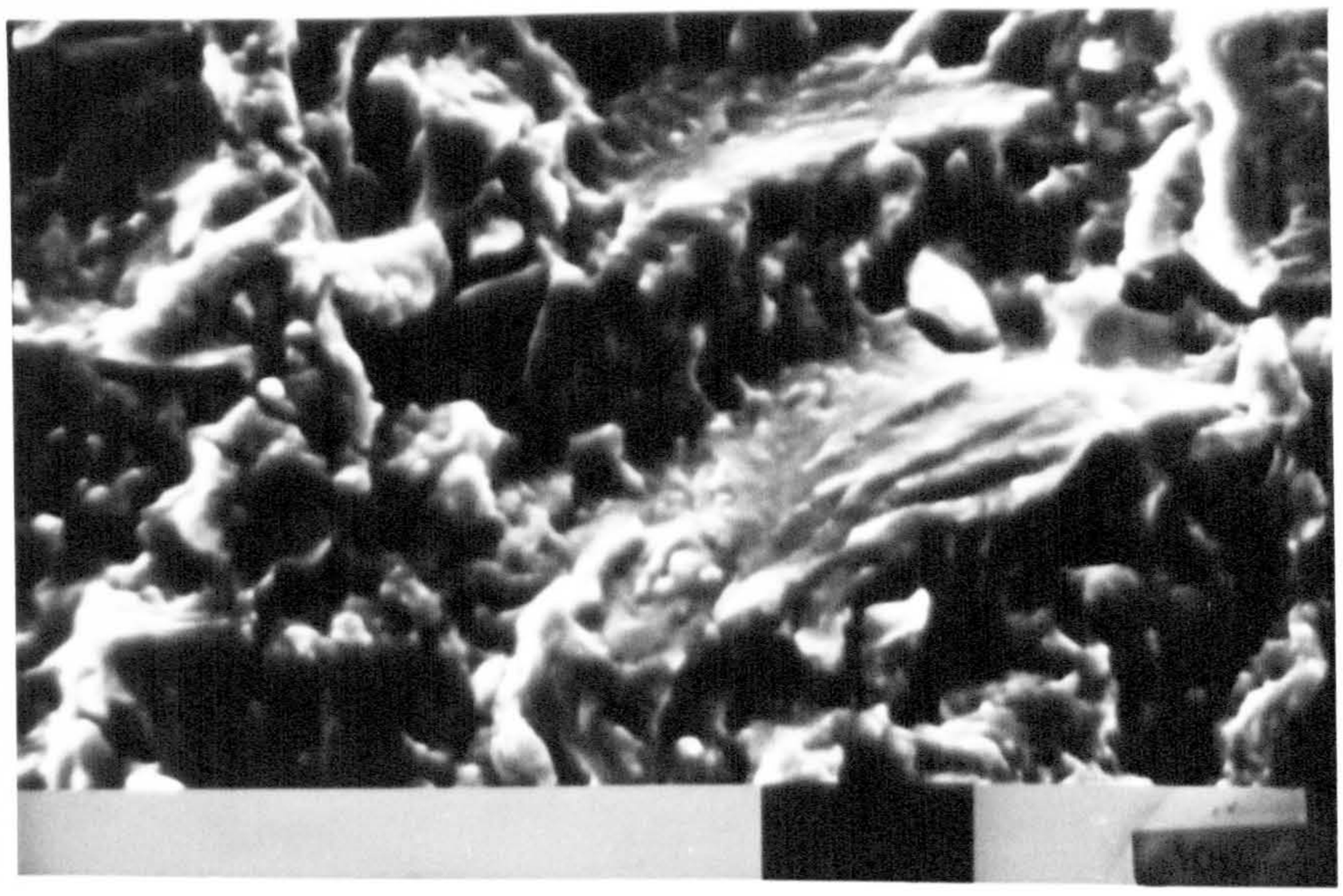

CFA 6 : arsenate, -1V(sce)
x2000 : 0^{o} tilt : crack direction ↑
$\Delta K = 17.7 MPa\sqrt{m}$
Transgranular cleavage facets
Figure 4.42

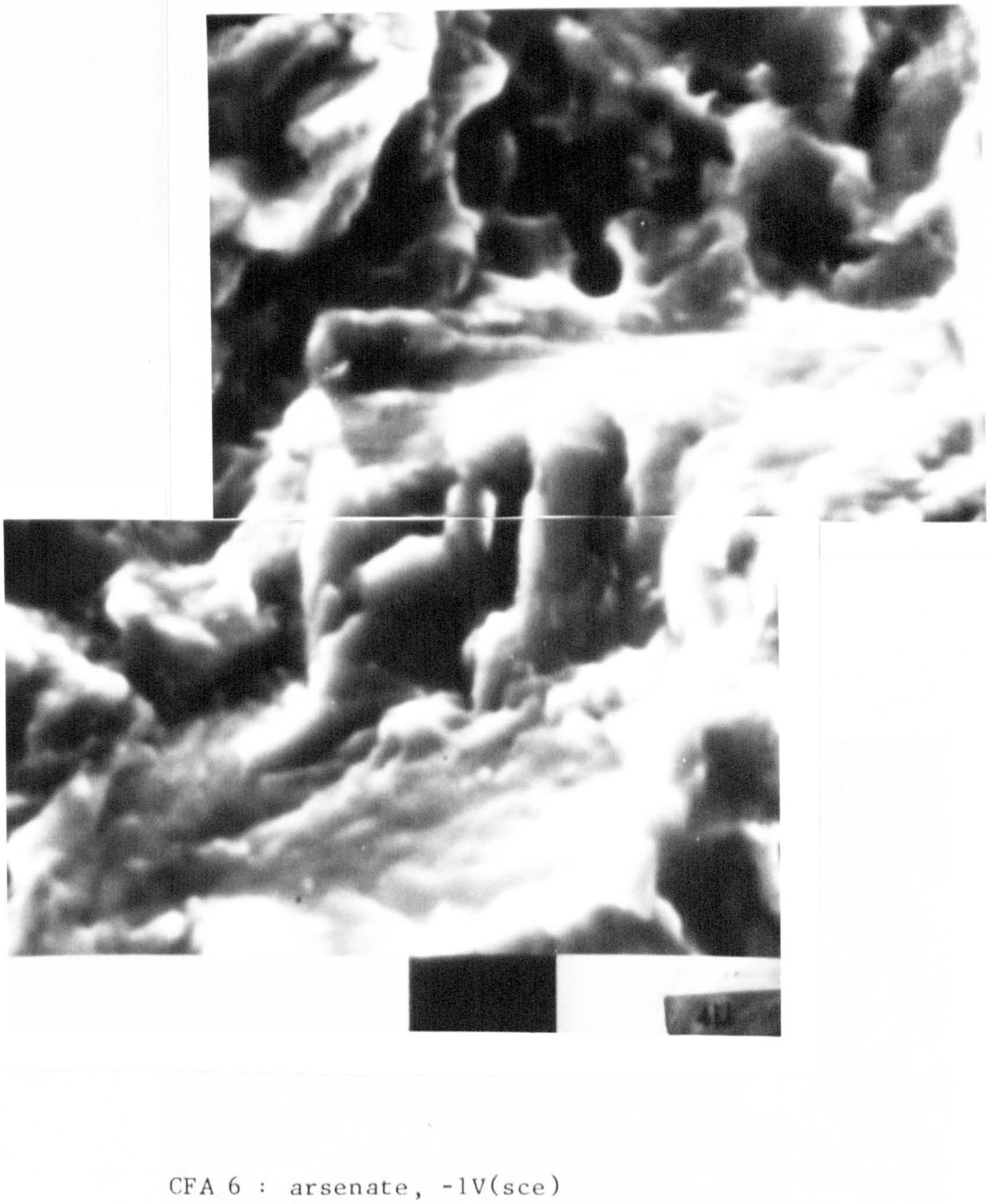

CFA 6 : arsenate, -1V(sce)

x5000 : 0^{o} tilt : crack direction ↑

$\Delta K = 17.6\ MPa\sqrt{m}$

Figure 4.43

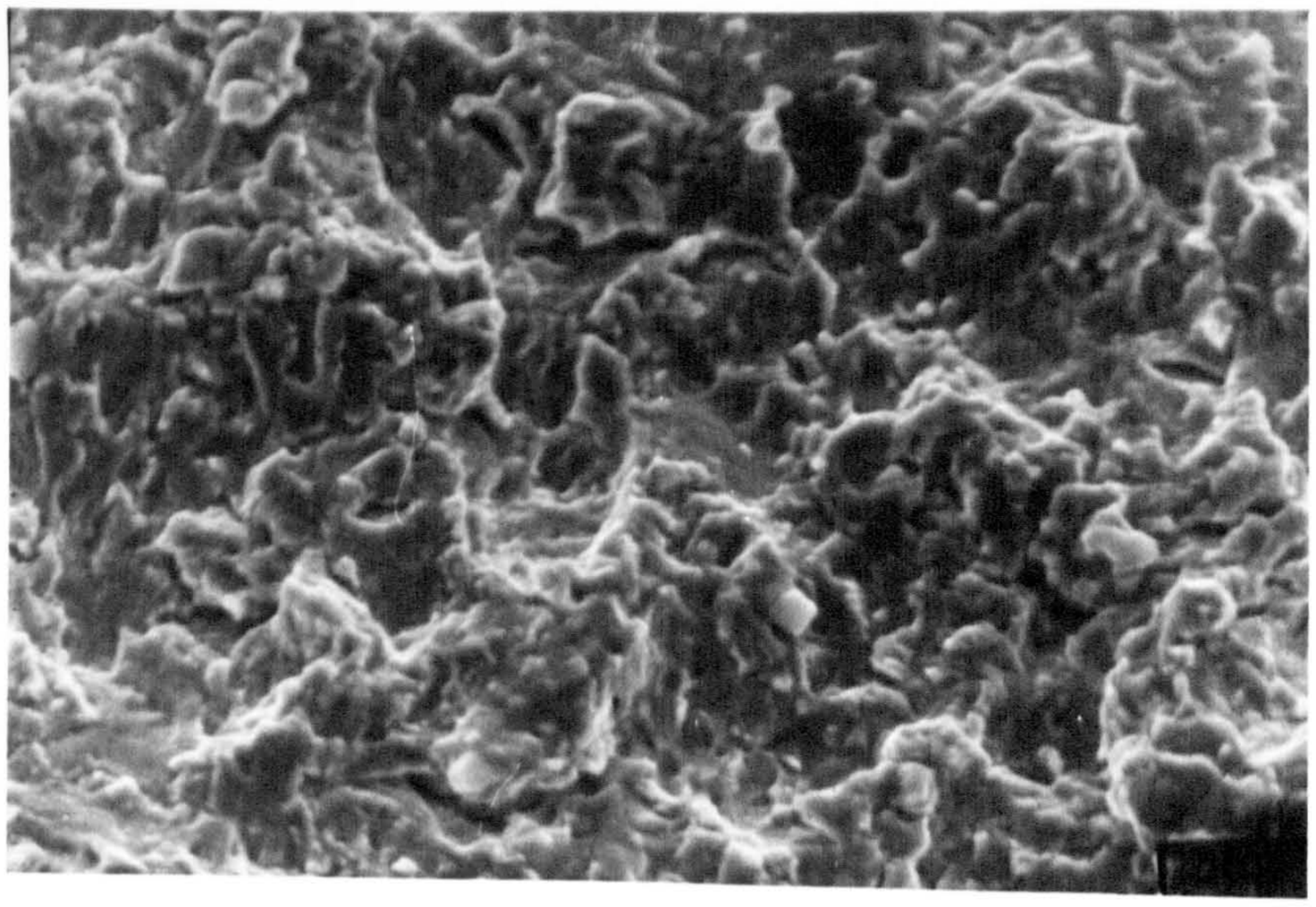

DOE 6 : ASTM, -0.85V(sce)

x1000 : 0^{o} tilt : crack direction ↑
$\Delta K = 29.6\ MPa\sqrt{m}$
Figure 4.44

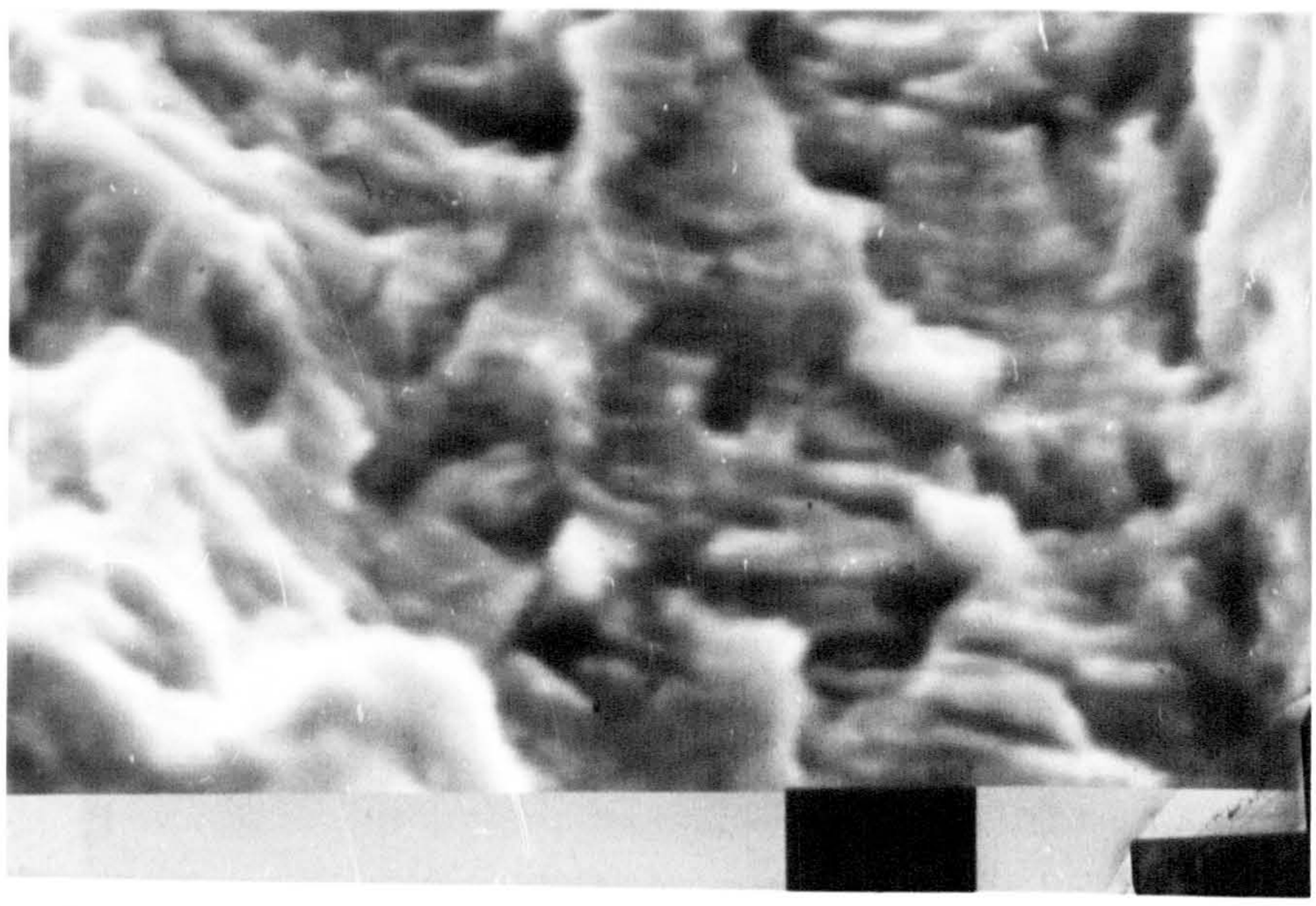

DOE 6 : ASTM, -0.85V(sce)

x5000 : 0^{o} tilt : crack direction ↑
ductile striations
Figure 4.45

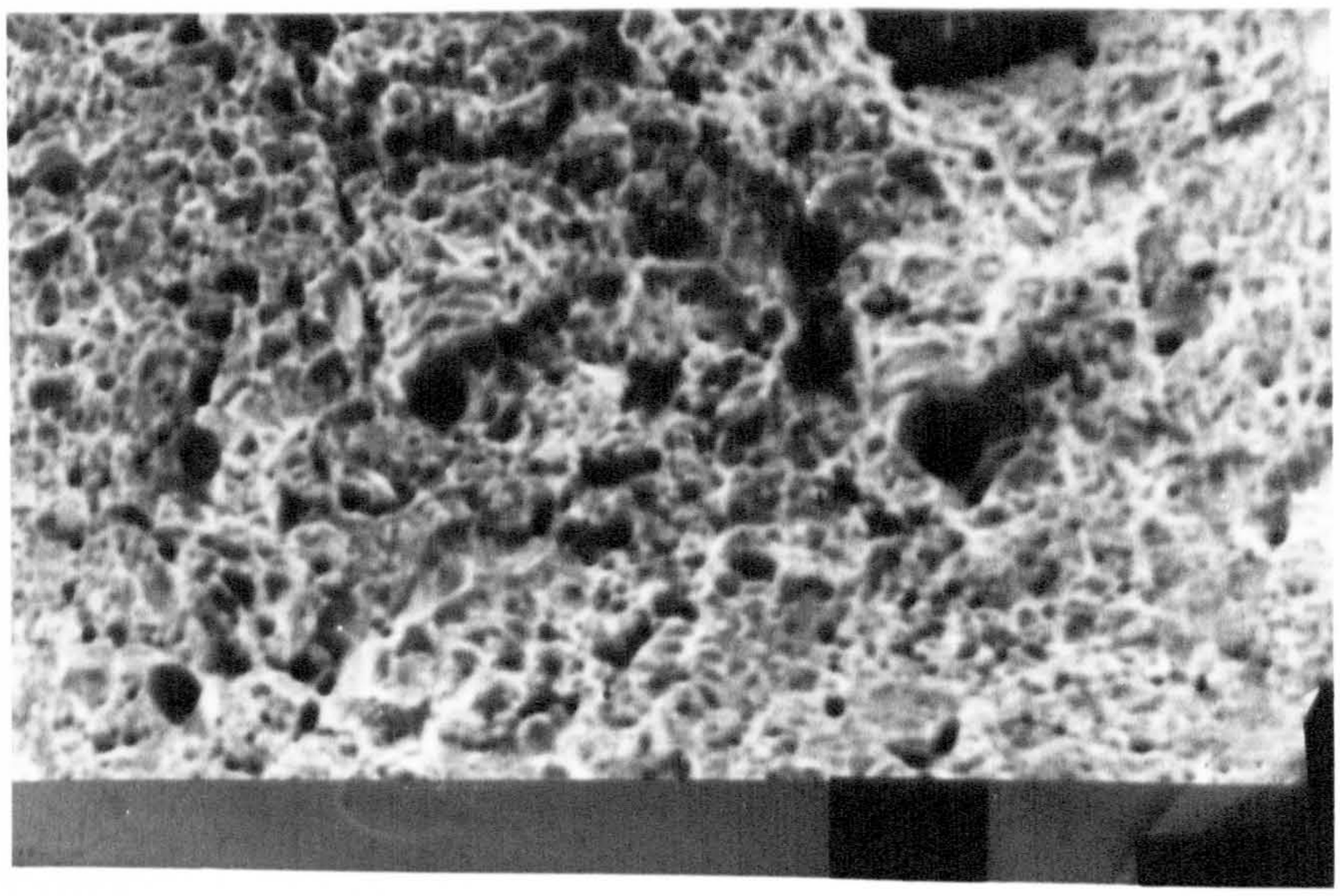

Slow strain rate test : air

x1000 : 0^{o} tilt
ductile fracture in middle of cup
Figure 4.46

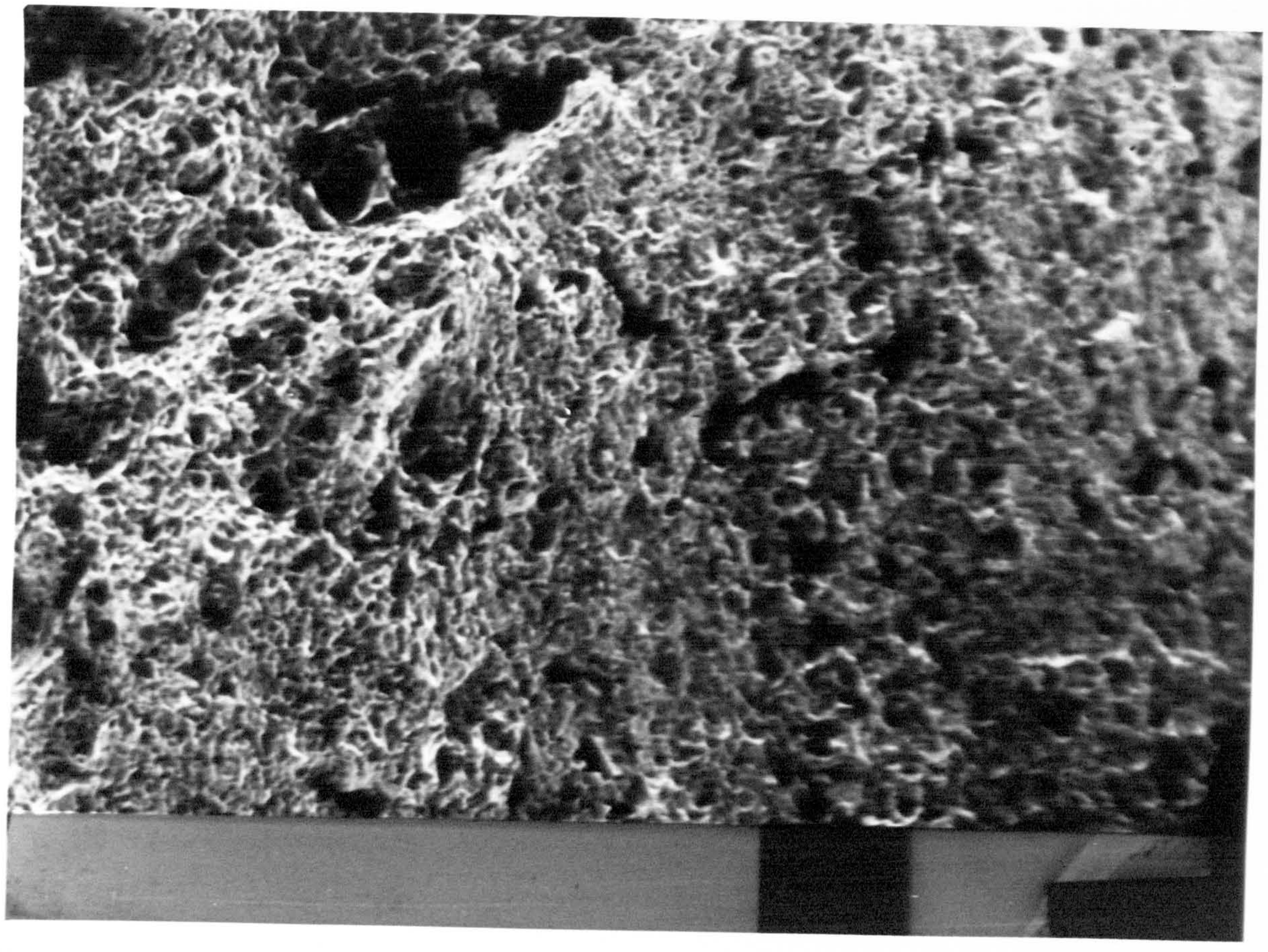

Slow strain rate test : air : x500 : 20° tilt
general view of middle part of cup

Figure 4.47

figures 4.49 and 4.50

figure 4.54

figures 4.51 → 4.53

Slow strain rate test : NaCl,-1.2V(sce)

x20 : 0^{o} tilt

top view of fracture surface

Figure 4.48

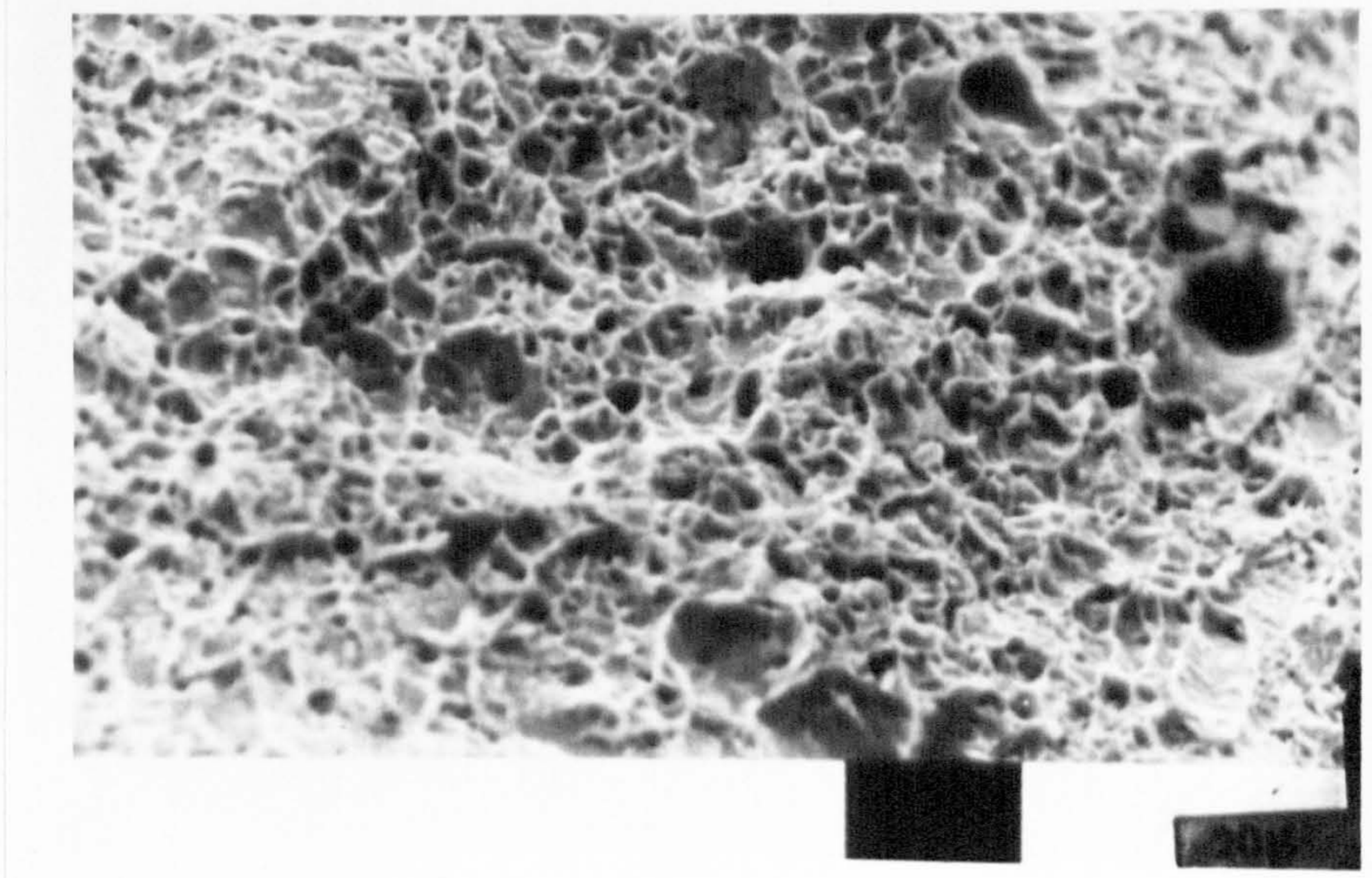

Slow strain rate test : NaCl, -1.2V(sce)

x1000 : 0^{o} tilt
ductile fracture
Figure 4.49

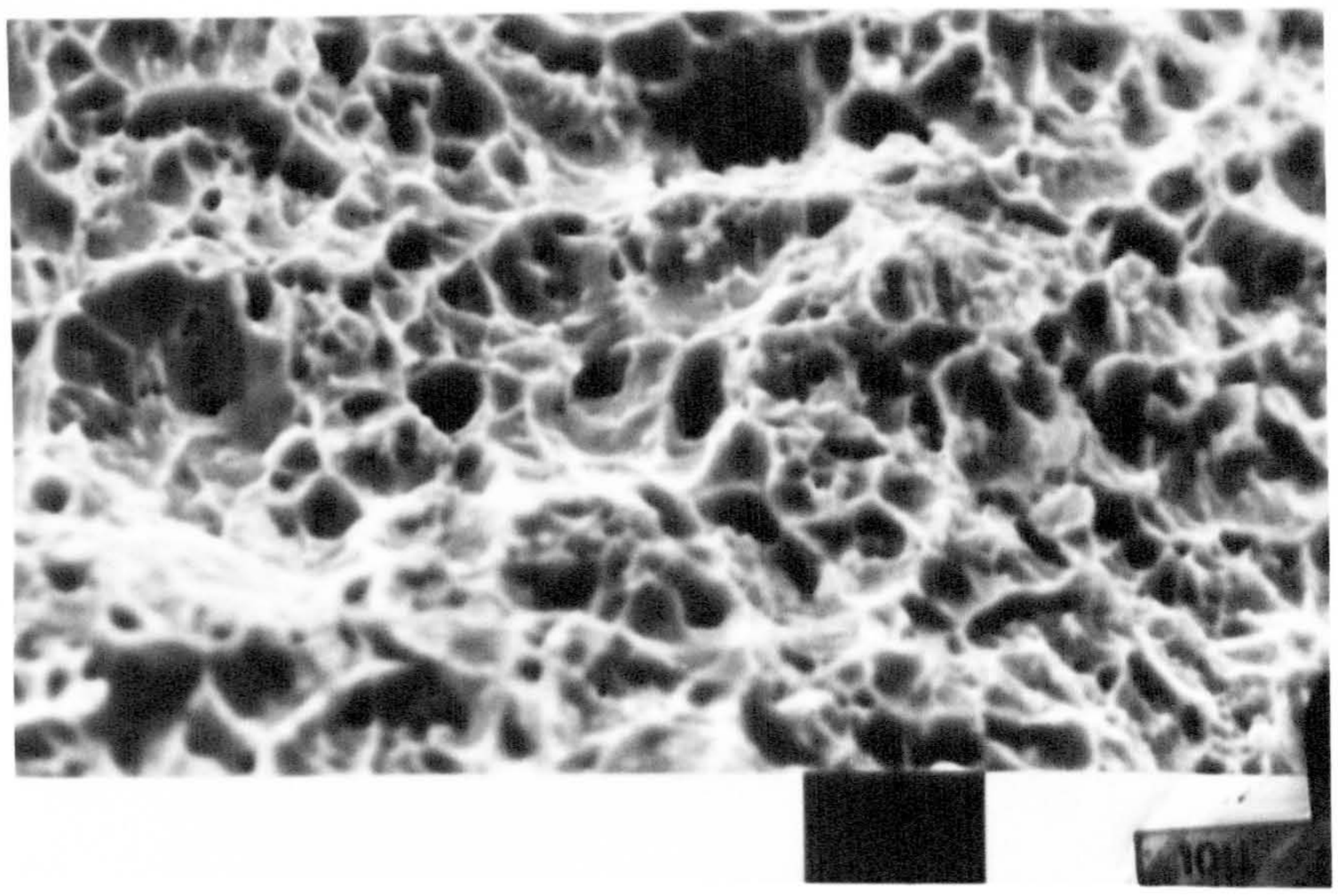

Slow strain rate test : NaCl, -1.2V(sce)

x2000 : 0^{o} tilt
detail of figure 4.49
Figure 4.50

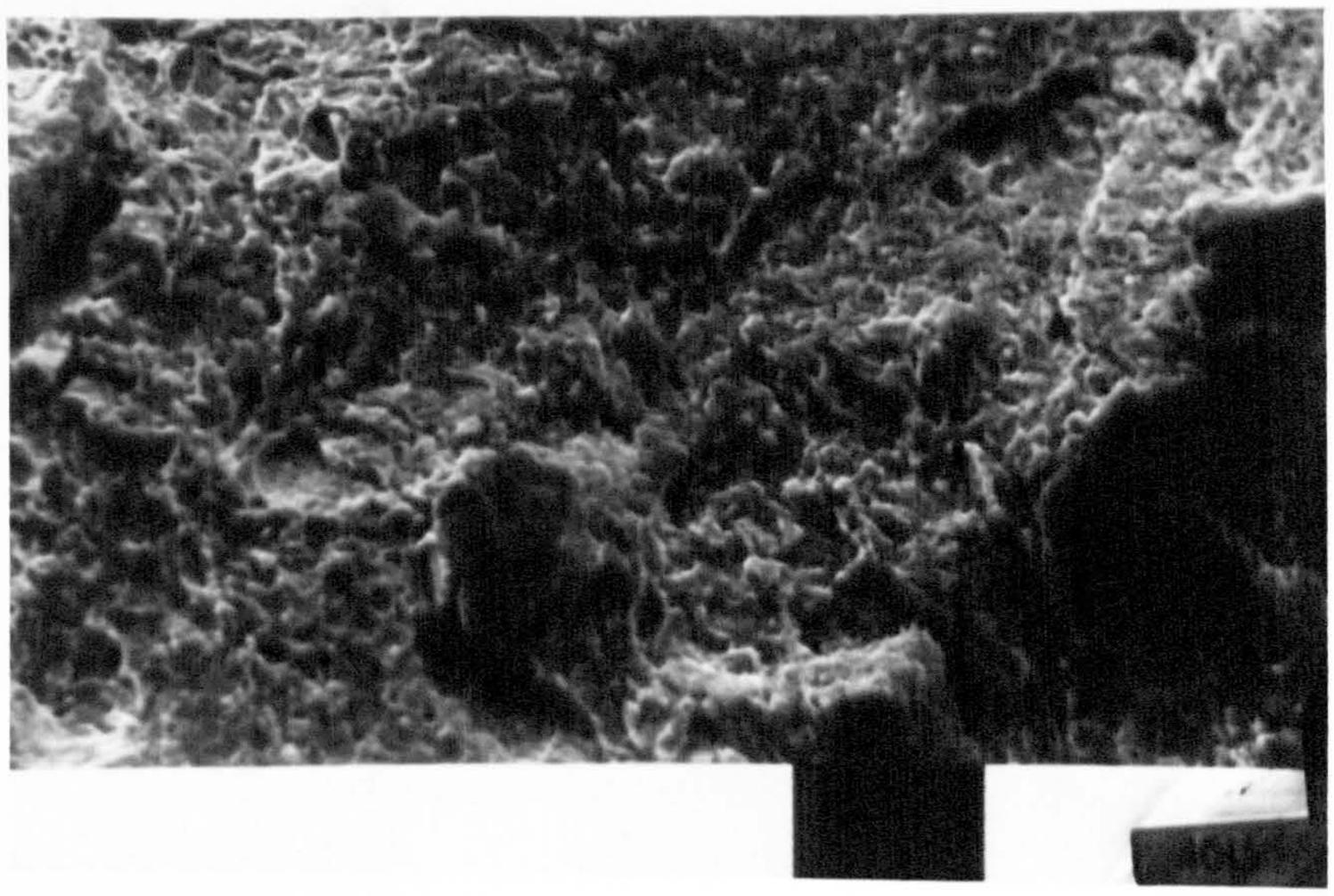

Slow strain rate test : NaCl, -1.2V(sce)

x500 : 0^{o} tilt

Figure 4.51

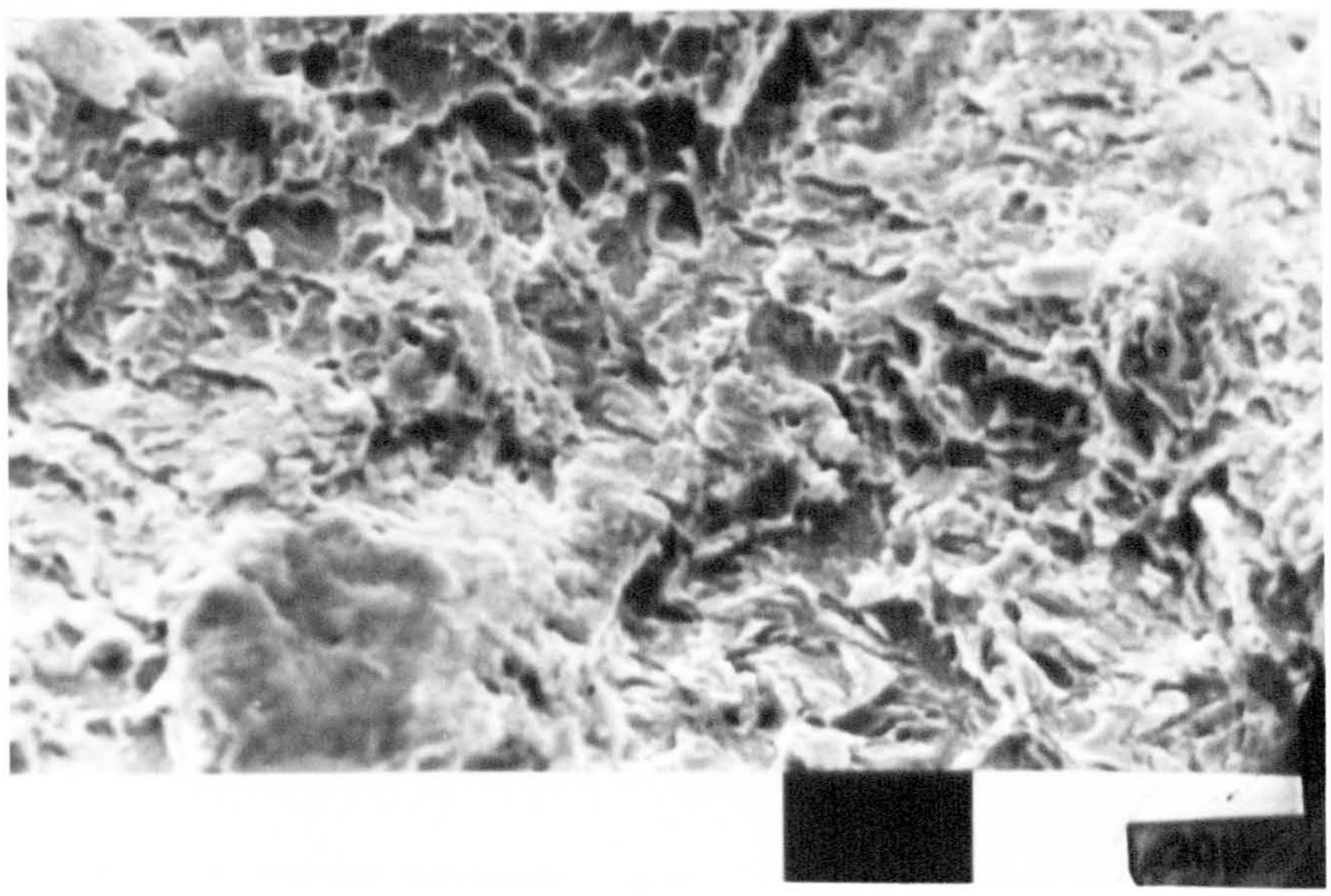

Slow strain rate test : NaCl, -1.2V(sce)

x1000 : 0^{o} tilt

detail of figure 4.51

Figure 4.52

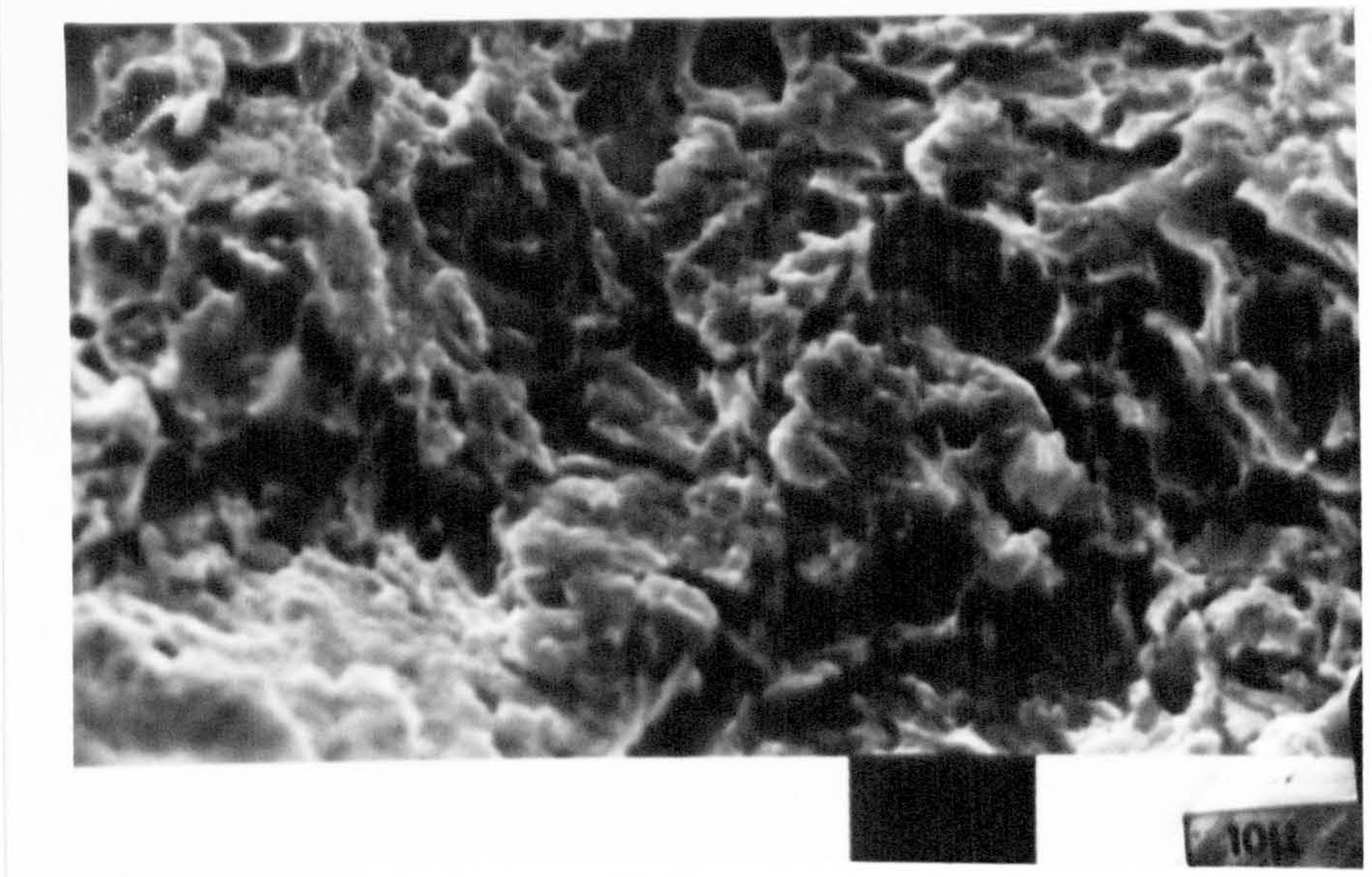

Slow strain rate test : NaCl, -1.2V(sce)

x2000 : 0^{o} tilt
detail of figure 4.52
Figure 4.53

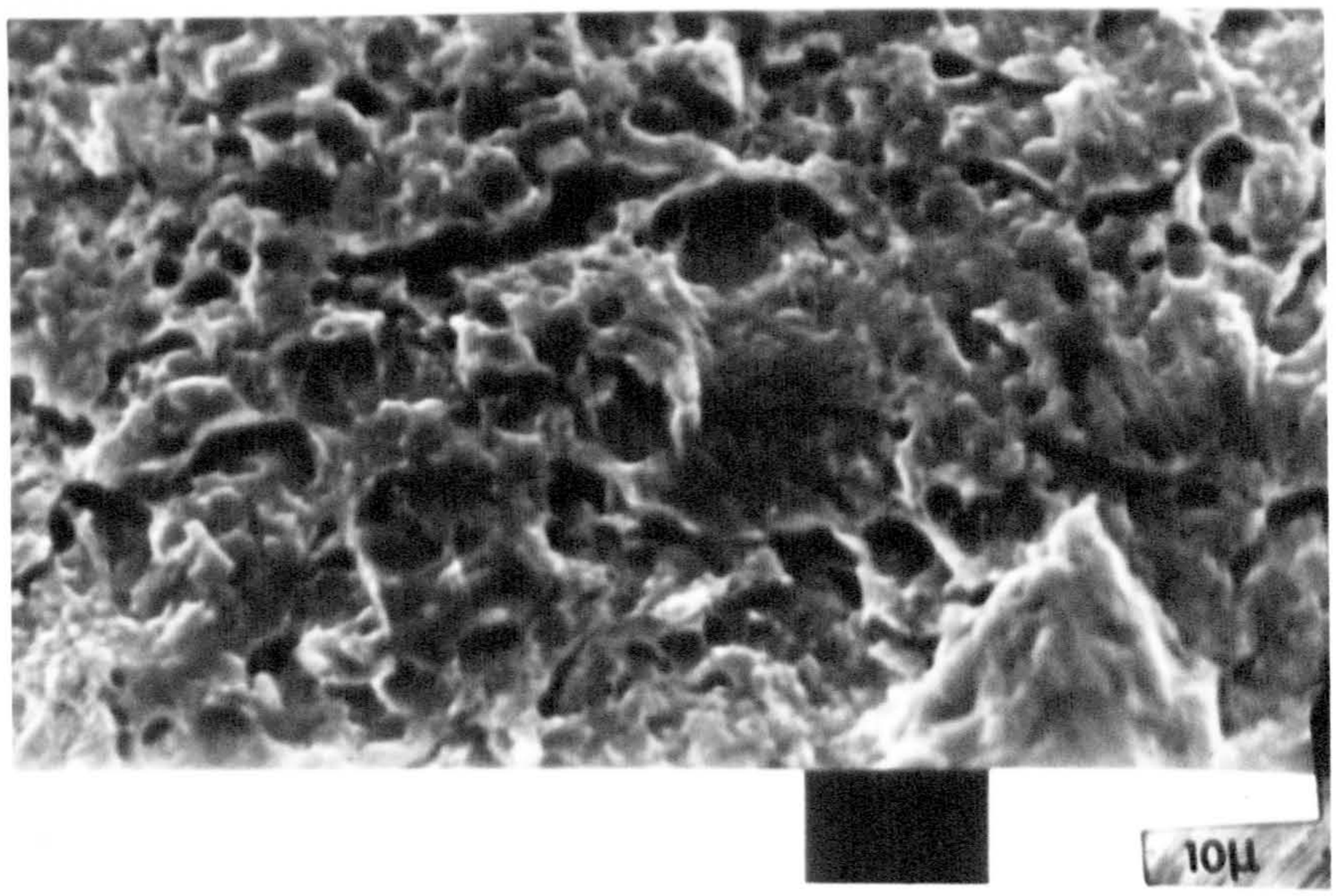

Slow strain rate test : NaCl, -1.2V(sce)

x2000 : 0^{o} tilt
Figure 4.54

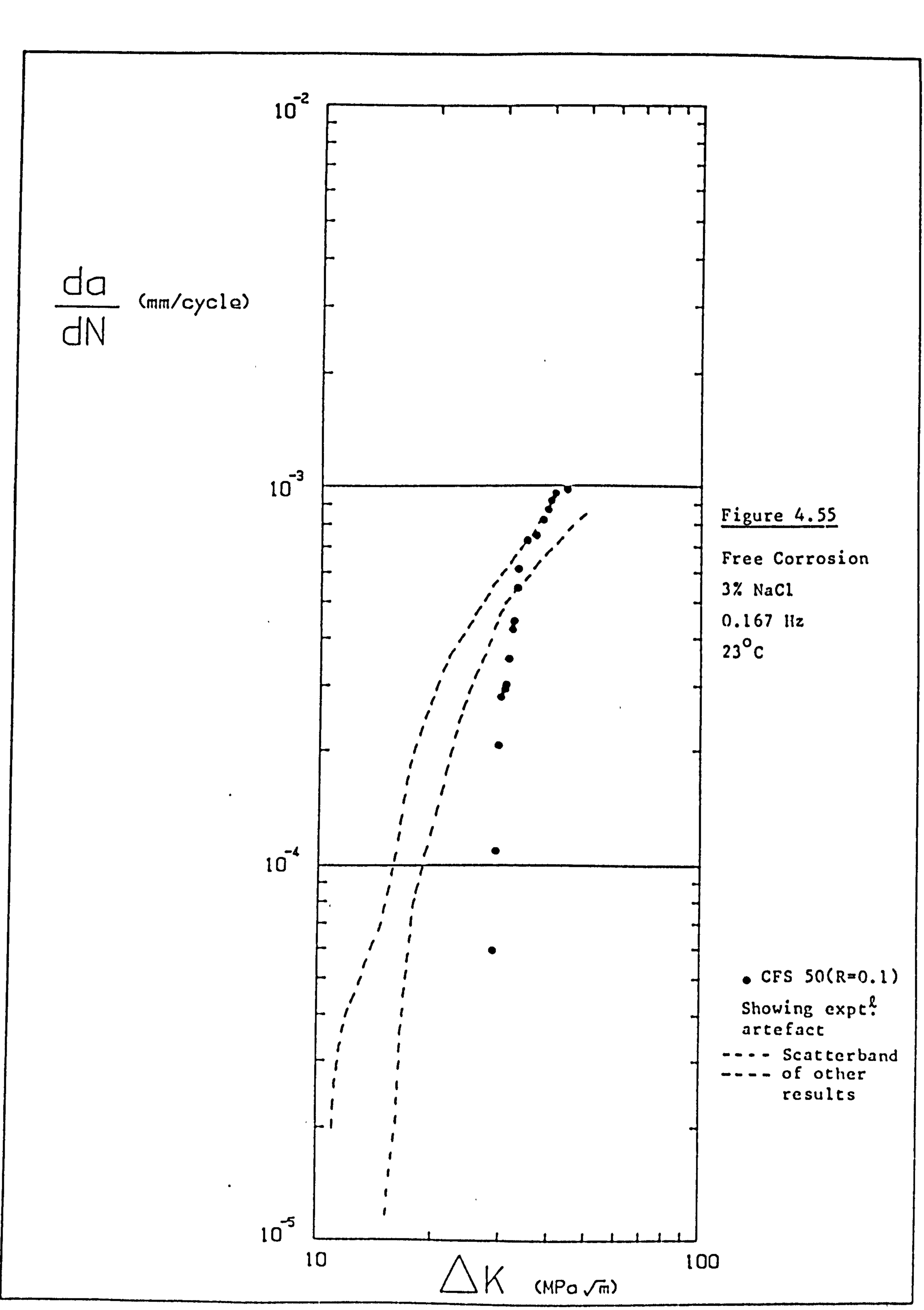

Figure 4.55

Free Corrosion

3% NaCl

0.167 Hz

23°C

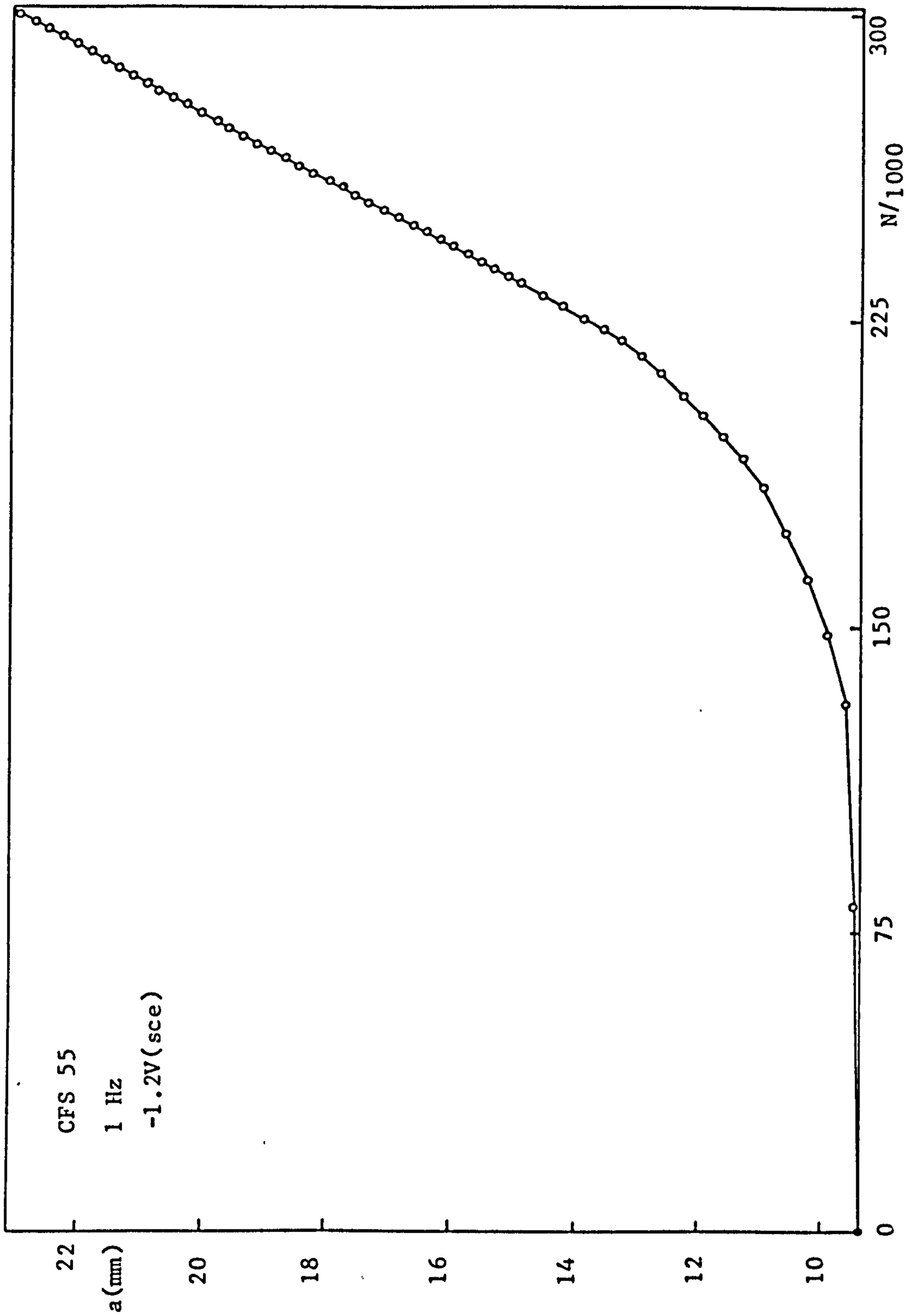

Figure 4.56

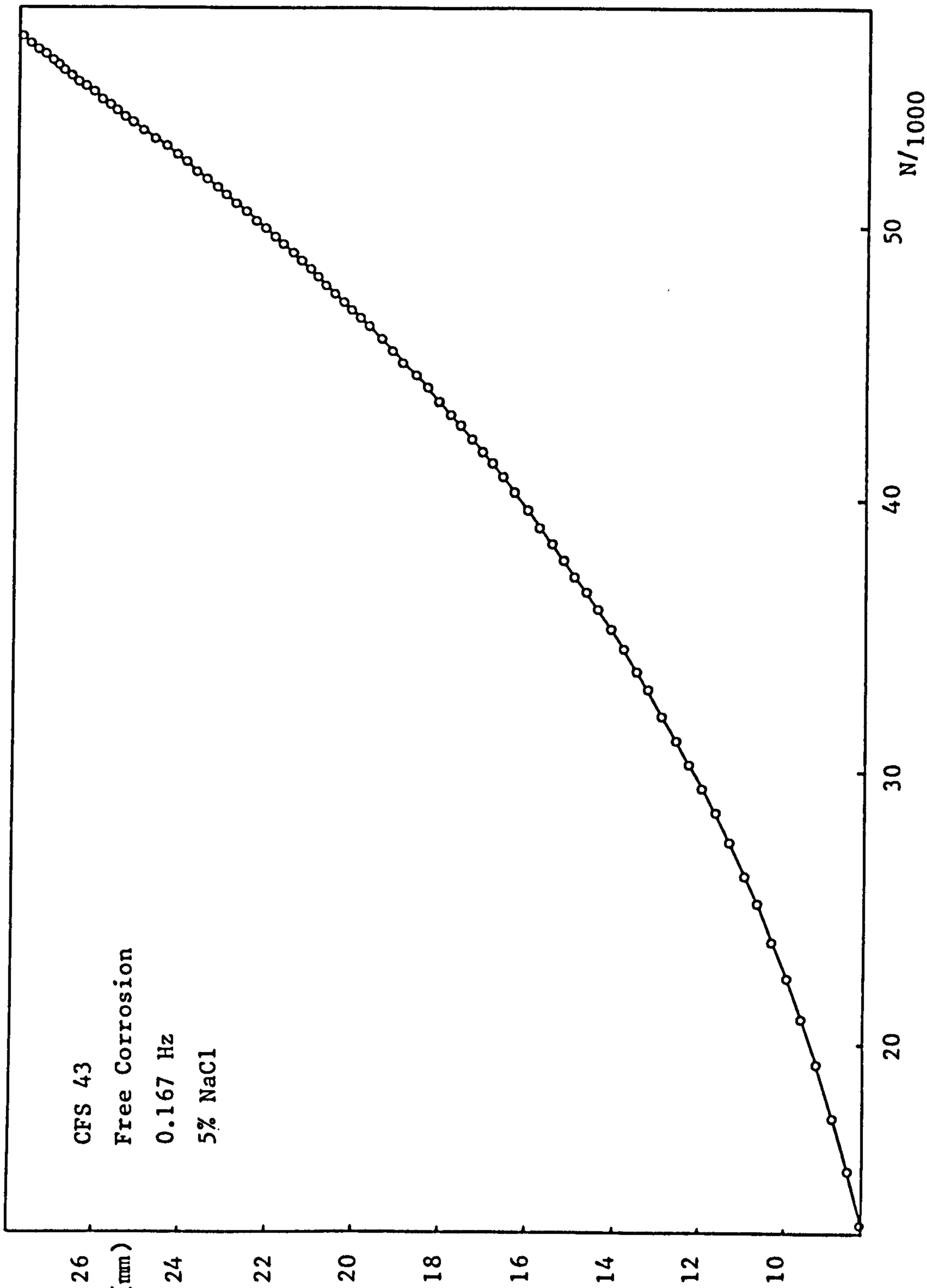
CFS 43
Free Corrosion
0.167 Hz
5% NaCl
a(mm)
26
24
22
20
18
16
14
12
10
20
30
40
50
N/1000

Figure 4.57

5.0 Discussion

5.1 Mechanisms of environmentally assisted crack growth.

The effects of the solution additives show that both hydrogen embrittlement and anodic dissolution can cause enhancement of corrosion fatigue crack growth rates.

From figures 4.1, 4.2, 4.5 and 4.7 it is seen that the crack growth rates were the same for the following conditions:

NaCl : +0.25V(sce) and free corrosion
Chloroplatinic acid : +0.25V(sce), free corrosion and -1V(sce)
Arsenate : +0.25V(sce)

This implies that the mechanism of enhanced crack growth is the same for all of these conditions. In particular it appears that the potential does not affect the crack growth rate in the chloroplatinic acid, that is for potentials within the range used this study.

Thus for free corrosion the addition of chloroplatinic acid to the solution does not alter the crack growth rate, even though it reduces the flux of hydrogen entering the metal. This behaviour shows that the mechanism of environmentally assisted crack growth during corrosion fatigue in 3% NaCl at the free corrosion potential appears to be anodic dissolution. This conclusion is reinforced by the results obtained in free corrosion for the thiourea solution. The presence of thiourea leads to a reduction in the crack growth rate for $\Delta K > 16 MPa\sqrt{m}$. This is due to the inhibition of the corrosion reactions by thiourea. It is significant that for $\Delta K > 20 MPa\sqrt{m}$ the thiourea results show little environmental effect as thiourea should only hinder the dissolution mechanism. Indeed, because of its poisoning action on the hydrogen recombination reaction, thiourea should aid the operation of a hydrogen embrittlement mechanism (cf. section 3.2.3).

An addition of arsenate to the solution caused the crack growth rate for free corrosion to be greater than in the NaCl, for $\Delta K < 25 MPa\sqrt{m}$. This indictes that the arsenic sufficiently enhances the flux of hydrogen into the metal to enable a hydrogen embrittlement mechanism to occur. As mentioned in section 3.2.3 the free corrosion potential of -0.65V(sce) is at the most positive end of the potential range over which arsenate poisons the hydrogen recombination reaction. This

would account for the irreproducibility of the results for $\Delta K<25MPa\sqrt{m}$: the variation in crack growth rate reflects the variation in the promotion of hydrogen entry into the metal by the arsenic. For $\Delta K>25MPa\sqrt{m}$ the crack growth mechanism in the arsenate solution appears to be the same as for the NaCl and chloroplatinic acid solutions, viz. anodic dissolution.

Polarizing the specimen to -1V(sce) should promote hydrogen embrittlement, and suppress anodic dissolution. However this does not happen in the chloroplatinic acid solution. The concentration of dissolved platinum is sufficient to deposit enough platinum black on the crack surface near the crack tip region to completely counter the effect of specimen polarization. (The rate of hydrogen entry into the metal may be not greatly increased by polarizing to -1V(sce) due to the platinum deposit.) The crack growth mechanism in the chloroplatinic acid solution at -1V(sce) remains that of anodic dissolution, as seen in figure 4.5. A dissolution mechanism is able to operate at this potential for two reasons :

(a) the bare surface reversible potential is more negative than for a filmed surface. As mentioned in section 2.3.1 the bare surface reversible potential is expected to be between ≈-0.8V and ≈-1V(sce).

(b) a large potential drop may exist within the crack as a result of hydrogen gas bubbles (cf. section 2.2.1), which are formed on the platinum deposited on the crack faces.

At -1V(sce) the crack growth rates in the NaCl and arsenate solutions are very different from those in the chloroplatinic acid solution. This is consistent with the operative mechanism of crack growth in these solutions being hydrogen embrittlement. The plateau is caused by a limit existing in the rate at which hydrogen can be supplied to the region at which the embrittlement occurs. Thus the plateau occurs at a greater value of da/dN in the NaCl than for the arsenate or thiourea solutions as both arsenate and thiourea can inhibit the corrosion reactions (cf. 3.2.3), so reducing the hydrogen flux into the metal. The reason that the crack growth rate in the arsenate solution is the same as in air for values of $\Delta K>32MPa\sqrt{m}$, is that the normal mechanical striation mechanism that occurs in air is then capable of producing crack growth at a rate that outstrips the

supply of hydrogen to the embrittlement zone.

At an externally applied potential of +0.25V(sce) the crack tip potential is only ≈-0.55→0.6V(sce) (cf. section 2.2.1). This is sufficient to prevent any action by arsenate in promoting hydrogen entry into the metal. Consequently the crack growth mechanism in the NaCl, arsenate and chloroplatinic acid solutions is the same, viz. anodic dissolution. However the anodic production of H_2S from the thiourea (cf. section 3.2.3) at this potential results in the stimulation of hydrogen entry into the steel. This could cause a hydrogen embrittlement phenomena to be responsible for the environmentally assisted crack growth. The crack growth rate decrease as ΔK increases may be caused by transport limitations down the crack. As the crack length increases the crack tip becomes increasingly remote from the sites at which H_2S is produced, and so the transport of H_2S along the crack could then limit the stimulation of hydrogen entry into the steel. As observed for the arsenate solution at -1V(sce) the crack growth rate follows the air upper bound line when a striation mechanism causes faster crack growth then the hydrogen embrittlement mechanism.

Thus it is seen that the effect of the solution additives is entirely consistent with the hypothesis that both anodic dissolution and hydrogen embrittlement occur as mechanisms of environmentally assisted crack growth, for the corrosion fatigue of BS4360:50D steel.

The conclusions reached as a result of using the solution additives are corroborated by the effects of specimen potential upon the crack growth rate. Scott and Silvester [139] obtained the results shown in figure 5.1 (for BS4360:50D at 0.1Hz, 20°C, R<0.1, 20<ΔK<40MPa$\sqrt{m}$, in seawater). Similar results were obtained in this study, as shown in figure 5.2 (this is based on the data shown in figure 4.23). These results show that the crack growth rate enhancement is at a minimum for potentials between -0.7 and -0.8V(sce), in both seawater and sodium chloride solution. As the potential is lowered beyond -0.8V(sce) the crack growth rate enhancement increases. This is due to the formation of a greater amount of hydrogen at the crack tip as a result of the overprotection. The increased amount of hydrogen entering the metal causes a greater amount of hydrogen embrittlement to occur. At potentials more positive than -0.7V(sce) the increase in crack growth rate enhancement is consistent with the occurrence of a dissolution mechanism.

The presence of oxygen at the crack tip should allow the oxygen reduction reaction :

$$O_2 + 2H_2O + 4e^- \rightarrow 4OH^- \qquad (5.1)$$

to occur as well as, or instead of, the hydrogen evolution reaction. This would provide an increase in metal dissolution at the crack tip without increasing the formation of hydrogen there. Thus a lowering of the oxygen concentration at the crack tip should only reduce the crack growth rate if a dissolution mechanism is operating. For BS4360:50D in seawater it has been reported [192-194] that lowering the oxygen content of the bulk solution does in fact reduce the crack growth rate enhancement under free corrosion conditions, but not at -0.85V or -1V(sce). Again this is consistent with the hypothesis that both anodic dissolution and hydrogen embrittlement can cause enhanced crack growth rates in this system. At free corrosion the anodic dissolution mechanism is dominant, but for potentials below -0.85V(sce) the hydrogen embrittlement mechanism predominates.

For X65 in 3.5% NaCl solution the results of Hinton and Procter [195,196] suggest that hydrogen embrittlement would only occur at impressed potentials lower than -0.8V(sce). The slow strain rate testing performed in the present study on BS4360:50D in 3% NaCl solution has produced results that are broadly similar to those of Hinton and Procter, as seen from figure 5.3. This provides yet more evidence that hydrogen embrittlement does not significantly affect corrosion fatigue crack growth rates for potentials more positive than -0.75V(sce).

The slow strain rate results given in figure 4.15 show a significant effect of the solution additives, except for the arsenate. The chloroplatinic acid reduced the deleterious effect of cathodic polarization, in accordance with the description of its action given in section 3.2.3. These results also show that although the deposition of platinum black upon the specimen surface does reduce the flux of hydrogen entering the metal, it does not entirely suppress it. The addition of thiourea to the solution led to a marked increase in embrittlement during these tests for potentials below -1V(sce). This is consistent with the poisoning action of thiourea upon the hydrogen recombination reaction, as desribed in section 3.2.3. The severity of the effect of the thiourea addition indicates that decomposition to form H_2S may well be occurring at these large negative potentials [184]. For potentials more positive than -0.9V(sce) the thiourea has

little effect compared to in air.

In many fields of science processes are envisaged as being the result of the simultaneous action of two or more different mechanisms. Parkins [74] has pointed out that there is no reason why this should not be true for environmentally assisted cracking. Thus although cracking in some systems appears to be unequivocally associated with either hydrogen embrittlement, (eg. high strength steels in hydrogen forming environments) or dissolution (eg. C-Mn steels in CO_3^{2-}/HCO_3^- solutions), the crack tip conditions for many systems may be such that both hydrogen embrittlement and anodic dissolution mechanisms are possible. This is true for BS4360:50D in 3% NaCl solution. He concluded that both mechanisms were operative in the stress corrosion cracking of a low strength ferritic steel in phosphate solutions, and of a high strength maraging steel in chloride solutions. At cathodic potentials hydrogen embrittlement was held to be responsible for the crack growth, but at sufficiently noble potentials a dissolution mechanism occurred. At intermediate potentials it was suggested that a mixed mechanism operates. The possibility was discussed that in such a case the crack moves forward with regions of the crack front advancing as a result of a dissolution mechanism, and adjacent portions of the crack front undergoing advance via a hydrogen embrittlement mechanism.

In a study utilizing Mode I/III loading techniques Green et. al. [150] concluded that SCC of Ti-8Al-1Mo-1V in 3.5% NaCl was caused purely by hydrogen embrittlement, but α-brass in aqueous ammonia failed by a dissolution mechanism. However for a 7075-T6 Al alloy in 3.5% NaCl + 3% $K_2Cr_2O_7$, pH=3.2, solution the results suggested that both mechanisms could occur. The addition of 10ppm As to the solution enhanced cracking in Mode I, but retarded it in Mode III. This is consistent with hydrogen embrittlement being the predominant cracking mechanism under Mode I loading, but being suppressed under Mode III. Thus for Mode III, cracking by the slower dissolution mechanism can be observed. Arsenic reduces the crack growth rate in Mode III because of its inhibitiary action on the cathodic reaction.

Although in his earlier work Scott [192] agrees with the concept of two operative mechanisms, with anodic dissolution dominant at the free corrosion potential, he later retracted this viewpoint [140]. His original assertion had acknowledged that the effects of bulk oxygen concentration upon the fatigue crack growth rate were difficult to interpret in terms of a hydrogen embrittlement mechanism. The

subsequent change of opinion appears to have been based on the observation that the crack growth rate exhibits a slow transition to its new value upon altering the cyclic frequency. Also initial hydrogen charging was held to be responsible for the incubation time observed in experiments (cf. section 4.5). It was suggested [140] that as a result of the incubation periods observed corrosion fatigue experiments should last longer than about 1 month. In the present work incubation times were only observed in those conditions where hydrogen embrittlement was held to be responsible for the environmentally assisted crack growth, as illustrated by figures 4.56 and 4.57. However, the observed transients and incubation times are not necessarialy just a result of the establishment of an equilibrium distribution of hydrogen around the crack tip [30,158]. Time is also needed to establish the steady state values of potential and pH at the crack tip (cf. section 2.2), this may take 2-4 days and so account for some of the transient behaviour [30,158]. In seawater an additional factor is the time dependent deposition of calcareous deposits on the metal surfaces [30,158]. For free corrosion conditions the rate at which the steady state value of oxygen concentration is attained is important. This could explain the transients observed by Scott for an experiment at free corrosion and a constant ΔK of 12MPa$\sqrt{m}$ (no transients were seen in a similar experiment with ΔK=14.5MPa$\sqrt{m}$, possibly as a result of increased pumping at the higher value of ΔK). Thus it appears that Scott has not presented any results that conflict with the hypothesis presented earlier that both hydrogen embrittlement and anodic dissolution can cause enhanced crack growth rates for BS4360:50D in chloride solutions.

Austen has also discounted anodic dissolution as a mechanism of environmentally assisted crack growth [17,78,197,198]. His objection is primarily based upon a short study [199] in which he concluded that the necessary current densities would be too high. As will be shown later in this thesis this objection is not valid for the system studied in this work. Also it should be noted that Austen and West overestimated the required current densities by assuming that the dissolution mechanism only operates during 1/10th of the fatigue cycle. Austen has produced a model [17,198] of corrosion fatigue crack growth in which the enhanced crack growth rate is assumed to be caused by hydrogen embrittlement. The role of anodic dissolution is taken to be that of blunting the crack tip, and so causing the effective applied ΔK to be reduced. This model would not be able to

predict the form of figure 5.2 as increasing the amount of cathodic protection should decrease the blunting effect, so leading to a larger crack growth rate. As hydrogen transport through the lattice is assumed to govern the amount of crack growth caused by hydrogen embrittlement, the hydrogen embrittlement component of the model should be unaffected by cathodic protection. The inability of Austen's model to predict the form of figure 5.2 must raise doubts about its validity. In addition, in order to fit the model to experimental data a very high value has to be assumed for the hydrogen diffusion coefficient, together with a rather low value of the bare surface current density [198]. It will be shown in the next chapter that the hypothesis presented in this section enables a phenemonological model of corrosion fatigue behaviour of BS4360:50D in 3% NaCl to be constructed. Thus Austen's rejection of anodic dissolution as a mechanism of crack growth for BS4360:50D in chloride solutions [198] is not substantiated by the available evidence.

Before this point the discussion has not made any reference to the available fractographic evidence. In air the fatigue crack growth was observed to involve the formation of ductile striations. Secondary cracking was also observed. These features can be seen in figures 4.34 to 4.36, and are in accord with the results of reference [200]. At low values of ΔK ($\approx$10MPa$\sqrt{m}$) some intergranular failure has been found in air [200], and at high values of ΔK the static ductile failure mechanism of void nucleation and growth also occurrs [200]. Thus for the range of values of ΔK used in this study ($\approx$12$\rightarrow$40MPa$\sqrt{m}$) crack growth in air occurred mainly by the classical plasticity induced fatigue crack growth mechanism.

For crack growth under free corrosion conditions in seawater patches of intergranular failure were seen at ΔK=14MPa$\sqrt{m}$ [193]. Misawa et. al. [201] have observed similar patches of intergranular failure at low values of ΔK for a 0.5Cr-0.5Mo-0.25V low alloy steel in distilled water at free corrosion. At a value of ΔK=32MPa$\sqrt{m}$ for BS4360:50D in seawater, free corrosion, indistinct ductile striations were seen [200]. The fracture mode was reported [200] to be generally little changed by the seawater environment, as opposed to in air. Some results from this study are shown in figures 4.37 and 4.38 for the free corrosion case. Although the resolution of the microscope was not adequate to resolve significant details on the fracture surface figures 4.37 and 4.38 do have a brittle appearance. This may be seen by comparing them to figure 4.39, which shows part of the surface

created when the fatigue specimens were cooled in liquid nitrogen and broken open. It is possible that dissolution along strain generated active paths modifies the effect of crack tip plasticity, and so produces a more brittle looking fracture surface.

With cathodic protection to below -0.85V(Ag/AgCl) in seawater small cleavage facets were found, sometimes with evidence of regular parallel markings [200]. Such facets were also seen in this work as shown in figures 4.40 and 4.41. Some workers [139,196] have reported that the number of these facets increases as ΔK increases towards the value at which the plateau region of crack growth begins. At -1V(Ag/AgCl) failure was by both intergranular cleavage and transgranular cleavage [200], with intergranular cleavage and ductile failure below about ΔK=20MPa$\sqrt{m}$, but by mixed ductile transgranular failure and transgranular cleavage at higher values of ΔK. Possible regions of transgranular cleavage were seen in this study as shown in figure 4.42. Figure 4.44 shows a fracture surface produced in ASTM artificial seawater at -0.85V(sce). It has a similar appearance to figure 4.52, and the majority of the fracture surface shows signs of quasi-cleavage as the failure mode. For cathodically protected specimens the crack growth rates at higher values of ΔK were within the air scatterband due to the operation of a normal striation mechanism as shown in figure 4.45.

Thus it appears that the effects of solution additives, bulk oxygen content and specimen potential are consistent with the dual mechanism hypothesis. The limited fractographic evidence available would also suggest that the mechanism of crack growth at free corrosion and -1V(sce) may not be the same [200]. It appears that anodic dissolution controls the environmental component of crack growth at free corrosion, and hydrogen embrittlement that at -1V(sce).

5.2 Effects of loading/environmental variables.

Following on from the investigation into the mechanisms of environmentally assisted crack growth a study was undertaken into the influence of several environmental and loading variables. The factors investigated were potential, frequency, R ratio (ie. K_{min}/K_{max}), waveform, NaCl concentration and temperature. The influence of each of these variables (except potential) upon fatigue crack growth was determined at both free corrosion and -1V(sce). It was decided to use both free corrosion and -1V(sce) potentials as these corresponded to regimes in which the environmentally enhanced crack growth rates were caused by anodic dissolution and hydrogen embrittlement respectively.

5.2.1 Air data.

A reliable base line for crack growth in air is obviously of importance for corrosion fatigue studies. Figure 4.20 compares the crack growth data in air for BS4360:50D obtained by several workers [190,192,193,202]. It is found that a good agreement exists between the data obtained by Bretherton et. al. [202] and that obtained at Glasgow University (GU) [190]. The results given by Bretherton et. al. consist of two straight lines on the log da/dN vs. log ΔK plot, intersecting at $\Delta K \approx 25 MPa\sqrt{m}$. These lines lay within the scatterband obtained at GU over the whole range of ΔK that was used in this study. The air upper bound line obtained at $R<0.1$ by Scott and Silvester [192] lay within the scatterband for the GU data for values of ΔK less than $22 MPa\sqrt{m}$. However this line lies above the GU data for higher values of ΔK. The line for $R>0.1$ obtained from ECSC sponsored research [203] does not agree with the GU data, or that of Bretherton et. al. In view of the aforementioned agreement between the data obtained by Bretherton et. al. and at GU the latter data was accepted as a reasonable air base line for the purposes of this study.

The values of the constants obtained at GU for the Paris law :

$$\frac{da}{dN} = A\,\Delta K^{m} \qquad (1.6)$$

were : $m = 2.92$

$A = 8.02 \times 10^{-9}$ (mean)
$A = 1.12 \times 10^{-8}$ (upper bound)
$A = 5.77 \times 10^{-9}$ (lower bound)

5.2.2 Potential.

The results obtained with different specimen polarization were presented in figure 4.23. Figure 5.2 shows how the crack growth enhancement alters with potential at constant values of ΔK. It is seen that a minimum occurs in the crack growth enhancement for a specimen polarization around -0.8V(sce). The work of Scott and Silvester [139] shown in figure 5.1 also shows a similar minimum, although this is at the slightly more positive potential of -0.7 to -0.75V(sce). The difference in the potential at which the minima occur is possibly due to the different frequencies used. It is unlikely to be due to the different R ratios, but another cause could be that Scott and Silvester used seawater as opposed to the 3% NaCl used in this work. This possibility that the potential at which the minimum occurs is different depending on whether 3%-3.5% NaCl or seawater is used has some experimental backing. In a study into the corrosion fatigue behaviour of Q1N steel at different potentials Galsworthy [204] obtained similar minima in both 3.5% NaCl and seawater. When the effects of calcareous deposits (at R=0 in seawater) are ignored both the R=0 and R=0.5 data show that the minimum in the 3.5% NaCl occurs at a potential that is about 50mV more negative than for the seawater. . The 50mV shift in the potential at which the minima occur is approximately the same as the difference between the potential observed in 3% NaCl from this work and that from Scott and Silvester's work [139] in seawater. It is not clear as to why this difference between seawater and NaCl solutions should exist. A comparison between figures 5.1 and 5.2 shows that the relative enhancement at free corrosion and -0.7V(sce) is unaffected by the differences in the solutions. However there is a difference at -0.8V(sce) which indicates that the seawater enhances the crack growth compared with 3% NaCl at this potential. A similar effect is also seen in the Q1N study [204]. The possibility therefore exists that the difference in the potential at which the minimum occurs could be explained on the basis that the seawater marginally increases the amount of hydrogen embrittlement that occurs at potentials around -0.8V(sce), when compared to 3% or 3.5% NaCl.

In the previous section the presence of the minimum was taken as further evidence that for BS4360:50D in chloride solutions the mechanism of corrosion fatigue crack growth could be either anodic dissolution or hydrogen embrittlement. Whilst this is the most

rational explanation, bearing in mind the supporting evidence, it has been suggested that a minimum could be caused by the effects of specimen polarization upon a hydrogen embrittlement mechanism [30,158]. Figure 5.4 (taken from reference [30]) illustrates this. However, the pH at which the minimum due to hydrogen embrittlement would occur is approximately 5.4 for BS4360:50D in 3.5% NaCl [30]. For free corrosion in seawater the crack tip pH is 7-8 rising to 11 or more at cathodic protection levels of -1V(sce) [49]. Turnbull [25] found little difference between 3.5% NaCl or seawater for the pH near the tip of an artificial crevice. His work also suggests that at free corrosion the crack tip pH is ≈7 rising to ≈11 at -1V(sce). Also a small difference in pH was observed between seawater and 3.5% NaCl at external polarizations below -0.9V(sce). This was held to be a result of the calcareous deposition that occurred in the seawater. Thus any explanation of the minimum in figure 5.2 based solely upon a hydrogen embrittlement mechanism limited by the rate of production of hydrogen at the crack tip would appear to be now ruled out.

In figure 4.23 the results obtained for the plateau at -1.2V(sce) lie only slightly above the results for the plateau at -1.1V(sce). This is entirely consistent with the large potential drop expected down the crack for external specimen polarization below ≈-1.1V(sce) [25,26], as mentioned in section 2.2.1. Thus the apparent limit in the fatigue crack growth rate at very negative potentials merely represents a limiting electrochemical state at the crack tip. It does not represent any mechanical limit to the possible rate of crack growth, a point that does not always appear to be appreciated [205].

Another important effect of cathodic protection is the formation of calcareous deposits. This is only applicable to the seawater situation. Calcareous deposits are caused by :

(a) during cathodic polarization the pH increases as a result of the following reactions :

$$O_2 + 2H_2O + 4e^- \rightarrow 4OH^- \qquad \text{(oxygen reduction)} \qquad (5.1)$$

$$2H_2O + 2e^- \rightarrow 2OH^- + H_2 \qquad \text{(reduction of water)} \qquad (5.2)$$

(b) as a result of the increase in pH the CO_3^{2-}/HCO_3^- equilibrium is moved towards the carbonate side :

$$HCO_3^- + OH^- \rightarrow CO_3^{2-} + H_2O \qquad (5.3)$$

(c) Calcium and magnesium salts are precipitated as their solubility products are exceeded :

$$Ca^{2+} + CO_3^{2-} \rightarrow CaCO_3(s) \qquad (5.4)$$

$$Mg^{2+} + 2OH^- \rightarrow Mg(OH)_2(s) \qquad (5.5)$$

The formation of calcareous deposits is encouraged by a lower flowrate, higher seawater temperature and more negative potentials [206]. As mentioned earlier the presence of calcareous deposits appears to slightly reduce the crack tip pH at specimen potentials below -0.9V(sce). The reason for this is that the calcareous deposit reduces the total cathodic reduction current in the crack, and thus lessens the formation of a high pH through reactions (5.1) and (5.2) [25]. It is unlikely that the small change in pH caused by calcareous deposits would significantly affect the fatigue crack growth rate (the change induced is about 0.5 of a pH unit, eg. from about 11.5 to 11).

The other effect of calcareous deposits is that they can induce crack closure, so reducing the crack growth rate due to the reduced applied alternating stress intensity. This has been proposed as an explanation for potential effects observed in E355 steel in ASTM artificial seawater [207]. Loss of adherence of the deposits was assumed to be the cause of the crack growth rates increasing with an increase in the degree of cathodic protection, at high levels of cathodic protection. The similar potential effects observed in this study, and by Galsworthy [204], using NaCl solutions show that this is not the case. Crack closure is discussed in more detail in section 5.2.4.

The shapes of the fatigue crack growth curves shown in figure 4.23 are similar to those obtained by Vosikovsky for X65 in 3.5% NaCl [72]. Region I, II and III behaviour can be seen in figure 4.23, although the tests were not performed with a sufficiently low starting value of ΔK so as to enable the region I behaviour to be defined. From figure 4.23 it is evident that the specimen polarization affects the region II behaviour, as discussed in this section, but not the region III behaviour. Whilst figure 4.23 shows that the slope of the region I line is obviously different for a hydrogen embrittlement mechanism as opposed to an anodic dissolution mechanism (see also reference [72]), the data is not sufficient to determine how the slope of the region I line varies with potential (or if it does at all) for the same crack growth enhancement mechanism. However Hinton and Procter [146,196] have reported that for X65 in 3.5% NaCl solution the slope of the

region I line does vary with potential, even over potential ranges at which hydrogen embrittlement is expected to dominate the cracking process. The different regions of the fatigue crack growth rate curves are discussed in more detail later in sections 5.3 and 5.4.

5.2.3 Frequency.

Frequency is widely recognized as an important variable for corrosion fatigue. Many workers have reported an effect of frequency upon corrosion fatigue crack propagation rates [14,72,140,192,196, 208-212]. The effect of frequency upon corrosion fatigue is a reflection of the time dependence of the chemical reactions and transport processes that cause the phenomena.

In his work on X65, X70 and HY130 Vosikovsky [72,166,208] has demonstrated the existence of distinct regions of behaviour on the da/dN vs. ΔK plot (although a correction for stress ratio effects in air was made for the X70 and HY130 data by plotting da/dN against ($\Delta K+xR$), where x is a numeric factor). The form of the crack growth rate curves found in the X65 and X70 are shown in figures 5.5 and 5.6. The region I behaviour was observed to be independent of frequency, for both the free corrosion and -1V(sce) potentials. The frequency independence of region I crack growth rates, which includes near threshold crack growth rates [72], explains Bardal's [213,214] observation of a lack of frequency dependence for very slow crack growth rates in DS52 steel in NaCl. 'A strong frequency effect was observed in the region II behaviour at both potentials. Vosikovsky's X65 data [72] showed that a small effect of frequency existed during region III, which was only observed at -1V(sce). The observed region III crack growth rates were within, or just above, the scatterband for crack growth in air.

The effect of frequency on crack growth rates in BS4360:50D was shown in figures 4.21 and 4.22. For the free corrosion condition region I and II behaviour is clearly observed, with the data obtained at 5Hz also indicating that at high values of ΔK the crack growth rate is the same as for the air lowerbound line. At a specimen potential of -1V(sce) region II and III behaviour was observed. Region I behaviour was not positively observed because the fatigue tests were not begun at a low enough value of ΔK. The data does however suggest that a similar region I exists, but is not sufficient to prove it. No frequency effect was observed for region III and the data lay within the air scatterband, this is in contrast to Vosikovsky's observations on X65 [72]. The results from this study are shown plotted on a time basis (as recommended for corrosion fatigue work [98]) in figures 5.7 and 5.8. Figure 5.7 shows that for free corrosion the transition between region I and region II behaviour occurs at a velocity between

1.5 and 2 μm/s. The crack growth velocities during the region II are not similar. This behaviour indicates that although the onset of region II is governed by a time dependent process, in region II the crack growth mechanism includes a contribution from a time-independent process. This point is taken up further in section 5.3. At an impressed potential of -1V(sce) the region II crack velocities also lay within a narrow range of values, viz. 1.6-3 μm/s. Thus the region II crack velocities are governed by a time dependent process, unlike those of regions I and III. Even when using a load stepping technique such as Vosikovsky's [208] the time needed for tests at very low frequencies is considerable. Consequently the most comprehensive investigations into the effect of frequency on corrosion fatigue crack growth rates have used a constant ΔK method of testing.

In a very useful piece of work Gallagher et. al. [215] showed that for 4340 steel the effect of frequency differed for the above K_{1SCC} and below K_{1SCC} cases. Some of his results are shown in figures 5.9(a) and 5.9(b). For the above K_{1SCC} case the crack growth velocity became independent of frequency at very low frequencies. This behaviour reflects the ability of the cracks to grow by stress corrosion cracking under a constant load (ie. frequency=0Hz). The superposition model of Wei and Landes [15] was found to underestimate the experimental results by up to a factor of 2 over the intermediate frequency range. This is because of the model's failure to include any component of environmental crack growth at $K_{max}<K_{1SCC}$, which in practice occurs to a significant extent over this intermediate range of frequencies.

At very low frequencies for the below K_{1SCC} case the crack growth was found to be cycle dependent, with the environmental contribution to the crack growth independent of frequency. This is the same as for the region I data observed by Vosikovsky [72] and in this work. At high frequencies the crack growth velocity was the same as in air, as expected. However, over an intermediate range of frequencies, the environmental component of crack growth increased as the frequency decreased. The intermediate frequency range was similar to the one mentioned above for which the superposition model underestimated the above K_{1SCC} crack growth velocities; this would tend to confirm the reason given above as to the model's shortcoming. Gallagher et. al. interpreted the cyclic dependency of the environmental component of corrosion fatigue crack growth at very low frequencies as meaning that "fatigue action is a prerequisite for environmental attack for below K_{1SCC} corrosion fatigue". This is in agreement with the concept of

K_{1SCC} as representing the K value at which a statically loaded crack can just maintain a sufficiently rapid rate of straining at the crack tip, so as to avoid crack arrest as a result of film growth at the crack tip. Thus K_{1SCC} is seen merely as a result of the competition between crack tip strain and repassivation of the bare surface [62], rather than as representing the kind of material property envisaged by Oriani in his hydrogen embrittlement model [101].

Obviously Gallagher et. al.'s observations for the below K_{1SCC} case are of most interest from the point of view of this work. For the below K_{1SCC} case intuition would suggest that as the frequency is reduced to extremely low levels the crack growth behaviour should approach that in air, ie. no environmental component of crack growth is expected at ultra-low frequencies. This is because for SCC (ie. f=0Hz) no environmental crack growth occurs, and as mentioned in section 1.2.3 SCC is only a limiting case at one end of the corrosion fatigue spectrum. Although Gallagher et. al.'s work did not show the expected behaviour it is possible that they did not use sufficiently low frequencies (it is reported that for these tests K_{max} was close to K_{1SCC}, which suggests that an ultra-low frequency would be needed to observe the expected effect). Also in a separate study on HY80 below K_{1SCC} in 3.5% NaCl [14] the environmental component of crack growth did appear to decrease below 0.01Hz. Other similar work [60,61,157] has shown that the expected behaviour can occur. Atkinson and Lindley [60,61,142] have studied a number of systems and for an aqueous environment they found that the crack growth rate increased as the frequency decreased, until a critical frequency was reached. Below the critical frequency the crack growth rate decreased with decreasing the frequency. One system studied was a C-Mn structural steel in lakewater and distilled water [61], at free corrosion. As in this work no effect of chloride concentration was noticed, as regards corrosion fatigue under free corrosion conditions, these results should be directly comparable to the present work. Two different values of ΔK were used by Atkinson and Lindley, and the results are shown in figure 5.10. At low values of ΔK the results of this work, and those of Vosikovsky [72], show the aforementioned region I behaviour, with a consequent range of frequency existing over which the environmentally assisted crack growth rate remains constant. Atkinson and Lindley's results showed no such region : it is not obvious why the discrepancy arises between their results and those of the present work. One possibility is that for the steel used by

Atkinson and Lindley region I crack growth occurs at lower values of ΔK than for X65 or BS4360:50D, ie. the region I is displaced to the left on the da/dN vs. ΔK plot. However, at the higher ΔK value used by Atkinson and Lindley, 50MPa√m, their results agree very well with those of Vosikovsky [72] on X65. Unfortunately Vosikovsky's results do not extend to frequencies below 0.01Hz, so it is not possible to see if the decrease in crack growth rate with decreasing frequency found by Atkinson and Lindley applies to X65 in 3.5%NaCl. At a value of ΔK of 50MPa√m Vosikovsky's work showed that X65 would exhibit region I behaviour at frequencies just below 0.01Hz, that is if the effect found by Atkinson and Lindley does not occur. More experimental work is required before the corrosion fatigue behaviour of steels such as BS4360:50D and X65 at ultra-low frequencies is understood.

Work done on a 2Ni-Cr-Mo-V rotor steel [96,157], and on A533B [142], both in hydrogen gas (at 2.4 bar and 1 bar respectively), showed frequency behaviour of the form shown in figure 5.11. This is of the same form as for BS4360:50D or X65 at ΔK=25MPa√m (cf. figure 5.10), except for the fall in environmental crack growth at frequencies below 0.01Hz. None of these studies reported the use of methods for removing any traces of water vapour or oxygen in the high purity hydrogen used, and Stewart [96] has acknowledged that the fall off in crack growth rate at very low frequencies may be due to the trace impurities present. On the other hand it could well be a true effect, reflecting the lack of SCC behaviour for these materials in hydrogen gas.

Although this discussion of frequency effects has concentrated on the free corrosion condition, for BS4360:50D and X65 in 3% or 3.5% NaCl the frequency behaviour at -1V(sce) is similar to that at free corrosion. This can be seen from figure 5.12. The similarity occurs despite the crack growth being enhanced by a dissolution mechanism at free corrosion and by hydrogen embrittlement at -1V(sce), and is another manifestation of the rate limiting processes that are common to both mechanisms. As both the dissolution rate and the rate of hydrogen entry into the metal at the crack tip are enhanced by the presence of a bare surface at the crack tip, both mechanisms of environmental enhancement of crack growth may be controlled by the competition between passivation and film rupture at the crack tip.

After a piece of bare surface is formed at the crack tip repassivation occurs, and the resultant decay of current can be described by :

$$i = i_a \left[\frac{t}{t_o}\right]^{-n} \qquad (5.6)$$

where n = 0.5 for BS4360:50D in seawater [11].
i_a = bare surface current.

When the crack tip strain rate is fast enough to maintain a bare surface continuously at the crack tip then the rate of hydrogen entry into the metal at the crack tip, or the rate of dissolution at the crack tip, should occur at a constant rate. Thus the crack growth velocity da/dt should remain essentially constant as the frequency alters. (In practice da/dt varies slightly with frequency, this is possibly due to transport phenomena (cf. chapter 6). Therefore for this case :

$$\frac{da}{dN} \propto f^{\alpha} \qquad (5.7)$$

where $\alpha \to 0$

but : $$\frac{da}{dt} = 2f.\frac{da}{dN} \qquad (5.8)$$

(assuming that only the opening part of the fatigue cycle is significant).

Thus : $$\frac{da}{dN} \propto f^{(\alpha-1)} \qquad (5.9)$$

or : $$\log (da/dN) \propto (\alpha-1).\log(f) \qquad (5.9a)$$

As the term $(\alpha-1)$ is negative equation (5.9a) is seen to provide a description of region A in figure 5.11. Thus the increase in environmentally assisted crack growth rate as the frequency is decreased, within region A, is due to the increased time available for dissolution or hydrogen attack to occur.

When the crack tip strain rate is slow sufficient time exists for complete passivation to occur between each film rupture event. In such circumstances a constant charge is passed during the repassivation transient. Thus associated with each film rupture event is either a constant amount of dissolution or of hydrogen entry.

Therefore for these circumstances equation 2.1 applies, viz :

$$\frac{da}{dt} \propto \frac{Q}{t^*} \qquad (5.10)$$

where t^* is the periodicity of the film rupture event.

As mentioned above, at slow frequencies, Q can be taken as constant. The time between film rupture events, t^*, is governed by the failure strain of the film and the crack tip strain rate.

ie. :
$$t^* \propto \frac{\gamma_f}{\dot{\gamma}} \qquad (5.11)$$

where γ_f is the failure strain of the film
and $\dot{\gamma}$ is the crack tip strain rate

The failure strain of the film would be expected to be approximately constant, which leads to :

$$\frac{da}{dt} \propto \dot{\gamma} \qquad (5.12)$$

It has been shown [59,216] that $\dot{\gamma}$ depends on frequency :

$$\dot{\gamma} \propto f \qquad (5.13)$$

When equations 5.8, 5.12 and 5.13 are combined it can be seen that for this case da/dN is expected to be independent of frequency. Region B in figure 5.11 can therefore be explained on this basis.

There is not a sudden transition between regions A and B as for frequencies that lie near the boundary of the two regions a partial repassivation transient occurs after each film rupture event. This results in there being a smooth transition between the two regions.

It is much harder to explain why region C occurs. One possibility is that at very low frequencies equation 5.11 no longer holds. This could be caused by the film being able to accommodate straining, either as a result of lattice diffusion in the film, or as a result of film growth occurring in a manner that reduces the applied strain.

On the subject of frequency a final comment needs to be made about figure 5.11. During the preceeding few paragraphs the form of figure 5.11 has been shown to result from the competition between the passivation behaviour and rate of formation of bare surface at the crack tip. Obviously this discussion was only relevent to corrosion fatigue in an aqueous environment. However the form of figure 5.11 was mentioned earlier as occurring during cracking in hydrogen gas

[96,142,157]. For this situation the analysis of region A behaviour is still valid (equations 5.7 to 5.9a), but da/dt is limited by the hydrogen flux entering the metal at the crack tip. If dislocation transport (cf. section 2.4.3) controls the rate at which hydrogen enters the metal at the crack tip, then region A behaviour is expected at frequencies that produce a crack tip strain rate greater than the critical strain rate for which the dislocation's velocity exceeds the velocity at which an associated hydrogen cloud can move. Below the frequency at which this critical strain rate occurs a disloction transport mechanism of hydrogen entry would result in the flux of hydrogen entering the metal at the crack tip being proportional to the crack tip strain rate (cf. section 2.4.3). Thus equation 5.12 is still valid and so a region B occurs. A possible reason for the occurrence of region C in hydrogen gas is that at ultra-low frequencies some hydrogen is able to diffuse away from the dislocations transporting it, or away from the embrittlement zone.

In conclusion in this section the frequency behaviour of corrosion fatigue of BS4360:50D in chloride solutions was described. This was followed by a comparison with other studies into frequency effects in corrosion fatigue. The final part of this section provided a rationale for the observed frequency behaviour.

5.2.4 R ratio.

The results of this study shown in figures 4.24 and 4.25 show that, within the limits of experimental scatter, no effect of R ratio exists for BS4360:50D in 3% NaCl. This is true for both a dissolution mechanism (ie. at free corrosion) and a hydrogen embrittlement mechanism (ie. at -1V(sce)) of corrosion fatigue crack growth. (The data points obtained for R=0.3 and -1V(sce) at values of da/dN below the plateau are different from those obtained with R=0.5 or R=0.7 because they represent experimental artifacts, as discussed in section 4.5).

The results of the UKOSRP I crack propagation studies were reported as showing that the R ratio is a major variable for corrosion fatigue [192,193]. At free corrosion the crack growth rates for BS4360:50D in seawater were reported to increase with increasing R ratio [160]. The effect was believed to saturate for R in the range 0.5 to 0.7. Similar effects were reported to occur with cathodic protection. It should be noted that the amount of scatter in these results was large, and this must bring into question whether the reported effect of R is genuine or not.

In a study using ABS EH36 ship steel in 3.5% NaCl under free corrosion conditions no difference was observed in the crack growth rates obtained with R ratios of 0.1 and 0.5 [217]. This steel is a normalized C-Mn steel of yield stress about 350MPa, and so is similar to BS4360:50D. Consequently this finding lends confirmation to the results of the present study.

Under cathodic protection conditions the formation of a calcareous deposit on the crack surfaces may cause crack closure effects to occur (cf. section 2.4.4). Crack closure effects are more severe at low R ratios, and so the presence of a calcareous deposit on the crack surface may lead to an effect of R ratio being noticed [218]. This is the most likely reason for the different effects of R ratio reported in this work and in the UKOSRP I studies [160,193], and some evidence of such deposits was presented [140]. Calcareous deposits cannot form in a pure NaCl solution as used in this work, but can form in the seawater used for the UKOSRP I programme. Other workers have noticed very slow crack growth rates at values of ΔK just below 10MPa$\sqrt{m}$, for BS4360:50D in either natural or ASTM artifical seawater [219]. This could be caused by a similar crack closure effect. The work of Galsworthy on QIN [204] shows very clearly that R ratio effects

occur in seawater with applied cathodic protection, but do not occur in 3.5% NaCl at similar applied potentials. Crude measurements of compliance showed that crack closure could be responsible for the R ratio effect. However the reduction in crack growth rates was so severe that it seemed likely that the calcareous deposit also prevented fluid access to the crack tip, so preventing corrosion fatigue mechanisms from operating.

Crack closure effects may also occur as a result of corrosion products accumulating on the crack surfaces. This has been shown to be important in the near threshold region of crack growth [71]. It is to be expected that the amount of corrosion product formed on the crack surface would be greatest under free corrosion conditions, and this is what was qualitatively observed during this work. Thus the R ratio effects observed under free corrosion conditions during the UKOSRP I programme [160,193] may have resulted from the build up of corrosion debris in the crack, causing both crack closure and restricted fluid access to the crack tip. In this work a difficulty arose in that care was needed to obtain test results for R=0.1 under free corrosion conditions. If the specimen was precracked wrongly the residual compressive stress at the crack tip retarded the crack growth sufficiently long enough to allow a build up of corrosion product in the crack, resulting in an anomalously slow rate of crack growth. This is illustrated by figure 5.13. Similar problems were not encountered at higher R ratios, or with cathodic protection to -1V(sce).

On the basis of theoretical modelling of the crack tip environment Turnbull [220] states that the R ratio affects the solution composition at the crack tip. For a dissolution mechanism, with the dissolution confined to the crack tip region, higher R ratios make transport to and from the crack tip more difficult. However, for conditions where the electrochemical reactions are rate controlled by a reaction that occurs along the whole crack face the situation is more complicated. The two effects of R ratio (altering the mean crack opening and the position of maximum fluid ingress) counterbalance each other. The experimental results from this study indicate that any changes in the environmental composition at the crack tip, caused by R ratio effects, do not affect the rate controlling process of environmentally enhanced crack growth.

The lack of an R ratio effect in this work has several practical consequences. Firstly, as mentioned earlier it was experimentally

easier to use an R ratio greater than 0.1, thus the experimental technique could justifiably be simplified by the use of an R ratio above 0.1. Secondly, it was stated in the UKOSRP I study [221] that corrosion fatigue would only be expected to occur in the presence of tensile residual stresses around welded joints. Because of the possibility of calcareous deposits forming in cracks this is probably usually true. However the present work shows that in the absence of any deposits within the crack a high residual stress is not necessary in order for corrosion fatigue crack propagation to occur. Scott [128] mentions that in cold seawater the solubility of the calcareous deposits increases. This means that the results from the present work provide an adequate and safe fatigue design line, as the beneficial (but unreliable) effects of calcareous deposition have been eliminated from the data.

As mentioned in section 1.2.3 as R→1 the crack growth behaviour must approach that found under SCC conditions. Such an effect has been observed for Al alloys in 3.5% NaCl [222]. The foregoing discussion of R ratio effects therefore does not necessarily apply for values of R greater than 0.85. No results are known to the author for BS4360:50D in seawater or 3%-3.5% NaCl, for values of R greater than 0.85.

5.2.5 Waveform.

Some studies have shown that the shape of the loading waveform may profoundly affect corrosion fatigue crack growth rates [60,61,157, 223]. Barsom [223] concluded that for 12Ni-5Cr-3Mo maraging steel in 3% NaCl environmental enhancement of the crack growth only occurred during the rising load portion of the applied waveform. He also pointed out that his conclusions do not necessarily apply to other material/environment systems. In their study of 4340 steel in 3.5% NaCl at different frequencies, Gallagher et. al. [215] observed that for $K_{max}<K_{1SCC}$ a square waveform, unlike a sinusoidal waveform, showed no environmental effect. This result suggests that Barsom's conclusions could apply as well to 4340 in 3.5% NaCl. For the $K_{max}>K_{1SCC}$ case a square waveform showed a larger environmental effect, compared to a sinusoidal waveform. This is because of the ocurrence of SCC during the hold part of the cycle. A similar effect has been observed for Cr-Mo steels in hydrogen gas [224].

For the case of A533B-1 in 1 bar hydrogen gas at 25°C (ie. a below K_{1SCC} condition) a square waveform was observed to yield identical results compared with a triangular waveform [142]. A hold at peak load of up to 2000s was not found to affect the crack growth rate compared with a simple triangular waveform (hold time=0s). Stewart [96] observed similar crack growth rates for sinusoidal,triangular and square waveforms in his study of a 2Ni-Cr-Mo-V rotor steel in 2.4 bar hydrogen gas at 23°C. However both Atkinson and Lindley [60] and Stewart and Smith [157] found that similar effects of waveform did not occur when the environment was changed to distilled water. Atkinson and Lindley [60,209] showed that for both En56C and A533B-1 in water the amount of environmental attack is governed by the time during which the load increases. Stewart and Smith [157] found that no environmental enhancement occurred for a square waveform and distilled water environment (a surprising result as they report that this is an above K_{1SCC} case). These studies indicate that Barsom's conclusions are widely applicable for steel/water systems, but not for a hydrogen gas environment.

The available data for C-Mn structural steels in water is very limited. In a further study Atkinson and Lindley showed that, for a C-Mn structural steel in lakewater or distilled water and in free corrosion, the cycle rise time controlled the degree of environmental enhancement of crack growth rate that was observed (cf. figure 5.10).

In his work on X65 in 3.5% NaCl Vosikovsky [72] includes a result for a square waveform at 0.1Hz, -1V(sce) for which an environmental effect is seen. Scott et. al. [140] report some results for BS4360:50D in seawater. It is claimed that these results are in general agreement with Barsom's conclusions, although they are recognized as being unable to explain all of the observed effects. However, the lack of plateaus in the results for triangular and positive sawtooth waveforms at cathodic protection levels of -0.85V(Ag/AgCl) and -1.1V(Ag/AgCl), as well as the discrepancy in the potential dependency of the crack growth rate with the various waveforms (compared to that obtained with a sinusoidal waveform [139]), must again call into question the validity of these workers results. In particular for a sinusoidal waveform the crack growth rate was fastest at -1.1V(Ag/AgCl), and slowest at -0.85V(Ag/AgCl) (for R=0.1). For a triangular waveform the crack growth rate was found to be fastest at -0.85V(Ag/AgCl) and slowest for free corrosion (for R=0.5). (The difference in R ratio cannot explain these differences, cf. section 5.2.4.) Furthermore for a positive sawtooth waveform little effect of potential was observed over most of the range of ΔK studied. Finally the negative sawtooth results gave the free corrosion crack growth rate as faster than those for -0.85V(Ag/AgCl) or -1.1(Ag/AgCl); also the free corrosion results were as fast as any observed with a sinusoidal waveform. The difference in behaviour between a sinusoidal and a triangular waveform is particularly surprising.

The results from the different waveforms used in this study are shown in figures 4.26 and 4.27. (The results marked _/_ are for a triangular waveform at 0.167Hz with a hold at peak load of 500s). Because of derivative control on the fatigue machines the gain on the machine had to be reduced to its minimum level, the resulting square waveform is illustrated in figure 5.14 and had a rise time of approximately 10ms. For free corrosion conditions the triangular and sinusoidal waveforms gave identical results, with the triangular wave with hold at peak load showing an even greater degree of environmental enhancement of crack growth rate. The square waveform showed no environmental enhancement of crack growth, and indeed at the higher values of ΔK used the crack growth rate was slower than in air. A test was carried out without the gain on the machine reduced, resulting in an overshoot on the square waveform, when the overshoot is accounted for (it was ≈5kN either way) the results agree with those for a true square waveform, figure 5.15. Thus the load at which the hold occurs

does not appear to be significant for a "square" waveform. The free corrosion results are consistent with an increasing stress being necessary for environmental enhancement of crack growth to occur. Because of the very fast passivation of any bare surface formed at the crack tip (less than 10 to 15ms [48]) a continuously increasing stress is necessary to provide fresh bare surface at the crack tip, for any significant crack growth to occur by the dissolution mechanism shown to operate at free corrosion (cf. section 5.1). The retardation of crack growth with square waveforms below those found in air may be caused by the dissolution reaction causing some crack blunting.

At -1V(sce) the results of this study show a significant environmental effect with a square waveform. A plateau was found to exist, with the plateau crack growth rate being half of that found using a sinusoidal waveform. The results from the triangular waveform were just below those for a sinusoidal waveform for the plateau region, the difference could be a result of scatter in the experimental results (eg. compare figures 4.27 and 4.25). Figures 5.16 and 5.17 compare the square wave results with those obtained by Vosikovsky [72] for X65 in 3.5% NaCl, both on a cycle and a time basis. Figure 5.17 shows very good agreement between these results. In section 5.1 it was shown that hydrogen embrittlement was the mechanism by which environmentally enhanced crack growth occurs for BS4360:50D in 3% NaCl at -1V(sce). As discussed in section 5.4 the plateau region of the da/dN vs. ΔK diagram corresponds to a limiting rate of entry of hydrogen into the metal at the crack tip. The presence of a film at the crack tip severely restricts the rate of hydrogen entry into the metal there [225]. In addition strain may aid hydrogen entry via dislocation transport. Thus the waveform effects observed at -1V(sce) in this study reflect the smaller amount of hydrogen entry with a square waveform as opposed to triangular or sinusoidal waveforms. Sufficient hydrogen to cause an embrittlement effect is able to enter the metal with a square waveform, despite the fast formation of a film on a bare surface, because a large amount of bare surface is suddenly formed. Subsequent diffusion of hydrogen to the embrittlement site then occurs. Stewart's work [96] provides some supporting evidence for this explanation of waveform effects at -1V(sce). In his work on below K_{1SCC} fatigue in hydrogen gas he studied the effects of air additions to the hydrogen, using both square and triangular waveforms. The results are reproduced in figure 5.18. The square waveform gave faster crack growth rates over a range of air partial pressures. This

was held to be a result of the more rapid creation of bare surface at the crack tip with the square waveform. Oxygen absorping onto the metal surface is known to reduce the rate of hydrogen entry [126,226], and so the amount of hydrogen entering the metal is governed by the competition between the rate of creation of fresh bare surface, and the rate at which oxygen can reach and poison such a surface. This is obviously similar to the situation encountered in this work, in that the total amount of hydrogen that enters the metal is governed by the rate of production of bare surface, and the rate at which such a surface is poisoned. The difference is that in the NaCl solution the more rapid poisoning of the surface means that it is necessary to continuously create fresh bare surface if the amount of hydrogen entry is to be maximized.

Figure 4.28 shows the effect of potential on the crack growth rates obtained using a square waveform. The results at -0.85V(sce) lie just below those obtained at free corrosion, and show no environmental enhancement of crack growth because the square waveform reduces to nothing the (small) effect of hydrogen embrittlement at this potential. The difference in the effect of the square waveform for free corrosion and -1V(sce) is yet more evidence that the predominant mechanisms of environmentally enhanced crack growth are not the same for these two conditions.

Significant effects of a 500s hold time at K_{max} were seen in figures 4.26 and 4.27. This is in stark contrast to the results of Atkinson and Lindley [60,61,142] in which no effects of hold time were observed for a C-Mn structural steel in lakewater and A533B-1 in hydrogen gas, and for A533B-1 at free corrosion in 90°C distilled water the crack growth rate decreased as the hold time increased. The reduction in crack growth rate for the A533B-1 in water could be caused by crack blunting [60]. All of Atkinson and Linley's results were consistent with the intuititive idea that for $K_{max}<K_{iscc}$ the hold time should not cause any greater enhancement of crack growth. However the results of this study for free corrosion are not inconsistent with the idea that the additional crack growth enhancement is caused by the occurrence of creep at the crack tip during the hold time. Creep at crack tips has been shown to be important in other cases of environmentally enhanced cracking [11,62]. Creep occurring at the crack tip during the hold time may also explain the results obtained at -1V(sce), but the dramatic increase in the crack growth rate caused by the hold time must bring into question whether this is an adequate

explanation. Unfortunately the machine used for this test exhibited intermittent noise in its control signal and, whilst this caused errors in the load applied that were too small to affect testing performed with other waveforms, it could have caused some extra creep to occur at the crack tip during the hold time.

In air waveform effects are not generally observed [168]. Modification of the slip reversibility at the crack tip (cf. section 2.5) may therefore explain why fatigue crack growth rates are larger in air than in vacuum, but the existence of waveform effects invalidates it as a mechanism of environmentally assisted crack growth for the systems investigated in this work. Also, the different effects of square waveforms noticed at free corrosion and -1V(sce) provides yet more evidence that both anodic dissolution and hydrogen embrittlement may cause environmentally enhanced crack growth for BS4360:50D in 3% NaCl.

5.2.6 Salt concentration.

In a study into the SCC and corrosion fatigue behaviour of aluminium, magnesium and titanium alloys, Speidel et. al. [227] found that bromide and iodide ions caused a greater environmental effect than chloride ions for a 7079 Al alloy. Sulphate ions were found to have no effect compared with pure distilled water. As the presence, or absence, of different anions was found to be important in that study it was decided to investigate the effect of NaCl concentration on corrosion fatigue crack growth for BS4360:50D in water. Practically this is of value because such steels may be considered for use in freshwater, and because the salt content of the world's seas differs [228].

Vosikovsky [72] noticed no difference in crack growth rates obtained with 0% and 3.5% NaCl for X65 at free corrosion. Atkinson and Lindley report no difference between the crack growth rates at 90°C, free corrosion, for 0% and 3% NaCl solutions for both A533B-1 and EN56C steels [60].

For the free corrosion case figure 4.30 shows that varying the NaCl concentration between 0% and 5% has no effect on the fatigue crack growth rate. Thus for BS4360:50D undergoing environmentally enhanced crack growth as a result of a dissolution mechanism the concentration of NaCl does not affect the crack growth rate (up to a concentration of >5%).

Figure 4.31 shows the results obtained at -1V(sce), ie. in the regime of enhanced crack growth caused by hydrogen embrittlement. It appears that there is no increase in the crack growth rate with an increased NaCl concentration from 3% to 5%. At concentrations below 3% it appears that the plateau crack growth rate is reduced by a factor of approximately 1.5. Thus seas with a higher salinity should not prove to be more aggressive environments, and waters less saline than normal seawater may be less aggressive than normal seawater.

5.2.7 Temperature.

As environmentally assisted crack growth occurs as a result of chemical reactions taking place at the crack tip, the solution temperature would be expected to be an important factor in determining the crack growth rate. Temperature was indeed shown to be a significant variable by the preliminary studies for the UKOSRP I programme [192]. It is important to realize that the repassivation reaction will also increase in rate with a higher temperature, as well as the hydrogen entry reactions and dissolution reaction. Diffusion processes are also thermally activated, and so the transport of species to and from the crack tip is affected by temperature.

Several workers have measured activation energies for corrosion fatigue crack growth, and "identified" the activation energy as being that of a particular process [180,229,230]. This is not a valid procedure as the activation energy reflects the temperature dependency of a conglomeration of processes eg. transport, oxygen concentration, passivation, hydrogen entry and dissolution. Thus the activation energy may be affected by more than one process [158].

Figure 4.32 shows the results obtained during this study at free corrosion. At 7°C the crack growth rate was the same as in air over most of the range of ΔK studied, thus the environmental effect was much smaller at 7°C than at 23°C or higher. The region I behaviour was seen to be little affected by temperature, except for $\Delta K<20MPa\sqrt{m}$ at 60°C where the crack growth rate was just above the air upper bound line. The region II behaviour was strongly dependent on temperature. As discussed in section 5.3 region II crack growth rates are partly governed by the bare surface current density, and as this increases with temperature the region II crack growth rates also increase with temperature. Because region I behaviour results from a mechanical limitation of the dissolution mechanism, figure 4.32 shows that the net effect of temperature changes upon the passivation, bare surface current density, film rupture strain, etc., is that the same amount of dissolution occurs per cycle over the temperatures studied. An exception to this is for $\Delta K<20MPa\sqrt{m}$ and 60°C where the enhancement of the passivation reaction coupled with the slower crack tip strain rates at low values of ΔK [216], leads to the suppression of any environmental effect upon the crack growth rate. Atkinson and Lindley [60] found that for En56C in distilled water, or 3.5% NaCl, at free corrosion the crack growth rate decreased with increasing temperature

at low frequencies, but increased with increasing temperature at higher frequencies. This could be caused by a similar effect of temperature on passivation behaviour leading to less environmentally assisted crack growth at slow crack tip strain rates and higher temperatures.

Figure 5.19 presents the results obtained at free corrosion in the form of an Arrhenius plot. The apparent activation energy was found to be ≈15.1 kJ/mole. (Unlike Atkinson and Lindley [61] the total crack growth rate, rather than an "environmental" one, (where $da/dN_{env} = da/dN_{total} - da/dN_{air}$), was found to yield an Arrhenius type relationship.) Their data is the only known comparative data for C-Mn structural steels at free corrosion, and showed an activation energy of 19.2 kJ/mole for the "environmental" component of crack growth.

Ficalora et. al. [231,232] have shown that the rate of absorption of hydrogen gas exhibits a maximum at about room temperature as the temperature varies. (They account for this by a model of adsorption as a two-stage process). Figure 5.20 illustrates their expected variation of crack growth rate in hydrogen with temperature, assuming that diffusion is not a controlling process. A similar temperature dependency has been reported for stage II crack growth in SCC studies performed in hydrogen gas [97,107,233], an example is shown in figure 5.21. For fatigue in hydrogen several studies [96,142] have shown a decrease in the crack growth rate as the temperature increased, for the range 23°C to 90°C. Obviously the environmental enhancement of crack growth in hydrogen is dependent on the supply of hydrogen to the embrittlement zone, and this in turn depends upon the adsorption of hydrogen. Thus the temperature dependence of the crack growth rate mirrors that of the supply of hydrogen to the crack tip.

For crack growth by hydrogen embrittlement in water environments a similar temperature dependence has been found [234] to that observed by Ficalora et. al. [231,232] for the absorption of hydrogen gas (cf. figure 5.22), but the maximum crack growth rate occurred at about 200°C rather than room temperature. The change in the temperature at which the maximum occurs is a reflection of the different kinetics involved in the entry of hydrogen into the metal from hydrogen gas or aqueous environments. Thus for temperatures between ambient and over 100°C the crack growth rates are expected to increase with increasing temperature for aqueous environments, but decrease with increasing temperature in hydrogen. It was indeed found in this study that the plateau crack growth rate in an aqueous environment increased with

temperature over the range 8°C to 60°C.

From the results shown in figure 4.33 it is seen that for BS4360:50D in 3% NaCl the region I crack growth behaviour is unaffected by temperatures within the range studied. This is for a similar reason to that given for the free corrosion case, the increase in hydrogen entry rate caused by the higher temperatures is counterbalanced by faster passivation behaviour. The region II crack growth rates obeyed an Arrhenius type relationship, as shown in figure 5.23. The apparent activation energy was found to be 25.6 kJ/mole. As the region III crack growth rates are controlled by the normal mechanical fatigue mechanisms they were found to be independent of temperature. Saito's work [180] on steels ST22 and ST28 in 3.5% NaCl at a potential of -1.05V(Ag/AgCl) gave results that are very similar to those of this study, they are shown in figure 5.24. Both of these steels showed an apparent activation energy of 40 kJ/mole.

In concluding this section it is useful to point out that the effects of frequency and temperature act conjointly, as seen in figure 5.25, taken from the work of Smith and Stewart [157].

5.2.8 Oxygen concentration.

As was mentioned earlier in section 5.1 an effect of bulk solution oxygen content has been observed for BS4360:50D in seawater [192]. At the free corrosion potential lower crack growth rates were observed with 1ppm of oxygen, as compared to the normal level of 7-8ppm. No effect of dissolved oxygen concentration was found at -0.85V(Ag/AgCl) or -1V(Ag/AgCl). These results suggest that only the dissolution mechanism of crack growth is affected by the solution's oxygen content, which is as expected. The presence of oxygen at the crack tip would enhance the dissolution reaction by allowing oxygen reduction (cf. equation 5.1) as a cathodic reaction. The only possible effects of oxygen on the hydrogen embrittlement mechanism would be to reduce environmental crack growth by its preferential absorption onto any bare surface formed at the crack tip (so reducing the amount of hydrogen that enters the metal there), and by the consumption of hydrogen ions via the reaction :

$$\frac{1}{2} O_2 + 2H^+ + 2e^- \rightarrow H_2O \qquad (5.14)$$

An oxygen inhibition model, where oxygen inhibits the extent of

hydrogen embrittlement, has been proposed as an explanation of the behaviour of short cracks in 4340 steel in 3% NaCl [235].

For free corrosion the corrosion potential may alter as the oxygen concentration decreases, this has been found to affect the results for simulated PWR conditions with extremely low oxygen levels [236,237]. For the present study decreasing the dissolved oxygen content to 3ppm did not affect the free corrosion potential (cf. chapter 10). The oxygen concentration present in water is a function of temperature; at room temperature the equilibrium (saturated) concentration is ≈8ppm, falling to ≈3ppm at 80 C.

Turnbull [220] has modelled numerically the transport of oxygen down a corrosion fatigue crack. His results predict that the crack tip oxygen concentration will increase as ΔK increases, be affected by the R ratio and be relatively insensitive to crack depth (for a>3mm) and specimen geometry (ie. SEN, CTS or 3 pt. bend)

In part II of this thesis some results are presented for BS4360:50D in ASTM artificial seawater (figures 10.3 and 10.5). At free corrosion the region I crack growth rate was unaffected by a change in the oxygen content from 8ppm to 5ppm. However at a lower concentration of 3ppm the region I crack growth rate was reduced by a factor of about 1.5. In a similar manner the region II crack growth rate was less with 3ppm of dissolved oxygen than for 8ppm. At a potential of -0.85V(sce) a slight effect of oxygen concentration was found for the plateau crack growth rate. It is possible that this is caused by a small dissolution contribution to the crack growth rate being prevented by the change in oxygen content from 8ppm to an estimated 3ppm.

5.2.9 Miscellaneous.

In a study on corrosion fatigue of A516-60 in 3.5% NaCl Sullivan and Crooker [238] reported that the solution flowrate affected the crack growth rate. In a still solution coupling the specimen to a zinc anode resulted in a plateau being observed, but in a flowing solution the results with a zinc anode were identical to results obtained at free corrosion. Subsequently Crooker et. al. [170] have included recommendations on flowrate as part of a proposed US Navy standard testing method for corrosion fatigue work. However it is unlikely that Sullivan and Crooker's results [238] were caused by

effects of flowrate, such as rate of oxygen supply (this has been found to be important for PWR environments [236]). It is more likely that because they used sacrificial zinc anodes the increased flowrate caused a loss of polarization to occur, hence the similarity with the free corrosion results. This could not happen when the potential is controlled with a potentiostat.

Figure 4.29 shows that altering the bulk solution pH, from approximately 6.5 to 5, does not affect the region I crack growth rate under free corrosion conditions. This is not suprising as the crack tip conditions should be relatively independent of the bulk solution pH [49]. Scott and Silvester [192] have reported differences in the results obtained in seawater, acidified seawater and 3.5% NaCl especially with a large amount of cathodic protection. Again as mentioned in part II of this thesis the addition of nutrients for bacteria to ASTM artificial seawater resulted in a doubling of the value of da/dN at which the plateau occurred, this was at -0.85V(sce). It is possible that the resulting acidification of the solution was partly, or wholly, responsible for this effect. Further experimental work, especially with cathodic protection, is needed before definite conclusions can be drawn about the effect of bulk solution pH.

In a review of corrosion fatigue Scott [128] reports that Crooker had found that differences in fatigue crack growth rates in air, for different production and tempers of a 17-4PH steel, disappeared in a seawater environment. The steel used in the present study was normalized and so little effect of orientation is seen upon the grain shape, although the sulphide inclusions are elongated in the rolling direction [200]. Thus little effect of crack growth direction would be expected, unless the inclusions affect the crack growth rate. Although microstructure is generally not an important variable for fatigue in air it is possible that for corrosion fatigue crack growth by a hydrogen embrittlement mechanism it is highly significant. In particular inclusions may affect the uptake of hydrogen from the environment [239,240]. Sulphur content has been found to be important in PWR steels [236], as well as the morphology and distribution of MnS inclusions [240]. For crack growth by a dissolution mechanism the insensitivity of the bare surface current density to the exact steel composition [48], as well as the chemical machining nature of the crack extension process, means that microstructural or compositional changes in the steel should not affect the crack growth rate. Some experimental backing for this can be obtained from the work of Cheng

[217]. No difference was observed between the crack growth rates for both the TL and LT orientations, in air and in 3.5% NaCl at free corrosion. The steel used was an ABS EH36 ship steel, which was normalized and was manufactured with sulphide shape control.

In concluding this section about the effect of different environmental/loading factors upon corrosion fatigue crack growth rates it seems in order to briefly discuss the choice between constant ΔK testing and constant ΔP testing. The advantage of constant ΔK testing is that the same specimen may be used to obtain more than one result, and that it is possible to survey a number of environmental conditions more quickly than possible with constant ΔP testing [191]. Also it is possible to study transient effects of changing the testing conditions, such as frequency, more easily with constant ΔK tests. Constant ΔK tests can be used as well to investigate crack depth effects in corrosion fatigue. However constant ΔP tests are a necessary adjunct to constant ΔK tests if a full picture of corrosion fatigue behaviour is to be developed, as can be seen from the discussion in sections 5.2.3 and 5.2.7. It must be borne in mind that constant ΔP tests may show initial experimental artifacts [191] (cf. section 4.5). A load stepping technique [170,208] may be used to accelerate constant ΔP tests. Ideally constant ΔP testing would be performed to form a general view of corrosion fatigue behaviour for a new material/environmental system, and constant ΔK tests performed to extend the results into regimes of frequency, etc. that would be impracticable to cover using constant ΔP tests.

5.3 The anodic dissolution mechanism.

Following the work of Ford on aluminium alloys [42,54] other workers have concluded that a dissolution mechanism may explain the corrosion fatigue behaviour of other material/environment systems [241,242]. As the crack growth rate by a dissolution mechanism is Faradaically related to the current density at the metal surface at the crack tip it is necessary to determine the magnitude of the current density before a dissolution model can be compared quantitatively with experimental data. The relevant current density is that on a freshly created patch of bare metal surface, as mentioned earlier in section 2.3. Trant [48] found that for iron and steels in 1M caustic solution the exact composition of the metal did not significantly affect the bare surface current density, a result that is intuitively expected. His data for iron in 1M chloride solutions at 20°C is therefore applicable for the system studied in this work. For potentials more positive than -0.8V(sce) the bare surface current density was found to be of the order of 0.4 to 0.7 A/cm^2. It is to be expected that this is only an approximate value for the bare surface current density, as large amounts of experimental scatter are usual in measuring it [158]. No indication was given by Trant [48] as to the scatter in the experimental data.

In a similar manner to Ford [42,54] the "environmental" component of crack growth is plotted as a function of specimen potential (with ΔK constant) in figure 5.26. The behaviour shown in figures 5.26 and 5.27 is similar between the free corrosion potential and about -0.8V(sce) to that observed by Ford for an aluminium alloy. The behaviour for this range of potentials is consistent with a dissolution mechanism, and the crack growth rates are much less than the maximum theorectical rate for a dissolution mechanism determined by Trant [53]. At potentials more negative than -0.8V(sce) the presumed increased amount of hydrogen embrittlement causes the crack growth rates to increase, until at potentials below ≈-1V(sce) the crack growth rate exceeds the maximum possible from a dissolution mechanism. Figure 5.27 is similar to figure 5.26 except that the total crack growth rate has been used, rather than the "environmental" component. It can be seen from figures 5.26 and 5.27 that for potentials between the free corrosion potential and about -0.8V(sce) a dissolution mechanism may yield the observed crack growth rates, irrespective of whether the dissolution and air mechanisms are assumed to act

competitively or conjointly.

In figure 5.7 the results obtained in this study at free corrosion were presented with the crack growth rate plotted on a time basis. The crack growth rate at which the transition from region I to region II behaviour occurred was found to be relatively independent of frequency, and was in the range 1.4×10^{-4} mm/s to 2.1×10^{-4} mm/s. If the "environmental" component of crack growth rate is plotted on the same basis it is found that the correlation in crack growth rates at which the region I/II transition occurs is not quite as good. This is seen from figure 5.28. Thus a comparison of figures 5.7 and 5.28 suggests that the region I/II transition occurs at an approximately constant *total* crack growth rate, rather than a constant "environmental" crack growth rate. In turn this must suggest that for this metal/environment system the air and environmental mechanisms are competitive at the point where the transition between regions I and II occurs.

If in equation 2.2 :

$$\frac{da}{dt} = \frac{Mi_a}{n\rho F}$$

we use : M = 56 g/mole
n = 2
ρ = 7.83 g/cm^3
F = 96,500 C/mole

then a bare surface current density of 0.4 A/cm^2 yields a crack velocity of 1.48×10^{-4} mm/s, and for a current density of 0.7 A/cm^2 this velocity would be 2.59×10^{-4} mm/s. Thus it appears that the transition between region I and region II behaviour corresponds with a crack growth rate that is entirely due to the dissolution of metal at a bare surface formed at the crack tip.

It was observed (figure 4.21) that the region I behaviour was independent of frequency, and also almost independent of temperature (figure 4.32), cf. figure 5.29. This would suggest that the region I behaviour is not controlled by an environmental process, but rather by a mechanical process. Also it should be noted that the region I crack growth rates are less than those given by equation 2.2 using the bare surface current densities found by Trant [48]. It is now proposed that the region I crack growth rates are controlled by the crack tip strain resulting from the applied loading.

It has been recognized that the crack tip strain rate is important for a dissolution mechanism of crack growth [59], as described in

section 5.2.3. However, at low crack tip strain rates, where passivation occurs, it is obvious from equations 5.10 to 5.13 in section 5.2.3 that the total strain at the crack tip determines the number of film rupture events that occur, and so controls the amount of dissolution that occurs during each cycle. Several attempts have been made to calculate the crack tip strain rate [216]. One approximate calculation was by Scott et. al. [59] and they proposed the expression for the average crack tip normal strain rate $\dot{\epsilon}_{av}$:

$$\dot{\epsilon}_{av} = -\frac{1}{T} \ln(1- 0.5[1-R]^2) \qquad (5.15)$$

where T is the cyclic period.

This is obviously not correct as $\dot{\epsilon}_{av}$ should →0 as ΔK→0. Lidbury [216] has proposed an alternative expression :

$$\langle \Delta\dot{\gamma}_p \rangle = \frac{2\gamma_o}{T} \left[\left[\frac{\xi}{\xi-1} \right] \ln(\xi) - 1 \right] \qquad (5.16)$$

where $\gamma_o = \frac{2(1+\nu)E}{3\sigma_y}$

and $\xi = \left[\frac{\Delta K}{\Delta K_{th}} \right]^2$

$\langle \Delta\dot{\gamma}_p \rangle$ = average crack tip shear strain rate

T = cyclic period.

It is seen that this expression does depict a variation of crack tip strain rate as ΔK increases. However $\langle \Delta\dot{\gamma}_p \rangle$ is approximately proportional to log ΔK, and so this would suggest that the environmental crack growth rate should also increase linearly with log ΔK. Ford [243] mentions that Shoji has related the crack tip strain rate to the fatigue crack propagation rate in an inert environment [244], ie. :

$$\dot{\epsilon} = B \left(\frac{da}{dt} \right)_{\text{inert env.}} \qquad (5.17)$$

This was held to be a valid procedure because of the nature of the mechanism of fatigue striation formation. Ford mentions that he has used equation 5.17 in his work on PWR pressure vessel steels, also a similar equation was derived by Shoji from the elastic/plastic analyses of Rice et. al. [245]. In that $da/dt_{(\text{inert env})}$ obeys the Paris law (equation 1.6) then the approach of equation 5.17 means that $\dot{\epsilon}$ and ΔK are related via :

$$\dot{\epsilon}_{av} \propto \Delta K^m / (\text{rise time}) \qquad (5.18)$$

Experimental evidence exists supporting the relationship given in equation 5.18 [241], the applied cyclic loading rate having been found to dominate the crack tip strain rate as expected, rather than any effect of the advancing crack tip. Equally importantly the observed crack tip strains were independent of cracking morphology (intergranular vs. transgranular failure). The rationale behind equation 5.17 leads therefore to the conclusion that the crack tip strain varies in a similar manner with ΔK as does the crack growth rate in vacuum, and for BS4360:50D that means it is not a function of R ratio.

Thus it is proposed that the region I crack growth rate is controlled by the crack tip strain, which determines the number of film rupture events that occur, and so the total amount of dissolution caused crack growth. As the crack length increases the crack growth rate increases according to a Paris type relationship (equation 1.6) as the crack tip strain obeys a similar dependency on ΔK. However as ΔK increases the crack tip strain rate increases in the same way as the crack tip strain. When ΔK becomes sufficiently large the crack tip strain rate is such that no passivation occurs, and the crack growth rate is then related to the bare surface current density, via equation 2.2. As mentioned earlier in this section this should correspond to the transition point between region I and region II behaviour. It is obvious that as ΔK increases above the value of ΔK at which the region I/II transition occurs, for a fixed frequency, the crack growth rate can no longer increase as a result of an increase in the amount of dissolution occurring during each cycle, and so region I behaviour is no longer observed.

In section 5.2.3 three regimes were identified on a graph of log da/dN vs. log f, cf. figure 5.11. The preceeding discussion, along with that in section 5.2.3, indicates that the region B behaviour in figure 5.11, and the region I behaviour of figure 5.5 are both the result of passivation occurring between each film rupture event with the subsequent control of the crack growth rate by the crack tip strain. It was also noted in section 5.2.3 that as the crack tip strain rate increases towards the value for which a bare surface is continuously maintained at the crack tip, there would be a smooth transition between region A and region B behaviour on figure 5.5, as only partial passivation would occur between each film rupture event.

A similar smooth transition could be expected between region I and region II crack growth, and was often (but not always) observed.

As seen in figure 5.29 the results obtained with different temperatures displayed a similar region I behaviour to those results obtained at different frequencies and 23°C. In terms of the model proposed this implies that the total charge passed during each film rupture event is not significantly affected by temperature. This was discussed in more detail in section 5.2.7. The apparent increase in the bare surface current density seen in figure 5.7 with frequency could be caused by the greater pumping that occurs with a higher frequency. A similar effect has been reported elsewhere [241].

For the observed region II of crack growth behaviour it is obvious that the crack growth rate is not caused solely by the operation of the dissolution mechanism. An additional component of crack growth must exist, and it is proposed that this is the normal mechanical fatigue striation mechanism found in air. At the transition point between regions I and II the contribution to the total crack growth rate from a striation mechanism is small but this increases at higher values of ΔK as the dissolution of metal at the crack tip cannot keep pace with the rate of creation of bare surface. If the crack growth region I/II transition occurs at a value of ΔK denoted by $\Delta K_{I/II}$ then the expected crack growth rate, from the previous discussion and equation 5.8, is :

$$\frac{da}{dN_{I/II}} = \frac{1}{2f} \cdot \frac{Mi_a}{n\rho F} \qquad (5.19)$$

For $\Delta K > \Delta K_{I/II}$ if the increase in crack growth rate is caused by the increase in the crack growth rate caused by a striation mechanism, as in air, then from equations 5.19 and 1.6 the crack growth rate is given by :

$$\frac{da}{dN} = \left[\frac{Mi_a}{2fn\rho F} \right] + C \left(\Delta K^m - \Delta K^m_{I/II} \right) \qquad (5.20)$$

It can be seen from figure 5.30 that equation 5.20 fits the experimental data very well for 0.167Hz and 1Hz, and da/dN less than $2.da/dN_{I/II}$. (The reference air line was taken as the air upper bound line). The reason for the failure of equation 5.20 to correctly predict the crack growth rates for $da/dN > 2.da/dN_{I/II}$ is that at these high crack growth rates ($da/dt \approx 3 \times 10^{-4}$ mm/s in both cases) the rate of solution renewal becomes a limiting factor. This can be seen by rewriting equation 5.20 as :

$$\frac{da}{dN} = \alpha\left[\frac{Mi_a}{2fn\rho F}\right] + C\,(\Delta K^m - \Delta K^m_{I/II}) \qquad (5.21)$$

The value of α necessary to make equation 5.21 fit the experimental data is shown in figures 5.31 and 5.32, both as a function of ΔK and of da/dt. The different behaviour observed at 5Hz was possibly due to a similar effect of solution renewal (for this case da/dt was $\approx 2.1 \times 10^{-4}$ mm/s at the end of the region I regime). Figure 5.33 summarizes schematically the reasons proposed in this discussion as to the observed region I/II behaviour.

For values of ΔK that are much greater than $\Delta K_{I/II}$ the crack growth rate lies within the air scatterband, and so is presumably caused entirely by the normal striation mechanism found in air. It may be possible that some crack blunting occurs as the 5Hz data lies along the air lowerbound line.

Tomkins [63,64] has proposed that the maximum possible enhancement of crack growth rate by a dissolution mechanism is given by $\delta/2$, where δ is the crack tip opening displacement. It was postulated that if the crack growth rate was larger than this the crack would blunt, as it could not completely resharpen upon unloading. Vosikovsky's work on X65 shows no dependency of the crack growth rate on either $\delta/2$ or $\Delta\delta/2$, as seen in figure 5.34. Furthermore although Tomkins [64] backs his hypothesis by comparison with Atkinson and Lindley's work [60], it is clear from some of their other work that the maximum crack growth enhancement for a dissolution mechanism does not always correspond to $\delta/2$. Thus it is suggested that Tomkins' hypothesis is not valid for the system studied in this work, and that factors other than $\delta/2$ govern the amount of crack growth caused by a dissolution mechanism.

It is hard to see why $\delta/2$ should present a limit to dissolution controlled crack growth, as the very fast passivation of a bare surface (within 10-15 ms [48]) means that a dissolution mechanism may in effect be an "electrochemical knife". This would cause enhanced crack growth, without causing significantly greater blunting at the crack tip. Thus it appears that crack growth greater than $\delta/2$ can occur during each cycle without any problems arising as to how a sharp crack tip is maintained.

Tomkins [63,64] also suggested that the region I/II transition could be caused by a change between stage I and stage II cracking, allowing greater solution access to the crack tip. This arguement does not fit the data for low strength steels in chloride solutions, and ignores the known effect of environment upon stage I cracking

[246]. It also does not explain the definite applicability of the Paris law (equation 1.6) to the region I crack growth data. The stage I/II transition depends upon the R ratio, and as no effect of R was observed upon the crack growth rates in this study it is concluded that this suggestion does not explain the behaviour of the system studied.

The similarity found between the region I crack growth rate for BS4360:50D, X65 and ABS EH36 steels (cf. section 6.1) provides more evidence that dissolution processes are the cause of these environmentally enhanced crack growth rates at free corrosion. Also the observation of striations upon a fracture surface obtained for BS4360:50D [200], immersed in seawater under free corrosion conditions at a value of ΔK that lies within region II, provides some more experimental backing for the proposed cause of region II behaviour.

One final point about the dissolution mechanism is that the rationale behind equations 5.17 and 5.18 for determining the crack tip strains and strain rates explains the different effects of R upon corrosion fatigue crack growth rates in BS4360:50D, X70 and HY130. Vosikovsky [166,208] found that R affected the corrosion fatigue crack growth rates in both X70 and HY130 in 3.5% NaCl, but the R ratio also affected the crack growth rate in air in a similar fashion. Thus when the results were plotted against a parameter $(\Delta K+xR)$, where x is a constant, such that the effects of R in air are removed the data for the 3.5% NaCl solution also lay on one curve [166,208,247].

5.4 Hydrogen embrittlement.

Although it was concluded in section 2.3.1 that the fundamental mechanism(s) of hydrogen embrittlement are poorly understood, attempts have been made to produce quantitive models of crack growth associated with hydrogen embrittlement [137]. Wei and others have shown that the rate of crack growth for 4130 steel in various environments may be controlled by any of several factors : transport of the environment to the crack tip, diffusion of hydrogen ahead of the crack, and the rate of reactions at the surface of the metal in the crack tip region [126,248,249].

In figure 4.22 an essentially frequency independent regime of crack growth at -1V(sce) is observed at the lower values of ΔK, similar to that observed by Vosikovsky for X65 [72]. A similar region is also seen in figure 4.33. Thus it appears that an analogous regime of crack growth occurs as a result of hydrogen embrittlement to that resulting from a dissolution mechanism. (In section 5.1 the mechanism of environmentally assisted crack growth at -1V(sce) was shown to be hydrogen embrittlement). This region I crack growth behaviour does not depend significantly upon frequency or temperature as it is governed by the same mechanical parameters as for a dissolution mechanism, namely the crack tip strain and strain rate. If the crack growth rate is proportional to the amount of hydrogen that enters the steel each cycle, an assumption that has elsewhere been found to produce reasonable results [249], then the crack tip strain should control the amount of hydrogen entering the metal at low values of ΔK. This is because the amount of crack tip strain determines how many film rupture events occur, and so how much bare surface is created where hydrogen entry can occur.

Although the region I crack growth rates obey a Paris law (equation 1.6) because of the relationship between crack tip strain and ΔK discussed in section 5.3, it should be realized that the environment determines the value of the exponent m in equation 1.6. This is a result of the more severe hydrogen bearing environments causing more hydrogen to enter the metal during each film rupture event than the less severe environments. Thus increasing the amount of cathodic protection increases m, as seen by Hinton [146]. The value of m is also increased if hydrogen sulphide is present in the environment [129,250].

The plateau, or region II crack growth behaviour, is caused by the

rate at which hydrogen can be supplied to the embrittlement zone being the rate determining step. This is seen from figure 5.8. The rate of hydrogen supply may be limited either by the rate of the surface reactions, or by the rate of entry of hydrogen from the surface into the metal. Hydrogen may enter the metal either by diffusion, or by dislocation transport [251], both of which display a maximum rate. The fact that the plateau rate increases with temperature and increasing degree of cathodic protection, suggests that it is the surface reactions that limit the rate of supply of hydrogen. This would agree with the observation that the plateau rate increases slightly with frequency [72], figure 5.8, a phenomena that has been attributed to be a result of the increased pumping of fresh solution down the crack at higher frequencies. Furthermore, although region I type behaviour is observed for steels in hydrogen gas, plateau type crack growth is not always seen [93,94].

From figures 4.22 and 4.33 it can be seen that the region III crack growth rates lie within the air scatterband, and so presumably result from the operation of the same striation mechanism as in air. The rate of supply of hydrogen to the embrittlement zone is not rapid enough to enable any hydrogen embrittlement to occur before the crack grows past the zone as a result of the mechanical mechanism of striation formation. It should be noted that for X65 both Vosikovsky [72] and Hinton [146] obtained some region III results that lay above the air scatterband.

In section 5.1 it was mentioned that small cleavage facets have been found on the fracture surface of specimens polarized to -0.85V(sce) or below. Coupled with the conclusions reached in section 5.1 as to mechanisms of environmentally assisted crack growth it would appear that these facets are a result of the operation of a hydrogen embrittlement mechanism.

It can be seen from figures 4.16 to 4.19 that an increasing amount of failure along a plane at 45° to the specimen axis occurred as the degree of embrittlement of the specimen increased. Also a larger degree of embrittlement was associated with a larger number of cracks nucleated in the vicinity of the neck, although the cracks opened more in some of the less severely embrittled specimens (with the exception of the cracks that caused the specimen failure). This was presumably because an increased number of cracks nucleated, and an increased degree of embrittlement, were both associated with the severity of the environment in promoting hydrogen entry into the metal. The overall

"cup and cone" type tensile failure was associated with the ductile failure mechanism, as expected. Figures 4.46 and 4.47 confirm that failure was a result of void growth and coalescence. As can be seen from figures 4.48 and 4.49 the middle portion of the specimens that were embrittled failed by this process of void growth and coalescence, ie. the nature of that mechanism was not affected by the environment. (Figure 4.50 shows part of figure 4.49 at a higher magnification). Figures 4.18 and 4.19 show that the effect of environment upon the specimen ductility was a surface effect. This would not necessarily be the case for slower strain rates [195,196]. Cracks in material that was in contact with the environment and contributed to the embrittlement of the specimen exhibited a different failure mechanism (cf. figures 4.48 and 4.51 to 4.54). Figures 4.51 to 4.53 show the surface of one of these cracks at different magnifications. It is seen that the whole of the surface has a pronounced "flaky" appearance. This probably is a result of the embrittlement of the metal by hydrogen produced as a consequence of the environmental conditions. In this region of the specimen some evidence of a ductile shearing mechanism would be expected. In figure 4.53 some voids are apparent, although voids and void growth are more obvious in figure 4.54. Hydrogen seems to alter the appearance of the fracture surface of the slow strain rate specimens, from that of a ductile void growth and coalescence mechanism to one including quasi-cleavage.

As mentioned ealier in section 5.1 figure 4.44, which shows part of the fatigue fracture surface obtained in ASTM artificial seawater at -0.85V(sce), shows some similarity with figure 4.52. Thus the effect on the fracture mechanism of a hydrogen producing environment, coupled with an applied strain rate, may be the same for both slow strain rate tests and fatigue tests [196]. Because of the differences in the crack tip environment and applied strain rates, as well as the existence of a reversed plastic zone at the tip of a fatigue crack, this is not always true [196].

Evidence that the fracture mode does not control corrosion fatigue crack growth rates comes from the work of Hinton and Procter [196]. The region I crack growth is seen to occur via a number of different fracture modes. It is suggested that the fracture mode observed is a result of the crack tip strain and strain rate imposed by the applied loading [83]. However mainly brittle failure modes such as intergranular fracture and cleavage occurred in region I, with region III crack growth being a result of the occurrence of mainly ductile

fracture modes.

Some workers [207,254,255] have reported that the size of the reverse plastic zone may be dramatically altered by the application of cathodic protection. Very little work appears to have been published about such effects, although they are probably worth further study.

It may also be that some insight into the applicability of the models of hydrogen embrittlement can be gained from the fatigue crack propagation data. For instance, the fact that crack growth enhancement due to hydrogen embrittlement has been obtained using a square waveform suggests that a surface phenomena, such as Lynch's proposed mechanism [114-120], is not the cause of embrittlement.

Tomkins [64] has postulated that a mechanics controlled upper limit exists to crack growth by a hydrogen embrittlement mechanism. This limit is taken to be a fraction of the cyclic plastic zone size, and so the maximum crack growth rate is said to be a function of R and ΔK^2. The work of Vosikovsky [256] for X65 in crude oil containing H_2S is quoted by Scott et. al. [140] as supporting evidence for this idea. However Vosikovsky and Rivard [129] have explained the results obtained in crude oil saturated with H_2S on the basis that solution renewal down the crack is the rate controlling process for intermediate values of ΔK. (It was suggested [129] that at higher values of ΔK a ductile dimple type fracture process becomes dominant and hydrogen diffusion through the metal can then limit the maximum crack growth rate). In addition Austen [164] has obtained results for BS4360:50D in H_2S saturated seawater that show crack growth rates greatly in excess of those found by Vosikovsky for X65 in sour crude oil. As seen in the next chapter the corrosion fatigue crack growth rates for BS4360:50D and X65 are similar, and so this result suggests that Vosikovsky's frequency independent results were the consequence of limited solution renewal, rather than of a fundemental mechanics controlled limit to the hydrogen embrittlement mechanism. Austen's results also significantly exceed the $3\Delta 6$ limit found empirically for some steels in low pressure hydrogen gas [142]. Thus it appears that if a mechanics controlled limit to crack growth by a hydrogen embrittlement mechanism exists it is too great to form a useful design parameter.

5.5 Miscellaneous.

Wei and Landes [15] proposed that for corrosion fatigue above K_{1SCC} the crack growth rate is given by a summation of the crack growth rates due to SCC and fatigue in an inert environment. Subsequently a "process competition model" [17,78,257] has been proposed in which the two mechanisms of crack growth are assumed to be competitive, rather than additive. Both of these models describe the above K_{1SCC} data fairly well, and because one process tends to dominate crack growth the two models usually give fairly similar results. However as seen from the data of Gallagher et. al. [215] the superposition model [15] underestimates the crack growth rate by up to a factor of two, over an intermediate range of frequencies at a constant value of ΔK. This reveals a defect of both the superposition and process competition models, namely that no crack growth is assumed to occur when $K<K_{1SCC}$. Dynamic loading affects the crack tip strain and strain rate and so alters K_{1SCC}. It has been shown that "K_{1SCC}" is lowered by dynamic loading [62].

From figures 4.22 and 4.33 it appears that the normal fatigue mechanism in air of striation formation, and the hydrogen embrittlement mechanism act competitively. The situation is not so clear as regards striation formation and a dissolution mechanism, although in section 5.3 the two processes were taken to be competitive during region I crack growth and additive during region II. The results of this study shown in figures 5.2 and 10.5 indicate that the dissolution and hydrogen embrittlement mechanisms may be additive. Also it is certainly possible that a crack may grow with one portion of the crack front advancing via a dissolution mechanism and adjacent portions of the crack front advancing as a result of hydrogen embrittlement [74].

5.6 Conclusions.

During this chapter it has been shown that for the material/environment system studied both anodic dissolution and hydrogen embrittlement may operate as mechanisms of crack growth. This mechanistic knowledge was then used to explain the effects of several environmental and loading variables upon the fatigue crack growth rate. The chapter was concluded with a more detailed disussion of these mechanisms of environmentally assisted crack growth.

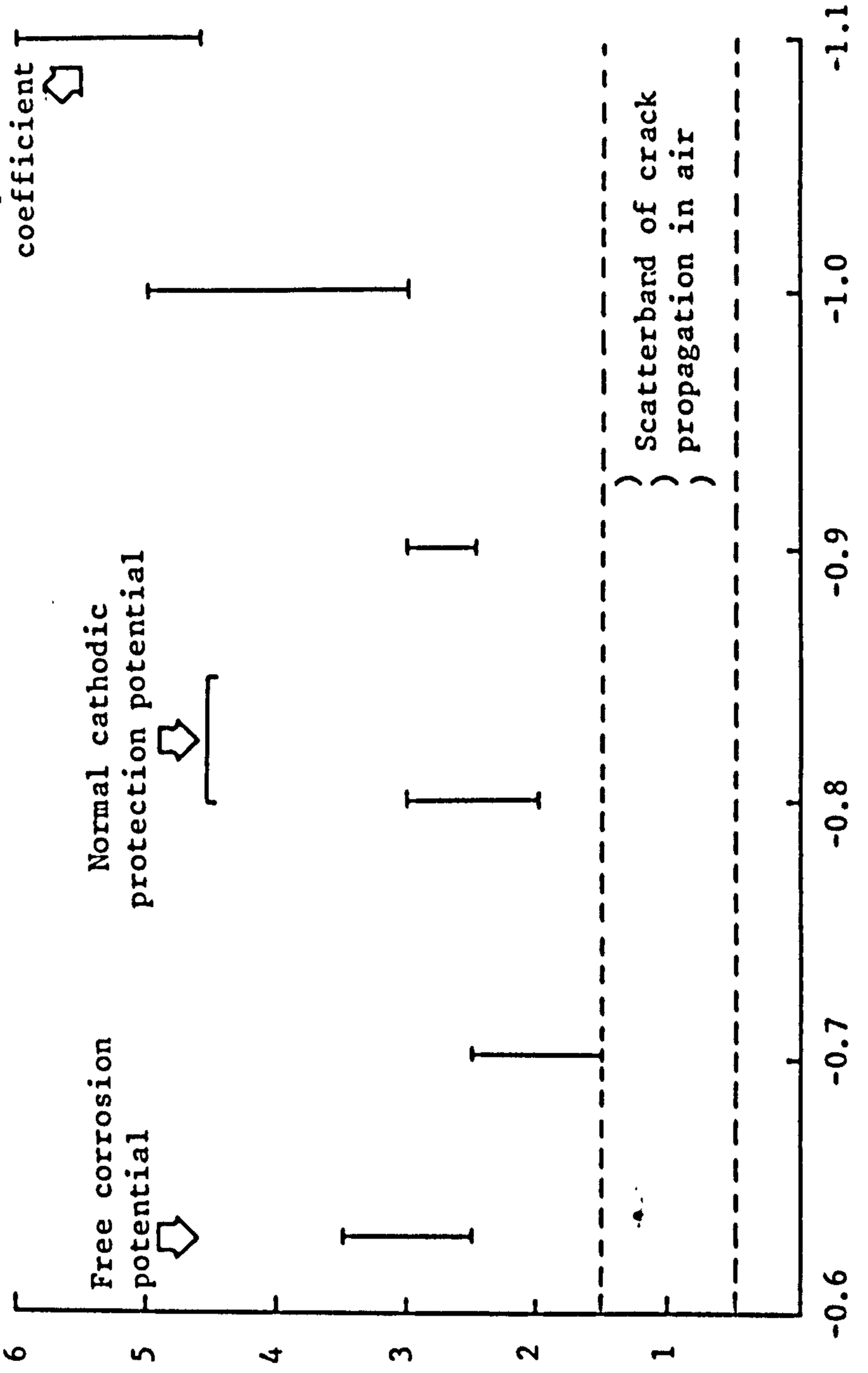

Figure 5.1 Effect of specimen potential on crack growth rate relative to air data (139)

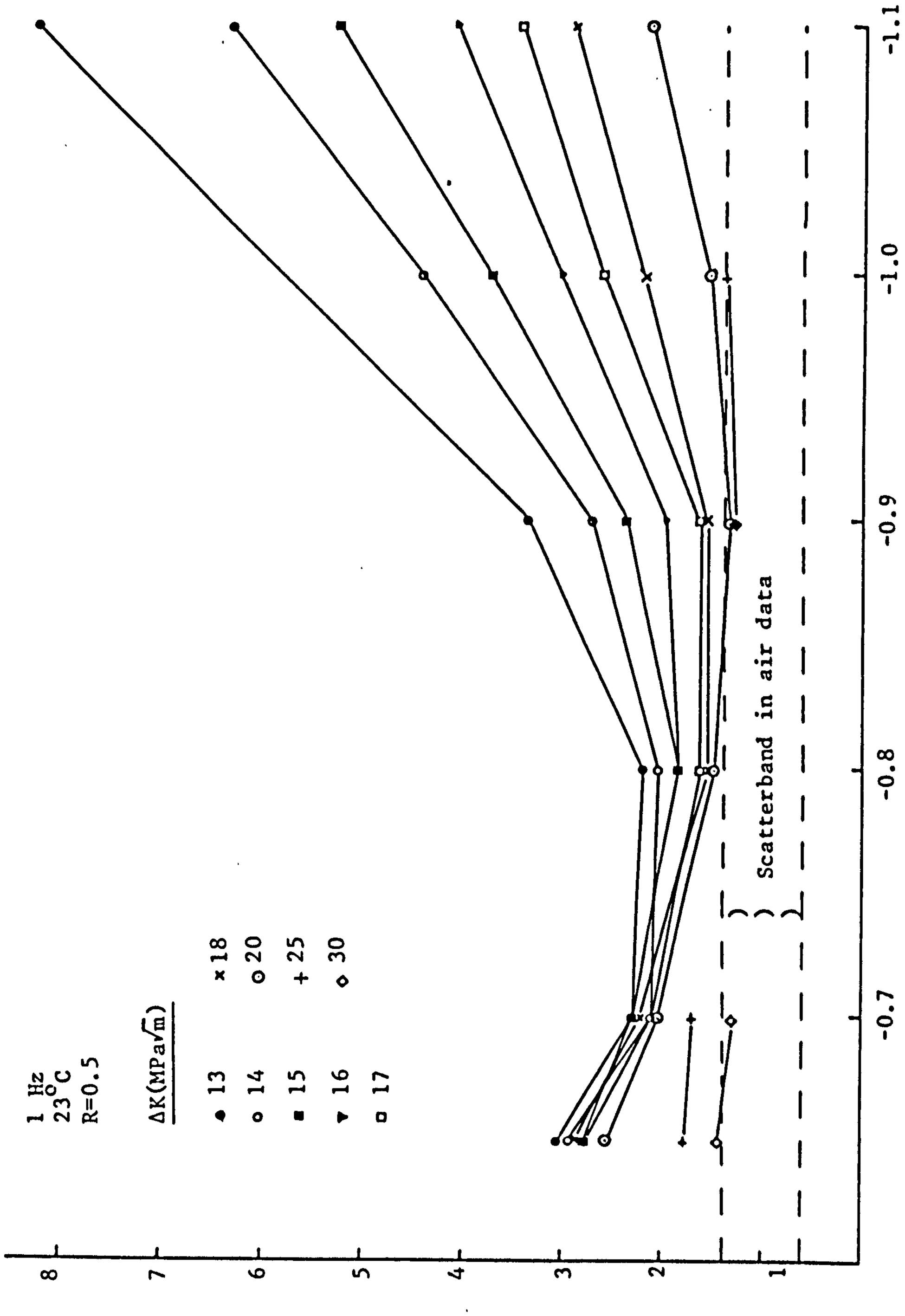

Figure 5.2 Effect of specimen potential on crack growth rate relative to air data

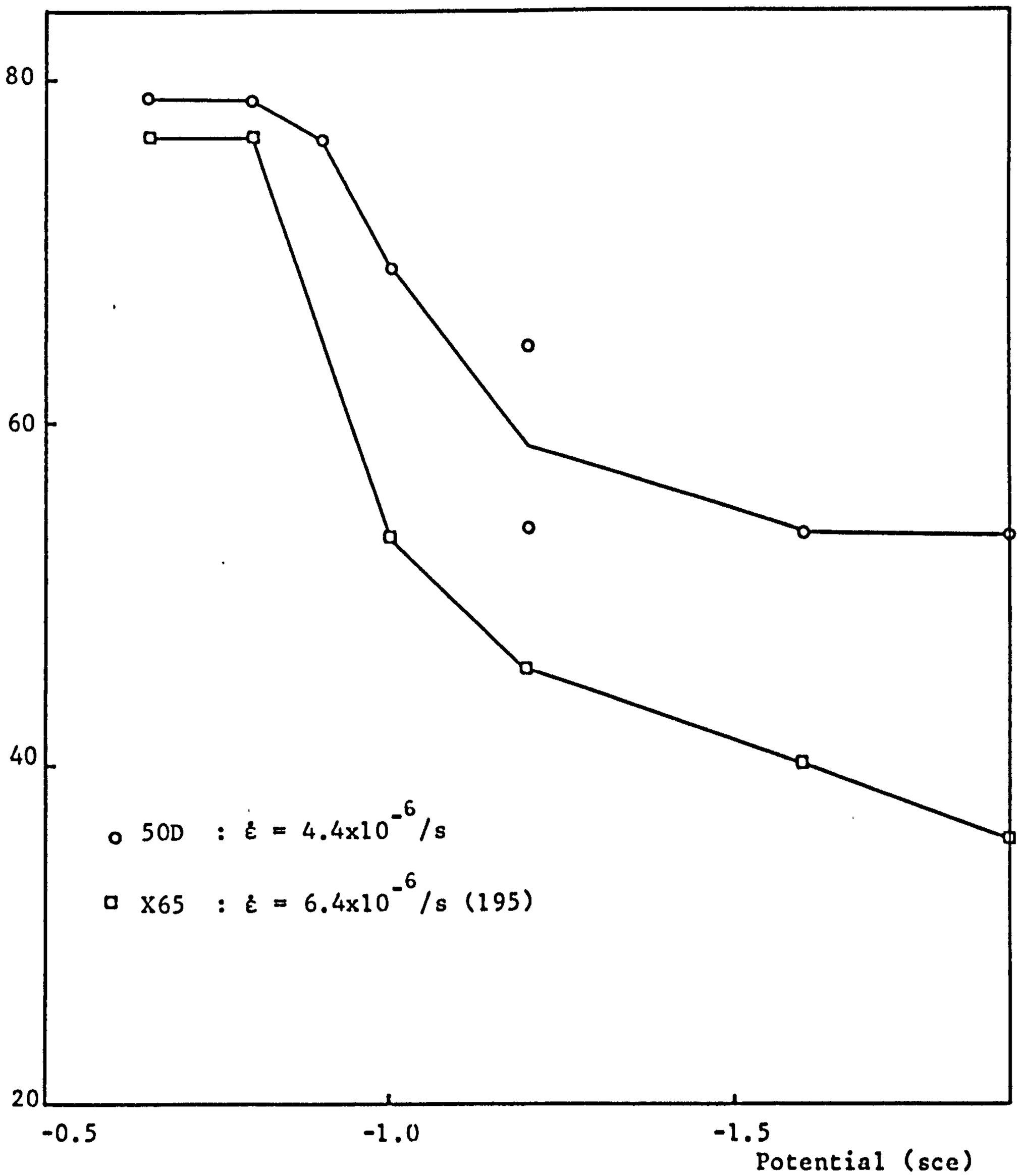

Figure 5.3 Comparison of slow strain rate results

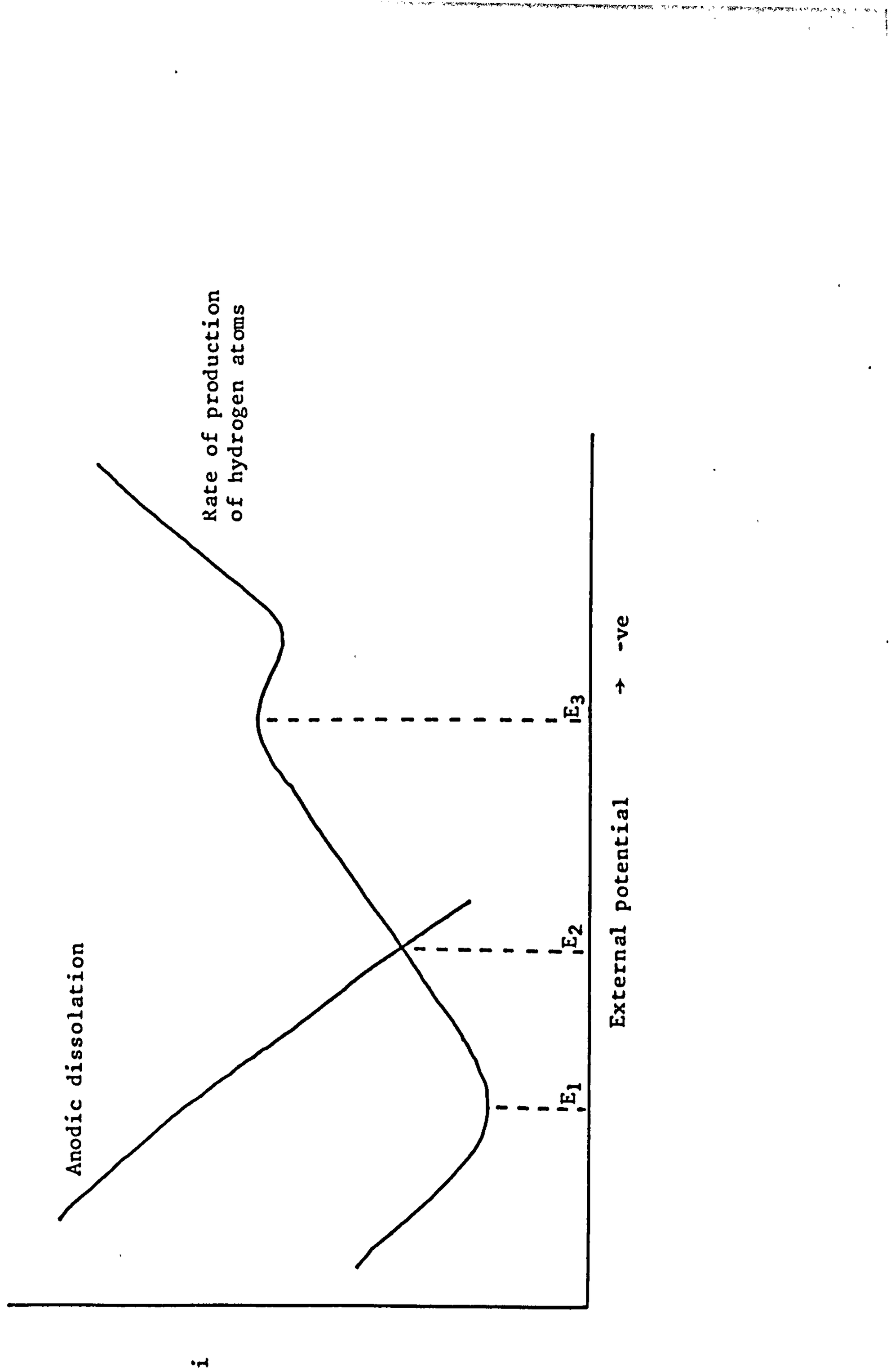

Figure 5.4 Schematic illustration of the variation of the current density $\vec{i}$ with applied external potential, from Turnbull (30)

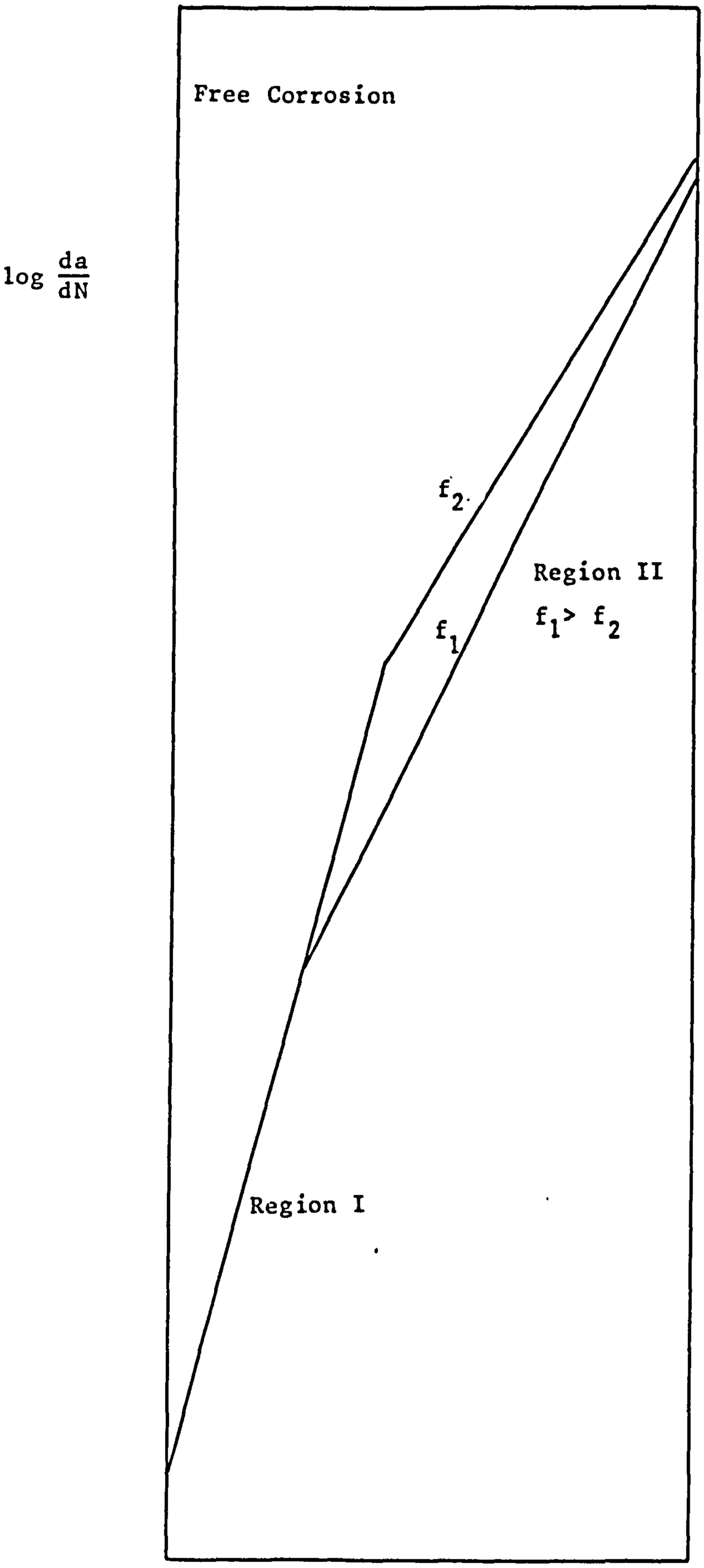
Free Corrosion
$\log \frac{da}{dN}$
f_2
f_1
Region II
$f_1 > f_2$
Region I
log ΔK

Figure 5.5

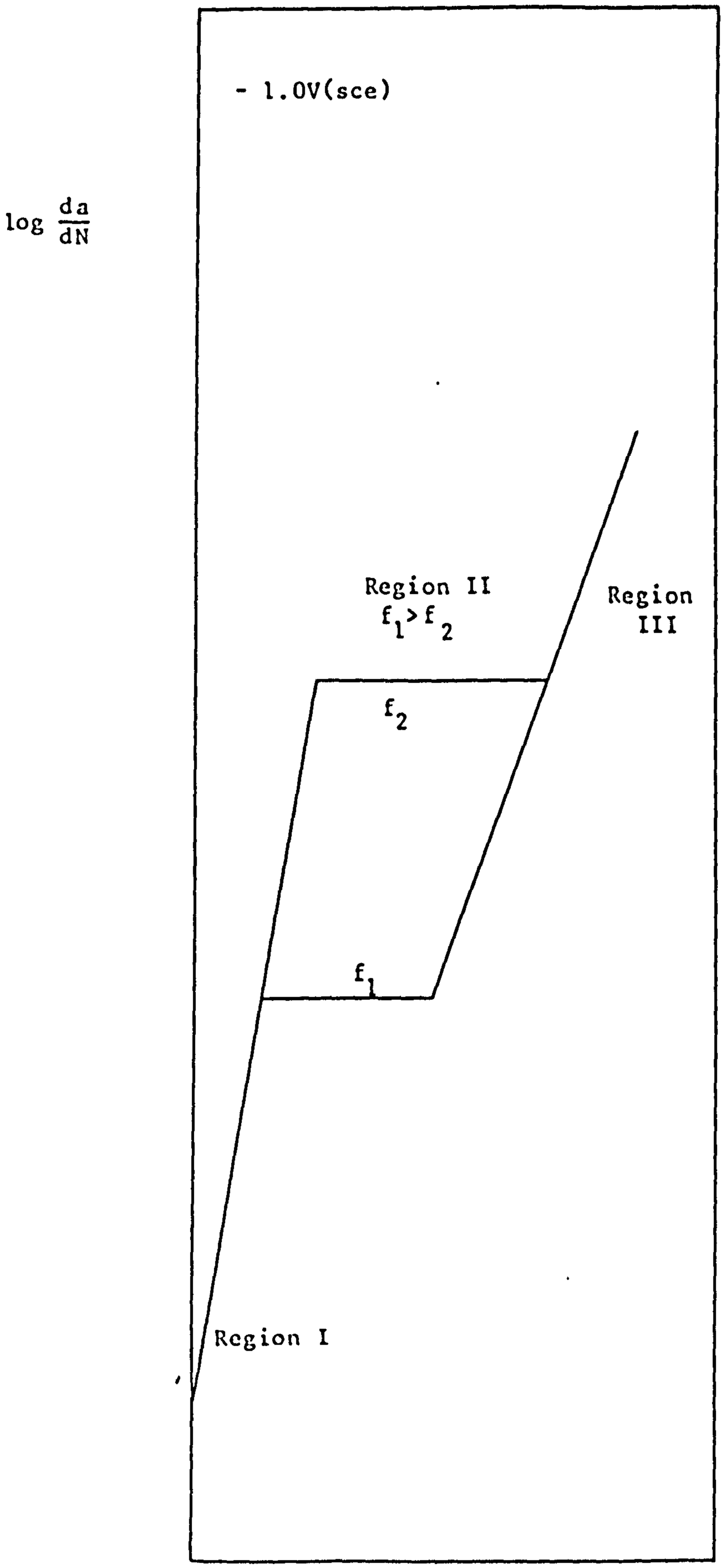
- 1.0V(sce)
log da/dN
Region II
f1>f2
Region
III
f2
f1
Region I
log ΔK

Figure 5.6

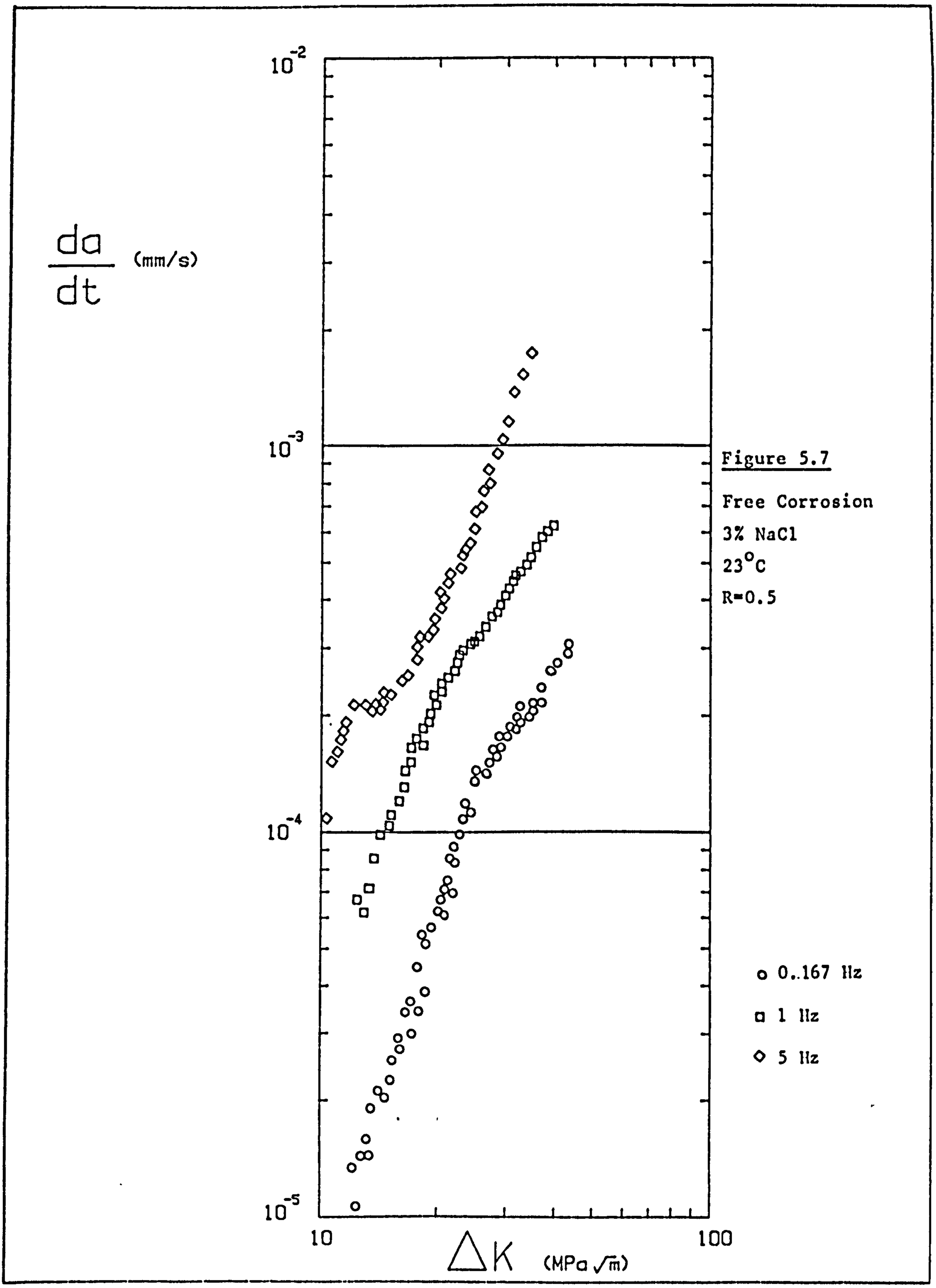
da/dt (mm/s)
10^-2
10^-3
10^-4
10^-5
10
100
ΔK (MPa √m)
Free Corrosion
3% NaCl
23°C
R=0.5
0..167 Hz
1 Hz
5 Hz

Figure 5.7

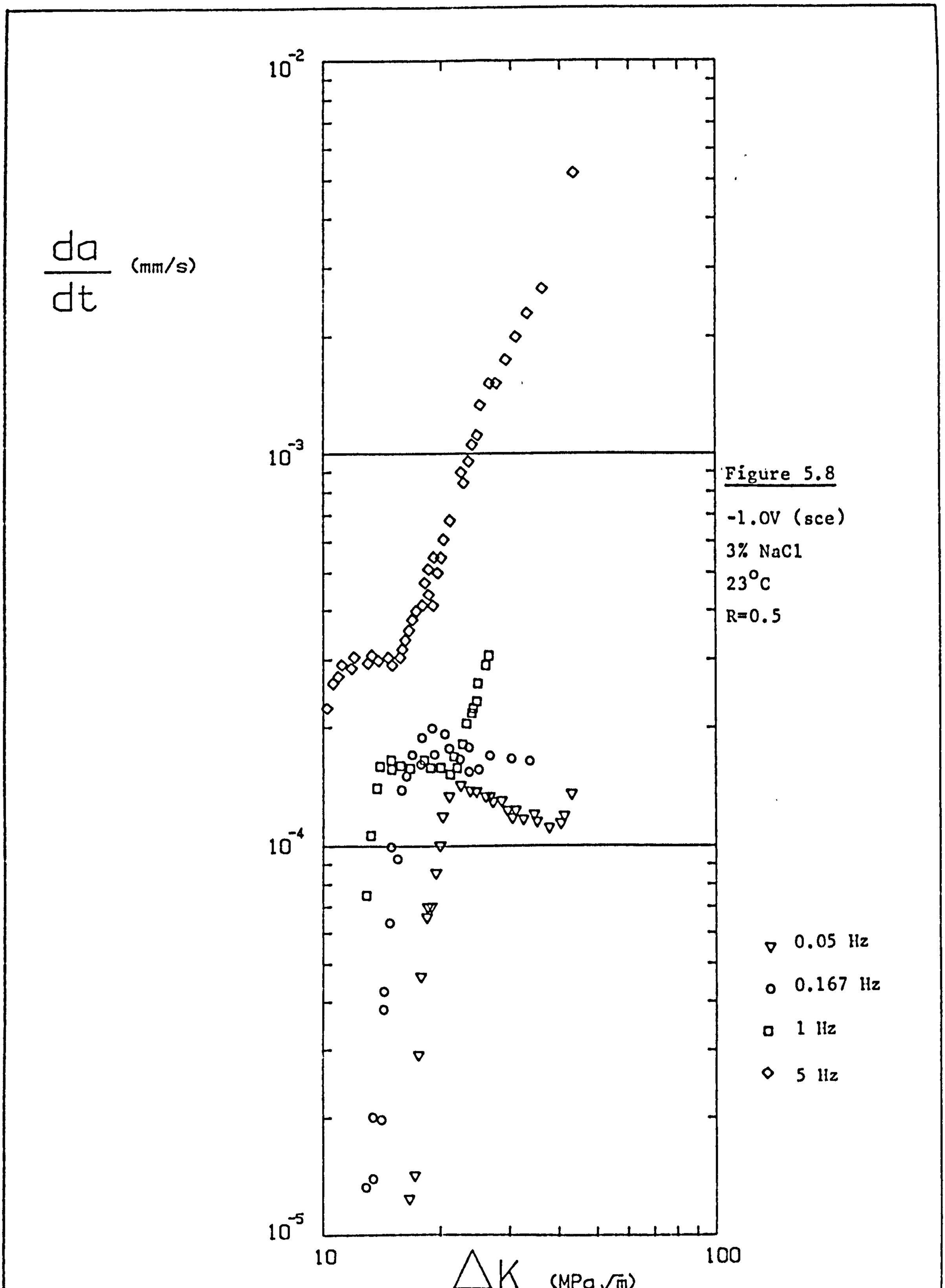
10^{-2}
10^{-3}
10^{-4}
10^{-5}
$\frac{da}{dt}$ (mm/s)
10
100
ΔK (MPa $\sqrt{m}$)
-1.0V (sce)
3% NaCl
23°C
R=0.5
0.05 Hz
0.167 Hz
1 Hz
5 Hz

Figure 5.8

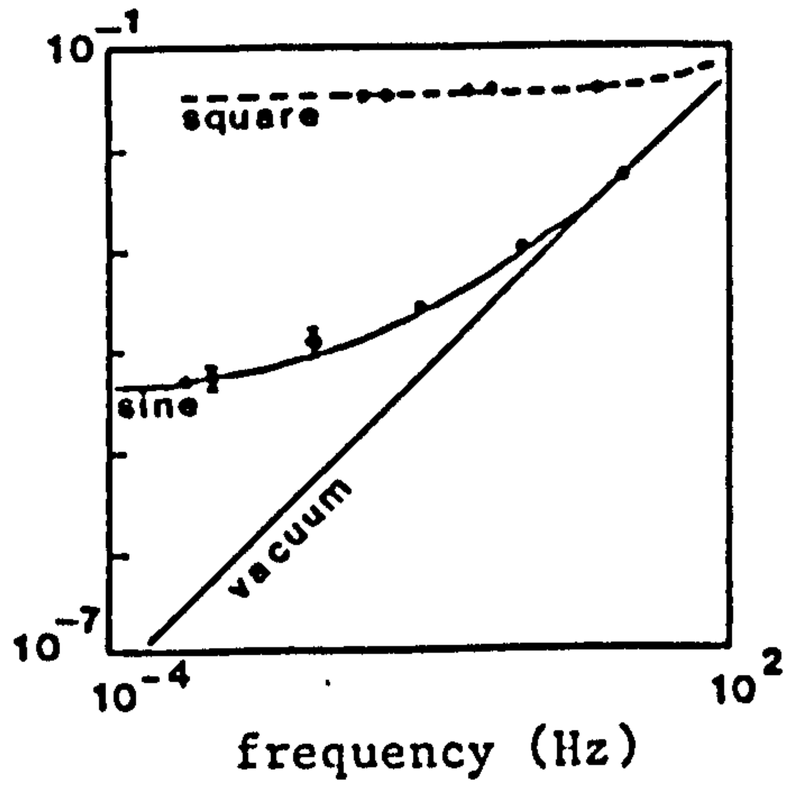

(a) above K_{1SCC} : $\Delta K = K_{max} = 40 ksi\sqrt{in}$
(σ_y=220ksi for square wave loading)

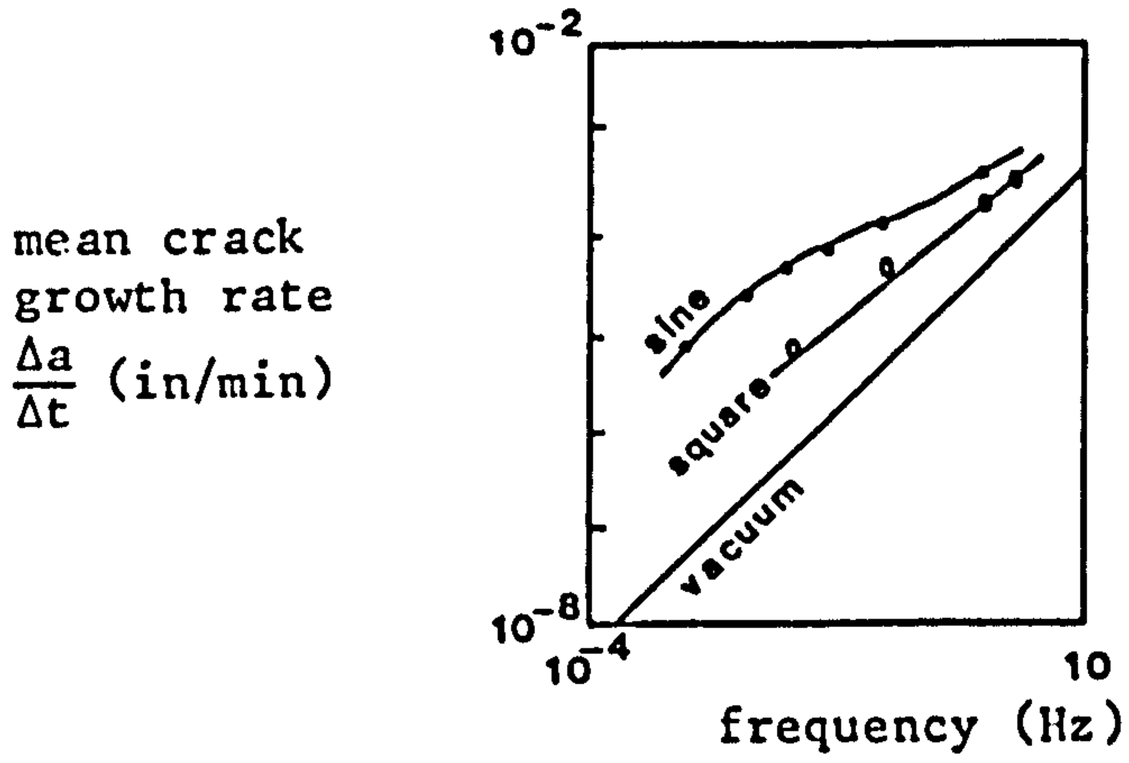

(b) below K_{1SCC} : $\Delta K = K_{max} = 20 ksi\sqrt{in}$

Figure 5.9 : above and below K_{1SCC} corrosion fatigue behaviour of 4340 steel (σ_y=190ksi) in 3.5% NaCl, from reference (215)

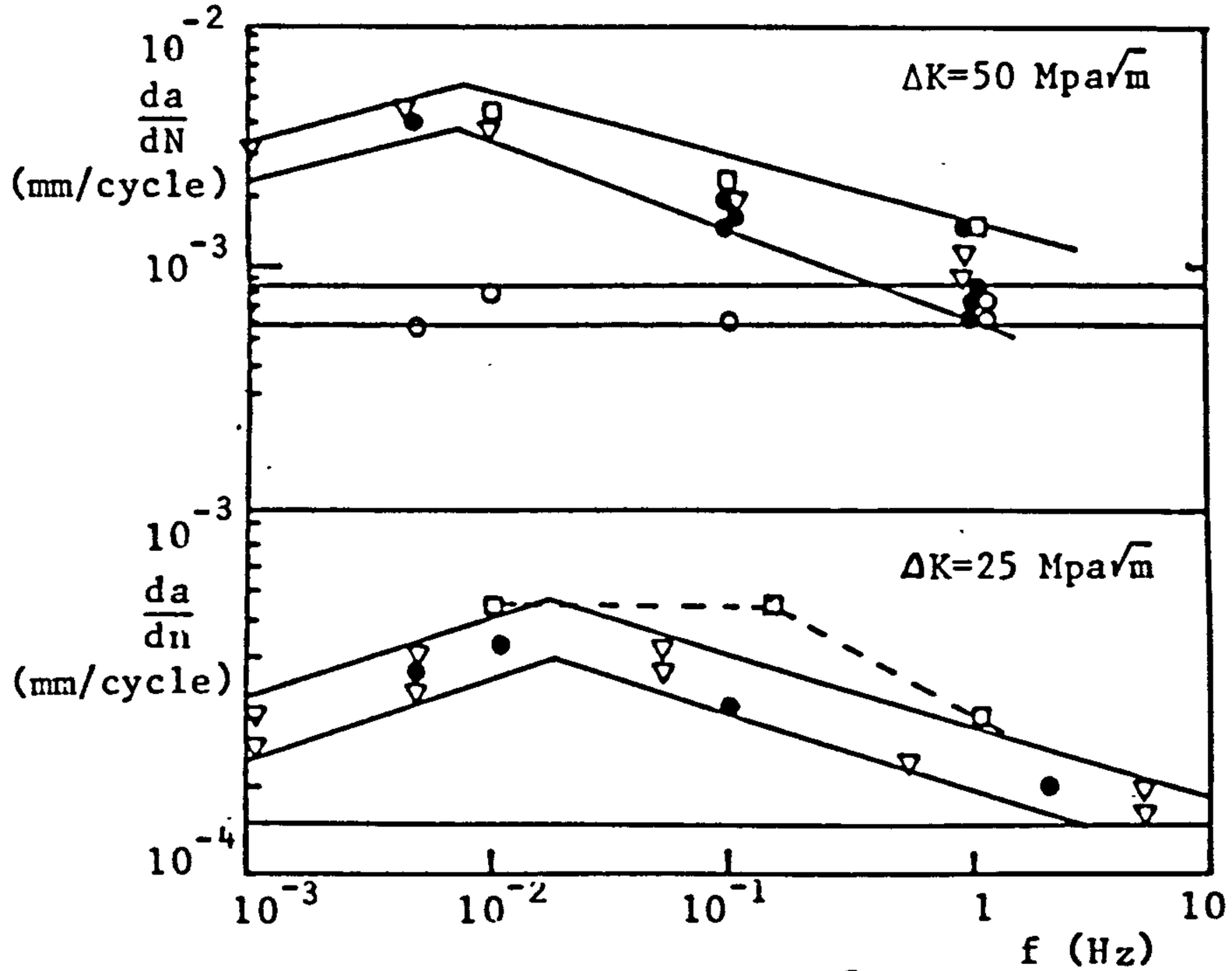

▫ 3.5% NaCl, X 65, 23°C (72)

● Lakewater, 25°C)
) C-Mn steel
▽ Distilled water, 30°C)

Effect of frequency on fatigue crack growth rate in water, triangular waveform (61)

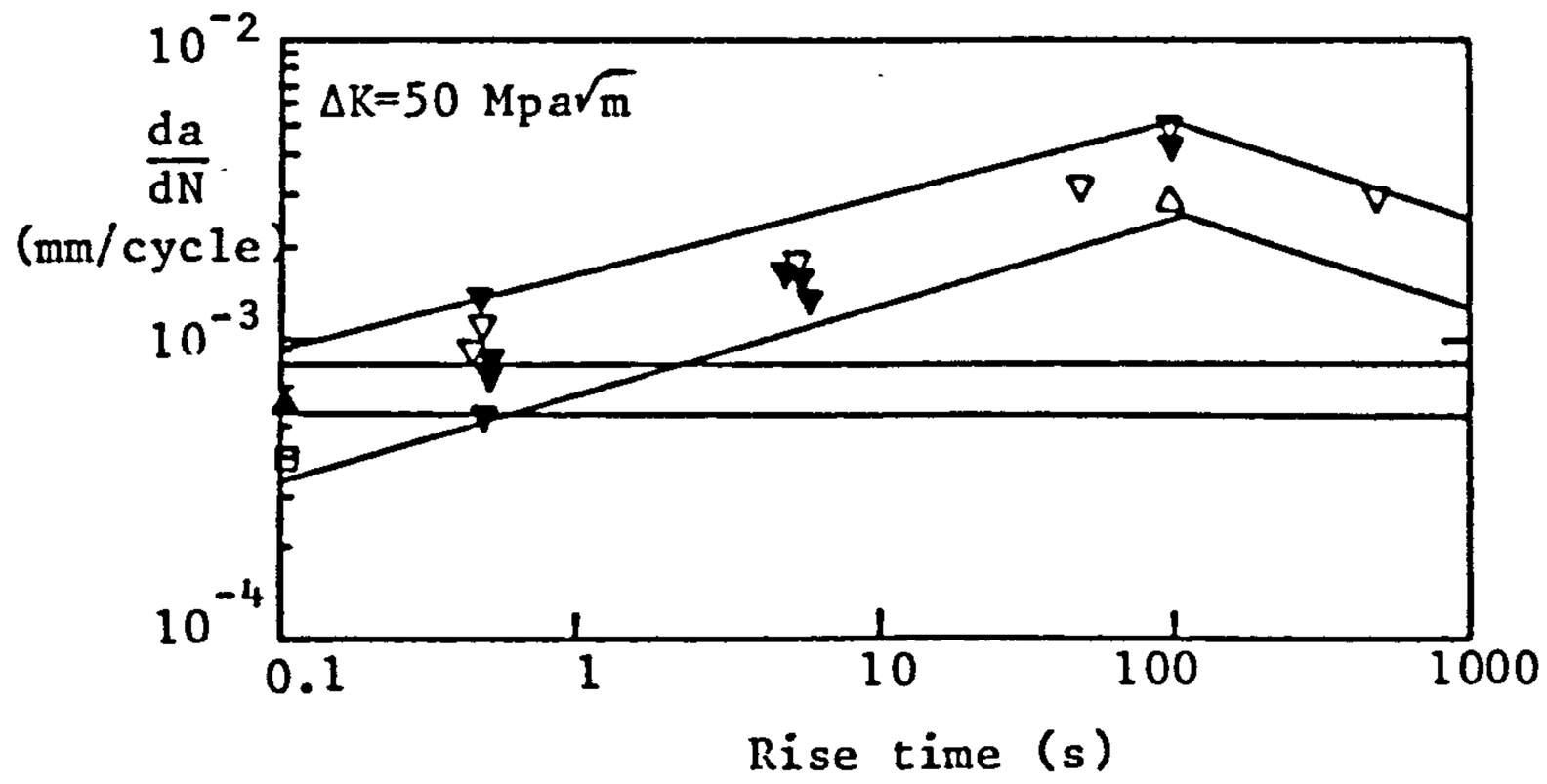

▼ Triangular, Lakewater, 25°C
▽ Triangular, Distilled water, 30°C
△ Positive sawtooth)
) Lakewater, 25°C
▲ Negative sawtooth)
▫ Squarewave)

Effect of waveform on fatigue crack growth rate in water (61)

Figure 5.10

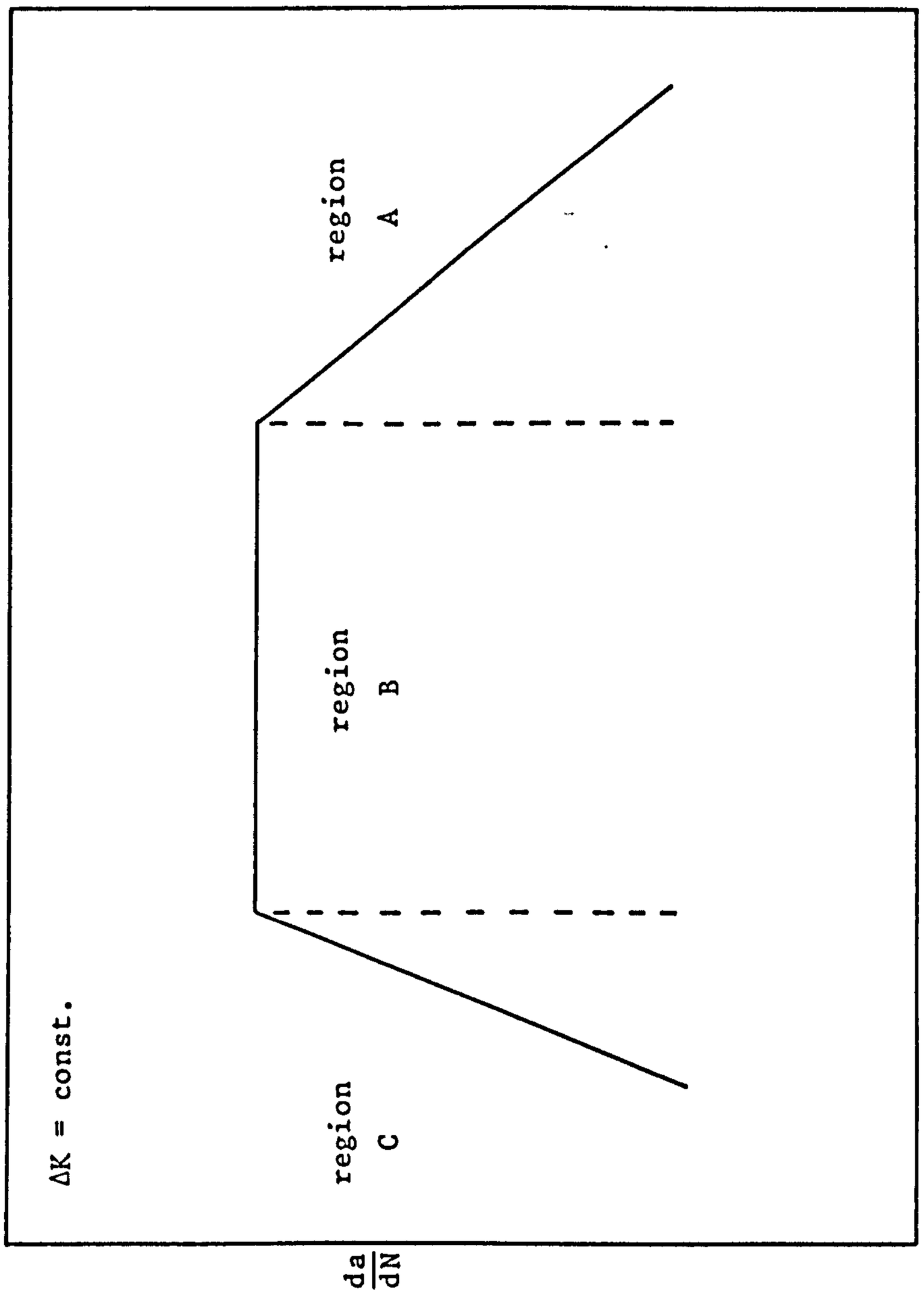

Figure 5.11 Schematic diagram showing dependence of da/dn on frequency, f, at constant ΔK

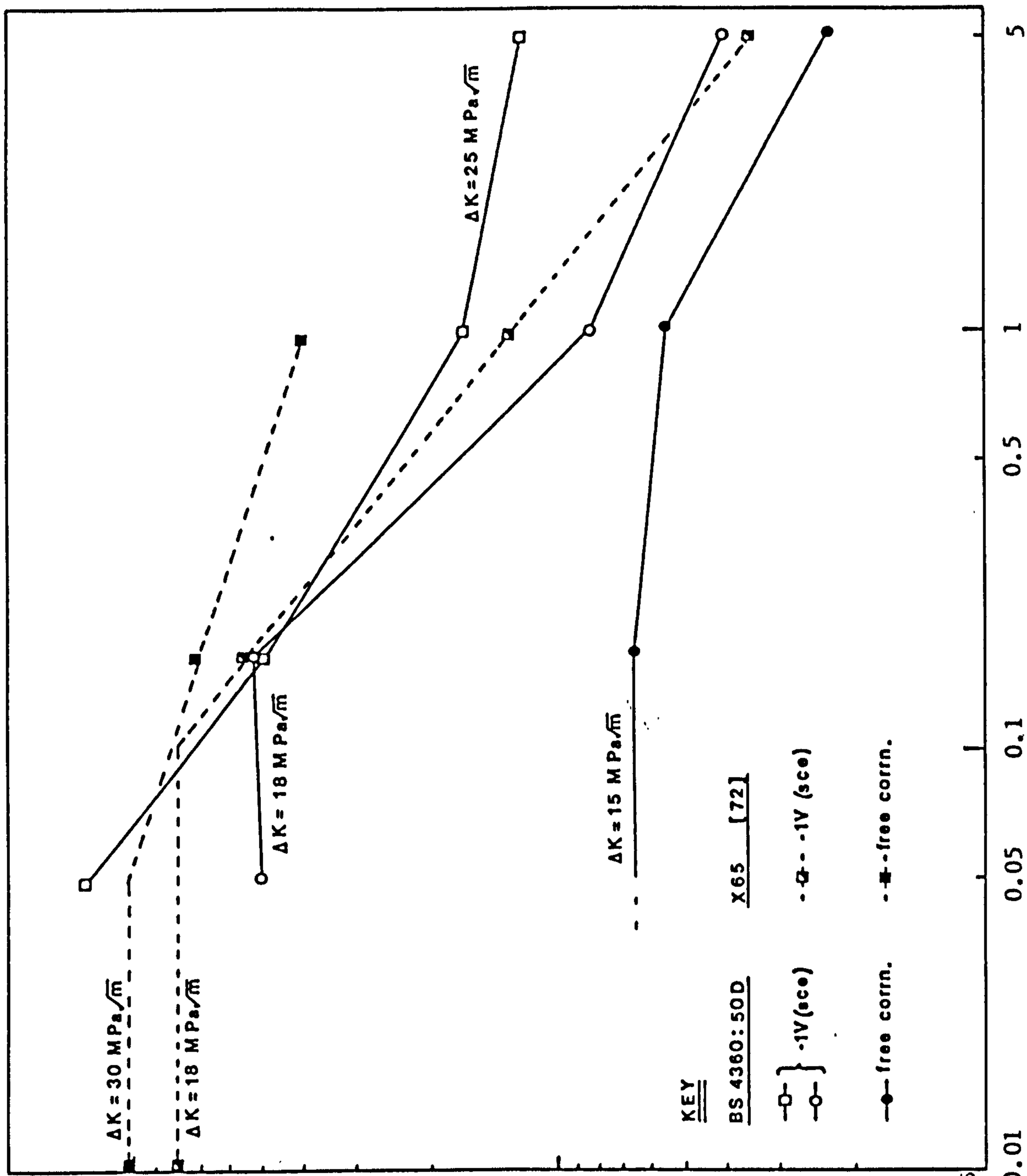
ΔK=25 MPa√m
ΔK=30 MPa√m
ΔK=18 MPa√m
ΔK = 18 MPa√m
ΔK=15 MPa√m
KEY
BS 4360: 50D
X65 [72]
-1V(sce)
-1V (sce)
free corn.
free corn.
5
1
0.5
0.1
0.05
0.01
10-3
10-4
10-5
da/dN (mm/cycle)
frequency (Hz)

Figure 5.12

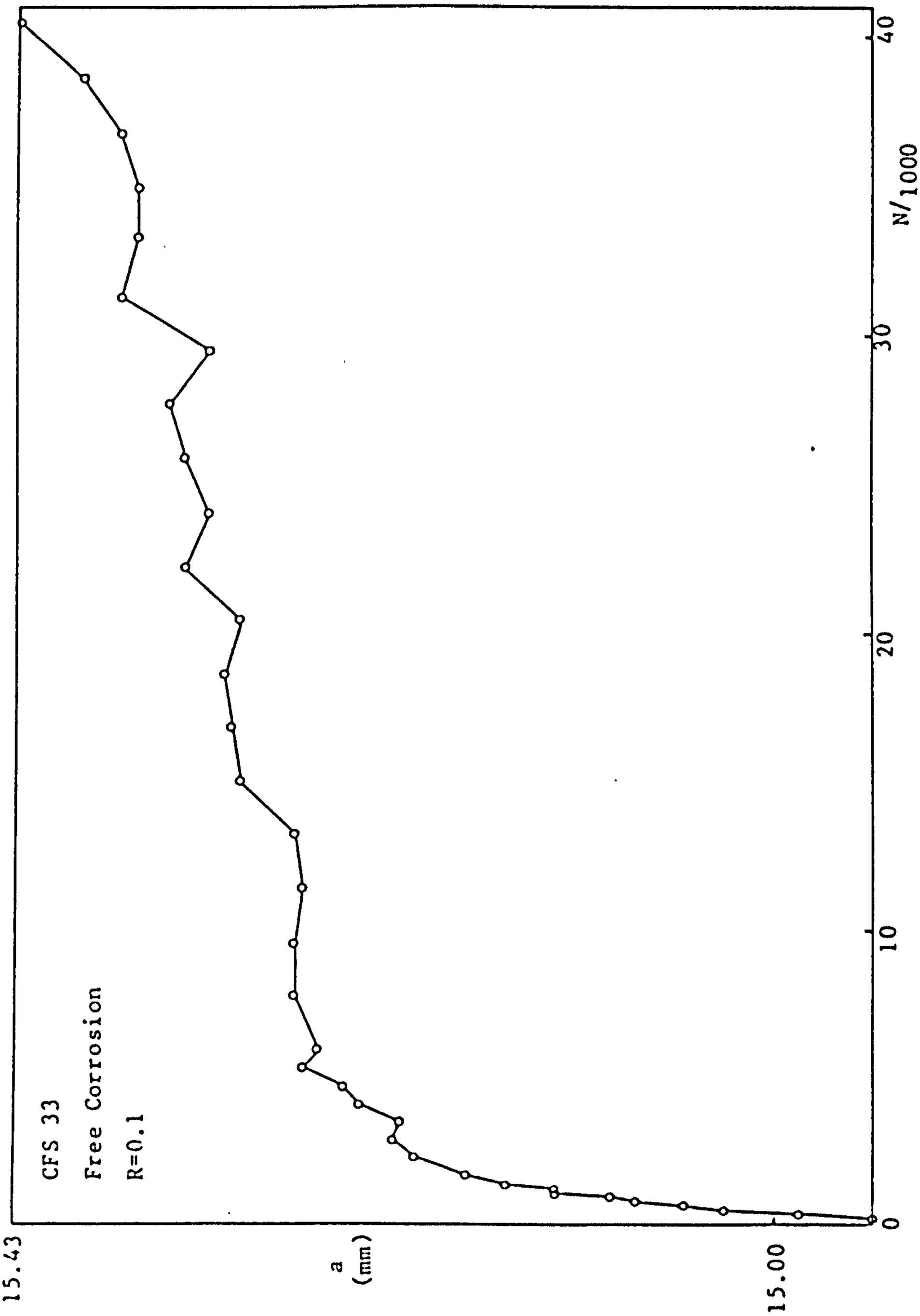

Figure 5.13

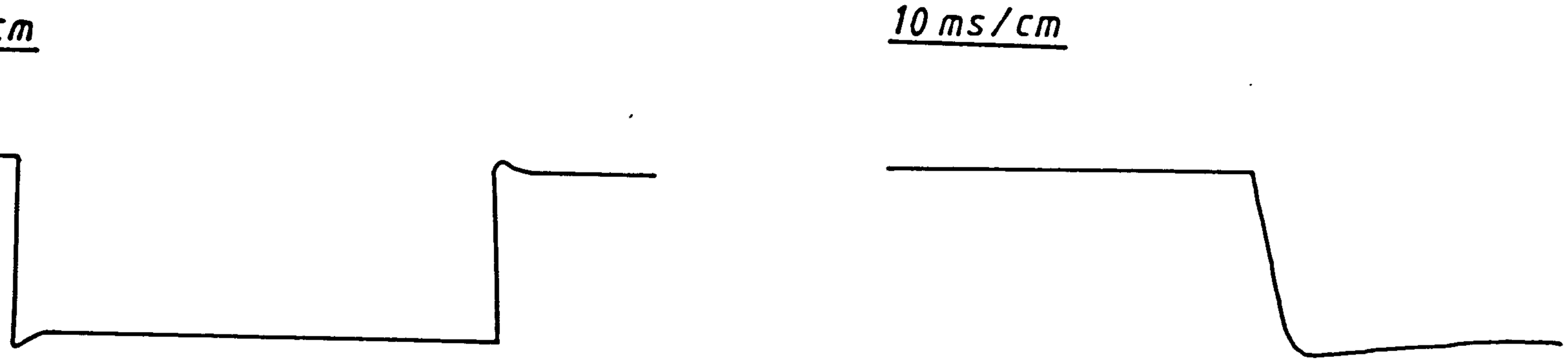

CFS 36 : -1V, 0·167 Hz

Tracing of square wave load signal.

Figure 5.14

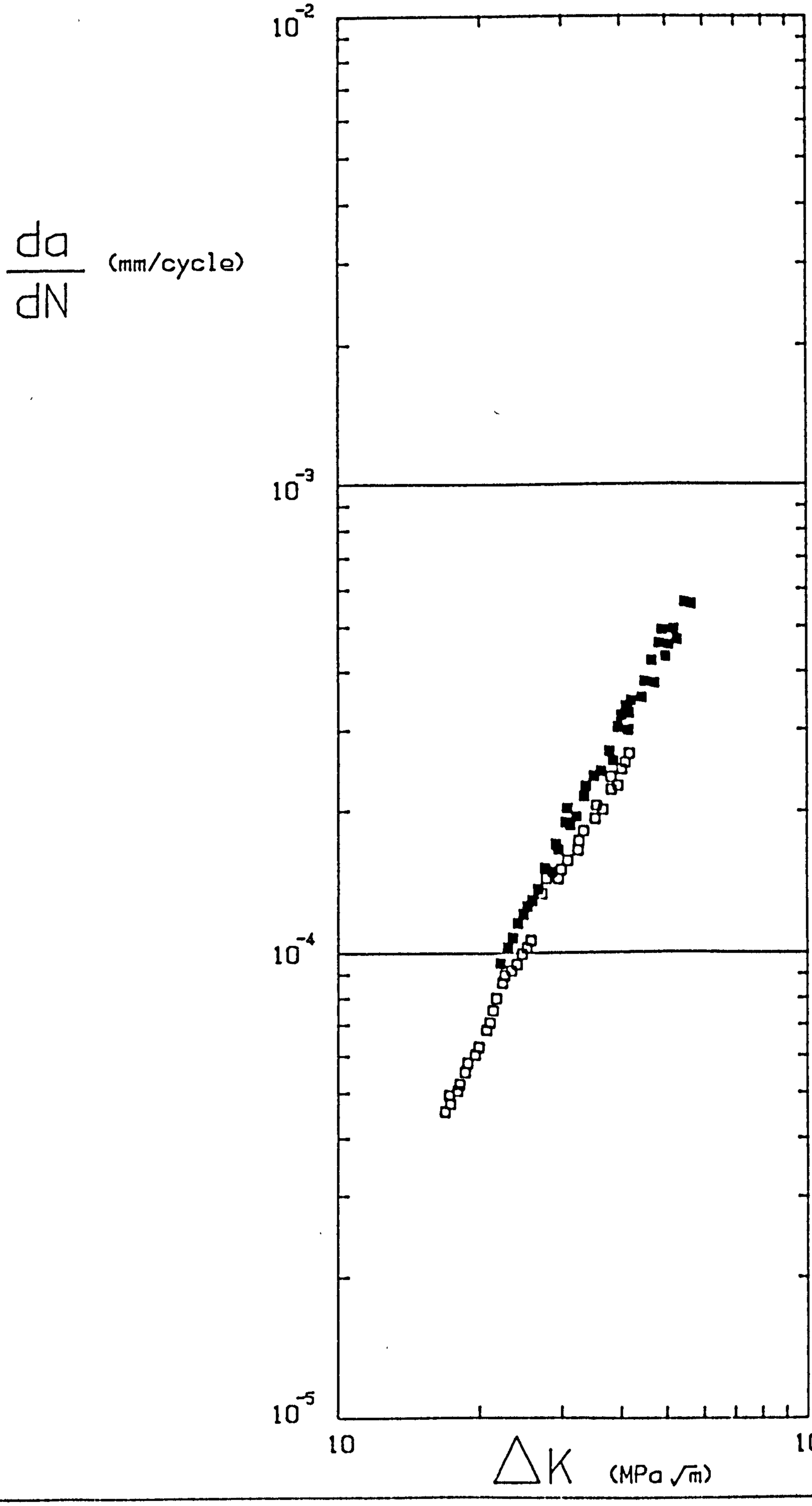

Figure 5.15

Free Corrosion

3% NaCl

0.167 Hz

23°C

R=0.5

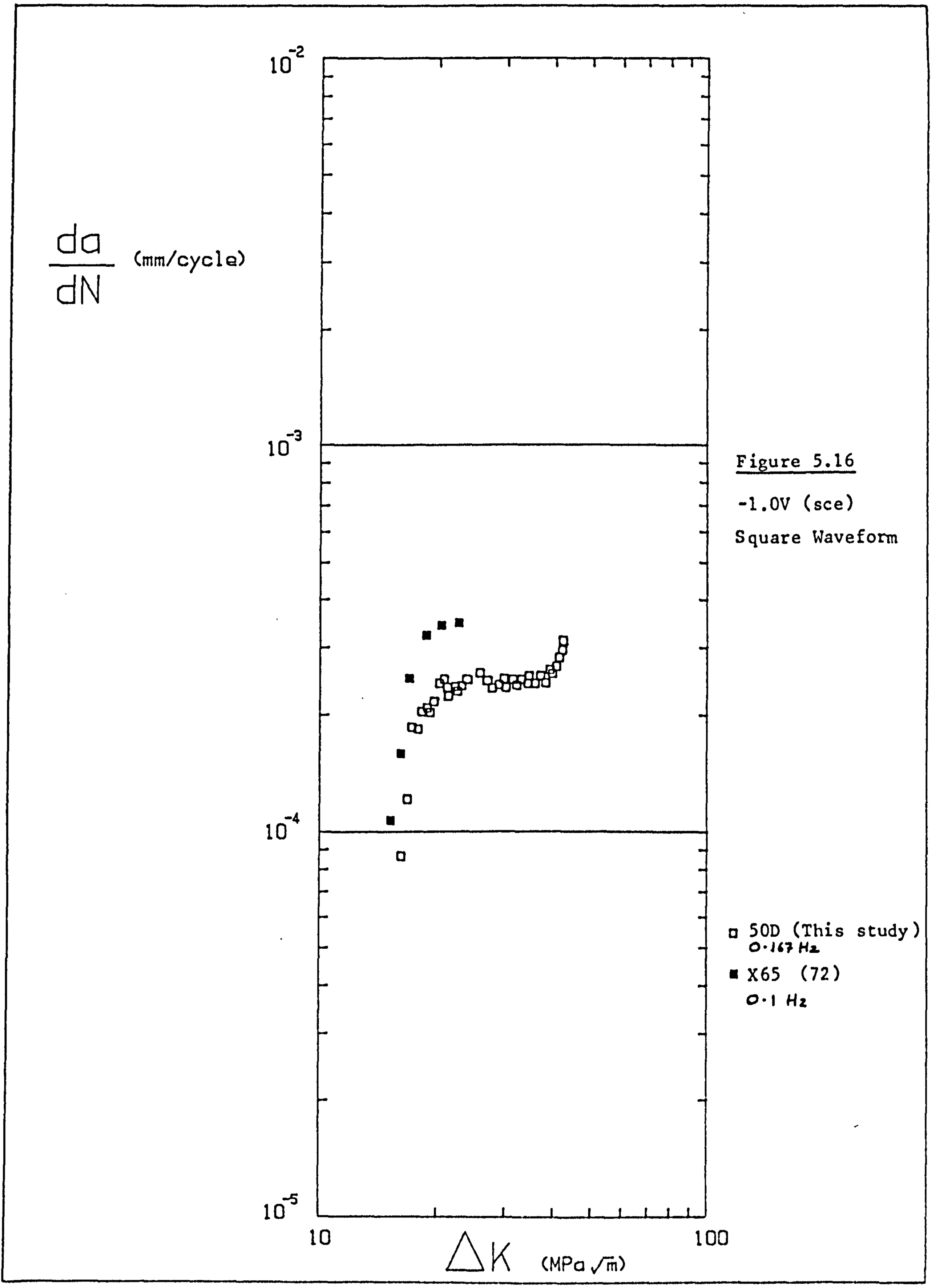

Figure 5.16

-1.0V (sce)

Square Waveform

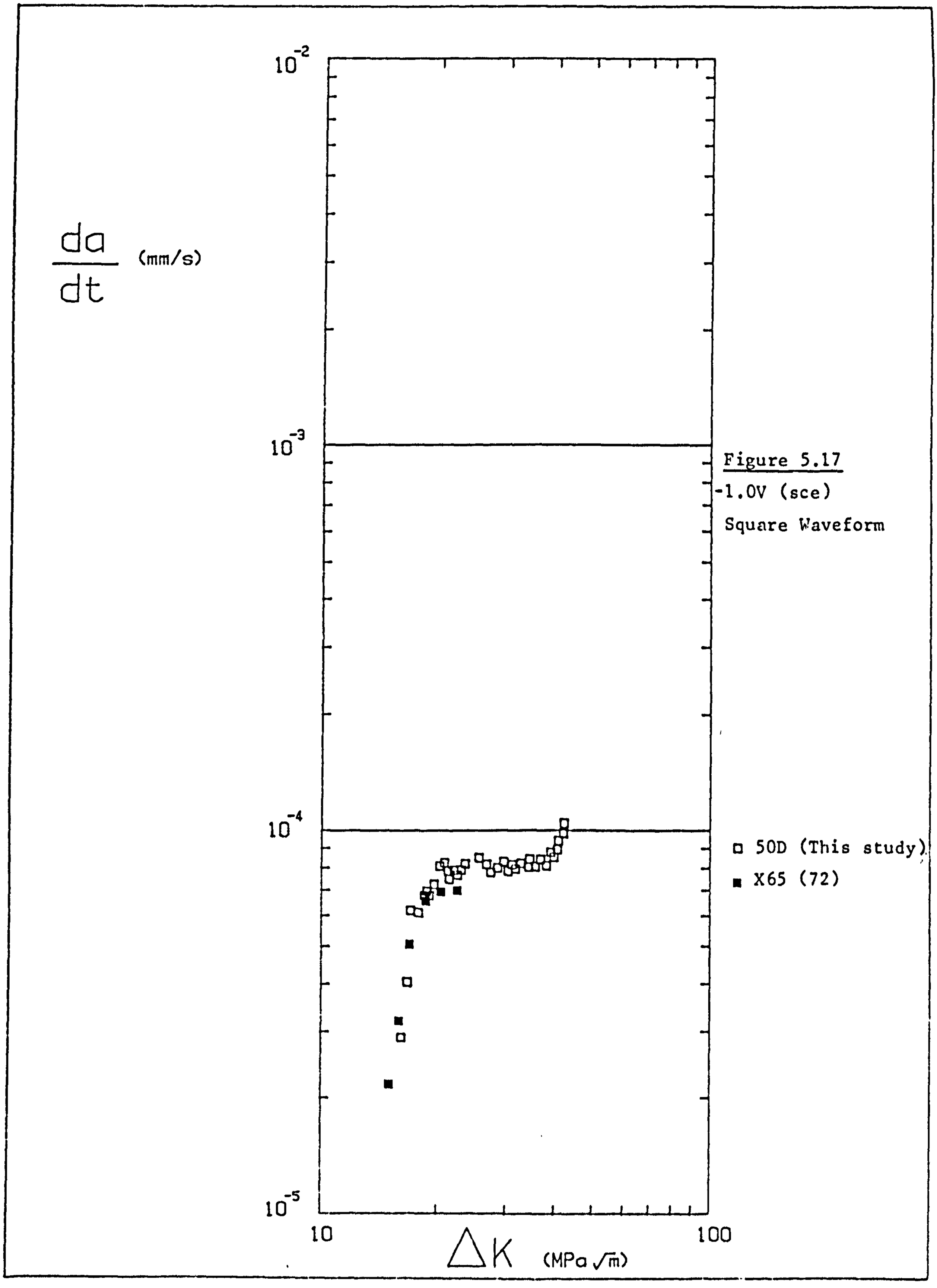
da/dt (mm/s)
10^-2
10^-3
10^-4
10^-5
10
100
ΔK (MPa √m)
-1.0V (sce)
Square Waveform
50D (This study)
X65 (72)

Figure 5.17

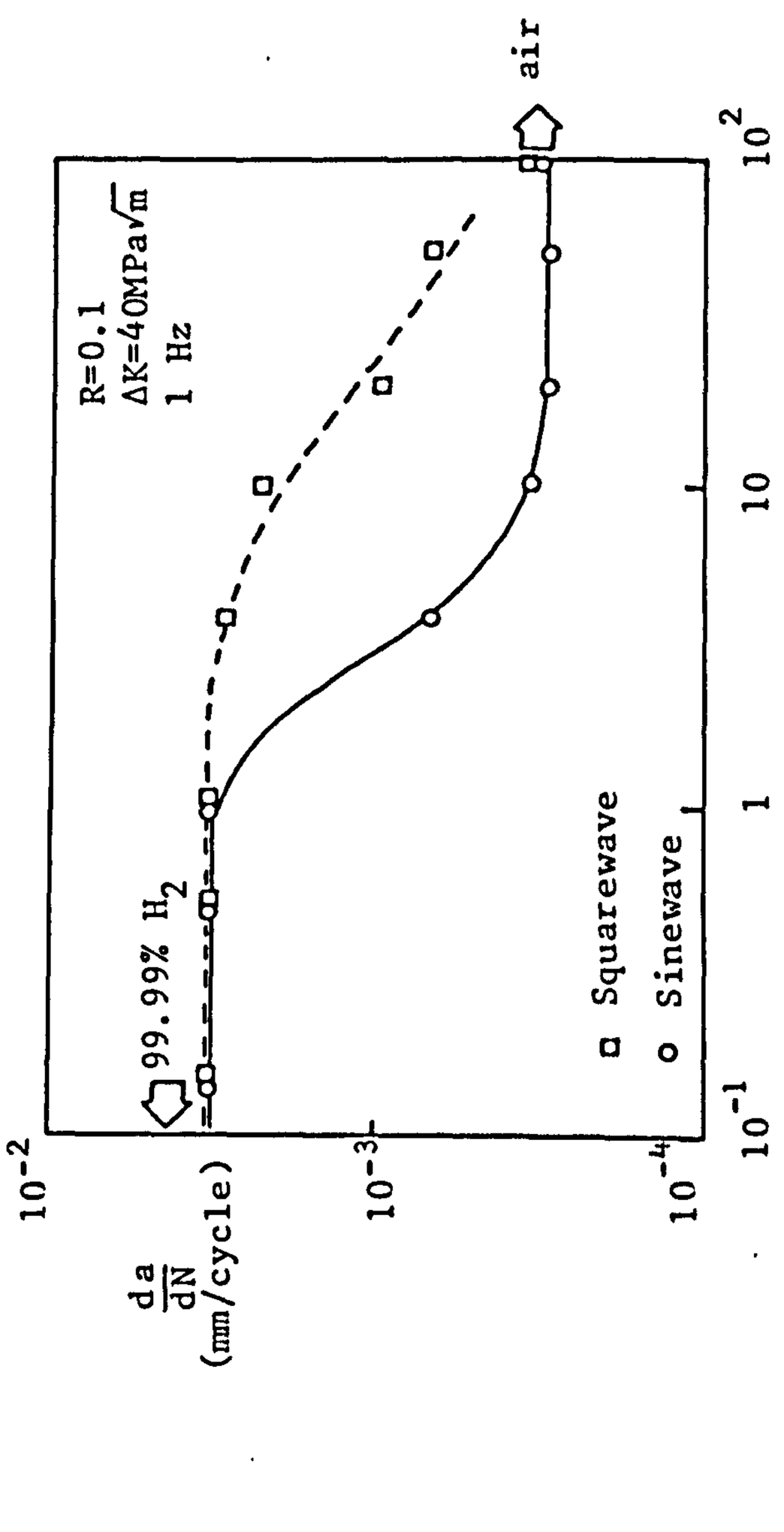

Figure 5.18 Effect of air additions on fatigue crack growth rate in hydrogen for a 2Ni-Cr-Mo-V steel, (96)

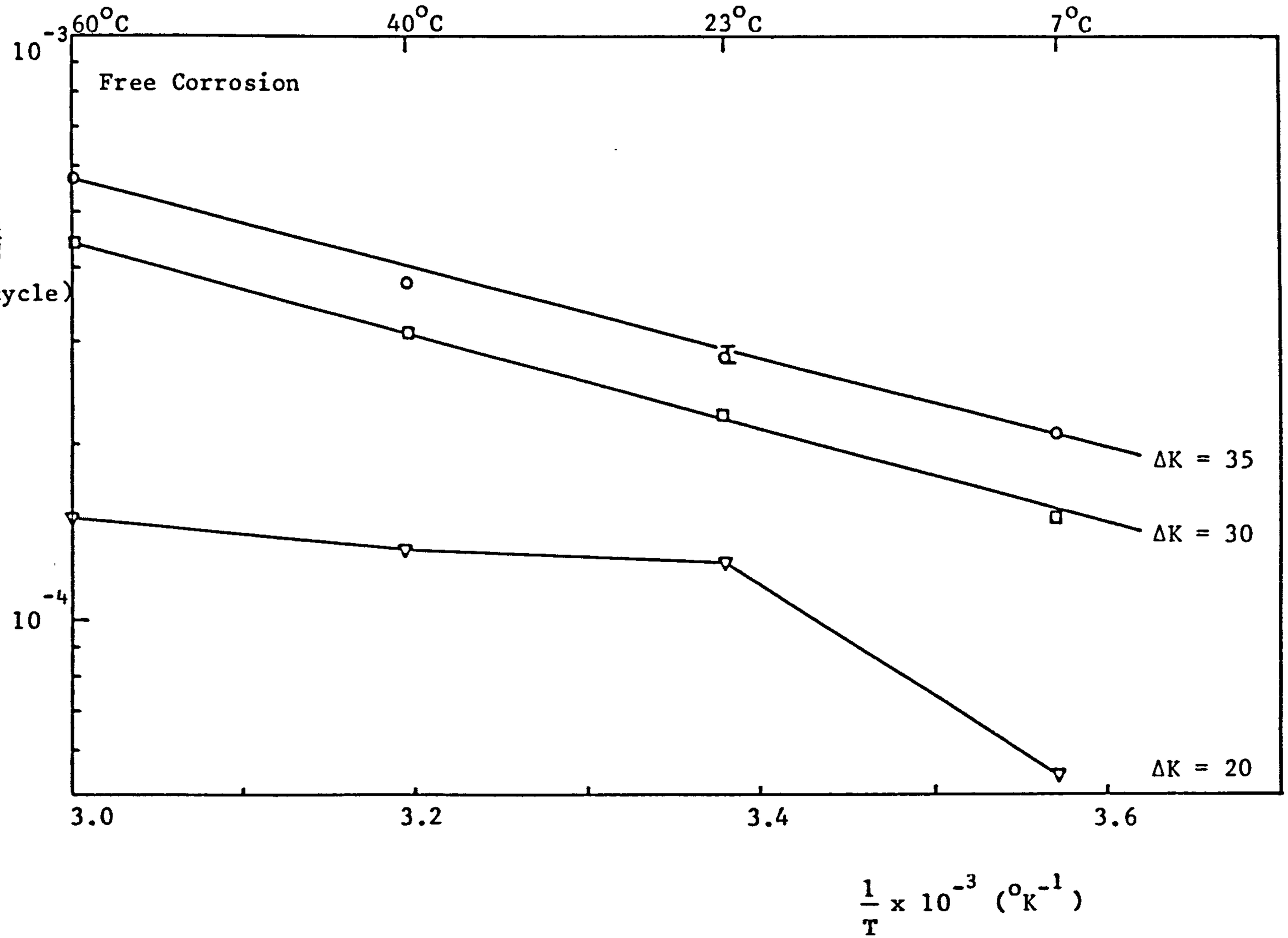
60°C
40°C
23°C
7°C
10^-3
Free Corrosion
da/dN
(mm/cycle)
ΔK = 35
ΔK = 30
ΔK = 20
10^-4
3.0
3.2
3.4
3.6
1/T x 10^-3 (°K^-1)

Figure 5.19

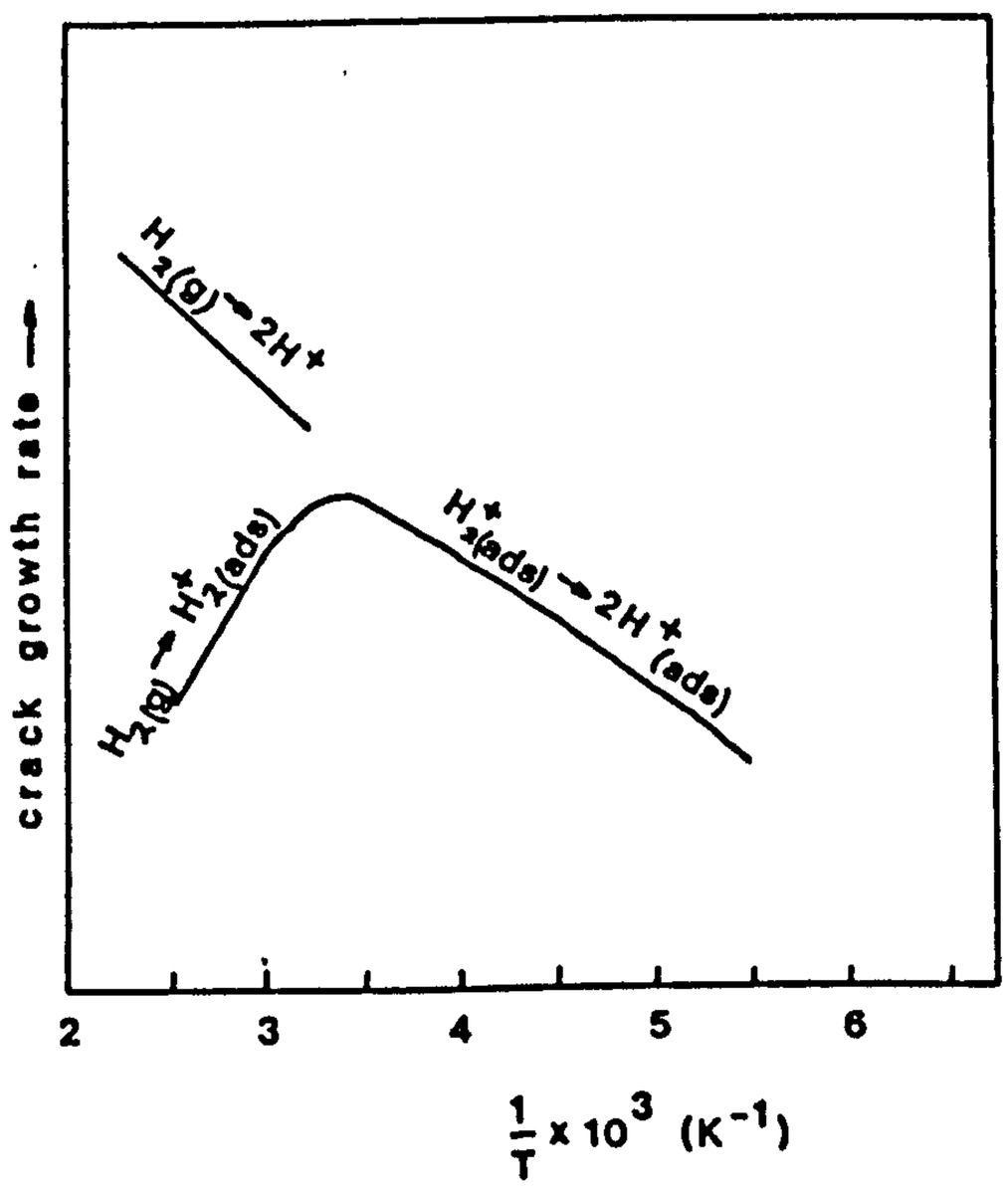

Figure 5.20 Schematic of crack growth rate considering the controlling adsorption process step, from reference (232)

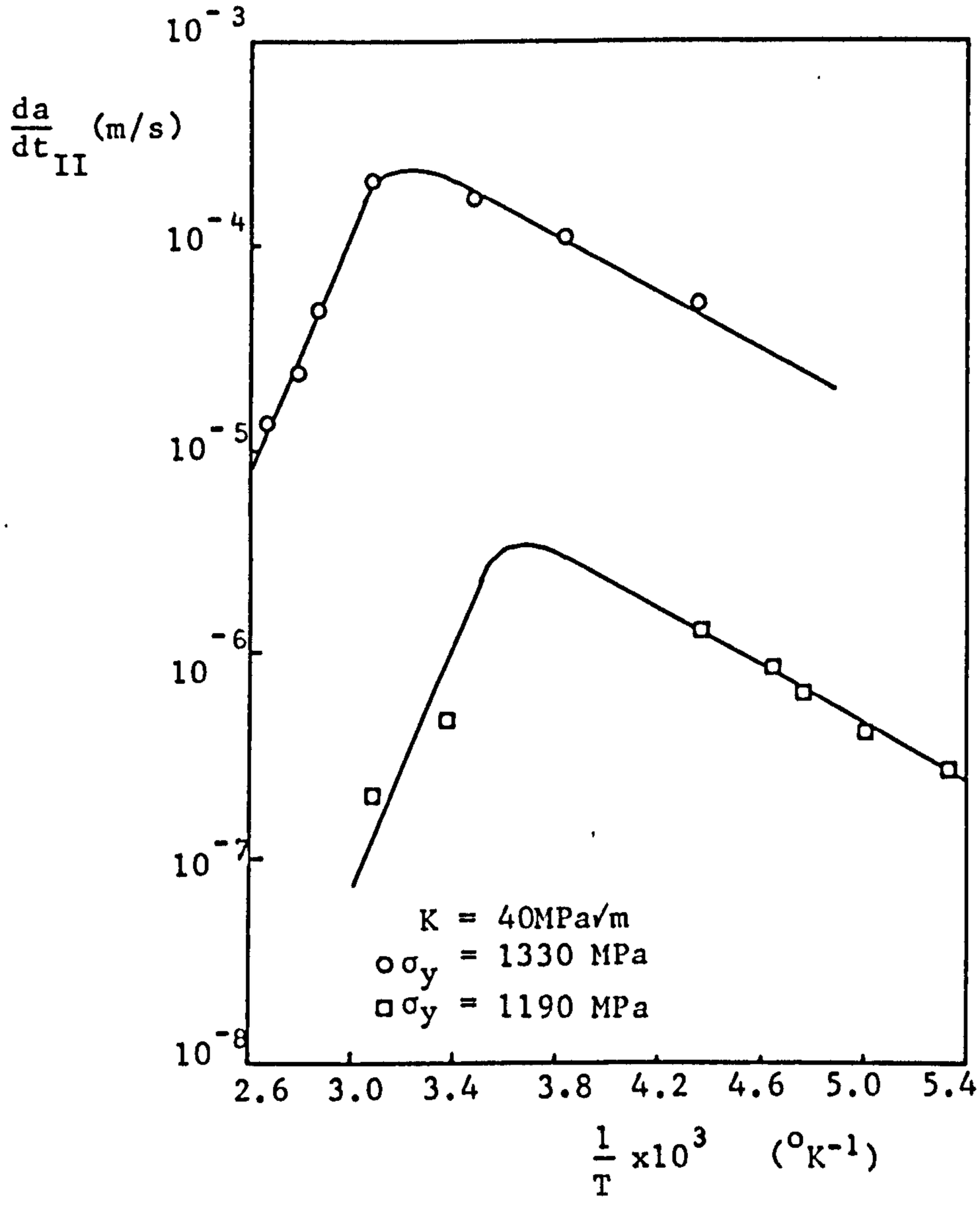

Figure 5.21 An Arrhenius plot of the temperature dependence of $\frac{da}{dt}_{II}$ at a constant K in 77.3 KPa hydrogen for 4130 steel (107)

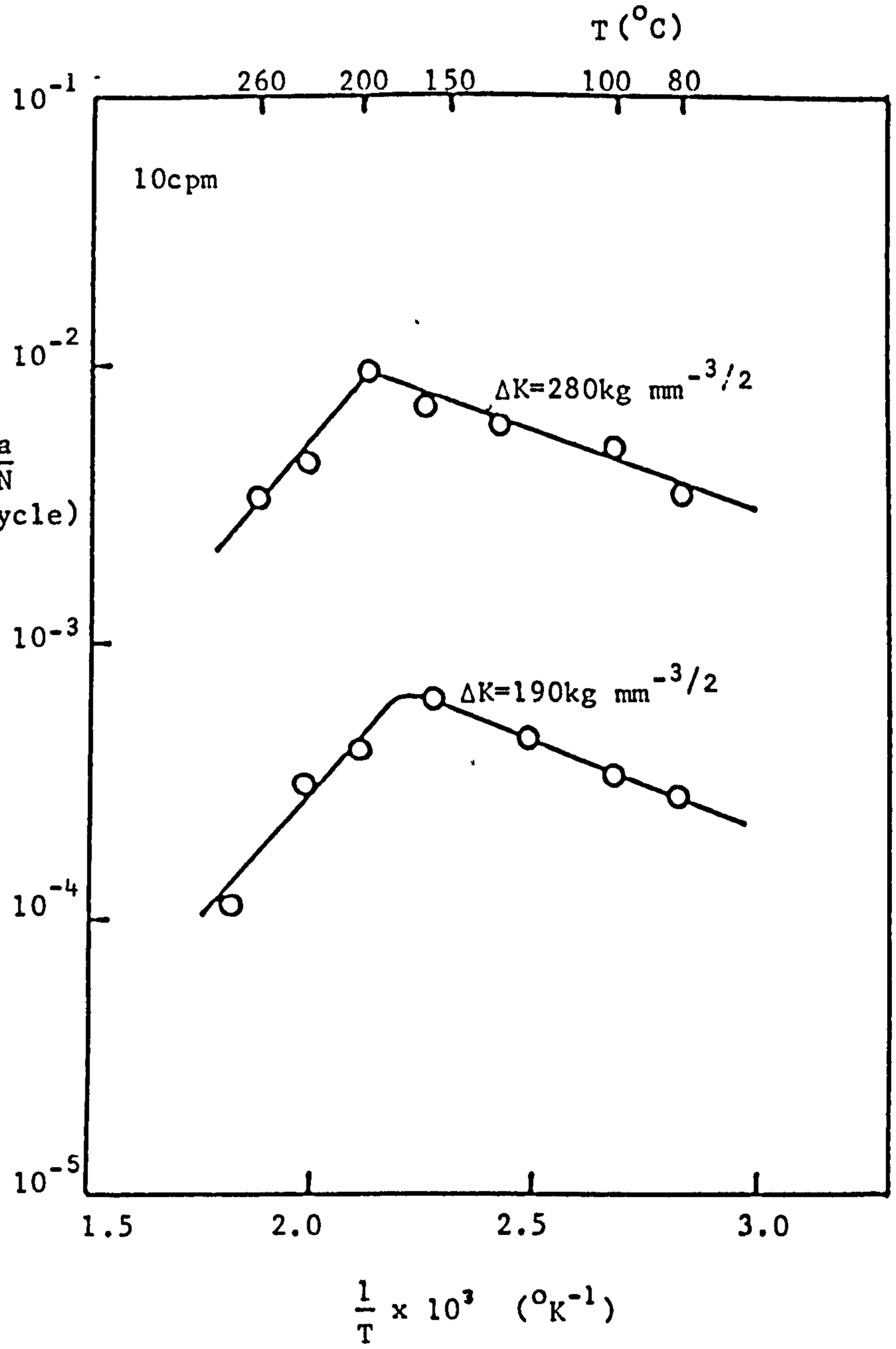

Figure 5.22 Effect of temperature on fatigue crack growth rate in deionized water for A302B steel clad with stainless steel (234)

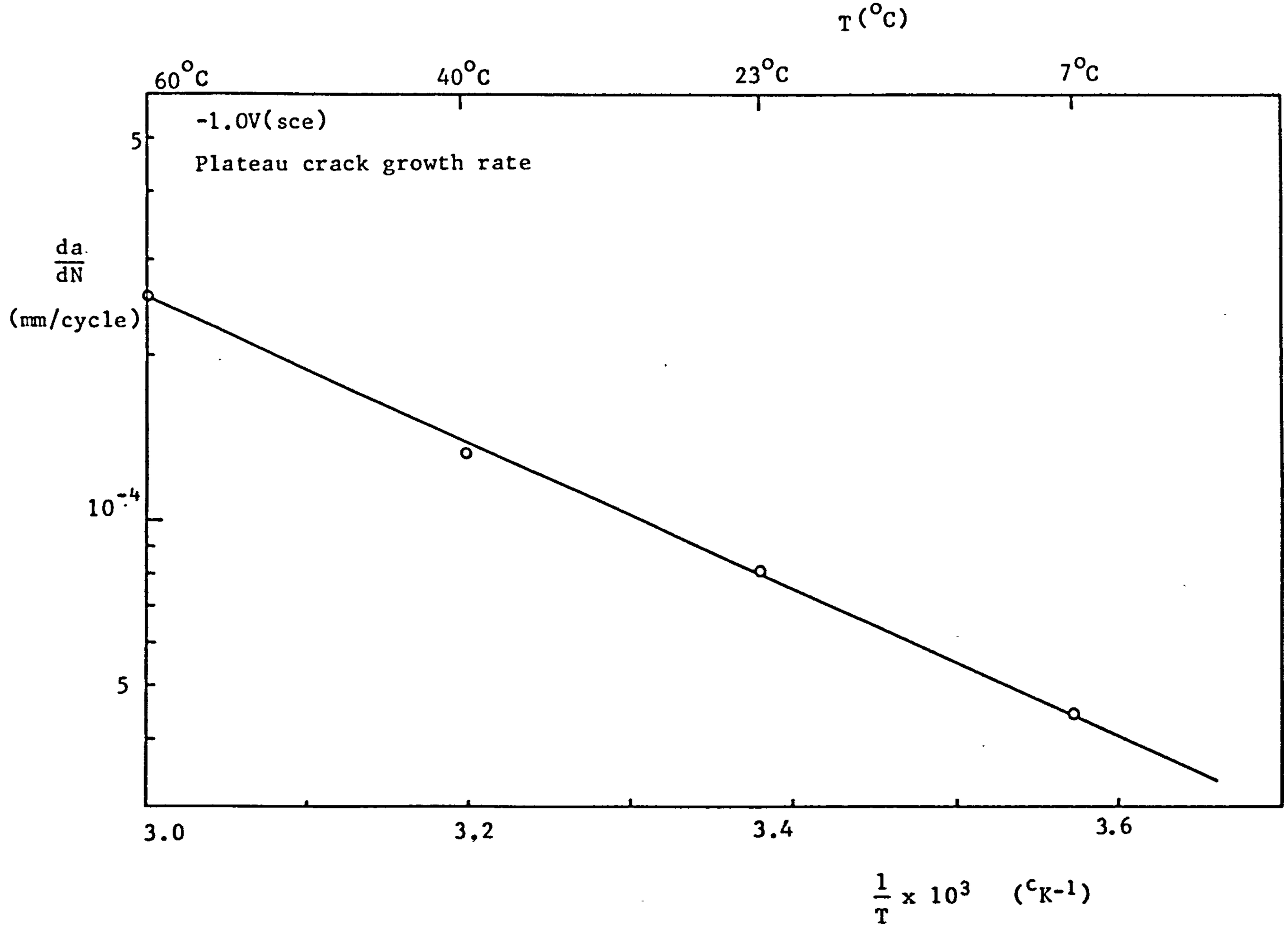
T (°C)
60°C
40°C
23°C
7°C
-1.0V(sce)
Plateau crack growth rate
da/dN
(mm/cycle)
5
10⁻⁴
5
3.0
3.2
3.4
3.6
1/T x 10³ (°K⁻¹)

Figure 5.23

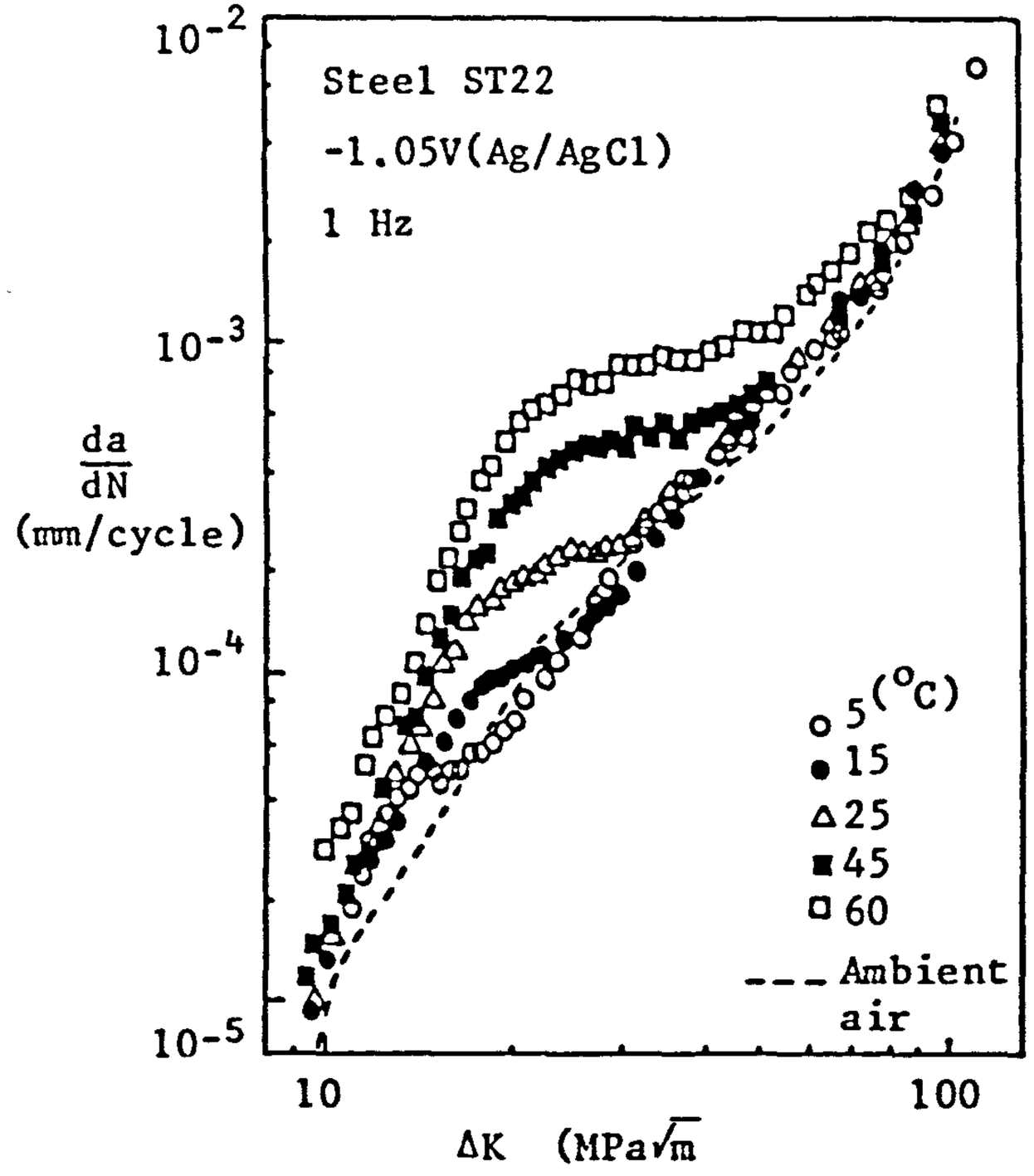

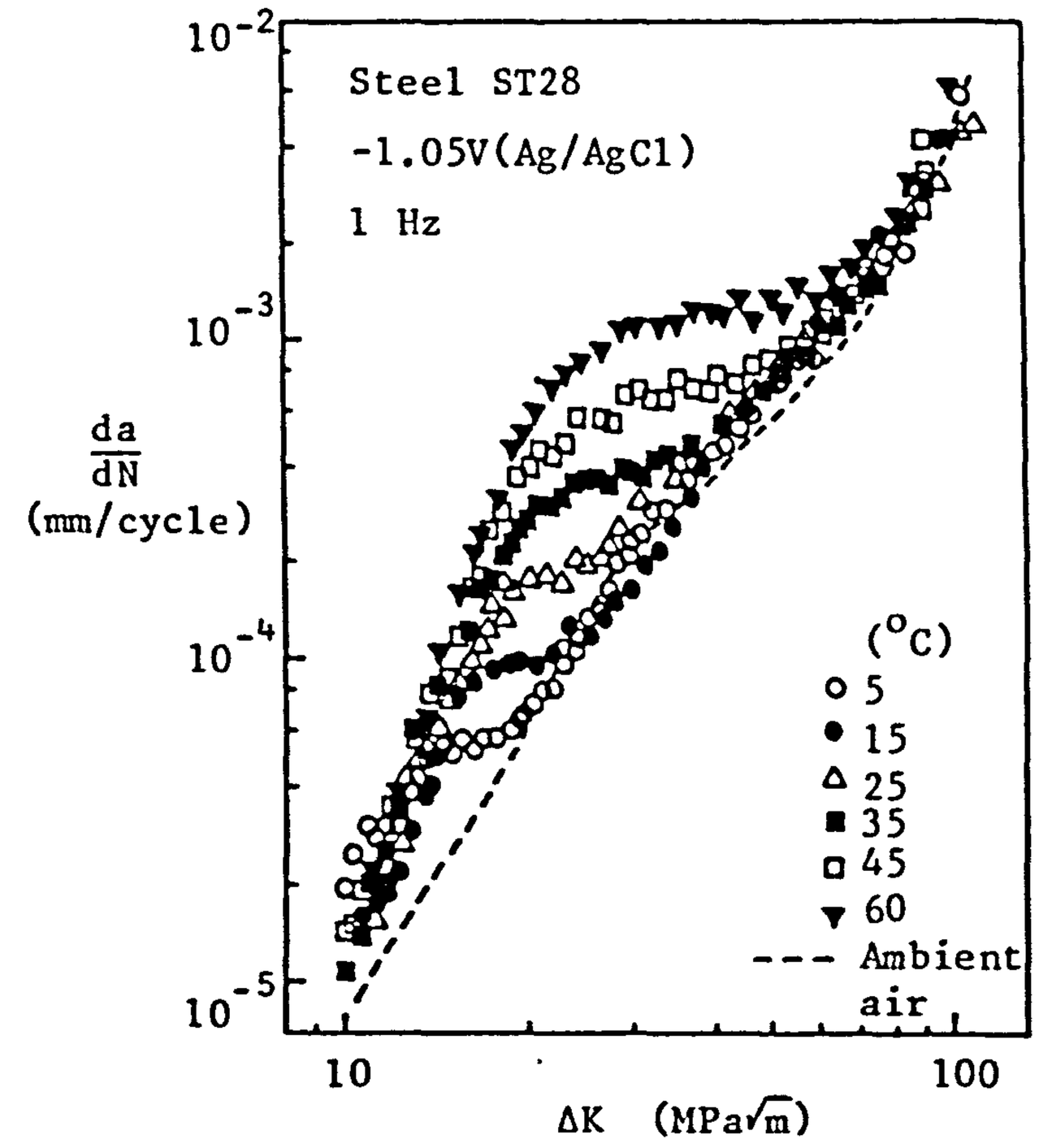

Figure 5.24 Effect of temperature on the corrosion fatigue behaviour of two steels in 3.5% NaCl (180)

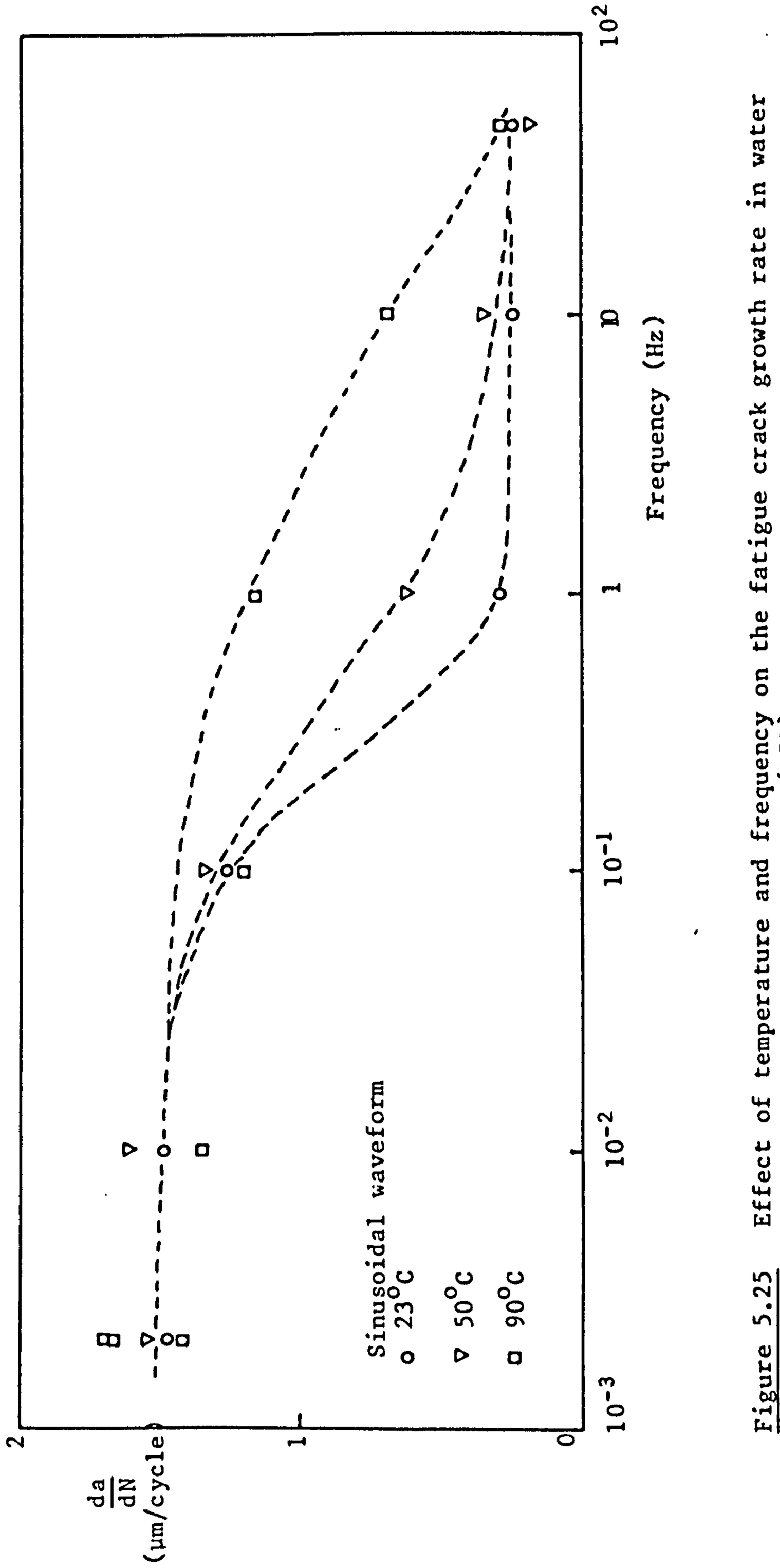

Figure 5.25 Effect of temperature and frequency on the fatigue crack growth rate in water for a 2Ni-Cr-Mo-V rotor steel (157)

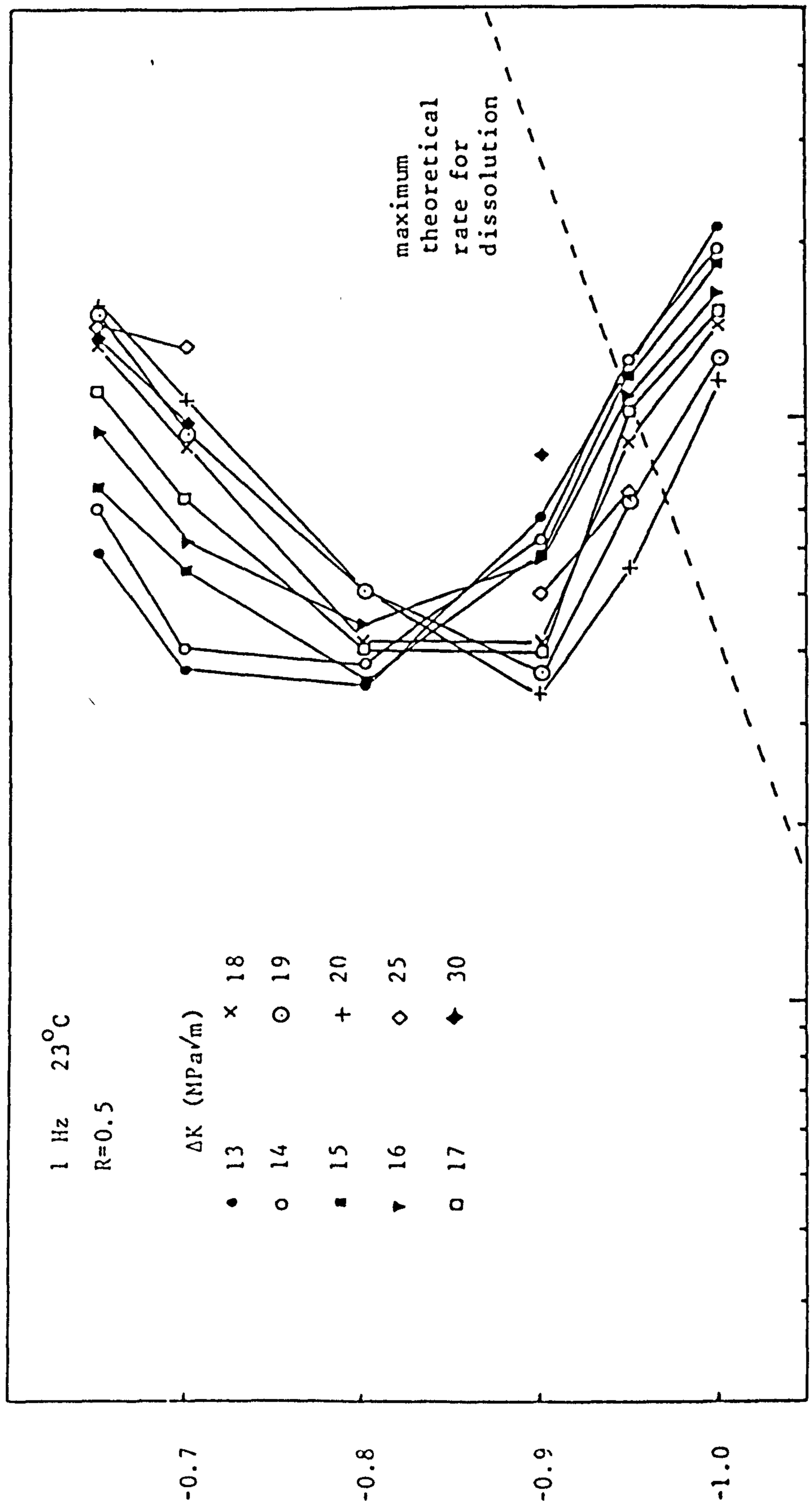
da/dt environment (mm/s)
maximum theoretical rate for dissolution
1 Hz 23°C
R=0.5
ΔK (MPa√m)
13
14
15
16
17
18
19
20
25
30
10^{-4}
10^{-5}
-0.7
-0.8
-0.9
-1.0
crack tip potential (sce)

Figure 5.26

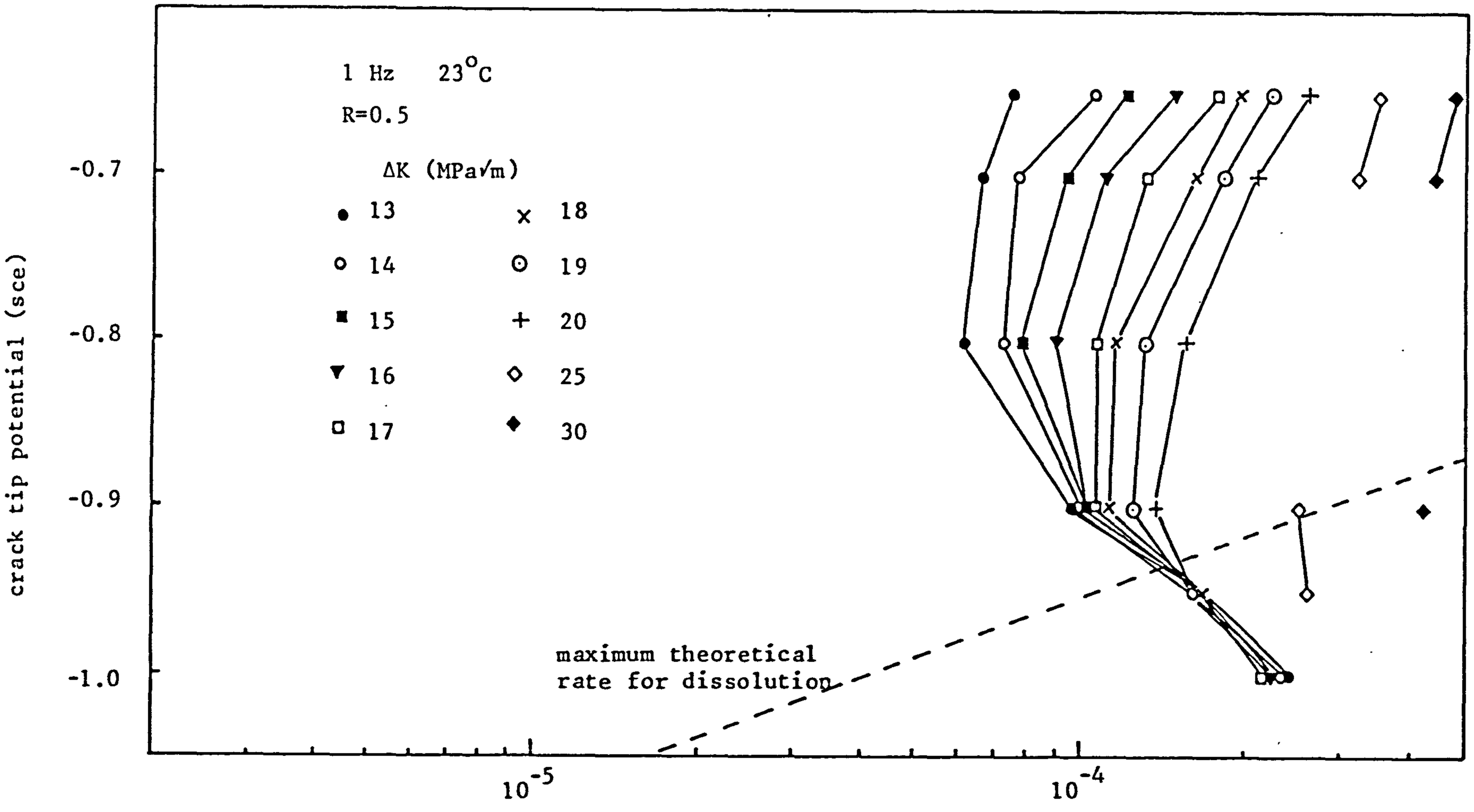
1 Hz 23°C
R=0.5
ΔK (MPa√m)
13
14
15
16
17
18
19
20
25
30
-0.7
-0.8
-0.9
-1.0
crack tip potential (sce)
maximum theoretical
rate for dissolution
10^{-5}
10^{-4}
da/dt total (mm/s)

Figure 5.27

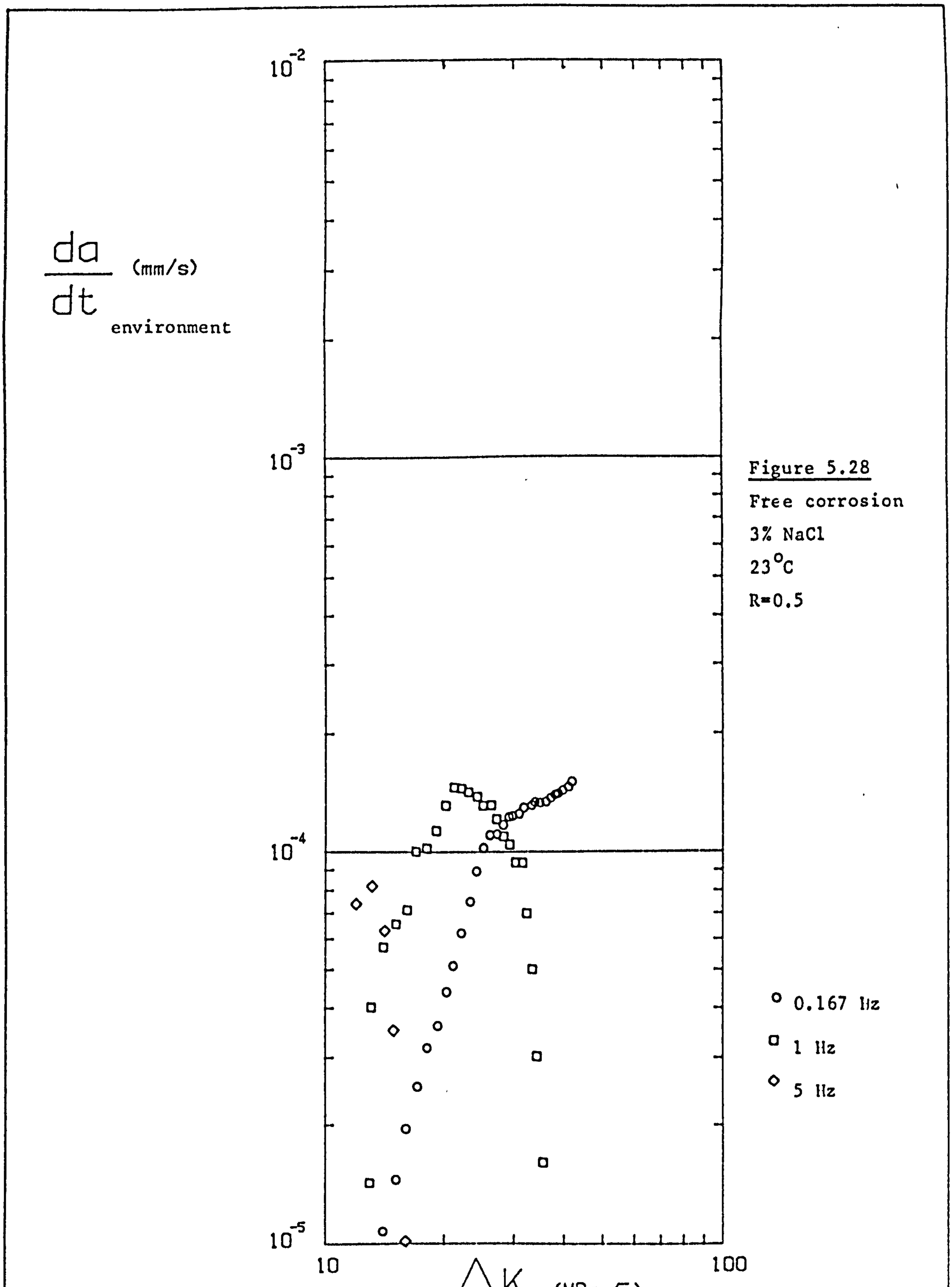

Figure 5.28

Free corrosion

3% NaCl

23°C

R=0.5

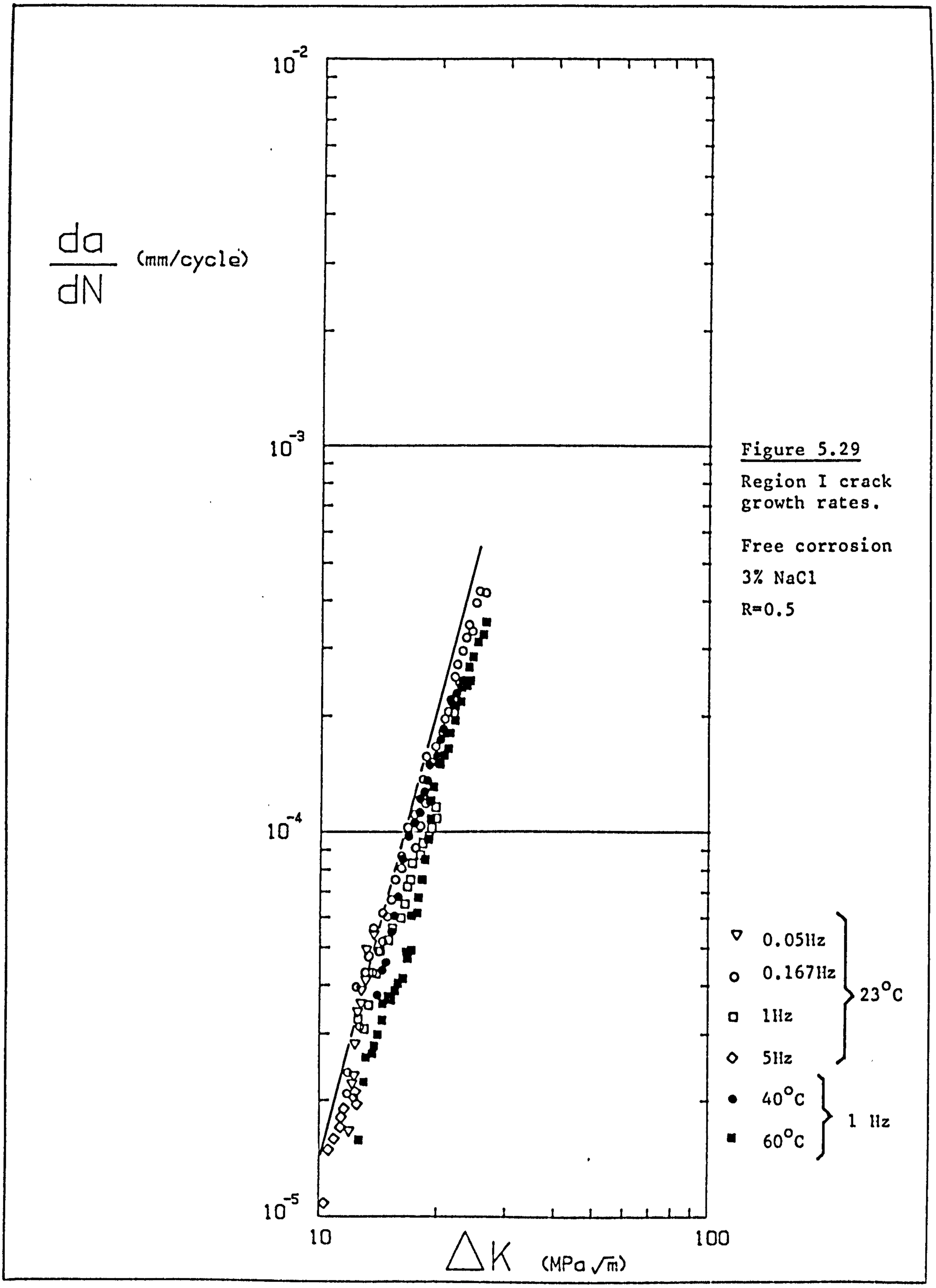

Figure 5.29

Region I crack growth rates.

Free corrosion

3% NaCl

R=0.5

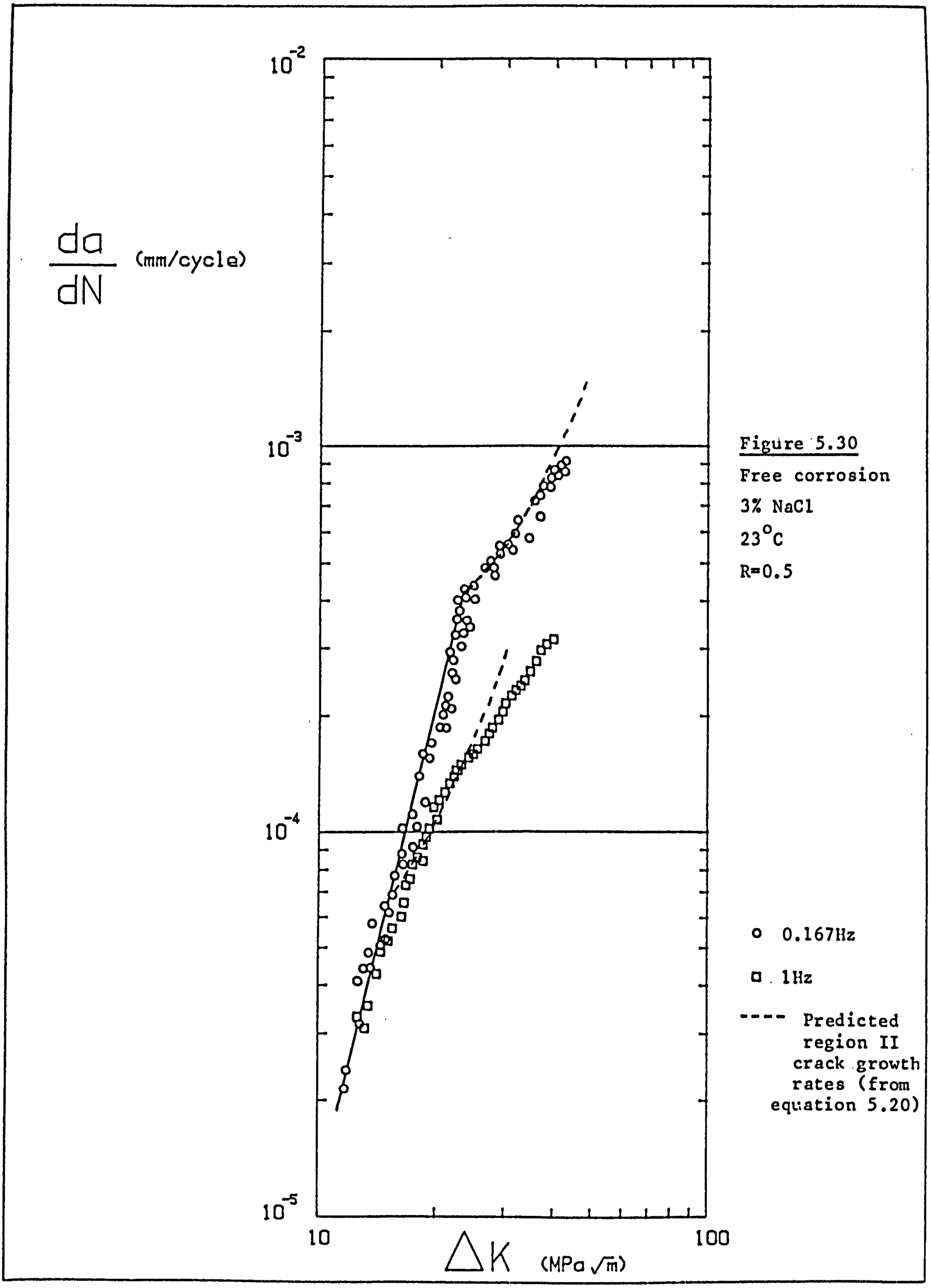

Figure 5.30

Free corrosion

3% NaCl

23°C

R=0.5

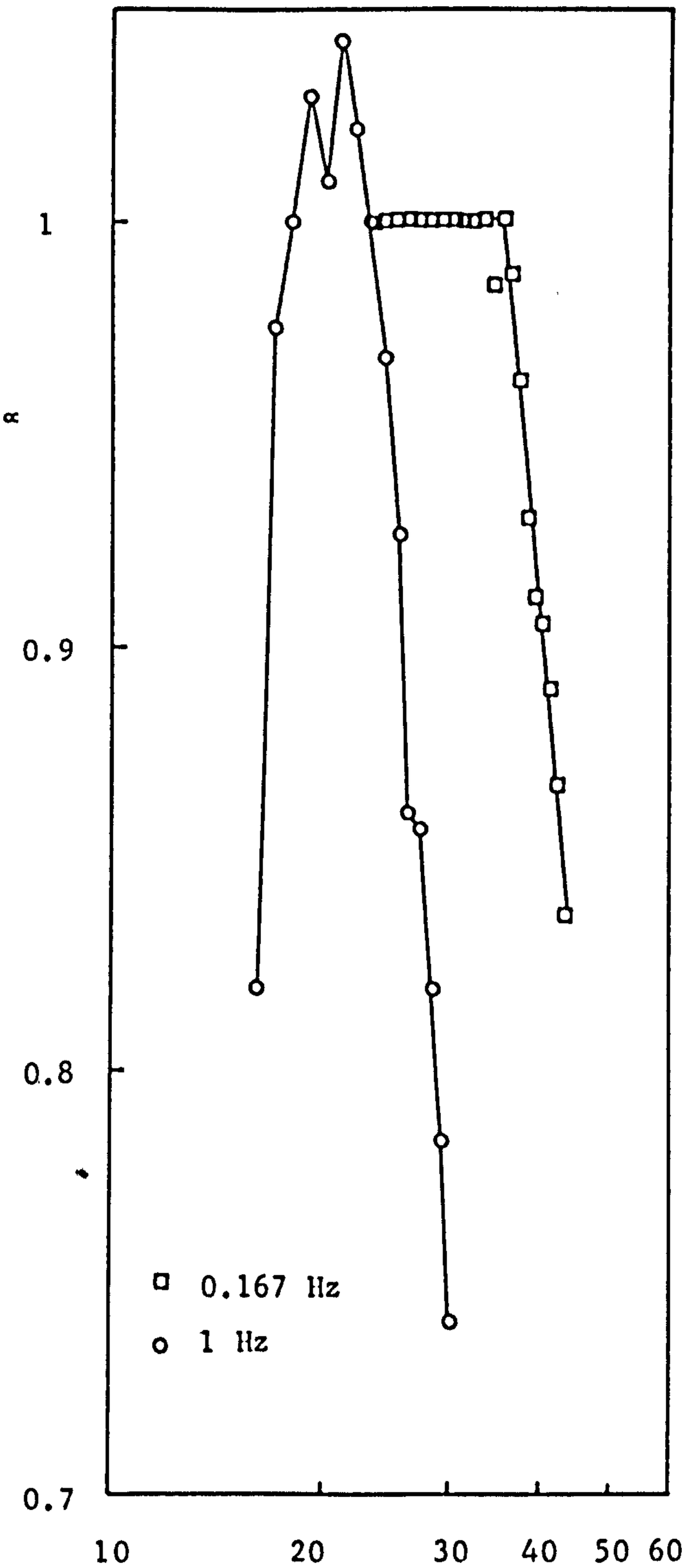

Figure 5.31

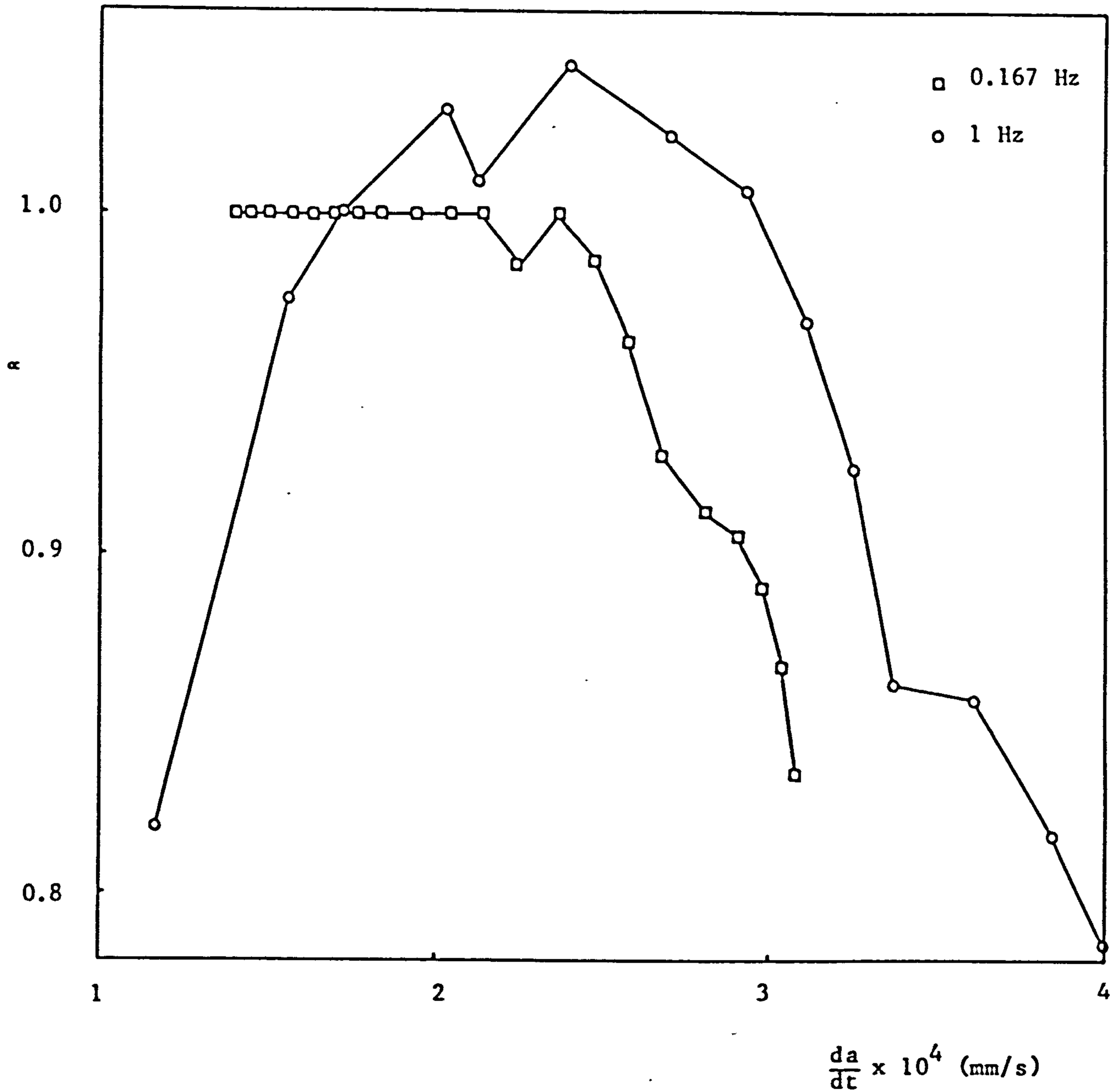

Figure 5.32

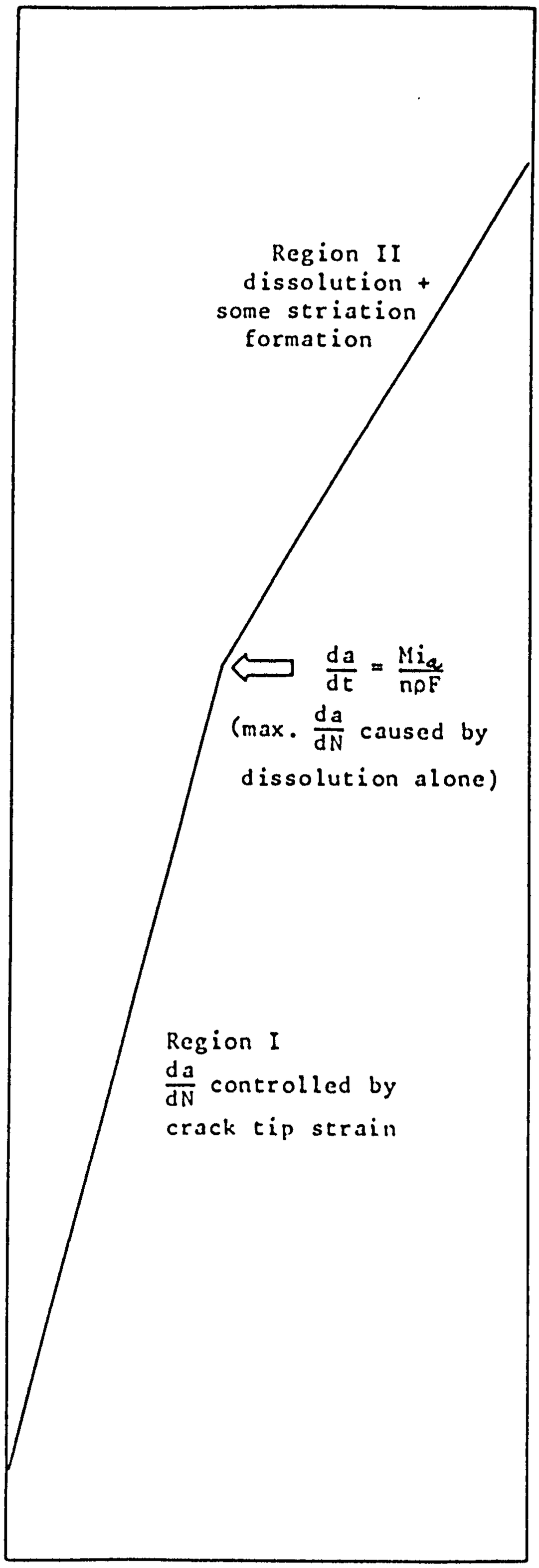
log $\frac{da}{dN}$
Region II
dissolution +
some striation
formation
$\frac{da}{dt} = \frac{Mi_a}{n\rho F}$
(max. $\frac{da}{dN}$ caused by
dissolution alone)
Region I
$\frac{da}{dN}$ controlled by
crack tip strain
log ΔK

Figure 5.33

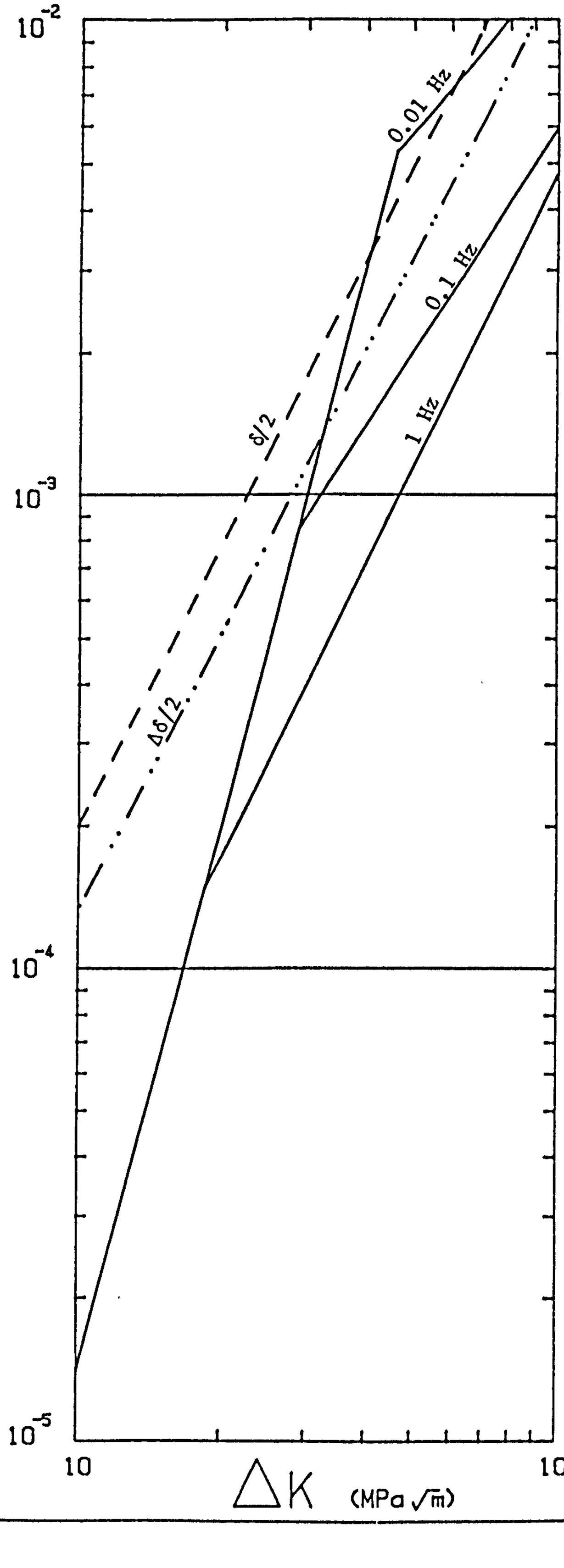

Figure 5.34

X65

Free corrosion

3.5% NaCl

Ambient Temp.

Triangular wave

Lines are Vosikovsky's fit to his X65 data (72)

6.0 Phenomenology.

In 1977 Staehle [258] commented that the research into environmentally assisted crack growth up to that date had failed to provide many useful models suitable for engineering applications. As was mentioned in section 1.1 the research work reported in this thesis was undertaken in the political and economic context of the continuing exploitation of the North Sea oil reserves. Thus it is appropiate that the following discussion on phenomenology is included.

6.1 Crack growth by a dissolution mechanism.

In chapter 5 the region I crack growth rates were seen to be mostly independent of frequency and temperature over the ranges 0.05-5Hz, and 23-60°C. Figure 6.1 shows that the region I crack growth rates found in this study were almost identical to those measured for X65 in 3.5% NaCl [72]. Thus the region I crack growth rates for BS4360:50D in 3% NaCl can be adequately represented by the same relationship described by Vosikovsky for those in X65 :

$$\frac{da}{dN} = 1.5 \times 10^{-9} \Delta K^{3.95} \text{ mm/cycle} \qquad (6.1)$$

ABS EH36 ship steel immersed in 3.5% NaCl at free corrosion has also been found to exhibit a similar form of crack growth behaviour as BS4360:50D. Both regions I and II were observed, and the region I crack growth rate was virtually coincident with that given by equation 6.1.

Figure 6.1 shows that the region II crack growth rates are less for BS4360:50D than for X65. The results of this work suggest that the different R ratios and salt concentrations used are not the cause. The most likely possibility, apart from steel composition and processing, is the effect of the different specimen thicknesses used, 12.7mm by Vosikovsky [72] and 25.4mm in this work. The different specimen thickness would alter the relative amount of fresh solution drawn into the crack through the crack sides as opposed to the crack mouth. Further experiments are required in order to see if this is the case. One useful experiment would be to prevent the ingress of solution into the crack through the crack sides. Certainly the equations fitted by Vosikovsky [72] to his data provide a safe upper bound to the crack growth rates measured for BS4360:50D in this study.

6.2 Crack growth by a hydrogen embrittlement mechanism.

Offshore structures are usually cathodically protected to -0.85V(sce) or lower. In order to ensure that the whole structure is protected at -0.85V(sce) some parts of the structure would be at potentials as low as -1V(sce). As discussed in chapter 5 corrosion fatigue crack growth by a hydrogen embrittlement mechanism occurs at these potentials. Thus a phenemenological description of crack growth rates due to a hydrogen embrittlement mechanism could be of direct relevance to the design of such structures, as well as the assesment of any defects found in them.

Figure 6.2 compares the results of this study, obtained in 3% NaCl at -1V(sce), R=0.5, with those found by Vosikovsky [72] for X65 in 3.5% NaCl at -1.04V(sce), R=0.2. Good agreement is seen between these results, except possibly at 1Hz. It can also be seen from figures 4.33 and 6.2 that the region I crack growth rates are the same. Thus the region I crack growth rates are given by the relationship obtained by Vosikovsky [72], viz. :

$$\frac{da}{dN} = 1.3\times10^{-11}\ \Delta K^{6.2}\ \text{mm/cycle} \qquad (6.2)$$

Several different experiments gave the same plateau crack growth rate at 1Hz for BS4360:50D, and so the discrepancy in the 1Hz data is not due to experimental error. It is possible that some form of hydrogen/trap interaction may be occurring at 1Hz in BS4360:50D that reduces the rate of supply of hydrogen to the embrittlement zone. This would not be suprising in view of the complexity of hydrogen/iron interactions, and the range of general frequency dependent effects that occur in materials [259].

In view of the similarity between the crack growth rates obtained in BS4360:50D and X65 (see also figure 5.17) a comparison was made with the results from other steels. Figure 6.3 shows that the plateau crack growth rates obtained for a number of similar steels (at -1 to -1.04V(sce) and 20-23°C) lie on a common line. Data taken from Austen's work [17,260] on higher strength steels in free corrosion shows the same effect. (The higher plateau crack growth rates observed by Austen at 0.25Hz occur because the steels used by him are susceptible to SCC, with a K_{iscc} of 14.3 MPa$\sqrt{m}$.) The agreement between plateau crack growth rates for BS4360:50D in 3% NaCl, X65 and X70 in 3.5% NaCl [72,208] and hot rolled DS52III in ASTM artificial seawater [261] suggested that the results from these studies could be

combined to form a phenomenological description of the corrosion fatigue behaviour of these steels.

The model assumes that the crack growth rate behaviour shows the three regions on a log da/dN vs. log ΔK plot described in sections 5.2.3 and 5.4. Equation 6.2 was used to describe the region I behaviour. Hinton [146] observed an effect of specimen potential upon the region I crack growth rates, but no such effect was included in the model for two reasons :

(a) his results were unavailable when the model was constucted.

(b) the use of results obtained at -1V(sce) should mean that equation 6.2 represnts a safe upperbound line. This is because it is not possible to polarize the crack tip much below -1V(sce) (cf. section 2.2.1).

The results of this study showed that the region III crack growth rates were the same as in air, and so the region III behaviour was described by the air upperbound line (cf. section 5.2.1) :

$$\frac{da}{dN} = 1.12\times10^{-11}\ \Delta K^{2.92}\ \text{mm/cycle} \qquad (6.3)$$

The region II crack growth rates have been shown to be a function of temperature and specimen potential [261], as well as of frequency [72,208]. The relationship given by Vosikovsky [72] for the region II crack growth rates was shown in figure 6.3, and is :

$$\frac{da}{dN} = 1.3\times10^{-4}\ (f)^{-0.8}\ \text{mm/cycle} \qquad (6.4)$$

Figure 6.4 shows equation 6.4, and the corresponding relationship for the data of Austen shown in figure 6.3, plotted on a time basis. In both cases the crack growth velocity increases as the frequency increases, an effect that is probably due to the increased pumping action of the crack at higher frequencies. Increased pumping at higher frequencies was advocated by Vosikovsky and Rivard as an explanation of the frequency effects observed in sour crude oil [129]. From figure 6.4 it is seen that :

$$\frac{da}{dt_2} = \frac{da}{dt_1} \cdot \left[\frac{f_2}{f_1} \right]^{m_f} \qquad (6.5)$$

where $m_f = 0.2$.

Maahn and Noppenau [261] studied the plateau crack growth rate as a function of temperature and potential. They used a hot-rolled DS52III steel in ASTM artificial seawater, at a frequency of 0.04Hz. From their results, shown in figure 6.5, it is seen that there is a synergistic effect of potential and temperature upon the plateau crack growth rate. The results are described by :

$$\frac{da}{dt_2} = \frac{da}{dt_1} \cdot 10^{m_p(\Phi_2 - \Phi_1)} \qquad (6.6)$$

where Φ is the crack tip potential
and m_p is a function of temperature.

Scott et. al. [140] commentating on this behaviour claimed that the rate of crack growth should be proportional to the flux of hydrogen entering the metal, and that this should be linearly related to the crack tip potential. This is not true as the partial pressure of hydrogen at the crack tip should be proportional to the square root of the hydrogen evolution current density, rather than the hydrogen evolution current density itself [158]. For the time being the behaviour found by Maahn and Noppenau has to be accepted as an empirical finding.

Although m_p in equation 6.6 was a function of temperature it is found from figure 6.6 that m_p is given by :

$$m_p = 0.082.T - 26.17 \qquad (6.7)$$

where T is the absolute temperature.

No data was known that detailed whether m_p is also a function of frequency so it was assumed that m_p is frequency independent.

Figure 6.7 illustrates that the plateau crack growth rates reported by Maahn and Noppenau fit an Arrhenius type relationship :

$$\frac{da}{dt_2} = \frac{da}{dt_1} \cdot 10^{m_t(1/T_2 - 1/T_1)} \qquad (6.8)$$

where m_t is a function of potential.

Figure 6.8 shows that m_t is given by :

$$m_t = -7620.\Phi - 8829 \qquad (6.9)$$

where Φ is the crack tip potential.

Again no data exists to determine the relationship between m_t and frequency, and so m_t was assumed to be independent of frequency. (Because of the anomalous behaviour observed at 1Hz for BS4360:50D it

was not possible to use the potential and temperature data obtained in this study to determine the effect of frequency upon m_p and m_t).

The crack tip potential is not necessarily the same as the potential applied to the specimen (cf. section 2.2.1). The crack tip potential was calculated from the potential applied to the specimen by reference to the experimental work done on crevices of BS4360:50D in 3.5% NaCl and seawater by Turnbull [25,26].

The plateau crack growth rate is then given by combining equations 6.5 to 6.9 :

$$\frac{da}{dt_2} = \frac{da}{dt_1} \cdot 10^{m_t(1/T_2 - 1/T_1)} \cdot 10^{m_p(\phi_2 - \phi_1)} \cdot \left[\frac{f_2}{f_1} \right]^{m_f} \qquad (6.10)$$

where $m_f = 0.2$
$m_t = -7620.\phi_1 - 8829$
$m_p = 0.082.T_2 - 26.17$

The reference plateau crack growth rate, da/dt_1, was taken from Maahn and Noppenau's work as being 6.4×10^{-5} mm/s at 0.04Hz, 20°C and a specimen potential of -1V(sce).

Figures 6.9 to 6.14 compare the predictions of the model with some experimental results. The agreement is very promising, although the 5Hz data indicates that m_p decreases with frequency. Unfortunately it was not possible to develop the model further because of the limited experimental time available.

For a phenomenological model it is important that the range of environmental conditions over which it is applicable is known. For the model proposed here the limits are :

environment : 3% to 3.5% NaCl or ASTM artificial seawater (the effect of the organic chemicals found in real seawater is unknown).

material : BS4360:50D, X65, X70 and DS5211. It is anticipated that the model would also apply to other similar structural and pipeline steels.

frequency : greater than 0.01Hz. As discussed in section 5.2.3 there is uncertainty about the crack growth behaviour at lower frequencies.

potentials : more negative than approximately -0.85V(sce). The model describes crack growth rates due to a hydrogen

embrittlement mechanism, and so only applies for potentials at which crack growth via a dissolution mechanism is negligable.

temperature : 0-60°C. Maahn and Noppenau investigated the effects of temperature between 0°C and 30°C. However the results of figure 4.33 indicated that Arrhenius type behaviour is observed to temperatures greater than 60°C.

waveform : sinusoidal and triangular. The data from this and other studies suggests that no significant difference exists between crack growth rates measured with either of these waveforms. The results shown in figure 4.27 indicate that a square waveform gives crack growth rate enhancements one half of those predicted by the model.

R ratio : no effect of R ratio upon corrosion fatigue crack growth rates was found in this study for BS4360:50D.

The phenomenological model proposed here provides a reasonably accurate, yet simple (3 piece linear), approximation to the constant amplitude data. Several studies [217,219,262] have shown that for narrowband random loading interaction effects are not significant for corrosion fatigue crack growth in structural steel immersed in chloride solution. In such a situation a Monte-Carlo simulation of the random fatigue crack growth provides a reasonably accurate description of it [262]. The Monte-Carlo simulation requires constant amplitude crack growth rate data obtained under the relevant environmental conditions. Thus the simultaneous use of the above model to provide a description of the constant amplitude data, and the Monte-Carlo technique to simulate the effects of a random loading, should enable a prediction to be made of crack growth in a wide range of practical situations.

The further development of such models would be of immediate use to the engineering community, although more work needs to be done on crack depth effects [214,235,263-265] and the corrosion fatigue behaviour of more realistic semi-elliptic surface cracks.

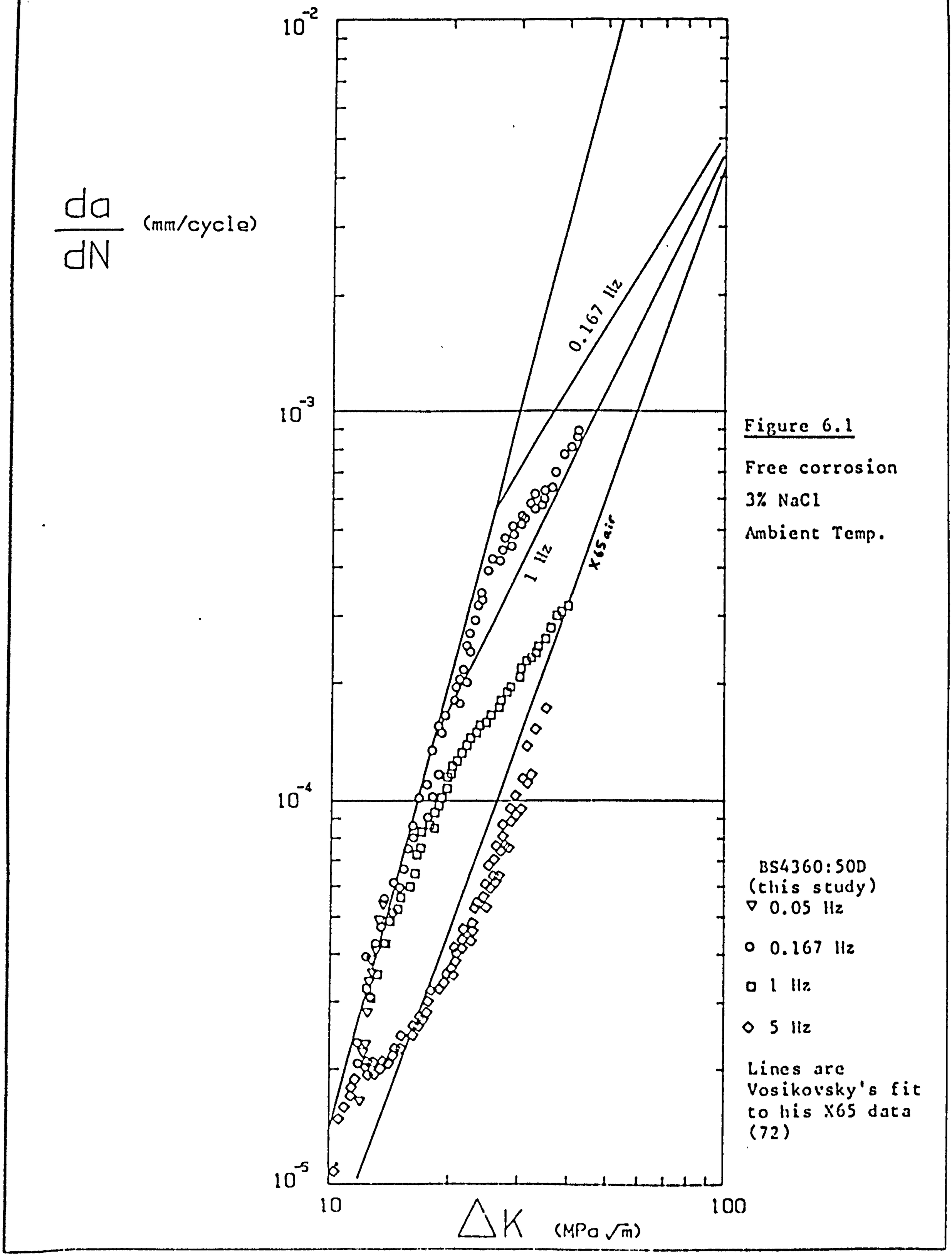

Figure 6.1

Free corrosion

3% NaCl

Ambient Temp.

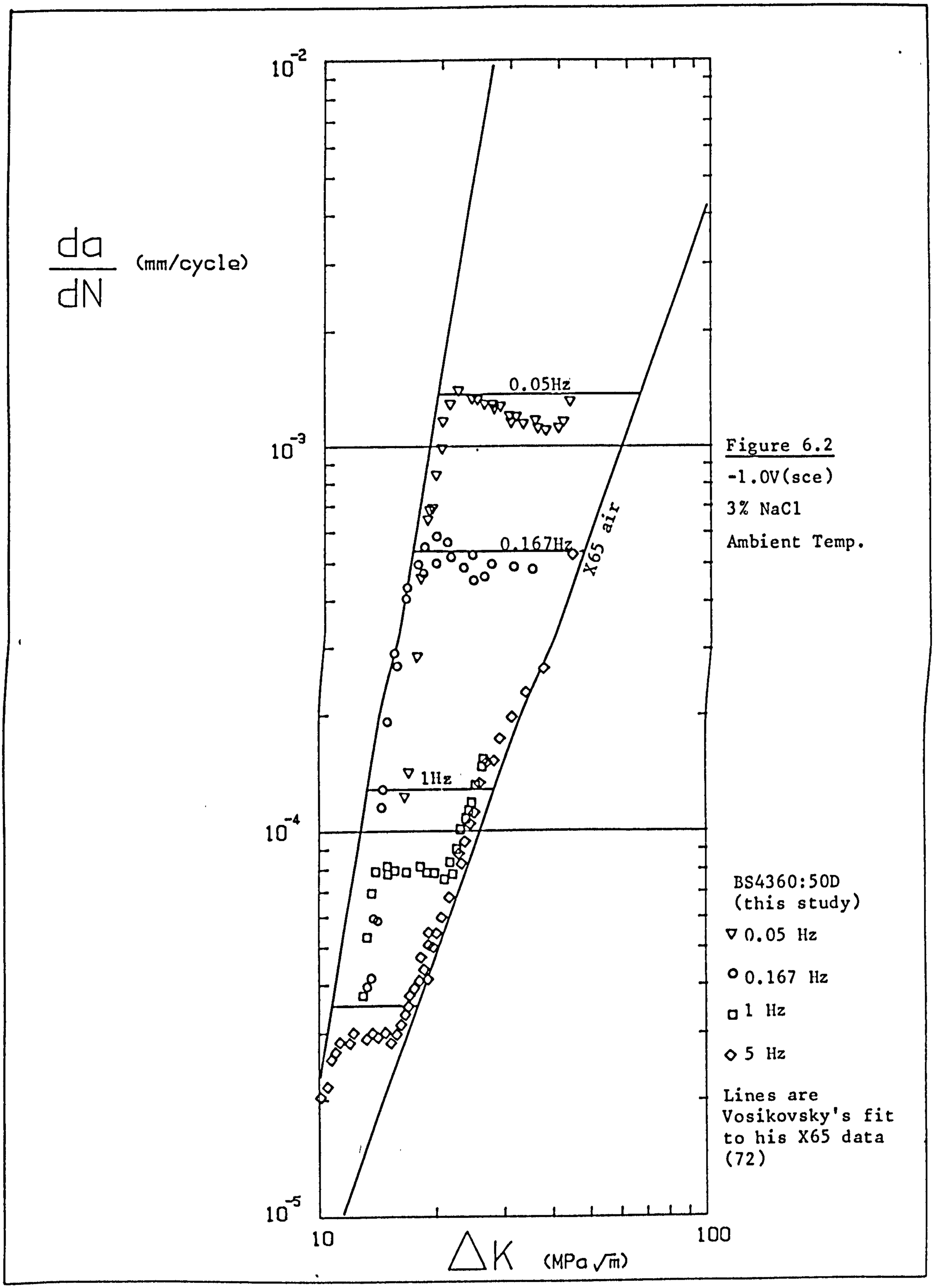
da/dN (mm/cycle)
10^-2
10^-3
10^-4
10^-5
0.05Hz
0.167Hz
1Hz
X65 air
10
100
ΔK (MPa √m)
-1.0V(sce)
3% NaCl
Ambient Temp.
BS4360:50D
(this study)
0.05 Hz
0.167 Hz
1 Hz
5 Hz
Lines are
Vosikovsky's fit
to his X65 data
(72)

Figure 6.2

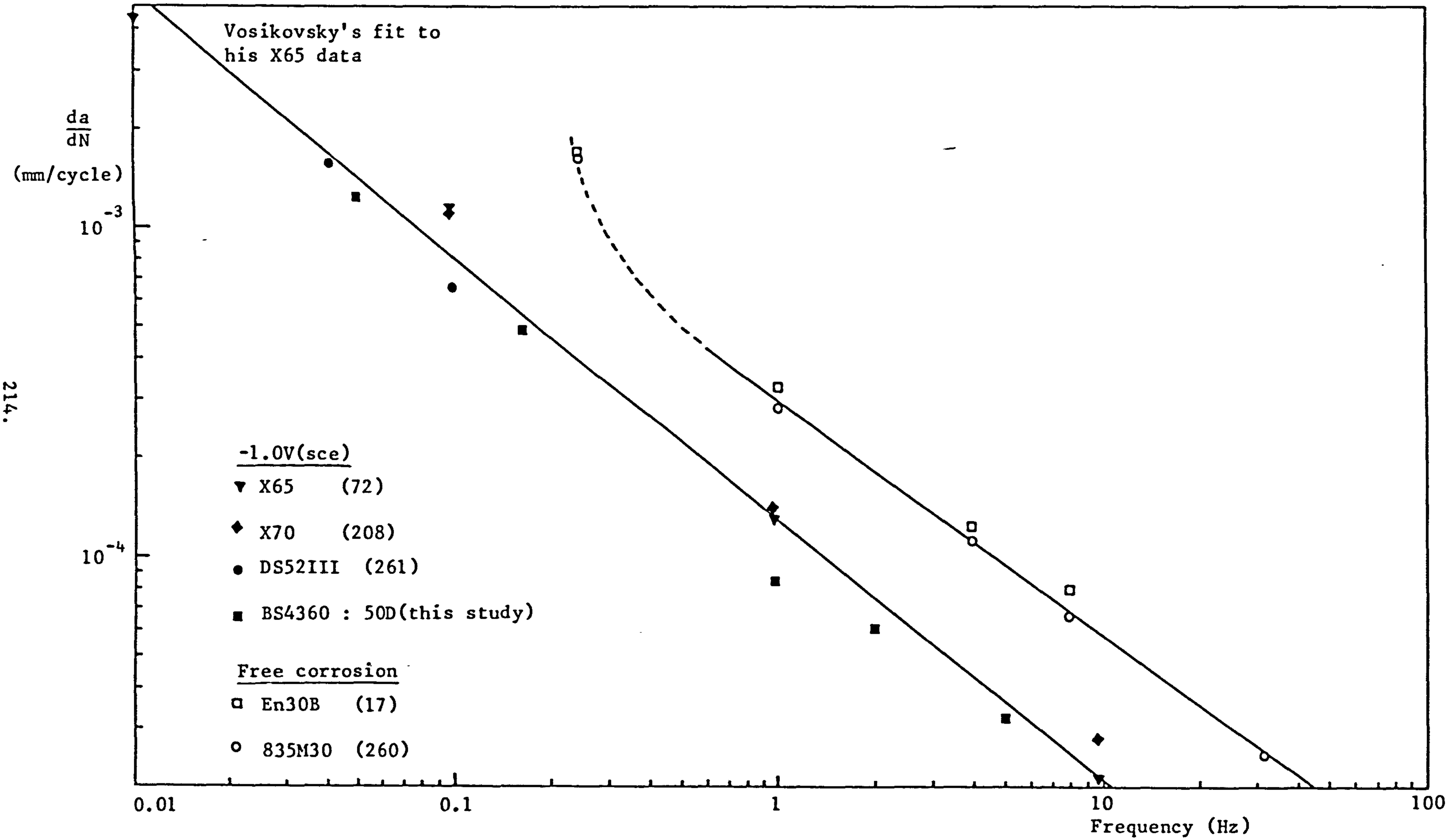
Vosikovsky's fit to
his X65 data
da/dN
(mm/cycle)
10^-3
10^-4
B
-1.0V(sce)
X65 (72)
X70 (208)
DS52III (261)
BS4360 : 50D(this study)
Free corrosion
En30B (17)
835M30 (260)
0.01
0.1
1
10
100
Frequency (Hz)

Figure 6.3

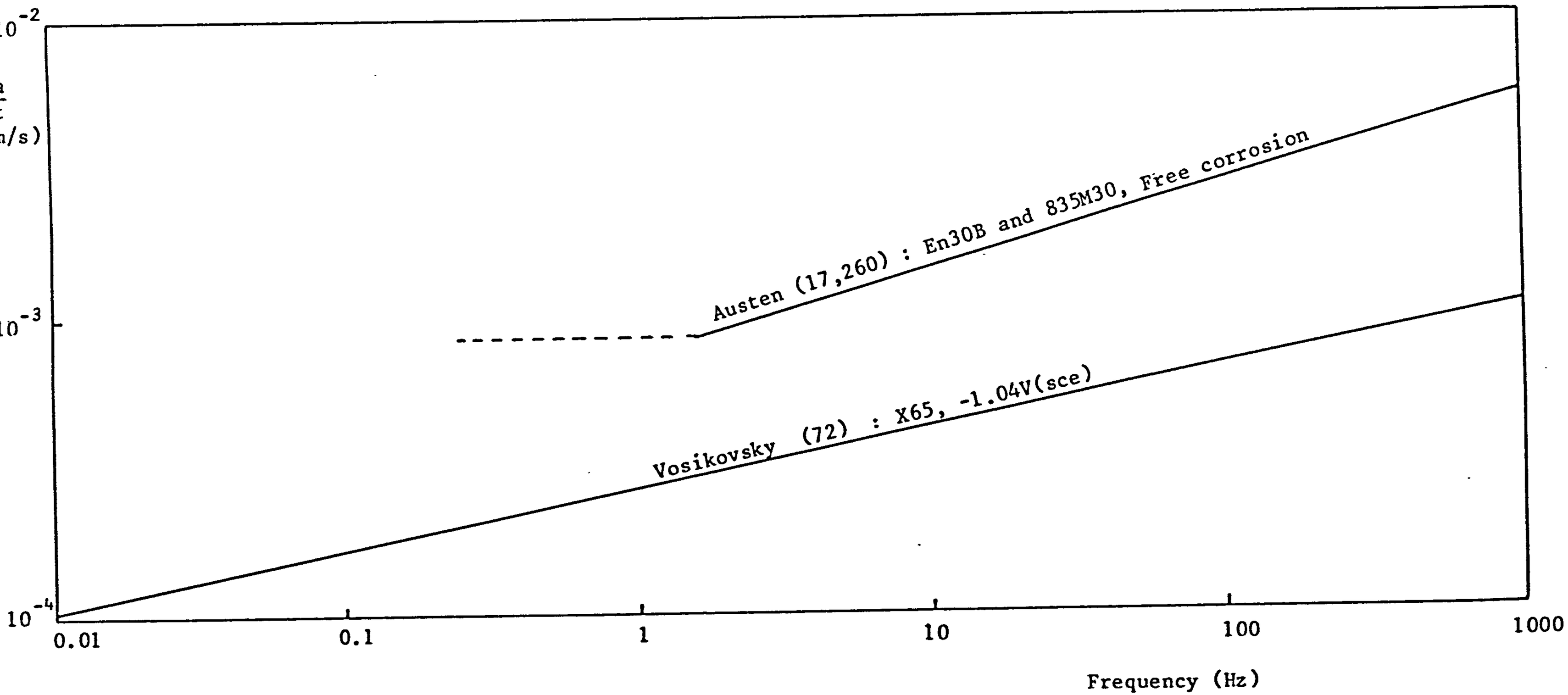
10^{-2}
$\frac{da}{dt}$ (mm/s)
10^{-3}
10^{-4}
Austen (17,260) : En30B and 835M30, Free corrosion
Vosikovsky (72) : X65, -1.04V(sce)
0.01
0.1
1
10
100
1000
Frequency (Hz)

Figure 6.4

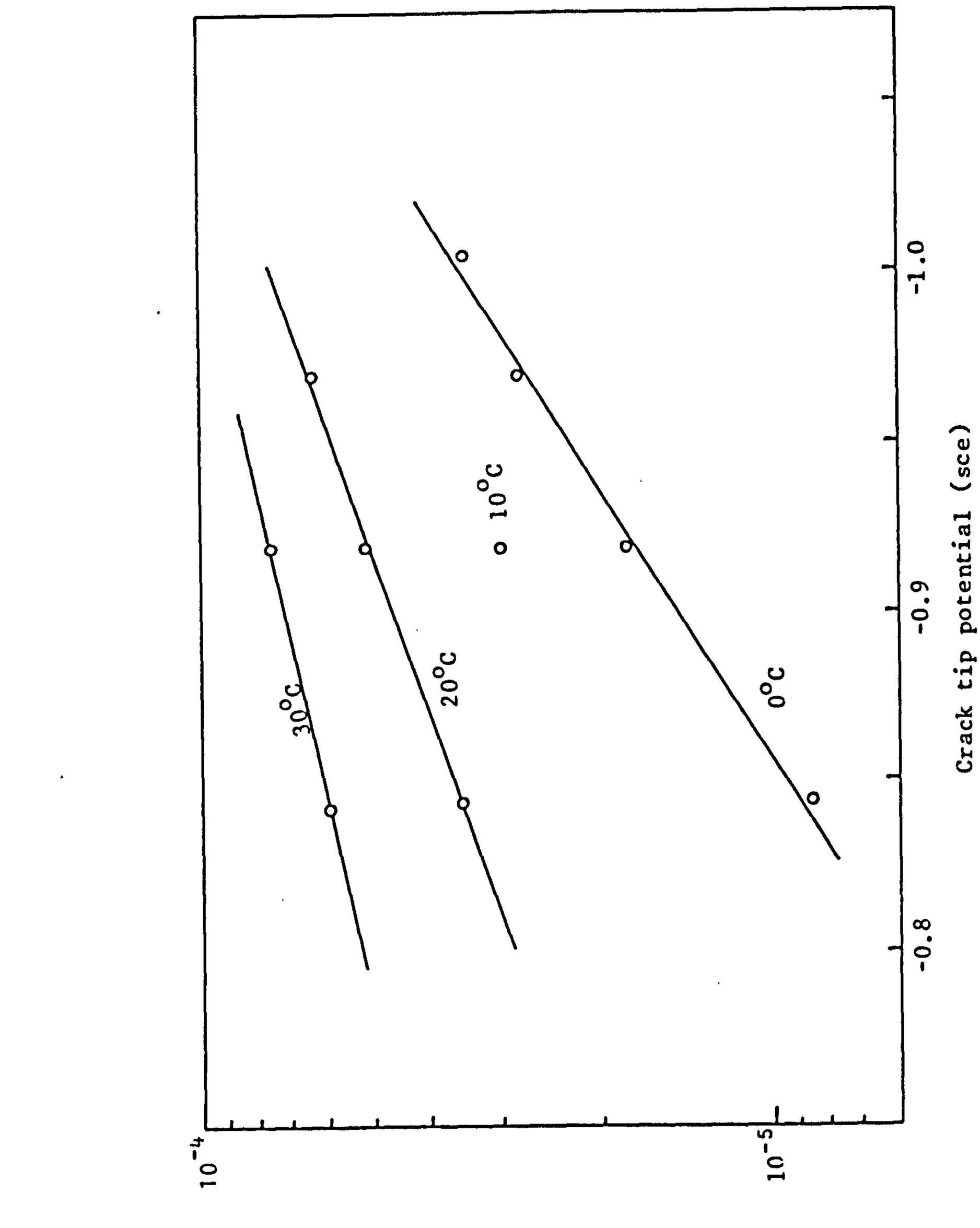

Figure 6.5 Variation in plateau crack growth rate with crack tip potential for DS52III, from Maahn and Noppenau (261)

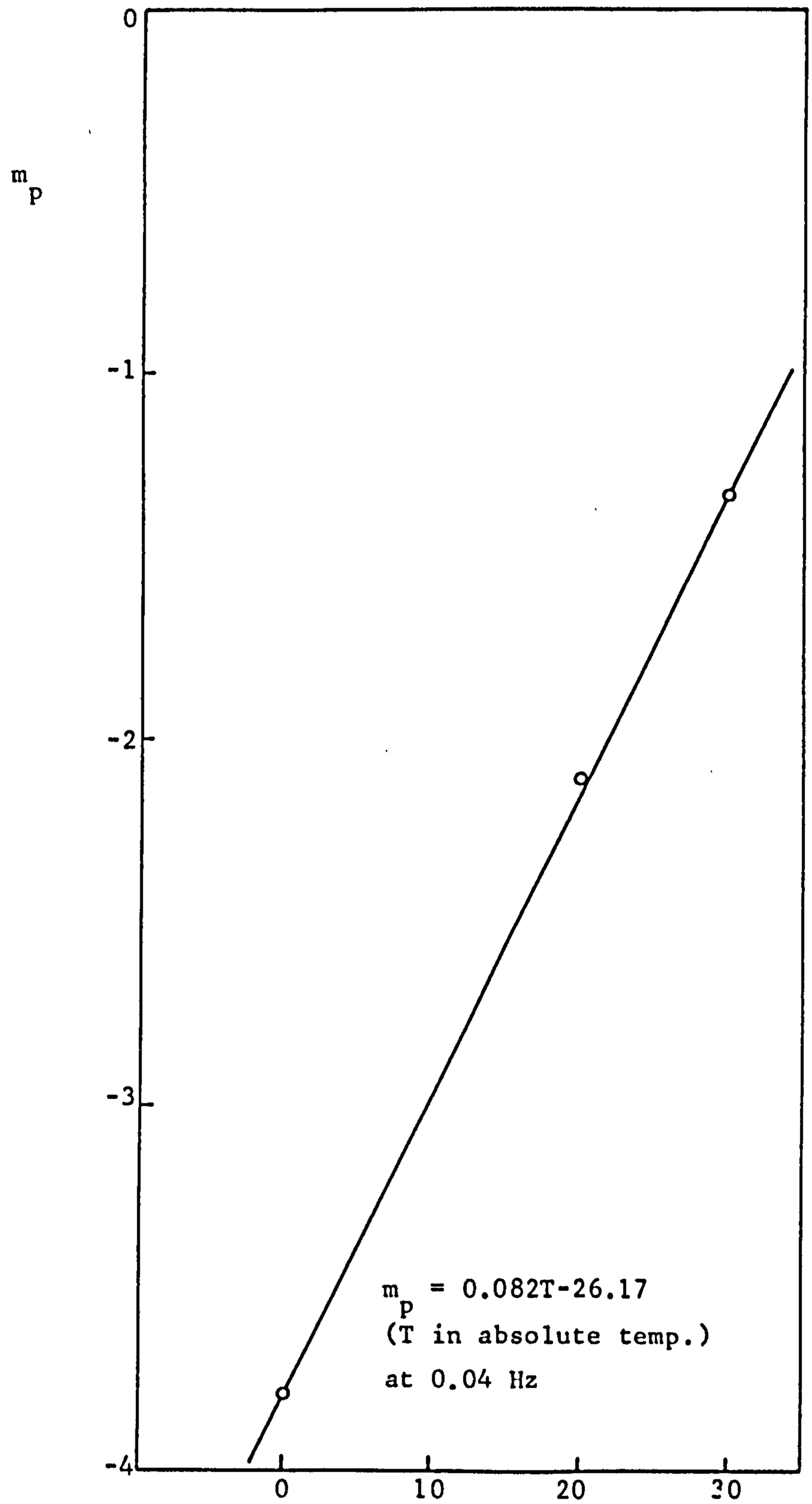
0
-1
-2
-3
-4
m_p
m_p = 0.082T-26.17
(T in absolute temp.)
at 0.04 Hz
0
10
20
30
Temperature (°C)

Figure 6.6

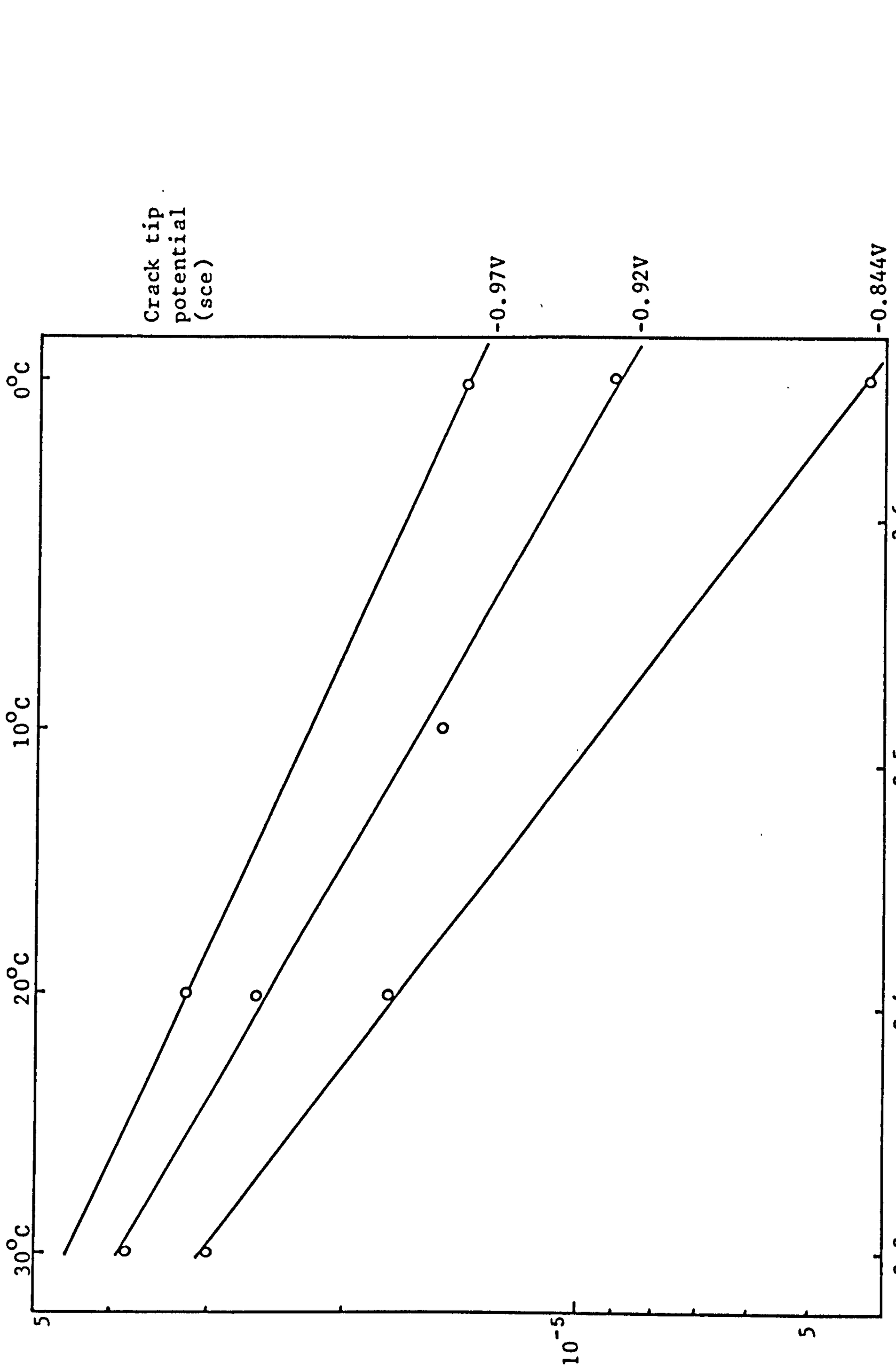
Crack tip potential (sce)
-0.97V
-0.92V
-0.844V
0°C
10°C
20°C
30°C
3.5
3.6
3.4
3.3
$\frac{1}{T} \times 10^3$ (K^{-1})
$\frac{da}{dt}$ (mm/s)
10^{-5}
5

Figure 6.7

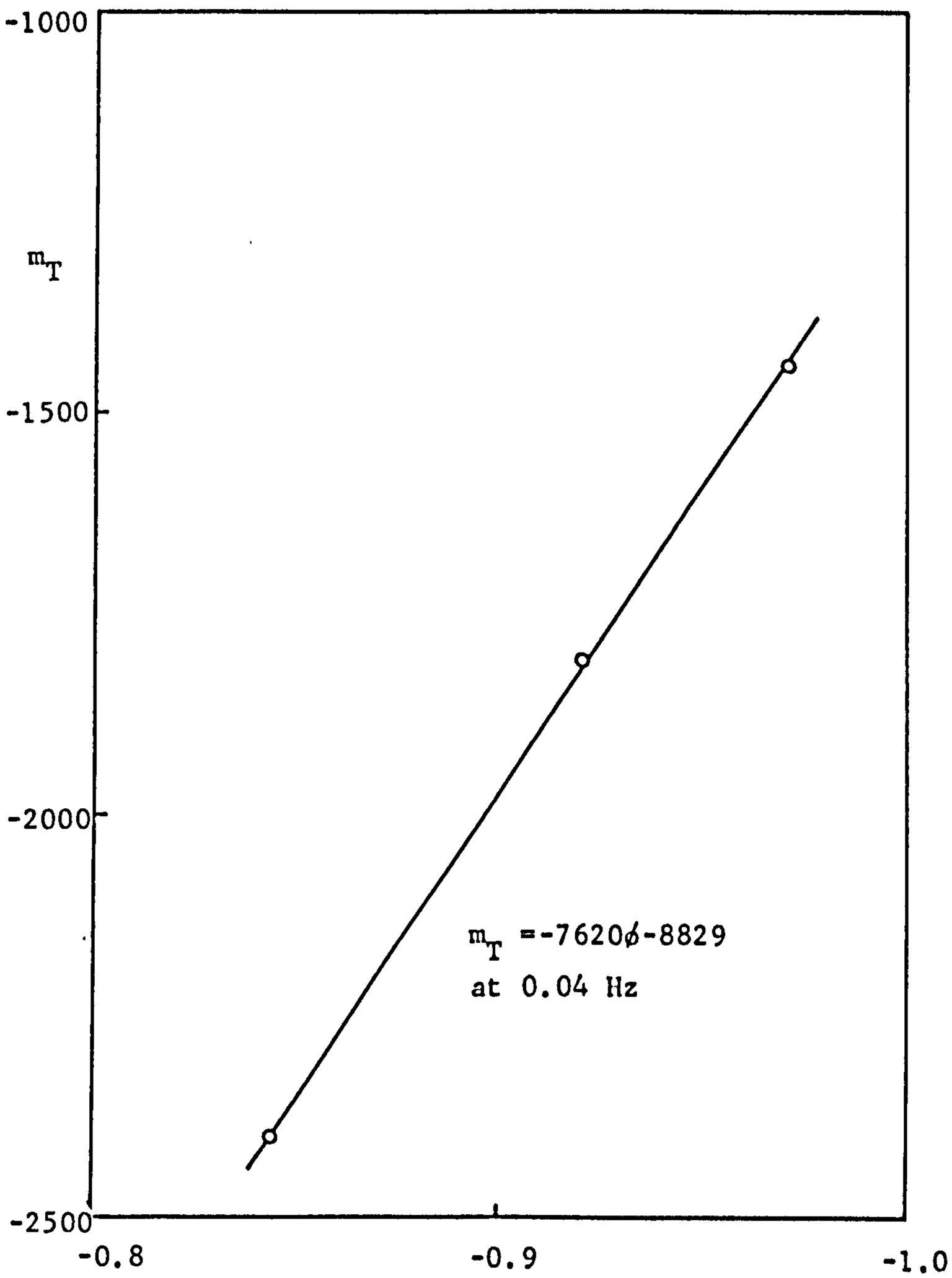
-1000
m_T
-1500
-2000
-2500
m_T =-7620ϕ-8829
at 0.04 Hz
-0.8
-0.9
-1.0
ϕ, Crack tip potential (sce)

Figure 6.8

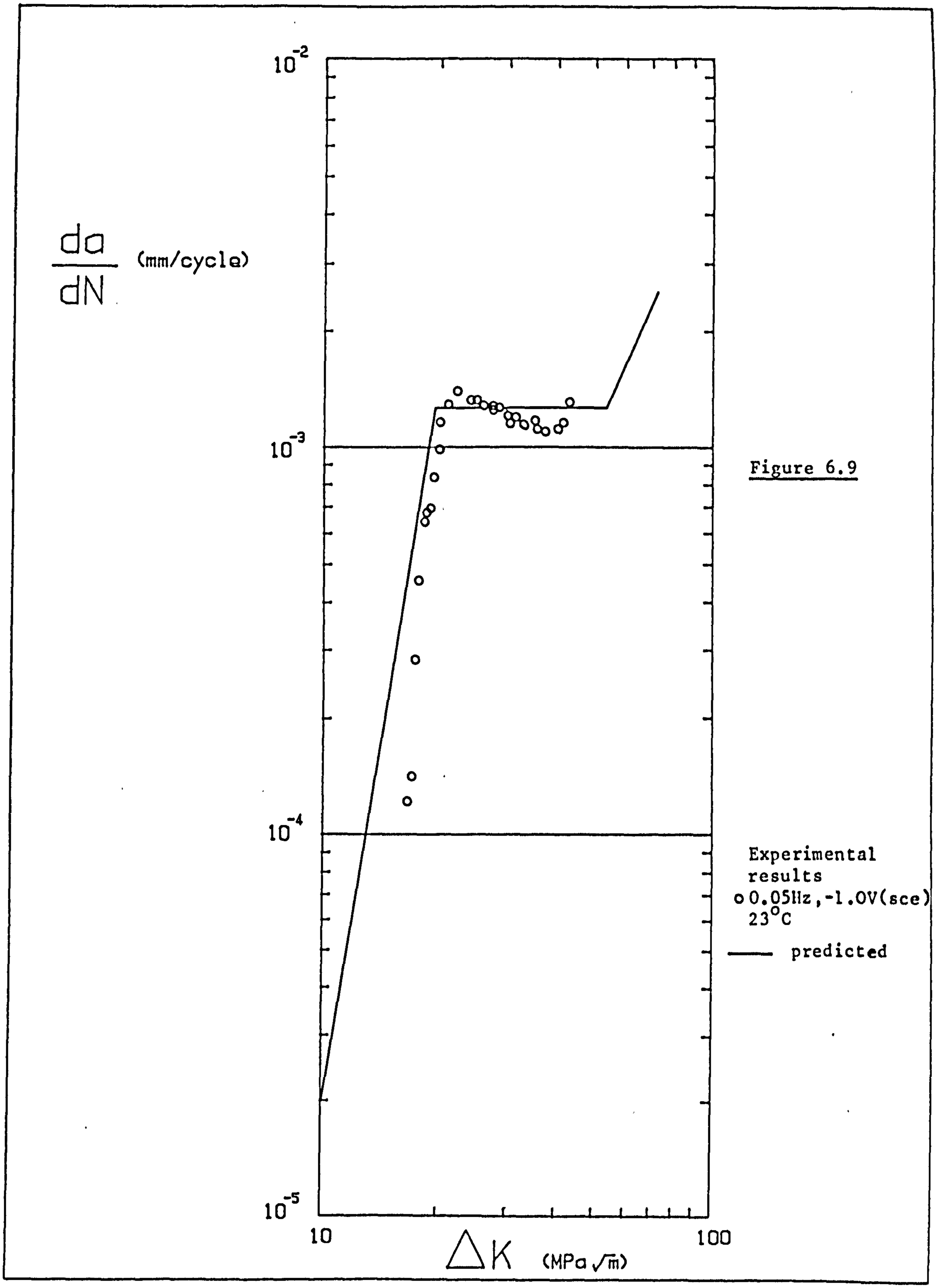
10^{-2}
10^{-3}
10^{-4}
10^{-5}
$\frac{da}{dN}$ (mm/cycle)
10
100
ΔK (MPa $\sqrt{m}$)
Experimental results
o 0.05Hz, -1.0V(sce) 23°C
—— predicted

Figure 6.9

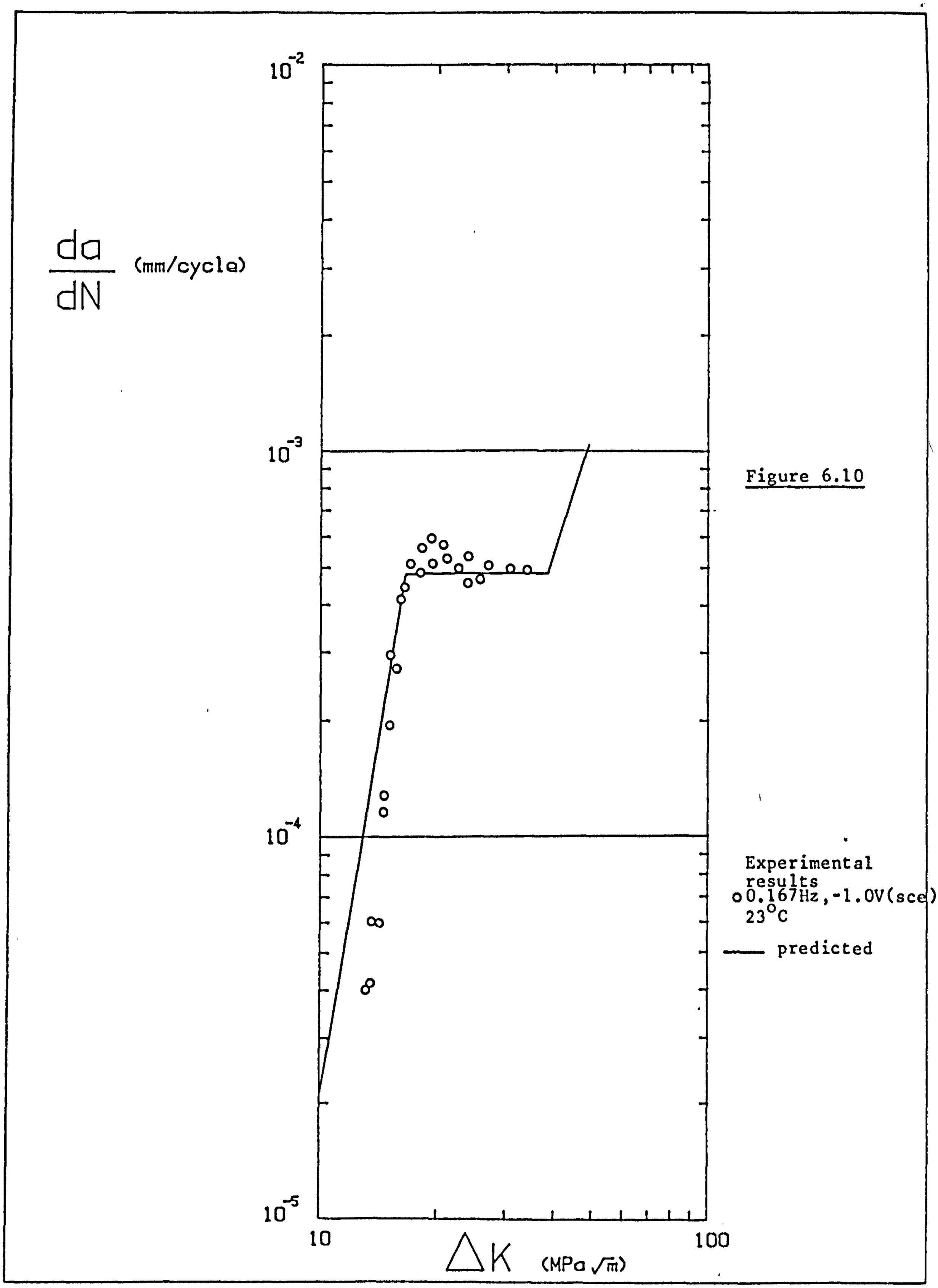
$\frac{da}{dN}$ (mm/cycle)
10^{-2}
10^{-3}
10^{-4}
10^{-5}
10
100
ΔK (MPa $\sqrt{m}$)
Experimental results
o 0.167Hz, -1.0V(sce) 23°C
—— predicted

Figure 6.10

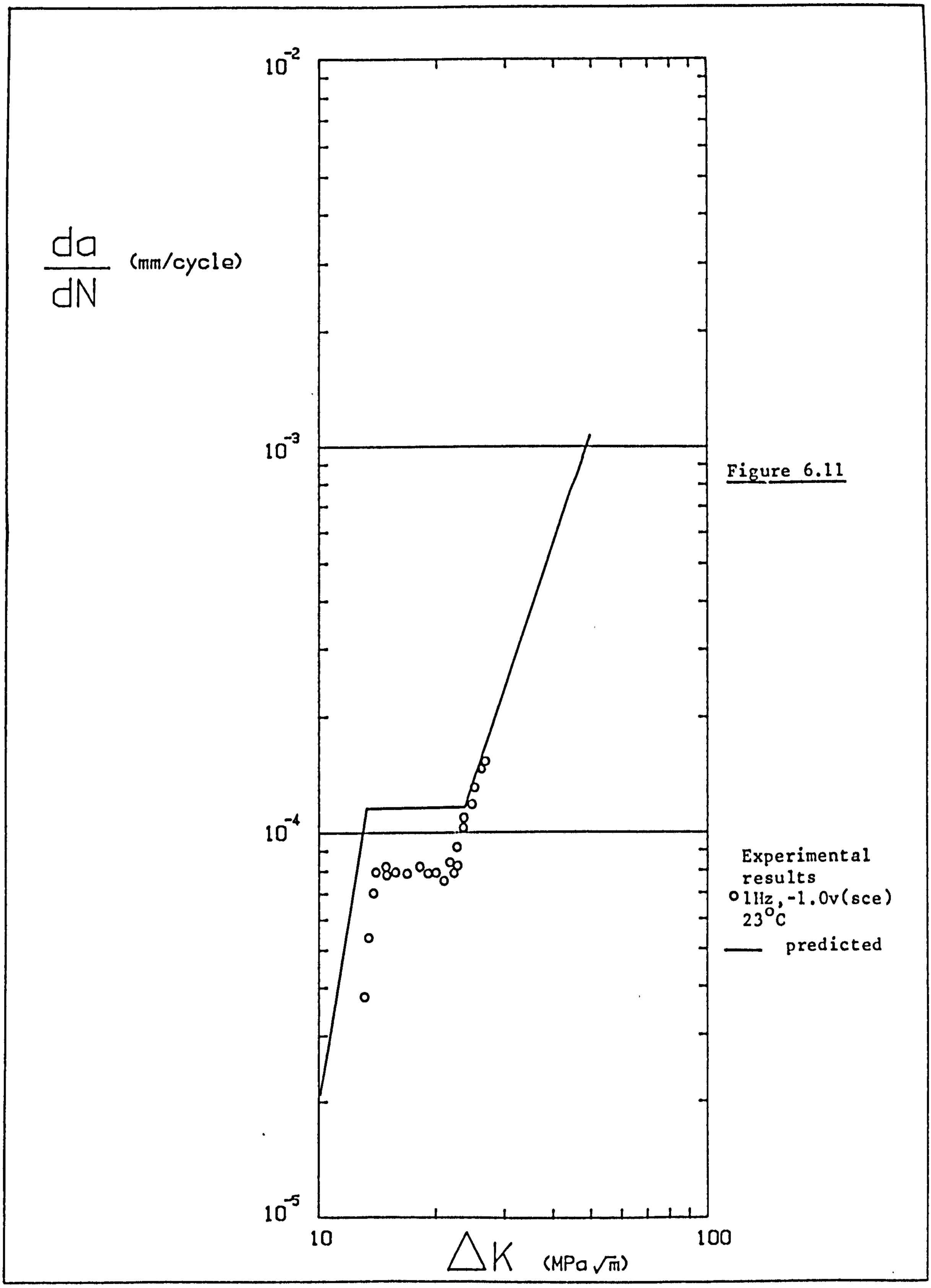
10^{-2}
10^{-3}
10^{-4}
10^{-5}
$\frac{da}{dN}$ (mm/cycle)
10
100
ΔK (MPa $\sqrt{m}$)
Experimental results
o 1Hz, -1.0v(sce) 23°C
—— predicted

Figure 6.11

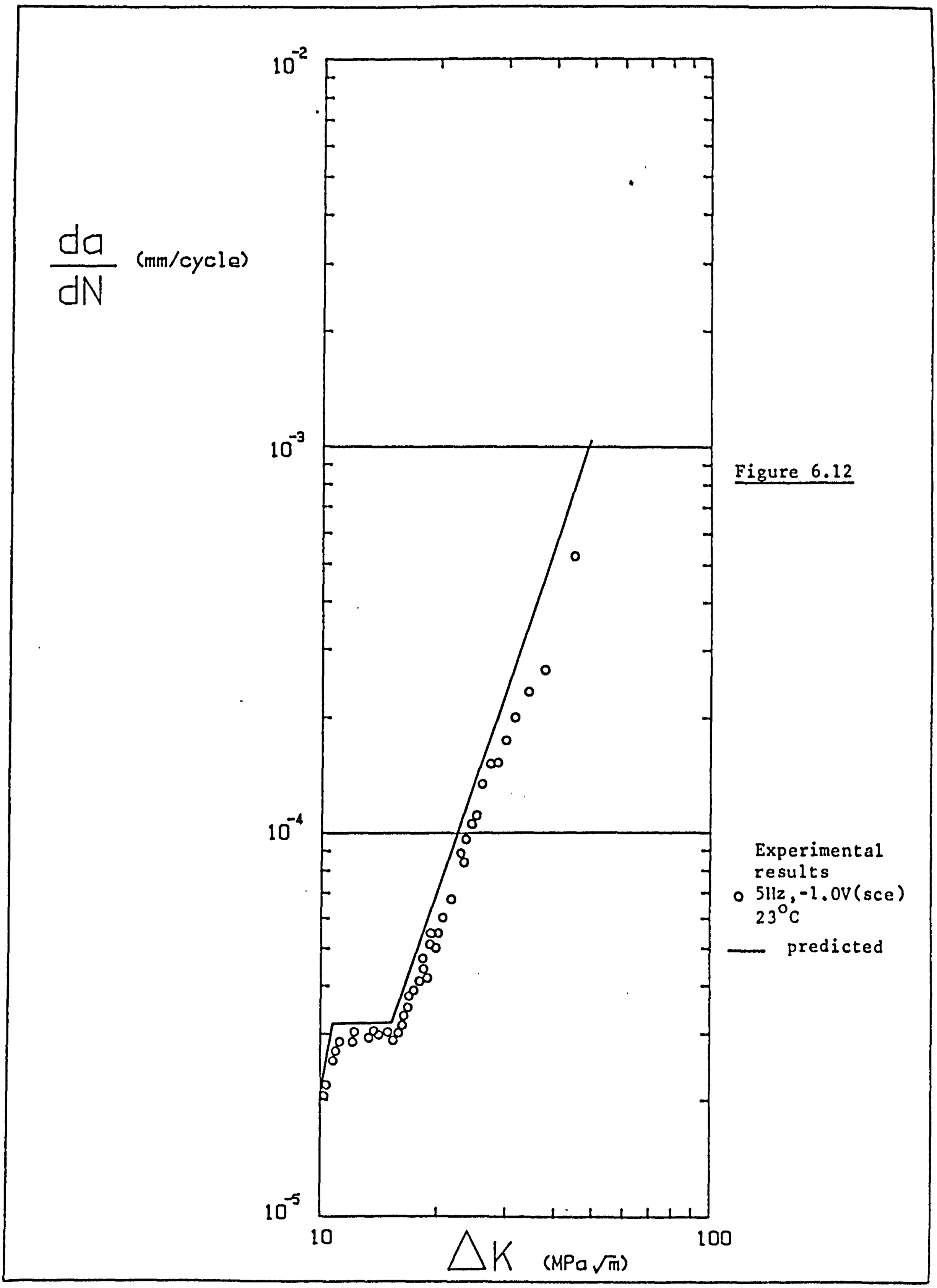
da/dN (mm/cycle)
10^-2
10^-3
10^-4
10^-5
10
100
ΔK (MPa √m)
Experimental results
o 5Hz, -1.0V(sce) 23°C
predicted

Figure 6.12

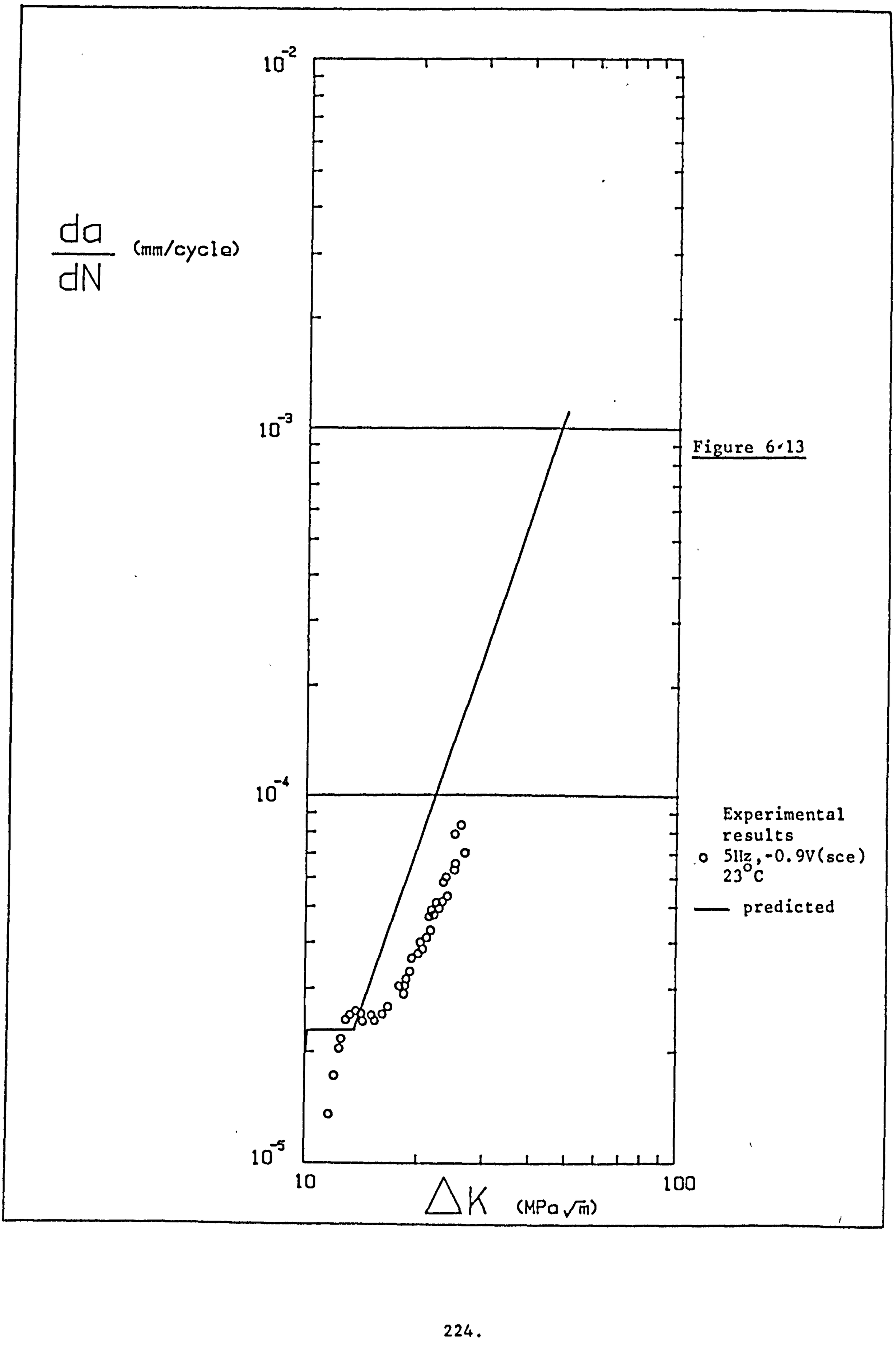
10^{-2}
10^{-3}
10^{-4}
10^{-5}
$\frac{da}{dN}$ (mm/cycle)
10
100
ΔK (MPa $\sqrt{m}$)
Experimental results
o 5Hz, -0.9V(sce) 23°C
predicted

Figure 6·13

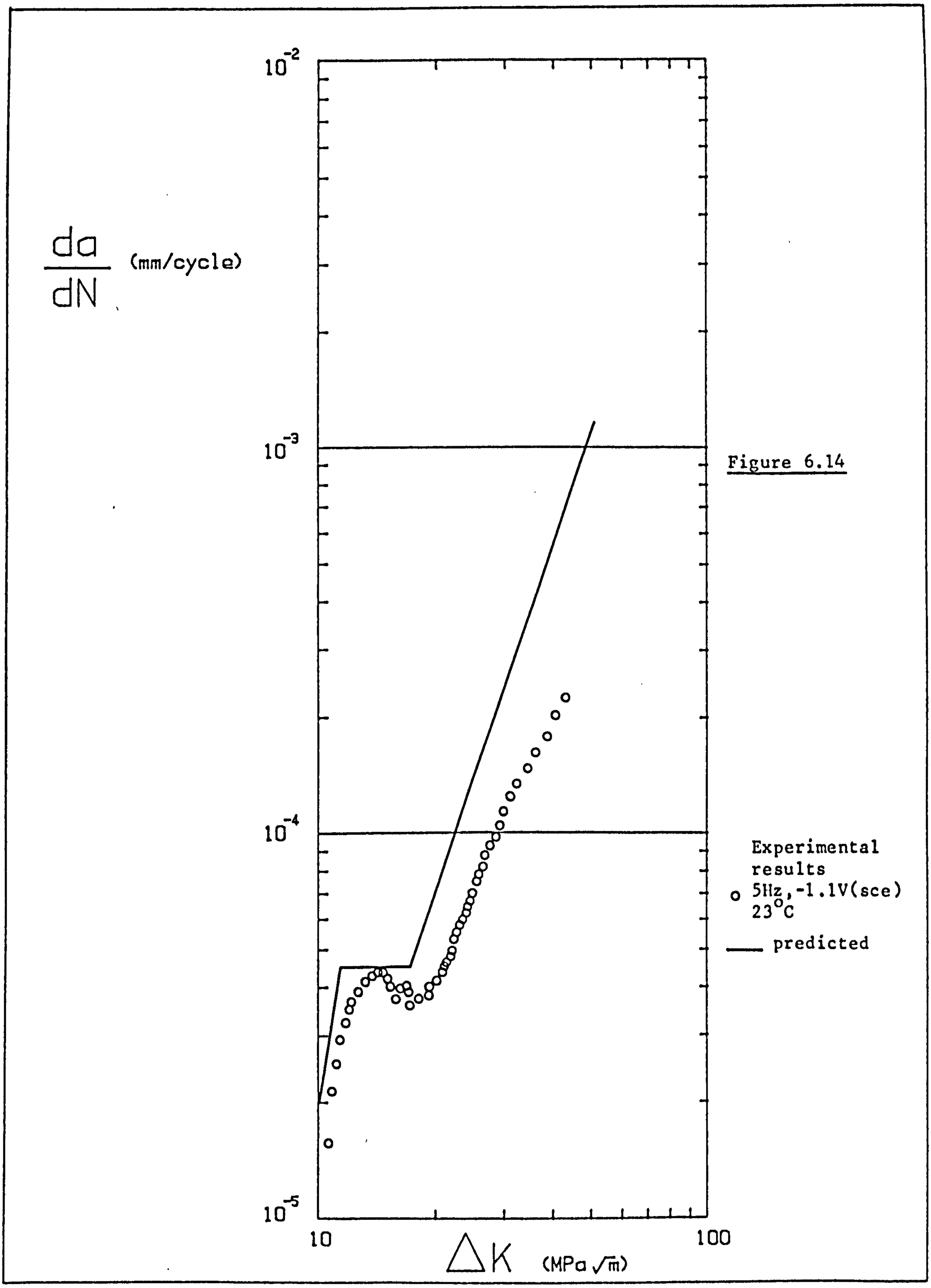
$\frac{da}{dN}$ (mm/cycle)
10^{-2}
10^{-3}
10^{-4}
10^{-5}
10
100
ΔK (MPa $\sqrt{m}$)
Experimental results
5Hz, -1.1V(sce)
23°C
predicted

Figure 6.14

Part II

Corrosion fatigue in a biologically active environment.

7.0 Introduction.

Part I of this thesis described a study of the corrosion fatigue behaviour of BS4360:50D in sodium chloride solution. This involved the evaluation of the fundamental mechanisms of environmentally assisted crack growth. Although the crack growth rates in 3%-3.5% NaCl and artificial seawater were held to be nearly identical concern has been expressed as to whether they are similar for real seawater. One study [264] has found no difference for Q1N steel. However this study used bulk seawater from the English Channel which would be expected to contain far smaller amounts of organic chemicals than water adjacent to the steel surface of any offshore structure. This is because a significant change in the seawater chemistry would be expected to occur as a result of the fouling present on such structures. One result of the alteration of the seawater chemistry is that an anaerobic zone may exist adjacent to the steel surface. Anaerobic bacteria will grow in these zones, and indeed evidence has been found for the presence of sulphate reducing bacteria on the steel jacket surface [266]. As these bacteria produce hydrogen sulphide as a by-product of their metabolism it has been postulated that they may cause significant increases in the rate of crack growth [267].

The work reported in this part of this thesis was designed as a preliminary study to investigate whether sulphate reducing bacteria affect the fatigue crack growth rate significantly. In particular an objective of the study was to discover if further research would be required into the effects of biological organisms upon fatigue crack growth rates, and whether chemically produced sulphide could be used to simulate the effect of sulphate reducing bacteria.

8.0 Theory.

8.1 Seawater chemistry.

Natural seawater is a complicated medium constituted by many organic and inorganic chemicals [228,268]. Over 77 elements are present in seawater, although 99.95% of the total solutes are accounted for by only 11 of the constituent ions. Although models of the chemistry of seawater have been produced some aspects of it are still unresolved [228]. As mentioned in Part I the presence of the inorganic constituents (above that of a 3.5% NaCl solution) has almost no effect on the fatigue crack growth rate, except where the formation of calcareous deposits causes crack closure effects. Thus the observed crack growth rates in 3%-3.5% NaCl and artificial seawater are usually the same. This is in accord with Turnbull's work on the electrochemical conditions within crevices of BS4360:50D, in which seawater had essentially the same effect as 3.5% NaCl [25,26] (cf.section 2.2.2).

The pH of natural seawater is approximately 8.2, as opposed to about 6.5 for 3.5% NaCl. Unlike NaCl solution seawater posseses several buffering systems [228]. Although the long term stability of the ocean's pH is determined by the presence of a buffering reaction involving aluminosilicates, for the time scales of interest in this study the seawater would be buffered by the carbonate/bicarbonate system [228]. It should be noted that the carbonate/bicarbonate system has only a limited buffering capacity.

The major difference between the artificial seawaters used [269,270] and real seawater is that real seawater contains many organic chemicals in addition to the inorganic constituents. These result from biological processes and comprise about 2ppm of the total solution. Over 100 organic compounds have been found in seawater, and surfaces exposed to seawater are covered with a layer of these chemicals [268]. This layer affects the surface/liquid chemical reactions, including corrosion. The presence of organic materials in seawater has been postulated as a cause of differences between the corrosion/SCC behaviour observed in seawater and NaCl solutions [271,272]. The organic content of the seawater next to the surface of a steel jacket is expected to be high due to the marine fouling present.

8.2 Marine fouling.

Marine fouling endangers steel jacket platforms by increasing the dead weight and wave loading on each member, obstructing visual and NDT inspection of welds and by creating favourable conditions for the growth of sulphate reducing bacteria (SRB). The types of fouling present on the platforms varies with their geographical location and the water depth, but fouling is commonly 0.1-0.2m thick, and can be up to 3m thick [273,274]. An example of the fouling found is shown in figure 8.1.

It is expected [266] that the fouling organisms create favourable conditions for the growth of SRB as :

(i) their waste products form a source of nutrients.

(ii) they deplete the concentration of dissolved oxygen, so forming an anaerobic zone at the metal surface.

This is illustrated in figure 8.2.

Periodically the fouling on structures is removed, either to reduce structural loading, or to facilitate inspection of welds [273,274].

8.3 Sulphate reducing bacteria.

8.3.1 Characteristics.

anaerobic : SRB are strict anaerobes [266,275], and so as the whole of the North Sea water column is aerated [276] they will only be active under special circumstances. As mentioned previously marine fouling can create a suitable environment for their growth, but anaerobic zones also exist in places such as the seabed sediments [276], underneath corrosion products [267], in crevices [267] or within the drilling mud that accumulates on the structural members [266].

require a low redox potential : SRB require a redox potential below about -100mV [275,277]. Whereas growth media for SRB are poised so as to lower the redox potential a natural environment may not be so favourable. However the sulphide produced by SRB lowers the redox potential, and so once these organisms become active they can adjust the local environment so as to encourage further growth. Other organisms found in the natural environment may also lower the redox potential [277].

require a limited range of carbon sources : pure cultures of SRB may only be grown on a limited range of carbon sources [266,275]. However a much wider range of carbon sources can be utilized when the SRB form one constituent of a mixed microbial community [278]. The presence of SRB on North Sea oil platform structures indicates that the layer of marine fouling can supply sufficient nutrient for their growth to occur [276].

sulphate is used as a terminal electron acceptor : sulphate reducing bacteria conduct *dissimilatory sulphate reduction* in which the sulphate ion acts as an oxidizing agent for the dissimilation of organic matter, as does oxygen during conventional respiration. The process has been called "sulphate respiration" and is analogous to the "nitrate respiration" found amongst nitrate reducing and denitrifying bacteria. During sulphate respiration the breakdown of the carbon sources produces electrons, which are transported with the production of ATP. The final part of the process involves an oxidative process during which sulphate becomes reduced to sulphide. Thus the sulphate

ion is a terminal electron acceptor for the respiratory process. Further details of the metabolism of SRB can be found in reference [275].

produce sulphide : although a wide variety of micro-organisms may excrete H_2S into the environment SRB are unique in that they produce H_2S as a result of dissimilatory sulphate reduction [275,277]. The sulphide produced in the environment leads to enhanced rates of corrosion as described below.

utilize and produce hydrogen : many SRB can utilize molecular hydrogen as an electron donor [275,277]. Such SRB contain hydrogenase enzymes which catalyze the reaction :

$$H_2 \rightarrow 2H^+ + 2e^- \qquad (8.1)$$

The electrons are then used in the reduction of SO_4^{2-} to S^{2-}. The utilization of molecular hydrogen in this way may affect corrosion fatigue crack growth rates, as well as corrosion processes. The reduction of sulphate to sulphide can occur in the absence of hydrogenase enzymes.

In the absence of sulphate hydrogen may be produced by these bacteria [275,278].

grow in communities with other bacteria : several workers have emphasized the fact that SRB are found as part of a bacterial community [278,279]. The properties of such communities may be very different from those of pure cultures, as a result of the inter-species interactions that occur [279]. SRB are usually found in mixed communities [278], often with aerobic organisms that can scavange any oxygen present. SRB and sulphur oxidizing bacteria, such as Thiobacillus, may work together to produce acidic environments, sometimes as acidic as pH=1.0 [276,280].

ubiquitous : although SRB are anaerobic they can survive for long periods in an aerobic environment. They are also to be found widely, both on land [275] and throughout the North Sea water column and bottom sediments [276]. These organisms would be in a quiescent state, ready to become active if they land within a suitable environment.

8.3.2 Results of SRB activity.

corrosion and pitting : SRB may cause corrosion and pitting in both ferrous and non-ferrous alloys [281]. They have often been identified as a source of corrosion in land pipelines [275]. Even stainless steels are pitted and corroded as a result of SRB activity [282]. SRB are often found inside the tubercules formed as a result of the growth of iron bacterium [275,283], severe pitting is then found [275]. In the natural environment corrosion and pitting attack usually occurs as the result of the activity of a mixed culture of organisms, sulphate reducing bacteria forming one constituent of the community.

blistering of high strength steels : hydrogen blisters have been reported to occur in a high strength steel as a result of SRB activity [284]. Such effects have not been widely reported, probably because studies involving SRB have been directed towards their effect upon corrosion rates, rather than investigating the acknowledged possibility [285,286] that biogenic sulphide could cause hydrogen embrittlement. Some doubt has been expressed as to whether it was really hydrogen blisters that were observed [287].

graphitization of cast irons : SRB can cause the graphitization of cast irons [275] by the corrosion of the iron.

sour oil and gas : SRB activity can cause an oil or gas reservoir to become "sour", with large economic consequences for the operators [266]. Microbial communities are able to degrade oil held in storage, and SRB are involved in this process [288].

death : hydrogen sulphide is highly toxic (safe working limit ≈10ppm). Three deaths from H_2S poisoning on the Spar buoy in the North Sea have been reported [289]. The H_2S accumulated in an oil storage area as a result of the action of SRB. Sulphide concentrations of 50 to 100ppm have been found in crude oil storage tanks [266], this can give H_2S concentrations of up to an order of magnitude greater in the overgas [266]. Aqueous sulphide concentrations of more than 2000ppm have been found in studies on SRB [290]. Thus it is seen that lethal concentrations of H_2S may develop quite easily as a result of the growth of SRB.

8.3.3 SRB population density.

Very little data has been released as to the exact environmental conditions found on the external surfaces of a steel jacket structure. Similarly very little data is freely available as to the numbers of SRB to be found on such surfaces.

Evidence of SRB activity has been found on the external surfaces of North Sea structures [266]. Tiller [287] found 10^1 SRB/ml in the Thames at Teddington, increasing to 10^3 SRB/ml below London at Tilbury, then falling to 10^1 SRB/ml in the sea. Sanders [266] gives 10^3 SRB/ml as a high value for open seawater. Hamilton et. al. [276] give 10^4 SRB/ml as a high number, found in nutritionally enriched sediments. They also found populations between 10^3 and 10^6 SRB/ml in the sediments around offshore platforms, the high numbers were attributed to the presence of an increased organic loading of the sediment due to domestic wastes, drilling muds and biological debris removed from the structure during cleaning and inspection. Tiller [287] obtained 10^4 to 10^6 SRB/ml in sludge after 1 year, and Sanders [266] gave 10^6 SRB/ml as a "high" number. As a guess Tiller [287] suggested that 10^3 to 10^4 SRB/ml would be a reasonable estimate of SRB numbers present on the surface of an offshore structure.

8.4 Mechanisms of microbial corrosion.

Although many different types of organism are present in the fouling of an offshore structure the layer of micro-organisms attached directly to the surface probably has the greatest effect upon the corrosion of the structure.

The accelerated corrosion of metals by microbes does not involve any new corrosion processes [282,283], it is caused by :

(a) production of differential aeration and concentration cells
(b) production of corrosive metabolites
(c) cathodic depolarization

8.4.1 Production of differential concentration and aeration cells.

An adherent microbial growth on the metal surface creates a zone underneath it in which oxygen and other nutrients are depleted. This zone is then anodic to the rest of the metal, like that at the bottom of a pit or crevice. Once the concentration cell has developed the layer of microbes acts as a physical barrier to the ingress of oxygen, and so the microbes do not have to remain alive for the enhanced corrosion to continue [291].

Some aerobic bacteria ("iron oxidizing bacteria") can form tubercles, the interior of which become anaerobic, leading to the growth of sulphate reducing bacteria and consequential pitting [275,283], an example is shown in figure 8.3.

Also, in conditions with an aerobic/anaerobic interface elemental sulphur may be formed, and pitting may then possibly be caused by the action of a sulphur concentration cell that is analogous to a differential aeration cell [283]. Figure 8.4 illustrates and compares the oxygen and sulphur concentration cells.

8.4.2 Production of corrosive metabolites.

Organic acids are produced by fungi and bacteria and are corrosive [291]. Additionally certain aerobic bacteria (of the genus Thiobacillus) can produce harmful amounts of sulphuric acid, especially when an aerobic/anaerobic boundary exists. (This is because the H_2S produced in the anaerobic zone by sulphate reducing bacteria is oxidized at the boundary to H_2SO_4.) Thiobacillus is often

implicated in corrosion problems in areas such as acid mine drainage water [292], and buried pipes [291]. In mines the presence of Thiobacillus can cause the pH of the water to become ≈2. Corrosive metabolites may also be produced as the end products of fermentation processes [293].

8.4.3 Cathodic depolarization.

Although both of the previous mechanisms would be expected to play a part in the microbial enhancement of corrosion of offshore structures the most important one is probably cathodic depolarization, brought about by the activity of the sulphate reducing bacteria. These are anaerobic bacteria that utilize sulphate as an oxidizing agent for the dissimilation of organic matter, producing sulphide as a waste product. As a result a layer of iron sulphide forms on the steel surface, and as iron sulphide is cathodic to mild steel [281] it becomes the cathode of the corrosion cell. The depolarization of mild steel by an iron sulphide layer depends on its non-stoichiometry [294]. In the absence of sulphate reducing bacteria the depolarization decreases with time, because atomic hydrogen becomes bound within the sulphide lattice. Sulphate reducing bacteria utilize hydrogen during their growth, and by removing hydrogen from the iron sulphide they maintain its depolarizing effect, so maintaining a high rate of corrosion. Booth and Tiller [295-298] conducted early polarization studies for mild steel in cultures of SRB. More detailed accounts of the mechanism by which SRB enhance corrosion rates can be found in the work of Tiller [282,283]. Extremely rapid corrosion can occur in metals that are exposed to aerated conditions after being in contact with a biogenically produced sulphide film [299,300], or chemically prepared sulphides [301].

It has been suggested [298,302] that corrosion due to SRB could be prevented by an additional 100mV of cathodic protection being applied, ie. protect the rig at -0.95V(Ag/AgCl). Such a strategy if applied to offshore structures would promote fatigue crack growth by a hydrogen embrittlement mechanism, as discussed in Part I of this thesis.

Finally, although biological enhancement of corrosion does occur it appears that the corrosion rates experienced offshore are still tolerable [303]. Therefore the only problem that microbial activity poses for the integrity of these structures is its possible effect on the growth of fatigue cracks.

8.5 Effect of hydrogen sulphide on fatigue.

Hydrogen sulphide poisons the hydrogen recombination reaction (equation 3.7) and so enhances the entry of hydrogen into the metal. Thus for 4130 steel it has been shown [304] that sulphide stress cracking is caused solely by the enhanced entry of hydrogen. As well as promoting hydrogen entry the presence of hydrogen sulphide causes enhanced corrosion of the metal [282,301,304]. This is because of the action of the sulphides in facilitating the cathodic reaction [282,301]. In a 3.5% Ni steel evidence has been found that sulphide stress cracking is caused by this enhancement of the corrosion process [305].

The role of inclusions is important [240,306] both as sites of hydrogen accumulation, and in enhancing hydrogen entry. Manganese sulphide inclusions can dissolve in contact with water :

$$MnS + 2H^{+} \rightarrow H_2S + Mn^{2+} \qquad (8.2)$$

The hydrogen sulphide that results from this reaction can enhance hydrogen entry into the metal [240], this may be significant for situations where the bulk environment does not contain sulphide. Similar effects may occur during pitting [30], but the sulphide encourages growth of pits by enhancement of the rate of corrosion. Other microstructural features such as carbides may also affect the uptake of hydrogen in environments containing hydrogen sulphide [239].

Although hydrogen sulphide is known to exacerbate fatigue crack growth rates very few relevant studies of its effect upon fatigue crack growth rates are known to the author. Bristoll and Roeleveld [250] gave the fatigue crack growth rates for steel 52 in H_2S saturated seawater as :

$$\frac{da}{dN} = 2.98 \times 10^{-4.96} \text{ mm/cycle} \qquad (8.3)$$

They also reported that the fatigue threshold appeared to be the same as that found in air. Results were only obtained under free corrosion conditions, and some scatter exists in the data - possibly as a result of the use of an optical crack length measurement technique.

Vosikovsky [129,256] has studied the corrosion fatigue behaviour of X65 in sour crude oil environments. This data has then been used in investigating crude oil pipeline failures [307]. Plateaus were only seen with low concentrations of H_2S, and the plateau crack growth rate increased as the frequency increased, suggesting that the plateau

could be caused by a restriction on the rate of supply of oil to the crack tip [129]. The crude oil only contained <0.01% water, it is to be expected that transport of fresh H_2S solution to the crack tip would be much faster in a fully aqueous environment. Thus although Vosikovsky's results are not directly comparable to the present work they do illustrate the deleterious effect of H_2S upon fatigue crack growth rates.

Austen [164,308] has investigated the growth of fatigue cracks for BS4360:50D in H_2S saturated artificial seawater (≈3150ppm). Unfortunately it is not possible to define the region I crack growth behaviour from these results because the initial value of ΔK was generally greater than 10 MPa√m. Figure 8.5 compares Austen's results with those of Bristoll and Vosikovsky discussed earlier.

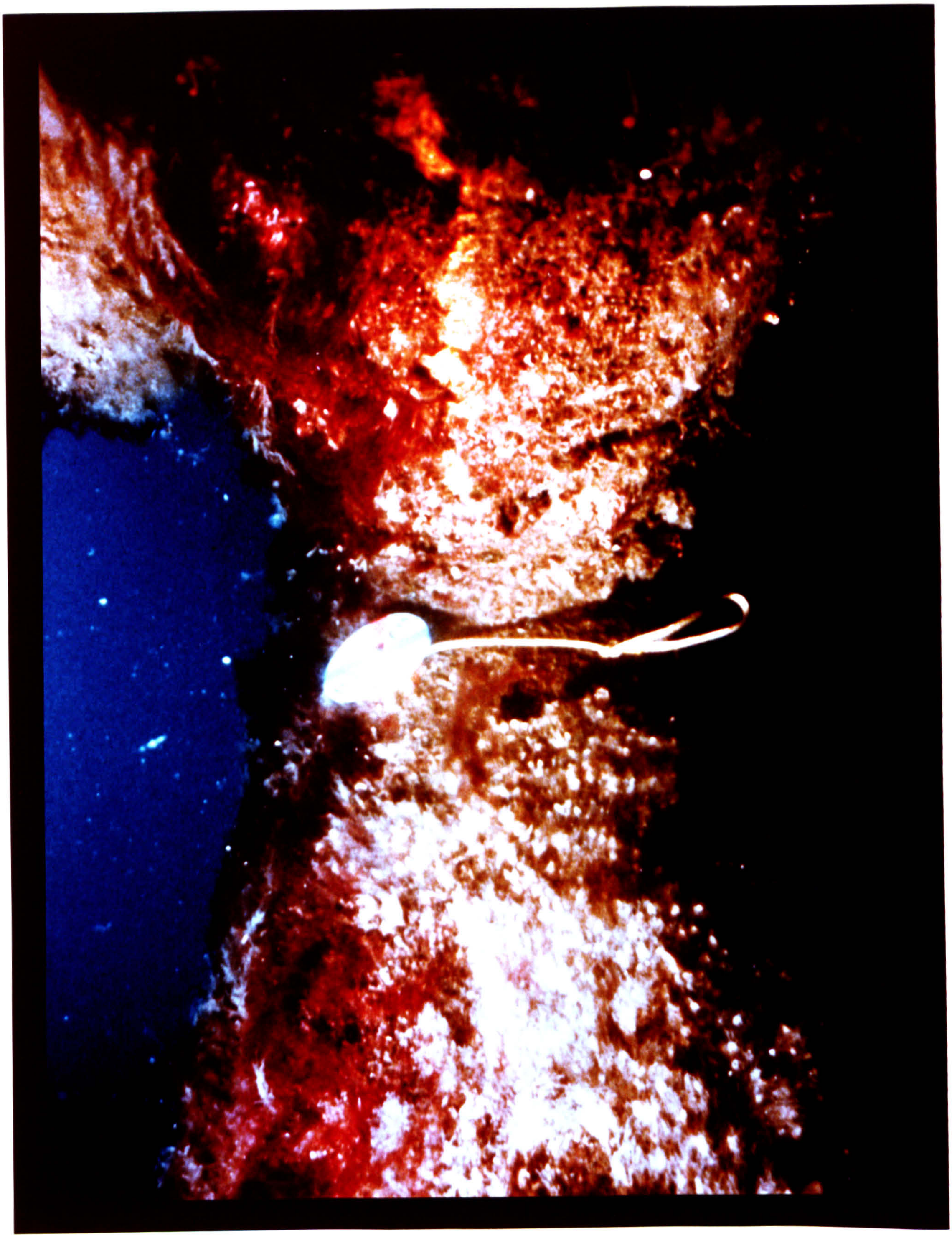

Figure 8.1 Photograph of fouling on a steel jacket (courtesy of P. Sanders)

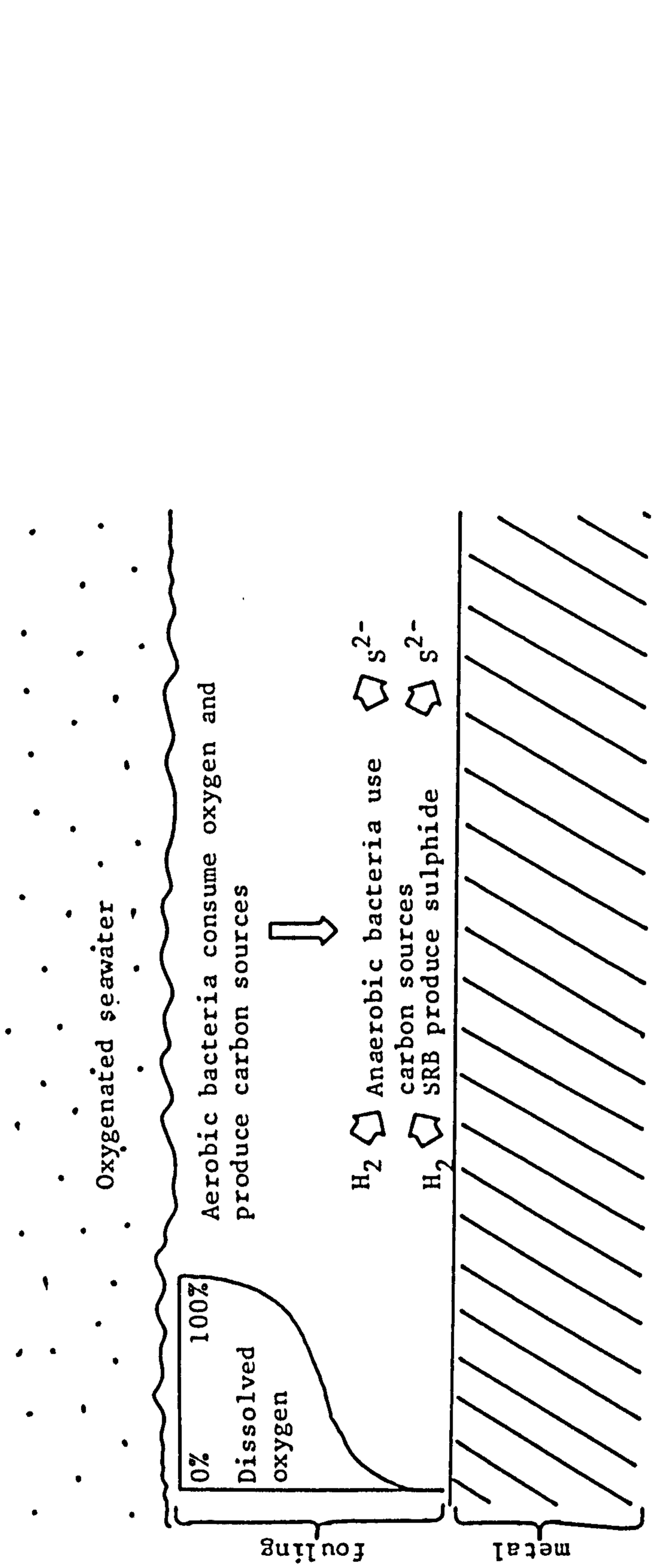

Figure 8.2 Schematic diagram showing effect of fouling layer, from reference (309)

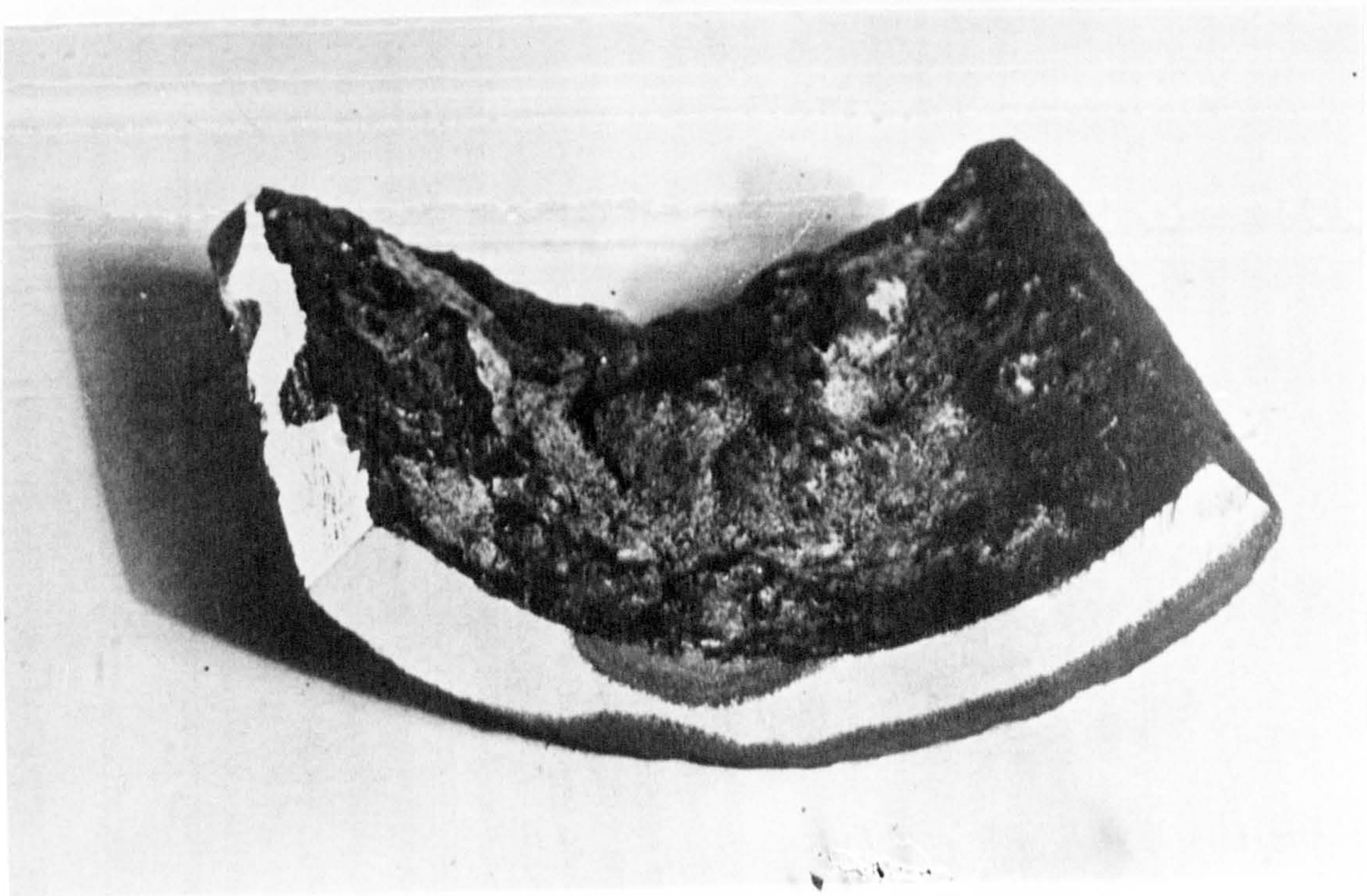

Figure 8.3 Anaerobic corrosion of a spun steel water pipe. The corroded pipe has been cut to show characterisitc corrosion beneath tubular deposits on the inner surface. Corrosion tends to be localized; some attack has been initiated from the outer surface. The darkening is "graphitization", loss of iron, leaving the carbon skeleton of the steel. From reference (275).

Autocatalytic pitting mechanisms.

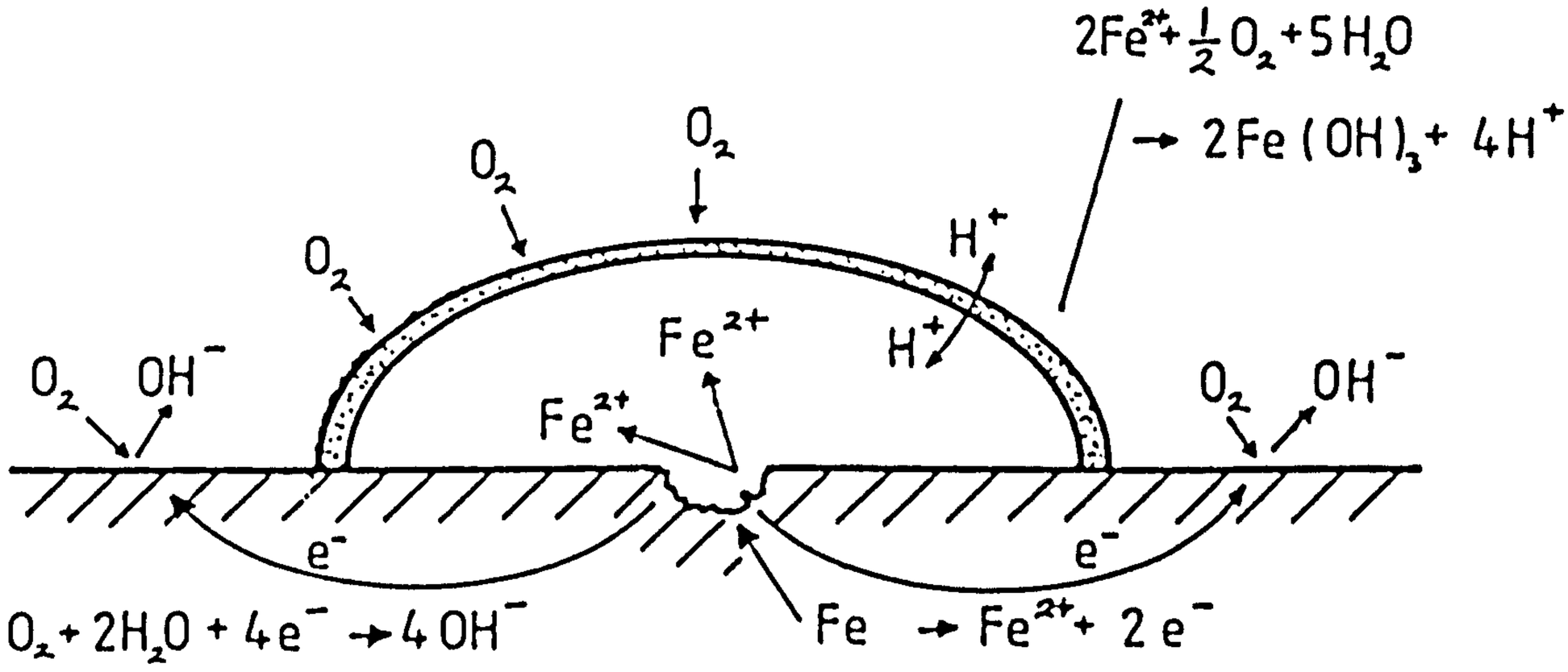

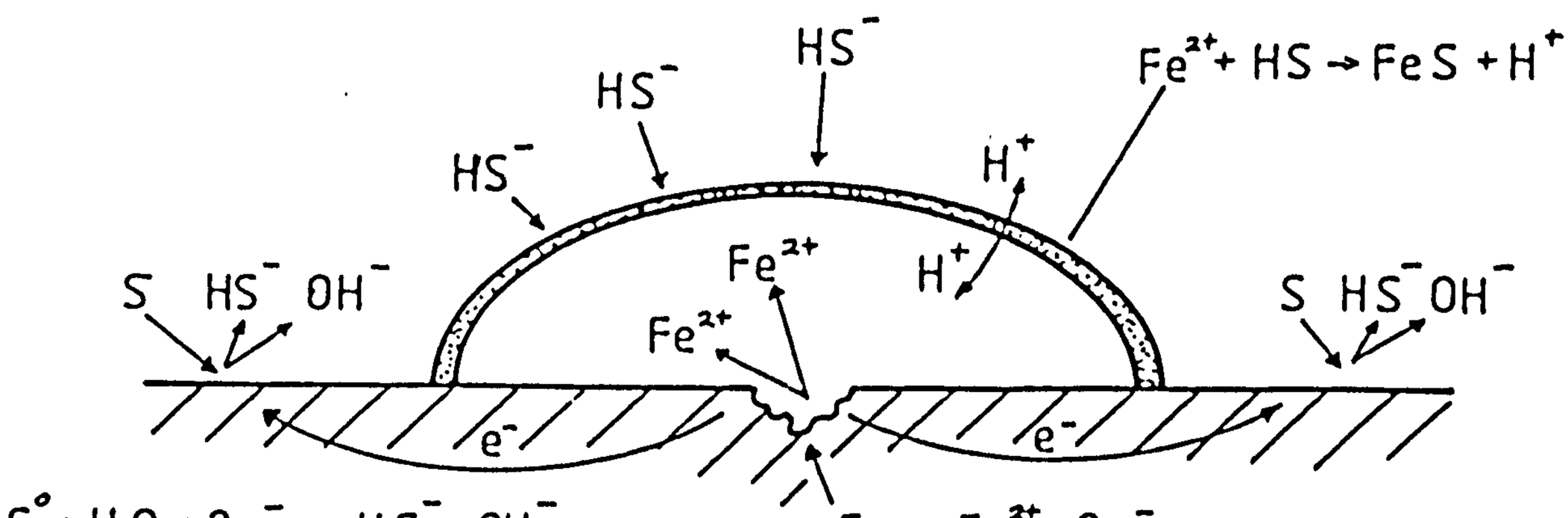

Figure 8.4

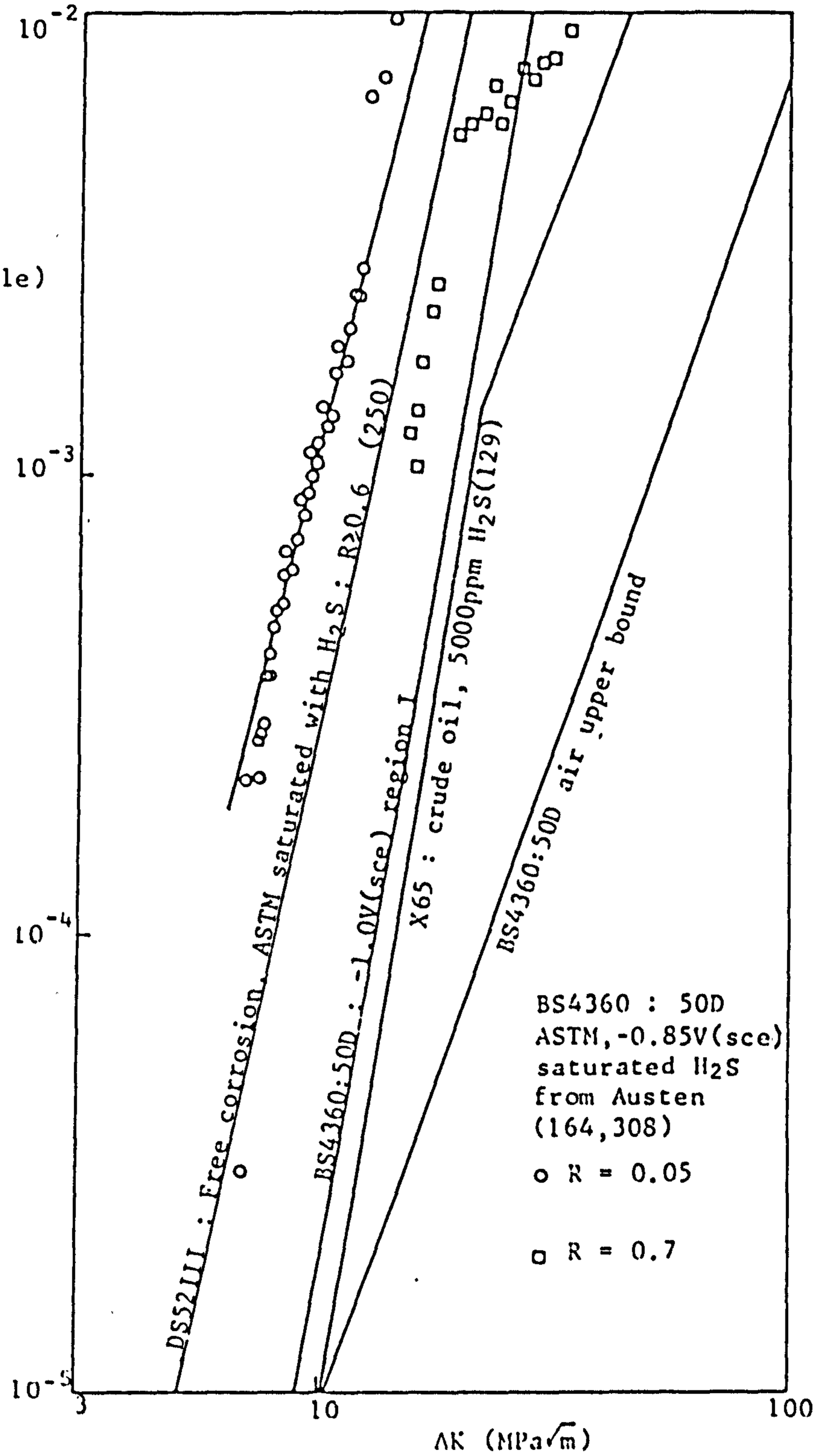
10^{-2}
10^{-3}
10^{-4}
10^{-5}
da/dN (mm/cycle)
3
10
100
ΔK (MPa√m)
DS2111 : Free corrosion, ASTM saturated with H_2S : R≥0.6 (250)
BS4360:50D : -1.0V(sce) region I
X65 : crude oil, 5000ppm H_2S(129)
BS4360:50D air upper bound
BS4360 : 50D
ASTM, -0.85V(sce)
saturated H_2S
from Austen
(164,308)
o R = 0.05
□ R = 0.7

Figure 8.5

9.0 Experimental.

Corrosion fatigue experiments conducted in a biologically active environment should ideally satisfy both the corrosion fatigue and microbiological testing criteria. It is extremely difficult to do this in practice, and so one or the other set of criteria may be contravened [287]. In this work the ideal microbiological criteria were not satisfied. This may be justified on the grounds that this study was an engineering "first look" at a potential problem, which did not warrent the same scientific experimental rigour as a more fundamental study [287].

9.1 SRB inoculum.

For microbiological work pure cultures are usually used, although some studies have used simple mixed cultures [279]. However pure cultures of SRB's have historically proved difficult to obtain and maintain [275]. It would also be extremely difficult, if at all possible, to prepare a fatigue test under asceptic conditions, which means that if a pure culture was used contamination would probably occur during the setting up of the corrosion fatigue test. Because SRB are present on offshore structures as part of a microbial community, and because interactions between different types of bacteria can occur [278,303], it was decided to use a mixed culture of bacteria for this work. Whereas for corrosion studies it is possible to do in situ experiments offshore [309] this was not a viable option for this work, and so a source of bacteria had to be found. It was chosen to use about 10mls of mud as the inoculum for each test : the mud was obtained as seabed core samples from the lower Clyde estuary (Ballochmartin bay, Cumbrae) taken by the University Marine Biological Station at Millport, Isle of Cumbrae. The mud was stored, in some cases for months, before being used and so the bacteria in it became senescent. This was not a problem because of the incubation time allowed for each test, as described later.

The penalty of the approach adopted is that, although it is easy to obtain and grow the mixed culture it does represent an impure microbiological system and so is not well characterized [287]. This does raise the probability that the microbiological system was different for each test, and the differences are difficult to quantify

[287]. Different organisms may give different effects. One beneficial effect of a mixed culture is that the aerobic bacteria present should scavange any oxygen present, in a similar manner to their proposed action offshore [309].

9.2 Environment.

It was specified by the funding body sponsoring this work [219] that the environment should be based upon ASTM artificial seawater [269], at a temperature in the range 5-10°C. As the artificial seawater would not support the growth of SRB it was fortified with additional nutrients to make it up to being equivalent to Postgate's medium "B" [275]. Because the iron content of the medium is only present as an indicator [310] for sulphide the high iron content of the medium was reduced to that of Postgate's medium "E" [275]. Other workers have also used Postgate's medium "B" modified by reducing the iron content [311]. Table 9.1 details the compostion of the resultant medium. (The thioglycollic acid in Postgate's medium is a poising agent for the redox potential, other media may use less acidic poising agents such as sodium sulphide [275,312]). The medium was kept in the dark to avoid growth of unwanted organisms [310].

The composition of the growth medium for the bacteria is important, as for a mixed culture situation the medium will determine which strains of bacteria multiply. This is because the bacteria present, for which the medium is similar to their natural environment, would obviously out compete those for which it is not. Thus the use of a different medium would result in a different pattern of microbial activity [287,312].

The medium used for this study contained 0.35g/l PO_4^{3-}, whereas the ASTM artificial seawater has no phosphate present. In Turnbull's review on electrochemical conditions in cracks [30] he reports that variations in the organic and phosphate content of seawater may cause changes in the precipitation rate for calcareous deposition of more than an order of magnitude. Thus the rate of calcareous deposition in the medium could be very different from that in plain ASTM artificial seawater. Biofouling would also cause variations in the organic and phosphate content of the water.

9.3 Determination of hydrogen sulphide concentration.

Ideally for a rigorous scientific approach the concentrations of fatty acids, sulphide and sulphate should have been monitored for the liquid environment and the concentrations of CO_2, CH_4, H_2 and H_2S in the overgas measured [312]. This would have enabled an idea to be obtained as to the activity of various types of bacteria [266]. The equipment and time necessary for such an undertaking were not available. Because the major effect of bacteria upon fatigue crack growth rates is expected to result from the production of hydrogen sulphide some measurements of hydrogen sulphide concentration were made.

Although iodimetric methods [313] have been used by other workers [314] the method used in this study was that of Truper and Schlegel [315]. This method was chosen as the amount of sulphide was expected to be less than 100ppm [314]. Both methods measure the total sulphide content (H_2S, S^{2-} and HS^-).

The sulphide determination method used is a colourmetric method involving methylene blue. The sample (1ml) is added to a zinc acetate solution to fix the sulphide as ZnS. In a 100ml volumetric flask the volume is increased to about 80ml with distilled water. 10ml of a dimethyl-p-phenylenediamine sulphate solution (0.2% in 20% H_2SO_4) is then added and the solution is swirled to mix. The solution is then complexed by the addition of 0.5ml of a $FeNH_4(SO_4)_2$ solution (10% in 2% H_2SO_4), and the mixture is shaken and left to stand for 10 minutes while the colour develops. The flask is then filled up to the mark with distilled water, and the density of colour determined using a Beckman DB/GT spectrophotometer at 670μm. The optical density is linearly related to sulphide concentration for concentrations up to approximately 120ppm. For sulphide concentrations greater than 120ppm a smaller sample size was used. As the sample was diluted by at least 100x the bacterial cells did not significantly affect the photometric determination. It was necessary to ensure that the method was not subject to interference by the constituents of the medium or seawater [316], no effect was found as shown in figure 9.1. A calibration curve had to be obtained before each sample run, this was done using sodium sulphide weighed out and diluted into known concentrations. Figure 9.2 shows an example calibration curve. The use of this method of sulphide analysis did mean that the sulphide concentration was not known instantly, most importantly the

concentration was not known during the test itself but was only available subsequently.

As mentioned earlier the method used determined the total sulphide content. Hydrogen sulphide in solution may be present as H_2S, HS^- or S^{2-} depending on the pH [30]. The ratio of H_2S to HS^- can be found from [30] :

$$\log \frac{[HS^-]}{[H_2S]} = -7 + [pH] \qquad (9.1)$$

Thus the proportion of H_2S increases as the pH is decreased.

9.4 Determination of SRB numbers.

Samples of liquid from the tests were sent to the National Collection of Industrial and Marine Bacteria (NCIMB), Torry Research Station, Aberdeen for aerobic plate counts and extinction dilution counts of SRB. It was not possible to count the number of bacteria present on the specimen surface, although this would be expected to be greater than the free swimming population. However the number of bacteria found in the liquid should roughly correlate with the number found attached to the surfaces. The counting methods used were plate counts for the aerobic bacteria and extinction dilution counts for SRB, in which quintuplicate bottles at each dilution were incubated at 30°C for up to 14 days. Blackening of the bottles indicated growth of SRB's, and after 14 days the most probable number of SRB was estimated [317].

9.5 Experimental arrangement.

The experimental arrangement is illustrated diagrammatically in figure 9.3. Because SRB are anaerobic, and also because they produce toxic hydrogen sulphide, the testing had to be performed inside a purpose built anaerobic chamber. The chamber was constructed out of 12.5mm thick Perspex sheet glued together and sealed around the base with a rubber gasket. Another rubber gasket was used to seal around the window of the chamber, and the movement of the testing machine ram was accommodated by a flexible tube manufactured from a lorry inner tube. Additionally the inside joints of the chamber were sealed with a silicone sealant. A photograph of a fatigue testing machine which

shows an anaerobic chamber in position is given as figure 9.4.

A tube was taken from the tank through the wall of the chamber in order to permit sampling of the liquid around the test specimen. Other leads through the chamber wall were made for the DC current supply, cooling water supply, etc. Each wire or tube through the chamber wall was carefully sealed.

The anaerobic atmosphere inside the chamber was maintained by slowly passing a N_2/CO_2 mixture through it. The gas contained 300vpm CO_2, an equivalent amount to that of CO_2 in air, so as not to strip the seawater of its carbonate buffering system [49]. All the tubing used was made from butyl XX rubber because of its impermeability to oxygen [312].

A miniture peristaltic pump was mounted on the side of the chamber to feed fresh medium into the tank. The flow rate was approximately 5mls/hr. Thus the dilution rate was about 0.0125hrs^{-1} (dilution rate=flow rate/volume, and should not exceed 0.03hrs^{-1} in order to avoid the sweeping of bacteria out of the tank [312]).

9.6 Dissolved oxygen concentration and pH measurement.

The dissolved oxygen content was measured using a YSI model 58 meter. As this used a membrane type probe a stirrer was required to be used with the probe. The stirrer was too large to fit inside the tank around the fatigue specimen, and so an auxillary tank was made for the stirrer and probe. The auxillary tank remained outside of the anaerobic chamber with the seawater constantly circulated between the two tanks by a peristaltic pump.

The pH of the environment was measured by a glass electrode in the tank around the fatigue specimen. The calibration of the electrode was checked before and after each test, but no significant drift was observed during any test. The pH meter used was a Beckman model 3500.

9.7 Testing procedure.

The fatigue testing was performed in the same manner as described in section 3.1. The temperature was maintained at about 7°C, in the middle of the desired range of 5-10°C. However, the testing procedure

differed for the "live" tests in that once the test was set up on the machine it was left under a constant load whilst the bacterial community developed, rather than load cycling beginning immediately. A period of just over a week was usually required for the bacteria to become active. The end of this incubation time was marked by a blackening of the solution due to the reaction of bacterially produced sulphide with dissolved iron to form iron sulphide. After the solution had turned black the cycling was begun, and the crack length monitored as before.

9.8 Miscellaneous.

Because of the toxicity of hydrogen sulphide an alarm system had to be installed in the testing laboratory before "live" testing could be commenced.

As part of the research programme testing was performed in ASTM artificial seawater, and in the "live" environment, using two different types of random load signal. This was in addition to the constant amplitude testing. The author was responsible for providing the environmental conditions for these tests, as well as monitoring them. The results of the random fatigue tests are not included in this thesis as their analysis and interpretation were the work of others [318,319].

The environment/growth medium used consisted of :

1 litre ASTM artificial seawater

plus :

0.1g	Ascorbic acid
0.004g	$FeSO_4.7H_2O$
0.5g	KH_2PO_4
1.0g	NH_4Cl
14g	Sodium lactate
0.4g	Thioglycollic acid
1.0g	Yeast extract

Table 9.1

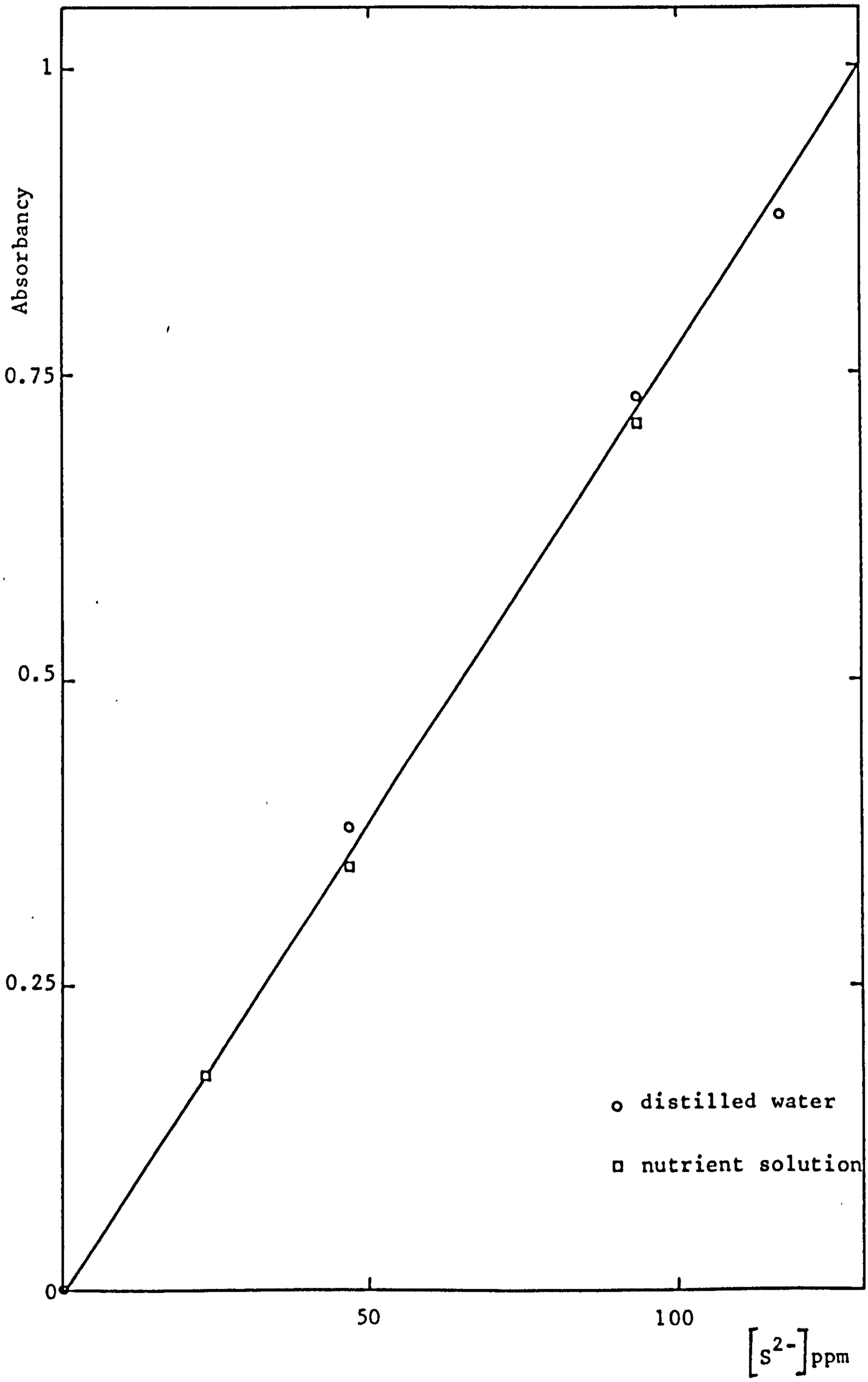
Absorbancy
1
0.75
0.5
0.25
0
50
100
[S2-]ppm
o distilled water
□ nutrient solution

Figure 9.1

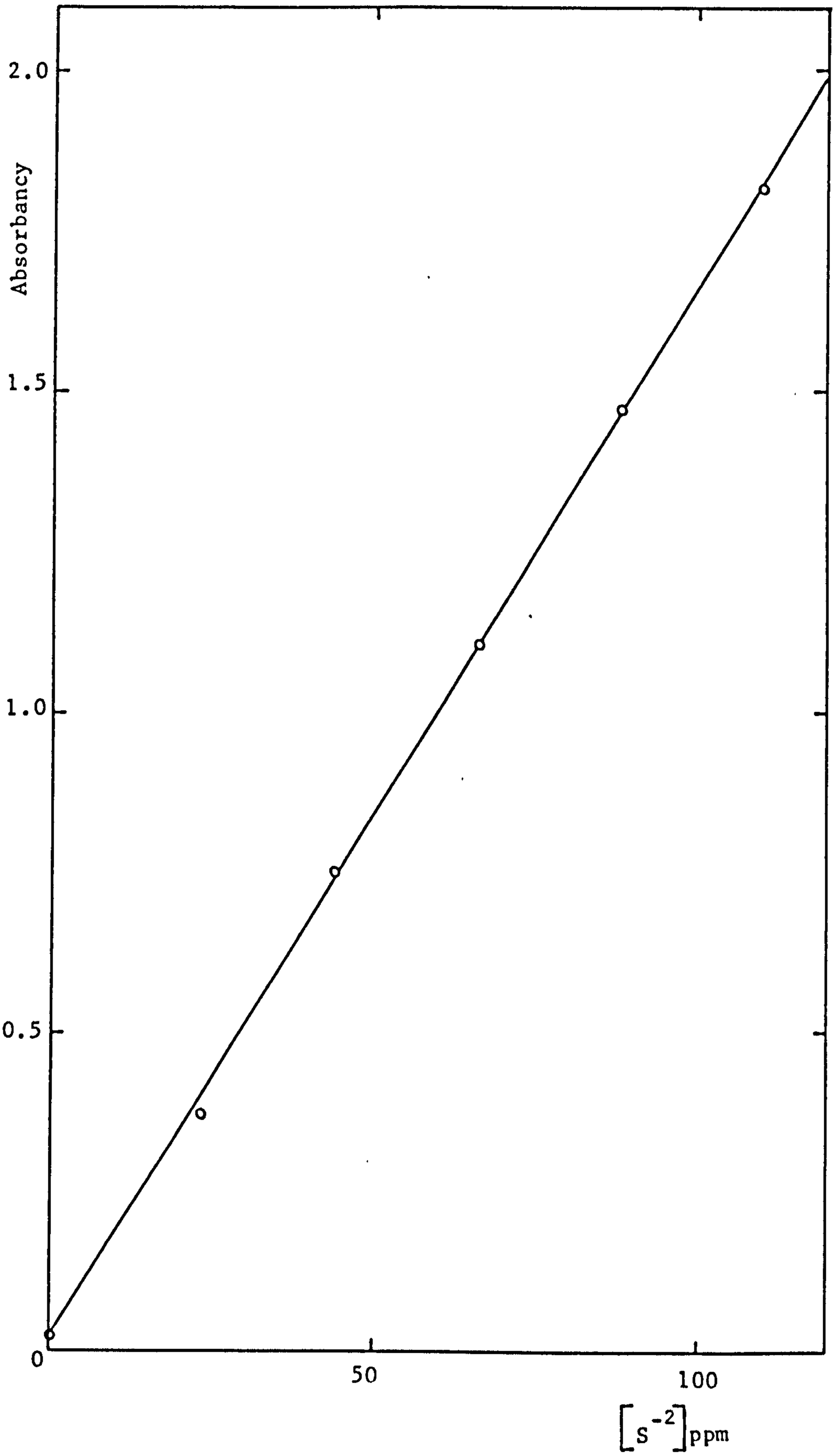

Figure 9.2

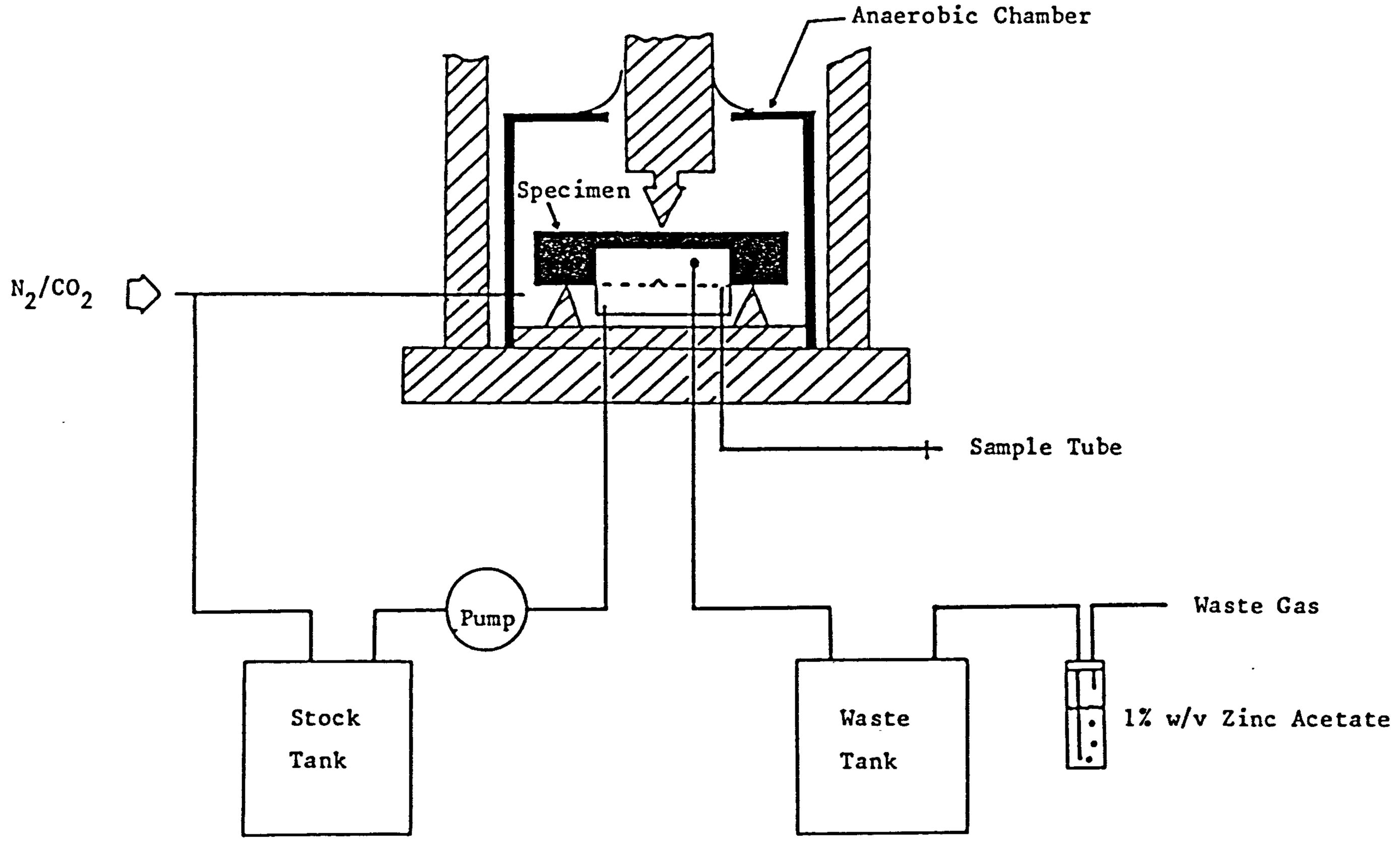

Figure 9.3 Experimental arrangement

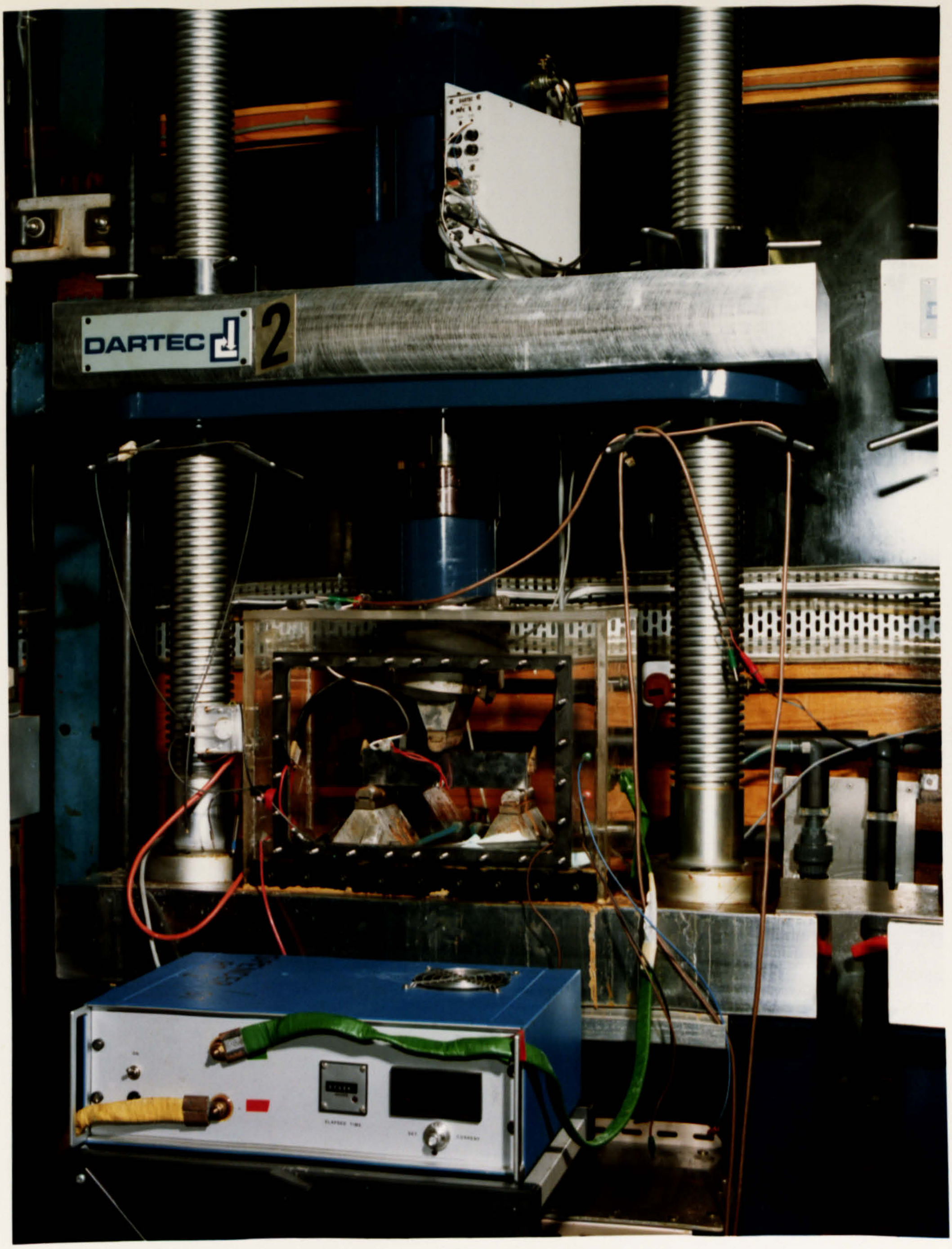

Figure 9.4 Photograph of fatigue testing machine showing anaerobic chamber in position

10.0 Results and discussion.

10.1 Calibrations.

As part of the research contract, of which this work formed part, it was specified that several calibration results were necessary [219]. This was to enable the present results to be compared with those of other workers, particularly the results obtained in the UKOSRP I programme. It was also necessary to segregate the effects of microbial growth from those of the ASTM artificial seawater plus nutrients without bacteria present.

10.1.1 Free corrosion.

In figure 10.1 the results obtained in ASTM artificial seawater at 13/14°C, and under free corrosion conditions, are compared with the results presented in Part I of this thesis (3% NaCl at approximately 23°C). The results are very similar for both regions I and II, bearing in mind the slight temperature difference. Results obtained in ASTM artificial seawater (free corrosion, 0.167Hz and 5/6°C) are compared with those obtained during the UKOSRP I project (ie. for real seawater, 5-10°C, and 0.1Hz [139]) in figure 10.2. Although no region I or II can be discerned from the UKOSRP I results figure 10.2 does show that the results obtained during this study are broadly in agreement with those from UKOSRP I.

Figure 10.3 compares all of the data obtained at free corrosion using ASTM artificial seawater. It is seen that the region I crack growth rate is unaffected by changes in temperature between 5°C and 14°C, and that a similar change in temperature causes the region II crack growth rates to differ by a factor of 1.3. These observations are in accord with the results discussed in section 5.2.7. The region I crack growth rate is also unaffected by lowering the dissolved oxygen level to approximately 5ppm. However, when the dissolved oxygen content is reduced to around 3ppm both the region I and region II crack growth rates are diminished : the region I crack growth rate was reduced by a factor of 1.7 compared to the results obtained with about 8ppm dissolved oxygen. The specimen potential was measured to be -0.68 to -0.70V(sce) for the test conducted with ≈3ppm dissolved

oxygen. Thus the different dissolved oxygen concentrations used did not materially affect the specimen potential. This would not necessarily be true for lower levels of dissolved oxygen [142]. For the test conducted with approximately 8ppm dissolved oxygen (naturally aerated) the dissolved oxygen content was measured as being in the range 7.7→8.4ppm, and the pH of the artificial seawater was within the range 7.5→8.2.

10.1.2 Cathodically protected to -0.85V(sce).

Figure 10.4 shows the results from this study for sinusoidal loading at 0.167Hz in ASTM articifical seawater at 6°C, R=0.5 cathodically protected to -0.85V(sce). The data from a previous investigation [139] (seawater, 5→10°C, R=0.5, 0.1Hz) is also shown. The seawater in the previous investigation was taken from the English Channel and stored on site. The two data sets are broadly similar, with the enhanced crack growth rates and plateau regions virtually coincident, although for region III crack growth the results of the previous study lie above the upper bound air data line. The results from this work show a region III crack growth regime that is coincident with the air upper bound line, in agreement with the results presented in Part I of this thesis. Both sets of data showed a plateau region, with $da/dN \approx 1.6 \times 10^{-4}$ mm/cycle. Because of the slightly different frequencies employed in these studies a small difference in the plateau crack growth rate was expected (compare chapter 6). It should be noted that the previous study [139] had reported a variation in the plateau crack growth rate with R ratio, a result that is in contradition with the results obtained in Part I of this thesis (cf. section 5.2.4).

The effect of dissolved oxygen content upon crack growth rates at an applied potential of -0.85V (sce) is shown in figure 10.5. The amount of dissolved oxygen was not measured during the "low oxygen" test, but was estimated to be about 3 to 4 ppm. It is seen that the plateau crack growth rate is reduced upon lowering the amount of dissolved oxygen. This could result from the reduction of any crack growth caused by a dissolution mechanism as the level of dissolved oxygen is lowered. From sections 5.2.2 and 5.5 it is seen that at a potential of -0.85V(sce) the crack growth is predominently caused by a hydrogen embrittlement mechanism, although a small amount of crack

growth may occur as a result of the dissolution mechanism. In this context it is significant that the low oxygen results shown in figure 10.5 yield almost the same plateau crack growth rate as predicted by the phenemonological model of chapter 6, figure 10.6 illustrates this. The plateau crack growth rates were 1.6×10^{-4} mm/cycle for the naturally aerated specimen (≈8ppm dissolved oxygen), and 1.15×10^{-4} mm/cycle for the low oxygen test.

Because of the alteration of the composition of the ASTM artificial seawater used for the "live" testing, a calibration test was performed in the nutrient solution with no active SRB (the test was naturally aerated, ie. ≈8ppm O_2, and conducted at 6°C). Care had to be taken during this test to ensure that no algae or other organisms grew in the solution during the duration of the test, in particular the stock solution and the test specimen were kept in the dark, and the stock solution was regularly changed. The results of all three calibrations performed at -0.85V(sce) are shown in figure 10.7. The "dead" nutrient solution gave a plateau crack growth rate of 3.2×10^{-4} mm/cycle, compared to 1.6×10^{-4} mm/cycle for similar conditions and ASTM artificial seawater. The twofold increase in the plateau crack growth rate caused by the nutrient additions to the ASTM seawater is probably a result of enhanced hydrogen entry as a consequence of the addition of thioglycollic and ascorbic acids to the solution. In Part I of this thesis it was observed that increased hydrogen entry caused the plateau crack growth rate to increase. Whereas the pH of ASTM artificial seawater remains between 7.5 and 8.2 during fatigue tests the pH of the nutrient solution is significantly lower, it was 5.71 at the beginning of the test and rose slowly to 6.11. (In figure 10.7 the gap in the results from the test conducted in the "dead" nutrient solution is due to a failure of the computerized data logging system, the actual fatiguing was not interrupted.)

10.2 Biologically active environments.

In addition to the fatigue tests performed in a biologically active environment some work was undertaken to provide an understanding of the biological environment. This work is discussed before the actual fatigue results are presented.

10.2.1 The biological environment.

Two 1 litre flasks of nutrient solution were purged of oxygen and innoculated with SRB in order to study the build up of sulphide with time. The results are shown in figures 10.8 and 10.9. A long incubation time was observed as the senescent cells reactivated themselves. This was followed by a rapid increase in the amount of sulphide in the liquid as the bacteria grew and multiplied. After this phase the amount of sulphide remained approximately constant, presumably because the bacteria had used up all of the available nutrient. Although the precise time was undertermined the flasks turned black sometime just after the rapid increase in sulphide concentration had begun. After the last sample was taken the final number of both SRB's and aerobic bacteria were determined. The build up of sulphide in these flasks followed a pattern typical of batch cultures of bacteria.

In some ways the solution around the fatigue specimens resembled a batch culture situation, in that an incubation period was required for the senescent cells to reactivate. After the incubation period was over the sulphide concentration increased rapidly, in a similar manner to in the batch culture flasks. During the time of rapid multiplication of bacteria within the tank around the fatigue specimen the nutrients initially present within the tank were used up. Thus the bacterial activity slowed down as it became governed by the provision of fresh nutrients, as mentioned in chapter 9 fresh nutrient was supplied at a rate of ≈5ml/hr. The build up of sulphide during the course of a test, as well as the increase in SRB population, is shown in figure 10.10. Again the tank was observed to turn black at the beginning of the steep increase in sulphide concentration, and the fatigue cycling occurred during this increase. The lag between the growth of the bacteria and the build up of sulphide concentration has been observed in other studies [320]. One point worthy of note is the relatively short duration of the fatigue experiments.

An attempt was made to correlate the numbers of SRB present with the sulphide concentration. The results for various batch culture situations are given in table 10.1 and shown in figure 10.11. At best only a general trend exists for higher numbers of SRB resulting in a greater concentration of sulphide. No correlation existed for the solutions from actual fatigue tests, as seen in figure 10.12. A high count of SRB population was often accompanied by a high count of

aerobic bacteria, as shown in figure 10.13. However, the inverse of this was not true as low SRB counts were sometimes accompanied by high aerobic counts. These results reflect the fact that growth of the SRB only occurred because the aerobic bacteria scavanged the oxygen within the test chamber. The lowest dissolved oxygen content obtained within the chamber by use solely of the inert overgas was ≈3ppm, which is too high for the growth of SRB [275]. Thus the aerobic bacteria present mirrored the postulated action of the fouling layer present on offshore structures, in that they created suitably anaerobic conditions for the growth of the SRB.

For the batch cultures the level of sulphide concentration attained was about 300 to 450ppm (compare table 10.1). Some bottles of nutrient solution taken out of the fatigue testing chamber and stored at room temperature for several months contained much higher levels of sulphide, namely 537, 691 and 1018ppm. These figures compare favourably with the limited amount of comparable data. For pure cultures of SRB grown in a lactate media concentrations of sulphide greater than 2000ppm have been observed [290]. Batch cultures of SRB grown on decomposing algae have been found to yield 500 to 900ppm, depending on the solution temperature [308]. Similar studies by other workers had previously been reported as showing sulphide concentrations of the order of 50 to 150ppm [300]. Wilkinson [320] has reported that for stagnant seawater the maximum sulphide concentration offshore is ≈5ppm, but for seawater contaminated with oil concentrations of sulphide between 50 and 100ppm have been found offshore.

The sulphide concentrations measured during the fatigue testing were much lower, with a maximum value being attained of between 131 and 137ppm. The reproducibility of the maximum amount of sulphide present is significant with respect to the use of a mixed culture for these experiments. The lower concentration of sulphide attained during the fatigue tests as opposed to the batch cultures is a result of the removal of sulphide from the environmental chamber during the test. The sulphide was removed both by the overgas passing through the chamber and by the excess solution that passed out of the testing tank.

10.2.2 Fatigue testing.

Figure 10.14 shows the results from four different fatigue tests. It is seen that the different amounts of sulphide present did not greatly affect the crack growth rate. This is because the tests were all performed just after the solution had turned black, during the period when the amount of sulphide present in the liquid increased rapidly (figure 10.10). Thus the tests were all performed in a situation in which the sulphide layer on the specimen surface would depolarize the specimen, leading to increased hydrogen entry into the metal. (For one of the random fatigue tests performed in the biologically active environment the cycling begun about 1 week after the solution had turned black, and as the rapid build up in sulphide had finished by then very little enhancement of the crack growth rate, compared to the dead nutrient solution, was seen.) The maximum crack growth rates observed were between $1x10^{-3}$ mm/cycle and $1.4x10^{-3}$ mm/cycle, and this represents a crack growth rate approximately 10 times that in ASTM artificial seawater and 5 times that in the dead nutrient solution. A consequence of this extremely rapid crack growth was that after the crack growth incubation period was over (compare section 4.5) the specimen broke within a day, compared to 1.5 to 2 weeks for in 3% NaCl solution. Although the initial pH of the nutrient solution was about 5.8 it gradually increased during the incubation time of the bacteria (cf. figure 10.10). The pH was usually about 6.1 to 6.2 when the cycling was begun.

For comparison a test was performed in ASTM artificial seawater with some added inorganic sulphide. The result is shown in figure 10.15. The crack growth rate is much lower than for the biologically active solution, with a plateau crack growth rate of $4.6x10^{-4}$ mm/cycle being found. The lower crack growth rate is because a continuing depolarizing effect of the sulphide layer on the metal surface only occurs with actively growing SRB present [282]. This viewpoint is reinforced by the results shown in figure 10.16. The maximum crack growth rate, caused by the biologically active solution, shown in figure 10.16 is $4.5x10^{-4}$ mm/cycle. This is a lot less than those shown in figure 10.14, and is only 1.4 times the plateau crack growth rate obtained in the dead nutrient solution. The reason for the low crack growth rate seen in figure 10.16 for the biologically active solution is that the SRB population was determined as only 32 bacteria/ml, as opposed to 10^5 to 10^6 bacteria/ml for the tests shown

in figure 10.14. Thus only a limited amount of depolarization could occur because of the few bacteria present.

Another interesting feature of the results obtained in the biologically active solutions is that after the maximum crack growth rate is attained the crack growth rate decreases as ΔK increases, rather than remaining at a constant value as for the dead solutions. Figures 10.14 to 10.16 clearly illustrate the difference in the behaviour in the biologically active solutions and the dead solutions. In Part I of this thesis the plateau observed in the dead solutions was taken as indicating that the rate of entry of hydrogen into the metal was the rate limiting step in the crack propagation process. The rate of hydrogen entry into the metal at the crack tip was assumed to be unaffected by the crack depth. It is clear that for the biologically active solutions the rate of hydrogen entry is not sufficiently fast to maintain the extremely fast crack growth rate observed, and so the crack growth rate decreases as the crack length increases. It is not clear whether the maximum crack growth rate is due to prior hydrogen charging of the specimen during the incubation period of the bacteria, or whether it is caused by the instantaneous reactions of the bacteria and the iron sulphide film on the specimen. If it is the latter then the crack growth rate decreases as the crack length increases, as the crack tip moves sufficiently far enough away from the specimen surface for the sulphide layer there not to affect the entry of hydrogen into the metal at the crack tip. It is of note that in figure 10.16 the maximum crack growth rate reappears upon restarting the test after a machine failure. This phenomena has practical ramifications as mentioned later.

During one test no crack growth was observed at an initial value of ΔK of 6.4MPa$\sqrt{m}$. The crack growth rate was less than 5×10^{-7} mm/cycle, as opposed to 2.5×10^{-6} mm/cycle expected in air. Thus it is possible that some form of crack closure occurred, probably due to calcareous deposits plugging the crack. Other workers have had difficulties growing cracks in BS4360:50D immersed in ASTM seawater at -0.85V(sce) when $\Delta K<10$MPa$\sqrt{m}$ [219].

The only other work on fatigue in biologically active environments known to the author is that of Edyvean et. al. [308]. For RQ701 steel (presumably at free corrosion) the results from a solution with 150ppm of biologically produced sulphide lay above those obtained in natural seawater. The crack growth rate obtained with 150ppm of sulphide was approximately 2×10^{-4} mm/cycle at $\Delta K=20$MPa$\sqrt{m}$. For 500ppm of

biologically produced sulphide the results were very similar to those obtained in natural seawater saturated with H_2S, a crack growth rate of approximately $1x10^{-3}$ mm/cycle was observed at $\Delta K=20MPa\sqrt{m}$. No indication is given as to the activity of the biological environment during the fatigue testing. Also no decrease in crack growth rate with increasing crack length was seen. Thus a much larger effect of biologically produced sulphide at a concentration of about 150ppm was observed in this study, although the form of the crack growth behaviour was noticeably different between these two studies.

On the basis of their result obtained with 500ppm of biologically produced sulphide Edyvean et. al. suggest that H_2S saturated seawater might be an adequate representation of the effects of the biological environment found offshore. Figure 10.17, which compares the results obtained in this study in the biologically active environment with results obtained in H_2S saturated seawater [164,250,308], suggests that this is true for $\Delta K<12MPa\sqrt{m}$. At higher values of ΔK the H_2S saturated seawater results significantly exceed those obtained in the biologically active solution. Also the lack of crack growth observed at a ΔK of $6.4MPa\sqrt{m}$, mentioned earlier, would suggest that even at values of $\Delta K<10MPa\sqrt{m}$ H_2S saturated seawater may produce much faster crack growth rates compared to biologically active solutions.

It appears that the crack growth rates found in H_2S saturated seawater do not occur in practice for jacket structures in the North Sea. Thus any effect of SRB on crack growth rates in real structures is less than that observed in this study for laboratory conditions. There are several possible reasons for this :

(i) there may be only a very small probability of SRB growth being found at a critical site where a pre-existing crack is located.

(ii) the numbers of SRB found on the surface of the structure may be a lot less than the number of bacteria on the surface of the laboratory specimen. As noted earlier a much smaller effect of SRB was observed in this study when their concentration was vastly reduced. Whereas the conditions in the laboratory tests were made favourable for the growth of SRB, the environment around an offshore structure is unlikely to be so favourable. Consequently lower numbers of SRB would be expected for the real life situation.

(iii) the concentration of H_2S at the steel surface could be less for the real life situation compared to the laboratory tests. The cause of this may be an effective mixing of water at the metal surface with bulk seawater. If too much mixing occurs the growth of the SRB would be inhibited by dissolved oxygen.

(iv) the absence of any growth at a value of ΔK of 6.4MPa$\sqrt{m}$ in the laboratory suggests that crack closure, caused by the plugging of cracks with deposits, may be extremely beneficial for real structures.

The reproducibility of the crack growth rates shown in figure 10.14 vindicates our experimental method, and in particular the use of a mixed culture (compare section 9.1). Because the nutrients used favour the growth of some bacteria over that of others a useful piece of future work would be to utilize a different nutrient solution, so altering the microbial community present during the fatigue testing.

10.3 Conclusions

The first objective of this study was met in that it was confirmed that SRB do affect the corrosion fatigue behaviour of steel. Crack growth rates were enhanced by up to an order of magnitude compared with a plain seawater environment. Thus further work is needed to develop a fuller understanding of how, and by how much, SRB affect fatigue crack growth rates.

It appears that H_2S saturated seawater may not provide an adequate simulation of biological activity for $\Delta K > 12$MPa$\sqrt{m}$. However for values of $\Delta K < 12$MPa$\sqrt{m}$ the results of this study suggest that H_2S saturated seawater may provide a satisfactory test environment.

At high values of ΔK the crack growth rate decreased as ΔK increased, but an interruption to the load cycling led to the crack growth rate being restored to its peak value upon the resumption of cycling. This has important ramifications for real structures, which experience calm periods between storms. Such effects require further study.

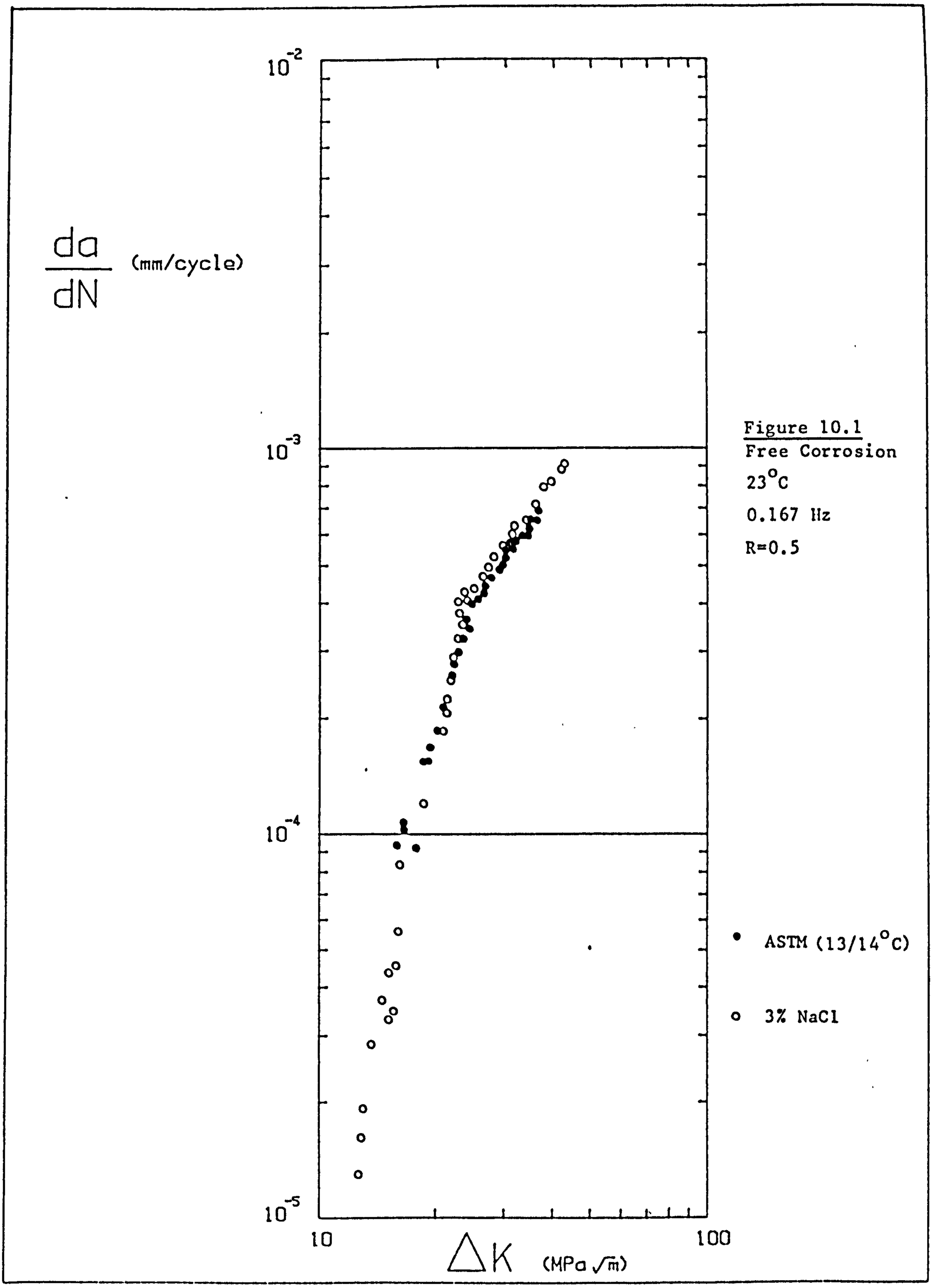

Figure 10.1
Free Corrosion
23°C
0.167 Hz
R=0.5

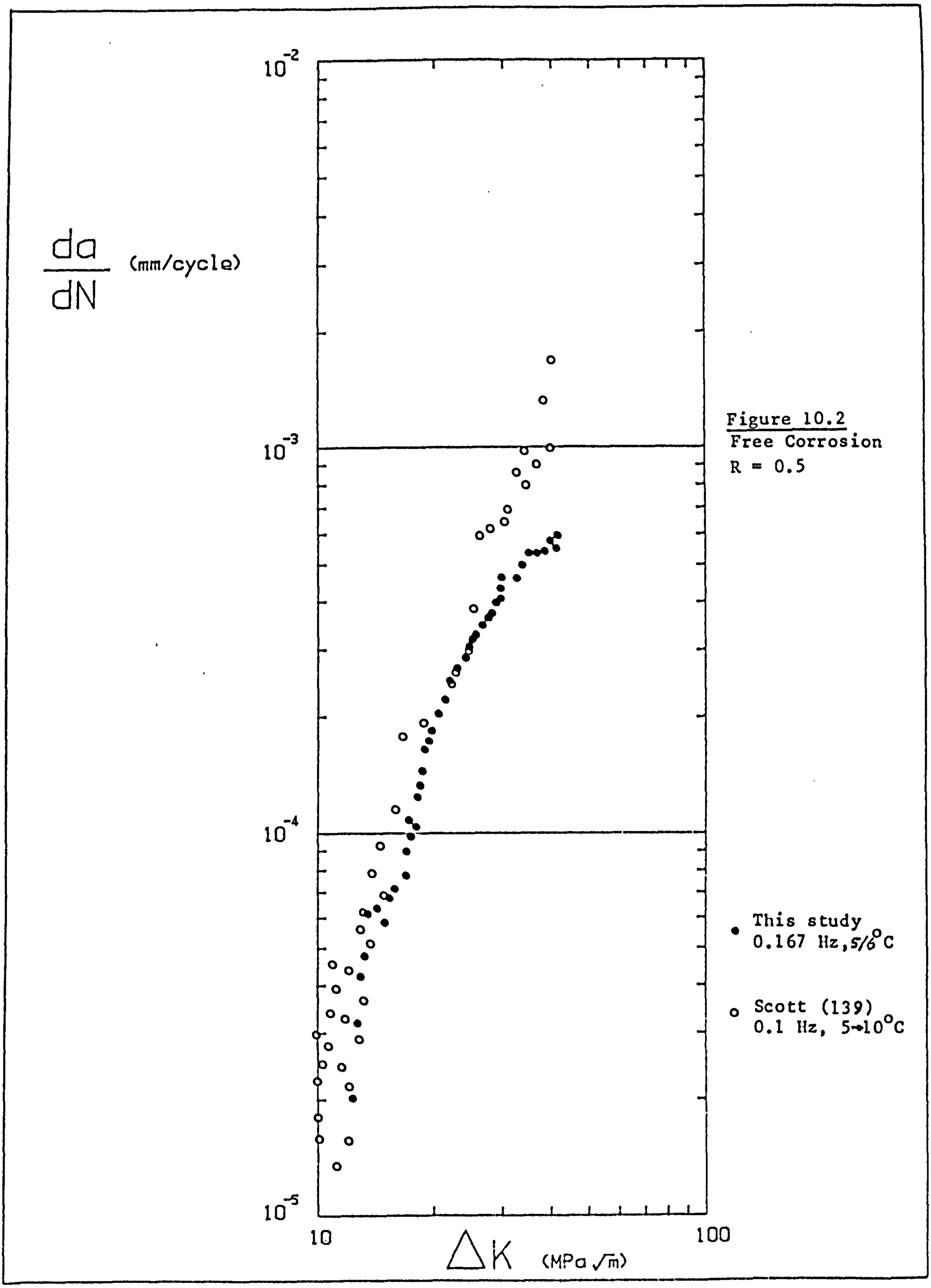

Figure 10.2
Free Corrosion
R = 0.5

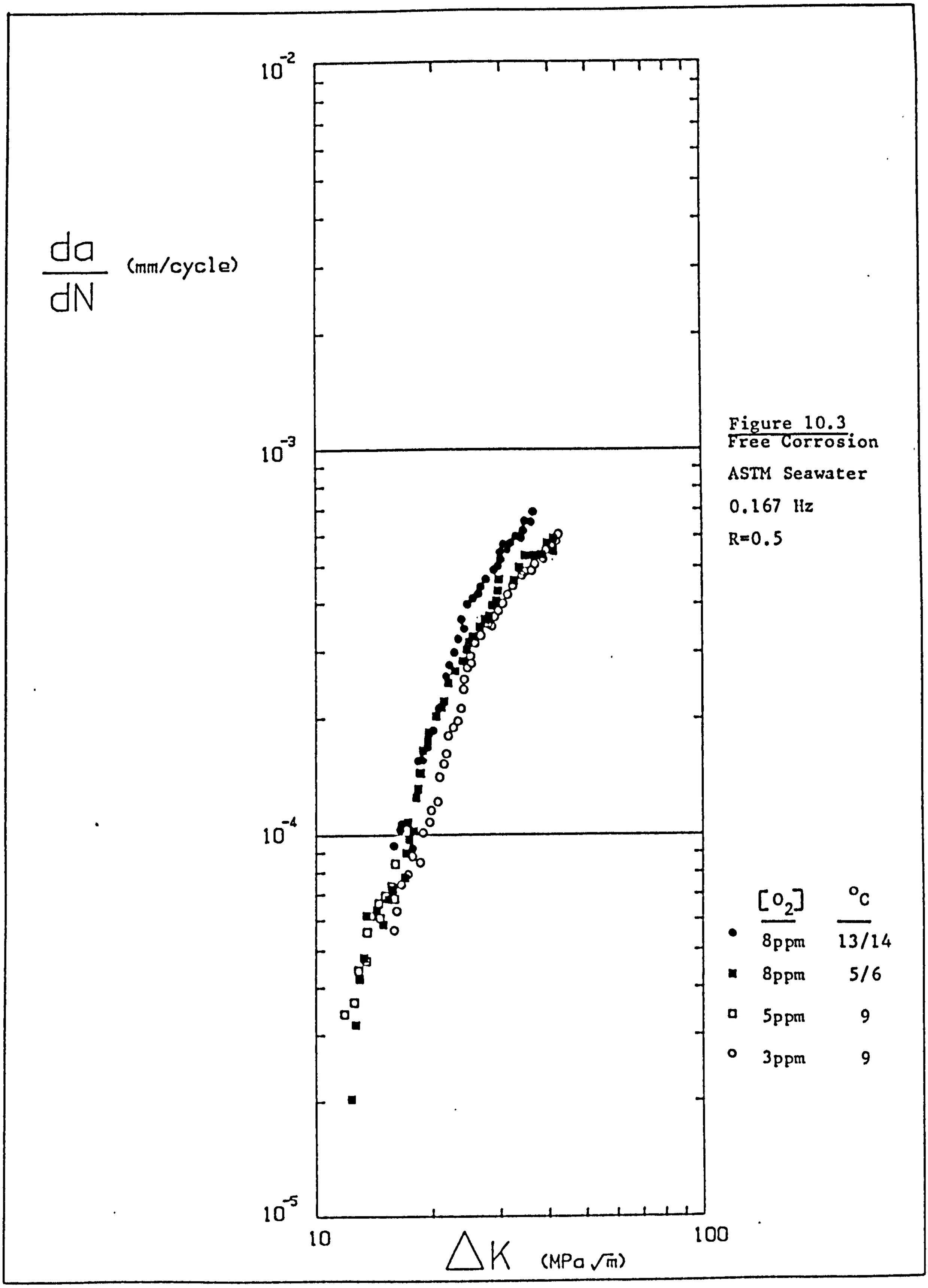

Figure 10.3
Free Corrosion
ASTM Seawater
0.167 Hz
R=0.5

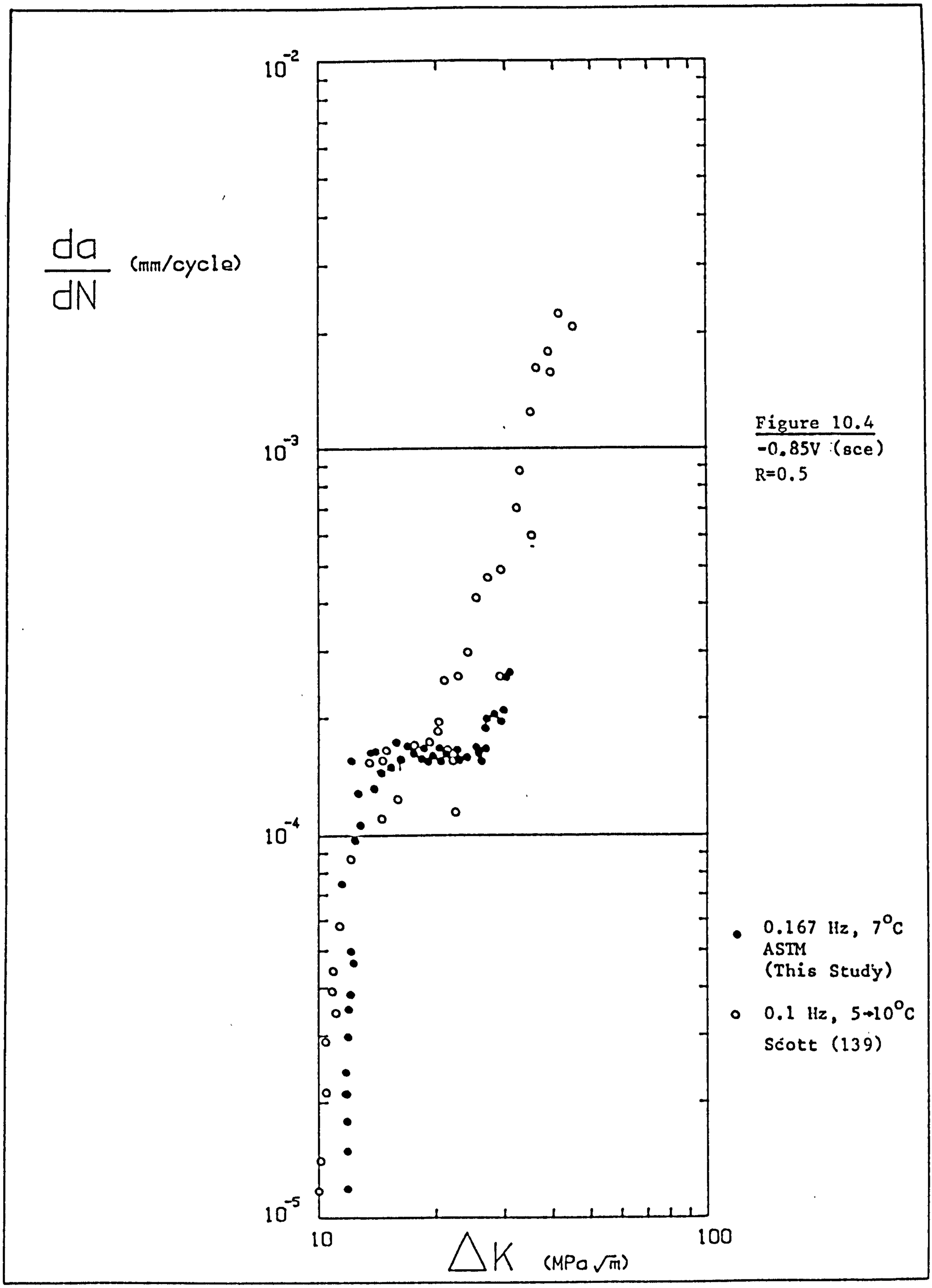
$\frac{da}{dN}$ (mm/cycle)
10^{-2}
10^{-3}
10^{-4}
10^{-5}
10
100
ΔK (MPa $\sqrt{m}$)
-0.85V (sce)
R=0.5
• 0.167 Hz, 7°C ASTM (This Study)
o 0.1 Hz, 5→10°C Scott (139)

Figure 10.4

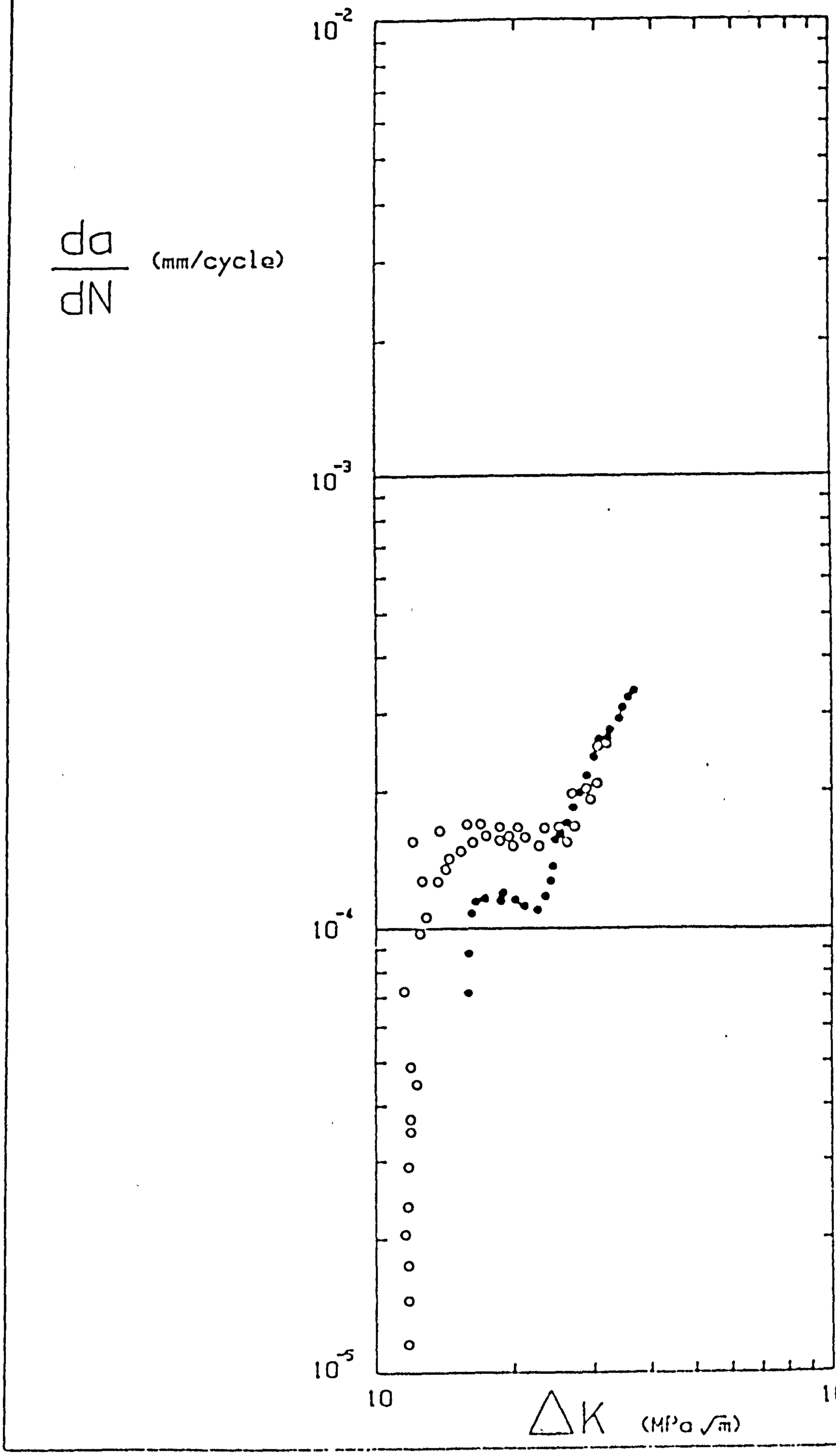

Figure 10.5
-0.85V (sce)
ASTM Seawater
0.167 Hz
R=0.5

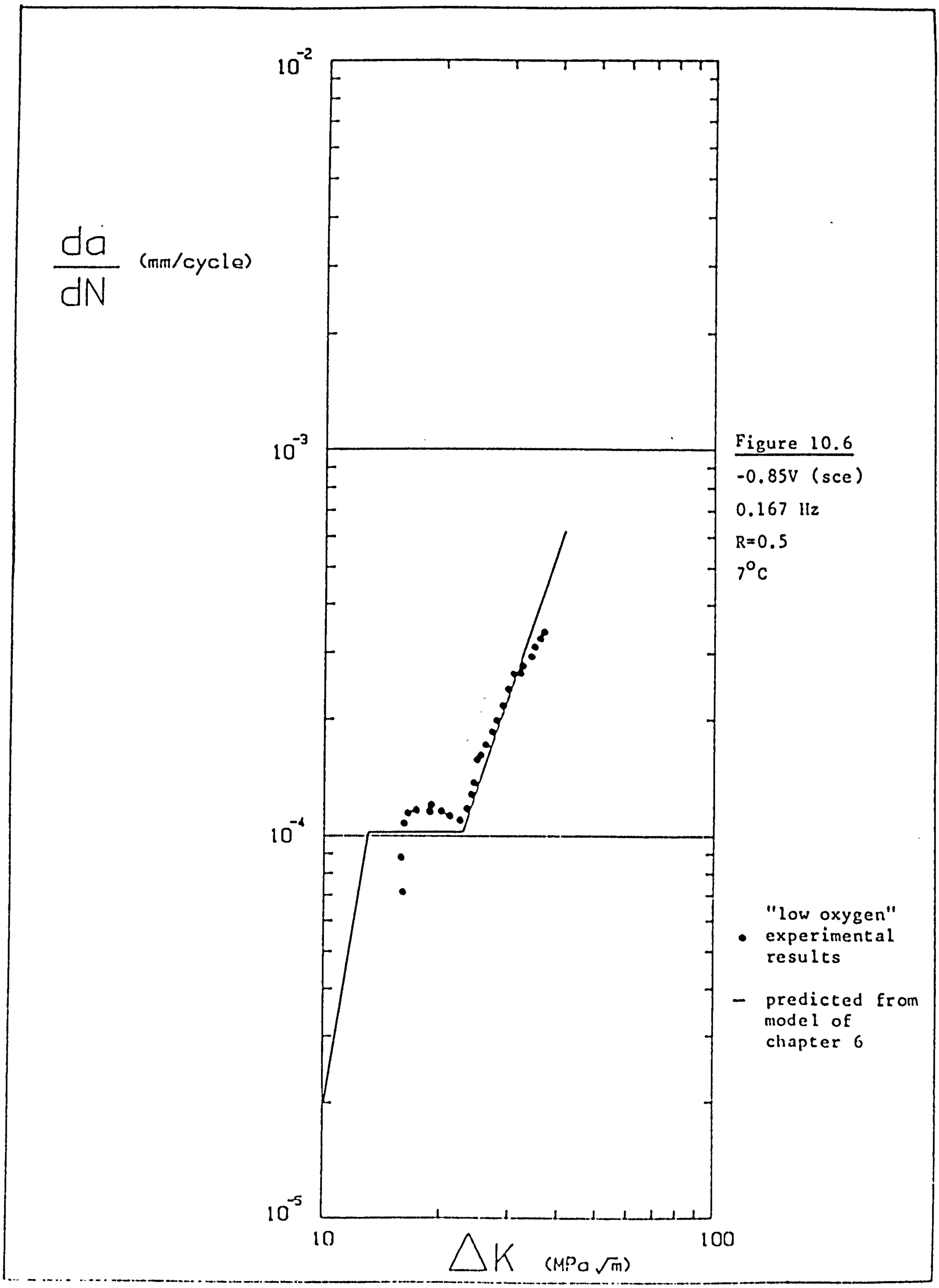
10^{-2}
10^{-3}
10^{-4}
10^{-5}
$\frac{da}{dN}$ (mm/cycle)
10
100
ΔK (MPa $\sqrt{m}$)
-0.85V (sce)
0.167 Hz
R=0.5
7°C
"low oxygen"
• experimental results
— predicted from model of chapter 6

Figure 10.6

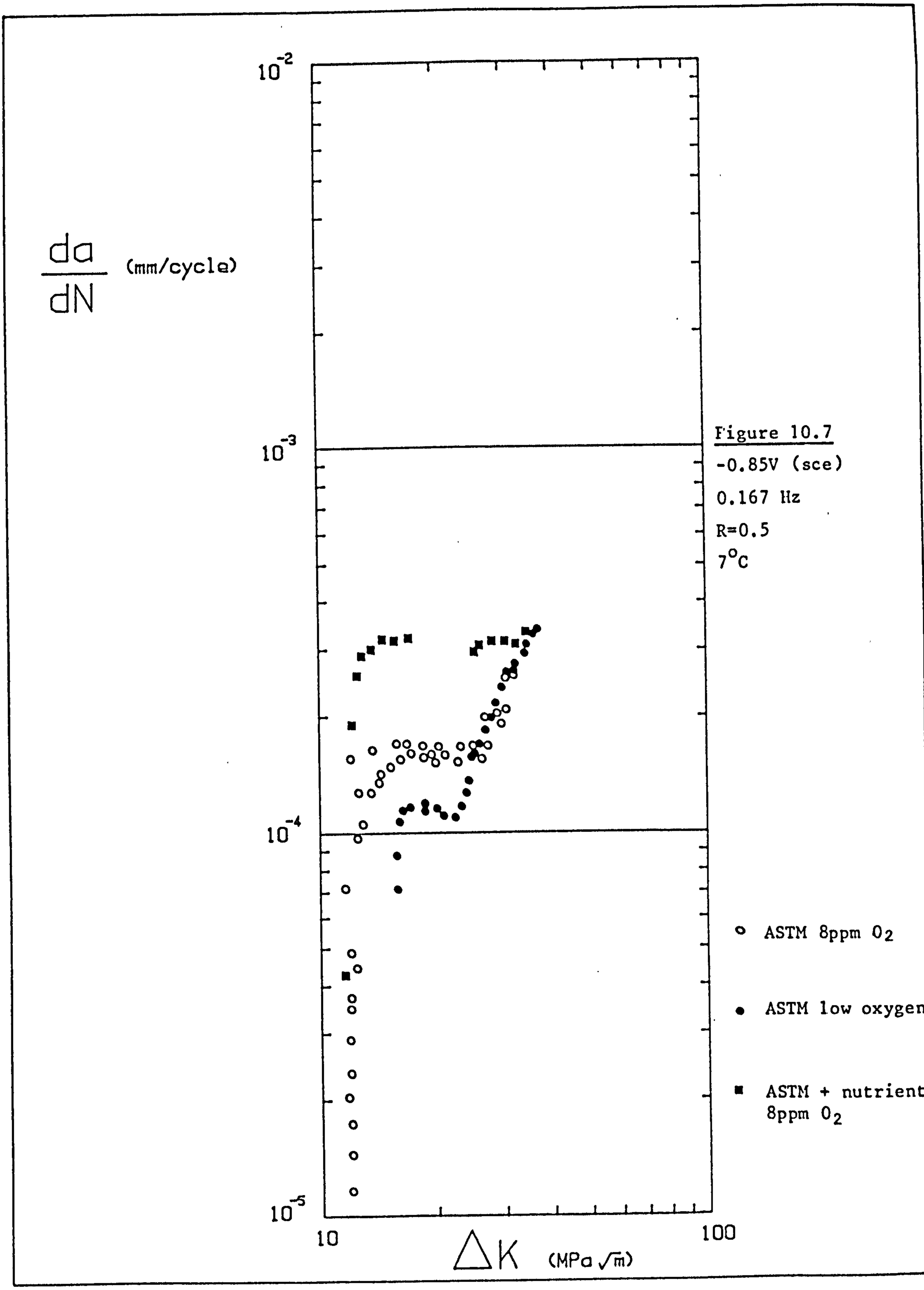
10^{-2}
10^{-3}
10^{-4}
10^{-5}
$\frac{da}{dN}$ (mm/cycle)
10
100
ΔK (MPa $\sqrt{m}$)
-0.85V (sce)
0.167 Hz
R=0.5
7°C
ASTM 8ppm O_2
ASTM low oxygen
ASTM + nutrient 8ppm O_2

Figure 10.7

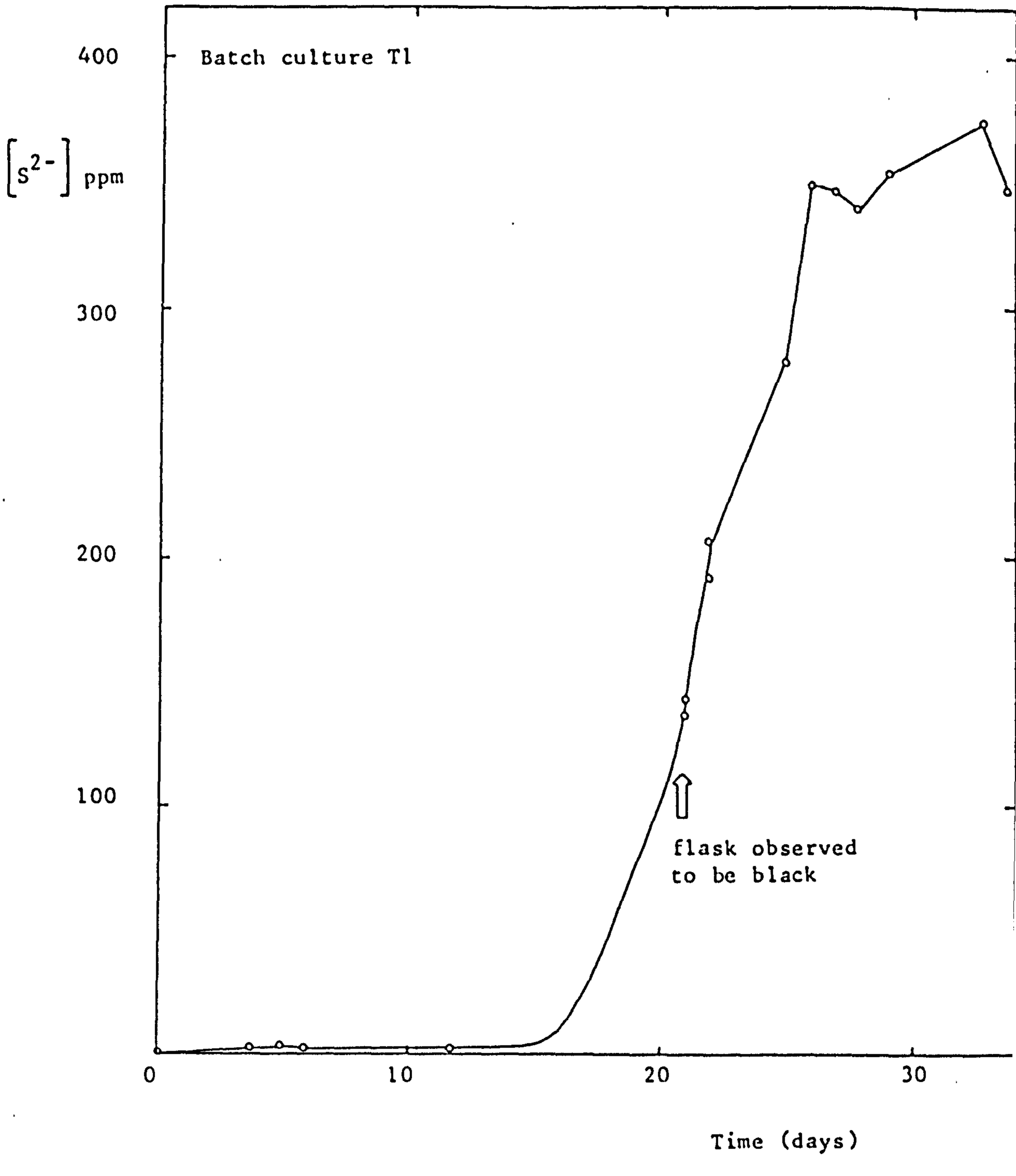
Batch culture T1
400
300
200
100
$[S^{2-}]$ ppm
0
10
20
30
Time (days)
flask observed
to be black

Figure 10.8

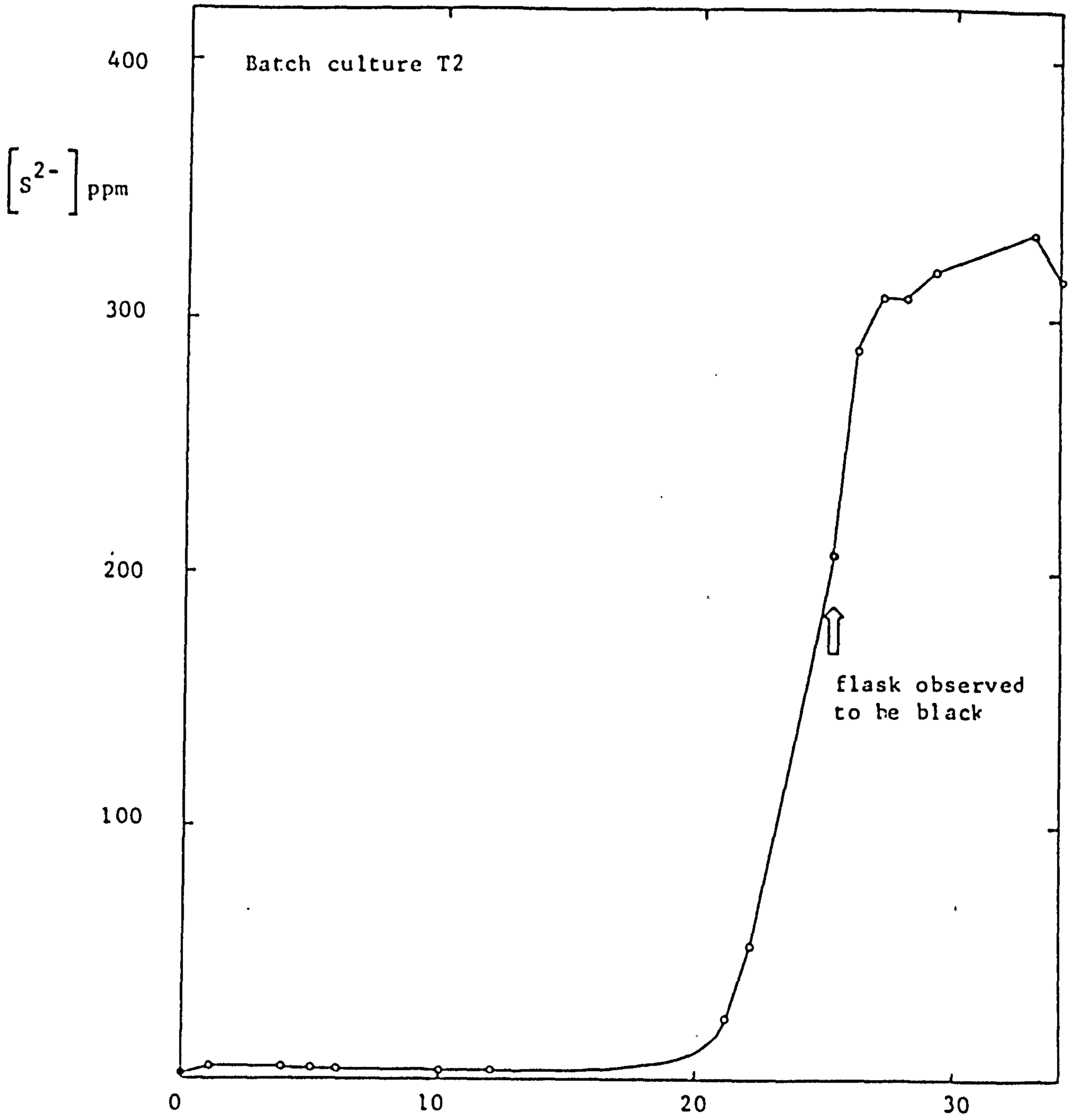
Batch culture T2
400
300
200
100
0
10
20
30
$[S^{2-}]$ ppm
flask observed
to be black
Time (days)

Figure 10.9

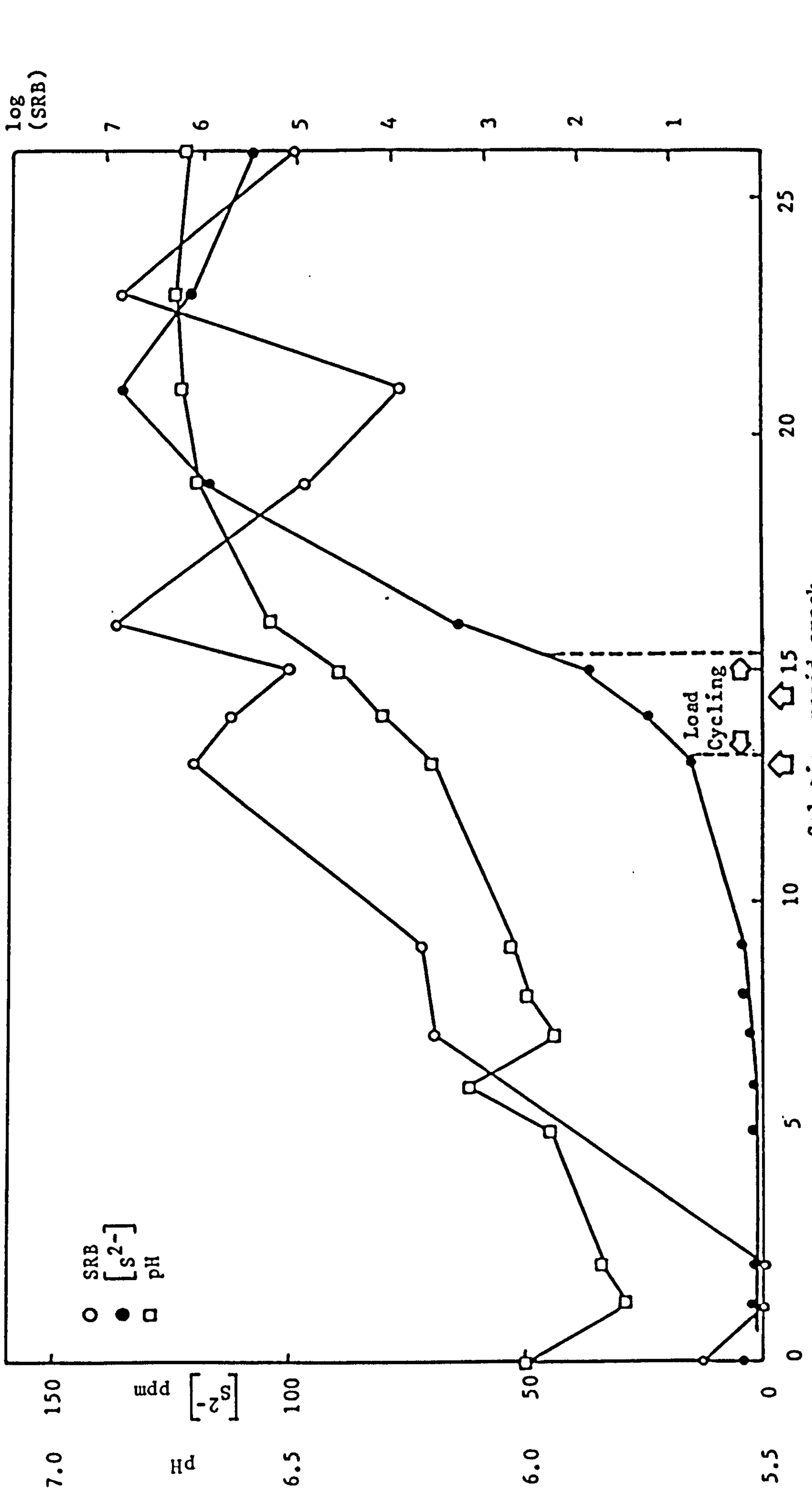
log (SRB)
7
6
5
4
3
2
1
Time (days)
25
20
15
10
5
0
Load Cycling
Solution rapid crack
Black growth begun
SRB [S2-]
pH
150
100
50
0
ppm [S2-]
7.0
6.5
6.0
5.5
pH

Figure 10.10

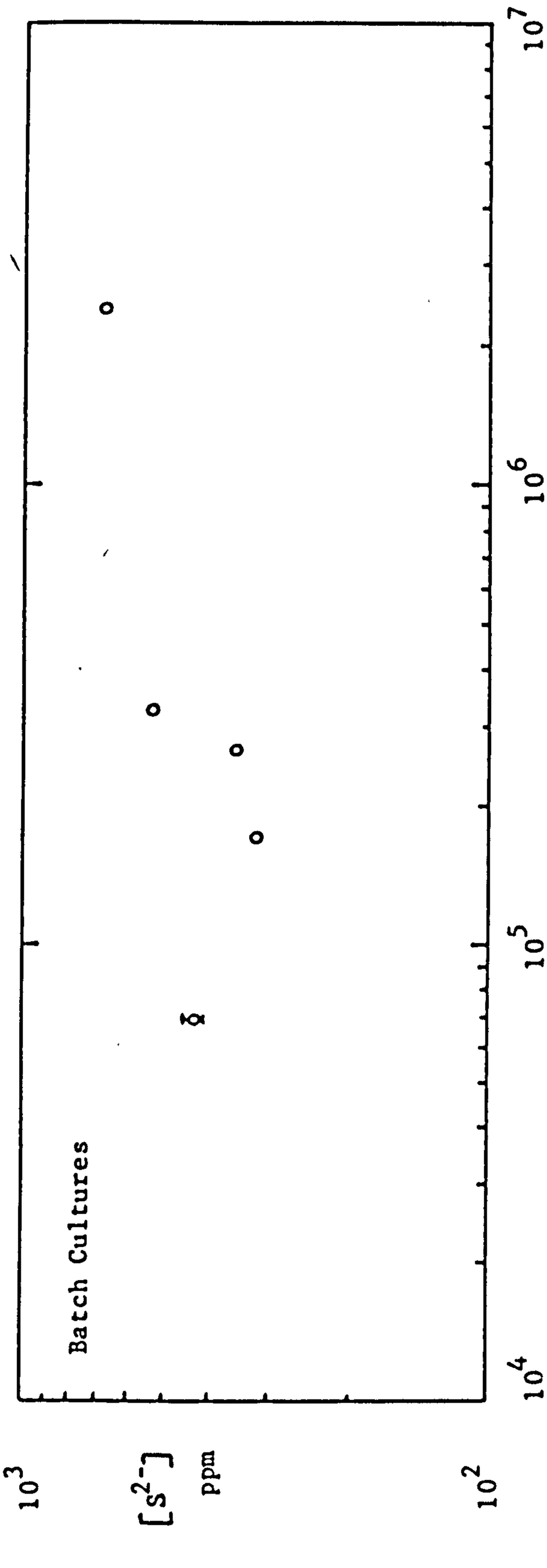

Figure 10.11

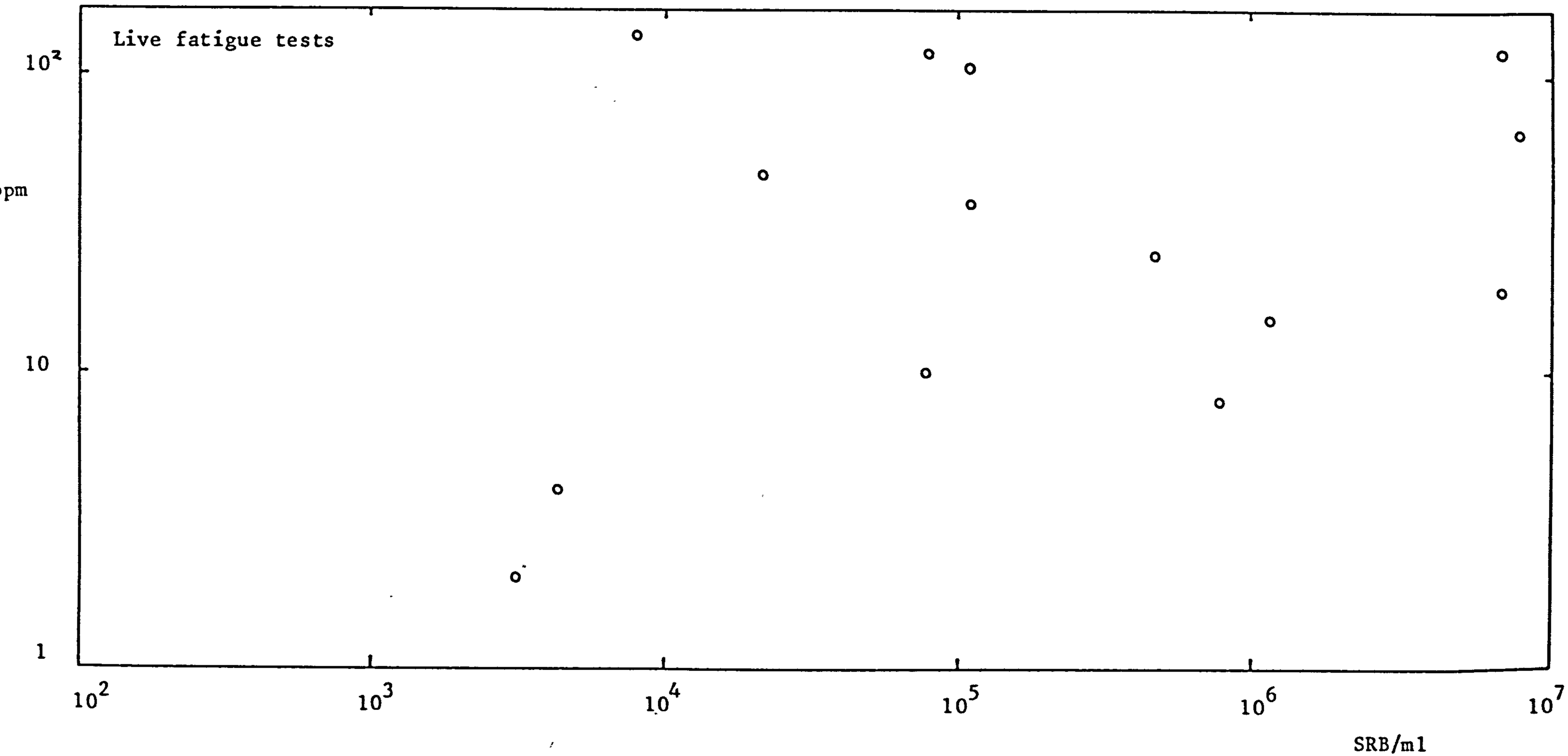
Live fatigue tests
10^2
10
1
$[S^{2-}]$ ppm
10^2
10^3
10^4
10^5
10^6
10^7
SRB/ml

Figure 10.12

Figure 10.13

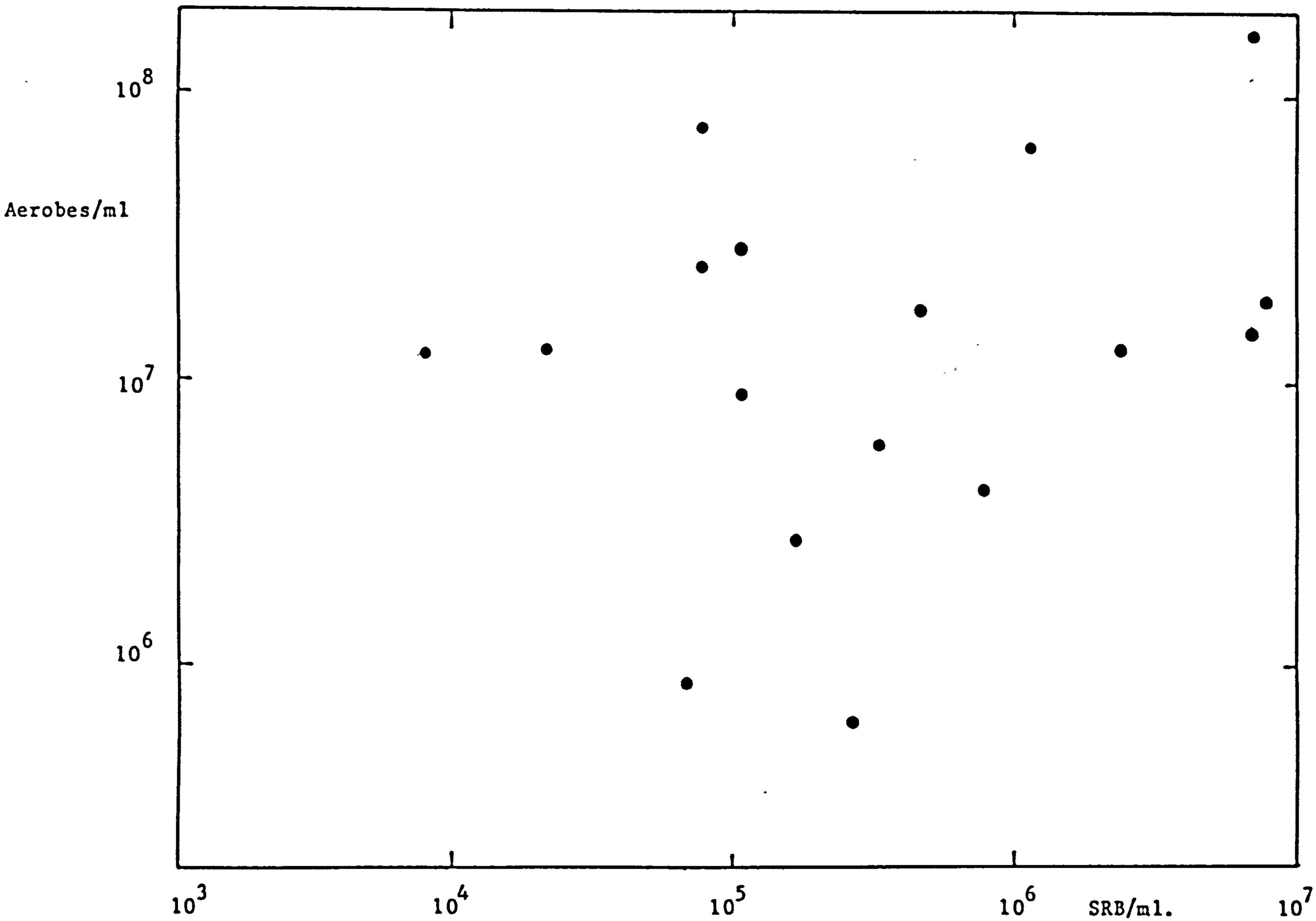

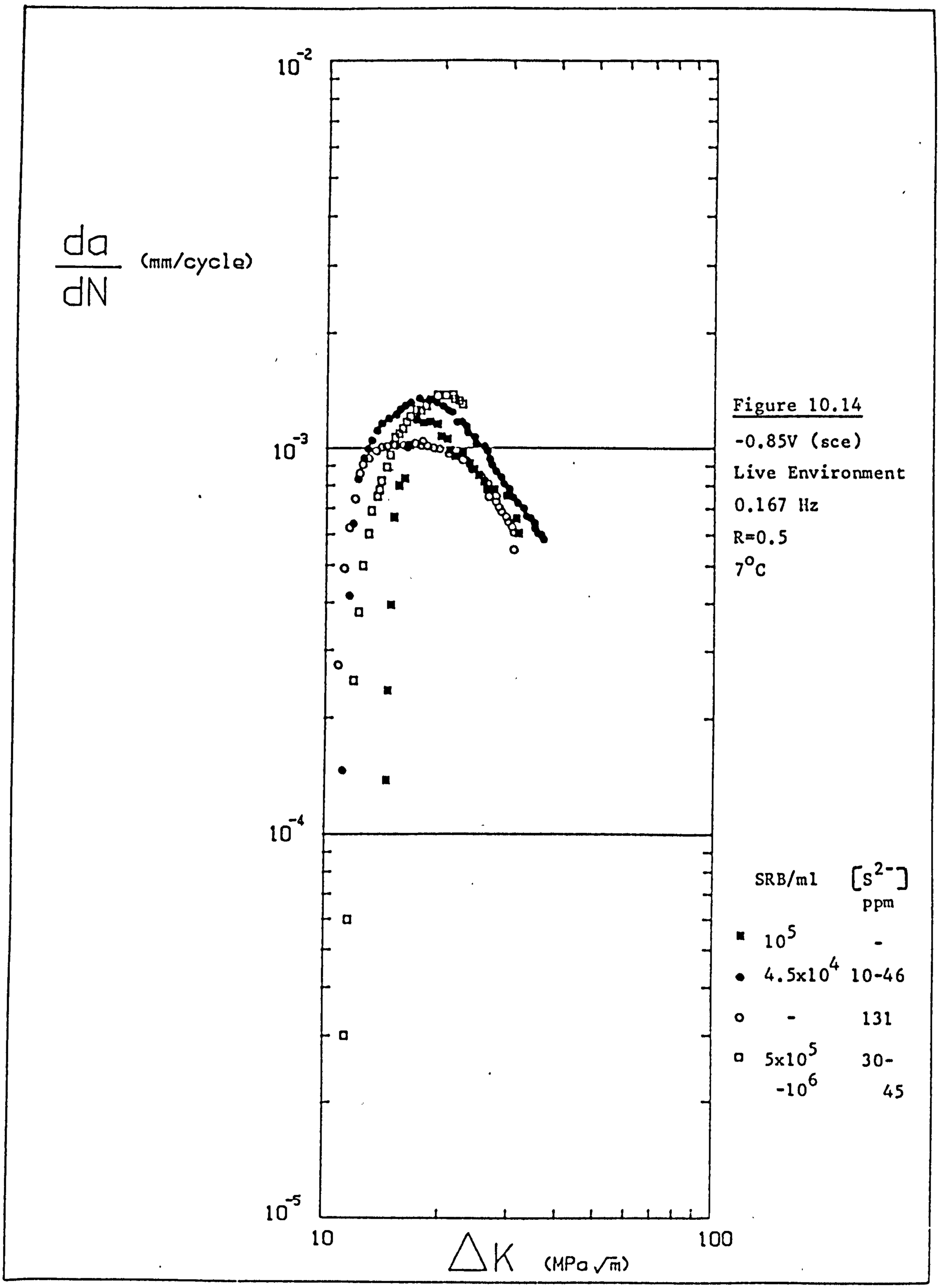
10^{-2}
10^{-3}
10^{-4}
10^{-5}
$\frac{da}{dN}$ (mm/cycle)
10
100
ΔK (MPa $\sqrt{m}$)
-0.85V (sce)
Live Environment
0.167 Hz
R=0.5
7°C
SRB/ml
$[S^{2-}]$ ppm
■ 10^5 -
● $4.5x10^4$ 10-46
○ - 131
□ $5x10^5$ - 10^6 30-45

Figure 10.14

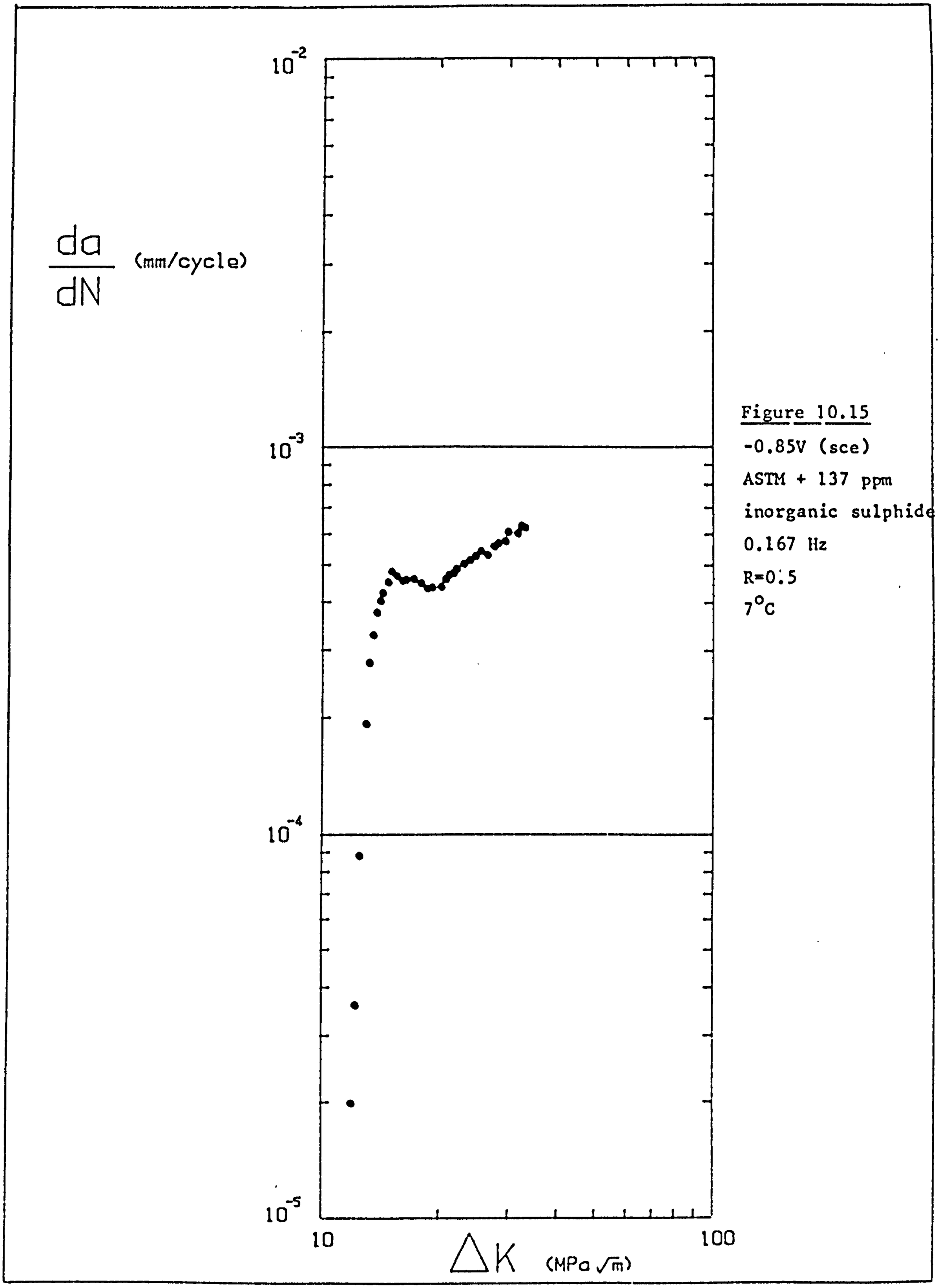

Figure 10.15

-0.85V (sce)

ASTM + 137 ppm

inorganic sulphide

0.167 Hz

R=0.5

7°C

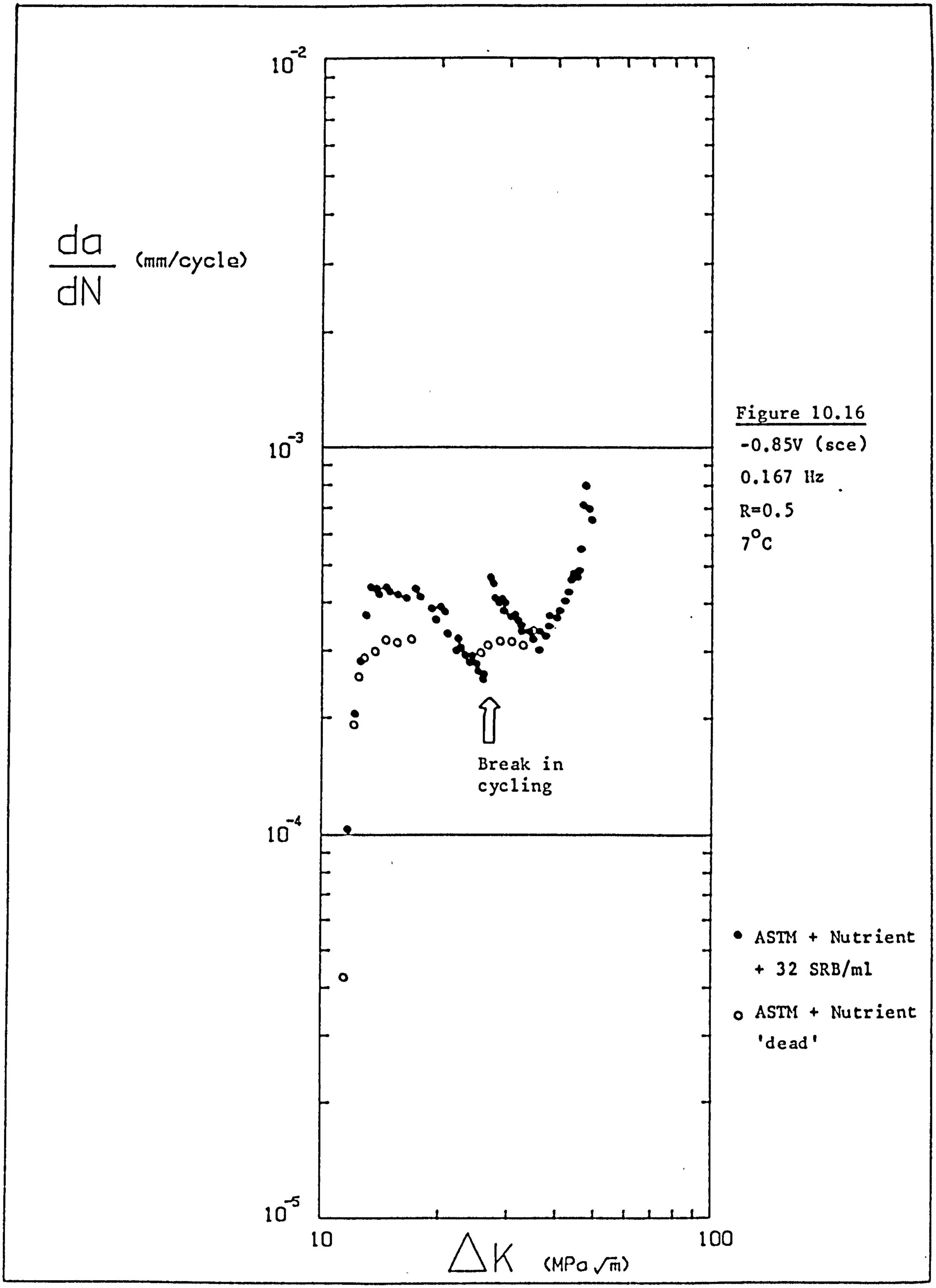
$\frac{da}{dN}$ (mm/cycle)
10^{-2}
10^{-3}
10^{-4}
10^{-5}
Break in cycling
-0.85V (sce)
0.167 Hz
R=0.5
7°C
• ASTM + Nutrient + 32 SRB/ml
o ASTM + Nutrient 'dead'
10
100
ΔK (MPa $\sqrt{m}$)

Figure 10.16

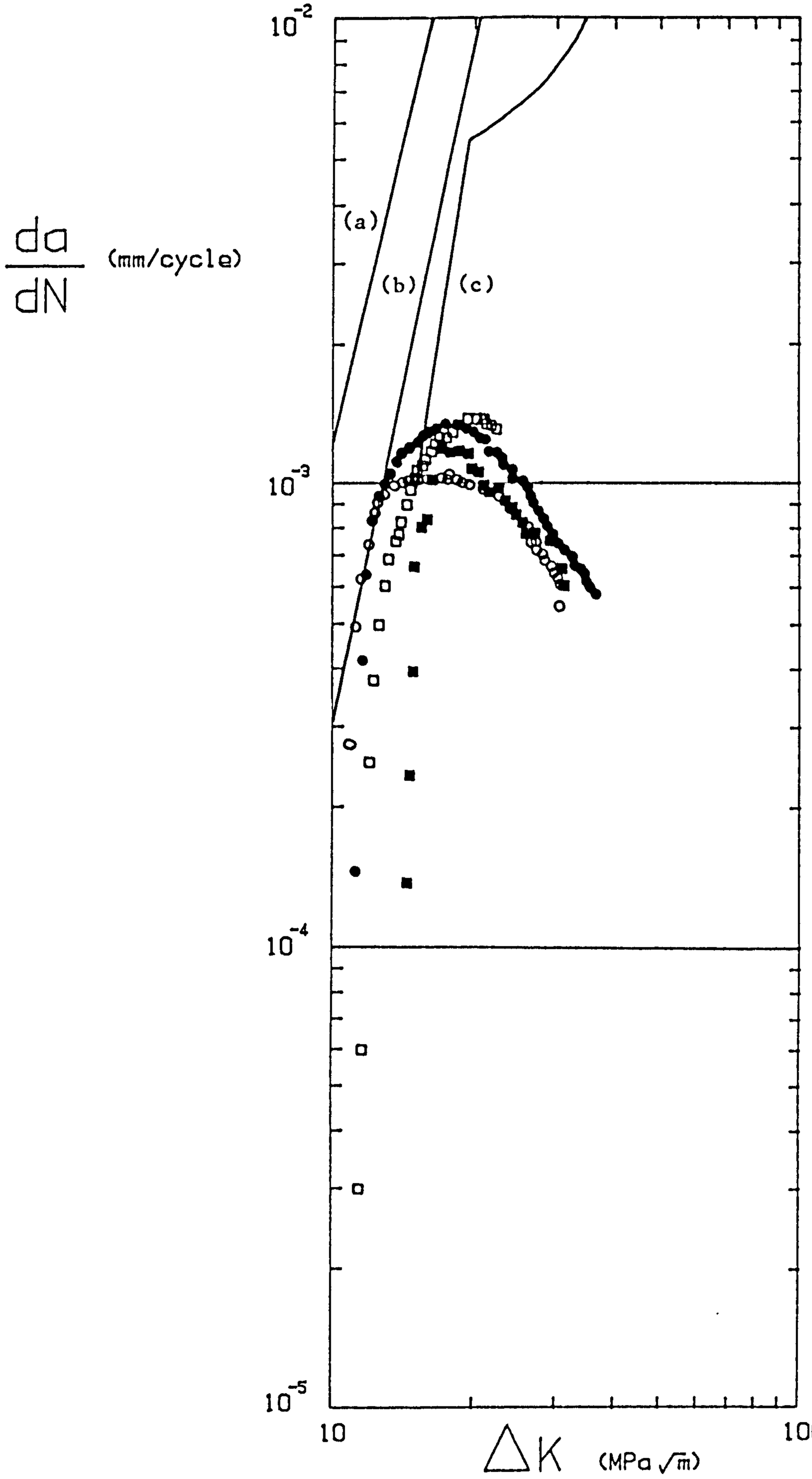

Figure 10.17

Comparison of results obtained in the live environment and H_2S saturated seawater.

H_2S sat. seawater

(a) 50D:-0.85V (Ag/AgCl)(308)

(b) DS52 : Free corrosion(250)

(c) 50D : -0.85V (Ag/AgCl)(164)

Live environment

■ ● ○ □ as in figure 10.14

Part III

Development of surface breaking cracks.

11.0 Stress intensity factors and crack development.

11.1 Introduction.

Parts I and II of this thesis described experimental studies of corrosion fatigue crack propagation. Before the results of such studies can be applied to real engineering situations using the principles of LEFM an adequate calibration for the stress intensity factor has to be obtained pertaining to the situation of interest. This chapter descibes the small amount of work that was done in the area of stress intensity factor calibrations.

11.2 Semi-elliptic cracks.

Surface breaking cracks are one of the most common types of crack found in engineering structures. Consequently it is important that accurate stress intensity calibrations are available for these defects. Many solutions have been published for the stress intensity factors relating to semi-elliptical surface breaking cracks in a tensile stress field [321-327]. There are substantial differences between some of these solutions, and so a basis has to be found for determining which solution is nearest to the exact answer. Newman [328] investigated this problem and ranked 14 different solutions according to how well they correlated with fracture data obtained from specimens made out of a brittle epoxy material. Scott and Thorpe [329,330] used the experimentally observed fact that these cracks grow such that they tend to a preferred shape as a basis for comparison of the solutions. A third method is that used by Aboutorabi and Cowling [331] where experimentally measured crack growth rates for various positions around the crack front were compared with those predicted by using the different solutions for the stress intensity factor in conjunction with the Paris law (equation 1.6).

Following the example of Scott and Thorpe [330] the solution obtained by Raju and Newman [326] was numerically integrated to illustrate the profile development of semi-elliptical cracks under tensile loading. The Raju-Newman solution was used as both Newman [328] and Scott and Thorpe [329,330] had concluded that it was one of the more accurate solutions available, and as well as that the results

were presented in a tabular form suitable for computational use. Figure 11.1 illustrates the notation used.

For a crack of depth a, and for a small amount of crack growth Δa during ΔN cycles, if Δa is small enough then :

$$\frac{\Delta a}{\Delta N} \approx \frac{da}{dN} \qquad (11.1)$$

Combining equations 11.1 and 1.6 gives :

$$\Delta a \approx C.\Delta N.\Delta K^m \qquad (11.2)$$

For a semi-elliptical crack the stress intensity factor can be expressed as :

$$K = \alpha\sigma\sqrt{(\pi a/Q)} \qquad (11.3)$$

where $\alpha = f(a/t, a/c, c/w, \Phi)$

and $Q \approx 1 + 1.464.\left[\frac{a}{c}\right]^{1.65}$ for $(a/c) \leq 1$ [328]

Substituting equation 11.3 into equation 11.2 leads to :

$$\Delta a \approx (C.\Delta N.\Delta\sigma^m.\pi^{m/2}) \left[\frac{\alpha^2 a}{Q} \right]^{m/2} \qquad (11.4)$$

As ΔN and $\Delta\sigma$ were taken to be constant for this work equation 11.4 may be rewritten as :

$$\Delta a \approx k \left[\frac{\alpha^2 a}{Q} \right]^{m/2} \qquad (11.5)$$

The value of α was obtained by linear interpolation between the values given by the Raju and Newman solution [326] at set values of (a/t) and (a/c) for both $\Phi=0^\circ$ and $\Phi=90^\circ$. Figures 11.2 and 11.3 illustrate that linear interpolation was sufficiently accurate. If the constant k is too large equation 11.1 would no longer hold true. The method was checked by using a value of k that was 1/10th of its original value : no difference in the results was observed.

For each iteration the crack growth at both the deepest point ($\Phi=90^\circ$) and the surface point ($\Phi=0^\circ$) was calculated. The current values of (a/t) and (a/c) were then updated, and the calculation terminated when (a/t) reached 0.8 as this is the limit of applicability for the Raju-Newman solution [326]. The crack growth at other parts of the crack front was assumed to be such that a semi-elliptical crack shape was maintained. No finite area correction factor was used [332] as this only affects the absolute crack growth rate, not the crack

shape development.

The results are shown in figures 11.4 to 11.6. It is clearly seen that a preferred crack shape is to be expected during the growth of semi-elliptic cracks, if the Raju-Newman solution is correct. Figure 11.7 shows the various results combined, and illustrates that the preferred crack shape alters for different values of the exponent m in equation 1.6. The preferred ratio of (a/c) is less for higher values of m, especially at greater values of (a/t).

11.3 Cast node specimens.

Following on from the work with semi-elliptic cracks under tension loading described in the previous section it was decided to attempt a similar calculation for the cast node specimen illustrated in figure 11.8 [333]. (These specimens were designed to aid the study of the fatigue properties of cast nodes for steel jacket structures). The intention was to compare the predicted crack development with that actually observed on specimens tested at BSC Swinden laboratories, Rotherham [334]. Before the same procedure could be followed it was necessary to develop solutions for the stress intensity factor for realistic cracks within these specimens.

11.3.1 FE methods for obtaining stress intensity factors.

Several methods exist for using the finite element calculation technique to determine stress intensity factors [335]. Fawkes et. al. [336] have compared the results obtained with different methods of formulating elements which incorporate the stress singularity present at a crack tip. The use of strain energy release methods (including the method of virtual crack extensions [337]) and displacement extrapolation techniques [338] were not able to be used, due to limitations on the time available for processing the computer output and on the computer time allowed. (The finite element package available, PAFEC 75 level 4.3, did not output the strain energy, or calculate a value for the J-integral). However, the package did incorporate crack tip elements, where the singularity was modelled by moving the midside nodes adjacent to the crack tip to the quarterpoint position [335]. For this case it can be shown [335] that the Mode I stress intensity factor should be given by the expression :

$$K_1 = \frac{2\mu}{(\kappa+1)} \left[\frac{2\pi}{L} \right]^{0.5} (4v_2 - v_3 - 3v_1) \qquad (11.6)$$

where μ = shear modulus
L = length of element side
κ = $3 - 4\nu$ for plane strain
ν = Poisson's ratio
v_1, v_2, v_3 = nodal displacements normal to the crack face (cf. figure 11.9)

Several 2D situations with known solutions were modelled in order to check that equation 11.6 gave reasonable results. (It was found that

equation 11.6, which corresponds to the $\theta=180^{\circ}$ case, gave better results than the similar equations for the situation where θ was 0° or 90°). The results are shown in figure 11.10. It is seen that this method usually underestimates the stress intensity factor by between about 2% to 14% compared to the solutions given by reference [339]. For the case of the 3 point bend specimen an effect of element size was noticed, because with very large elements the displacements due to the specimen bending dominate the displacements due to the crack tip. The results for the center cracked plate with h/b=0.4 are not as good as for h/b=1 because of the fewer elements used between the crack plane and the plane at which the uniform stress was applied. A similar effect of element size, and comparable errors were obtained by Banks-Sills and Bortman using the same method of calculating the stress intensity factor. Other workers [340] have used "correction factors" for finite element results, if such a factor of about 1.05 were to be used in the present situation the results of figure 11.10 suggest that the present method of calculating the stress intensity factor would be sufficiently accurate for the majority of engineering applications, especially in view of the ease with which the PAFEC package may be used. (In many situations engineering estimates of K_I still have to be made [341]).

The grid of figure 11.11 was used to assess the accuracy of the method used to determine K_I for a 3D situation. The results are compared with other workers results for a semi-elliptical crack in figure 11.12. The results show a similar trend as θ varies as those of Raju and Newman [326], except for at $\theta=0^{\circ}$ where surface effects are not properly modelled by the coarse mesh enforced by the limitations of the PAFEC package (ie. minimum angle between two element sides is 15° [342]). However, at the deepest point ($\theta=90^{\circ}$) the results obtained using PAFEC showed an excellent agreement with those given by the solution of Newman [323]. The experimental results of Aboutorabi and Cowling indicated that for the deepest point the Newman solution [323] gave very good results. Thus this method of determining stress intensity factors appeared to be suitable for a preliminary investigation of crack shape effects in the cast node specimens.

The results from the determination of the stress concentration along the (uncracked) specimen surface are shown in figures 11.13 to 11.15. The stress used to normalize the stress concentration factors in figure 11.15 was the bending stress expected at point C (cf. figure 11.13), as calculated from simple beam theory. The peaks in the

stress concentration factor results shown in figure 11.15 corresponded to points A and B given in figure 11.13.

The first attempt to calculate stress intensity factors for 3D cracks in a cast node specimen used the grid shown in figure 11.16. However problems arose in obtaining satisfactory results which remained unresolved. It may be that a more sophisticated finite element package is required for applications involving cracked structures before the original aim can be pursued further.

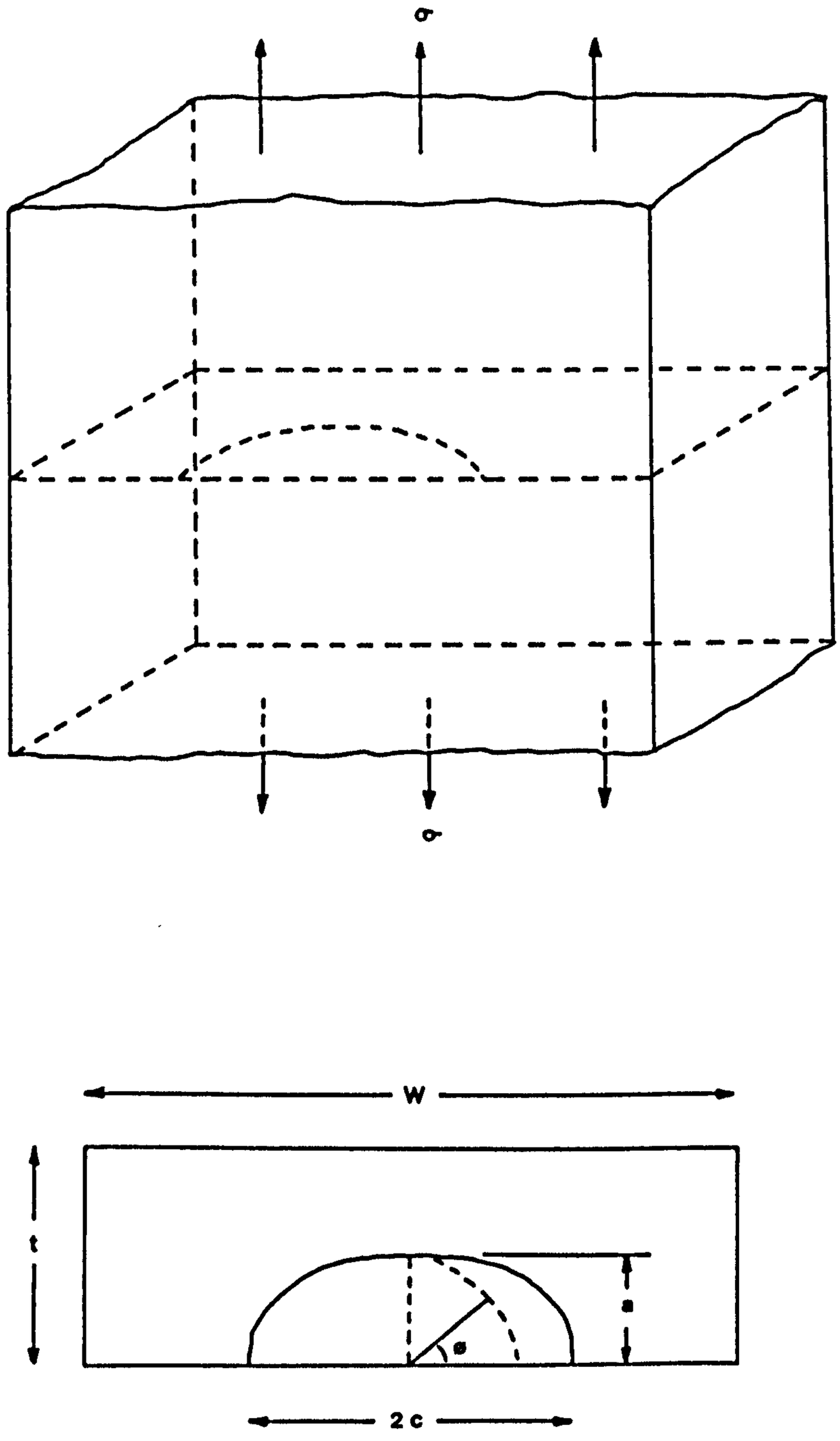

Figure 11.1 Notation used

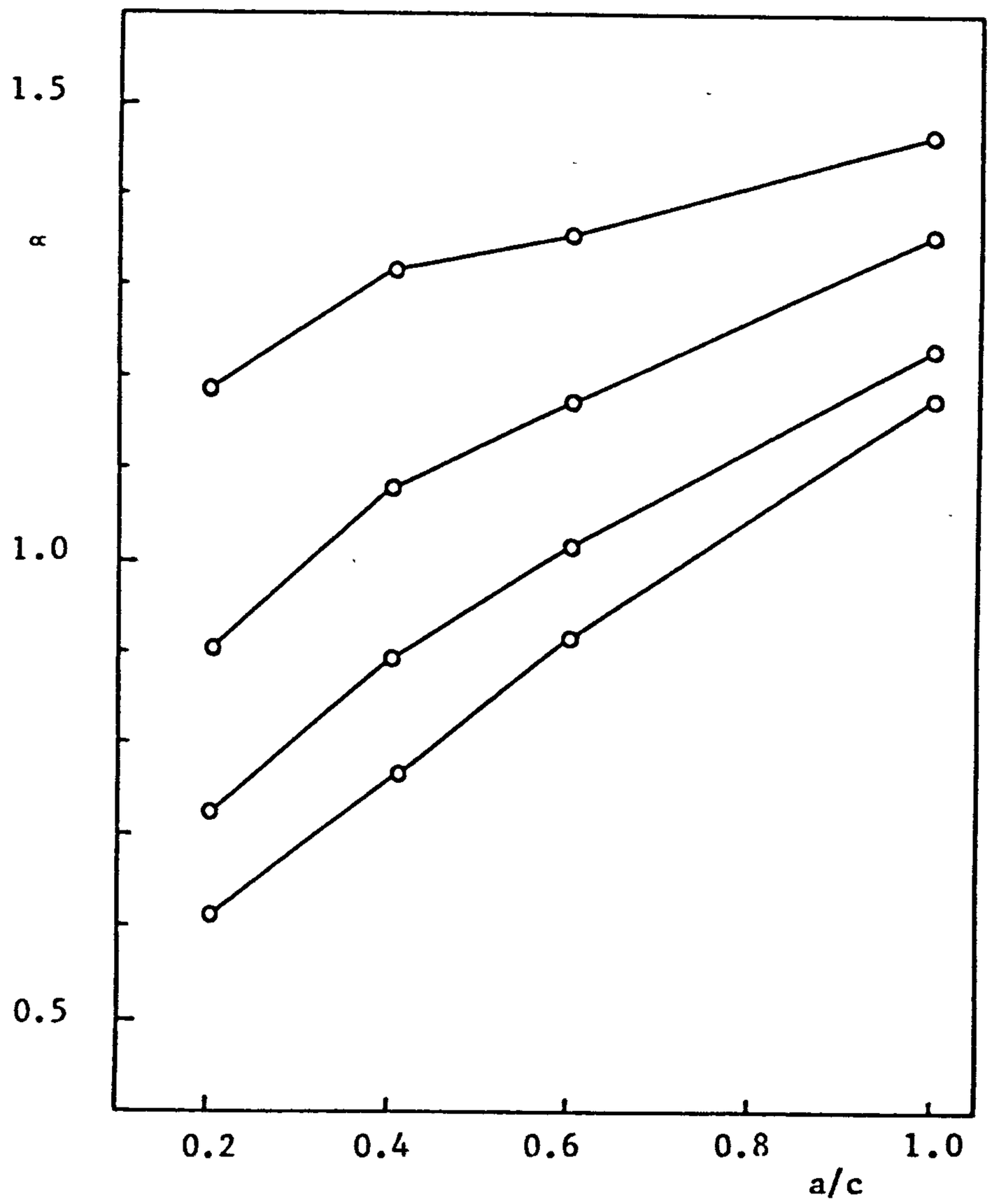

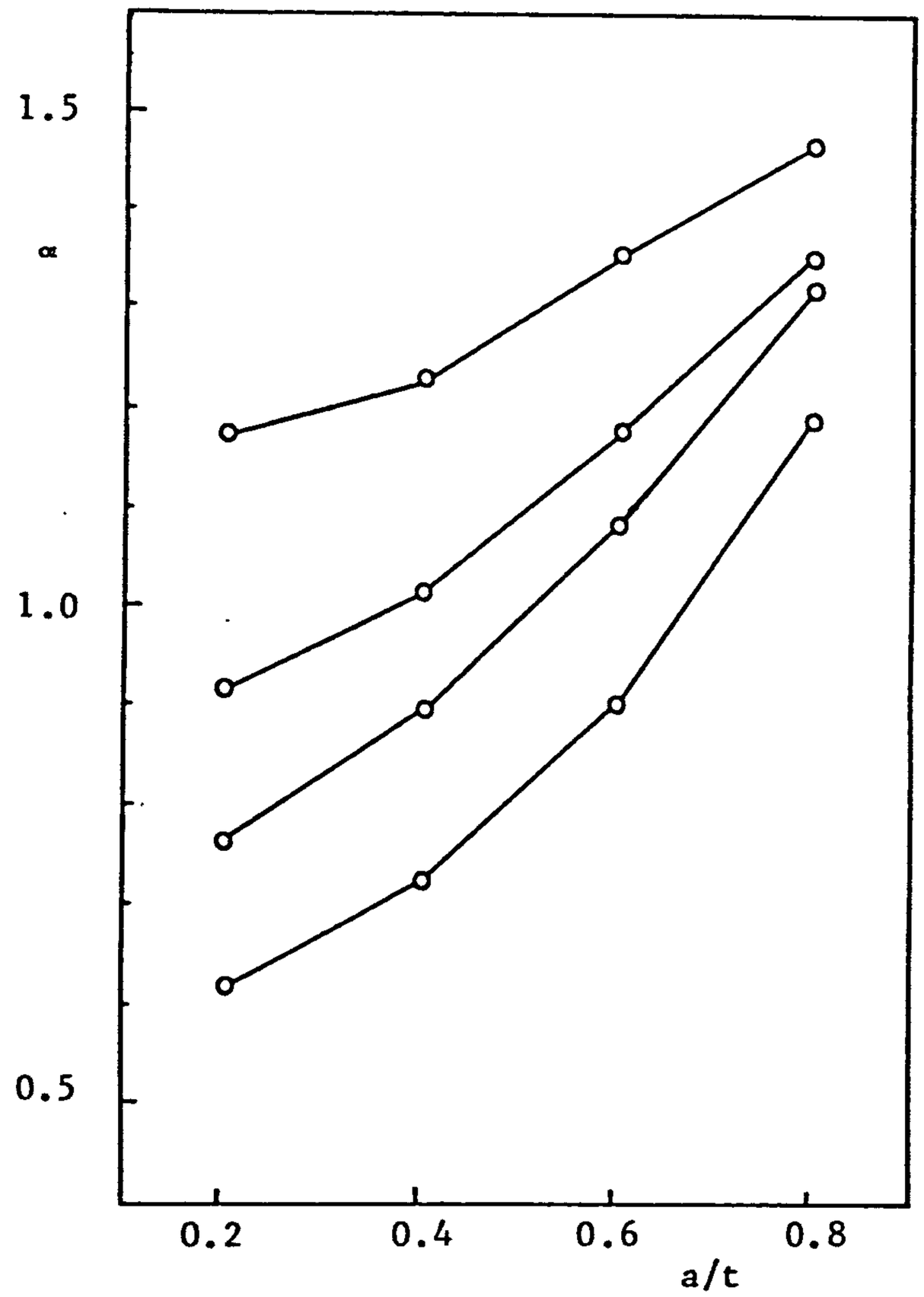

Figure 11.2 $\propto$ for $\phi = 0^{\circ}$ as given by Raju and Newman (326)

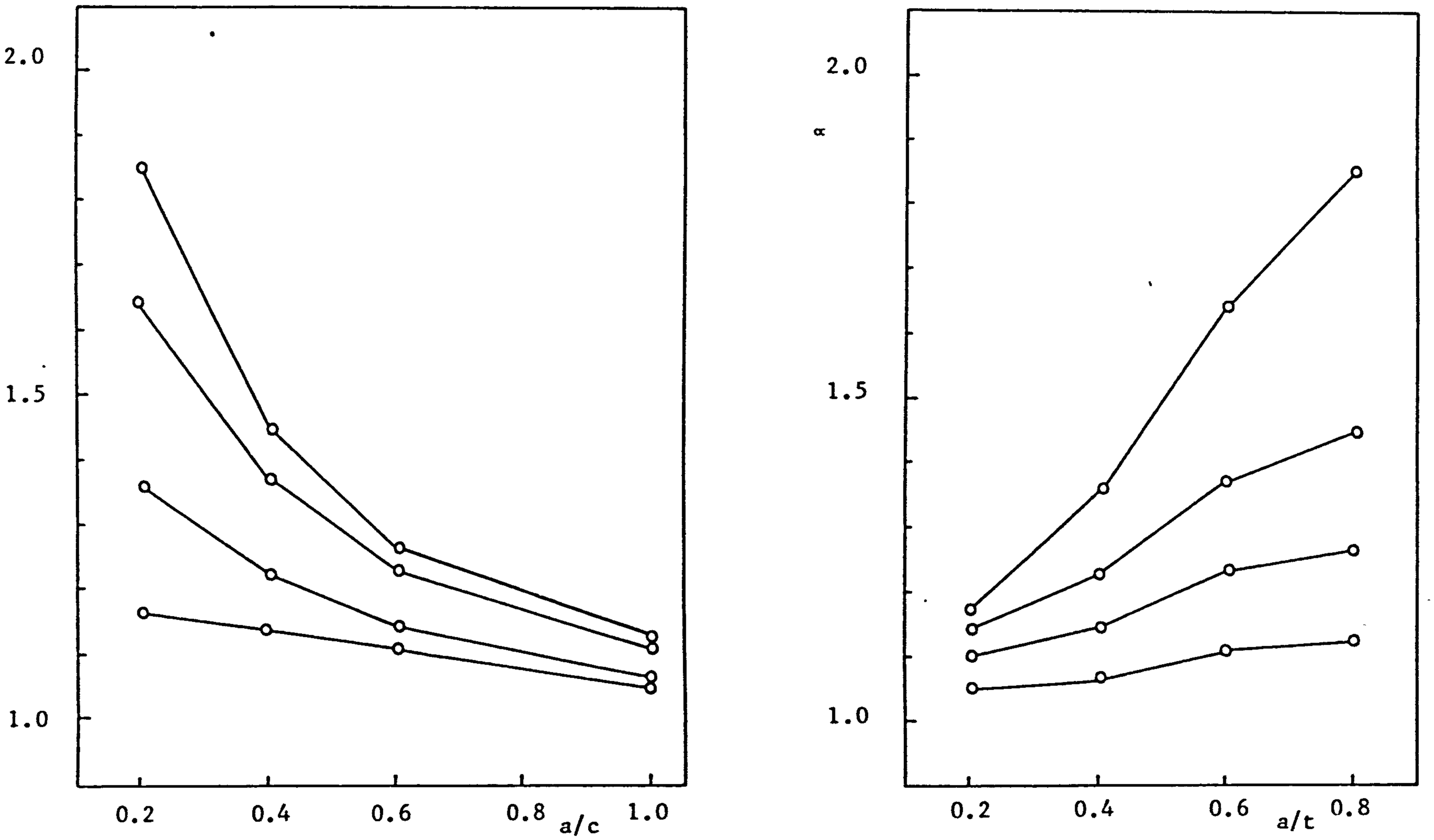

Figure 11.3 α for $\phi = 90^{\circ}$ as given by Raju and Newman (326)

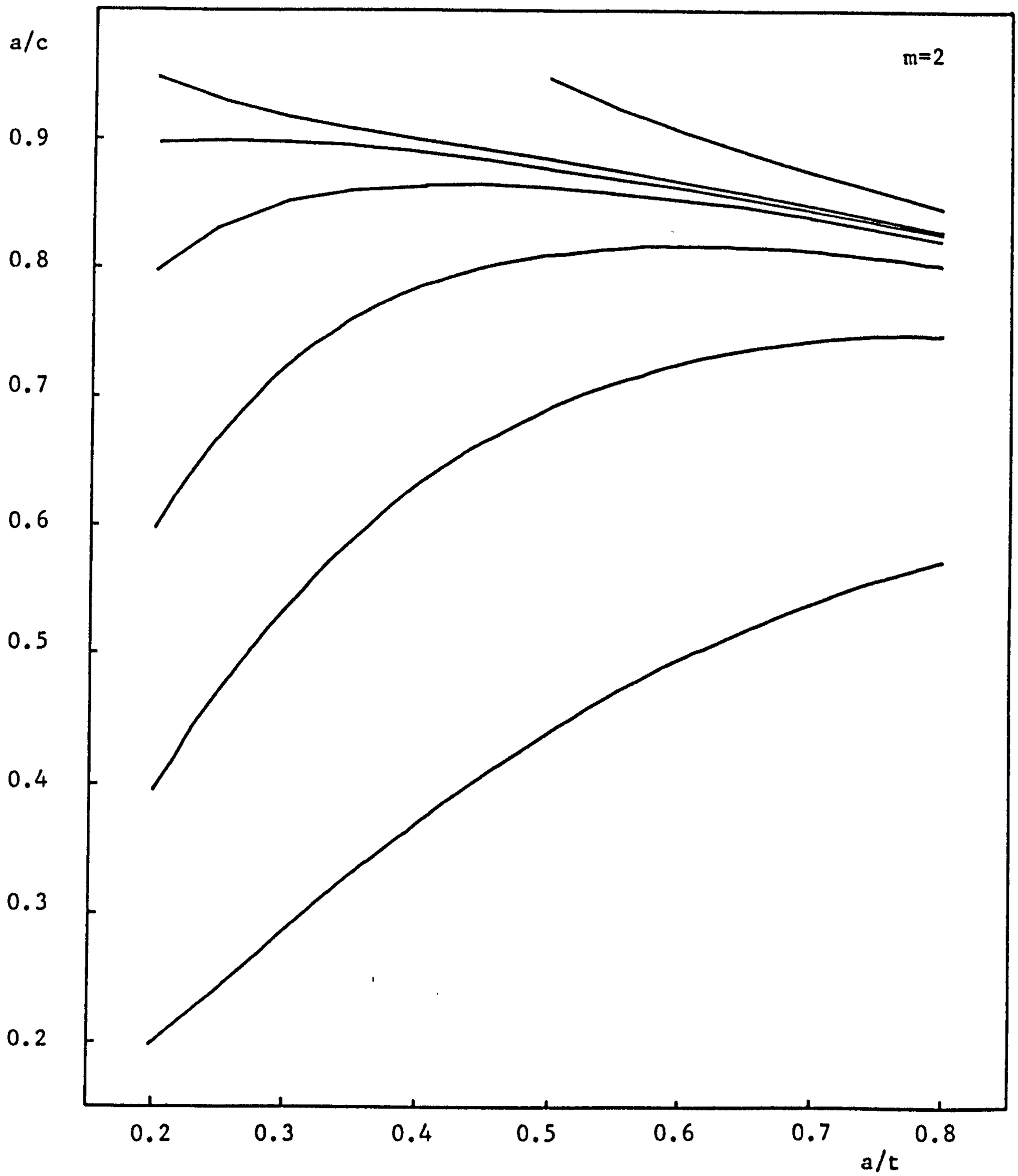

Figure 11.4

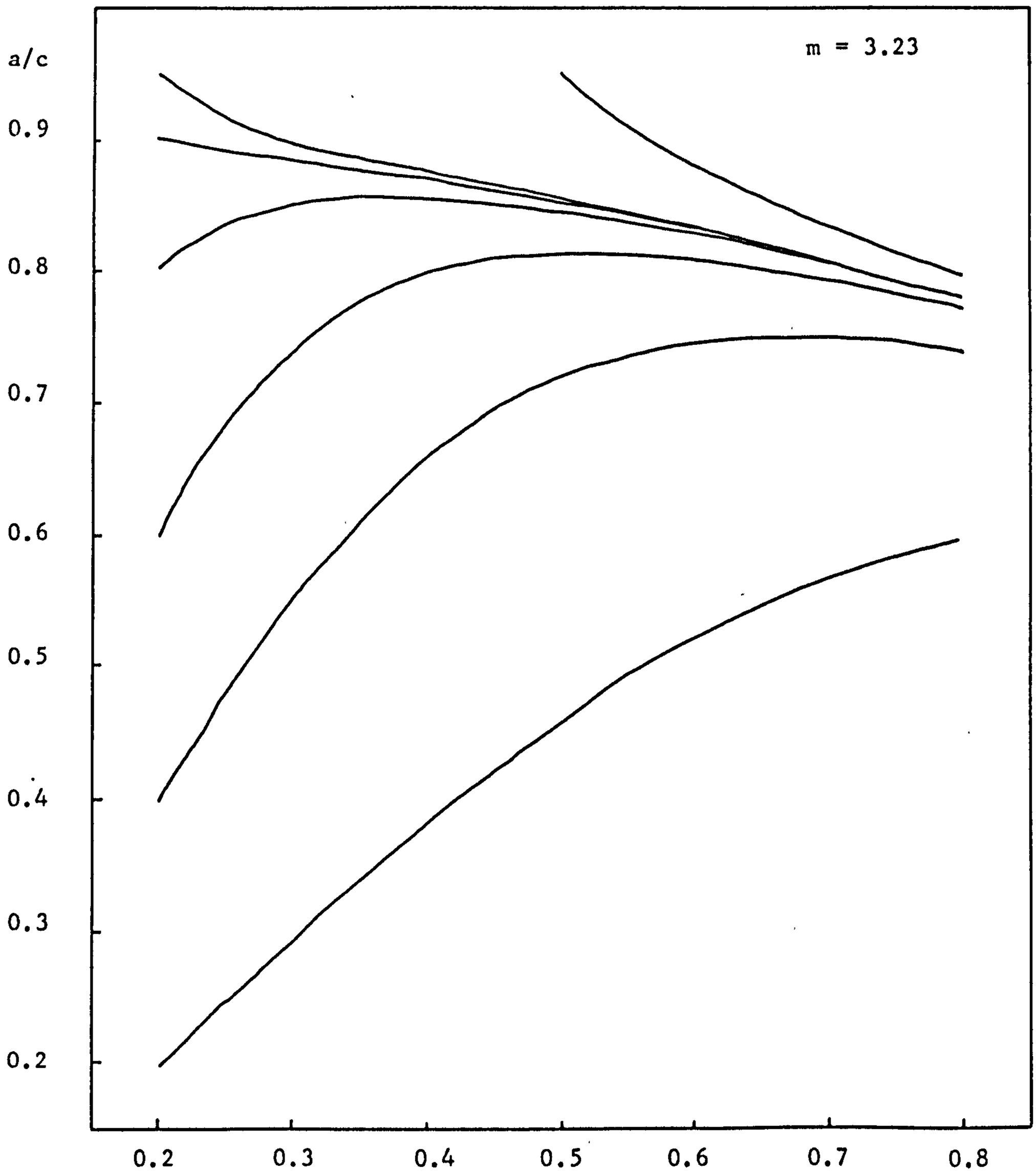

Figure 11.5

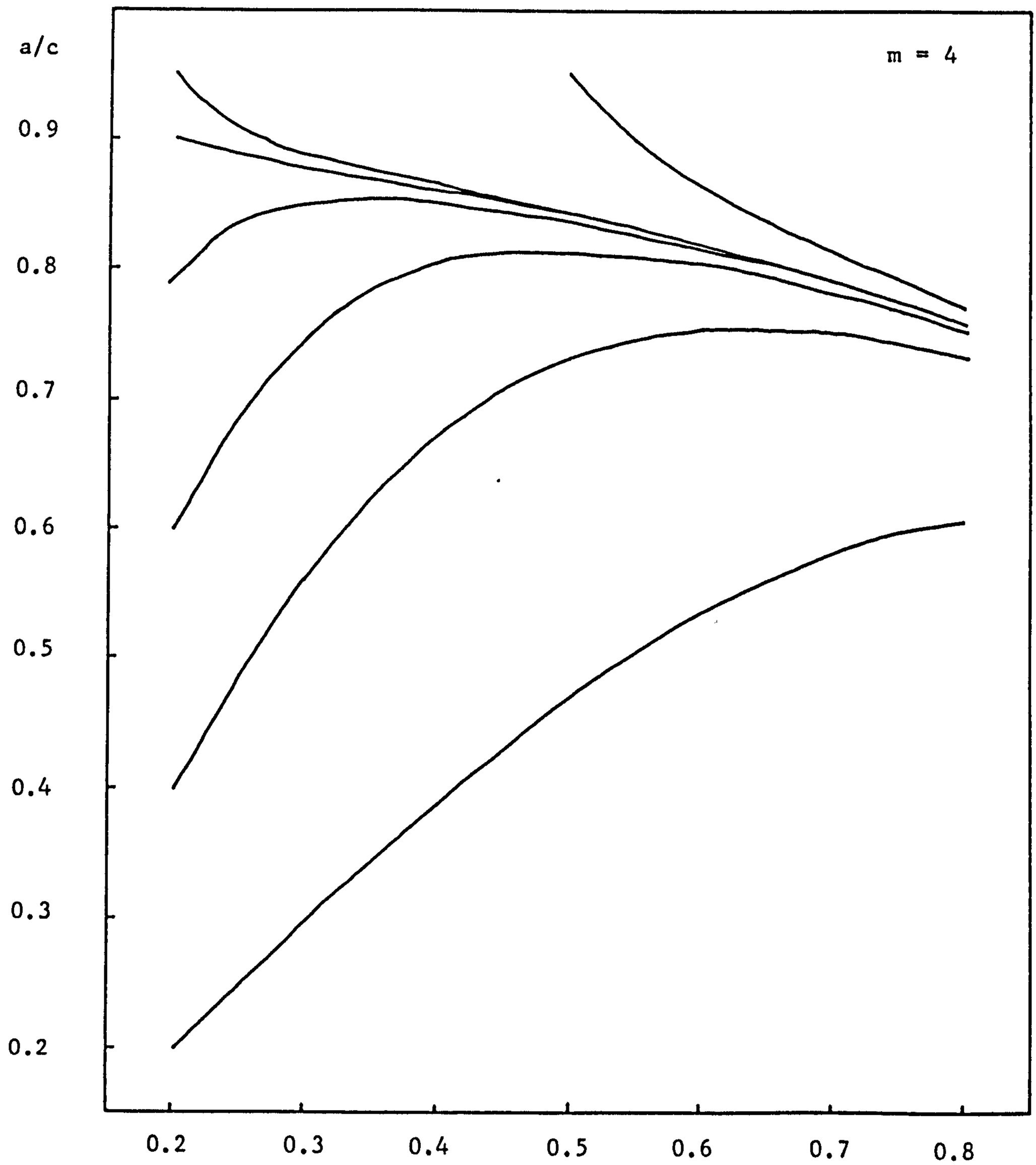

Figure 11.6

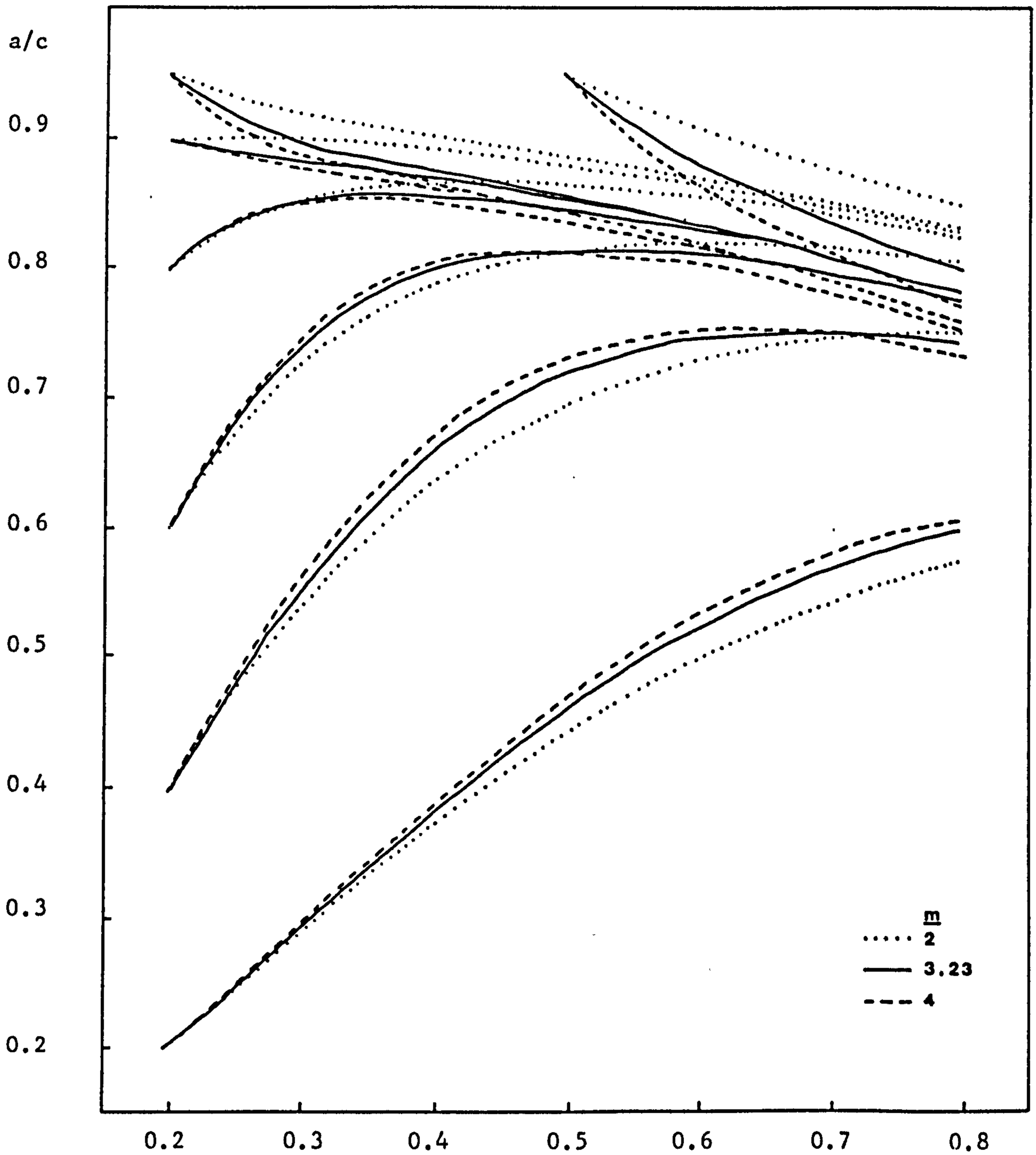

Figure 11.7

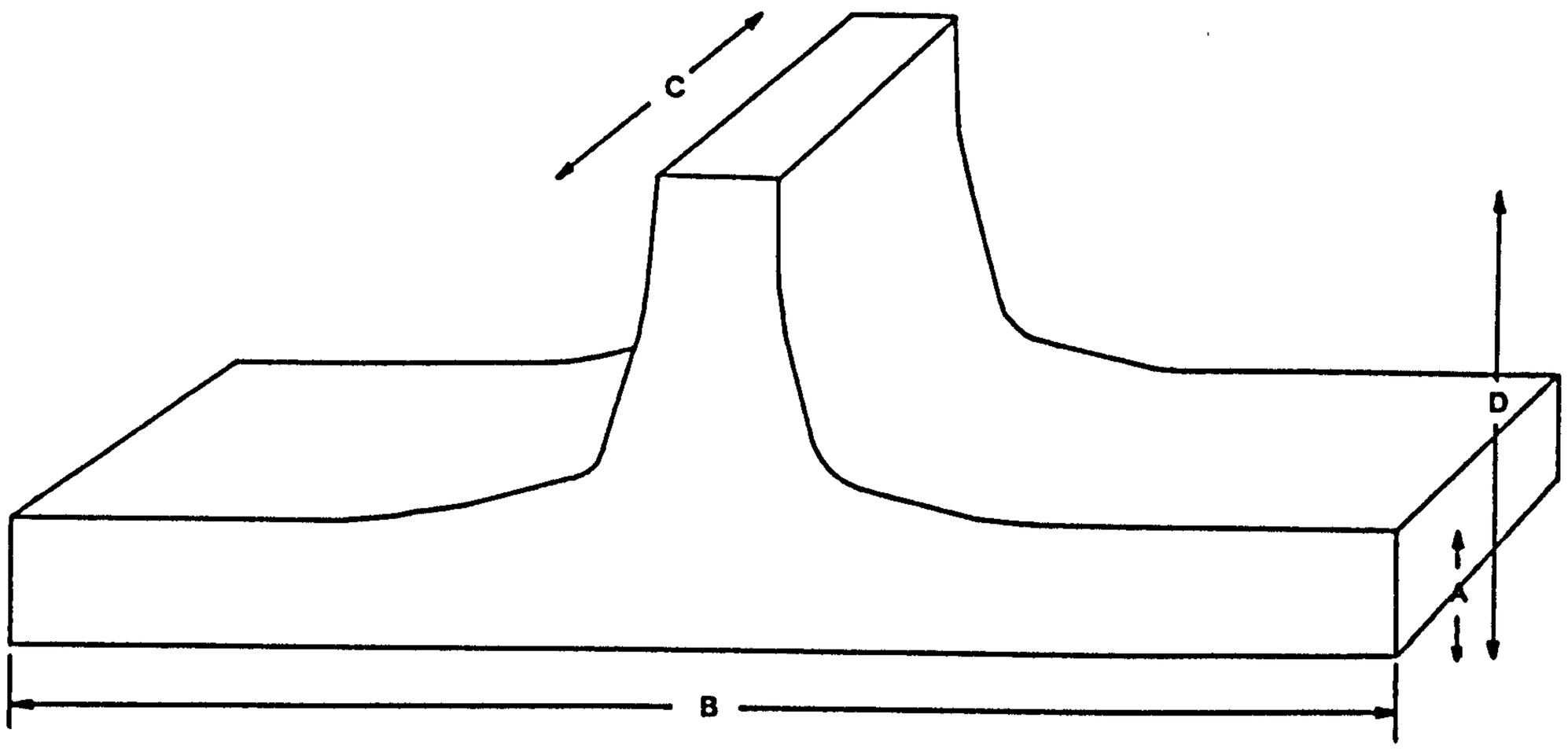

A = 100mm

B = 1300mm

C = 325mm

D = 380mm

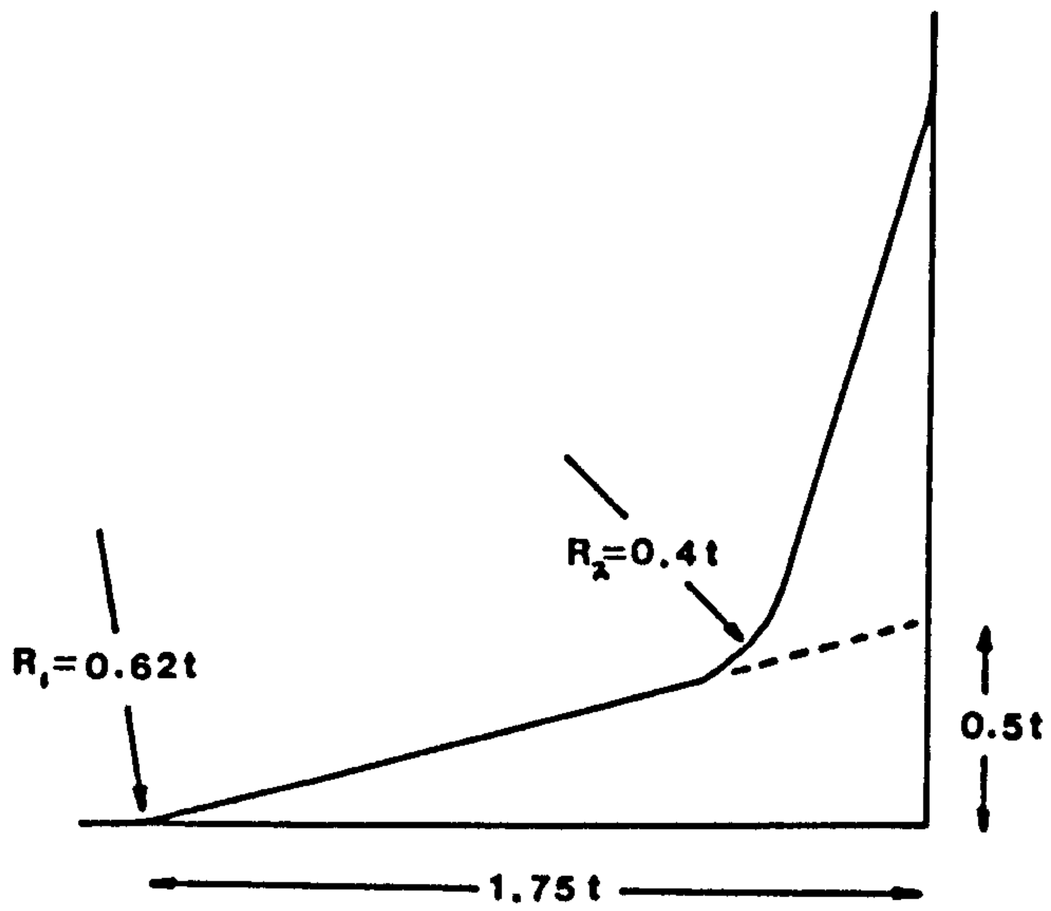

Figure 11.8 Castnode specimen geometry

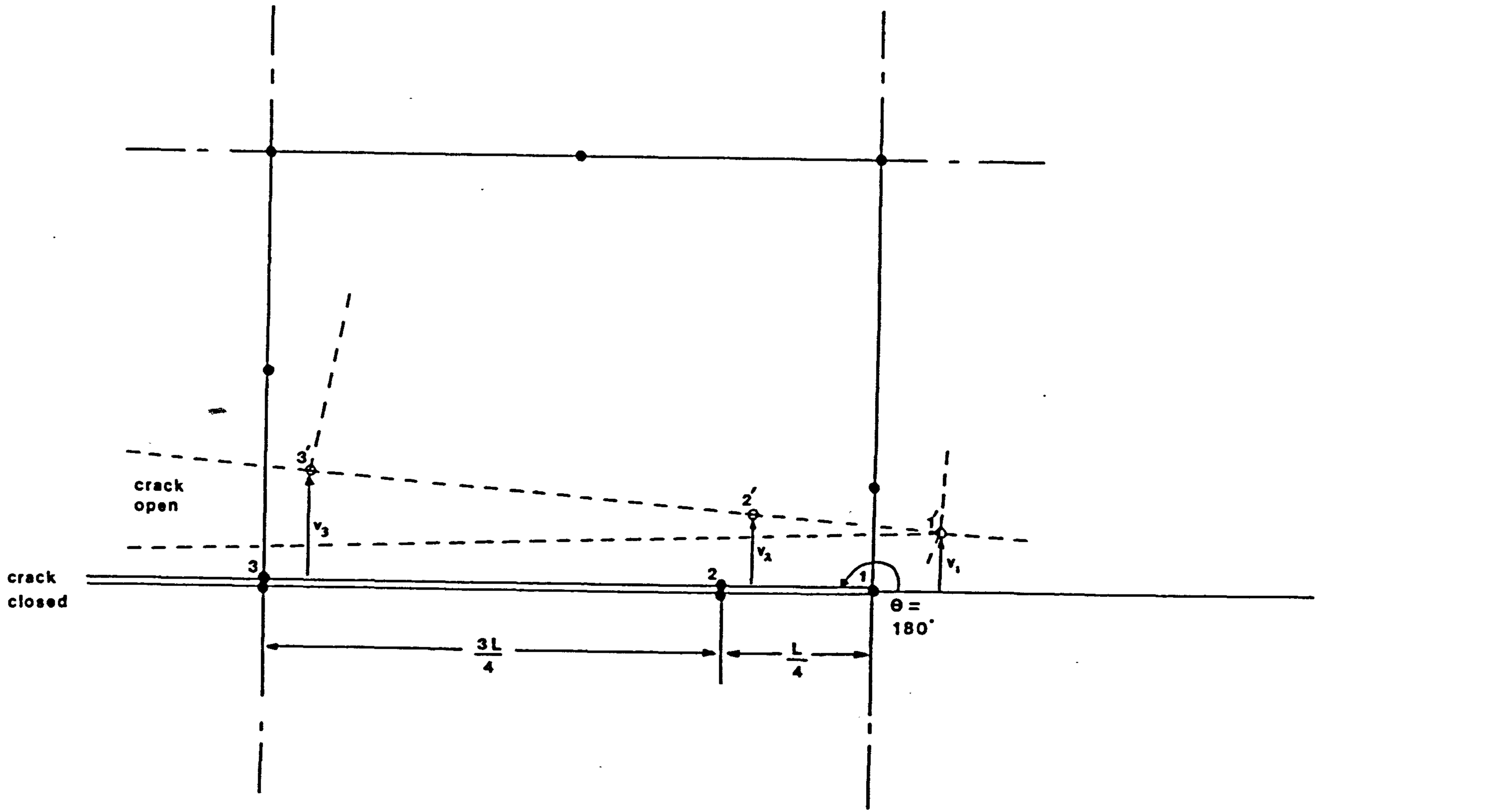

Figure 11.9 Diagram of quarterpoint crack tip element, illustrating notation used

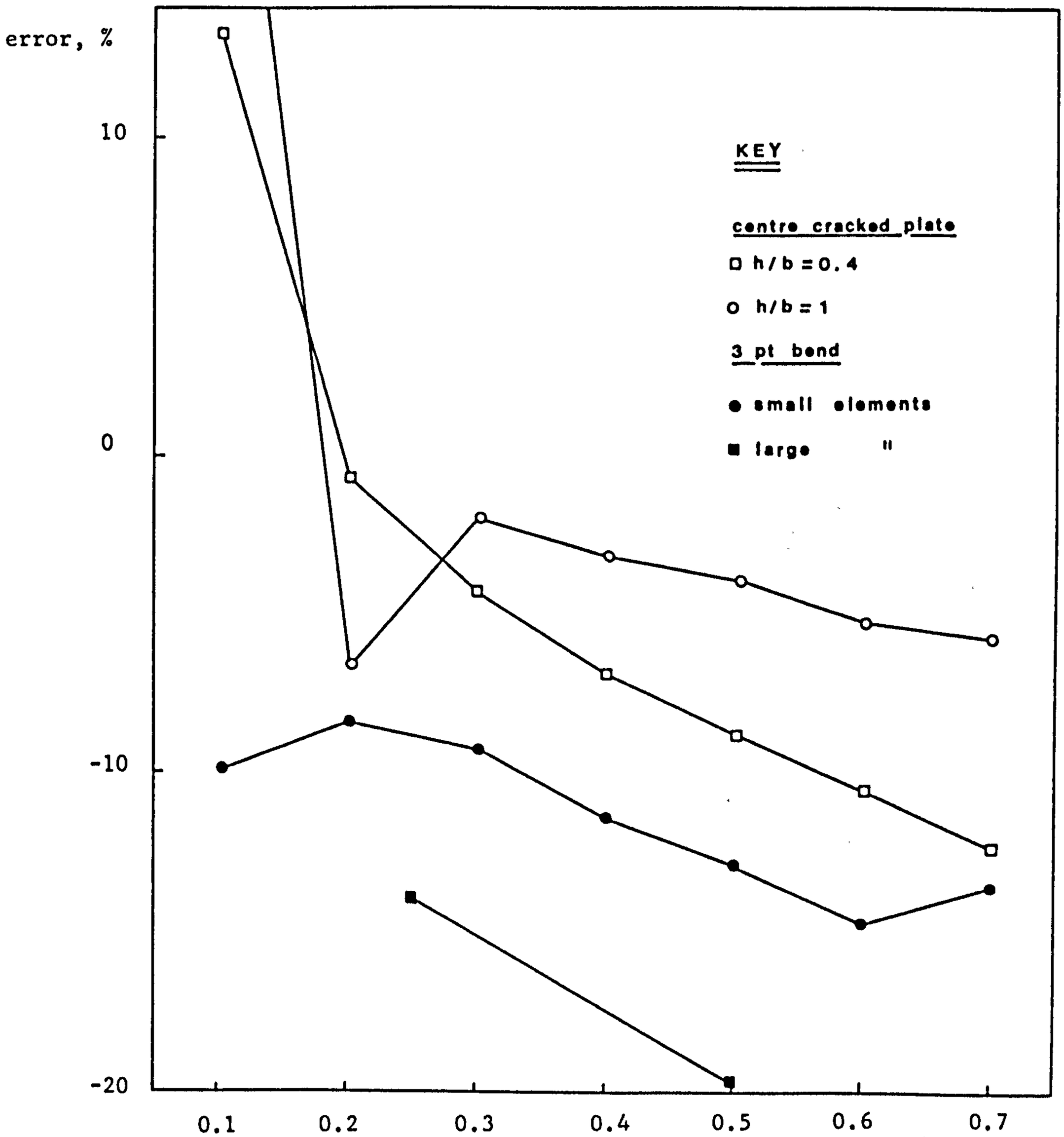

Figure 11.10 2D calibration results

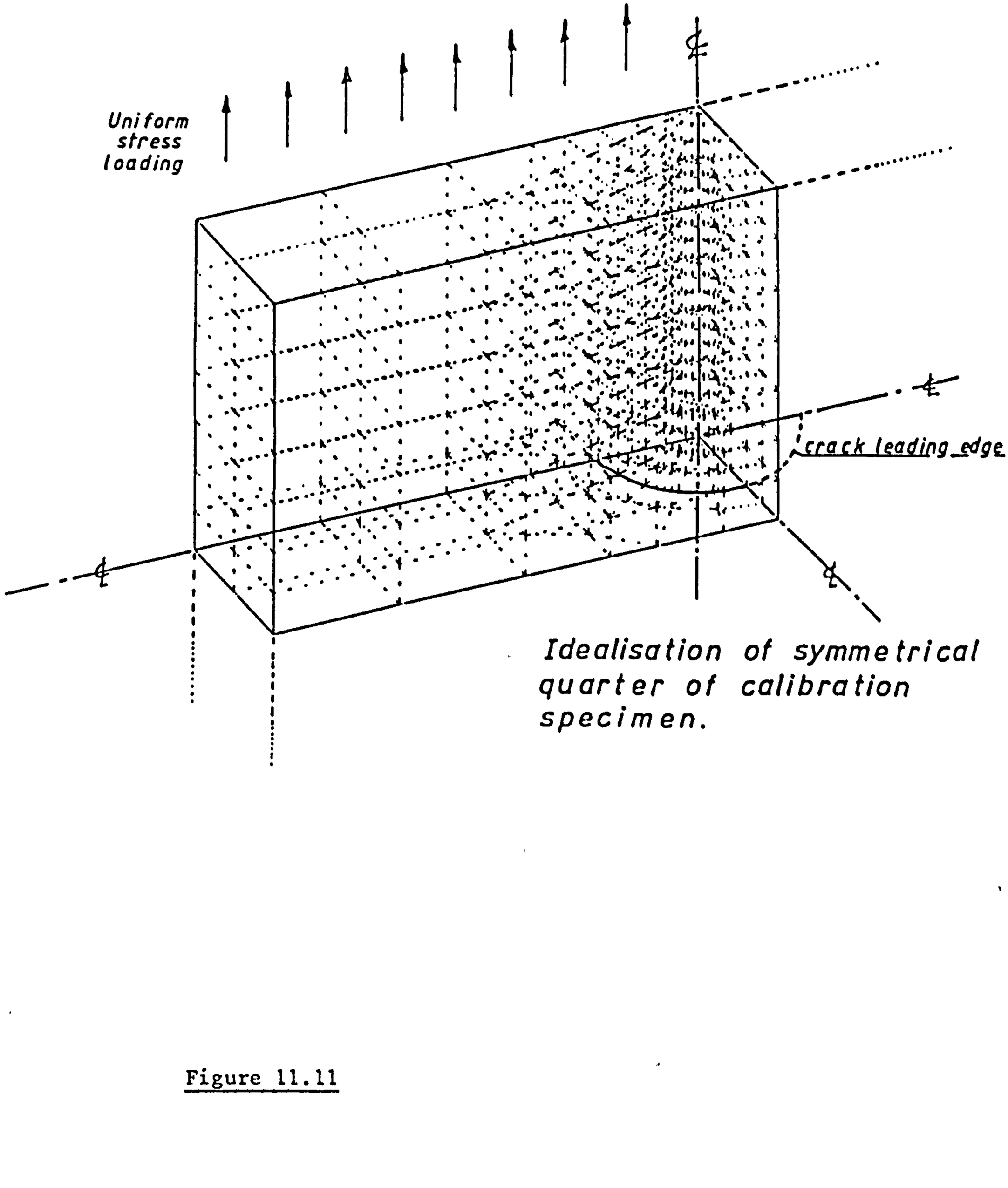

Idealisation of symmetrical quarter of calibration specimen.

Figure 11.11

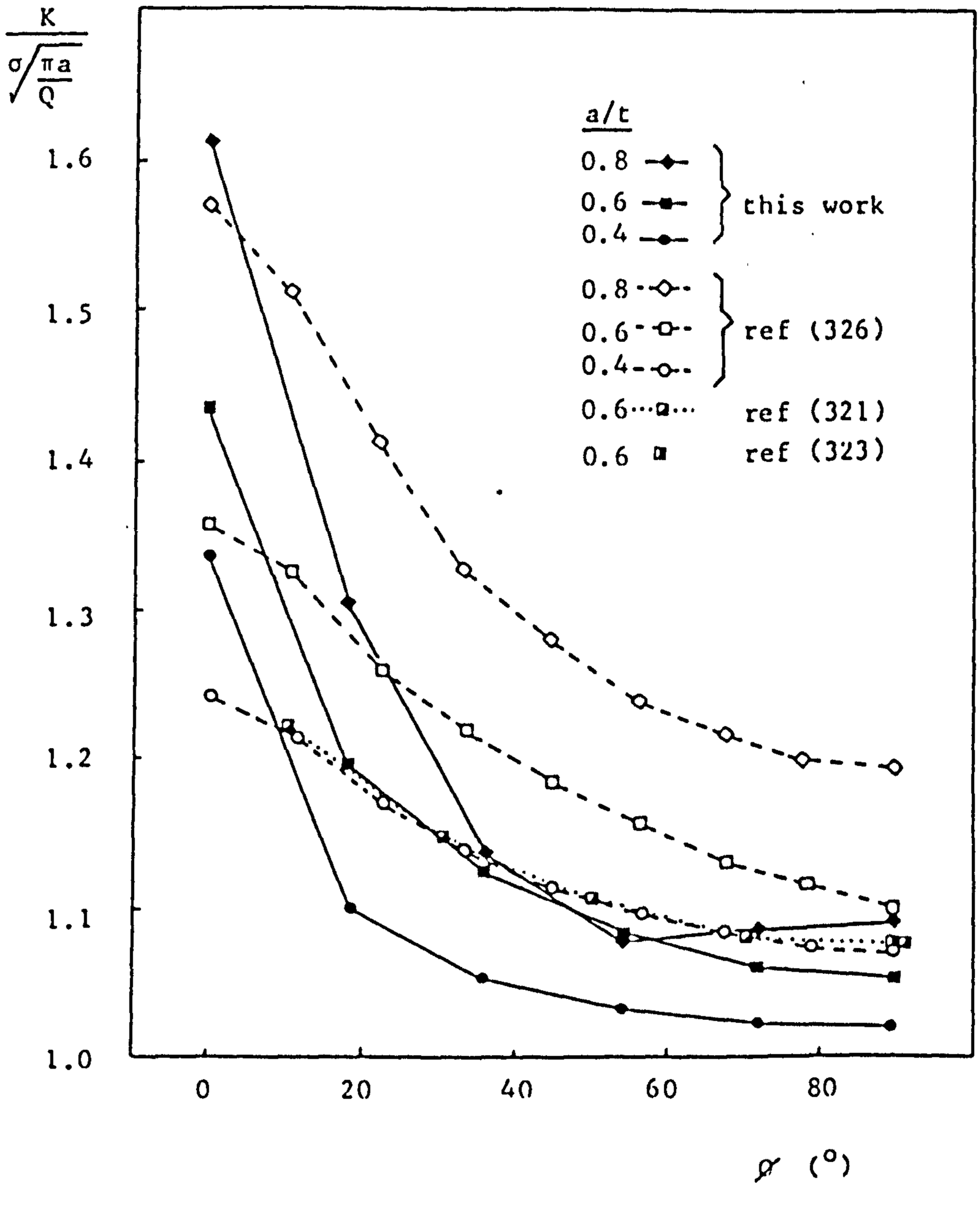

Figure 11.12 Comparison of 3D calibration results with those of other workers. (Where necessary the finite area correction of reference 332 was used)

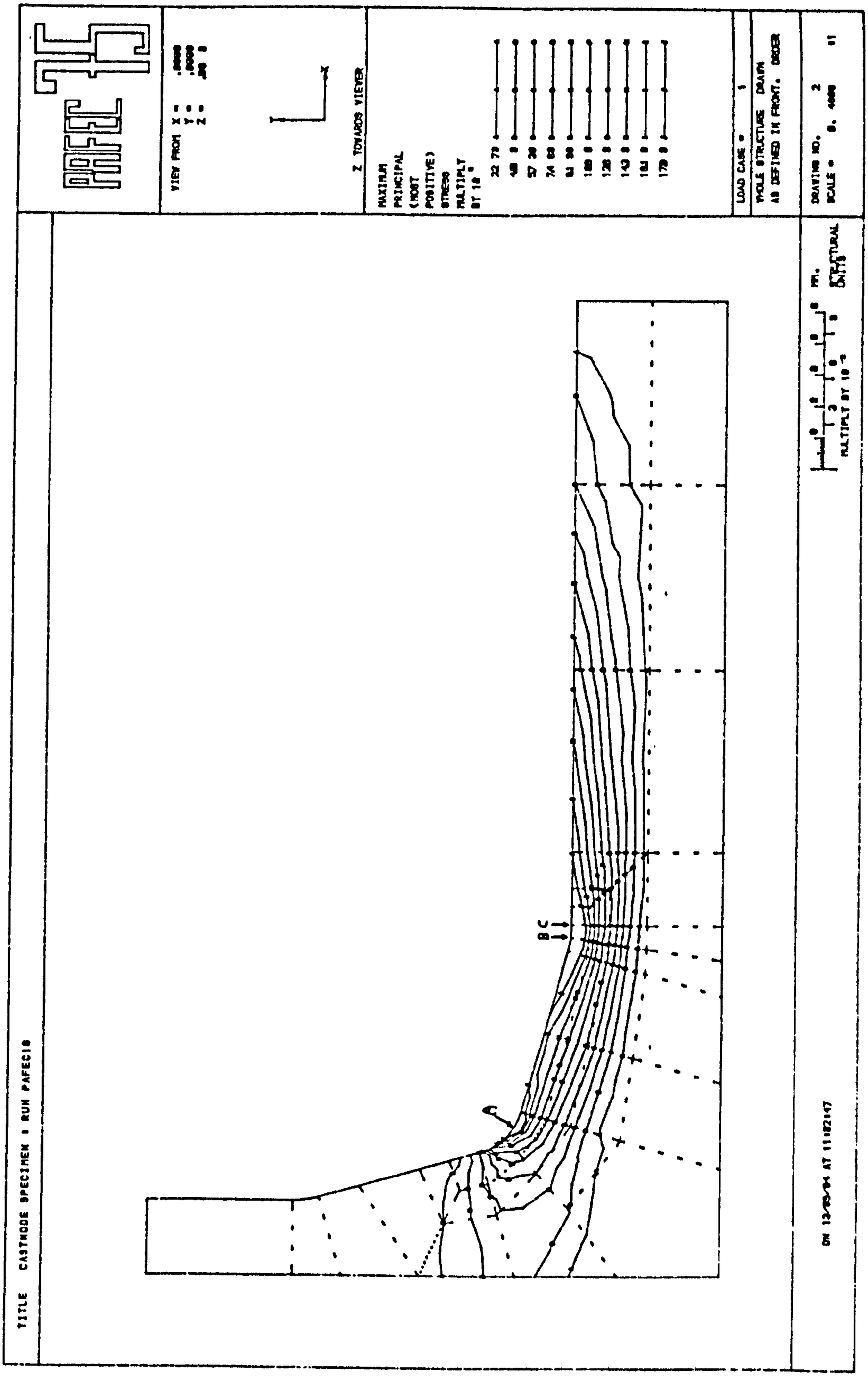
PAFEC 75
VIEW FROM X = .0000
Y = .0000
Z = .00 0
Z TOWARDS VIEWER
MAXIMUM PRINCIPAL (MOST POSITIVE) STRESS MULTIPLY BY 10**
22.79
45 0
67 20
74 00
91 00
100 0
120 0
140 0
160 0
179 0
LOAD CASE = 1
WHOLE STRUCTURE DRAWN AS DEFINED IN FRONT. ORDER
DRAWING NO. 2
SCALE = 0. 4000 11
FT.
STRUCTURAL UNITS
MULTIPLY BY 10**
BC
TITLE CASTNODE SPECIMEN 1 RUN PAFEC18
ON 12/05/84 AT 11:52:47

Figure 11.13

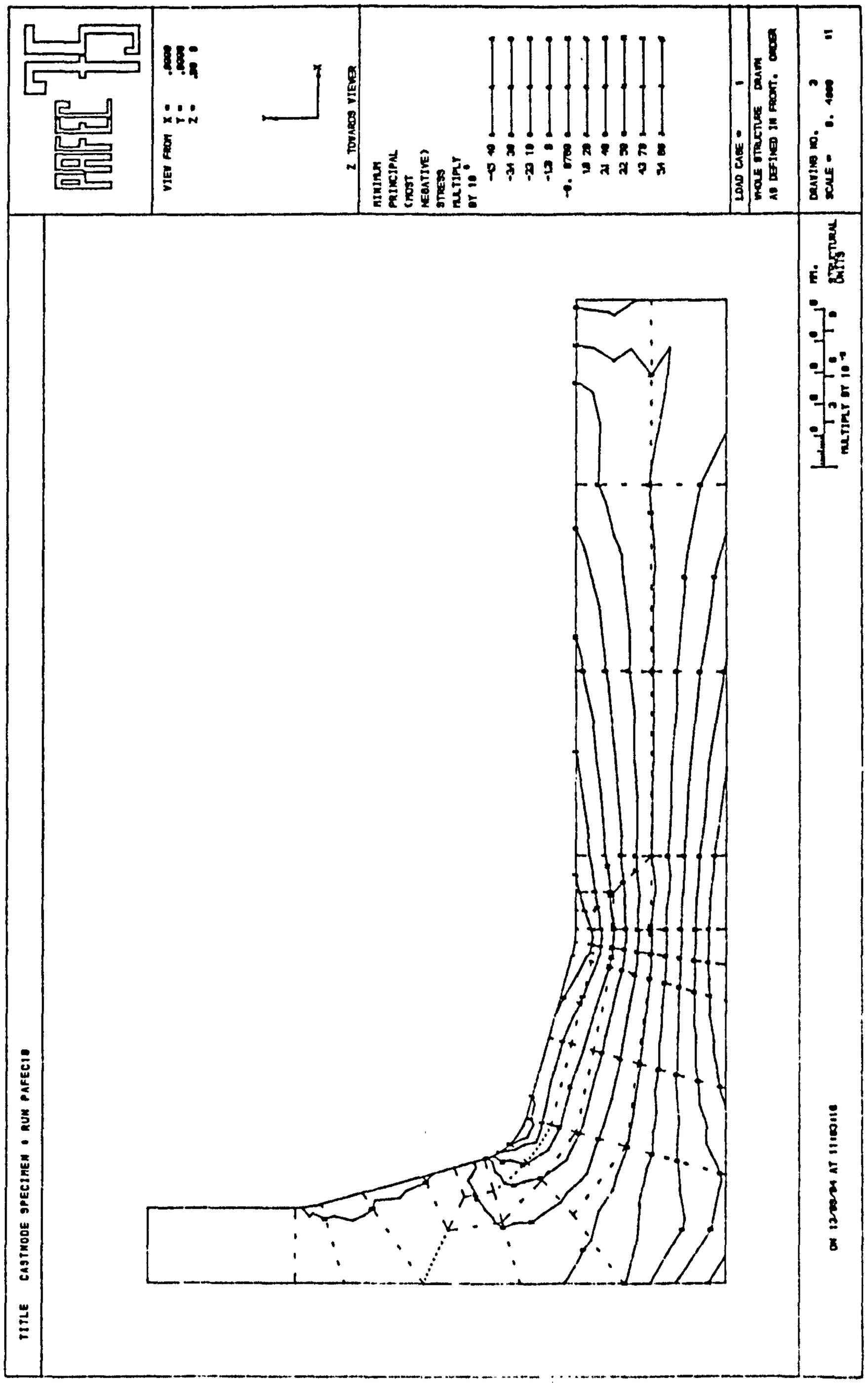
PAFEC 75
VIEW FROM X = .0000
Y = .0000
Z = .000 0
Z TOWARDS VIEWER
MINIMUM
PRINCIPAL
(MOST
NEGATIVE)
STRESS
MULTIPLY
BY 10
-43 40
-34 30
-25 10
-15 0
-6. 8760
18 20
21 40
22 50
43 70
54 80
LOAD CASE = 1
WHOLE STRUCTURE DRAWN
AS DEFINED IN FRONT. ORDER
DRAWING NO. 2 11
SCALE = 0. 4000 IN
0 1 2 3 4
MULTIPLY BY 10**0
TITLE CASTNODE SPECIMEN + RUN PAFEC18
ON 12/08/84 AT 11:50:18

Figure 11.14

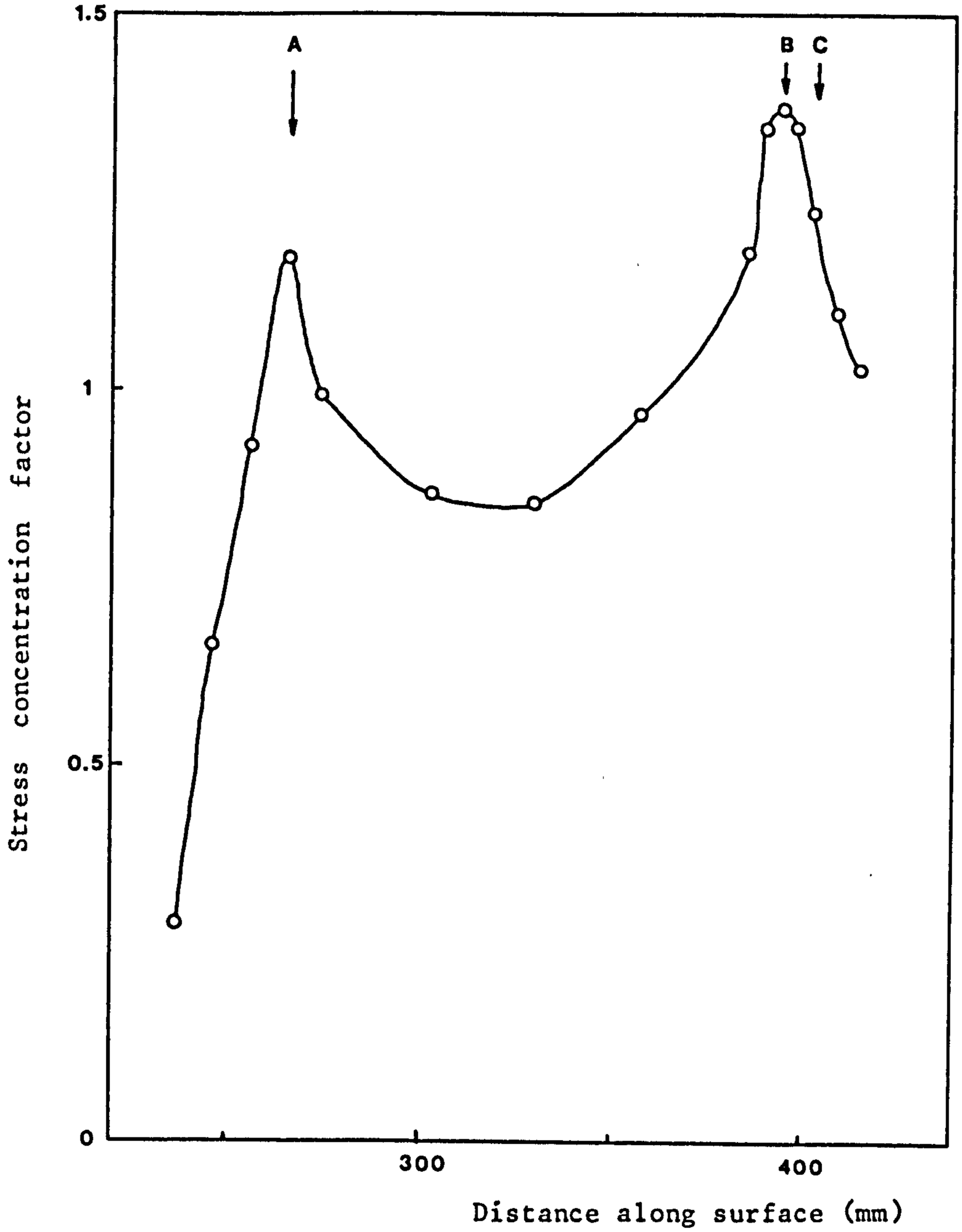

Figure 11.15 Stress concentration factor for castnode specimen in 3pt. bending.
(Reference stress is that expected at point C from simple beam theory)

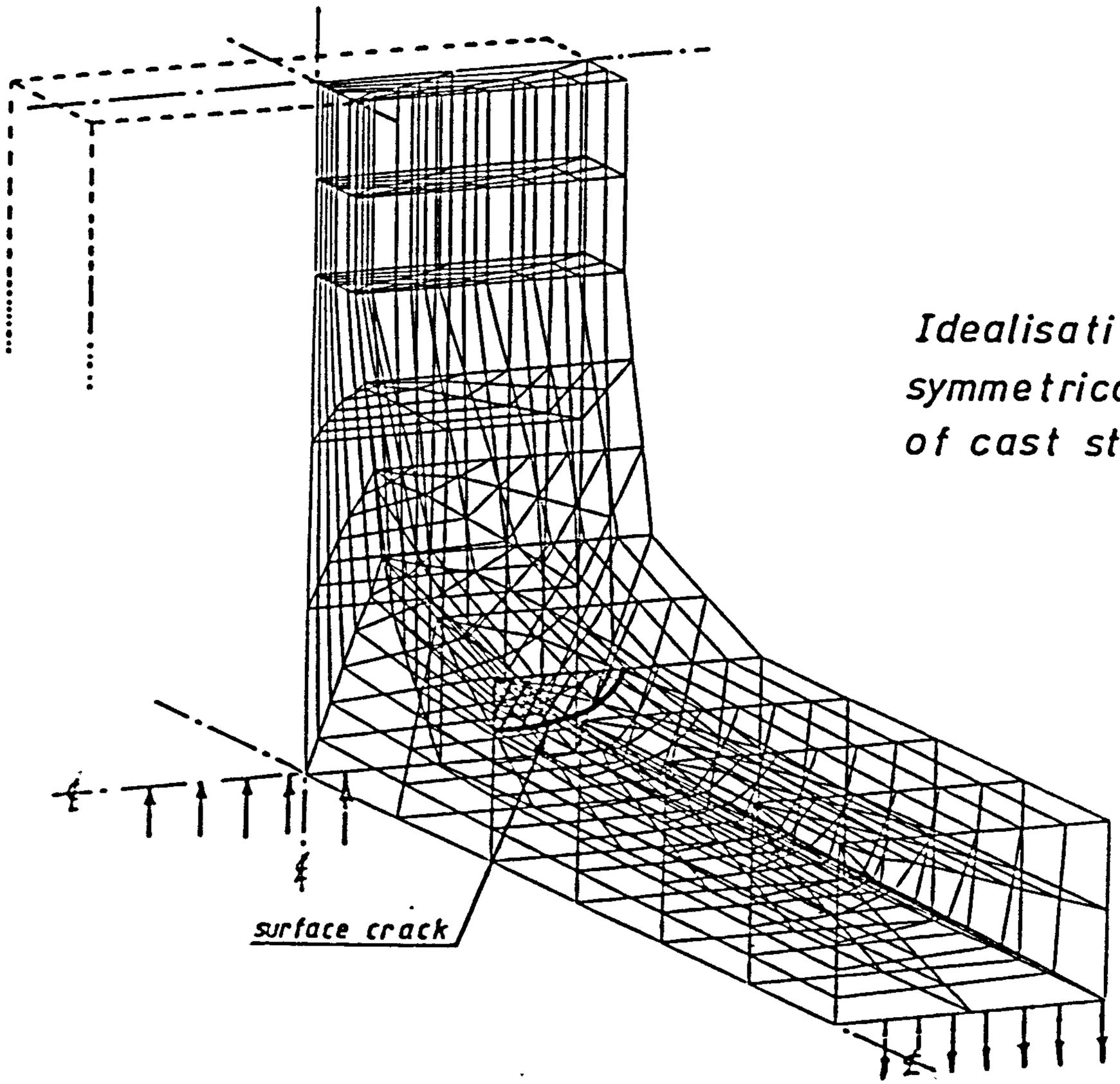

Idealisation of symmetrical quarter of cast steel specimen

Figure 11.16

References

References.

[1] H.M.Westergaard : *J. Appl. Mech. A* : 49 : (1939)

[2] G.R.Irwin : *Fracture* : Encyclopedia of Physics Vol VI : Springer, Berlin : (1958)

[3] G.R.Irwin, J.A.Kies, H.L.Smith : *Proc. ASTM* : 58 : (1958) : p640

[4] British Standards Institution : BS 5447 : (1977)

[5] P.C.Paris : Proc. *10th Sagamore conf.* : Syracuse University Press, Syracuse, New York : (1964) : p107

[6] P.C.Paris, F.Erdogan : *J. Basic Engng. - Trans. ASME(D)* : 85 : (1963) : p528

[7] S.R.Swanson, F.Cicci, W.Hoppe : *ASTM STP 415* : (1967) : p312

[8] R.C.Bates, W.G.Clark : *Trans. Quart., ASM* : 62 : (1969) : p380

[9] C.E.Richards, T.C.Lindley : *Eng. Fract. Mechs.* : 4 : (1972) : pp951-978

[10] C.J.Beevers, R.J.Cooke, J.F.Knott, R.O.Ritchie : *Metal Sci.* : 9 : (1975) : pp119-126

[11] R.N.Parkins : *A general introduction to fracture mechanics* : Mechanical Engineering Publications Ltd. : (1978) : ISBN 0/85298/383/2 : chapter 9

[12] R.N.Parkins : Proc. *ICM 3* : (1979) : Cambridge : Vol.1 : pp139-164

[13] A.J.McEvily, R.P.Wei : Proc. int. conf. *Corrosion fatigue : chemistry, mechanics and metallurgy* : 14-18 June 1971 : Univ. Connecticut, Connecticut : NACE-2 : pp381-393

[14] J.P.Gallagher, R.P.Wei : ref. 13 : pp409-419

[15] R.P.Wei, J.D.Landes : *Mat. Res. and Std. ASTM* : 9 : (1969) : p25

[16] I.M.Austen, E.F.Walker : Proc. conf. *Effect of environment on fatigue* : 18-19 May 1977 : I.Mech.E, London : ISBN 0/85298/376/X p1

[17] I.M.Austen : Draft final report of ECSC contract 7210.KE/806 (BSC ref. FR 70-7 821) : July 1982

[18] I.M.Bernstein, H.W.Pickering : *Corrosion* : 31 : (1975) : pp105-107

[19] D.Harris, H.W.Pickering : *Effect of hydrogen on the behaviour of materials* : eds. A.W.Thompson & I.M.Bernstein : TMS-AIME, Metals Park, Ohio : (1975) : pp229-230

[20] H.W.Pickering, A.Valdes : Proc. int. symp. *Embrittlement by the localized crack environment* : 4-5 Oct 1983 : Philadelphia : ed. R.P.Gangloff : TMS-AIME : pp33-48

[21] B.G.Ateya, H.W.Pickering : *J. Electrochem. Soc.* : 122 : (1975) : pp1018-1025

[22] K.Landles, J.Congleton, R.N.Parkins : ref. 20 : pp59-74

[23] R.N.Parkins, I.H.Craig, J.Congleton : *Corrosion sci.* : 24 : (1984) : pp709-730

[24] R.N.Parkins : submitted to *Metals Sci. Tech.* : (1985)

[25] A.Turnbull, M.K.Gardner : *Br. Corros. Jnl.* : 16 : (1981) : pp140-144

[26] A.Turnbull, A.T.May : NPL report DMA(A) 45 : June 1982

[27] T.Hodgkiess, M.J.Cannon, A.McLachlan : Conf. *Corrosion chemistry within pits, crevices and cracks* : Oct 1984 : NPL, Teddington : (to be published by HMSO)

[28] A.Turnbull : *Corrosion sci.* : 23 : (1983) : pp833-870

[29] A.Turnbull : ref. 20 : pp3-31

[30] A.Turnbull : *Reviews in coatings and corrosion* : 5 : (1982) : pp43-171

[31] A.Turnbull, M.K.Gardner : *Corrosion sci.* : 22 : (1982) : pp661-673

[32] G.Sandoz, C.T.Fujii, B.F.Brown : *Corrosion sci.* : 10 : (1970) : pp839-845

[33] J.A.Smith, M.H.Peterson, B.F.Brown : *Corrosion* : 26 : (1970) : pp539-542

[34] A.Alavi, R.A.Cottis : ref. 20 : pp75-87

[35] J.C.Scully : Proc. int. conf. *Mechanisms of environment sensitive cracking of materials* : 4-7 April 1977 : University of Surrey : Metals Society, London : pp1-18

[36] D.A.Vermilyea : *J. Electrochem. Soc.* : 119 : (1972) : pp405-407

[37] R.N.Parkins : *Br. Corros. Jnl.* : 7 : (1972) :pp15-28

[38] J.F.Newman : ref. 35 : pp19-31

[39] F.P.Ford : ref. 12 : Vol. 2 : pp431-444

[40] F.P.Ford : *ASTM STP 821* : (1984) : pp32-51

[41] D.A.Vermilyea, R.B.Diegle : *Corrosion* : 32 : (1976) : pp26-29

[42] F.P.Ford : ref. 35 : pp125-146

[43] D.Howard, T.Pyle : *Phil. Mag.* : 14 : (1966) : pp1179-1189

[44] D.Howard, T.Pyle : *Br. Corros. Jnl.* : 3 : (1968) : pp301-304

[45] T.Pyle, V.Rollins, D.Howard : *J. Electrochem. Soc.* : 122 : pp1445-1453

[46] F.P.Ford : ref. 35 : discussion p346

[47] G.T.Burstein, D.H.Davies : *Corrosion sci.* : 20 : (1980) : pp1143-1155

[48] P.J.Trant : private communication : (1985)

[49] T.Hodgkiess : private communications : (1981-1985)

[50] G.T.Burstein, D.H.Davies : *J. Electrochem. Soc.* : 128 : (1981) : pp33-39

[51] M.G.Alvarez, C.Manfredi, M.Giordano, J.R.Galvele : *Corrosion sci.* : 24 : (1984) : pp769-780

[52] F.P.Ford : *J. Electrochem. Soc.* : 120 : (1973) : pp1013-1019

[53] P.J.Trant : ref. 16 : pp57-63

[54] F.P.Ford : PhD thesis : Cambridge University : (1973)

[55] J.C.Scully : *Corrosion sci.* : 15 : (1975) : pp207-224

[56] R.N.Parkins : *Metal Sci.* : 13 : (1979) : pp381-386

[57] R.N.Parkins : *ASTM STP 665* : (1979) : pp5-25

[58] C.D.Kim, B.E.Wilde : ref. 57 : pp97-112

[59] P.M.Scott, A.E.Truswell, S.G.Druce : *Corrosion* : 40 : (1984) : pp350-357

[60] J.D.Atkinson, T.C.Lindley : ref. 16 : pp65-74

[61] J.D.Atkinson, T.C.Lindley : *Metal Sci.* : 13 : (1979) : pp444-448

[62] R.N.Parkins, B.S.Greenwell : *Metal Sci.* : 11 : (1977) : pp405-413

[63] B.Tomkins : ref. 16 : pp111-116

[64] B.Tomkins : *Metal Sci.* : 13 : (1979) : pp387-395

[65] J.C.Radon, C.M.Branco, L.E.Culver : *Int. Jnl. Fracture* : 12 : (1976) : pp467-469

[66] S.J.Gill, K.M.Htun, M.I.Jolles, T.W.Crooker : ref. 20 : pp471-483

[67] J.K.Musuva, J.C.Radon : Proc. conf. *Fatigue '81* : 24-27 March 1981 : Warwick University : pp106-116

[68] S.Suresh, G.F.Zamiski, R.O.Ritchie : *Metall. Trans.* : 12A : (1981) : pp1435-1443

[69] R.O.Ritchie, S.Suresh, C.M.Moss : *J. Engng. Mater. Technol. - Trans. ASME* : 102 : (1980) : pp293

[70] J.L.Yuen, C.G.Schmidt, P.Roy : *Fatigue Fract. Engng. Mater. Struct.* : 8 : (1985) : pp65-76

[71] S.Suresh, M.Parks, R.O.Ritchie : Proc. int. conf. *Fatigue thresholds, fundamentals and engineering applications* : EMAS, Warley, Birmingham : (1981) : pp391-408

[72] O.Vosikovsky : *J. Engng. Mater. Tech. - Trans. ASME* : 97 : (1975) : pp298-304

[73] J.Congleton, R.A.Olieh, R.N.Parkins : *Metals technol.* : 9 : (1982) : pp94-103

[74] R.N.Parkins, I.H.Craig : ref. 35 : pp32-52

[75] F.A.McClintock : ref. 13 : pp289-302

[76] H.L.Marcus, J.C.Williams, N.E.Paton : ref. 13 : pp346-358

[77] H.G.Nelson, A.S.Tetelman, D.P.Williams : ref. 13 : pp359-365

[78] I.M.Austen, E.F.Walker : ref. 35 : pp334-347

[79] R.N.Parkins, I.H.Craig : *Br. Corros. Jnl.* : 19 : (1984) : pp3-16

[80] D.J.Duquette : ref. 35 : pp305-321

[81] A.W.Thompson, I.M.Bernstein : Proc. int. conf. *Fracture '77 ICF 4* : 19-24 June 1977 : Waterloo, Canada : Vol.2 : pp249-254

[82] A.W.Thompson, I.M.Bernstein : Proc. 2nd. int. conf. *Hydrogen in metals* : June 1977 : Paris : paper 3A6

[83] A.W.Thompson : *Environment sensitive fracture of engineering materials* : Warrendale Pa. (USA) : ed. Z.A.Foroulis : TMS-AIME : (1979) : pp379-410

[84] A.W.Thompson : ref. 19 : pp 467-479

[85] C.Zappfe, C.Sims : *Trans. AIME* : 145 : (1941) : pp225-261

[86] A.S.Tetelman, W.D.Robertson : *Trans. TMS-AIME* : 224 : (1962) : pp775-783

[87] F.de Kazinsky : *J. Iron Steel Inst.* : 177 : (1954) : pp85-92

[88] G.G.Hancock, H.H.Johnson : *Trans. TMS-AIME* : 236 : (1965) : pp513-516

[89] J.K.Tien, A.W.Thompson, I.M.Bernstein, R.J.Richards : *Metall. Trans.* : 7A : (1976) : pp821-829

[90] J.K.Tien : ref. 19 : pp309-326

[91] H.H.Johnson, J.P.Hirth : *Metall. Trans.* : 7A : (1976) : pp1543-1548

[92] N.J.Petch, P.Stables : *Nature* : 169 : (1952) : pp842-843

[93] N.J.Petch : *Phil. Mag.* : 1 : (1956) : pp331-337

[94] A.A.Griffith : *Phil. Trans. R. Soc.* : A221 : (1920) : p163

[95] R.A.Oriani, P.H.Josephic : *Acta. Metall.* : 25 : pp979-988

[96] A.T.Stewart : ref. 35 : pp400-411

[97] H.H.Johnson : Proc. conf. *Stress corrosion cracking and hydrogen embrittlement of iron base alloys* : eds. R.W.Staehle, J.Hochman, R.D.McCright, J.E.Slater : NACE, Houston Tx. : (1977) : NACE-5 : pp382-389

[98] R.N.Parkins : private communication : (1984)

[99] S.P.Lynch : *Metals Forum* : 2 : (1979) : pp189-200

[100] A.R.Troiano : *Trans. ASM* : 52 : (1960) : pp54-80

[101] R.A.Oriani : ref. 97 : pp351-358

[102] R.A.Oriani : *Berichte der Bunsen-Gesellschaft fur Physikalische*

Chemie : 76 : (1972) : pp848-857

[103] R.A.Oriani : *Ann. Rev. Mater. Sci.* : 1978.8 : pp327-357

[104] R.A.Oriani, P.H.Josephic : *Scripta metall.* : 6 : (1972) : pp681-688

[105] R.A.Oriani, P.H.Josephic : *Acta. Metall.* : 25 : (1977) : pp979-988

[106] H.P.Van Leeuwen : *Corrosion* : 32 : (1976) : pp34-37

[107] H.G.Nelson, D.P.Williams : ref. 97 : pp390-404

[108] J.R.Rice : *Corrosion* : 32 : (1976) : pp22-26

[109] J.R.Rice : ref. 19 : pp455-466

[110] C.D.Beachem : ref. 97 : pp376-381

[111] C.D.Beachem : *Metall. Trans.* : 3 : (1972) : pp437-451

[112] J.P.Hirth : *Metall. Trans.* : 11A : (1980) : pp861-890

[113] M.Cornet, S.Talbot-Besnard : ref. 35 : pp538-546

[114] S.P.Lynch, N.E.Ryan : ref. 82 : paper 3D12

cf. also : *Hydrogen Damage* : ed. C.D.Beachem : ASM source book : pp369-376

[115] S.P.Lynch : ref. 35 : pp201-212

[116] S.P.Lynch : ref. 81 : pp859-866

[117] S.P.Lynch : *Scripta metall.* : 13 : (1979) : pp1051-1056

[118] S.P.Lynch : *Acta. Metall.* : 32 : (1984) : pp79-90

[119] S.P.Lynch : *ASTM STP 675* : (1979) : pp174-203

[120] S.P.Lynch : Proc. conf. *Hydrogen effects in metals* : eds. I.M.Bernstein & A.W.Thompson : Warrendale Pa (USA) : TMS-AIME : (1981) : pp863-871

[121] J.A.Clum : *Scripta metall.* : 9 : (1975) : pp51-58

[122] J.Eastman, T.Matsumato, N.Narita, F.Heubaum, H.K.Birnbaum : ref. 120 : pp397-409

[123] D.G.Westlake : *Trans. ASM* : 62 : (1969) : pp1000-1006

[124] H.G.Nelson : *Corrosion* : 32 : (1976) : p17

[125] S.Gahr, M.L.Grossbeck, H.K.Birnbaum : *Acta. Metall.* : 25 : (1977) : pp125-133

[126] R.P Wei : ref. 120 : pp677-689

[127] J.C.Scully : ref. 19 : pp129-149

[128] P.M.Scott : *Offshore Technology Paper 2* : Dept. of Energy : (1977) : ISSN 0309-8184

[129] O.Vosikovsky, A.Rivard : *Corrosion* : 38 : (1982) : pp19-22

[130] H.Vehoff, W.Rothe : *Acta. Metall.* : 11 : (1983) : pp1781-1793

[131] C.Q.Bowles, J.Schijve : *ASTM STP 801* : (1983) : pp96-114

[132] A.R.Troiano : *Hydrogen in metals* : eds. I.M.Bernstein &

A.W.Thompson : ASM : Library Congress cat. no. 73-86455 : pp1-15

[133] I.M.Bernstein, A.W.Thompson : ref. 35 : pp412-425

[134] W.A.Oates : *Metals Forum* : 2 : (1979) : pp138-148

[135] M.F.Ashby : private communication : (1981)

[136] C.F.StJohn, W.W.Gerberich : *Metall. Trans.* : 4 : (1973) : pp589-594

[137] H.P.Van Leeuwen : *Eng. Fract. Mechs.* : 6 : (1974) : pp141-161

[138] H.E.Townsend : *Corrosion* : 26 : (1970) : pp361-362

[139] P.M.Scott, D.R.V.Silvester : *UKOSRP interim technical report 3/02* : May 1977 : Dept. of Energy

[140] P.M.Scott, T.W.Thorpe, D.R.V.Silvester : *Corrosion sci.* : 23 : (1983) : pp559-575

[141] C.S.Carter : *Eng. Fract. Mech.* : 3 : (1971) : pp1-13

[142] J.D.Atkinson, T.C.Lindley : Presentation to the Int. Cyclic crack growth rate (PWR) meeting : UKAEA Risley, Warrington : May 1984 : (to be published in *Fatigue of Engng. Struct.*)

[143] C.Laird : ref. 7 : p139

[144] A.J.McEvily : *ASTM STP 811* : (1982) : pp283-312

[145] P.Neumann, H.Fuhlrott, H.Vehoff : ref. 119 : pp371-395

[146] B.R.W.Hinton : PhD thesis : University of Manchester : (1980)

[147] B.F.Brown : *Problems in the load carrying application of high strength steels* : Defense metals information center : Report no. 210 : (1964)

[148] H.J.Bhatt, E.H.Phelps : *Corrosion* : 17 : (1961) : pp430-434

[149] A.W.Thompson, I.M.Bernstein : *ASTM STP 821* : (1984) : pp114-127

[150] J.A.S.Green, H.W.Hayden, W.G.Montague : ref. 19 : pp200-217

[151] J.A.S.Green, H.W.Hayden : ref. 132 : pp234-245

[152] H.W.Hayden, S.Floreen : *Corrosion* : 27 : (1971) : pp429-433

[153] C.F.StJohn : *Scripta metall.* : 9 : (1975) : pp141-144

[154] R.E.Swanson, I.M.Bernstein, A.W.Thompson : *Scripta metall.* : 16 : (1982) : pp321-324

[155] J.R.Pickens, J.R.Gordon, J.A.S.Green : *Metall. Trans.* : 14A : (1983) : pp925-930

[156] R.E.Swanson, A.W.Thompson, I.M.Bernstein, J.L.Maloney : ref. 120 : pp459-466

[157] P.Smith, A.T.Stewart : *Metal Sci.* : 13 : (1979) : pp429-435

[158] A.Turnbull : private communication : (1985)

[159] J.F.Knott : *Fundamentals of fracture mechanics* : Butterworth, London : (1979) : ISBN 0/408/70789/5

[160] T.W.Thorpe, P.M.Scott, A.Rance, D.R.V.Silvester : *Int. J. Fatigue* : 5 : (1983) : pp123-133

[161] A.A.Aboutorabi : private communication : (1985)

[162] M.D.Halliday, C.J.Beevers : *The measurement of crack length and shape during fracture and fatigue* : ed. C.J.Beevers : EMAS, Warley, Birmingham : (1980) : pp85-112

[163] R.P.Gangloff : *Advances in crack length measurement* : ed. C.J.Beevers : EMAS, Warley, Birmingham : (1981) : pp175-229

[164] I.M.Austen, E.F.Walker : Proc. int. conf. *Fatigue '84* : Sept 1984 : EMAS, Warley, Birmingham : pp1457-1469

[165] M.J.Cannon : private communication : (1985)

[166] O.Vosikovsky : *J. Testing and Evaluation* : 6 : (1978) : pp175-182

[167] S.G.Druce, G.S.Booth : ref. 162 : pp136-163

[168] J.W.Hancock : private communication : (1981)

[169] A.C.Pickard, M.A.Hicks : ref. 163 : pp97-113

[170] T.W.Crooker, S.J.Gill, G.R.Yoder, F.D.Bogar : ref. 40 : pp415-425

[171] B.Mukherjee : *Int. J. Fract. Mech.* : 8 : (1972) : pp449-452

[172] I.M.Austen : ref. 162 : pp164-189

[173] I.M.Austen : BSC research report SH/PT/7422/8/79/B : (1979)

[174] R.P.Wei, W.Wei, G.A.Miller : *J. Testing and Evaluation* : 7 : (1979) : pp90-95

[175] W.G.Clark, S.J.Hudak : *Application of fatigue crack growth rate data to design* : Plenum press, New York : (1978) : pp67-81

[176] L.P.Pook : NEL report RE 40301 500 6/75 NEL 595 CL : Presented at SEE fatigue group symp. *Statistical aspects of fatigue testing* : 12th Feb 1975 : Warwick University

[177] L.P.Pook : *The role of crack growth in metal fatigue* : Metal Society, London : ISBN 0/904357/63/5 : chapter 5

[178] A.McMinn : *Fatigue Engng. Mater. Struct.* : 4 : (1981) : pp235-251

[179] A.McMinn : UKAEA report ND-R-526(S) : (1980) : ISBN 0/85/356132/X

[180] T.Saito : *Trans. ISIJ* : 24 : (1984) : pp1055-1062

[181] M.Pourbaix : *J. Less Common Metals* : 28 : (1972) : pp51-65

[182] D.R.Crow : *Principles and applications of electrochemistry* : Chapman and Hall, London : (1974) : ISBN 0/412121/808

[183] H.W.Pickering, M.Zamanzadeh : ref. 120 : pp143-152

[184] M.Smialowski : *Hydrogen in steel* : Pergammon, London : (1962)

[185] T.P.Radhakrishnan, L.L.Shrier : *Electrochima Acta* : 11 : (1966) : pp1007-1021

[186] U.R.Evans : *An introduction to metallic corrosion* : 3rd edn. : ISBN 0/7131/2758/9 : p155

[187] J.O'M.Bockris, J.McBreen, L.Nanis : *J.Electrochem. Soc.* : 112 : (1965) : pp1025-1031

[188] *J. Electrochem. Soc.* : 113 : (1966) : pp637-638 : discussion of ref. 187

[189] K.Chandrasekara-Pillai, R.Narayan : *Corrosion sci.* : 23 : (1983) : pp151-166

[190] J.W.Hancock, D.S.Gall, R.J.Appleton : unpublished work

[191] W.A.Van der Sluys, D.S.de Miglio : ref. 170 : pp443-469

[192] P.M.Scott, D.R.V.Silvester : UKAEA report HL 75/2552 : (1975)

[193] H.G.Morgan, T.W.Thorpe : Proc. conf. *Fatigue in offshore structural steel* : ICE, London : (1981) : pp19-27

[194] P.M.Scott, D.R.V.Silvester : *UKOSRP interim technical report 3/03* : (1977) : Dept. of Energy

[195] B.R.W.Hinton, R.P.M.Procter : *Corrosion sci.* : 23 : (1983) : pp101-123

[196] B.R.W.Hinton, R.P.M.Procter : ref. 120 : pp1005-1015

[197] I.M.Austen : private communication : (1984)

[198] I.M.Austen : BSC research report SH/PROD/EM/7422/11/81/B : (1981)

[199] I.M.Austen, J.M.West : *Eng. Fract. Mechs.* : 4 : (1972) : pp181-183

[200] R.Johnson, H.G.Morgan, I.Bretherton : *UKOSRP interim technical report 3/07* : (1980) : Dept. of Energy

[201] T.Misawa, N.Ringshall, J.F.Knott : *Corrosion sci.* : 16 : (1976) : pp805-818

[202] R.Johnson, I.Bretherton : *UKOSRP interim technical report 3/04* : (1979) : Dept. of Energy

[203] H.G.Crisp : ECSC Contract no. 7210.KE/8/801 Draft final report : (1980)

[204] J.C.Galsworthy : AMTE(M) tech. memo. TM83205 : AMTE(Holton Heath), Poole, Dorset BH16 6JU : (1983)

[205] I.M.Austen : BSC research report SH/PROD/EM/8247/1/82/A : (1982)

[206] P.E.Francis, A.S.Dolphin : NPL report DMA(A)55 : (1982)

[207] M.Habashi, G.Philipponeau, S.Widawski, J.Galland : Proc. int. conf. *ICF 6* : New Dehli, India : (1985) : pp2521-2528 : ISBN 0/08/029309/3

[208] O.Vosikovsky : *J. Testing and Evaluation* : 8 : (1980) : pp68-73

[209] J.D.Atkinson, T.C.Lindley : Central Electricity Research Laboratories : laboratory note RD/L/N 40/77 : (1977)

[210] J.J.W.Nibbering : *Corrosion sci.* : 23 : (1983) : pp645-662

[211] J.M.Barsom : *Eng. Fract. Mechs.* : 3 : (1971) : pp15-25

[212] J.M.Barsom : *Int. J. Fract. Mech.* : 7 : (1971) : pp163-182

[213] E.Bardal : Proc. int. conf. *7th Int. congress on metallic corrosion* : 4-11 Oct 1978 : Rio de Janeiro, Brazil : paper 121 : pp902-914

[214] E.Bardal, J.M.Sondenfor, P.O.Gartland : Proc. symp. *European offshore steels research* : 27-29 Nov 1978 : Welding Inst., Cambridge : pp415-438

[215] J.P.Gallagher, J.T.Ryder, J.C.Chadley : Proc. int. conf. *Mechanical behaviour of materials* : (1972) : Kyoto, Japan : pp328-341

[216] D.P.G.Lidbury : ref. 20 : pp149-172

[217] Y.W.Cheng : *Int. J. Fatigue* : 7 : (1985) : pp95-100

[218] T.W.Thorpe, A.Rance, D.R.V.Silvester, P.M.Scott : ref. 193 : pp35-43

[219] J.Tweed : private communication : (1985)

[220] A.Turnbull : submitted to *Metal Sci. Tech.* : (1985)

[221] R.Johnson, I.Bretherton : UKAEA report ND-R-151(S) : (1978)

[222] K.Endo, K.Komai,K.Minoshima : ref. 67 : pp77-86

[223] J.M.Barsom : ref. 13 : pp424-433

[224] K.Hirano, Y.Kobayashi, H.Nakazawa : ref. 222 : pp87-96

[225] R.W.Staehle : ref. 13 : p434 (discussion)

[226] R.W.Pasco, K.Sieradzki, P.J.Ficalora : ref. 20 : pp375-381

[227] M.O.Speidel, M.J.Blackburn, T.R.Beck, J.A.Feeney : ref. 13 : pp324-345

[228] D.F.Martin : *Marine chemistry* : Marcel Dekker Inc. : (1970) : Library of congress cat. no. 68-27532

[229] H.H.Johnson, P.C.Paris : *Eng. Fract. Mechs.* : 1 : (1968) : pp3-45

[230] M.O.Speidel : Proc. conf. *Theory of stress corrosion cracking in alloys* : NATO, Brussels : (1971) : ed. J.C.Scully : pp289-344

[231] L.Pecora, P.J.Ficalora : *Metall. Trans.* : 8A : (1977) : pp1841-1848

[232] C.M.Ransom, P.J.Ficalora : *Metall. Trans.* : 11A : (1980) : pp801-807

[233] S.J.Hudak, R.P.Wei : *Metall. Trans.* : 7A : (1976) : pp235

[234] T.Kondo, T.Kikuyama, H.Nakajima, M.Shindo, R.Nagasaki : ref. 13 : pp539-549

[235] R.P.Gangloff : ref. 20 : pp265-290

[236] J.D.Atkinson : private communication : (1985)

[237] P.M.Scott : UKAEA report AERE-R-11385 : (1984)

[238] A.M.Sullivan, T.W.Crooker : *Fracture mechanics and technology* : eds. G.C.Sih, C.L.Chow : Sijthoff & Nordhoff : ISBN 90/286/0637/8 : Vol.1 : pp687-698

[239] Y.Yoshino : *Corrosion* : 39 : (1983) : pp435-444

[240] H.Hanninen, K.Torronen, M.Kemppainen, S.Salonen : *Corrosion sci.* : 23 : (1983) : pp663-679

[241] S.J.Hudak, D.L.Davidson, R.A.Page : ref. 20 : pp173-198

[242] P.S.Maiya, W.J.Shack : ref. 20: pp199-209

[243] F.P.Ford : ref. 20 : pp117-147

[244] T.Shoji, H.Takahashi, M.Suzuki, T.Kondo : *J. Engng. Mater. Tech. - Trans. ASME* : 103 : (1981) : pp298-304

[245] J.R.Rice, W.J.Drugan, T.L.Sham : *ASTM STP 700* : (1980) : pp189-195

[246] P.Neumann, H.Verhoff, H.Fuhlrott : ref. 81 : p1313

[247] O.Vosikovsky : *Eng. Fract. Mechs.* : 11 : (1979) : pp595-602

[248] R.Brazill, G.W.Simmons, R.P.Wei : *J. Engng. Mater. Tech. - Trans. ASME* : 101 : (1979) : pp199-204

[249] R.P.Wei, G.Shim, K.Tanaka : ref. 20 : pp243-263

[250] P.Bristoll, J.A.Roeleveld : ref. 214 : pp439-458 (paper 18)

[251] J.K.Tien, R.J.Richards, O.Ruck, H.L.Marcus : *Scripta metall.* : 9 : (1975) : pp1097-1101

[252] H.J.Cialone, J.H.Holbrook : *Metall. Trans.* : 16A : (1985) : pp115-122

[253] W.G.Clark : ref. 132 : pp149-164

[254] N.J.Holroyd, G.M.Scamans, R.Hermann : ref. 20 : pp327-347

[255] D.L.Davidson, J.Lankford : ref. 81 : pp897-904

[256] O.Vosikovsky : *Corrosion* : 32 : (1976) : pp472-475

[257] I.M.Austen, P.McIntyre : *Metal Sci.* : 13 : (1979) : pp420-428

[258] R.W.Staehle : ref. 35 : pp574-602

[259] A.H.Cottrell : *The mechanical properties of matter* : Wiley, New York : (1964) : ISBN 0/471/17676/1

[260] I.M.Austen : BSC research report PT/7422/1/77/B : (1977)

[261] E.Maahn, H.Noppenau : Proc. int. conf. *Steel in marine structures* : (1981) : Paris : ECSC : paper 5.3

[262] D.S.Gall, J.W.Hancock : private communication : (1985)

[263] B.F.Jones : *J. Mater. Sci.* : 17 : (1982) : pp499-507

[264] B.F.Jones : ref. 20 : pp453-469

[265] R.P.Gangloff : *Res. mechanica letters* : 1 : (1981) : pp299-306

[266] P.Sanders : private communications : (1983-1985)

[267] A.Turnbull : NPL report DMA(D)234 : (1980)

[268] W.F.McIlhenny, M.A.Zeibun : *Chemical Engineering* : 3/11/69 pp81-86 and 17/11/69 pp251ff.

[269] ASTM standard D1141-52 : (1971) : (reapproved 1980)

[270] British Standards Institution : BS 3900

[271] J.E.Castle, S.Parvizi, A.H.Chamberlain : Proc. conf. *Microbial corrosion* : 8-10 March 1983 : NPL, Teddington : pp36-45

[272] R.L.Jones : private communication : (1983)

[273] *Offshore technology paper 4* : (1980) : Dept. of Energy : ISBN 0/86017/141/8

[274] D.G.Oldfield : *Offshore technology paper 6* : (1980) : Dept. of Energy : ISBN 0/86017/142/6

[275] J.R.Postgate : *The sulphate reducing bacteria* : 2nd edn : CUP : (1984) : ISBN 0/521/25791/3

[276] W.A.Hamilton, J.A.Hardy, H.R.Rosser : notes from course *Sulphate reducing bacteria - relevance to the offshore industry* : 9-12 Dec 1980 : Inst. Offshore Engng., Heriot-Watt Univy., Edinburgh

[277] C.M.Brown : ref. 276

[278] W.A.Hamilton : ref. 271 : pp1-5

[279] J.W.Hopton : Proc. microbiology group symp. : Inst. Petroleum, London : 5th Oct 1983 : pp32-49

[280] P.D.Gilbert, A.D.Steele, T.D.B.Morgan, B.N.Herbert : ref. 279 : pp71-80

[281] R.A.King, J.D.A.Miller : Proc. *1st int. conf. internal and external protection of pipes* : 9-11 Sept 1975 : University of Durham : paper F2

[282] A.K.Tiller : ref. 271 : pp54-65 and pp104-107

[283] A.K.Tiller : ref. 279 : pp1-31

[284] J.A.Hardy : private communication : (1983)

[285] J.A.Hardy : ref. 279 : pp57-63

[286] M.Walch, R.Mitchell : Proc. conf. *Corrosion '83* : (1983) : Anaheim, California : paper 249

[287] A.K.Tiller : private communication : (1985)

[288] R.J.Watkinson : ref. 279 : pp50-56

[289] T.G.Wilkinson : private communication : (1983)

[290] R.L.Starkey : *Producers monthly* : 22 : (1958) : pp12-30

[291] J.D.A.Miller : *Microbial biodeterioration* : Economic Microbiology, Vol. 6 : ed. A.H.Rose : Academic Press : (1981) : chapter 6

[292] P.Bos, J.G.Kuenen : ref. 271 : pp18-27

[293] D.C.White : Proc. conf. *Corrosion '82* : 22-26 March 1982 : Houston, Texas : paper 55

[294] D.D.Mara, D.J.A.Williams : *Biodeterioration of materials* : Applied Sci. Publ. : (1971) : eds. A.H.Walters, E.H.Hueck van der Plas : ISBN 0/85334/530/4 : Vol. 2 : pp103-113

[295] G.H.Booth, A.K.Tiller : *Trans. Faraday Soc.* : 56 : (1960) : pp1689-1696

[296] A.K.Tiller, G.H.Booth : *Trans. Faraday Soc.* : 58 : (1962) : pp110-115

[297] G.H.Booth, A.K.Tiller : *Trans. Faraday Soc.* : 58 : (1962) : pp2510-2516

[298] G.H.Booth, A.K.Tiller : *Corrosion sci.* : 8 : (1968) : pp583-600

[299] J.A.Hardy, J.L.Brown : *Corrosion* : 40 : (1984) : pp650-654

[300] K.D.Efird, T.S.Lee : *Corrosion* : 35 : (1979) : pp79-83

[301] R.L.Martin, R.R.Annand : *Corrosion* : 36 : (1981) : pp297-301

[302] D.Kirkwood, J.Hosie : ref. 276

[303] W.A.Hamilton : private communication : (1984)

[304] B.J.Berkowitz, F.H.Heubaum : *Corrosion* : 40 : (1984) : pp240-245

[305] A.K.Dunlop : *Corrosion* : 34 : (1978) : pp88-96

[306] T.V.Venkatasubramanian, T.J.Baker : *Metal Sci.* : 18 : (1984) : pp241-247

[307] O.Vosikovsky, R.J.Cooke : *Int. Jnl. Pressure vessels and piping* : 6 : (1978) : pp113-129

[308] R.G.J.Edyvean, C.J.Thomas, R.Brook, I.M.Austen : paper presented at int. conf. *Biologically induced corrosion* : 10-12 June 1985 : Gaithersburg, Maryland : NACE

[309] P.F.Sanders, S.Maxwell : ref. 271 : pp74-83

[310] R.Miller : private communication : (1984)

[311] B.N.Herbert, F.D.J.Stott : ref. 271 : pp7-17

[312] E.Senior : private communication : (1983)

[313] I.M.Kolthoff, E.B.Sandell, E.J.Meehan, S.Bruckenstein : *Quantitative chemical analysis* : 4th edn. : Macmillan, London : (1969) : Library congress cat. no. 69-10291

[314] R.G.J.Edyvean : private communications : (1983-1985)

[315] H.G.Truper, H.G.Schlegel : *Antonie van Leeuwenhoek* : 30 : (1964) : pp225-238

[316] I.McNeil : private communication : (1985)

[317] P.N.Green : private communication : (1985)

[318] D.S.Gall : MSc thesis : University of Glasgow : (in preparation)

[319] D.S.Gall, J.W.Hancock : Dept. of Energy, Petroleum Engng. Div. : research project OT/F/918 : draft final report : (1985)

[320] T.G.Wilkinson : ref. 271 : pp117-122

[321] M.Isida, H.Noguchi, T.Yoshida : *Int. J. Fract.* : 26 : (1984) : pp157-188

[322] F.W.Smith, M.J.Alavi : Proc. *1st int. conf. pressure vessel technology* : (1969) : Delft : ASME : pp793-800

[323] J.C.Newman : *Eng. Fract. Mechs.* : 5 : (1973) : pp667-689

[324] J.R.Rice, N.Levy : *J. Appl. Mechs. - Trans. ASME* : 94 : (1972) : pp185-194

[325] R.C.Shah, A.S.Kobayashi : *Int. J. Fract. Mechs.* : 9 : (1973) : pp133-146

[326] I.S.Raju, J.C.Newman : *Eng. Fract. Mechs.* : 11 : (1979) : pp817-829

[327] F.W.Smith, A.F.Emery, A.S.Kobayashi : *J. Appl. Mechs. - Trans. ASME* : 89 : (1967) : pp953-959

[328] J.C.Newman : *ASTM STP 687* : (1979) : pp16-42

[329] P.M.Scott, T.W.Thorpe : *Fatigue Engng. Mater. Struct.* : 4 : (1981) : pp291-309

[330] P.M.Scott, T.W.Thorpe : UKAEA report AERE-R10104 : (1981)

[331] A.A.Aboutorabi, M.J.Cowling : *Int. J. Fract.* : to be published

[332] S.J.Holdbrook, W.D.Dover : *Eng. Fract. Mechs.* : 12 : (1979) : pp347-364

[333] M.J.Cowling : private communication : (1984)

[334] S.E.Webster : BSC final report for ECSC agreement no. 7210.KG/801 : June 1984

[335] D.R.J.Owen, A.J.Fawkes : *Engineering fracture mechanics : numerical methods and applications* : Pineridge Press Ltd., Swansea : (1983) : ISBN 0/906674/26/3

[336] A.J.Fawkes, D.R.J.Owen, A.R.Luxmore : *Eng. Fract. Mechs.* : 11 : (1979) : pp143-159

[337] T.K.Hellen : *Int. J. for numerical methods in engineering* : 9 : (1975) : pp187-207

[338] R.D.Henshell, K.G.Shaw : *Int. J. for numerical methods in engineering* : 9 : (1975) : pp495-507

[339] D.P.Rooke, D.J.Cartwright : *Stress intensity factors* : HMSO, London : (1976) : ISBN 0/11/771336/8

[340] R.S.Barsoum : *Int. J. for numerical methods in engineering* : 10 : (1976) : pp25-37

[341] H.Tada, P.Paris : discussion at end of ref. 328

[342] PAFEC 75 : level 4 data preparation manual

Appendix

Program "AIM 65"

```
1000 REM ************************************************************
1010 REM *                                                          *
1020 REM *   Program to convert times from the AIM 65 into number of *
1030 REM *   elapsed fatigue cycles (also a data file for use with the *
1040 REM *   program "Fatigue" is produced).                        *
1041 REM *                                                          *
1050 REM *   R.J.Appleton                                           *
1060 REM *   Glasgow University                                     *
1070 REM *   15/3/1984                                              *
1080 REM *                                                          *
1090 REM ************************************************************
1100 OPTION BASE 0
1110 PRINTER IS 701
1119 REAL PD(200),cycles(200)
1120 INTEGER length(12)
1121 DISP "Enter test name  ";@ INPUT name$
1122 DISP "Enter R ratio    ";@ INPUT R
1123 DISP "Enter max. load (in kN)";@ INPUT test_load
1124 DISP "Enter potentiostat setting (V) ";@ INPUT potential
```

```
1125 CLEAR @ j=-1
1130 FOR i=1 TO 12 @ READ length(i)@ NEXT i
1140 DISP "Enter first date  : day,month,year"
1150 INPUT day1,month1,year1
1160 DISP "Enter first time  : hours,mins,secs"
1170 INPUT hours1,mins1,secs1
1180 DISP "Enter first cycles  :"
1190 INPUT cycles1
1200 time1=hours1*3600+mins1*60+secs1
1210 DISP "Enter second date : day,month,year"
1220 INPUT day2,month2,year2
1230 DISP "Enter second time : hours,mins,secs"
1240 INPUT hours2,mins2,secs2
1250 DISP "Enter second cycles :"
1260 INPUT cycles2
1270 time2=hours2*3600+mins2*60+secs2
1280 GOSUB days
1290 dt=time2-time1+86400*number
1300 dN=cycles2-cycles1
1310 frequency=dN/dt
1320 GOSUB titles
1330 lasttime=0
1340 number=0
1350 repeat: j=j+1
1360 DISP "Enter P.D., time  (hours,mins,secs)              (0,0,0) to stop run"
1370 INPUT PD(j),hours,mins,secs
1380 IF hours=0 AND mins=0 AND secs=0 THEN GOTO file_data
1390 newtime=hours*3600+mins*60+secs+number*86400
1400 IF newtime<lasttime THEN GOSUB newdate
1410 lasttime=newtime
1420 cycles(j)=INT ((newtime-time1)*frequency+.5)+cycles1
1430 PRINT USING one ; hours,":",mins,":",secs,newtime,PD(j),cycles(j)
1440 GOTO repeat
```

```
1450 REM ************************************************************************
1460 titles:
1470 PRINT USING two ; 1,hours1,mins1,secs1,time1,day1,month1,year1,cycles1
1480 PRINT USING two ; 2,hours2,mins2,secs2,time2,day2,month2,year2,cycles2
1490 PRINT
1500 PRINT "Frequency = ";dN;"/";dt;" = ";frequency;" Hz."
1510 PRINT
1520 day=day1 @ month=month1 @ year=year1
1530 GOSUB heading
1540 RETURN
1550 REM ************************************************************************
1560 newdate:
1570 newtime=newtime+86400
1580 number=number+1
1590 day=day1 @ month=month1 @ year=year1
1600 FOR n=1 TO number
1610 day=day+1
1620 IF INT (year/4)=year/4 THEN length(2)=29 ELSE length(2)=28
1630 IF day>length(month) THEN day=1 @ month=month+1
1640 IF month>12 THEN month=1 @ year=year+1
1650 NEXT n
1660 heading:
1670 PRINT "
1680 PRINT USING three ; day,"/",month,"/",year
1690 PRINT "
1700 PRINT USING four ; "Time","secs.","cycles"
1710 PRINT "
1720 RETURN
```

```
1730 REM ************************************************************
1740 days:
1750 number=0
1760 days=day1 @ month=month1 @ year=year1
1770 loop:
1780 IF days=day2 AND month=month2 AND year=year2 THEN EXIT FN
1790 number=number+1
1800 days=days+1
1810 IF INT (year/4)=year/4 THEN length(2)=29 ELSE length(2)=28
1820 IF days>length(month) THEN days=1 @ month=month+1
1830 IF month>12 THEN month=1 @ year=year+1
1840 GOTO loop
1850 one: IMAGE DD,A,DD,A,DD,2X,8D,2X,3D.D,2X,8D
1860 two: IMAGE "Time ",D," : ",DD,":",DD,":",DD,"  (",8D," secs )  on ",DD,"/",
DD,"/",DD,"  is ",8D," cycles"
1870 three: IMAGE DD,A,DD,A,DD
1880 four: IMAGE AAAAAAAA,2X,AAAAAAAA,2X,AAAAAAAA
1890 DATA 31,28,31,30,31,30,31,31,30,31,30,31
7040 file_data:
7050 CLEAR
7060 DISP "File data ?" @ INPUT a$@ IF a$ <> "Y" THEN STOP
7070 DISP "Filing ";name$;" data."
7080 CREATE name$,j+3.15
7090 ASSIGN# 1 TO  name$
7100 PRINT# 1 ; potential,R,test_load,j-1
7110 FOR i=0 TO j-1 @ PRINT# 1 ; cycles(i),PD(i) @ NEXT i
7120 ASSIGN# 1 TO  *
7130 BEEP @ STOP
```

Program "Patigue"

```
1000 REM ************************************************************************************************
1010 REM *                                                                                              *
1011 REM *     ==========================                                                               *
1020 REM *     Fatigue data analysis program                                                            *
1030 REM *     ==========================                                                               *
1031 REM *                                                                                              *
1040 REM *     R.J.Appleton                                                                             *
1050 REM *     Glasgow University                                                                       *
1060 REM *     15th. December 1984                                                                      *
1070 REM *                                                                                              *
1071 REM *     =======                                                                                  *
1072 REM *     Notes :                                                                                  *
1073 REM *     =======                                                                                  *
1074 REM *                                                                                              *
1075 REM *          Line 5250 plots air data upper bound for BS4360:50D                                 *
1076 REM *                                                                                              *
1080 REM *          FNa(x) (lines 8050 to 8080) gives the crack length as                               *
1090 REM *          a function of microvolts for 3pb specimens made from                                *
1100 REM *          BS4360;50D.                                                                         *
1110 REM *                                                                                              *
1111 REM *          FNdK(a) returns the value of /\K as a function of                                   *
1112 REM *          crack length for a 8"x2"x1" 3pb specimen. The value of                              *
1113 REM *          "constant" is calculated in line 3450.                                              *
1114 REM *                                                                                              *
1120 REM ************************************************************************************************
```

```
1130 REM
1140 REM
1150 GOSUB start
1160 GOSUB load_data
1170 GOSUB a_vs_N
1180 GOSUB dadN_vs_dK
1190 GOSUB results_printout
1200 GOSUB file_data
1210 REM ask for rerun
1220 END
2000 REM
2010 REM ==========
2020 REM      Subroutine to initialize computer and arrays
2030 REM ==========
2040 REM
2050 start: CLEAR
2060 OFF TIMER# 1 @ OFF TIMER# 2 @ OFF TIMER# 3 @ OFF KEY# @ OFF ERROR
2070 PRINTER IS 701 @ PLOTTER IS 705 @ PEN 1
2080 LIMIT 0,251,7,187
2090 REAL N(200),PD(200),dK(200),a(200),dadN(200)
2100 RETURN
2110 REM
3000 REM ==========
3010 REM      Subroutine to enter test data
3020 REM ==========
3030 REM
3040 load_data: CLEAR @ DISP " "
3050 DISP "Press <k1> to load data from disk, or <k2> to enter new data"
3060 ON KEY# 1,"Disk" GOTO disk_data  @ ON KEY# 2,"New data" GOTO new_data
3070 KEY LABEL
3080 wait_for_key_input: GOTO wait_for_key_input
3090 REM ----------
3100 REM   Enter data from either disk or keyboard
3110 REM ----------
3140 REM
```

```
3170 REM
3180 REM ------------------------------------------------
3190 REM       Routine to enter data from keyboard
3200 REM ------------------------------------------------
3210 REM
3220 new_data: CLEAR @ DISP "Enter test name  ";@ INPUT name$
3230 DISP "Enter R ratio    ";@ INPUT R
3240 DISP "Enter max. load (in kN) ";@ INPUT test_load
3250 DISP "Enter potensiostat setting (V) " @ INPUT potential
3260 CLEAR @ j=-1
3270 DISP "Enter P.D. , cycles  "
3280 repeat: j=j+1 @ INPUT PD(j),N(j)@ IF PD(j)<> 0 OR N(j)<> 0 THEN repeat
3290 j=j-1 @ GOTO calculate
3300 REM
3310 REM ------------------------------------------------
3320 REM       Routine to retrieve data from disk
3330 REM ------------------------------------------------
3340 REM
3350 disk_data: CLEAR
3360 DISP "Enter test name ";@ INPUT name$
3370 ASSIGN# 1 TO  name$
3380 READ# 1 ; potential,R,test_load,j
3390 FOR i=0 TO j @ READ# 1 ; N(i),PD(i)@ NEXT i
3400 ASSIGN# 1 TO  *
3410 GOTO calculate
3420 REM
```

```
3430 REM ---------- ---------- ---------- ----------
3434 REM Choose method of differentiating a vs N data
3435 REM ---------- ---------- ---------- ----------
3440 REM
3450 calculate: constant=test_load*.001*6*(1-R)*2*87.338228
3455 FOR i=0 TO j @ a(i)=FNa(FD(i)) @ NEXT i
3460 ON KEY# 1,"difference" GOTO method1  @ ON KEY# 8,"3pt linear" GOTO method1
3470 ON KEY# 2,"7pt p^bla" GOTO method2  @ ON KEY# 9,"ASTM" GOTO method2
3480 ON KEY# 3,"polynomial" GOTO method3  @ ON KEY# 10,"3pt fitted" GOTO method3

3490 CLEAR @ KEY LABEL
3500 DISP "Press function key to select required method of numerically
          differentiating the a vs. N data."
3510 waiting: GOTO waiting
3520 REM
3530 REM ---------- ---------- ---------- ----------
3540 REM   Branch to selected data reduction method
3550 REM ---------- ---------- ---------- ----------
3560 REM
3570 REM ---------- ---------- ---------- ----------
3580 REM   3pt linear difference method
3590 REM ---------- ---------- ---------- ----------
3600 method1: first=1 @ last=j-1 @ OFF KEY# @ CLEAR
3610 FOR i=first TO last
3620 dadN(i)=(a(i+1)-a(i-1))/(N(i+1)-N(i-1)) @ dK(i)=FNdK(a(i))
3630 NEXT i
3640 RETURN
3650 REM
3660 REM ---------- ---------- ---------- ----------
3670 REM   ASTM 7pt incremental fitted parabola
3680 REM ---------- ---------- ---------- ----------
3690 REM
```

```
3700 method2: n=3 @ first=n @ last=,-n @ N=2*n+1 @ OFF KEY# @ CLEAR
3710 REAL A(4,5),B(3),X(7),Y(7)
3720 FOR i=first TO last
3730 C1=.5*(N(i-n)+N(i+n)) @ C2=.5*(N(i+n)-N(i n))
3735 IF ABS ((N(i)-C1)/C2)>1 THEN STOP ELSE DISP i
3780 FOR k=1 TO N @ X(k)=N(i+k-n-1) C1)/C2 @ Y(k)=a(
3790 REM
3800 REM ##### start of least squares routine #######
3810 REM
3820 FOR l=1 TO 3 @ FOR m=1 TO 3
3830 S1,S2=0
3840 FOR I=1 TO N @ S1=S1+X(I)^(l-1)*X(I)^(m-1) @ S2=S2+X(I)^(l-1)*Y(I) @ NEXT I

3850 A(l,m)=S1 @ A(l,4)=S2
3860 NEXT m @ NEXT l
3870 row=3 @ col=4
3880 FOR k=1 TO row
3890 pivot=A(k,k) @ p=k
3891 FOR l=k+1 TO row
3895 IF ABS (A(l,k))<ABS (pivot) THEN skip1
3900 pivot=A(l,k) @ p=l
3910 skip1: NEXT l
3920 IF p=k THEN skip2
3930 FOR q=1 TO col @ temp=A(k,q) @ A(k,q)=A(p,q) @ A(p,q)=temp @ NEXT q
3931 skip2: NEXT k
3932 FOR J=2 TO col @ A(1,J)=A(1,J)/A(1,1) @ NEXT J
3933 FOR l=2 TO row @ FOR I=l TO row
3934 sum=0 @ FOR k=1 TO I-1 @ sum=sum+A(I,k)*A(k,1) @ NEXT k
3935 A(I,1)=A(I,1)-sum
3936 NEXT I
3937 FOR J=l+1 TO col @ sum=0
3938 FOR k=1 TO I-1 @ sum=sum+A(I,k)*A(k,J) @ NEXT k
```

```
3939 A(l,J)=(A(l,J)-sum)/A(l,l)
3940 NEXT J @ NEXT l
3941 B(row)=A(row,col)
3942 FOR m=1 TO row-1
3943 I=row-m @ sum=0
3944 FOR J=I+1 TO row @ sum=sum+A(I,J)*B(J) @ NEXT J
3945 B(I)=A(I,col)-sum
3946 NEXT m
3947 REM ####### End of least squares routine #######
3950 dadN(i)=(B(2)+2*B(3)*X(n+1))/C2
3960 dK(i)=FNdK(B(1)+B(2)*X(n+1)+B(3)*X(n+1)^2)
3970 NEXT i
3980 RETURN
4000 REM
4010 REM ================================================================
4020 REM      Subroutine to plot graph of crack length against cycles
4030 REM ================================================================
4040 REM
4050 a_vs_N: CLEAR @ ymin=50 @ ymax=0
4060 FOR i=0 TO j @ ymax=MAX (ymax,a(i)) @ ymin=MIN (ymin,a(i)) @ NEXT i
4070 xmin=N(0) DIV 1000 @ xmax=CEIL (N(j)/1000)
4080 FRAME
4090 LOCATE 5,135,5,95 @ SCALE xmin,xmax,ymin,ymax @ FXD 0
4100 PEN 2 @ LGRID (xmax-xmin) DIV 20,CEIL ((ymax-ymin)/10),0.0 @ PEN 1
4110 FRAME @ LORG 1 @ CSIZE FNz(.01,.9,"a(mm)",3)
4120 CSIZE FNz(.2,.9,name$,6) @ CSIZE FNz(.93,.02,"N/1000",7)
4130 LORG 5 @ L$="-" @ MOVE N(0)/1000,a(0) @ LABEL L$
4140 FOR i=1 TO j @ MOVE N(i-1)/1000,a(i-1) @ DRAW N(i)/1000,a(i) @ LABEL L$ @ N
EXT i
4150 BEEP @ RETURN
5000 REM
```

```
5010 REM ================================================================
5020 REM      Subroutine to plot logarithmic graph of da/dN against /\K
5030 REM ================================================================
5040 REM
5050 dadN_vs_dK: BEEP @ CLEAR
5060 DISP "Place new sheet of paper in plotter."
5070 DISP "Press <CONT> when paper is ready." @ PAUSE
5080 xmin=0 @ xmax=100 @ ymin=0 @ ymax=100
5090 LIMIT 0,251,7,187 @ PEN 1 @ FRAME @ SCALE xmin,xmax,ymin,ymax
5100 DEG @ LDIR 90 @ LORG 1
5110 RESTORE dadN_vs_dK_labels
5120 READ k@ FOR i=0 TO k @ READ y,x,L$,s@ CSIZE FNz(x,y,L$,s) @ NEXT i
5130 dadN_vs_dK_labels: DATA 15,.05,.19,da,6,.05,.23,dN,6,.53,.99,K,6,.58,.99,(M
Pa,3,.655,.99,m),3,.75,.97,100,3,.33,.97,10,3,.13,.2,(mm/cycle),3
5140 DATA .28,.95,10,3,.302,.938,-5,2,.28,.65,10,3,.302,.639,-4,2,.28,.35,10,3,.
302,.338,-3,2,.28,.05,10,3,.302,.038,-2,2
5150 CSIZE FNz(.2,.79,name$,6)
5160 MOVE 20,4 @ DRAW 20,11 @ MOVE 99,48 @ DRAW 99,52 @ DRAW 96,50 @ DRAW 99,48
5170 MOVE 98.75,63.75 @ DRAW 99.25,64 @ DRAW 98,65 @ DRAW 98,66
5180 LIMIT 238,10,68,144 @ SCALE -5,-2,1,2 @ FRAME
5190 PEN 2 @ MOVE -4,1 @ DRAW -4,2 @ MOVE  3,1 @ DRAW -3,2
5200 FOR k=-5 TO -3 @ FOR i=2 TO 9
5210 z=LGT (i*10^k) @ MOVE z,1 @ DRAW z,1.02 @ MOVE z,1.98 @ DRAW z,2
5220 NEXT i @ NEXT k
5230 FOR i=20 TO 90 STEP 10 @ z=LGT (i)
5240 MOVE -5,z @ DRAW -4.98,z @ MOVE -2,z @ DRAW -2.02,z @ NEXT i
5250 LINE TYPE 6 @ MOVE -4.1631963,1.30103 @ DRAW -2.8778497,1.69897
5260 LINE TYPE 1 @ LORG 5 @ L$="+" @ PEN 1
5270 MOVE LGT (dadN(first)),LGT (dK(first)) @ LABEL L$
5280 FOR i=first+1 TO last
5290 MOVE LGT (dadN(i-1)),LGT (dK(i-1)) @ DRAW LGT (dadN(i)),LGT (dK(i)) @ LABEL
 L$
5300 NEXT i
5310 BEEP @ RETURN
```

```
6000 REM
6010 REM ================================================================
6020 REM      Subroutine to print out results
6030 REM ================================================================
6040 REM
6050 results_printout: CLEAR
6060 PRINT @ PRINT "      ";name$ @ PRINT
6070 PRINT "      R=";R;" load=";test_load;"kN" @ PRINT
6080 PRINT USING line1 ; "========","====","======","======","=========="
6090 PRINT USING line1 ; " cycles ","P.D.","a(mm)"," dK "," da/dN  "
6100 PRINT USING line1 ; "========","====","======","======","=========="
6110 FOR i=0 TO first-1 @ PRINT USING line2 ; N(i),PD(i),a(i) @ NEXT i
6120 FOR i=first TO last
6130 PRINT USING line3 ; N(i),PD(i),a(i),dK(i),dadN(i)
6140 NEXT i
6150 FOR i=last+1 TO j @ PRINT USING line2 ; N(i),PD(i),a(i) @ NEXT i
6160 BEEP @ RETURN
7000 REM
7010 REM ================================================================
7020 REM      Subroutine to store data on disk
7030 REM ================================================================
7040 REM
7050 file_data: CLEAR
7060 DISP "File data ?" @ INPUT a$@ IF a$ <> "Y" THEN RETURN
7070 DISP "Filing ";name$;" data."
7080 CREATE name$,j+3,16
7090 ASSIGN# 1 TO  name$
7100 PRINT# 1 ; potential,R,test_load,j
7110 FOR i=0 TO j @ PRINT# 1 ; N(i),PD(i) @ NEXT i
7120 ASSIGN# 1 TO  *
7130 BEEP @ RETURN
```

```
8000 REM
8010 REM ================================================================
8020 REM       Function definitions and formatting statements
8030 REM ================================================================
8040 REM
8050 DEF FNa(x)
8060 x=x/100
8070 FNa=241.604992*(SQR (.0474565925^2-(1.362059-x)*.0042052113)-.0474565925)
8080 FN END
8090 REM ----------------------------------------------------------------
8100 DEF FNdK(a)
8110 a=a/50.8
8120 FNdK=constant*(1.93*a^.5-3.07*a^1.5+14.53*a^2.5-25.11*a^3.5+25.89*a^4.5)
8130 FN END
8140 REM ----------------------------------------------------------------
9150 DEF FNz(x,y,L$,s)
9160 x=xmin+(xmax-xmin)*x @ y=ymin+(ymax-ymin)*y @ CSIZE s
8170 MOVE x,y @ LABEL L$
8180 FNz=3
8190 FN END
8200 REM ----------------------------------------------------------------
8210 line1: IMAGE 5X,9A,2X,4A,2X,5A,3X,5A,3X,9A
8220 line2: IMAGE 5X,8D,2X,4D,2X,2D.2D
8230 line3: IMAGE 5X,3D,2X,4D,2X,2D.2D,3X,2D.2D,3X,D.2DE
```

Program "Readings"

This program was written to enable the A-D boards to be used in gathering experimental data. Each of the 16 input channels may be logged at a different time interval from the others.

```
10 DIM A(16)
20 DIM TI(16)
30 DIM TT(16)
35 FOR C=1 TO 16
36 TT(C)=0 : TI(C)=1430
37 NEXT C

40 INPUT "RESET CLOCK (Y/N)";A$
50 IF A$="Y" THEN GOSUB 1000
60 GOSUB 7000
70 GOSUB 5000

200 REM CHECK TIMES
206 GOSUB 6000
210 GOSUB 4000
220 PRINT T$
230 FOR C=1 TO 16
240 GOSUB 4000
250 T=60*T3+T2
260 IF T<TT(C) GOTO 310
270 IF T>TT(C)+3 GOTO 310
280 GOSUB 3000
290 TT(C)=TT(C)+TI(C)
300 IF TT(C)>1439 THEN TT(C)=TT(C)-1440
310 NEXT C
315 GET A$
316 IF A$<>"" THEN GOTO 40
320 GOTO 200
```

```
1000 REM CLOCK SET
1010 POKE 4,3
1020 POKE 5,208
1040 INPUT "DATE D,MO,Y";D,MO,Y
1050 IF Y>100 GOTO 1040
1060 INPUT "DAY OF WEEK";DW
1070 INPUT "TIME H,M";H,M
1080 POKE 28702,M
1090 POKE 28703,H
1100 POKE 28704,D
1110 POKE 28705,MO
1120 POKE 28706,Y
1130 POKE 28707,DW
1140 POKE 28710,65
1150 POKE 28711,24
1160 PRINT "PRESS A KEY TO START"
1165 GET A$
1166 IF A$="" GOTO 1165
1170 A=USR(0)
1180 RETURN

3000 REM TAKE READING
3010 POKE 4,0
3020 POKE 5,152
3030 A=USR(0)
3040 IF C=8 GOTO 3150
3050 INPUT *A(C),C,C,1
3060 IF A(C)<150 OR A(C)>5000 GOTO 3140
3070 B=0
3080 FOR J=0 TO 99
3090 INPUT *A(C),C,C,1
3100 B=B+A(C)
3110 NEXT J
3120 GOSUB 4000
3130 PRINT! C;INT(B/10+0.5)/10-5;T$
3140 GOTO 3180
3150 INPUT *A(C),C,C,2
3160 GOSUB 4000
3170 PRINT! "TEMP  :";INT(A(C)*10+0.5)/10;T$
3180 RETURN
```

```
4000 REM READ CLOCK
4010 POKE 4,0
4020 POKE 5,208
4030 A=USR(0)
4040 T1=PEEK(28701)
4050 T2=PEEK(28702)
4060 T3=PEEK(28703)
4070 T$=STR$(T3)+STR$(T2)+STR$(T1)
4080 RETURN

5000 REM PRINT DATE
5010 GOSUB 4000
5020 D=PEEK(28704)
5030 MO=PEEK(28705)
5040 Y=PEEK(28706)
5050 D1=PEEK(28708)
5060 D2=PEEK(28709)
5070 PRINT! " "
5080 PRINT! "************************"
5090 PRINT! "* ";CHR$(D1);CHR$(D2);TAB(7);D;MO;Y;TAB(19);"*"
5100 PRINT! "************************"
5110 PRINT! " "
5130 DL=D
5150 PRINT! "C  PD          TIME  "
5160 PRINT! "======================="
5170 RETURN

6000 REM CHECK DATE
6010 GOSUB 4000
6020 D=PEEK(28704)
6030 IF D<>DL THEN GOSUB 5000
6040 RETURN

7000 REM SET LOGGING INTERVALS
7010 INPUT "CHANNEL";C
7020 IF C=0 GOTO 7080
7030 INPUT "INTERVAL H,M";H,M
7040 TI(C)=60*H+M
7050 INPUT "START AT H,M";H,M
7060 TT(C)=60*H+M
```

```
7070 GOTO 7010
7080 PRINT! "CH. ";TAB(5);"INTVL";TAB(14);"START"
7090 FOR C=1 TO 16
7100 PRINT! C;TAB(5);TI(C);TAB(14);TT(C)
7110 NEXT C
7120 INPUT "SETTINGS OK (Y/N)";A$
7130 IF A$<>"Y" GOTO 7010
7140 RETURN
```